



東北医科薬科大学
TOHOKU MEDICAL AND PHARMACEUTICAL UNIVERSITY

東北医科薬科大学
分子生体膜研究所年報

二〇一七年度【平成二十九年】

東北医科薬科大学 分子生体膜研究所年報 2017年度 研究成果報告書

2017 Annual Report of
Institute of Molecular Biomembrane and Glycobiology



ご挨拶

分子生体膜研究所がその前身である癌研究所時代から発展させてきた糖鎖生物学は、我が国の糖鎖生物学研究拠点としての実績を築いており、本学の大きな特色となっております。これまでに、学術フロンティア推進事業「生体膜の糖鎖機能と疾患に関する薬学的研究」（平成 18～22 年度）、私立大学戦略的研究基盤形成支援事業「生体膜糖鎖異常に起因する生活習慣病発症機序の解明と臨床への応用」（平成 24～28 年度）に選定され、現代の主要疾患である糖尿病とその合併症、アレルギー・喘息、自己免疫疾患、がんなどにおいて、糖鎖機能異常が様々な機構で病態に関与することを見出してきました。2016 年の医学部開設、付属病院の開設と連携研究の強化により、分子生体膜研究所を中心として推進してきたこれまでの基礎研究の成果を、迅速に疾患の予防・診断・治療・創薬といった臨床への応用に結びつける研究実施体制が飛躍的に向上しつつあります。

2017 年度は、分子生体膜研究所名誉所長であります箱守仙一郎先生の米寿を記念して箱守仙一郎糖鎖科学シンポジウムを開催いたしました。箱守先生の特別講義のタイトルは、『糖鎖研究の回想と将来への展望』でありました。将来の展望として、

- ・ 糖鎖の新しい認識・結合様式の存在の検索
- ・ 糖鎖が細胞膜に組み込まれている様式の研究
- ・ 遺伝子に支配された糖鎖発現様式と疾患の関連性の検索
- ・ 糖鎖発現のエピジェネティック制御機構に関する研究
- ・ 糖鎖によるステム細胞表現型質コントロールの可能性

を挙げられました。さらに、特にがん研究においては、コーンハイムの迷芽説「将来、癌になるべき細胞（癌ステム細胞）は、個体発生の途上に作られ、組織の中に迷いこんで、潜んでいるが、ある時期に、あるきっかけによって、癌としての本来の能力を発揮するようになる（Cohnheim J. 1875, *Virchows Arch Pathol Anat Physiol Klin Med* 65: 64).」に多くを学ばなければならないとして、

- ・ 癌ステム細胞が組織の中に潜んでいる機構は何か？
- ・ 又、本来の癌機能を発揮する機構はなにか？
- ・ それらの機構に、糖鎖がどの様に関与するのか、今後の研究は興味深い
- ・ 従来の細胞レベルでの“cell glycobiology”から、組織や器官での周囲の細胞からの影響を含む“tissue/ organ glycobiology”の研究分野が益々盛んになると予想される

と述べられています。

今回の年報では、各研究部門の研究活動報告に加え、箱守仙一郎糖鎖科学シンポジウムおよび箱守仙一郎賞創設のご紹介をいたします。

皆様からのなお一層のご指導、ご鞭撻のほど衷心よりお願い申し上げます。

平成 30 年 3 月

東北医科薬科大学分子生体膜研究所・所長

東北糖鎖研究会・会長

井ノ口 仁一

目 次

■ 所長挨拶・・・・・・・・・・・・・・・・・・・・・・・・	1
分子生体膜研究所 所長 井ノ口 仁一	
■ 箱守仙一郎糖鎖科学シンポジウム開催報告・・・・・・・・	4
■ 箱守仙一郎賞 (Sen-itiroh Hakomori Glycoscience Award) ・・・・・・・・	6
東北医科薬科大学分子生体膜研究所「箱守仙一郎賞」規約	
平成 29 年度 箱守仙一郎賞	
奨励賞 山本 勇人 (弘前大学医学部)	
奨励賞 郷 慎司 (東北医科薬科大学)	
優秀論文賞 周 穎 (東北医科薬科大学)	
■ 研究報告・・・・・・・・・・・・・・・・・・・・・・・・	15
機能病態分子部門	
「スフィンゴ糖脂質の病態生理学的意義の解明に向けて」	
井ノ口 仁一、稲森 啓一郎、永福 正和、狩野 裕考	
生体膜情報部門	
「生活習慣病に関連した G タンパク質共役受容体の機能と糖鎖および受容体間相互作用による調節」	
東 秀好、中川 哲人、黒田 喜幸	
細胞制御部門	
「がん細胞における N-型糖鎖の機能解析と臨床への応用に向けて」	
顧 建国、福田 友彦、伊左治 知弥	
分子認識部門	
「レクチンのがん薬物治療への応用」	
細野 雅祐、菅原 栄紀、立田 岳生	
■ 学会発表・・・・・・・・・・・・・・・・・・・・・・・・	27
■ 学術論文・・・・・・・・・・・・・・・・・・・・・・・・	31

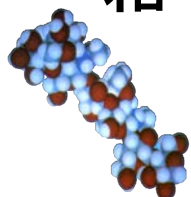
箱守仙一郎糖鎖科学シンポジウム開催報告

東北医科薬科大学附属分子生体膜研究所名誉所長であります恩師・箱守仙一郎先生におかれましては、2017年2月13日をもって88歳の米寿を迎えられました。箱守先生は、1959年（昭和34年）に東北大学の医学部から東北薬科大学附属癌研究所第一部（当時）教授として赴任され、研究所の充実発展に尽くされた後渡米し、糖脂質研究の世界的権威となりました。以来、多くの優れた門下生を世に送り出しつつ、一貫して癌研究所の指導にもご尽力下さいました。米国シアトルのワシントン州立大学、フレッドハッチンソン癌研究所、バイオメンブレンインスティテュートおよびパシフィックノースウェスト研究所において先生のご指導を受けた研究者が、本邦に限らず世界で糖鎖生物学をリードする存在となっていることは周知の事実であります。2006年4月、癌研究所が発展的に改組され分子生体膜研究所（以下分生研）となって以降も顧問・指導教授として研究のご指導を頂いております。

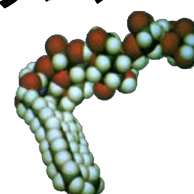
分生研では、米寿を迎えられた恩師箱守仙一郎先生の、多年にわたる世界の糖鎖生物学への比類のないご貢献ならびに私どもへの温かいご指導に対し、限りない尊敬と報恩の念を込めまして、箱守先生が長年追求してこられた糖鎖生命科学に関する最新の知識を共有できる場として箱守仙一郎糖鎖科学シンポジウム（Glycoscience Symposium with Gratitude to Dr. Sen-itiroh Hakomori）を開催いたしました。

2017年11月10日（金）13:30から東北医科薬科大学70周年記念講堂において開催されたシンポジウムには、門下生を中心に国内外から多くの参加者が訪れ盛況を博しました。また、箱守先生のご功績を長く後世に伝承すべく、分生研では後進研究者の育成を目的とした「箱守仙一郎賞（Sen-itiroh Hakomori Glycoscience Award）」を創設いたしました。シンポジウム懇親会会場において第一回の受賞式が執り行われ、受賞者には箱守先生より顕彰楯と副賞が贈られました。

箱守仙一郎糖鎖科学シンポジウム



Glycoscience Symposium with Gratitude to Dr. Sen-itiroh Hakomori



平成29年11月10日(金) 13:30-17:00
東北医科薬科大学70周年記念講堂

Opening remark

13:30-13:35



Roger A Laine (University of Louisiana)
Windows Opened to Many Research Directions by
Experiencing Postdoctoral Training with Hakomori-sensei

13:35-14:00



Reiji Kannagi (Academia Sinica)
Glycan markers for embryonic stem cells and human cancers

14:00-14:25



Kiyotoshi Sekiguchi (Osaka University)
An odyssey in the extracellular world:
From fibronectin to matrixome research

14:25-14:50

Coffee break



Yasuyuki Igarashi (Hokkaido University)
Run after Hakomori-sensei:
ten years in Seattle and 20 years afterward

15:10-15:35



Alessandro Prinetti (University of Milano)
GEMs from the Emerald City

15:35-16:00



Kazuhisa Iwabuchi (Juntendo University)
A paradigm shift in innate immunity has been the recent
evidence of carbohydrate-carbohydrate interactions

16:00-16:25



Masahiro Hosono
(Tohoku Medical and Pharmaceutical University)
A Half-century Story of the Frog Lectin:
from CRI to IMBG with Dr. Hakomori

16:25-16:50

Closing

Chair: **Jin-ichi Inokuchi**



東北医科薬科大学附属分子生体膜研究所
井ノ口 仁一, 東 秀好
願 建国, 細野 雅祐



箱守仙一郎先生の米寿を祝う会 平成29年11月10日 於 江陽グランドホテル

東北医科薬科大学分子生体膜研究所
「箱守仙一郎賞」(Sen-itiroh Hakomori Glycoscience Award) 規約

平成 29 年 11 月 10 日
東北医科薬科大学分子生体膜研究所
井ノ口 仁一

名称

箱守仙一郎賞

授与機関

東北医科薬科大学分子生体膜研究所

目的

生物系化学系を問わず広く糖鎖科学を専攻し、日夜努力を続けている東北エリアの研究者を顕彰することにより、日本の糖鎖科学研究の増進を図る。

賞の種別

奨励賞 1 名 顕彰楯および副賞
優秀論文賞 1 名 顕彰楯および副賞

対象

- (1) 奨励賞：東北エリア（新潟県および群馬県を含む）で研究に従事する 45 歳未満の研究者
 - (2) 優秀論文賞：同地域で研究に従事し、申請時点で大学院生もしくは博士研究員である者
- * いずれも指定された期間内に発表（accepted でも可）された学術論文に対して審査・授与する。

選考方法

自薦および他薦によるものとし、東北糖鎖研究会世話人が審査する。
評価を点数化（次項参照）して決する。

授賞方法

東北糖鎖研究会開催時に授賞および受賞講演を行う。

運用方法

顕彰楯および副賞の購入費は、箱守賞基金を原資とし、分子生体膜研究所がこれを支弁する。

その他

事務局は分子生体膜研究所内に置く。

審査

(1) 応募資格および応募方法

東北6県、新潟県および群馬県（東北糖鎖研究会エリア）で研究を行っている45歳未満の糖鎖科学研究者（大学院生、博士研究員は自動的に優秀論文賞へのノミネートとなる）。対象論文は、その年度内（ただし応募締切以前）にImpact factorが付与されている英文学術雑誌（査読有）に出版、または掲載が決定されている原著論文（acceptedでも可）とし、応募者が筆頭著者となっているものとする。要旨和訳と論文PDFを添えて既定のエントリーフォームに記入してメールにて応募する。化学系・生物系は問わない。自薦および他薦どちらでも受け付ける。応募期間等についてはその都度決定し、周知する。

書類送付先：東北医科薬科大学 分子生体膜研究所 所長 井ノ口 仁一

メールアドレス：jin@tohoku-mpu.ac.jp

(2) エントリーフォーム（別添）

(3) 審査委員および審査方法

- 1) 分子生体膜研究所所長が審査員長を務める。
- 2) 東北糖鎖研究会世話人が審査員となる。ただし、世話人が推薦者または自薦者の所属責任者あるいは論文の共著者である場合は審査に参加しない。
- 3) 期限内に提出された論文について事務局が一次審査（下記基礎点による）を行い、奨励賞および優秀論文賞それぞれ上位3報を選定する。
- 4) 上位3報について審査員が下記評価項目を採点し、全員（その都度人数は異なる）の評価平均点＋基礎点（100点満点、1点未満は四捨五入）から最上位者を受賞者として決定する。
- 5) 最高点が複数出た場合は審査員長の判断に委ねる。

基礎点

Impact factor	2.0 未満	10 点
	4.0 未満	20 点
	6.0 未満	30 点
	8.0 未満	40 点
	10 未満	50 点
	10 以上	60 点

評価最高点

独創性	10 点
インパクト（重要性）	10 点
論文構成	10 点
将来性	10 点

平成 29 年度 箱守仙一郎賞
(Sen-itiroh Hakomori Glycoscience Award)

奨励賞

山本 勇人 弘前大学医学部 附属病院泌尿器科 助教

新規ヒアルロン酸分解酵素 transmembrane protein 2 (TMEM2) の発見

A mammalian homolog of the zebrafish transmembrane protein 2 (TMEM2) is the long-sought-after cell-surface hyaluronidase

郷 慎司 東北医科薬科大学 機能病態分子学 助教（現：川崎医科大学 病態代謝学 講師）

ガングリオシドの微細構造変化が制御する筋分化機構

Altered expression of GM3 molecular species during myoblast differentiation, and its biological significance

優秀論文賞

周 穎 東北医科薬科大学 細胞制御学 (D3)

Inhibition of fucosylation by 2-fluorofucose suppresses human liver cancer HepG2 cell proliferation and migration as well as tumor formation

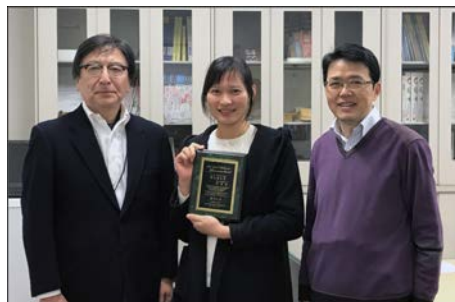
Scientific Reports 7(1):11563, 2017, doi:10.1038/s41598-017-11911-9



左より、井ノ口所長、山本勇人博士、箱守先生、郷慎司博士



奨励賞：郷 慎司博士



優秀論文賞：周 穎さん

奨励賞

新規ヒアルロン酸分解酵素transmembrane protein 2 (TMEM2) の発見

A mammalian homolog of the zebrafish transmembrane protein 2 (TMEM2) is the long-sought-after cell-surface hyaluronidase

山本 勇人 (弘前大学医学部 附属病院泌尿器科・助教)

ヒアルロン酸 (HA) は、細胞の様々な機能に関与する高分子多糖類である。HA の代謝に関しては、まず、細胞外または細胞表面の HA 分解酵素により細胞外にある高分子 (HMW) HA が切断される。次に切断された中分子量の HA が細胞内に取り込まれ、リソソーム内で単糖へ分解されると考えられている。細胞内における HA 分解酵素に関しては、HYAL1 と HYAL2 は主にリソソームに存在する HA 酸分解酵素であり、近年同定された CEMIP / KIAA1199 は、細胞内のクラスリン被覆小胞の経路において HA を分解すると考えられている。細胞外における HA 酸分解酵素についても様々研究されているが、依然として詳細は不明瞭なままである。今回我々は心内膜の発生において重要な役割を果たす Transmembrane protein 2 (TMEM2) が細胞表面に存在するである HA 分解酵素であることを証明した。まず Live staining および surface biotin assay を用いて TMEM2 が II 型膜貫通型タンパク質として細胞表面に発現していることを確認した。次に TMEM2 が、HMW-HA を約 5kDa の HA に分解すること、コンドロイチン硫酸またはデルマトン硫酸分解活性を持たないこと、 Ca^{2+} 依存性の HA 分解酵素であること、至適 pH が約 6~7 であることを確認した。さらには細胞内のクラスリン被覆小胞内で活性を有する CEMIP / KIAA1199 とは異なり、TMEM2 は細胞を必要とせずタンパク質のみで活性を有することを証明した。最後に in situ HA degradation assay を用いて、TMEM2 が細胞表面に接触している細胞外 HA を分解していることを確認した。これらの結果は、TMEM2 が細胞外において HMW-HA を中分子量の HA に切断する HA 分解酵素であることを示唆している (1)。

(1) Hayato Yamamoto, Yuki Tobisawa, Toshihiro Inubushi, Fumitoshi Irie, Chikara Ohyama, Yu Yamaguchi. *J. Biol. Chem.*, **292** (18), 2017. DOI 10.1074

【経歴】

平成 15 年 弘前大学医学部医学科卒業

平成 19 年 弘前大学大学院泌尿器科学講座入局

平成 23 年 弘前大学大学院医学研究科卒業

(膀胱癌の浸潤機構における invadopodia の意義について研究)

平成 27~29 年 5 月

Sanford Burnham Preby MEDICAL DISCOVERY INSTITUTE, Yamaguchi Laboratory へ客員研究員として研修。

(新規ヒアルロン酸分解酵素 TMEM2 について研究)

平成 29 年 6 月 弘前大学医学部附属病院泌尿器科配属

【受賞の感想と抱負】

この度、箱守仙一郎賞奨励賞を賜りましたこと大変光栄に存じます。箱守先生はじめ東北糖鎖研究会論文賞審査委員の先生方に深く御礼申し上げます。私の所属している弘前大学泌尿器科は、箱守先生の教室におられた福田穰、道子先生より指導を仰ぎ、現在の糖鎖研究に至っております。今回の受賞まで私自身、箱守先生とお会いする機会はありませんでしたが、箱守先生の多くのご功績を拝見しておりました。その箱守仙一郎先生のお名前がついた賞をいただけること、また今回は第一回記念として箱守先生の米寿を祝う会にお招きいただき、箱守先生とお会いすることができたこと、誠に身に余る光栄です。

受賞論文は2017年5月まで留学していた Sanford Burnham Prebys Institute、山口祐教授の教室での研究内容となります。当教室ではてんかん発作、自閉症などの脳神経疾患や多発性外骨腫（MHE）など多岐にわたる疾患と糖鎖との関連性について研究しておりますが、以前よりヒアルロン酸の代謝に関して興味を持っておりました。今回我々は細胞膜に存在するヒアルロン酸分解酵素に着目し、心内膜の発生において重要な役割を果たす Transmembrane protein 2 (TMEM2) が細胞表面に存在するヒアルロン酸分解酵素であることを証明しました。論文内容は以下の通りです。①TMEM2 が II 型膜貫通型タンパク質として細胞表面に発現している。②TMEM2 はヒアルロン酸を約 5kDa に分解し、コンドロイチン硫酸またはデルマタン硫酸分解活性を持たない。③Ca²⁺ 依存性の分解酵素である。④至適 pH が約 6~7 である。⑤実際に TMEM2 が細胞表面に接触している細胞外 HA を分解していることを確認。詳細などご興味のある方は J Biol Chem. 2017 May;292(18):7304-7313 を参照いただけると幸いです。

この研究が今後のヒアルロン酸代謝の研究の一助になればこれ以上の喜びはありません。また、TMEM2 が臓器の発生や悪性腫瘍の浸潤転移に関与していると考えており、泌尿器科の領域で更にヒアルロン酸の研究を進めていきたいと考えております。

最後に山口教授、大山教授をはじめ、両研究室のメンバーの支えなくして、今回の僥倖に恵まれることはなかったので、この場を借りまして御礼を申し上げさせていただきます。今後受賞者として恥じることのないよう、より一層精進して参りたいと思います。

山本 勇人

奨励賞

ガングリオシドの微細構造変化が制御する筋分化機構

Altered expression of GM3 molecular species during myoblast differentiation, and its biological significance

郷 慎司 (川崎医科大学 病態代謝学・講師)

スフィンゴ糖脂質は、セラミドにグルコース、ガラクトース、N-アセチルグルコサミン、N-アセチルガラクトサミン、シアル酸などの糖が酵素により段階的に付加された糖鎖構造を有した両親媒性の細胞膜構成脂質である。とくに糖鎖構造中にシアル酸を含むスフィンゴ糖脂質は「ガングリオシド」とよばれている。ガングリオシドは、細胞膜上で様々な分子と特異的に相互作用し機能的微小膜領域「マイクロドメイン (ラフト)」を形成し様々な生命現象を制御していることが報告されている。当研究室では、ガングリオシドの一つ「GM3」に注目し、GM3 がインスリンシグナル、免疫機能、聴覚機能、摂食行動などを制御していることを新たに見出してきた (1)。

近年、スフィンゴ糖脂質のセラミドの構造の多様性とその機能にも注目が集まってきている。セラミド構造中のアシル鎖およびスフィンゴイド塩基の構造 (鎖長、水酸化などの修飾、不飽和度) の組み合わせにより、約 40 種の多様な構造が天然で見出されている。我々はヒト血清中の GM3 分子種を LC-MS/MS を用いて解析した結果、炭素数 24 で水酸化修飾されたアシル鎖を持つ GM3 分子種の量が生活習慣病の様々なリスクファクターと強く相関していることを見出した (2)。この報告を含め、糖鎖部分とセラミド部分の両者の多様性の組み合わせによる「スフィンゴ糖脂質分子種の超多様性」が複雑に生命現象を制御していることが示唆されてきている。

筋細胞はその分化において、隣接する細胞間での認識・情報交換を行い、細胞膜融合を起こし多核の筋管細胞を形成する。この筋分化過程では細胞膜の劇的な変化がおこるため、細胞膜におけるスフィンゴ糖脂質およびマイクロドメインの機能を考えるうえで興味深い対象である。そこで本研究では、筋細胞分化モデルとして汎用されるマウス筋芽細胞 C2C12 細胞の分化過程におけるスフィンゴ糖脂質を解析した。分化前の筋芽細胞の段階では GM3 のシアル酸は「Neu5Ac」であるのに対し、分化進行 (筋管形成) に伴い、「Neu5Gc」へと変化した。また、GM3 のセラミドアシル鎖部分の構造は分化前には炭素数 24 のものが主要であったが、分化に伴い炭素数 16 のものが増加し主要なものへと変化した。見出したシアル酸分子種変化およびセラミドのアシル鎖構造変化は筋分化過程の様々なステップに重要であることが示唆された (3)。

つまり筋細胞は、同じ GM3 であっても、そのセラミド構造および糖鎖中のシアル酸の構造を変化させることで、その性質を変え、筋分化を適切に、繊細に制御していると考えられる。

シアル酸は一括りで考えられがちであるが、炭素 5 位の構造、各位の水酸基に対する多様な修飾によって多様な分子種が存在する。シアル酸の構造多様性も加味するとスフィンゴ糖脂質の多様性はさらに広がる。今後、これらスフィンゴ糖脂質構造多様性の発現制御機構、各構造の性質・機能、およびスフィンゴ糖脂質構造多様性の生物学的意義に関して解明を目指す。

(1) Inokuchi J. (2011) *Proc. Jpn. Acad., Ser. B.* 87, 179-198

(2) Veillon L, Go S, Matsuyama W, Suzuki A, Nagasaki M, Yatomi Y, Inokuchi J.,(2015) *PLoS*

One.,10(6):e0129645

- (3) Go S, Go S, Veillon L, Ciampa MG, Mauri L, Sato C, Kitajima K, Prinetti A, Sonnino S, Inokuchi J. (2017) *J. Biol. Chem.*, 292, 7040-7051

【経歴】

名古屋大学 農学部 卒業

名古屋大学大学院 生命農学研究科 博士課程修了 (博士(農学))

(生物機能開発利用研究センター 北島健教授のもと、シアル酸の代謝に関する研究)

東北薬科大学 (現・東北医科薬科大学) 分子生体膜研究所 学術フロンティア研究員

東北薬科大学 (現・東北医科薬科大学) 機能病態分子学教室 助教

(分子生体膜研究所 機能病態分子学 井ノ口仁一教授のもと、ガングリオシドの代謝制御機構および機能に関する研究)

2017年3月より、川崎医科大学 病態代謝学教室 講師

【受賞の感想と抱負】

この度、平成29年度箱守仙一郎賞 奨励賞を賜りましたこと、大変光栄に存じます。学生の時代、糖鎖研究を始めてからずっと教科書・論文で目にし続けてきた、箱守先生の御名前を冠した賞であることに恐縮しつつ、糖鎖科学の発展に寄与できる知見を得られるよう、研鑽を積んでまいりたいと存じます。

名古屋での学生時代、北島健先生、佐藤ちひろ先生のもとシアル酸の代謝制御の研究に取り組み、卒業後、東北薬科大学 分子生体膜研究所で井ノ口仁一先生のご指導のもとガングリオシドの機能および代謝制御機構に関する研究に取り組みできました。今回の受賞対象となった論文は、ガングリオシドの新機能解明に向け、新たに立ち上げた筋分化の系で思いがけず偶然見つかった現象です。ガングリオシド“GM3”のセラミド部分の構造とシアル酸部分の構造が筋分化に伴い大きく変化するという現象で、糖脂質の構造多様性の発現が厳密に制御されており、繊細に生命現象を制御し得る可能性を示唆したものでした。

マニアックな部分ではありますが、名古屋時代に見ていたシアル酸分子種と、仙台で見えてきた糖脂質がつながった研究でもあります。諸先生方、先輩方、同僚の皆様、学生さんとの出会い、そして皆様のご指導・ご協力・ご支援のおかげであると大変感謝しております。

東北ですごした約10年は大変すばらしい期間でした。東北糖鎖研究会にもほぼ毎回参加させていただき、様々な方々と活発で有意義な議論をさせていただきました。

縁あって2017年3月に岡山県にある川崎医科大学に移籍しました。東北での経験を生かし、糖鎖の生合成・分解の代謝バランス制御機構、そして機能に関して新たな視点で研究を展開しようと考えております。環境もこれまでとは大きく異なり、悪戦苦闘の日々が続いておりますが、できれば近い将来、大きな成果をもって東北の地を訪れることができるように…、今回の受賞を励みに研鑽を重ね、糖鎖科学研究に尽力しようと思っております。今後ともご指導ご鞭撻のほどよろしくお願い申し上げます。

郷 慎司

優秀論文賞

「Inhibition of fucosylation by 2-fluorofucose suppresses human liver cancer HepG2 cell proliferation and migration as well as tumor formation」

Scientific Reports 7(1):11563, 2017, doi:10.1038/s41598-017-11911-9

周 穎 （東北医科薬科大学・薬科学専攻博士後期課程(D3)）

【論文要旨】

α 1,6 フコース（コアフコース）転移酵素(Fut8)により生合成されるコアフコシル化糖鎖は、肝がんのバイオマーカーとして非常に特異性が高いことで注目されている糖鎖構造である。一方、我々は肝がんの発生・増殖にもコアフコシル化糖鎖の発現が重要であることを明らかにしている。しかし、治療を考える上では、Fut8 遺伝子の欠失やその酵素活性の阻害という方法は困難である。本研究では、コアフコシル化をがん組織特異的に抑制することを目的に、L-フコースのアナログである 2-fluorofucose (2FF)の有用性を検討した。2FF は細胞内に取り込まれて、GDP-fucose 合成の *de novo* 経路を阻害すると知られている。2FF の添加によりヒト肝がん由来 HepG2 細胞のコアフコシル化が劇的に抑制されることをレクチン検出や質量分析で確認した。細胞表面の重要な受容体である EGFR や β 1 インテグリンなど個別の分子でもコアフコシル化が消失することを確認した。また、これらの受容体を介したシグナルが減弱、細胞増殖や細胞遊走、軟寒天上でのコロニー形成能も有意に抑制された。一方、*in vivo* では、マウス皮下へ HepG2 細胞を移植し、定期的に移植部位近傍へ 2FF を投与したところ、腫瘍組織のコアフコシル化糖鎖の発現が強く抑制された。さらに、腫瘍サイズ並びに細胞内のシグナル伝達経路も有意に抑制されることがわかった。以上のことから、肝がん組織におけるコアフコシル化の重要性を示すと共に、2FF のような化合物が肝がんの新規治療薬になる可能性が強く示唆された。

【受賞の感想と抱負】

It's really a great honor for me to receive the Sen-itiroh Hakomori glycoscience award. This is the best affirmation and encouragement for my three years studying in Tohoku Medical and pharmaceutical University.

Here, I would like to show my heartfelt gratitude to Prof. Hakomori as well as the Prize committee members. Prof. Hakomori is an outstanding scientist in the world, who has made a great contribution to the glycobiology, the biochemistry and cell biology. As a student, I was very lucky to have several chances to listen to his lectures, and very impressed with his talk. Under the guidance of Prof. Hakomori, I had deeper understanding of glycobiology and became more and more interested in the glycobiology.

Time flies, I have been studying in Tohoku Medical and pharmaceutical University for nearly 3 years. I owe my deepest gratitude to President Motoaki Takayanagi to provide the opportunity to study in Tohoku Medical and Pharmaceutical University. I feel grateful to our university for providing us such a high-quality academic environment, a good academic atmosphere, plenty of academic resource and an extensive communication platform. During the 3-year staying, I have learned a lot of things, not only about science, but also Japanese habits, lifestyle and cultures.

I would also like to express my sincere thanks to Prof. Jianguo Gu, Dr. Tomohiko Fukuda and Dr. Tomaya Isaji. Their rigorous academic attitude, extensive academic knowledge as well as their enthusiasm for science deeply infected me and triggered my love for these marvelous experiments. Under their help, I gradually clarified my research direction with confidence, and finally I understood the value and charm of the glycan's world.

After graduation, I plan to go back to China to continue scientific research on glycobiology. I want to apply my basic knowledge that I have learned here to translational research, and try my best to introduce the importance of glycans to more and more researchers and clinical doctors. And also I would like to appreciate your advices and comments on my research in the future.

Thank you very much!

周 穎 (Zhou Ying)

研究報告

スフィンゴ糖脂質の病態生理学的意義の解明に向けて 機能病態分子部門 井ノ口 仁一

機能病態分子学教室の2017年最初のトピックは、11年間の研究生活を共にした郷慎司助教が3月に川崎医科大学の松田純子教授が新たに開設された病態代謝学教室の講師として栄転したことである。郷博士との仕事は、ガングリオシド GM3 と聴覚、筋分化とガングリオシド、シアル酸代謝、o-GlcNAc とスフィンゴ糖脂質代謝、などの多岐にわたっており現在も共同研究を継続している。10年間の研究成果をまとめた2編の総説「ガングリオシド GM3 合成酵素欠損症から見るスフィンゴ糖脂質機能」(1)および「Gangliosides and Hearing」(2)を出版した。また、最近の研究成果である「筋分化とガングリオシドの生理的意義」に関する原著論文をJBCに報告した(3)。マウス筋芽細胞 C2C12 細胞の分化過程におけるスフィンゴ糖脂質を解析したところ、分化前の筋芽細胞の段階では GM3 のシアル酸は「Neu5Ac」であるのに対し、分化進行（筋管形成）に伴い、「Neu5Gc」へと変化した。また、GM3 のセラミドアシル鎖部分の構造は分化前には炭素数 24 のものが主要であったが、分化に伴い炭素数 16 のものが増加し主要なものへと変化した。見出したシアル酸分子種変化およびセラミドのアシル鎖構造変化は筋分化過程の様々なステップに重要であることが示唆された(3)。つまり筋細胞は、同じ GM3 であっても、そのセラミド構造および糖鎖中のシアル酸の構造を変化させることで、その性質を変え、筋分化を適切に、繊細に制御していると考えられる。この研究で郷博士は、第一回箱守仙一郎賞（奨励賞）を受賞したのは大変喜ばしいことである。

郷博士の川崎医大転出に伴い、当研究室の博士研究員であった狩野裕考博士が2017年4月より助手として着任した。狩野博士は、私が北大薬学部のアシスタント教授時代の学部学生であり、今は亡き稲垣冬彦教授の下で構造生物学を学んで修士号を取得し、その後、東北大学薬学部の倉田教授の研究室でショウジョウバエの自然免疫で学位を取得した後、縁あってわたしの研究室に所属した。現在、自然免疫系におけるスフィンゴ糖脂質の病態生理学的意義について鋭意研究を進めている。我々の主研究課題である「メタ

ボリック症候群におけるスフィンゴ糖質病態生理学的意義」の解明において、自然免疫系の異常な活性化にもとづく炎症反応の誘導に、ガングリオシド GM3 分子種発現バランスの異常が原因であることを証明しつつある。図1に現在の知見に基づく作業仮説を示す。

研究員の穴戸は、医学部医化学教室の上村講師と共同でガングリオシド GM2 合成酵素におけるゴルジ体繫留機構の解析についての原著論文を発表した(4)。本研究では、GM2 合成酵素 (GM2S) が新規 mRNA バリエーションをもち、この新規 mRNA から逆行輸送シグナルとして機能する R-based motif をもつ M1-GM2S が翻訳されることを示した。さらに、R-based motif をもたない既知のアイソフォームである M2-GM2S と M1-GM2S がへ

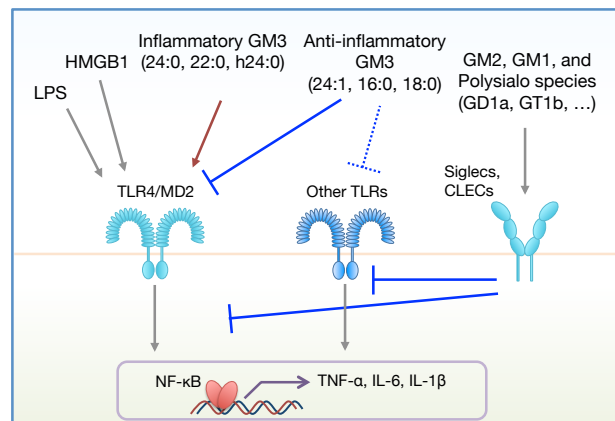


図1 ガングリオシドを介した炎症制御メカニズムの仮説

テロダイマーを形成することで、M2-GM2S ホモダイマーよりも高い安定性をもつことが示された。興味深いことに、この安定性の向上は小胞体への逆行輸送ではなくゴルジ体繫留に依存するものであり、GM2S において R-based motif がゴルジ体繫留シグナルとして機能することが示唆された (図 2)。また、GM3 合成酵素 (GM3S) の Exon3 ノックアウトマウスを用いた解析で、他組織では GM3 合成活性が消失するが、肝臓で GM3 合成活性が残存することを見出した。これまで、野生型マウスの解析において、肝臓組織で高い GM3 合成活性が認められるにも関わらず、mRNA の発現量が他臓器と比較して著しく低いことが示されていた。肝臓のみで高発現している新規 mRNA バリエント (c1-type) を同定し、肝臓での高い GM3 合成活性は c1-type の発現に由来することを示した。また、c1-type は Exon3 がスプライシングされても、新たに人工的なスプライシングアイソフォームが合成される。これが GM3S-Exon3-KO マウスの肝臓で GM3 合成活性が残存していた理由であることを示した(5)。

東京医科歯科大の横山博士との共同研究で、非常に興味深い結果が得られた(6)。セラミドアナログである 1-phenyl-2-decanoylamino-3-morpholino-1-propanol (PDMP) はスフィンゴ糖脂質の合成阻害剤として開発されたが、リソソームや小胞体の構造にも影響を与えることが知られていた。本研究では、PDMP が mTORC1 の細胞内局在を変化させることで mTORC1 の活性を制御する可能性に着目し、その検証を試みた。その結果 PDMP 処理により mTORC1 の小胞体との共局在率が有意に増加した。さらに mTORC1 をリソソーム膜に動員する足場となる Ragulator の構成要素 LAMTOR1 も、PDMP 処理によりリソソームから小胞体へと局在が変化することが判明した。これらの結果から、PDMP 処理により mTORC1 がリソソームから小胞体へ移行することが示された(6)。本研究は細胞内局在の変化という、今までに全く知られていない作用機序による mTORC1 阻害剤の開発にもつながると期待される。

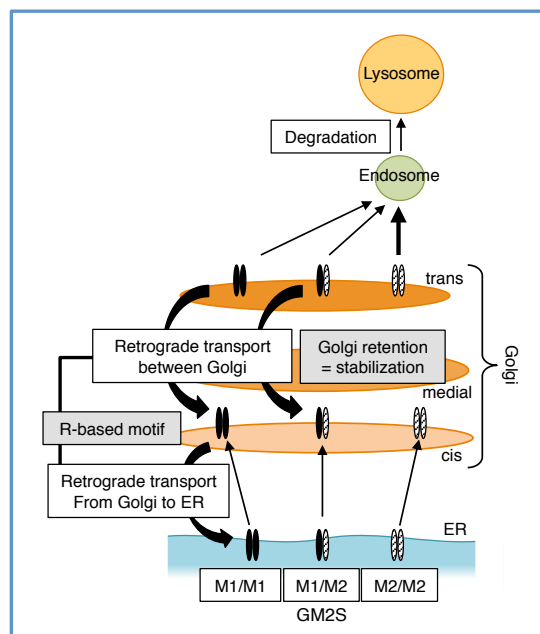


図 2 M1-GM2S の細胞質領域 N 末端に存在する R-based motif は、ゴルジ体から小胞体への逆行輸送とゴルジ体繫留に関する

2017年に発表した論文

1. ガングリオシド GM3 合成酵素欠損症から見るスフィンゴ糖脂質機能 郷慎司、井ノ口 仁一 「生化学」 2017
2. Gangliosides and hearing. Inokuchi J., Go S., Yoshikawa M. and Strauss K. *Biochim. Biophys. Acta*, 1861, 2485-2493, 2017
3. Altered expression of ganglioside GM3 molecular species and a potential regulatory role during myoblast differentiation. Go S., Go S., Veillon L., Ciampa M.G., Mauri L., Soto C., Kitajima K., Prinetti A., Sonnino S. and Inokuchi J. *J. Biol. Chem.*, 292, 7040-7051, 2017
4. Identification of a new B4GalNAcT1 (GM2/GD2/GA2 synthase) isoform, and regulation of enzyme stability and intracellular transport by arginine-based motif

Shishido F., Uemura S., Kashimura M. and Inokuchi J. *Biochim. Biophys. Acta*, 1859, 2001-2011, 2017

5. Identification of a new liver-specific c-type mRNA transcriptional variant for mouse ST3GAL5 (GM3/GM4 synthase). Shishido F., Uemura S., Niita T. and Inokuchi J. *Glycoconj. J.*, 34, 651-659, 2017
6. PDMP, a ceramide analogue, acts as an inhibitor of mTORC1 by inducing its translocation from lysosome to endoplasmic reticulum. Ode T., Podyma-Inoue K.A., Terasawa K., Inokuchi J., Kobayashi T., Watabe T., Izumi Y. and Hara-Yokoyama M. *Exp. Cell Res.* 350, 103-114, 2017

生活習慣病に関連した G タンパク質共役受容体の機能と糖鎖および受容体間相互作用による調節

生体膜情報部門 東 秀好

1. 肥満関連 GPCR の機能とそのネットワーク

我々が以前から注目しているリガンド不明の G タンパク質共役受容体 (GPCR) の一つである GPRC5B は、中枢神経系や脂肪細胞、膵臓 β 細胞に発現し、その多コピーが BMI 値と相関する肥満関連受容体である。mGluR 等と同じ Class C に属する GPRC5B は、高脂肪食摂取時の脂肪細胞の増大やインスリン分泌、血糖値の制御に関与する。膵臓 β 細胞の生存性やインスリン分泌が、GPRC5B を発現することで低下することが分かっており、糖尿病患者の膵臓 β 細胞では GPRC5B 発現が亢進している。しかし、GPRC5B がどのようなシグナルを介して、これらの現象を制御しているのかは明らかでない。そこで我々は、GPRC5B の発現により、細胞内でどのようなシグナル伝達が引き起こされるのかを検討した (1)。まず、HEK293 細胞に GPRC5B を発現させると、発現した細胞の増殖が亢進していることが分かった。次に、シグナル伝達分子の阻害剤を用いて、GPRC5B の発現による細胞増殖の亢進に関わるシグナル伝達経路を検討した。その結果、ラパマイシン標的シグナル (mTOR) とプロテインキナーゼ C (PKC) の阻害剤により、GPRC5B による細胞増殖が抑制された。さらに、三量体 G タンパク質の α サブユニットの阻害ペプチドにより、GPRC5B に結合する $G\alpha$ タンパク質を検討したところ、 $G\alpha_q$ の阻害により細胞増殖が抑制された。これらの結果から、GPRC5B のシグナルは、 $G\alpha_q$ および PKC を介して mTOR を活性化すると考えられた。mTOR シグナルは、脂肪細胞の増殖亢進により肥満を誘導する。また、mTOR シグナルが膵臓 β 細胞からのインスリン分泌を促進する一方、慢性的な活性化はインスリン分泌を低下させ、糖尿病の発症につながると考えられている。GPRC5B による脂肪細胞の増大やインスリン分泌の制御といった現象は、mTOR シグナルを制御することで引き起こされていると考えられた。

そこで、我々は、GPRC5B の過剰発現がマウスインスリノーマ (MIN6) 細胞のインスリン分泌に及ぼす影響を検討したところ、GPRC5B の過剰発現によって MIN6 細胞から培地中に放出されるインスリン量が上昇することを見出した (2)。次に、このインスリン分泌亢進のメカニズムを明らかにするため、インスリン遺伝子の発現をリアルタイム PCR により測定すると、GPRC5B を過剰発現した MIN6 ではインスリン遺伝子の発現が上昇していた。インスリン遺伝子は、転写因子の PDX-1 により転写が調節される。また、PDX-1 の発現は mTOR シグナルにより調節される。従って、GPRC5B の発現による MIN6 のインスリン分泌の亢進には、GPRC5B から mTOR シグナルを介したインスリンの増産が寄与していることが示唆された。

β 2-アドレナリン受容体 (β 2AR) は、カテコラミンをリガンドとする G タンパク質共役受容体 (GPCR) で、気管支や血管等の拡張・収縮、グリコーゲン分解を制御する。また、 β 2AR は脂肪細胞にも発現し、脂質代謝に関与する。近年、酵母の系を用いた解析結果から、 β 2AR と GPRC5B が相互作用することが報告された。我々は、GPRC5B が関与する現象が、 β 2AR と GPRC5B の相互作用により引き起こされているのではないかと考えた。そこで、HEK293T に β 2AR と GPRC5B を発現させ、免疫沈降をおこなったところ、両 GPCR は共沈降されたので、これらが哺乳動物細胞においても相互作用しているこ

とが明らかになった (3)。次に、活性化した GPCR は β アレスチンが結合することで脱感作されることから、 β 2AR と β アレスチンの結合を β ガラクトシダーゼの α 相補を利用して検出した。その結果、GPCR5B の存在により、 β 2AR と β アレスチンの結合が低下した。さらに、 β 2AR が持つ 2 本の N 結合型糖鎖が欠損した β 2AR は、アゴニスト刺激により脱感作されやすいが、GPCR5B が共存すると、糖鎖欠損 β 2AR と β アレスチンの結合も顕著に低下しており、脱感作が起こりにくくなると考えられた。このことから、 β 2AR と GPCR5B の相互作用は、アゴニスト刺激による β 2AR の脱感作を起こりにくくし、 β 2AR の G タンパク質経路の活性化が維持される可能性が示唆された。また、GPCR5B との相互作用に、 β 2AR の N 結合型糖鎖は関与しないと考えられた。特に、GPCR5B と β 2AR は脂肪細胞において共発現しているので、両分子が相互作用し β 2AR のシグナルを増強し、脂質代謝を亢進させることによって、脂肪細胞の増大に繋がっている可能性がある。

2. GPCR の N 結合糖鎖とジスルフィド架橋の機能、脂質ラフトとの関わり

上記のごとく、 β 2AR では N 結合糖鎖は脱感作の制御に関与していた。我々の研究室ではブラジキニン B2 受容体(B2R)が GT1b ガングリオシドとコンドロイチン硫酸 C の連続刺激により不応化されることと ATP/UTP 受容体 P2Y₂ (P2Y₂R)と共役することを見出した (4) ので、この現象における N 結合糖鎖の役割を含めた分子機構を解析している。B2R と P2Y₂R は共に G α q/11 を共役 G タンパク質とする Class A の GPCR で、炎症誘発、血圧低下、発痛に関与する。両者のヘテロオリゴマーはジスルフィド架橋による共有結合によるものと推定している。そこで、まず、両受容体の細胞における局在を調べた。両者は ER からゴルジ装置での糖鎖付加を経て細胞膜表面に発現されるが、細胞膜上でのマイクロドメインへの分布は少し異なり、P2Y₂R がほぼすべて脂質ラフトの画分に分画されるのに対して B2R はラフトと非ラフトの両画分にほぼ等量分画された。P2Y₂R の N 結合糖鎖は N 末端ドメインに 2 ヶ所あり、2 ヶ所の糖鎖を欠損させた変異体は細胞膜表面に輸送されずに ER に留まったが、脂質ラフト画分には分画された (6)。興味深いことに、P2Y₂R を共発現すると B2R はラフト画分へ多く分画され、両受容体の密な相互作用が示唆された (5)。一方、B2R はアゴニスト刺激によりホモダイマーを形成し、このホモダイマー形成やアレスチンリクルートには N 末端ドメインが不可欠である。我々は、P2Y₂R についてアゴニスト刺激とは無関係にホモダイマーが形成されることを見出し、それはジスルフィド架橋によるものであることを証明した (7)。P2Y₂R には N 末端ドメイン、第 1、第 2、第 3 細胞外ループにそれぞれ 1 ヶ所ずつ Cys 残基が存在する。細胞膜表面発現や活性化に必須な中央の 2 ヶ所の Cys 残基に加え、外側の 2 ヶ所の Cys 残基間の架橋がホモダイマー形成に関与することを明らかにした。B2R の N 結合糖鎖はホモダイマー形成に必要とされているが、P2Y₂R とのヘテロオリゴマー形成には糖鎖の小さい B2R が優先的に関わっていた (4)。P2Y₂R の場合、N 結合糖鎖が小さい方がホモダイマー・オリゴマーの形成率が高かった (8,9)。前述のごとく、2 ヶ所の N 結合糖鎖を欠失すると、細胞膜表面に発現されないが、2 ヶ所とも、あるいは、どちらか 1 ヶ所の糖鎖欠損変異体は野生型よりもホモダイマー・オリゴマーの形成率が高かった。さらに、Asn9 は欠失しても活性を保持したが、Asn13 の欠失は活性をほぼ失った。このように、同じ Class A に属する B2R と P2Y₂R であるが、これらの N 型糖鎖の機能は大きく異なっていた。

REFERENCES

1. 黒田 喜幸, 中川 哲人, 東 秀好 (2017) 肥満と関連する受容体 GPRC5B による mTOR シグナルの制御. 日本薬学会第 137 回年会, 仙台
2. 小松 伊織, 黒田 喜幸, 中川 哲人, 東 秀好 (2017) β 2-アドレナリン受容体と GPRC5B の相互作用による脱感作の制御. 日本薬学会第 137 回年会, 仙台
3. 黒田 喜幸, 中川 哲人, 東 秀好 (2017) オーフアン GPCR, GPRC5B によるインスリン分泌亢進とそのメカニズム. 第 36 回日本糖質学会年会, 旭川
4. Shimazaki, A., Nakagawa, T., Mitoma, J., and Higashi, H. (2012) Gangliosides and chondroitin sulfate desensitize and internalize B2 bradykinin receptors. *Biochem. Biophys. Res. Commun.* 420, 193-198
5. Nakagawa, T., Takahashi, C., Matsuzaki, H., Kuroda, Y., and Higashi, H. Membrane raft recruitment of bradykinin B2 receptor by ATP/UTP receptor P2Y₂ via their close association. *Manuscript in preparation.*
6. Nakagawa, T., Takahashi, C., Matsuzaki, H., Takeyama, S., Sato, S., Sato, A., Kuroda, Y., and Higashi, H. (2017) N-glycan-dependent cell-surface expression of the P2Y₂ receptor and N-glycan-independent distribution to lipid rafts. *Biochem. Biophys. Res. Commun.* 485, 427-431
7. Abe, M., Watanabe, K., Kuroda, Y., Nakagawa, T., and Higashi, H. (2018) Homodimer formation by the ATP/UTP receptor P2Y₂ via disulfide bridges. *J. Biochem., Tokyo.* in press.
8. 矢口 沙也子, 黒田 喜幸, 中川 哲人, 東 秀好 (2017) ATP/UTP 受容体 P2Y₂ の N 結合糖鎖の 2 量体形成に及ぼす効果: ブラジキニン B2 受容体との比較. 第 11 回東北糖鎖研究会, 桐生
9. 矢口 沙也子, 阿部 真耶, 黒田 喜幸, 中川 哲人, 東 秀好 (2017) ATP/UTP 受容体 P2Y₂ の細胞外 Cys 残基と N 結合糖鎖の機能. 第 90 回日本生化学会大会, 神戸

がん細胞におけるN-型糖鎖の機能解析と臨床への応用に向けて 細胞制御部門 顧 建国

糖タンパク質は糖鎖と蛋白質が共有結合した生体分子である。蛋白質上の糖鎖の結合様式は一般的にはN-型とO-型という2種類がある。N-型糖鎖は、ポリペプチド上にAsn-X-Ser/Thrモチーフのアスパラギン(Asn)のアミド基(-NH₂)にC-N結合でN-アセチルグルコサミン(GlcNAc)を還元末端とする糖鎖の総称である。糖鎖はタンパク質の物性に影響を与えると同時にタンパク質の機能、そして分子間の認識や細胞内シグナル伝達に大きな役割を持つ。私達は、図1に示すような分岐型糖鎖の生合成に関わるN-アセチルグルコサミン転移酵素III(GnT-III)、N-アセチルグルコサミン転移酵素V(GnT-V)、 α 1,6 フコース転移酵素(Fut8)の機能に注目して研究してきた。近年の研究によりそれらの糖鎖は、細胞機能に密接に関わっていることが明らかになりつつある。

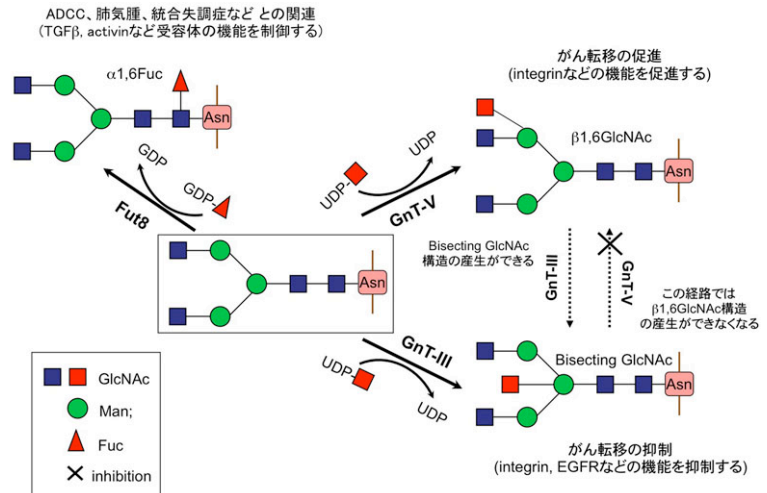


図1. 注目する分岐型N-型糖鎖の生合成と主な機能

I. 細胞接着および移動におけるインテグリン α 5上のN-型糖鎖の重要性について

細胞接着分子であるインテグリンは α 鎖と β 鎖から成るヘテロ二量体で、ECMへの細胞の接着を媒介する主要な糖蛋白質で、細胞内蛋白質のチロシンリン酸化や低分子量GTP結合蛋白質の活性化を通じて細胞内骨格系の再編成や増殖・分化のシグナル伝達に深く関わる(図2, A)。また、インテグリンと細胞増殖因子受容体との相互作用は、細胞の増殖・移動・生存などの生理的な過程のみならず、がん細胞の増殖・転移・浸潤など病理的な過程にも重要な役割を担うと考えられている。図2のようにインテグリン α 5に14カ所、 β 1鎖には12カ所の糖鎖付加部位があるが、これまで我々はそれぞれ3カ所の糖鎖がインテグリンの α と β 鎖ヘテロダイマー形成や機能発現に重要である

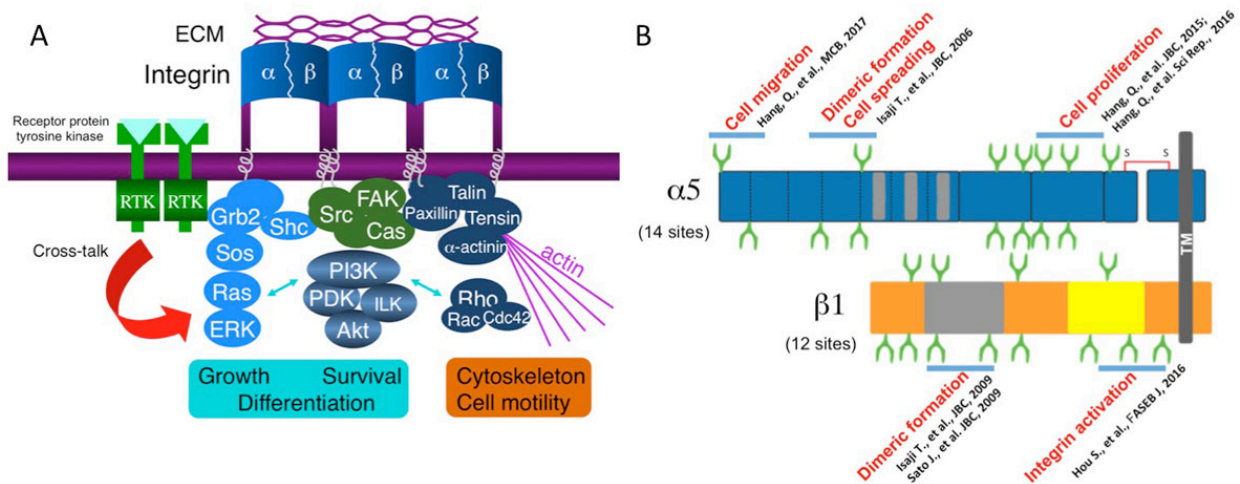


図2. A, インテグリンの機能; B, α 5 β 1にN-型糖鎖付加サイトと機能の特異性

ことを同定した (Isaji, T., et al. JBC. 2009)。最近、我々はさらにインテグリン $\alpha 5$ の N-型糖鎖に焦点を絞り、分子間複合体の形成および細胞内シグナル伝達の制御を解析し (図 2, B)、 $\alpha 5$ が lipid raft において EGFR と相互作用し、EGFR を介した細胞内シグナル伝達を負に制御することを明らかにした (Hang, Q., et al. JBC. 290, 29345-60, 2015)。また、部位特異的変異導入法を駆使して $\alpha 5$ の 11 番目の糖鎖が $\alpha 5$ と EGFR との相互作用に重要であり、その相互作用は EGFR の負の制御に重要であることを立証した (Hang, Q., et al. Sci. Rep. doi: 10.1038/srep33507, 2016)。その 11 番目サイトには他のサイトより分岐型糖鎖が多く付加されたことも分かった。また、インテグリン $\beta 1$ に対しても解析を行った。 $\beta 1$ が EGFR と相互作用において、 $\beta 1$ に付加されている糖鎖の中でも特に膜近傍の糖鎖が重要であることを明らかにした。さらに、それらの糖鎖構造に $\alpha 2,6$ シアリル化が必要である (Hou, S., FASEB J., 30, 4120-31, 2016)。それらの知見から、N-型糖鎖または特定の糖鎖構造が細胞膜上での分子間の相互作用に重要な役割を演じていると考えられる。

最近、私達は、細胞移動を制御するインテグリン $\alpha 5$ 上の重要な糖鎖付加部位 (1 と 2 番目) の同定に成功した (1)。その分子機序としては、1 と 2 番目に付加された糖鎖が細胞膜上 syndecan-4 分子と $\alpha 5$ との複合体形成に重要で、その糖鎖を無くすと $\alpha 5$ のエンドサイトーシスが抑制され、そして細胞移動が低下すると考えられる。さらに興味深いところに、その 1 と 2 番目の糖鎖の欠損でインテグリンからのシグナル伝達に重要な働きをする Focal adhesion kinase (FAK) が過剰に活性化された。実は FAK の活性化はインテグリンを介する細胞遊走に大事であるが、過剰な活性化は逆に細胞移動を阻害する。今後、これらの結果を *in vivo* でも検討し、インテグリンと他の受容体を介するシグナル伝達の Cross-talk の分子機序の解明や糖鎖による抗がん剤の開発に貢献する新知見の提供を目指す。

II. コアフコースによるがん性変化の制御について

一方、コアフコースは図 1 に示すようにフコース転移酵素 (Fut8) により生合成され、肝がんの特異的バイオマーカーや抗体医療とも深く関わっており、注目されている糖鎖の一つである。その Fut8 遺伝子が欠損させると、マウスは様々な病態を生じる。一方、我々は肝がんの発生・増殖にもコアフコシル化糖鎖の発現が重要であることを明らかにしている (Wang, et al., Sci Rep, 2015; FASEB J, 2015)。しかし、治療を考える上では、Fut8 遺伝子の欠失やその酵素活性の阻害という方法は困難である。最近、コアフコシル化をがん組織特異的に抑制することを目的に、L-フコースのアナログである 2-fluorofucose (2FF) の有用性を検討した (6)。2FF は細胞内に取り込まれて、GDP-fucose 合成の *de novo* 経路を阻害すると知られている。2FF の添加によりヒト肝がん由来 HepG2 細胞のコアフコシル化が劇的に抑制されることをレクチン検出や質量分析で確認した。細胞表面の重要な受容体である EGFR や $\beta 1$ インテグリンなど個別の分子でもコアフコシル化が消失することを確認した。また、これらの受容体を介したシグナルが減弱、細胞増殖や細胞遊走、軟寒天上でのコロニー形成能も有意に抑制さ

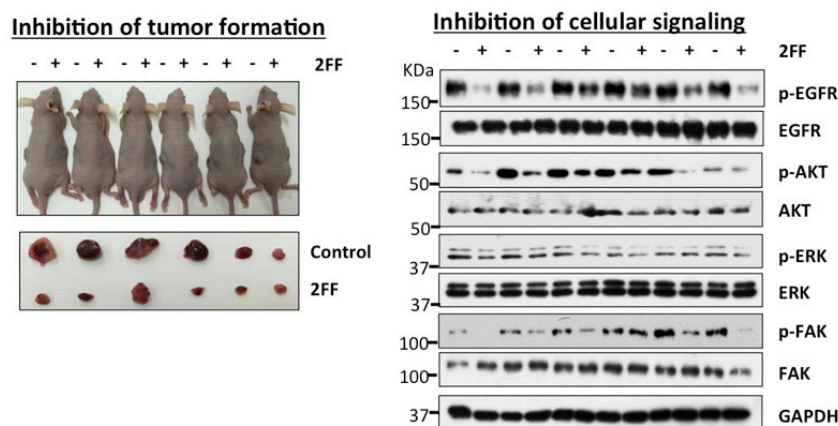


図 3. 2FF による腫瘍形成と細胞内シグナルの抑制

れた。一方、in vivoでは、マウス皮下へHepG2細胞を移植し、定期的に移植部位近傍へ2FFを投与したところ、腫瘍組織のコアフコシル化糖鎖の発現が強く抑制された。さらに、腫瘍サイズ並びに細胞内のシグナル伝達経路も有意に抑制されることがわかった (図3)。以上のことから、肝がん組織におけるコアフコシル化の重要性を示すと共に、2FFのような化合物が肝がんの新規治療薬になる可能性が強く示唆された。

2017年に発表した論文

1. A key regulator of cell adhesion: Identification and characterization of important N-glycosylation sites on integrin $\alpha 5$ for cell migration. Hang, Q., Isaji, T., Hou, S., Wang, Y., Fukuda, T. and Gu, J. *Mol. Cell. Biol.* 37: e00558-16, 2017
2. Alteration of N-glycan expression profile and glycan pattern of glycoproteins in human hepatoma cells after HCV infection. Xiang, T., Yang, Q., Liu, X., Zhou, Y., Lu, F., Gu, J., Taniguchi, N., Tan, Z., Chen, X., Xie, Y., Guan, F. and Zhang, X. *Biochim. Biophys. Acta*, 1861: 1036-1045, 2017
3. Chitosan oligosaccharides inhibit epithelial cell migration through blockade of N-acetylglucosaminyltransferase V and branched GlcNAc structure. Xu, Q., Wang, W., Qu, C., Gu, J., Yin, H., Song, L. and Du, Y. *Carbohydrate Polymers*, 170:241-246, 2017
4. Differential expression of ST6GAL1 in the tumor progression of colorectal cancer. Zhang, S., Lu, J., Xu, Z., Zou, X., Sun, X., Xu, Y., Shan, A., Lu, J., Yan, X., Cui, Y., Yan, W., Du, Y., Gu, J., Zheng, M., Feng, B., Zhang, Y. *Biochem Biophys Res Commun.* 486:1090-1096, 2017
5. Specific N-glycan alterations are coupled in EMT induced by different density cultivation of MCF 10A epithelial cells. Xu, Q., Niu, X., Wang, W., Yang, W., Du, Y., Gu, J., Song, L. *Glycoconj J.* 34:219-227, 2017
6. Inhibition of fucosylation by 2-fluorofucose suppresses human liver cancer HepG2 cell proliferation and migration as well as tumor formation. Zhou, Y., Fukuda, T., Hang, Q., Hou, S., Isaji, T., Kameyama, A., and Gu, J. *Sci Rep.* doi: 10.1038/s41598, 2017
7. Roles of Integrin $\alpha 6\beta 4$ Glycosylation in Cancer. Kariya, Y., Kariya, Y and Gu, J. *Cancers* 9: doi: 10.3390/cancers9070079, 2017

レクチンのがん薬物治療への応用 分子認識部門 細野 雅祐

(1) ナマズ卵レクチン (SAL) による抗がん剤排出抑制機構の解明

SAL は細胞膜表面の非還元末端 Gal α -結合糖鎖, 実際にはグロボトリアオシルセラミド (Gb3) を主とする, を特異的に認識して結合するレクチンである.

SAL は, ヒト子宮頸がん由来細胞株 HeLa のスニチニブ (スーテント, 主として腎がんに応用される分子標的薬) に対する感受性を高め, 単独処理に比べ細胞生存率を著しく減少させるが, この機序として, SAL の Gb3 を介した結合により, ①スニチニブの細胞内取り込み量が増加すること, ②SAL 処理により細胞内に形成される油滴状の膜構造物の周囲にスニチニブが集積する結果, この分子の排出が抑制されること, が分かっている.

本年度は, SAL により形成される膜構造物について解析を行った. この構造物は SAL 単独処理でも明視野像で明確に観察することができ, SAL と Gb3 との特異的相互作用により出現する. Nile Red では染色されないことから, いわゆる脂肪滴ではなく, ブレフェルディン A の前処理によって形成が減少した. また, 膜部分が 抗 LAMP1 抗体で染色され, かつ取り込まれたスニチニブと LAMP1 が共局在したことから, この構造物はリソソームである可能性が考えられた. 一方, この構造物は, リソソームマーカーである Lysotracker では染色されず, ニュートラルレッドで染色された. したがって SAL は, HeLa 細胞内にゴルジ体由来で内部が中性のリソソーム様構造物の形成を促進し, その膜部分に細胞内に取り込まれたスニチニブがトラップされることで排出が抑制されている可能性が示唆された (投稿準備中).

(2) SAL 受容体としての細胞膜 Gb3 分子の機能

バーキリンパ腫細胞 Raji の Gb3 欠損株 (Gb3-KO-Raji) および Gb3 の発現を誘導した慢性骨髄性白血病細胞株 K562 (Gb3-K562) 細胞を作製し, SAL 受容体分子としての Gb3 について検討した. Gb3-KO-Raji は, 親株と比較して細胞増殖スピードが遅くなるが, このとき細胞周期を負に制御する p21 と p27 の発現上昇およびリン酸化 ERK 量が増加していることが示された. Gb3-K562 では, 逆にわずかではあるが増殖速度が速くなり, p21 の発現低下およびリン酸化 ERK 量の低下が認められた. また, Gb3-KO-Raji および Gb3-K562 を SAL 処理しても, Raji で見られるような変化は観察されなかった. 以上の結果から, SAL の効果発現には, 受容体としての Gb3 分子が必要ではあるもののそれだけでは十分ではなく, Raji で見られる細胞応答には Gb3 以外の分子が関与している可能性が示唆された. 現在, この分子の探索を行っている.

(3) ウシガエル卵レクチン (cSBL) の悪性胸膜中皮腫 (MPM) に対する他剤併用効果

cSBLは, レクチン活性およびリボヌクレアーゼ (RNase) 活性を併せ持つ抗腫瘍性タンパク質である. cSBLはRNAをターゲットとした新規抗腫瘍メカニズムにより, MPMを含む多くのがん細胞株に対して, アポトーシスの誘導を介した細胞傷害作用を示すことを明らかにしている.

本年度は, *in vitro* における数種のMPM細胞株に対するcSBLの有効性, 既存治療薬との併用効果ならびにその作用機序について解析を行った. その結果, 既存治療薬と比較してcSBLは強い細胞増殖抑制効果および高いがん細胞選択性を示すことを明らかにした. また, H28細胞を用い, 2剤併用時の効果について検討したところ, pemetrexed + cSBL が, 既存レジメンと同等以上の抗腫瘍作用および相乗性を持つことが示唆された. この相乗効果は, pemetrexedの持つcyclin Aの持続

的活性化による細胞周期の停止作用とcSBLの持つcaspase-3の活性化を介したアポトーシスの誘導作用が協働することで引き起こされることが考えられる。

次に異種移植可能なH2452およびMSTOを用いて異種移植モデルマウスを作成し、*in vivo*におけるcSBLの抗腫瘍効果の検討を試みた。まず、*in vitro*における殺細胞メカニズムの解析を行ったところ、caspase-9、-8、-3 が順次活性化され、アポトーシスが誘導されることが示唆された。*in vivo*におけるcSBLの有効性の検討では、通常動物実験に用いられる濃度のpemetrexedと比較すると、cSBL処理群でより早期に腫瘍の増殖抑制が引き起こされ、同時にこの濃度においてマウスに有意な体重変化は生じず、有害作用は小さいことが示唆された。

さらに、MPMの治療障壁の一つとなっているpemetrexed耐性株への各薬剤の効果を比較した。H28およびH2452に対する効果では、pemetrexedおよびcisplatinと比較し、cSBL、TRAIL、およびEGFR-TKIs（チロシンキナーゼ阻害薬）はいずれも中皮腫細胞に対して高い選択性を示した。また、cSBLおよびEGFR-TKIsは、細胞株の違いによる増殖抑制効果にほとんど差がないことが明らかとなった。また併用効果の検討では、耐性細胞においてpemetrexed + cSBLが既存レジメンと比較しpemetrexedのDRIが2倍以上高く、耐性細胞株に対しても有効なレジメンとなる可能性が示された。3剤併用では、Combination Index (CI, 薬剤併用効果の指標) およびDRIの観点から、pemetrexed + cisplatin + cSBLが最も有効な組み合わせであることが示された。

2017年に発表した原著論文

(1) Catfish rhamnose-binding lectin induces G0/1 cell cycle arrest in Burkitt's lymphoma cells via membrane surface Gb3

Shigeki Sugawara, Changhun Im, Tasuku Kawano, Takeo Tatsuta, Yasuhiro Koide, Daiki Yamamoto, Yasuhiro Ozeki, Kazuo Nitta, Masahiro Hosono
Glycoconj. J., **34**, 127-138 (2017)

(2) Lissoclibadin 1, a Polysulfur Aromatic Alkaloid from the Indonesian Ascidian Lissoclinum cf. badium, Induces Caspase-Dependent Apoptosis in Human Colon Cancer Cells and Suppresses Tumor Growth in Nude Mice

Takeo Tatsuta, Masahiro Hosono, Henki Rotinsulu, Defny S. Wewengkang, Deiske S. Sumilat, Michio Namikoshi, Hiroyuki Yamazaki
J. Natl. Product., **80**, 499-502 (2017)

(3) Synergistic anti-tumor effect of bullfrog sialic acid-binding lectin and pemetrexed in malignant mesothelioma

Toshiyuki Satoh, Takeo Tatsuta, Shigeki Sugawara, Akiyoshi Hara, Masahiro Hosono
Oncotarget., **8**, 42466-42477 (2017)

(4) Sialidase NEU3 defines invasive potential of human glioblastoma cells by regulating calpain-mediated proteolysis of focal adhesion proteins

Kohta Takahashi, Sergei Proshin, Kazunori Yamaguchi, Yoji Yamashita, Ryuichi Katakura, Koji Yamamoto, Hiroshi Shima, Masahiro Hosono, Taeko Miyagi
Biochim. Biophys. Acta., **1861**, 2778-2788 (2017)

■学会発表記録

<機能病態分子部門>

- ・ **ガングリオシド欠損による肥満モデルマウスの病態改善および受容体機能に与える影響**

稲森 啓一郎, 伊藤 英樹, 田村 有美, 楊 燕華, 二瓶 渉, 宍戸 史, 突田 壮平^a, 山田 哲也^a, 片桐 秀樹^a, 井ノ口 仁一

(東北大・院医^a)

第59回日本脂質生化学会, 京都, 2017年6月, 要旨集 p.140-141

- ・ **ガングリオシド GM3 のアシル鎖構造に基づく新たな自然免疫応答と慢性炎症**

狩野 裕考, 郷 慎司, 新田 昂大, Lucas Veillon, 藤居 真優^a, 樺山 一哉^a, 下山 敦史^a, 深瀬 浩一^a, 安藤 弘宗^b, 石田 秀治^b, 名取 良浩^c, 吉村 祐一^c, 鈴木 明身, 井ノ口 仁一

(大阪大・院理^a, 岐阜大・応用生物科学^b, 東北医薬大・薬・分子薬科学^c)

第59回日本脂質生化学会, 京都, 2017年6月, 要旨集 p.137-139

- ・ **胸腺細胞の分化におけるスフィンゴミエリン発現とその機能的役割**

豊島 かおる, 永福 正和, 岡崎 俊郎^a, 井ノ口 仁一

(金沢医科大・血液免疫内科^a)

第59回日本脂質生化学会, 京都, 2017年6月, 要旨集 p.244-246

- ・ **ガングリオシド分子種による慢性炎症応答の新機軸**

井ノ口 仁一, 狩野 裕考

第36回日本糖質学会年会, 旭川, 2017年7月, 要旨集 p.103

- ・ **ガングリオシドは NPC1L1 を介した腸管からのコレステロール吸収を制御する**

二瓶 渉, 永福 正和, 狩野 裕考, 稲森 啓一郎, 新井 健太^a, 樺山 一哉^a, 深瀬 浩一^a, 井ノ口 仁一

(大阪大・院理^a)

第36回日本糖質学会年会, 旭川, 2017年7月, 要旨集 p.107

- ・ **New Insights into Ganglioside Functions from GM3S Knockout in Obese Mouse Models**

Kei-ichiro Inamori

Muscle Membrane Serendipity: Past, Present and Future Conference, Iowa City, IA, USA, July 2017, Program p.3

- ・ **New Paradigm for Chronic Inflammation Mediated by Ganglioside Molecular Species.**

Jin-ichi Inokuchi, Hirotaka Kanoh

24th International Symposium on Glycoconjugates, Korea, August 2017, p.61

- ・ **Gangliosides and Hearing**

Jin-ichi Inokuchi

International Conference on the Glycobiology of Nervous System: From the Genome Research Era to the Glycome, Korea, September 2017

- ・ **肥満糖尿病モデルにおけるガングリオシド GM3 欠損マウスから得られた新知見**

稲森 啓一郎, 伊藤 英樹, 田村 有美, 新田 昂大, 楊 燕華, 二瓶 渉, 宍戸 史, 突田 壮平^a, 山田 哲也^a, 片桐 秀樹^a, 井ノ口 仁一

(東北大・院医^a)

東北糖鎖研究会・東京糖鎖研究会 合同シンポジウム, 桐生, 2017年11月, 要旨集 p.52

- ・ **ガングリオシド分子種による慢性炎症制御の新機軸**

井ノ口 仁一

東北糖鎖研究会・東京糖鎖研究会 合同シンポジウム, 桐生, 2017年11月, 要旨集 p.22-24

- ・ **ガングリオシドのアシル鎖構造が制御する新たな慢性炎症メカニズム**

狩野 裕考, 郷 慎司, 新田 昂大, Lucas Veillon, 藤居 真優^a, 樺山 一哉^a, 下山 敦史^a, 深瀬 浩一^a, 安藤 弘宗^b, 石田 秀治^b, 名取 良浩^c, 吉村 祐一^c, 鈴木 明身, 井ノ口 仁一

(大阪大・院理^a, 岐阜大・応用生物科学^b, 東北医薬大・薬・分子薬科学^c)

東北糖鎖研究会・東京糖鎖研究会 合同シンポジウム, 桐生, 2017 年 11 月, 要旨集 p.87

・細胞膜スフィンゴリエリンは胸腺における自己反応性 T 細胞の除去に関与するか？

豊島 かおる, 永福 正和, 岡崎 俊郎^a, 井ノ口 仁一

(金沢医科大・血液免疫内科^a)

東北糖鎖研究会・東京糖鎖研究会 合同シンポジウム, 桐生, 2017 年 11 月, 要旨集 p.142

・慢性炎症によるガングリオシド分子種の発現変化

新田 昂大, 狩野 裕考, 郷 慎司, Lucas Veillon, 鈴木 明身, 井ノ口 仁一

東北糖鎖研究会・東京糖鎖研究会 合同シンポジウム, 桐生, 2017 年 11 月, 要旨集 p.134

・ガングリオシドによる NPC1L1 を介した腸管からのコレステロール吸収制御

二瓶 渉, 永福 正和, 狩野 裕考, 稲森 啓一郎, 新井 健太^a, 樺山 一哉^a, 深瀬 浩一^a, 井ノ口 仁一
(大阪大・院理^a)

東北糖鎖研究会・東京糖鎖研究会 合同シンポジウム, 桐生, 2017 年 11 月, 要旨集 p.79

・New Paradigm for Chronic Inflammation Mediated by Ganglioside Molecular Species.

Jin-ichi Inokuchi, Hirotaka Kanoh

9th Asian Community of Glycoscience and Glycotechnology Conference, Hong Kong, December 2017

・ガングリオシドの糖鎖・アシル鎖構造が制御する新たな慢性炎症メカニズム

狩野 裕考

ConBio2017, 神戸, 2017 年 12 月, ワークショップ 3PW24-4

・New Paradigm for Chronic Inflammation Mediated by Ganglioside GM3 Molecular Species.

Jin-ichi Inokuchi

2018 Gordon Research Conference on “Glycolipid and Sphingolipid Biology”, Galveston Texas USA, February 2018

<生体膜情報部門>

・オーファン GPCR, GPRC5B によるインスリン分泌亢進とそのメカニズム

黒田 喜幸, 中川 哲人, 東 秀好

第 36 回日本糖質学会年会, 旭川, 2017 年 7 月, 演題番号 3B-03

・ATP/UTP 受容体 P2Y2 の N 結合糖鎖の 2 量体形成に及ぼす効果：ブラジキニン B2 受容体との比較

矢口 沙也子, 黒田 喜幸, 中川 哲人, 東 秀好

第 11 回東北糖鎖研究会, 桐生, 2017 年 11 月

・ATP/UTP 受容体 P2Y2 の細胞外 Cys 残基と N 結合糖鎖の機能

矢口 沙也子, 阿部 真耶, 黒田 喜幸, 中川 哲人, 東 秀好

第 90 回日本生化学会大会, 神戸, 2017 年 12 月

<細胞制御部門>

・細胞接着における N-型糖鎖の機能発現と細胞内シグナルの制御

杭 慶雷, 伊左治 知弥, 侯 思聡, 福田 友彦, 顧 建国

第 69 回日本細胞生物学大会, 2017 年 6 月, 仙台, 要旨集 p61

・PI4KIIα による N-型糖鎖の調節とインテグリン α3β1 の機能制御細胞接着における N-型糖鎖の機能発現と細胞内シグナルの制御

伊左治 知弥, 福田 友彦, 顧 建国

第 69 回日本細胞生物学大会, 2017 年 6 月, 仙台, 要旨集 p96

・脳における α1,6 フコース転移酵素 Fut8 の機能とその役割

福田 友彦

第 16 回生物化学若手研究者セミナー, 仙台, 2017 年 7 月

・ **インテグリン $\alpha 5$ の糖鎖が細胞増殖・運動の鍵となる**

杭 慶雷, 伊左治 知弥, 侯 思聡, 福田 友彦, 顧 建国

第 36 回日本糖質学会年会, 旭川, 2017 年 7 月, 要旨集 p83

・ **コアフコシル化を欠損した肝細胞由来の細胞外小胞では, インテグリン $\alpha 3 \beta 1$ が増加した**

新居 瞳 ^a, 鎌田 佳宏 ^a, 赤松 佑香 ^a, 前田 恵 ^a, 福田 友彦, 顧 建国, 三善 英知 ^a
(大阪大学保健学科 ^a)

第 76 回日本癌学会学術総会, 横浜, 2017 年 9 月, 要旨集 p109

・ **2-フルオロフコースによるフコシル化の阻害はヒト肝がん細胞の細胞増殖・移動および腫瘍形成を抑制する**

周 穎, 福田 友彦, 杭 慶雷, 侯 思聡, 伊左治 知弥, 亀山 昭彦, 顧 建国

第 11 回東北糖鎖研究会・GlycoTOKYO 2017, 群馬, 2017 年 11 月, 要旨集 p111

・ **N-glycosylation in cell adhesion of cancer cells**

顧 建国

システム糖鎖生物学と展望国際シンポジウム, 和光市, 2017 年 11 月, 要旨集 p30

・ **N-glycosylation in cancer cells and towards application**

顧 建国

第 9 回南京腫瘍診断治療国際会議, 南京市, 2017 年 11 月, 要旨集 p102

・ **Importance of N-glycosylation in cell adhesion and EMT**

顧 建国

IUBMB Special Meeting Frontiers in Glycoscience II: Oncology, 台北市, 2017 年 12 月, 要旨集 p45-46

・ **Function of N-glycans in cancer cells and toward clinical application**

顧 建国

中国科学院 生物化学細胞研究所・国家重点研究拠点セミナー, 上海市, 2018 年 3 月

・ **Importance and complexity of N-glycosylation and its possibilities for clinical application**

顧 建国

復旦大学 中国衛生部複合糖質重点研究拠点セミナー, 上海市, 2018 年 3 月

<分子認識部門>

・ **SAL 処理による抗がん剤取り込み促進に関与する Gb3 分子種の解析**

菅原 栄紀, 石川 幼尋, 立田 岳生, 藤村 務, 細野 雅祐

第 36 回日本糖質学会年会, 旭川, 2017 年 7 月, 要旨集 p.117

・ **悪性中皮腫に対するレクザイムの *in vivo* における抗腫瘍効果およびペメトレキセドとの併用効果**

立田 岳生, 佐藤 稔之, 細野 雅祐

第 76 回日本癌学会学術総会, 横浜, 2017 年 9 月, 演題番号 P-1408

・ **ナマズ卵レクチン処理バーキットリンパ腫細胞において発現が変化する分子の探索**

石川 幼尋, 菅原 栄紀, 立田 岳生, 細野 雅祐

第 56 回日本薬学会東北支部大会, 青森, 2017 年 10 月, 要旨集 p.42

・ **ナマズ卵レクチンは腎癌細胞において sunitinib の効果を増強する**

伊藤 淳, 岩村 大径, 阿南 剛, 海法 康裕, 立田 岳生, 菅原 栄紀, 細野 雅祐, 佐藤 信

第 11 回東北糖鎖研究会, 桐生, 2017 年 11 月, P.31

・ **ナマズ卵レクチン処理細胞における薬物取り込みおよび排出機構について**

本田 捷太, 菅原 栄紀, 石川 幼尋, 立田 岳生, 伊藤 淳, 佐藤 信, 細野 雅祐

第 11 回東北糖鎖研究会, 桐生, 2017 年 11 月, P.47

・ナマズ卵レクチンによる抗がん剤排出抑制機構の解明

菅原 栄紀, 石川 幼尋, 本田 捷太, 立田 岳生, 細野 雅祐

2017 年度生命科学系学会合同年次大会, 神戸, 2017 年 12 月, 1P-0046

・悪性中皮腫に対するシアル酸結合性レクチン (cSBL) と他剤との併用効果

佐藤 稔之, 立田 岳生, 菅原 栄紀, 原 明義, 細野 雅祐

2017 年度生命科学系学会合同年次大会 (第 90 回日本生化学会大会), 神戸, 2017 年 12 月, 演題番号 2P-0914

・シアル酸結合性レクチン (cSBL) の EGFR pathway への影響

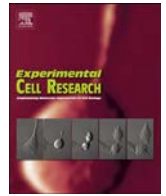
佐藤 稔之, 立田 岳生, 菅原 栄紀, 原 明義, 細野 雅祐

日本薬学会第 138 年会, 金沢, 2018 年 3 月, 演題番号 27J-am12S

・ナマズ卵レクチンの処理による細胞増殖抑制にかかわる分子の発現調節機構について

石川 幼尋, 菅原 栄紀, 立田 岳生, 細野 雅祐

日本薬学会第 138 年会, 金沢, 2018 年 3 月, 演題番号 27J-pm16



PDMP, a ceramide analogue, acts as an inhibitor of mTORC1 by inducing its translocation from lysosome to endoplasmic reticulum

Takashi Ode^{a,b}, Katarzyna A. Podyma-Inoue^c, Kazue Terasawa^c, Jin-ichi Inokuchi^d,
Toshihide Kobayashi^{e,f}, Tetsuro Watabe^c, Yuichi Izumi^a, Miki Hara-Yokoyama^{c,*}

^a Department of Periodontology, Graduate School of Medical and Dental Sciences, Tokyo Medical and Dental University (TMDU), 1-5-45 Yushima, Bunkyo-ku, Tokyo 113-8510, Japan

^b Research Fellow of the Japan Society for the Promotion of Science (JSPS), 5-3-1 Kojimachi, Chiyoda-ku, Tokyo 102-0083, Japan

^c Department of Biochemistry, Graduate School of Medical and Dental Sciences, Tokyo Medical and Dental University (TMDU), 1-5-45 Yushima, Bunkyo-ku, Tokyo 113-8510, Japan

^d Division of Glycopathology, Institute of Molecular Biomembrane and Glycobiology, Tohoku Medical and Pharmaceutical University, 4-4-1, Komatsushima, Aoba-ku, Sendai, Miyagi 981-8558, Japan

^e Lipid Biology Laboratory, RIKEN, 2-1 Hirosawa, Wako, Saitama 351-0198, Japan

^f CNRS, UMR 7213, University of Strasbourg, 67401 Illkirch, France

ARTICLE INFO

Keywords:

PDMP
mTOR
Subcellular localization
Lysosome
ER
Osteoblast

ABSTRACT

Mammalian or mechanistic target of rapamycin complex 1 (mTORC1) is a master regulator of cell growth, metabolism, and cell differentiation. Recent studies have revealed that the recruitment of mTORC1 to lysosomes is essential for its activation. The ceramide analogue 1-phenyl-2-decanoylamino-3-morpholino-1-propanol (PDMP), a well known glycosphingolipid synthesis inhibitor, also affects the structures and functions of various organelles, including lysosomes and endoplasmic reticulum (ER). We investigated whether PDMP regulates the mTORC1 activity through its effects on organellar behavior. PDMP induced the translocation of mTORC1 from late endosomes/lysosomes, leading to the dissociation of mTORC1 from its activator Rheb in MC3T3-E1 cells. Surprisingly, we found mTORC1 translocation to the ER upon PDMP treatment. This effect of PDMP was independent of its action as the inhibitor, since two stereoisomers of PDMP, with and without the inhibitor activity, showed essentially the same effect. We confirmed that PDMP inhibits the mTORC1 activity based on the decrease in the phosphorylation of ribosomal S6 kinase, a downstream target of mTORC1, and the increase in LC3 puncta, reflecting autophagosome formation. Furthermore, PDMP inhibited the mTORC1-dependent osteoblastic cell proliferation and differentiation of MC3T3-E1 cells. Accordingly, the present results reveal a novel mechanism of PDMP, which inhibits the mTORC1 activity by inducing the translocation of mTOR from lysosomes to the ER.

1. Introduction

Mammalian (mechanistic) target of rapamycin (mTOR) is a serine/threonine kinase that functions as the master regulator of cell metabolism and growth [1]. mTOR forms two distinct complexes, mTOR complex 1 (mTORC1) and mTOR complex 2 (mTORC2). mTORC1 regulates protein synthesis, cell proliferation, differentiation, and autophagy [1–3]. mTORC2 controls cytoskeleton organization and cell survival [1,2,4]. Recent studies revealed that mTORC1 also plays an important role in osteoblast differentiation, both in vitro and in vivo [5–9].

mTORC1 is activated in response to growth factors, amino acids, and energy status [1–3]. Recently, late endosome/lysosome (LE/Ly)

has been identified as the major intracellular site where the multiple signals are integrated to activate mTORC1 [10]. In the presence of amino acids, mTORC1 is recruited to LE/Ly membranes and activated by the mTORC1 activator Rheb, which is constitutively located on LE/Ly membranes [11]. The Ragulator complex and Rag GTPase are essential for the recruitment of mTORC1 to LE/Ly, and the Ragulator complex acts as a scaffold for mTORC1 at LE/Ly membranes [11–13]. Whereas the tethering of mTORC1 to LE/Ly membranes is required for mTORC1 activation, the inactivation of mTORC1 occurs through the dissociation of mTORC1 from LE/Ly and the recruitment of TSC2, a negative regulator of Rheb, to LE/Ly membranes in the absence of amino acids [14] or growth factors [15]. Thus, the association of mTORC1 with LE/Ly is essential for cell growth, proliferation, and

* Corresponding author.

E-mail address: m.yokoyama.bch@tmd.ac.jp (M. Hara-Yokoyama).

differentiation.

Ceramides, composed of a sphingosine base linked to a fatty acid, are the precursors of all sphingolipids, including sphingomyelin and glycolipids. In addition to their structural role, ceramides act as bioactive molecules that regulate various cellular responses, including metabolism, apoptosis, and differentiation [16–19]. Many studies have demonstrated the biological actions of ceramides on the “plasma” membrane. For example, studies on ceramides in insulin resistance suggested that ceramides suppress the activation of Akt/protein kinase B (PKB) on the plasma membrane, which plays a crucial key role in cell growth, proliferation, survival, and metabolism [20,21]. The ceramide-induced inhibition of the Akt/PKB signaling may also underlie the apoptosis-inducing effects of ceramides in numerous types of cancer cells [22]. One part of ceramides is generated from sphingomyelin by neutral sphingomyelinase 2 (nSMase2), localized in the plasma membrane. The deficiency of nSMase2 reportedly causes impaired bone and tooth mineralization in mice [23,24], suggesting the importance of the ceramides on the plasma membrane for osteogenesis [25].

Endogenous ceramides generated by *de novo* synthesis are rapidly converted into sphingolipid species, whereas exogenously added ceramide analogues that cannot be metabolized are accumulated within intracellular “organelles”. Ceramide analogues reportedly act on the mitochondrial membrane to induce apoptosis [26]. However, the biological actions of ceramides or ceramide analogues on other organelle membranes have not been sufficiently investigated.

The ceramide analogue 1-phenyl-2-decanoylamino-3-morpholino-1-propanol (PDMP) inhibits glucosylceramide synthase, leading to the suppression of glycosphingolipid biosynthesis [27]. PDMP prevents atherosclerosis and cardiac hypertrophy [28,29] and augments the activities of several anti-cancer agents, including the MEK/ERK inhibitor AZD-6244 [30,31]. Apart from the inhibitory effect on glucosylceramide synthase, PDMP has also been reported to alter the organization of LE/Ly [32,33] and the endoplasmic reticulum (ER) [34]. This action of PDMP on the organellar morphology can be clearly distinguished from that on the glycosphingolipid biosynthesis by the use of two distinct stereoisomers of PDMP. *D-threo*-PDMP (D-PDMP), but not its stereoisomer *L-threo*-PDMP (L-PDMP), inhibits glucosylceramide synthase [27], whereas both PDMP isomers affect organellar organization [33,34]. In addition, the inhibitory effect of PDMP on the mTORC1 activity has been reported [30]. Therefore, we considered PDMP to be an excellent material to evaluate the biological potential of ceramide analogues on intracellular organelles.

The objective of the present study was to clarify whether the

ceramide analogue PDMP regulates the mTORC1 activity by affecting its subcellular localization. We used the pre-osteoblastic cell line MC3T3-E1, in which PDMP suppressed the cell proliferation and the osteoblastic differentiation. We successfully linked the effects of PDMP on the mTORC1 activity and the intracellular organelles: PDMP causes the translocation of mTOR from LE/Ly membranes to the ER and the segregation of mTOR from its activator Rheb, leading to the inhibition of the mTORC1 activity. The present study provides a new perspective on the biological actions of ceramide analogues on LE/Ly membranes.

2. Materials and methods

2.1. Compounds

The syntheses of D-PDMP and L-PDMP, were performed as described previously [27]. *D-threo*-1-phenyl-2-benzoyloxycarbonylamino-3-pyrrolidino-1-propanol (PBPP), a newly developed glucosylceramide synthase inhibitor, was synthesized according to our previous report [35]. D-PDMP, L-PDMP, and PBPP were dissolved in water. The structures of D-PDMP, L-PDMP, and PBPP are shown in Fig. 1A. Rapamycin was purchased from Focus Biomolecules (Pennsylvania, USA).

2.2. Cell culture

The mouse pre-osteoblastic cell line (MC3T3-E1) was obtained from the RIKEN Bioresource Center (RCB1126). The cells were seeded and maintained in growth medium consisting of α -modified MEM (Sigma-Aldrich Japan, Tokyo, Japan), supplemented with 10% fetal bovine serum (Sigma-Aldrich Japan, Tokyo, Japan), 4 mM L-glutamine, L-penicillin (50 U/ml), and streptomycin (50 μ g/ml), at 37 °C in a 5% CO₂ atmosphere. To induce osteoblastic differentiation, MC3T3-E1 cells were cultured in osteogenic medium, consisting of growth medium supplemented with β -glycerophosphate (10 mM), ascorbic acid (50 μ g/ml), and dexamethasone (10 nM).

2.3. Immunocytochemistry

MC3T3-E1 cells were cultured on 15-mm round glass coverslips in 12-well plates (4×10^4 cells/well). After 24 h, the medium was exchanged from growth medium to osteogenic medium in the absence (control) or presence of the compounds. The cells were washed once with PBS and fixed with 3 or 4% paraformaldehyde (PFA) in PBS,

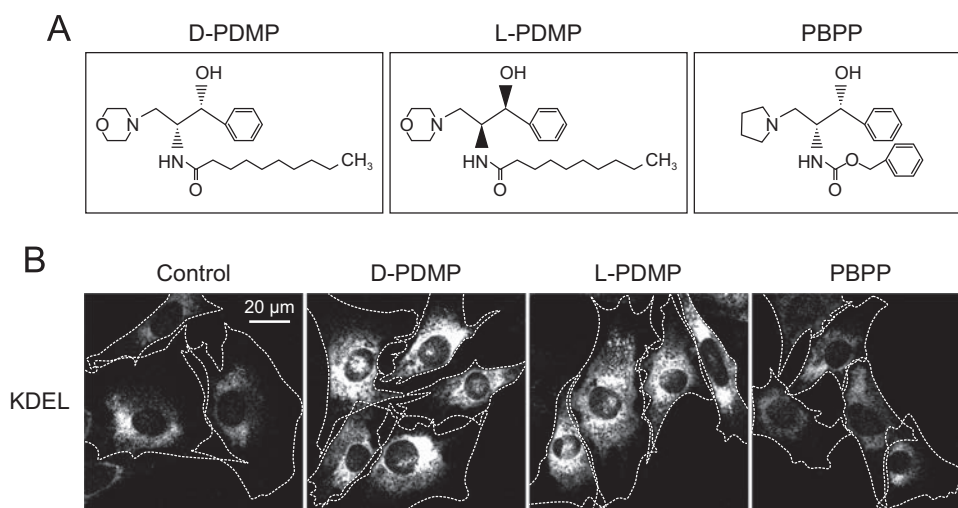


Fig. 1. D-PDMP and L-PDMP, but not PBPP, affect the ER morphology. (A) The structures of ceramide analogues. D-PDMP is an inhibitor of glucosylceramide synthase, but L-PDMP, a stereoisomer of D-PDMP, lacks this inhibitory activity. PBPP is a newly developed, more potent inhibitor of glucosylceramide synthase. (B) The ER morphology is altered by treatments with D-PDMP and L-PDMP, but not PBPP. MC3T3-E1 cells were seeded on 15-mm round glass coverslips in 12-well plates (4×10^4 cells/well). After 24 h, the cells were treated without or with 40 μ M D-PDMP, 40 μ M L-PDMP, or 40 μ M PBPP in osteogenic medium for 24 h. Untreated cells cultured in osteogenic medium for 24 h were used as the control. The cells were fixed with 4% PFA for 15 min, permeabilized with 0.1% Triton X-100 for 5 min, and then labeled with an anti-KDEL antibody. Cells are outlined with white dashed lines.

followed by permeabilization with 0.1% Triton X-100 or digitonin (50 or 100 µg/ml) in PBS containing 0.1 M glycine. The cells were then washed with PBS, blocked with 1% bovine serum albumin (BSA) in PBS for 30 min at RT, and then stained with the primary antibodies for 1 h at RT. The primary antibodies used in the present study were against the ER marker KDEL (sc-58774, 1:400; Santa Cruz Biotechnology, CA, USA), mTOR (2983, 1:400; Cell Signaling Technology, MA, USA), the LE/Ly marker LBPA (1:20; prepared as described [36]), LAMTOR1 (8975, 1:100; Cell Signaling Technology, MA, USA), and the autophagosome marker LC3 (PM036, 1:500; MBL, Nagoya, Japan). Subsequently, the cells were washed three times with 0.1% BSA in PBS and incubated with an Alexa Fluor 488-conjugated anti-rabbit antibody (A11008, 1:200; Invitrogen, OR, USA) and/or an Alexa Fluor 555-conjugated anti-mouse antibody (A21422, 1:200; Invitrogen, OR, USA). Images were captured using a FLUOVIEW FV10i laser confocal microscope (Olympus, Tokyo, Japan).

Co-localization analysis was performed using the FV10-ASW software (Olympus, Tokyo, Japan). The co-localization ratio was quantified as described [15,37,38]. Briefly, the ratio of the number of mTOR pixels co-localized with LBPA or KDEL pixels to the total number of mTOR pixels was calculated, as expressed as the percentage. At least 20 cells were randomly chosen for co-localization analysis for each experimental condition.

2.4. Co-immunoprecipitation

MC3T3-E1 cells were transfected with pRK7-Rheb (15888, Addgene, MA, USA), the plasmid encoding FLAG-tagged Rheb, using the FuGENE6 transfection reagent (Promega, WI, USA). The cells were washed with PBS and lysed with 1% Triton X-100 in buffer A (20 mM Tris-HCl, pH 7.5, 150 mM NaCl, 10 mM iodoacetamide, 2.5 mM NaF, 2.5 mM sodium pyrophosphate, 10 mM EDTA, 10 mM β-glycerophosphate, 1 mM sodium orthovanadate, 1 mM phenylmethylsulfonyl fluoride, 5 µg/ml leupeptin, 10 µg/ml pepstatin, and 10 µg/ml aprotinin, pH 7.5) for 60 min on ice. The lysates were then centrifuged for 15 min at 15,000g, and the supernatants were incubated with anti-FLAG M2 affinity gel (Sigma-Aldrich Japan, Tokyo, Japan) for 120 min at 4 °C with rotation. The immune-complexes were washed with PBS and subjected to immunoblotting. A biotinylated polyclonal rabbit anti-FLAG antibody (GTx77459, 1:1,000; GeneTex, CA, USA), a monoclonal anti-FLAG M2 antibody (F1804, 1:2,000; Sigma-Aldrich Japan, Tokyo, Japan), and the mTOR antibody (1:1,000) were used for the immunoblotting of immunoprecipitants (IP), cell lysates, and both, respectively.

2.5. Immunoblotting

The cells were lysed with 1% Triton X-100 in buffer A for 15 min on ice, and then centrifuged for 10 min at 15,000g. The supernatants were subjected to 10% SDS-PAGE, and then transferred to PVDF membranes. For the detection of ribosomal S6 kinase (S6K), phosphorylated S6K (P-S6K), or mTOR, the membranes were incubated with 5% BSA in TBS-T for 1 h, followed by an incubation with primary antibodies overnight at 4 °C. The membranes were then washed three times with TBS-T and incubated with secondary antibodies for 1 h. When the polyclonal rabbit biotinylated anti-FLAG antibody or the monoclonal anti-FLAG M2 antibody was used, the membranes were incubated with 1% BSA in TBS-T or with 4% Block Ace (Yukijirushi, Tokyo, Japan), respectively, for 1 h, and incubated with each primary antibody for another 1 h at RT. The primary antibodies against S6K (9202, 1:500; Cell Signaling Technology, MA, USA), P-S6K (9205, 1:500; Cell Signaling Technology, MA, USA), and α-tubulin (ab4074, 1:10,000; Abcam, Tokyo, Japan) were used. The secondary antibodies were an HRP-conjugated anti-rabbit antibody (1858415, Pierce, IL, USA) and an HRP-linked anti-biotin antibody (7075 S, Cell Signaling Technology, MA, USA). The immunoblot signals were visualized using the ECL Prime

Western Blotting Detection Reagent (GE Healthcare Japan, Tokyo, Japan). The band intensities of S6K and P-S6K were determined using the ImageJ software (NIH, MD, USA), and the intensities of the P-S6K bands relative to those of the S6K bands were calculated.

2.6. Cell proliferation assay

MC3T3-E1 cells were seeded in 96-well plates (2×10^3 cells/well) and treated without or with D-PDMP, L-PDMP, PBPP, or rapamycin in osteogenic medium for 1, 2, and 3 days. The cell proliferation assay was performed using a WST-8 assay (Cell Counting Kit-8, Dojindo, Kumamoto, Japan), according to the manufacturer's instructions with minor modifications. The absorbance was measured at 450 nm using a microplate reader (Model 680, Bio-Rad, CA, USA).

2.7. Alkaline phosphatase (ALP) staining

The cells were plated in 12-well plates (1×10^4 cells/well). After 24 h, the medium was exchanged from growth medium to osteogenic medium in the absence or presence of D-PDMP, L-PDMP, PBPP, or rapamycin, and the cells were then incubated for 12 days. The osteogenic medium without or with these compounds was changed every 3 days. The cells were washed three times with PBS and fixed with 4% PFA in PBS for 10 min at RT. Subsequently, the cells were incubated with ALP staining solution, consisting of 0.2 M Tris-HCl, pH 8.6, 50 mM MgCl₂, 0.01% naphthol AS-MX phosphate (Sigma-Aldrich Japan, Tokyo, Japan), and 0.06% Fast Blue BB Salt (Sigma-Aldrich Japan, Tokyo, Japan), for 30 min at RT, and then washed three times with MilliQ water.

2.8. Real-time RT-PCR

The cells were seeded in 6-well plates (2.25×10^4 cells/well). After 24 h, the medium was changed from growth medium to osteogenic medium in the absence or presence of D-PDMP, L-PDMP, PBPP, or rapamycin (Day 0), and the cells were then incubated for 14 days (Day 14). Total RNA was isolated using an RNAqueous-4PCR Kit (Ambion, TX, USA), according to the manufacturer's instructions. The cDNAs were obtained from 1 µg of RNA, using a High Capacity cDNA Reverse Transcription Kit (Applied Biosystems, CA, USA). Quantitative PCR was performed using SYBR Premix Ex Taq II (TaKaRa, Shiga, Japan) and a Thermal Cycler Dice Real-Time System II (TaKaRa, Shiga, Japan). The primers used were 5'-GCGTCAACACCATCATCTG-3' and 5'-CAGACCAGCAGCACTCCATA-3' (Runx2), 5'-AAGGCGTTG-GCAATAGTGG-3' and 5'-CCGCTCTAGCTCCTGACAGT-3' (Osx), and 5'-AGGACCAGGTTGTCTCTGT-3' and 5'-TTACTCCTTGGAGGCCATGT-3' (GAPDH). Amplification conditions were as follows: 95 °C for 5 s, 55 °C for 10 s, and 72 °C for 20 s, with 45 cycles. The mRNA expression levels of the target genes were normalized to those of GAPDH, and the relative ratios of the expression levels in the Day 14 group to those in the Day 0 group were calculated.

2.9. Statistical analysis

Differences between different groups were analyzed using the Student's *t*-test or Welch's *t*-test. All experiments were repeated at least twice, with triplicate samples.

3. Results

3.1. The alteration of ER morphology in MC3T3-E1 cells induced by PDMP is independent of its inhibitory action related to glycosphingolipid synthesis

PDMP has been widely used as an inhibitor of glucosylceramide synthase. In addition, PDMP affects the morphology of the ER in HeLa

cells [34] and the LE/Ly in human skin fibroblasts [33]. In the present study, we focused on the effects of PDMP on the organellar morphology. In order to discriminate between the inhibitor activity-dependent and -independent effects, we used three ceramide analogues, D-PDMP and its stereoisomer L-PDMP, as well as the newly developed glucosylceramide synthase inhibitor PBPP. D-PDMP and PBPP, but not L-PDMP, showed inhibitory activity against glucosylceramide synthase [27,35]. The glucosylceramide levels in the D-PDMP- and PBPP-treated MC3T3-E1 cells were significantly lower than that in the untreated control cells, while the glucosylceramide level in the L-PDMP-treated cells was similar to that in the control cells (Supplementary Fig. S1). In our system, MC3T3-E1 cells were treated without or with D-PDMP, L-PDMP, or PBPP, followed by an immunocytochemical analysis with the anti-KDEL (an ER marker) antibody. The anti-KDEL antibody recognizes the sequence Lys-Asp-Glu-Leu (KDEL) at the carboxy-terminus of the ER-resident proteins [39]. The staining pattern of KDEL in the D-PDMP- or L-PDMP-treated cells was altered, as compared with that in control cells, and the intensity was appreciably increased in the presence of PDMP (Fig. 1B), likely due to the PDMP-dependent restructuring of the ER [34]. In contrast, PBPP had no obvious effect on the KDEL-staining pattern. These results suggested that PDMP affects the ER architecture in MC3T3-E1 cells, and this effect is independent of the inhibition of glucosylceramide synthase.

3.2. Dissociation of mTOR from LE/Ly induced by PDMP

The recruitment of mTOR to LE/Ly membranes is required for its activation [11]. mTOR is dissociated from LE/Ly in the absence of amino acids [14] or growth factors [15]. In the present study, cell fractionation

experiments revealed the presence of mTOR in the membrane fraction, rather than the cytosolic fraction, under normal conditions (Supplementary Fig. S2). Since PDMP reportedly affects the function and morphology of LE/Ly [32,33], we investigated the effects of ceramide analogues on the subcellular localization of mTOR. MC3T3-E1 cells were co-stained with anti-mTOR and anti-LBPA (an LE/Ly marker) antibodies. In control cells, both mTOR and LBPA exhibited punctate staining patterns (Fig. 2A). In contrast, a non-punctate fluorescence pattern was observed in both the D-PDMP- and L-PDMP-treated cells. No appreciable changes were seen in the PBPP-treated cells, as compared to control cells. A co-localization analysis of mTOR and LBPA revealed that mTOR was specifically co-localized with LBPA in the control group (Fig. 2B). The co-localization ratio was significantly decreased in the D-PDMP-treated group and the L-PDMP-treated group, while no significant difference was observed between the control group and the PBPP-treated group, suggesting that PDMP induces the dissociation of mTOR from LE/Ly. Similar results were obtained in a mouse bone marrow-derived stromal cell line (ST2) and a mouse embryonic fibroblast cell line (NIH3T3) (Supplementary Fig. S3).

In order to study the kinetic actions of D-PDMP, we performed a time-course analysis of the decrease in the co-localization between mTOR and LBPA upon D-PDMP treatment. The decrease occurred significantly 12 h after D-PDMP treatment (Fig. 3). We also investigated the effects of the culture medium composition on the subcellular localization of mTOR, and found that the co-localization between mTOR and LBPA remained unchanged in MC3T3-E1 cells cultured in growth medium or osteogenic medium without D-PDMP at any time point (Supplementary Fig. S4).

As shown in Fig. 2A and Supplementary Fig. S3 A and C, the intensity

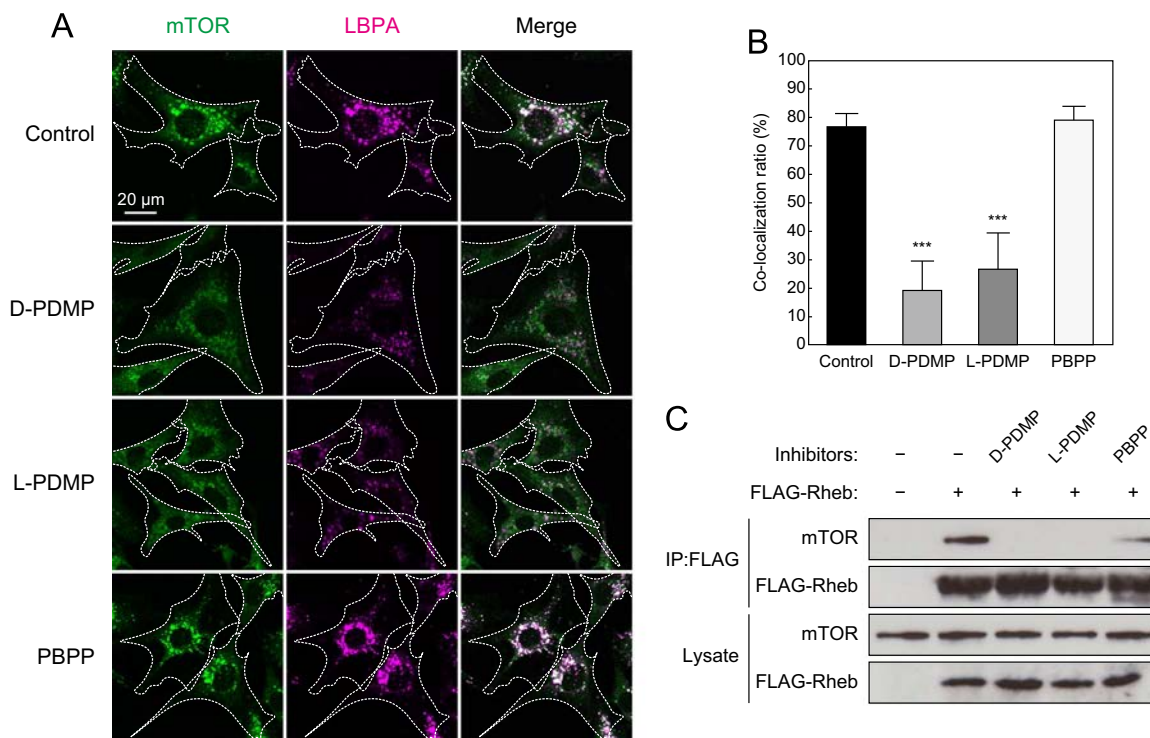


Fig. 2. mTOR is dissociated from LE/Ly by D-PDMP and L-PDMP treatments. (A) The co-localization of mTOR with LBPA is decreased in the presence of D-PDMP. MC3T3-E1 cells were seeded on 15-mm round glass coverslips in 12-well plates (4×10^4 cells/well). After 24 h, the cells were treated without or with 40 μ M D-PDMP, 40 μ M L-PDMP, or 40 μ M PBPP in osteogenic medium for 24 h. Untreated cells cultured in osteogenic medium for 24 h were used as the control. The cells were fixed with 3% PFA for 20 min, permeabilized with 50 μ g/ml digitonin for 5 min, and then labeled with an anti-mTOR antibody (green) and an anti-LBPA antibody (magenta). Cells are outlined with white dashed lines. (B) Quantification of the co-localization between mTOR and LBPA in MC3T3-E1 cells. (C) The interaction between FLAG-tagged Rheb (FLAG-Rheb) and endogenous mTOR is impaired by D-PDMP and L-PDMP treatments. MC3T3-E1 cells were seeded in 10-cm dishes (3×10^5 cells/dish). After 24 h, the cells were treated without or with 40 μ M D-PDMP, 40 μ M L-PDMP, or 40 μ M PBPP for 24 h, and then transfected or mock-transfected with the plasmid encoding FLAG-Rheb. Based on the results of preliminary experiments, we adjusted the amount of the plasmid encoding FLAG-tagged Rheb, so that comparable amounts of the FLAG-Rheb protein were expressed under the four conditions (control, D-PDMP, L-PDMP, and PBPP). After the immunoprecipitation of FLAG-Rheb, the co-immunoprecipitated mTOR was detected by immunoblotting. Data are expressed as means \pm SD. *** $P < 0.001$ compared with control group.

of the LBPA fluorescence was lower in the D-PDMP-treated cells than in the control cells. Using immunocytochemistry for LAMP-1, another lysosome marker, we analyzed whether this phenomenon was due to the decreased number of LE/Ly or the reduced reactivity of LBPA against the anti-LBPA antibody. The number of LAMP-1-positive dots was not decreased in the D-PDMP-treated cells (Supplementary Fig. S5), suggesting that D-PDMP does not affect the LE/Ly biogenesis. PDMP associates with the acidic compartment due to its positively charged amino group, where LBPA (a unique acidic phospholipid) is enriched [36]. Since PDMP induces the formation of multilamellar structures of the LBPA-containing membranes [33], PDMP may cause the decreased accessibility or reactivity of the anti-LBPA antibody to LBPA.

Furthermore, the staining for ICDH and GOLGA5, markers of mitochondria and Golgi, respectively, revealed that D-PDMP does not alter the subcellular localizations of mitochondria and Golgi (Supplementary Figs. S5 and S6). Considering the characteristic morphologies of mitochondria and Golgi, it is apparent that mTOR is not present on these organelles.

Since the localization of mTOR on the LE/Ly membranes is required for the interaction of mTORC1 with its activator Rheb [10,11], we investigated whether PDMP weakens the interaction between mTOR and Rheb. Co-immunoprecipitation assays of mTOR and Rheb in MC3T3-E1 cells demonstrated that the level of co-immunoprecipitated mTOR was decreased in the presence of D-PDMP or L-PDMP (Fig. 2C), suggesting that PDMP causes the dissociation of mTORC1 from LE/Ly and reduces the interaction between mTOR and Rheb.

3.3. mTOR translocation to ER upon PDMP treatment

D-PDMP treatment causes the dissociation of mTOR from LE/Ly, as shown in Figs. 2 and 3 and Supplementary Fig. S3. However, the cell fractionation experiments demonstrated that mTOR is not translocated to the cytosol and remained localized at the membrane after D-PDMP treatment (Supplementary Fig. S2). To identify the subcellular localization of the mTOR that dissociated from LE/Ly in ceramide analogue-

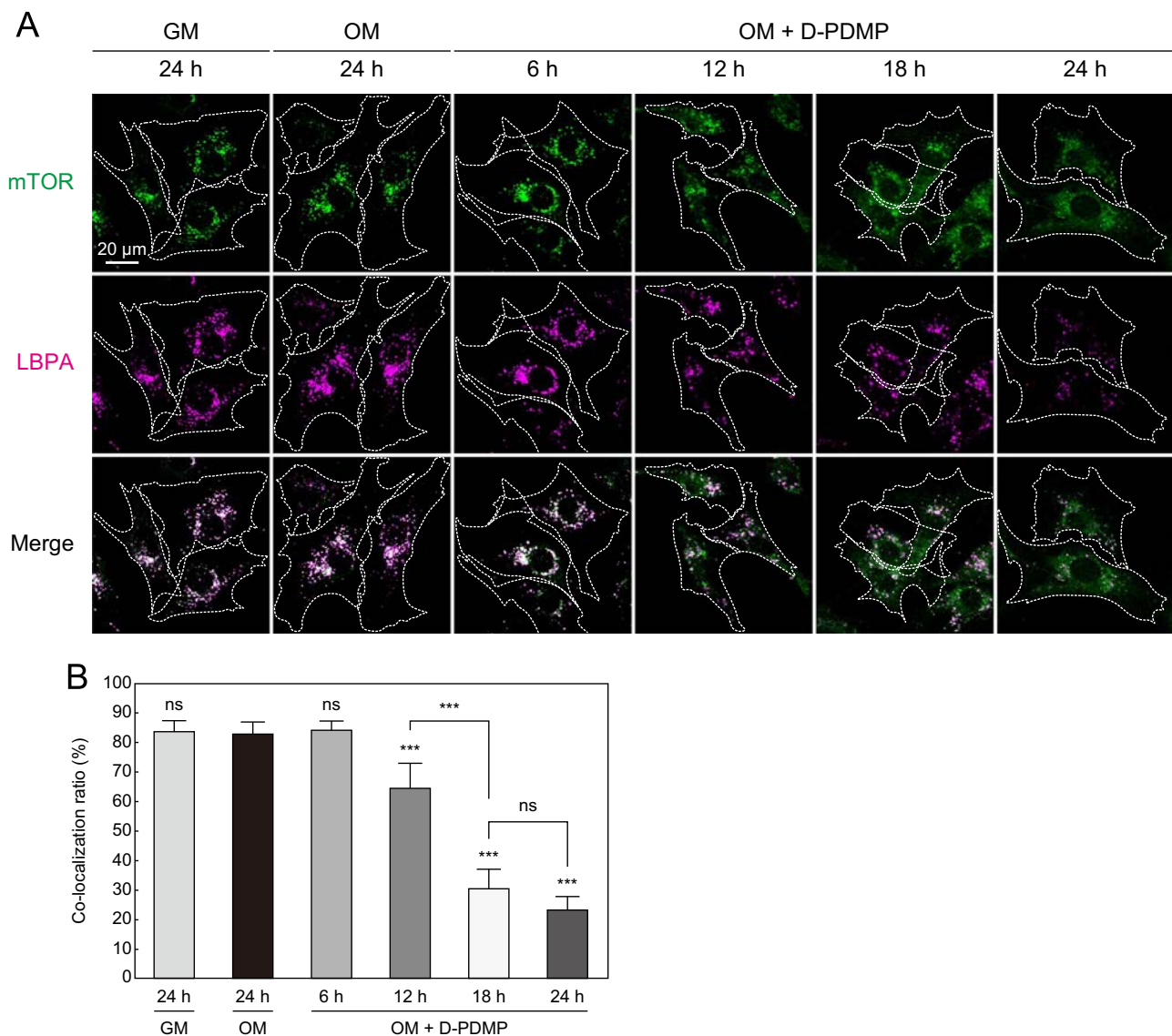


Fig. 3. Kinetics of mTOR dissociation from LE/Ly by D-PDMP. (A) Time-course analysis of the co-localization of mTOR with LBPA. MC3T3-E1 cells were seeded on 15-mm round glass coverslips in 12-well plates (4×10^4 cells/well). After 24 h, the cells were treated without or with 40 μ M D-PDMP in growth medium or osteogenic medium for the indicated times. The cells were fixed with 3% PFA for 20 min, permeabilized with 50 μ g/ml digitonin for 5 min, and then labeled with an anti-mTOR antibody (green) and an anti-LBPA antibody (magenta). Cells are outlined with white dashed lines. (B) Quantification of the co-localization between mTOR and LBPA in MC3T3-E1 cells. Data are expressed as means \pm SD. *** $P < 0.001$; ns (not significant), $P > 0.05$ compared with OM 24-h group. Abbreviations: GM, cells cultured in growth medium; OM, cells cultured in osteogenic medium.

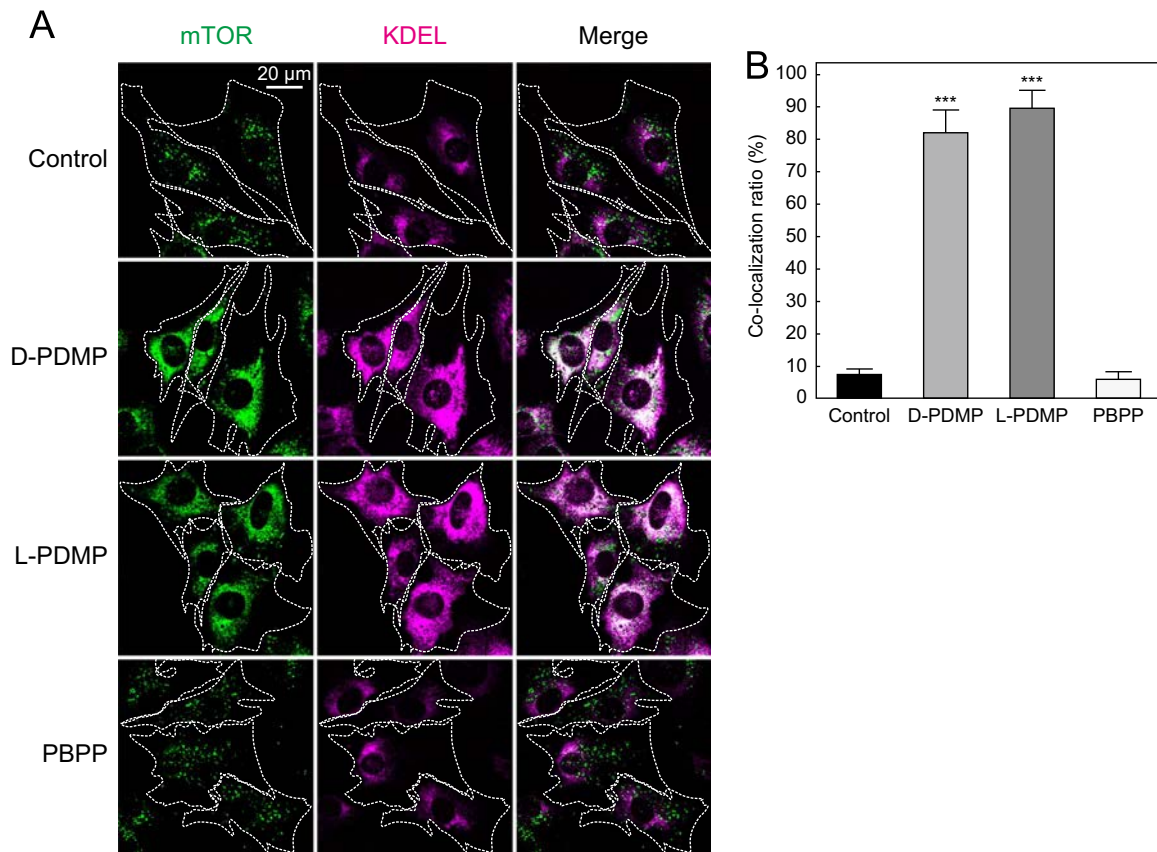


Fig. 4. mTOR is translocated to the ER by D-PDMP or L-PDMP treatment. (A) The co-localization of mTOR with KDEL is increased in the presence of D-PDMP and L-PDMP. MC3T3-E1 cells were seeded on 15-mm round glass coverslips in 12-well plates (4×10^4 cells/well). After 24 h, the cells were treated without or with 40 μ M D-PDMP, 40 μ M L-PDMP, or 40 μ M PBPP in osteogenic medium for 24 h. Untreated cells cultured in osteogenic medium for 24 h were used as the control. The cells were fixed with 4% PFA for 15 min, permeabilized with 0.1% Triton X-100 for 5 min, and then labeled with an anti-mTOR antibody (green) and an anti-KDEL antibody (magenta). Cells are outlined with white dashed lines. (B) Quantification of the co-localization between mTOR and KDEL in MC3T3-E1 cells. Data are expressed as means \pm SD. *** $P < 0.001$ compared with control group.

treated cells, the cells were co-stained with anti-mTOR and anti-KDEL antibodies, because the mTOR-staining pattern resembled the KDEL-staining pattern when the cells were treated with D-PDMP or L-PDMP, as shown in Figs. 1B and 2A. The immunofluorescence double staining and the subsequent co-localization analysis revealed that both mTOR and KDEL showed the non-punctate fluorescence patterns in D-PDMP-treated cells and L-PDMP-treated cells, and that the co-localization ratios between mTOR and KDEL were significantly increased in the D-PDMP-treated and L-PDMP-treated groups, as compared with the control group (Fig. 4), clearly indicating the translocation of mTOR from LE/Ly to the ER. Consistent with our mTOR and LBPA double staining results, PBPP had no apparent effect on mTOR localization. Similar effects of D-PDMP on the co-localization between mTOR and KDEL were also observed in ST2 cells and NIH3T3 cells (Supplementary Fig. S7). The increase in the co-localization between mTOR and KDEL upon D-PDMP treatment occurred significantly 12 h after D-PDMP treatment (Fig. 5), which inversely corresponds to the decreased co-localization of mTOR with LE/Ly. The co-localization between mTOR and KDEL remained unchanged in MC3T3-E1 cells cultured in growth medium or osteogenic medium in the absence of D-PDMP at any time point (Supplementary Fig. S8).

We noticed that the signal intensity of mTOR in the mTOR/LBPA staining decreased upon the PDMP treatment (Figs. 2 and 3), whereas that in the mTOR/KDEL staining increased (Figs. 4 and 5). The immunocytochemistry methods for the two staining procedures are different. Since the total surface area of the ER (~60%) is much larger than that of LE/Ly (~1%), the distribution of mTOR can become broader, when mTOR is translocated from LE/Ly to the ER. If the accessibility of the anti-mTOR antibody to mTOR is unchanged, then

the signal intensity of mTOR per unit area should be reduced. In contrast, if the accessibility of the antibody to a sparse antigen is significantly improved, then the signal intensity of mTOR per unit area would be increased. The difference in the signal intensities of mTOR may be explained by the possibilities that the accessibility of the antibody is unchanged for the mTOR/LBPA staining and increased for the mTOR/KDEL staining upon PDMP treatment.

3.4. Changes of LAMTOR1 subcellular localization upon PDMP treatment

LAMTOR1, also called p18, is an essential anchor protein of the Regulator complex. It functions as a scaffold to recruit mTORC1 to LE/Ly [13,40]. The subcellular localization analysis of LAMTOR1 demonstrated that the LAMTOR1-fluorescence signals that were co-localized with the LBPA-fluorescence signals were significantly decreased in the D-PDMP-treated cells, as compared to control cells (Fig. 6 A and B). In contrast, the D-PDMP treatment led to a significant increase in the co-localization ratio between LAMTOR1 and KDEL (Fig. 6 C and D), suggesting that not only mTOR but also LAMTOR1 is translocated from LE/Ly to the ER by the treatment with PDMP.

Since LAMTOR1 is reportedly associated with lipid rafts [13], we further analyzed the effects of PDMP on the raft-localization of LAMTOR1. Flotillin-1 was used as the raft marker of LE/Ly [41]. An analysis of detergent-resistant membranes (DRMs) demonstrated that the lipid rafts were dramatically affected by the D-PDMP treatment (Supplementary Fig. S9A), and that the proportion of LAMTOR1 in DRMs was increased upon the D-PDMP treatment (Supplementary Fig. S9 B and C). These results imply that the PDMP treatment exerts its

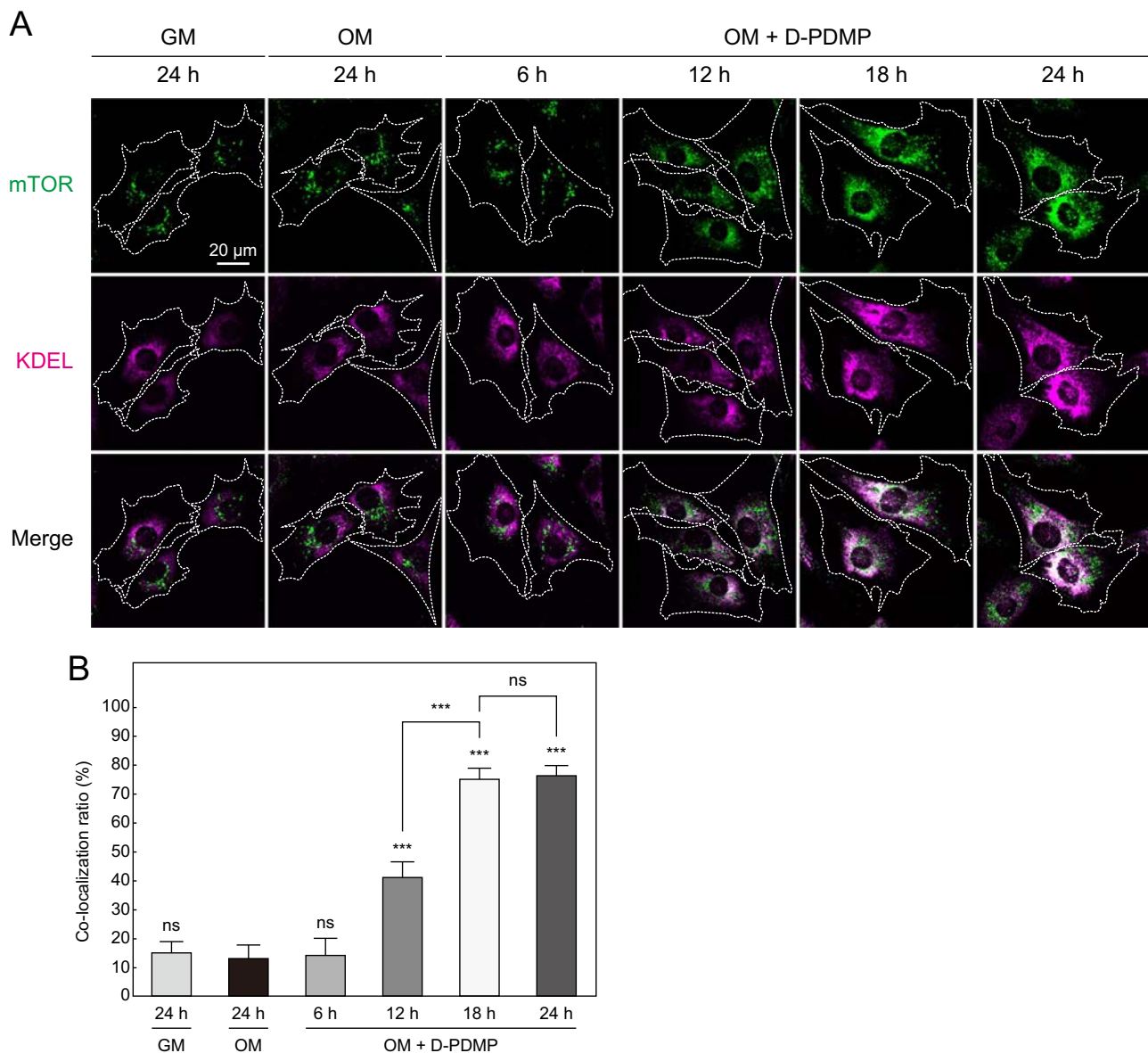


Fig. 5. Kinetics of translocation of mTOR to the ER by D-PDMP. (A) Time-course analysis of the co-localization of mTOR with KDEL. MC3T3-E1 cells were seeded on 15-mm round glass coverslips in 12-well plates (4×10^4 cells/well). After 24 h, the cells were treated without or with 40 μ M D-PDMP in growth medium or osteogenic medium for the indicated times. The cells were fixed with 4% PFA for 15 min, permeabilized with 0.1% Triton X-100 for 5 min, and then labeled with an anti-mTOR antibody (green) and an anti-KDEL antibody (magenta). Cells are outlined with white dashed lines. (B) Quantification of the co-localization between mTOR and KDEL in MC3T3-E1 cells. Data are expressed as means \pm SD. *** P < 0.001; ns (not significant), P > 0.05 compared with OM 24-h group. Abbreviations: GM, cells cultured in growth medium; OM, cells cultured in osteogenic medium.

effects on LAMTOR1 by modulating lipid rafts.

3.5. PDMP inhibits mTORC1 activity

The mTORC1 activity depends on its recruitment to the LE/Ly membranes [11,14,15]. Since PDMP caused the translocation of mTORC1 from LE/Ly to the ER (Figs. 2 and 4), we monitored the effects of PDMP on the mTORC1 activity based on the phosphorylation level of S6K, a downstream target of mTORC1. MC3T3-E1 cells were treated with D-PDMP, L-PDMP, or PBPP. Rapamycin was used as a positive control of mTORC1 inhibition. As shown in Fig. 7A, the D-PDMP and L-PDMP treatments, but not the PBPP treatment, dramatically decreased the level of P-S6K, indicating the inhibition of mTORC1 activity. The level of P-S6K was decreased in a dose-dependent manner in the D-PDMP- and L-PDMP-treated groups. In contrast, the PBPP-treated group showed no significant change even at a high concentration (50 μ M) (Fig. 7 B–D). The mTORC1 activity

increased in a time-dependent manner in the cells cultured in osteogenic medium (Fig. 7E, left panel). In contrast, in the D-PDMP- and L-PDMP-treated groups, the mTORC1 activity increased after a short-term treatment (6 h) and then decreased (Fig. 7E, middle and right panels, respectively), which implies that the inhibitory effect of PDMP is not one-step process, but requires several intermediate steps to take place. The mechanisms of the transient and stimulatory effects should be elucidated in future work. In the present study, the time-course experiments confirmed that the inhibition of the mTORC1 activity by D-PDMP and L-PDMP was evident after treatments for 24 h.

The inactivation of mTORC1 induces autophagy [1–3]. Hence, we assessed the activity of mTORC1 by monitoring the punctate formation of LC3 (an autophagosome marker). The results indicated that D-PDMP and L-PDMP, but not PBPP, induced the LC3 puncta formation (Fig. 7F). Taken together, PDMP inhibits the mTORC1 activity, regardless of the presence or absence of the glucosylceramide

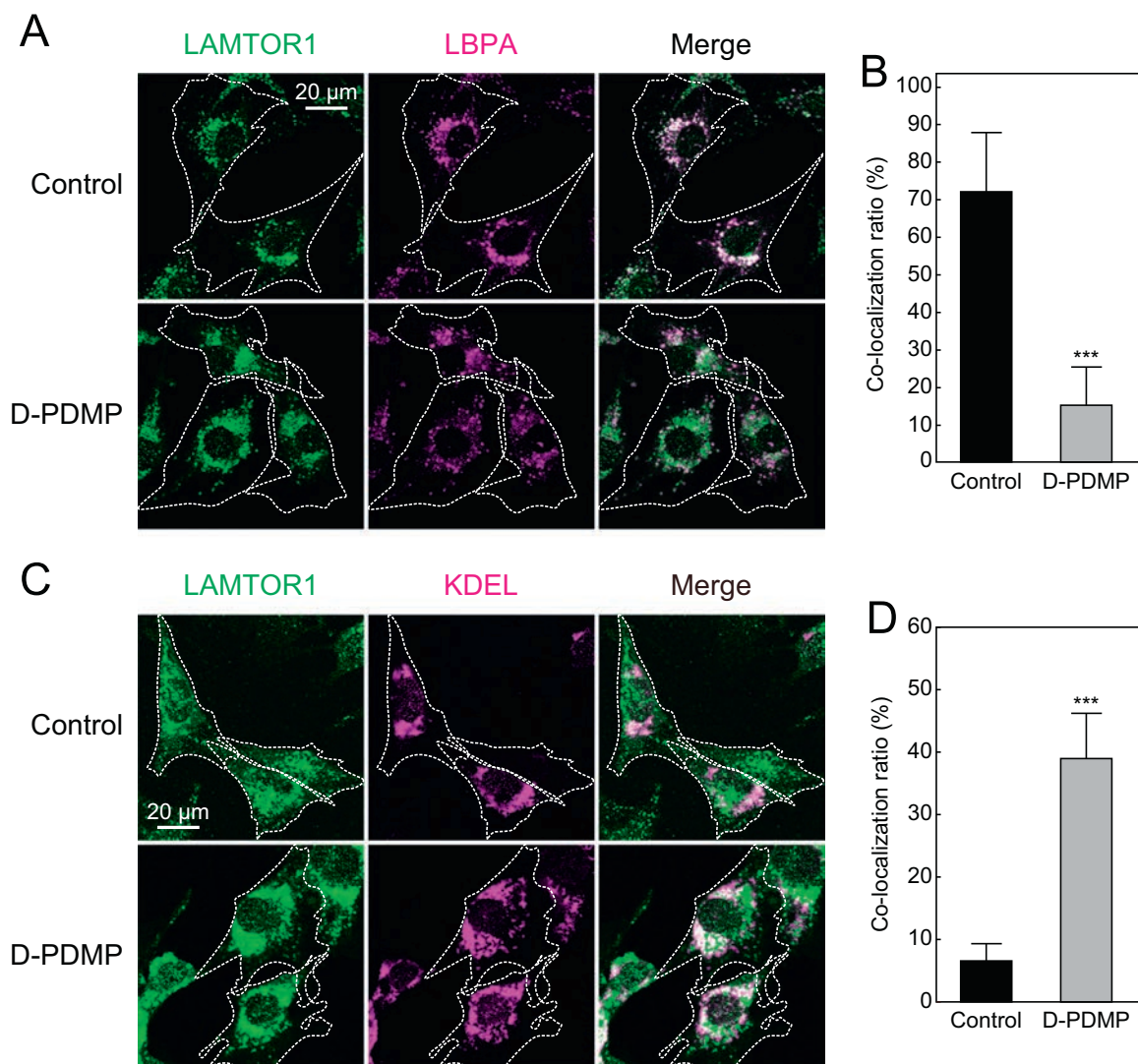


Fig. 6. LAMTOR1 is translocated from LE/Ly to ER by D-PDMP treatment. (A) The co-localization of LAMTOR1 with LBPA is decreased in the D-PDMP-treated MC3T3-E1 cells. MC3T3-E1 cells were seeded on 15-mm round glass coverslips in 12-well plates (4×10^4 cells/well). After 24 h, the cells were treated without or with 40 μM D-PDMP in osteogenic medium for 24 h. Untreated cells cultured in osteogenic medium for 24 h were used as the control. The cells were fixed with 3% PFA for 20 min, permeabilized with 50 μg/ml digitonin for 5 min, and then labeled with an anti-LAMTOR1 antibody (green) and an anti-LBPA antibody (magenta). Cells are outlined with white dashed lines. (B) Quantification of the co-localization between LAMTOR1 and LBPA in MC3T3-E1 cells. (C) The co-localization of LAMTOR1 with KDEL is increased in the D-PDMP-treated cells. MC3T3-E1 cells were seeded on 15-mm round glass coverslips in 12-well plates (4×10^4 cells/well). After 24 h, the cells were treated without or with 40 μM D-PDMP in osteogenic medium for 24 h. Untreated cells cultured in osteogenic medium for 24 h were used as the control. The cells were fixed with 3% PFA for 20 min, permeabilized with 100 μg/ml digitonin for 10 min, and then labeled with an anti-LAMTOR1 antibody (green) and an anti-KDEL antibody (magenta). Cells are outlined with white dashed lines. (D) Quantification of the co-localization between LAMTOR1 and KDEL in MC3T3-E1 cells. Data are expressed as means \pm SD. *** $P < 0.001$ compared with control group.

synthase-inhibitory activity.

3.6. Inhibition of mTORC1 activity by PDMP affects osteoblastic proliferation and differentiation

The contribution of mTORC1 inactivation to the inhibition of osteoblastic cell proliferation has been confirmed by several recent studies [7,8]. Thus, we investigated the effects of PDMP on osteoblastic cell proliferation and differentiation, using MC3T3-E1 cells. The proliferation rates of MC3T3-E1 cells treated with D-PDMP, L-PDMP, or rapamycin for 3 days were dramatically decreased, as compared with the control group, while no significant difference was observed in the PBPP-treated group (Fig. 8A). Both D-PDMP and L-PDMP inhibited the cell proliferation in dose-dependent manners (Fig. 8B). The decreased cell proliferation by the PDMP treatment is not due to cell death, as the amounts of LDH release in all treatment groups were not significantly different from that in the untreated control group (Supplementary Fig. S10).

We evaluated the effects of PDMP on the osteoblastic differentiation of MC3T3-E1 cells, using ALP staining as an indicator of osteogenesis. Control cells, cultured in osteogenic medium without any treatments with compounds for 12 days, exhibited strongly positive ALP staining (Fig. 9A). In contrast, ALP staining was negative in the cells treated with rapamycin for 12 days, suggesting the importance of the mTORC1 activity in the differentiation process. In addition, the ALP staining intensity was decreased by the treatment with D-PDMP or L-PDMP, but not PBPP (Fig. 9A), and in a dose-dependent manner with D-PDMP (Fig. 9B). Similar results were obtained in ST2 cells cultured in osteogenic medium for 21 days (Supplementary Fig. S11).

We measured the mRNA levels of two transcription factors, Runx2 and Osx, early-stage markers of osteoblastic differentiation, in MC3T3-E1 cells. Unlike the expression of the late-stage markers, the expression of the early-stage markers does not exclusively depend on the mTORC1 activity, since the expression is not affected by the deletion of Raptor (an essential component of mTORC1) [8]. Consistent with this notion, rapamycin failed to abolish the expression of Runx2 and Osx.

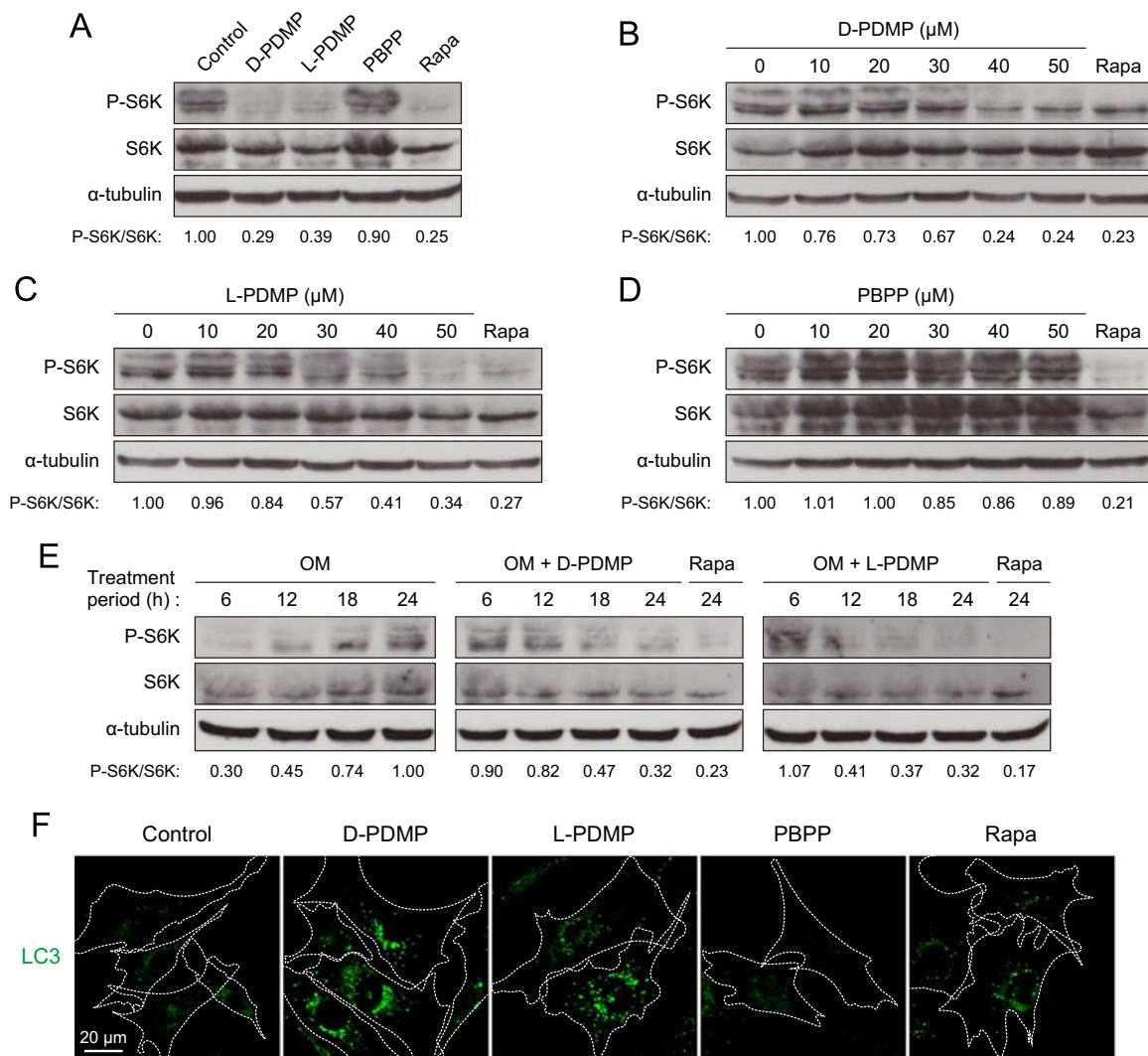


Fig. 7. The mTORC1 activity is inhibited by D-PDMP and L-PDMP. (A) D-PDMP and L-PDMP, but not PBPP, decrease the mTORC1 activity in MC3T3-E1 cells. MC3T3-E1 cells were seeded in 6-well plates (1.8×10^5 cells/well). After 24 h, the cells were treated without or with 40 μ M D-PDMP, 40 μ M L-PDMP, 40 μ M PBPP, or 100 nM rapamycin in osteogenic medium for 24 h. Untreated cells cultured in osteogenic medium for 24 h were used as the control. P-S6K/S6K is the ratio of the band intensity of P-S6K versus the total amount of S6K. Data are expressed as the relative values to the control group. The phosphorylation levels of S6K (P-S6K), a downstream target of mTORC1, were decreased in the D-PDMP- and L-PDMP-treated groups, as compared with the control group. (B–D) D-PDMP and L-PDMP, but not PBPP, decrease the mTORC1 activity in dose-dependent manners. MC3T3-E1 cells were seeded in 6-well plates (1.8×10^5 cells/well). After 24 h, the cells were treated without or with the indicated concentrations of D-PDMP, L-PDMP, or PBPP in osteogenic medium for 24 h. Rapamycin (100 nM for 24 h) was used as a positive control. Each P-S6K/S6K shows the relative ratio to that in the absence of drugs. (E) D-PDMP and L-PDMP time-dependently reduce the levels of P-S6K. MC3T3-E1 cells were seeded in 6-well plates (1.8×10^5 cells/well). After 24 h, the medium was exchanged from growth medium to osteogenic medium in the absence or presence of 40 μ M D-PDMP, 40 μ M L-PDMP, or 100 nM rapamycin for the indicated times. P-S6K/S6K shows the relative ratio to the OM 24-h group. (F) D-PDMP and L-PDMP, but not PBPP, induce the formation of LC3-positive puncta (autophagosomes). MC3T3-E1 cells were seeded on 15-mm round glass coverslips in 12-well plates (4×10^4 cells/well). After 24 h, the cells were treated without or with 40 μ M D-PDMP, 40 μ M L-PDMP, 40 μ M PBPP, or 100 nM rapamycin in osteogenic medium for 24 h. Untreated cells cultured in osteogenic medium for 24 h were used as the control. The cells were fixed with 4% PFA for 10 min and then permeabilized with 100 μ g/ml digitonin for 10 min. To detect the endogenous LC3 protein, the cells were labeled with an anti-LC3 antibody (green). Abbreviations: OM, cells cultured in osteogenic medium; Rapa, rapamycin.

Nonetheless, the expression levels of Runx2 and Osx were significantly reduced in the D-PDMP- and L-PDMP-treated groups, as compared with the control group (Fig. 9 C and D), suggesting that PDMP suppresses the early stage of osteoblastic differentiation by an mTORC1-independent mechanism.

It is noteworthy that L-PDMP tended to inhibit cell proliferation and osteoblastic differentiation more than D-PDMP (Figs. 8 and 9), whereas the apparent difference between these compounds was not observed in the P-S6K levels (Fig. 7A) (We will discuss this point later.). These results suggested that PDMP inhibits not only cell proliferation but also the early stage of osteoblastic differentiation, through the inactivation of mTORC1.

Collectively, PDMP suppresses the proliferation and osteoblastic differentiation of MC3T3-E1 cells in an mTORC1 activity-dependent manner. PDMP also exerts the mTORC1-independent action to inhibit

the early stage of osteoblastic differentiation.

4. Discussion

Accumulating evidence has revealed that the LE/Ly surface is a crucial site for the activation of mTORC1 [10]. In the present study, using an MC3T3-E1 model, we demonstrated that the ceramide analogue PDMP induces the translocation of both mTORC1 and its scaffold protein LAMTOR1 from LE/Ly to the ER, and suppresses the activation of mTORC1. The time-course experiments strongly support the proposal that mTOR is translocated from LE/Ly to the ER in the presence of PDMP, which is closely related to the inhibition of the mTORC1 activity (Figs. 3, 5, and 7E). We also found that PDMP impairs the association of mTORC1 with its activator Rheb, suggesting the PDMP-dependent spatial control of the mTORC1 signaling by the

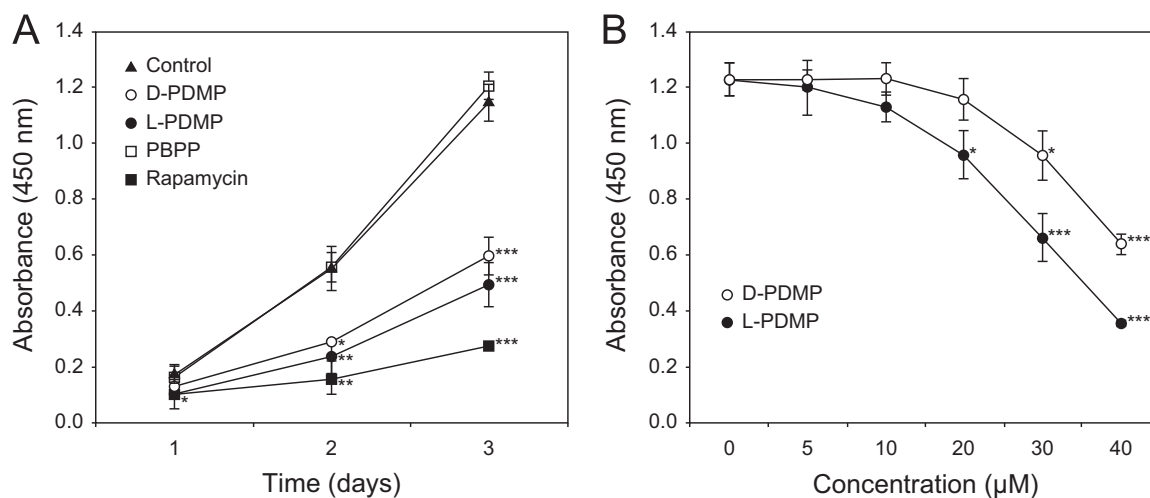


Fig. 8. MC3T3-E1 cell proliferation is inhibited by D-PDMP and L-PDMP. (A) Treatments with D-PDMP and L-PDMP, but not PBPP, for 3 days reduce the proliferation of MC3T3-E1 cells. MC3T3-E1 cells were seeded in 96-well plates (2×10^3 cells/well). After 24 h, the cells were treated without or with 40 μM D-PDMP, 40 μM L-PDMP, 40 μM PBPP, or 10 nM rapamycin in osteogenic medium for the indicated periods of time. Untreated cells cultured in osteogenic medium for the indicated periods of time were used as the control. (B) D-PDMP and L-PDMP inhibit the proliferation of MC3T3-E1 cells in dose-dependent manners. MC3T3-E1 cells were seeded in 96-well plates (2×10^3 cells/well). After 24 h, the cells were treated with the indicated concentrations of D-PDMP or L-PDMP in osteogenic medium for 3 days. Untreated cells cultured in osteogenic medium for 3 days were used as the control. The cell proliferation was determined by a Cell Counting Kit-8 assay. Data are expressed as means \pm SD. * $P < 0.05$; ** $P < 0.01$; *** $P < 0.001$ compared with control group.

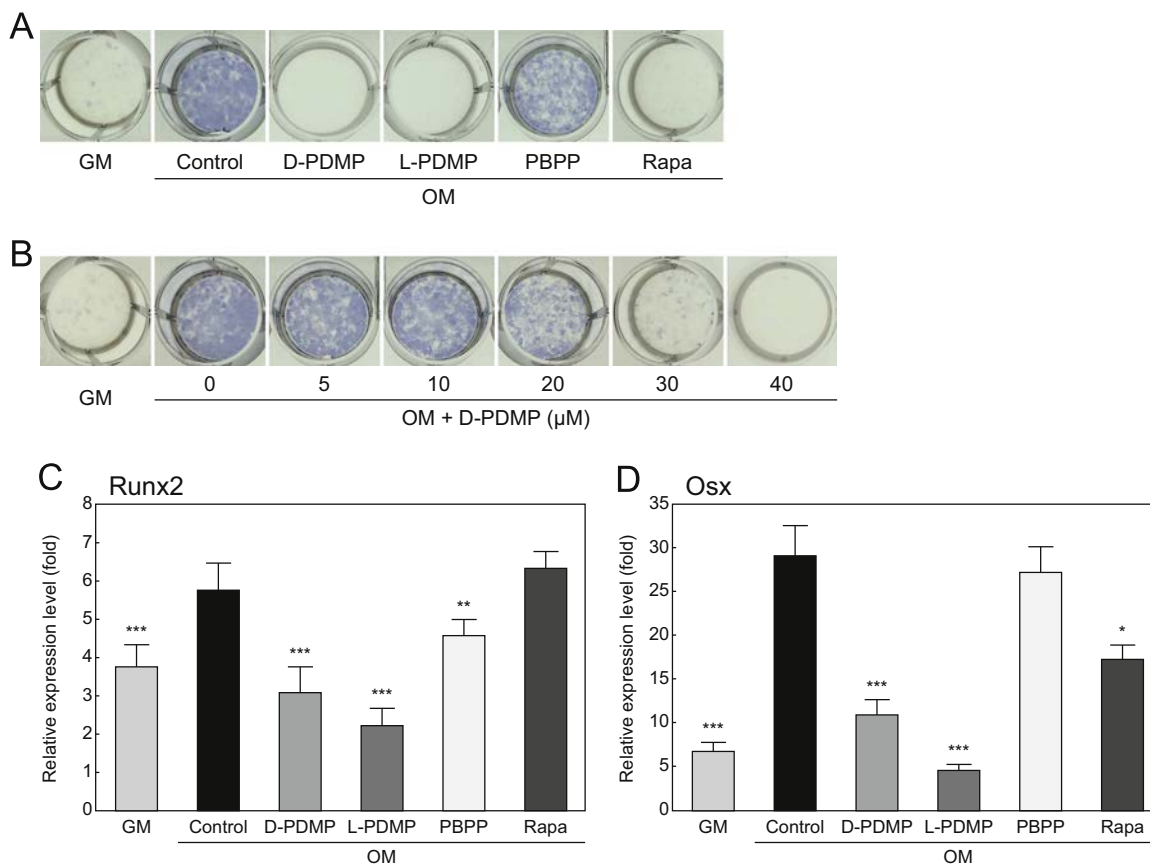


Fig. 9. The osteoblastic differentiation of MC3T3-E1 cells is inhibited by D-PDMP and L-PDMP. (A) ALP staining in MC3T3-E1 cells. MC3T3-E1 cells were seeded in 12-well plates (1×10^4 cells/well). After 24 h, the medium was exchanged from growth medium to osteogenic medium in the absence or presence of 40 μM D-PDMP, 40 μM L-PDMP, 40 μM PBPP, or 10 nM rapamycin for 12 days. Untreated cells cultured in osteogenic medium for 12 days were used as the control. Treatments with D-PDMP and L-PDMP, but not PBPP, decreased the ALP staining intensity, as compared with control groups. (B) MC3T3-E1 cells were seeded in 12-well plates (1×10^4 cells/well). After 24 h, the medium was exchanged from growth medium to osteogenic medium in the absence or presence of the indicated concentrations of D-PDMP for 12 days. Untreated cells cultured in osteogenic medium for 12 days were used as the control. D-PDMP decreased the ALP staining intensity of MC3T3-E1 cells in a dose-dependent manner. (C, D) mRNA expression of osteoblastic differentiation markers (Runx2 and Osx) in MC3T3-E1 cells. MC3T3-E1 cells were seeded in 6-well plates (2.25×10^4 cells/well), cultured in growth medium for 24 h (Day 0), and then treated without or with 40 μM D-PDMP, 40 μM L-PDMP, 40 μM PBPP, or 10 nM rapamycin in osteogenic medium for 14 days (Day 14). Untreated cells cultured in osteogenic medium for 14 days were used as the control. mRNA expression levels were determined by a quantitative real-time RT-PCR analysis. Target gene expression was normalized to GAPDH mRNA, and shown as relative ratios of the gene expression in the Day 14 group to that in the Day 0 group. The expression levels of the osteoblastic differentiation markers were decreased by the D-PDMP and L-PDMP treatments. Data are expressed as means \pm SD. * $P < 0.05$; ** $P < 0.01$; *** $P < 0.001$ compared with control group. Abbreviations: GM, cells cultured in growth medium; OM, cells cultured in osteogenic medium; Rapa, rapamycin.

segregation of mTOR from Rheb. Furthermore, the present study also suggests that the effects of PDMP treatment on LAMTOR1 are mediated via lipid rafts (Supplementary Fig. S9). Thus, we propose a novel mechanism of action for ceramide analogues that target mTORC1 on the LE/Ly membrane. This mechanism adds new insights to our current understanding of the biological actions of ceramides and ceramide analogues, which is mainly based on the Akt/PKB signaling on the plasma membrane.

PDMP reportedly induces the formation of an ER tubular network in a glycosphingolipid-independent manner [34]. Sprocati et al. proposed that PDMP induces ribosome clustering on the ER and leaves a large area available for tubular network formation. The exclusion of ribosomes from the ER membrane is a prominent feature of the membrane contact sites between the ER and other organelles [42]. Recent studies suggested the importance of the contact sites between the ER and LE/Ly in endosome trafficking and endosome fission, as well as the transport of cholesterol and ceramide [42,43]. Combining these studies, as an underlying mechanism for the translocation of mTORC1 from LE/Ly to the ER, we hypothesize that PDMP promotes the contacts between the ER and LE/Ly.

Impaired intracellular cholesterol transport is associated with the inhibition of the mTORC1 activity, in the cases of ezetimibe in human hepatocytes [41] and itraconazole in human endothelial cells and glioblastoma cells [44,45]. Coincidentally, ezetimibe also significantly increases the proportion of LAMTOR1 in DRMs [41], similar to PDMP. The oxysterol-binding protein ORP1L senses the cholesterol level in LE/Ly and interacts with the ER integral protein VAP (vesicle-associated membrane protein) [46], which may link the inhibition of intracellular cholesterol transport with the formation of ER-LE/Ly contact sites. We speculate that the molecular machinery of cholesterol transport, the ER-LE/Ly contact sites, and the association of LAMTOR1 to DRMs are converged for the translocation of mTORC1 from LE/Ly to the ER.

According to the results shown in Figs. 2 and 4, the translocation of mTORC1 from LE/Ly to the ER was induced by PDMP, but not PBPP. Morpholino and decanoylamino groups are present in PDMP, whereas pyrrolidino and benzyloxycarbonylamino groups exist at the corresponding positions in PBPP, respectively (Fig. 1A). The presence of the acyl chain in PDMP may be involved in its affinity to membrane lipids. It is also possible that an oxygen atom in the morpholino group has an affinity to a hydroxyl or amino group in the vicinal PDMP molecules, which allows the lateral association of the PDMP molecules to form distinct membrane domains similar to lipid rafts. Further studies are required to identify whether PDMP exerts its effects through alterations of local membrane structures or associations with distinct target proteins.

In the present study, we demonstrated the PDMP-dependent translocation of mTORC1 and its scaffold protein LAMTOR1 to the ER, and the PDMP-dependent dissociation of mTORC1 from Rheb. In the presence of PDMP, Rheb likely remains on the LE/Ly membrane, thus leading to the segregation of mTORC1 from Rheb. Then, the question arises: why is LAMTOR1, but not Rheb, translocated to the ER? The difference in the membrane association modes, such as the fatty acid modification of LAMTOR1 and the isoprenoid modification of Rheb, is likely to be responsible for the distinct effects of PDMP on LAMTOR1 and Rheb.

PDMP is a promising target for preventing atherosclerosis and cardiac hypertrophy [28,29] and for suppressing osteoclastogenesis [47,48] by inhibiting glycosphingolipid synthesis. PDMP is reportedly potent in combination therapies for cancer treatment [30,31]. Since the mTORC1 activity is enhanced in cancer cells to potentiate their survival, the inhibitory effect of PDMP on the mTORC1 activity could explain the sensitization of cancer cells to anti-cancer drugs. In the present study, we showed that PDMP suppresses osteoblastic proliferation and pre-osteoblastic cell differentiation by inhibiting the mTORC1 activity. The underlying mechanism is distinct from the

inhibition of glycosphingolipid synthesis. However, the effect of L-PDMP on osteoblastic differentiation was more potent than that of D-PDMP. Since glycosphingolipids such as GM3 inhibit osteoblastic differentiation [49,50], the effect of D-PDMP may have relieved the glycosphingolipid-mediated inhibition of differentiation. It is conceivable that the various effects of PDMP are opposing or additive in membrane property-dependent manners. Accordingly, the present study adds an important rationale to extend the utility of PDMP.

5. Conclusions

Our study revealed that PDMP induces the translocation of mTOR from LE/Ly to the ER through the effects on the organelles, which is independent of its well-known action as an inhibitor of glycosphingolipid synthesis. The translocation of mTOR results in the impaired interaction between mTOR and Rheb, an mTOR activator, leading to mTORC1 inactivation. The inactivation of mTORC1 leads to reductions in the proliferation and osteoblastic differentiation of MC3T3-E1 cells.

Acknowledgements

This study was supported by a Grant-in-Aid for the Japan Society for the Promotion of Science (JSPS) Fellows 16J07413 (to T.O.) and Grants-in-Aid for Scientific Research 22592060 and 25463072 (to M.H.) and 23650319 and 26463087 (to K.A.I.). T.O. was a recipient of the Iwadare Scholarship Foundation.

Appendix A. Supporting information

Supplementary data associated with this article can be found in the online version at doi:10.1016/j.yexcr.2016.11.011.

References

- [1] M. Laplante, D.M. Sabatini, mTOR signaling in growth control and disease, *Cell* 149 (2012) 274–293.
- [2] M. Laplante, D.M. Sabatini, mTOR signaling at a glance, *J. Cell Sci.* 122 (2009) 3589–3594.
- [3] M. Laplante, D.M. Sabatini, Regulation of mTORC1 and its impact on gene expression at a glance, *J. Cell Sci.* 126 (2013) 1713–1719.
- [4] E. Jacinto, R. Loewith, A. Schmidt, S. Lin, M.A. Ruegg, A. Hall, M.N. Hall, Mammalian TOR complex 2 controls the actin cytoskeleton and is rapamycin insensitive, *Nat. Cell Biol.* 6 (2004) 1122–1128.
- [5] T. Ogawa, M. Tokuda, K. Tomizawa, H. Matsui, T. Itano, R. Konishi, S. Nagahata, O. Hatase, Osteoblastic differentiation is enhanced by rapamycin in rat osteoblast-like osteosarcoma (ROS 17/2.8) cells, *Biochem. Biophys. Res. Commun.* 249 (1998) 226–230.
- [6] F. Vinals, T. Lopez-Rovira, J.L. Rosa, F. Ventura, Inhibition of PI3K/p70 S6K and p38 MAPK cascades increases osteoblastic differentiation induced by BMP-2, *FEBS Lett.* 510 (2002) 99–104.
- [7] U.K. Singha, Y. Jiang, S. Yu, M. Luo, Y. Lu, J. Zhang, G. Xiao, Rapamycin inhibits osteoblast proliferation and differentiation in MC3T3-E1 cells and primary mouse bone marrow stromal cells, *J. Cell Biochem.* 103 (2008) 434–446.
- [8] J. Chen, F. Long, mTORC1 signaling promotes osteoblast differentiation from preosteoblasts, *PLoS One* 10 (2015) e0130627.
- [9] B. Huang, Y. Wang, W. Wang, J. Chen, P. Lai, Z. Liu, B. Yan, S. Xu, Z. Zhang, C. Zeng, L. Rong, B. Liu, D. Cai, D. Jin, X. Bai, mTORC1 prevents preosteoblast differentiation through the notch signaling pathway, *PLoS Genet.* 11 (2015) e1005426.
- [10] R. Puertollano, mTOR and lysosome regulation, *F1000Prime Rep.* 6 (2014) 52.
- [11] Y. Sancak, L. Bar-Peled, R. Zoncu, A.L. Markhard, S. Nada, D.M. Sabatini, Regulator-Rag complex targets mTORC1 to the lysosomal surface and is necessary for its activation by amino acids, *Cell* 141 (2010) 290–303.
- [12] L. Bar-Peled, L.D. Schweitzer, R. Zoncu, D.M. Sabatini, Regulator is a GEF for the rag GTPases that signal amino acid levels to mTORC1, *Cell* 150 (2012) 1196–1208.
- [13] S. Nada, A. Hondo, A. Kasai, M. Koike, K. Saito, Y. Uchiyama, M. Okada, The novel lipid raft adaptor p18 controls endosome dynamics by anchoring the MEK-ERK pathway to late endosomes, *EMBO J.* 28 (2009) 477–489.
- [14] C. Demetriades, N. Doumpas, A.A. Teleman, Regulation of TORC1 in response to amino acid starvation via lysosomal recruitment of TSC2, *Cell* 156 (2014) 786–799.
- [15] S. Menon, C.C. Dibble, G. Talbot, G. Hoxhaj, A.J. Valvezan, H. Takahashi, L.C. Cantley, B.D. Manning, Spatial control of the TSC complex integrates insulin and nutrient regulation of mTORC1 at the lysosome, *Cell* 156 (2014) 771–785.
- [16] Y. Uchida, Ceramide signaling in mammalian epidermis, *Biochim. Biophys. Acta* 2014 (1841) 453–462.

- [17] R.N. Kolesnick, M. Kronke, Regulation of ceramide production and apoptosis, *Annu. Rev. Physiol.* 60 (1998) 643–665.
- [18] G. Yang, L. Badeanlou, J. Bielawski, A.J. Roberts, Y.A. Hannun, F. Samad, Central role of ceramide biosynthesis in body weight regulation, energy metabolism, and the metabolic syndrome, *Am. J. Physiol. Endocrinol. Metab.* 297 (2009) E211–E224.
- [19] B. Stancevic, R. Kolesnick, Ceramide-rich platforms in transmembrane signaling, *FEBS Lett.* 584 (2010) 1728–1740.
- [20] E. Hajdich, A. Balendran, I.H. Batty, G.J. Litherland, A.S. Blair, C.P. Downes, H.S. Hundal, Ceramide impairs the insulin-dependent membrane recruitment of Protein Kinase B leading to a loss in downstream signalling in L6 skeletal muscle cells, *Diabetologia* 44 (2001) 173–183.
- [21] S. Stratford, K.L. Hoehn, F. Liu, S.A. Summers, Regulation of insulin action by ceramide: dual mechanisms linking ceramide accumulation to the inhibition of Akt/protein kinase B, *J. Biol. Chem.* 279 (2004) 36608–36615.
- [22] F. Li, N. Zhang, Ceramide: therapeutic potential in combination therapy for cancer treatment, *Curr. Drug Metab.* 17 (2015) 37–51.
- [23] I. Aubin, C.P. Adams, S. Opsahl, D. Septier, C.E. Bishop, N. Auge, R. Salvayre, A. Negre-Salvayre, M. Goldberg, J.L. Guenet, C. Poirier, A deletion in the gene encoding sphingomyelin phosphodiesterase 3 (Smpd3) results in osteogenesis and dentinogenesis imperfecta in the mouse, *Nat. Genet.* 37 (2005) 803–805.
- [24] Z. Khavandgar, S. Alebrahim, H. Eimar, F. Tamimi, M.D. McKee, M. Murshed, Local regulation of tooth mineralization by sphingomyelin phosphodiesterase 3, *J. Dent. Res.* 92 (2013) 358–364.
- [25] Z. Khavandgar, M. Murshed, Sphingolipid metabolism and its role in the skeletal tissues, *Cell Mol. Life Sci.* 72 (2015) 959–969.
- [26] L.J. Siskind, R.N. Kolesnick, M. Colombini, Ceramide forms channels in mitochondrial outer membranes at physiologically relevant concentrations, *Mitochondrion* 6 (2006) 118–125.
- [27] J. Inokuchi, N.S. Radin, Preparation of the active isomer of 1-phenyl-2-decanoylamino-3-morpholino-1-propanol, inhibitor of murine glucocerebrosidase, *J. Lipid Res* 28 (1987) 565–571.
- [28] S. Chatterjee, D. Bedja, S. Mishra, C. Amuzie, A. Avolio, D.A. Kass, D. Berkowitz, M. Renahan, Inhibition of glycosphingolipid synthesis ameliorates atherosclerosis and arterial stiffness in apolipoprotein E^{-/-} mice and rabbits fed a high-fat and -cholesterol diet, *Circulation* 129 (2014) 2403–2413.
- [29] S. Mishra, D. Bedja, C. Amuzie, C.A. Foss, M.G. Pomper, R. Bhattacharya, K.J. Yarema, S. Chatterjee, Improved intervention of atherosclerosis and cardiac hypertrophy through biodegradable polymer-encapsulated delivery of glycosphingolipid inhibitor, *Biomaterials* 64 (2015) 125–135.
- [30] T. Wang, J. Wei, N. Wang, J.L. Ma, P.P. Hui, The glucosylceramide synthase inhibitor PDMP sensitizes pancreatic cancer cells to MEK/ERK inhibitor AZD-6244, *Biochem. Biophys. Res. Commun.* 456 (2015) 821–826.
- [31] H. Sietsma, R.J. Veldman, D. Kolk, B. Ausema, W. Nijhof, W. Kamps, E. Vellenga, J.W. Kok, 1-phenyl-2-decanoylamino-3-morpholino-1-propanol chemosensitizes neuroblastoma cells for taxol and vincristine, *Clin. Cancer Res.* 6 (2000) 942–948.
- [32] A.G. Rosenwald, R.E. Pagano, Effects of the glucosphingolipid synthesis inhibitor, PDMP, on lysosomes in cultured cells, *J. Lipid Res.* 35 (1994) 1232–1240.
- [33] A. Makino, K. Ishii, M. Murate, T. Hayakawa, Y. Suzuki, M. Suzuki, K. Ito, T. Fujisawa, H. Matsuo, R. Ishitsuka, T. Kobayashi, D-threo-1-phenyl-2-decanoylamino-3-morpholino-1-propanol alters cellular cholesterol homeostasis by modulating the endosome lipid domains, *Biochemistry* 45 (2006) 4530–4541.
- [34] T. Sprocati, P. Ronchi, A. Raimondi, M. Francolini, N. Borgese, Dynamic and reversible restructuring of the ER induced by PDMP in cultured cells, *J. Cell Sci.* 119 (2006) 3249–3260.
- [35] M. Jimbo, K. Yamagishi, T. Yamaki, K. Nunomura, K. Kabayama, Y. Igarashi, J.I. Inokuchi, Development of a new inhibitor of glucosylceramide synthase, *J. Biochem.* 127 (2000) 485–491.
- [36] T. Kobayashi, E. Stang, K.S. Fang, P. de Moerloose, R.G. Parton, J. Gruenberg, A lipid associated with the antiphospholipid syndrome regulates endosome structure and function, *Nature* 392 (1998) 193–197.
- [37] M. Oba, T. Kato, K. Furukawa, M. Tanaka, A cell-penetrating peptide with a guanidylethyl amine structure directed to gene delivery, *Sci. Rep.* 6 (2016) 19913.
- [38] T. Yamasaki, A. Suzuki, R. Hasebe, M. Horiuchi, Comparison of the anti-prion mechanism of four different anti-prion compounds, anti-PrP monoclonal antibody 44B1, pentosan polysulfate, chlorpromazine, and U18666A, in prion-infected mouse neuroblastoma cells, *PLoS One* 9 (2014) e106516.
- [39] H.R. Pelham, The retention signal for soluble proteins of the endoplasmic reticulum, *Trends Biochem. Sci.* 15 (1990) 483–486.
- [40] S. Nada, S. Mori, Y. Takahashi, M. Okada, p18/LAMTOR1: a late endosome/lysosome-specific anchor protein for the mTORC1/MAPK signaling pathway, *Methods Enzymol.* 535 (2014) 249–263.
- [41] T. Yamamura, Y. Ohsaki, M. Suzuki, Y. Shinohara, T. Tatematsu, J. Cheng, M. Okada, N. Ohmiya, Y. Hirooka, H. Goto, T. Fujimoto, Inhibition of Niemann-Pick-type C1-like1 by ezetimibe activates autophagy in human hepatocytes and reduces mutant alpha1-antitrypsin Z deposition, *Hepatology* 59 (2014) 1591–1599.
- [42] M.J. Phillips, G.K. Voeltz, Structure and function of ER membrane contact sites with other organelles, *Nat. Rev. Mol. Cell Biol.* 17 (2016) 69–82.
- [43] C. Raiborg, E.M. Wenzel, H. Stenmark, ER-endosome contact sites: molecular compositions and functions, *EMBO J.* 34 (2015) 1848–1858.
- [44] J. Xu, Y. Dang, Y.R. Ren, J.O. Liu, Cholesterol trafficking is required for mTOR activation in endothelial cells, *Proc. Natl. Acad. Sci. USA* 107 (2010) 4764–4769.
- [45] R. Liu, J. Li, T. Zhang, L. Zou, Y. Chen, K. Wang, Y. Lei, K. Yuan, Y. Li, J. Lan, L. Cheng, N. Xie, R. Xiang, E.C. Nice, C. Huang, Y. Wei, Itraconazole suppresses the growth of glioblastoma through induction of autophagy: involvement of abnormal cholesterol trafficking, *Autophagy* 10 (2014) 1241–1255.
- [46] N. Rocha, C. Kuijl, R. van der Kant, L. Janssen, D. Houben, H. Janssen, W. Zwart, J. Neefjes, Cholesterol sensor ORP1L contacts the ER protein VAP to control Rab7-RILP-p150 Glued and late endosome positioning, *J. Cell Biol.* 185 (2009) 1209–1225.
- [47] T. Iwamoto, S. Fukumoto, K. Kanaoka, E. Sakai, M. Shibata, E. Fukumoto, J. Inokuchi, K. Takamiya, K. Furukawa, Y. Kato, A. Mizuno, Lactosylceramide is essential for the osteoclastogenesis mediated by macrophage-colony-stimulating factor and receptor activator of nuclear factor-kappa B ligand, *J. Biol. Chem.* 276 (2001) 46031–46038.
- [48] S. Fukumoto, T. Iwamoto, E. Sakai, K. Yuasa, E. Fukumoto, A. Yamada, T. Hasegawa, K. Nonaka, Y. Kato, Current topics in pharmacological research on bone metabolism: osteoclast differentiation regulated by glycosphingolipids, *J. Pharmacol. Sci.* 100 (2006) 195–200.
- [49] S.M. Kim, J.U. Jung, J.S. Ryu, J.W. Jin, H.J. Yang, K. Ko, H.K. You, K.Y. Jung, Y.K. Choo, Effects of gangliosides on the differentiation of human mesenchymal stem cells into osteoblasts by modulating epidermal growth factor receptors, *Biochem. Biophys. Res. Commun.* 371 (2008) 866–871.
- [50] G. Moussavou, D.H. Kwak, M.U. Lim, J.S. Kim, S.U. Kim, K.T. Chang, Y.K. Choo, Role of gangliosides in the differentiation of human mesenchymal-derived stem cells into osteoblasts and neuronal cells, *BMB Rep.* 46 (2013) 527–532.



Gangliosides and hearing

Jin-ichi Inokuchi^{a,*}, Shinji Go^{a,b}, Misato Yoshikawa^{a,c}, Kevin Strauss^d

^a Division of Glycopathology, Institute of Molecular Biomembrane and Glycobiology, Tohoku Medical and Pharmaceutical University, 4-4-1 Komatsushima, Aoba-ku, Sendai, Miyagi 981-8558, Japan

^b Kawasaki medical school, 577, Matsushima, Kurashiki, Okayama 701-0192, Japan

^c School of Pharmacy, Shujitsu University, 1-6-1 Nishigawara, Naka-ku, Okayama-shi, Okayama 703-8516, Japan

^d Clinic for Special Children, 535 Bunker Hill Road, Strasburg, PA 17579, United States

ARTICLE INFO

Keywords:

Gangliosides
GM3 synthase
Auditory system
Deafness
Hair cells
Stereocilia

ABSTRACT

Severe auditory impairment observed in GM3 synthase-deficient mice and humans indicates that glycosphingolipids, especially sialic-acid containing gangliosides, are indispensable for hearing. Gangliosides associate with glycoproteins to form membrane microdomains, the composition of which plays a special role in maintaining the structural and functional integrity of hair cells. These microdomains, also called lipid rafts, connect with intracellular signaling and cytoskeletal systems to link cellular responses to environmental cues. During development, ganglioside species are expressed in distinctive spatial and temporal patterns throughout the cochlea. In both mice and humans, blocking particular steps of ganglioside metabolism produces distinctive neurological and auditory phenotypes. Thus each ganglioside species may have specific, non-overlapping functions within the cochlea, central auditory network, and brain.

1. Background

Deafness is the most common hereditary disability in humans, affecting 1 per 1000 newborns, and more than 40% of people older than 65 years suffer from age-related hearing loss. Cell-surface glycoconjugates—proteoglycans, glycoproteins, and glycosphingolipids (GSLs)—have specific spatial and temporal patterns of expression in the developing cochlea and appear to subserve important roles in hearing [1]. Gangliosides (sialic acid-containing GSLs) are abundant in mammalian brains, where they typically reside in the outer leaflet of cell membranes and cluster in microdomains (lipid rafts) specialized for adhesion and signaling [3,4]. They comprise 0.5% of mature human brain (~1.8% of non-water brain weight) [5], have 3-fold greater abundance in gray relative to white matter, and are requisite for the normal growth, differentiation, and maintenance of neural tissues [2].

GM3 synthase (a.k.a. lactosylceramide sialyltransferase; SIAT9, ST3GAL5) is encoded by *ST3GAL5* and mediates the sialylation of lactosylceramide (LacCer) to form GM3, the root structure for all downstream a- and b-series gangliosides (Fig. 1A) [6–8]. B4GALNT1 subsequently transfers *N*-acetylgalactosamine to LacCer, GM3, or GD3 to

form GA2, GM2 or GD2, respectively. Based on this enzymology, various patterns of systemic ganglioside deficiency have been modeled in transgenic mice [9].

St8sia1 $-/-$ (GD3 synthase null) mice lack b-series gangliosides (GD3 and its downstream derivatives) and suffer from thermal hyperalgesia and mechanical allodynia [10]. *B4galnt1* $-/-$ mice express only two ganglioside species (GM3 and GD3) and manifest delayed nerve conduction, axonal degeneration, and ataxia [11,12]. *B4galnt1* $-/-$: *St8sia1* $-/-$ double knockout animals express only GM3 and have fatal audiogenic seizures and peripheral neuropathy [7,13]. Knocking out both *St3gal5* and *B4galnt1* produces mice deficient of GM3 as well as all downstream a-, b-, and o-series gangliosides; these animals have lethal neurodegenerative disease characterized by micrencephaly, aberrant axon-glial interactions, and axonal degeneration [14].

We generated *St3gal5* $-/-$ mice lacking GM3 as well as a- and b-series gangliosides [9]. These animals have no overt neurodegenerative phenotype, perhaps owing to compensatory B4galnt1-mediated production of o-series gangliosides [14]. *St3gal5* $-/-$ mice do not startle in response to sound but startle normally to puffs of air, which suggests hearing impairment [15]. This is corroborated by electrophysiological and

* Corresponding author.

E-mail address: jin@tohoku-mpu.ac.jp (J.-i. Inokuchi).

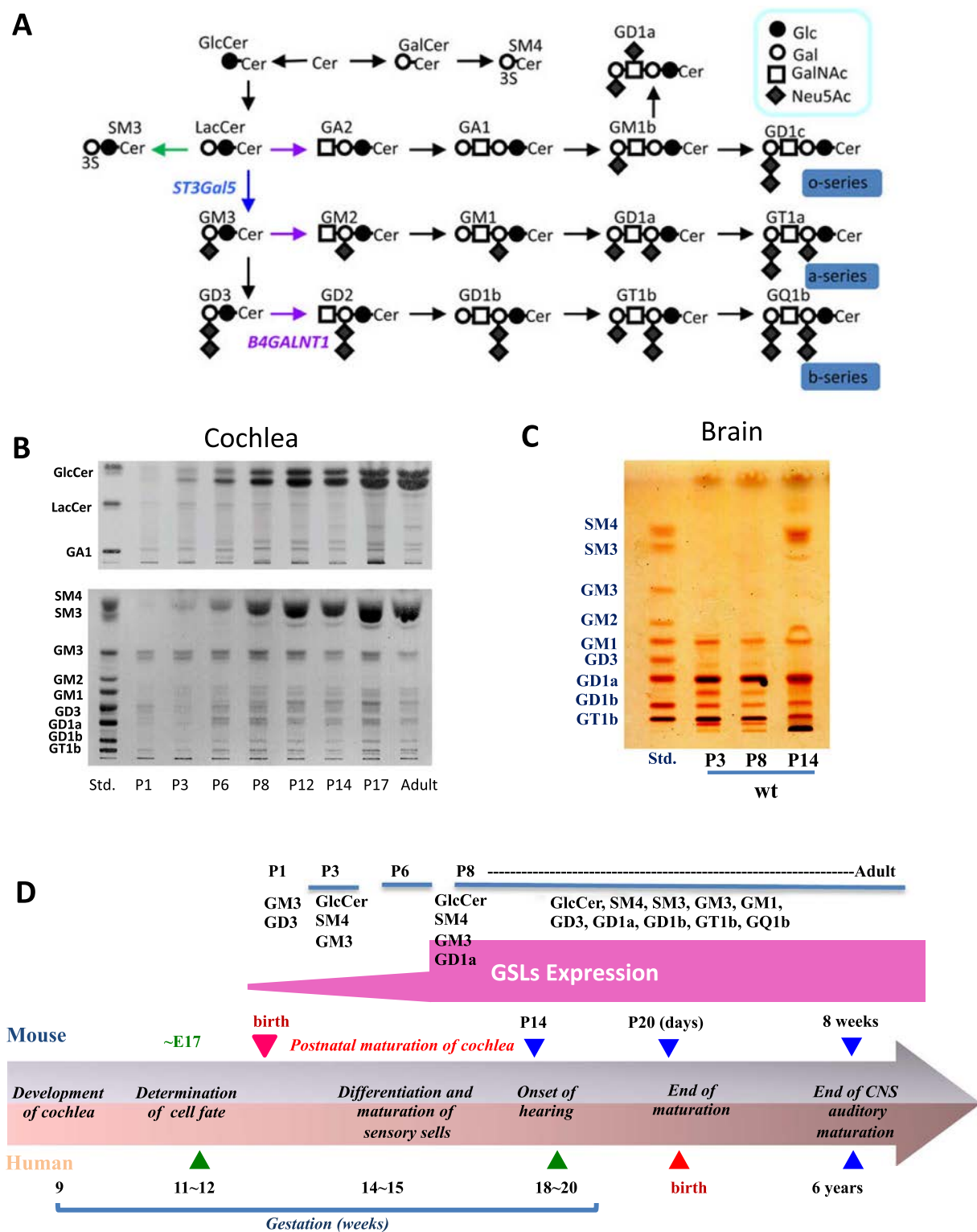


Fig. 1. Marked increase of GSLs in cochlea during postnatal maturation period. (A) Schematic presentation of GSL biosynthesis. (B) High performance-thin-layer chromatograms (HPTLC) analysis of gangliosides in cochlea of wild-type mice during the postnatal maturation period. Upper panel is neutral glycolipids and lower panel is acidic glycolipids. Cochlea were isolated and subjected for the purification of GSL analysis as described in ref. [16]. Each purified fraction was spotted as 2 mg protein per lane. (C) HPTLC analysis of gangliosides in whole brain of wild-type mice during the postnatal maturation period (D) Summary of stage-specific expression of GSLs during postnatal maturation of cochlea based on the information of Fig. 1B and LC-MS/MS analysis of ganglioside species reported in ref. [16]. Comparative development of the cochlea of both humans and mice are also shown.

histological analyses of the auditory system, which reveal selective degeneration of the organ of Corti [15,16]. Interestingly, auditory impairment is the herald sign of disease in newborns with ST3GAL5 deficiency [16], indicating that GM3 may be indispensable for murine and human hearing.

2. Scope of review

We provide an overview of glycoconjugate expression in the murine auditory system and consider the association between ganglioside deficiency and hearing, including recent auditory findings in ganglioside-

Table 1
Phenotypes of hearing loss in mice depleted enzymes related to glycoconjugate metabolism.

Mouse	Type of hearing loss	Symptom, histology	Ref.
Neu1 knockout (Lysosomal sialidase)	Conductive	Inflammation in middle ear Thickened mucosa	[51]
Fbs2 knockout (Ubiquitin ligase of glycoproteins)	Sensorineural	Reduce of endolymphatic potential	[52]
Cmah knockout (Sialic acid metabolism)	Sensorineural (progressive)	Degradation of supporting cells	[53]
	Sensorineural (reducing hearing ability with age)	Degradation of outer hair cells	[53]
Mucopolysaccharidosis type VII model (Lysosomal glucuronidase)	Hearing loss with age	No obvious cell loss	[54]
ST3GAL5 knockout (GM3 synthase)	Sensorineural	Degeneration and loss of outer and inner hair cells	[15,16]
Prosaposin knockout (Glycosphingolipid catabolism)	Sensorineural (progressive)	Hypertrophy of hair cells and dieters cells Loss of outer hair cells	[55]
SaposinB knockout (Glycosphingolipid catabolism)	Sensorineural	Degeneration of spiral ganglions	[56]

deficient mice and humans.

3. Major conclusions

3.1. Hearing loss in human and animals with disorders of glycoconjugate metabolism

Abundant glycans (carbohydrate portions of glycoconjugates) in cochlear tissue have been reported from 1980s using various stainings such as reagents, lectins and antibodies against specific glycan [15–18,36–50]. Further insights about the relationship between glycoconjugates and hearing emerged from studies of transgenic mice. Deletion of enzymes that synthesize (Cmah and St3Gal5) and catabolize (Neu1, Fbx2, glucuronidase, and Saposins) glycoconjugates cause hearing loss in mice, and each enzymopathy entrains a particular pattern and mechanism of hearing loss (Table 1) [15,16,51–56].

Mixed type (conductive and sensorineural) hearing loss is observed in humans with lysosomal storage diseases (LSDs) and congenital disorders of glycosylation (CDGs), which result from mutations that interfere with the catabolism and assembly of glycoconjugates, respectively. Nerve defects and middle ear disease are observed in these patients, but the molecular mechanisms of hearing loss may be more specifically related to alterations of glycoconjugate expression within the cochlea (Table 2, [57–66]).

The study of autosomal recessive ST3GAL5 (GM3 synthase) deficiency provides the strongest link between ganglioside metabolism and auditory function in humans. Biallelic damaging ST3GAL5 variants cause infantile-onset epileptic encephalopathy, slow brain growth, stagnant psychomotor development, growth failure, blindness, dyspigmentation, and deafness [19–23]. We examined eight children (ages 4.1 ± 2.3 years) from the Old Order Amish community who were homozygous for pathogenic ST3GAL5 c.694C > T variants [16].

Table 2
Hearing loss in human LSDs and CDGs.

Human diseases	Causative gene	Ref.
Lysosomal storage disorders		
• Gaucher disease	Glucocerebrosidase	[57]
• Fabry disease	Alpha-galactosidase	[58]
• Mucopolysaccharidosis	hydrolases of glycosaminoglycans	[59]
• Pompe disease	Alpha-glucosidase	[60]
• Sialidosis	Neuraminidase	[61]
• GM2 gangliosidosis	Beta-hexosaminidase	[62]
• Mannosidosis	Mannosidases	[63]
Congenital disorder of glycosylation		
• Type Ig	ALG12	[64]
• Type II	SLC35A2 (UDP-Gal transporter)	[65]
	SLC39A8 (Manganese transporter)	[66]

Plasma of affected children had undetectable GM3 and downstream a- and b-series derivatives accompanied by elevations of LacCer, globo-side, and paragloboside species. All ST3GAL5 c.694C > T homozygotes had the characteristic phenotype of slow postnatal head growth, intractable epileptic encephalopathy, severe psychomotor delay, visual impairment, and hearing loss; the latter manifesting as a failed newborn hearing screen.

Auditory brainstem responses (ABRs) had abnormal thresholds in all ears tested and cochlear microphonics (CM) were consistently absent (Table 3). One child had no reproducible ABR waves. Wave I was observed in one subject, questionable in another, and absent in remaining patients. In six children, only Waves III and V could be clearly defined. Wave latencies were normal (80 dB) in the majority of patients. In most ears, comparison of condensation and rarefaction responses revealed waveform phase reversals (Fig. 2). Although cortical auditory-evoked potentials (CAEPs) were detectable in all 8 ST3GAL5 c.694C > T homozygotes (Table 3), their morphology was abnormal in 7 (88%) and P2/N2 latency was delayed in 6 (75%).

3.2. Gangliosides and mammalian auditory development

3.2.1. Significant increase of glycosphingolipids during postnatal maturation of murine cochlea

We investigated the expression of GSLs in wild-type murine cochlea during the postnatal period of auditory system maturation. Healthy mice begin to recognize sound by postnatal day 12 (P12), designated the ‘onset of hearing’. As shown in Fig. 1B, GM3 is the dominant cochlear GSL at P1. After P3, there is marked increase of cochlear GM3 as well as other GSLs, including glucosylceramide, complex gangliosides (GM1, GD1a, GD3, GD1b, GT1b), and sulfatides (SM3 and SM4) (Fig. 1B). In contrast, expression of cerebral gangliosides reaches a stable, mature pattern as early as P3 (Fig. 1C).

Significant alterations of ganglioside expression in murine cochlea after P3 reveal the vital role these molecules play in hearing onset [16]. After auditory maturation, GM3 and GM1 are discretely distributed among inner hair (IHC), outer hair (OHC), Dieters, and pillar cells of the organ of Corti (Table 4). Both IHCs and OHCs express GM3, which is preferentially distributed to the apical surface, cuticular plate, and stereocilia. GM1 is the primary IHC ganglioside and predominates on the apical surface of supporting cells, but is largely absent from OHCs (Fig. 3) [16].

3.2.2. Glycocalyx integrity and membrane cycling in GM3 synthase-deficient mice

Apical membranes of stereocilia are covered with a glycocalyx composed of sialic acid-containing glycoproteins and glycolipids (including gangliosides) [24] to create a dense negative charge field that normally prevents fusion of adjacent stereocilia. In experimental animals, aminoglycoside administration reduces expression of sialo-

Table 3
Auditory brainstem responses and CAEPs in children homozygous for ST3GAL5 c.694C > T.

Age (years)	Auditory brainstem responses												CAEPs			
	CM		Morphology		Waves (80 dB)		Thresholds		Latency (80 dB)		Phase reversal		Morphology		Latency	
	Left	Right	Left	Right	Left	Right	Left	Right	Left	Right	Left	Right	Left	Right	Left	Right
1.6	Abs	Abs	–	–	Abs	Abs	–	–	–	–	–	–	Abn	Abn	D	D
2.0	Abs	Abs	Abs	Abs	I, III, V	I, III, V	50	50	N	N	No	Yes	Abn	Abn	D	D
2.8	Abs	Abs	Abs	Abs	III, V	III, V	70	70	D	D	Yes	Yes	Abn	Abn	D	D
3.1	Abs	Abs	Abs	Abs	III, V	III, V	80	80	N	N	No	Yes	Abn	Abn	D	D
3.6	Abs	Abs	Abs	Abs	III, V	III, V	80	80	N	N	Yes	Yes	Abn	Abn	D	D
4.5	Abs	Abs	Abs	Abs	I ^a , III, V	I ^a , III, V	DNT	DNT	N	N	Yes	Yes	Abn	Abn	N	N
7.2	Abs	Abs	Abs	Abs	III, V	III, V	60	50	N	N	No	Yes	N	N	N	N
7.9	Abs	Abs	Abs	Abs	III ^a , V ^a	III ^a , V ^a	80	80	N	D	No	a	Abn	Abn	D	D

Abn, abnormal; Abs, absent; CM, cochlear microphonic; D, delayed; N, normal; DNT, did not test.
^a Equivocal result.

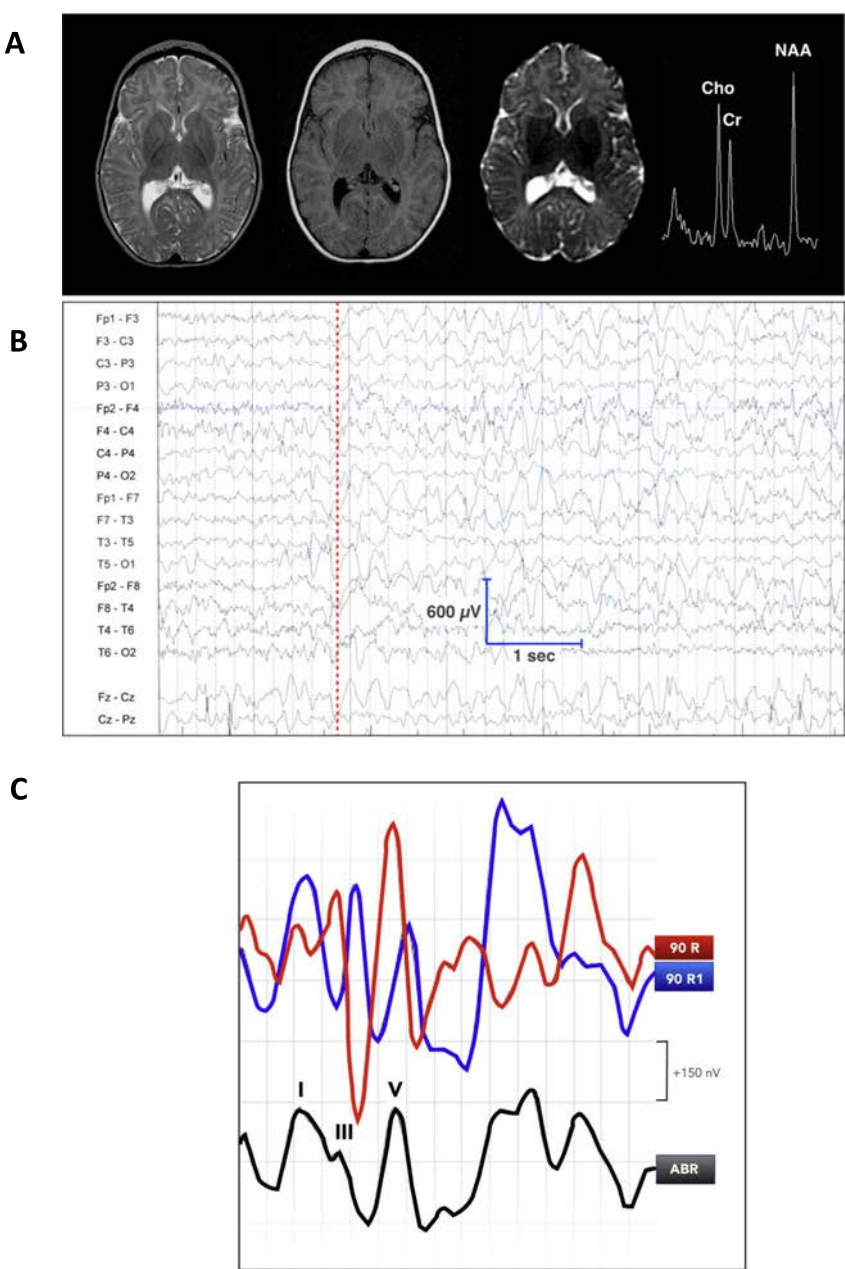


Fig. 2. Neurological and auditory phenotype of ST3GAL5 (GM3 synthase) deficiency in humans. (A) From left to right, T2, fluid-attenuated inversion recovery, diffusion-weighted, and 1H-MR spectroscopy at 1.5 T show normal cortical and subcortical structure, but severe hypomyelination and increased water diffusion throughout the corona radiata, as well as elevated choline (Cho) relative to creatine-phosphocreatine (Cr) and N-acetylaspartate (NAA) 1H signals (single voxel PRESS, TE 144/TR 1500). (B) Electroencephalogram of a 2 year-old child homozygous for ST3GAL5 c.694C > T shows a slow, chaotic background, absent posterior rhythm and no discernable change through a sleep-wake cycle. Beginning at the dashed red line, there is a burst of generalized, frontal predominant, 3 Hz spike-slow wave discharges in excess of 450 μ V. (C) In the majority of affected children, auditory brainstem responses show waveform reversals [16].

Table 4
Comparison of GM3 and GM1 expression of specific regions in the organ of Corti at P14.

	OHC			IHC			DC		PC
	Stereocilia	Cuticular plate	Cell body	Stereocilia	Cuticular plate	Cell body	Cell surface	Cell body	Cell body
GM3	++	+	–	++	+	–	–	+	–
GM1	–	–	–	++	+	+	++	+	+

OHC; outer hair cell, IHC; inner hair cell, DC; Deiters cell, PC; pillar cell.

glycoconjugates in the OHC glycocalyx and precipitates fusion of stereocilia [25,26].
To better define the role of various ganglioside species in hearing, we compared auditory function between *St3gal5* $-/-$ and *B4galnt1* $-/-$ mice, which have distinctive patterns of GSL expression within the organ of Corti (Fig. 4A). Murine *B4galnt1* $-/-$ cochlea has rich GM3 content, intact hair bundles, and normal auditory function whereas *St3gal5* $-/-$ cochlea, devoid of GM3, are associated with deafness (Fig. 4B). Using confocal laser microscopy with phalloidin staining, we observe normal IHC and OHC morphology in 4 week-old *B4galnt1* $-/-$ mice (Fig. 4C and D). In contrast, *St3gal5* $-/-$ OHCs have blebs and intracellular vesicles, the latter composed of membranous structures (Fig. 4E), indicative of unbalanced endocytosis and exocytosis [16]. As noted above, GM3 is expressed in both IHCs and OHCs of wild-type mice, whereas only IHCs express GM1 (Table 4). This may explain in part why OHCs degenerate in advance of IHCs in *St3gal5* $-/-$ mice.

3.2.3. GM3-enriched membrane organization, PTPRQ-myosin VI complex localization and hair cell morphology
Hair cells are specialized to mediate auditory and vestibular transduction. Projecting from their apical surface are filopodial processes called stereocilia, each filled with hundreds of cross-linked actin filaments. Certain proteins—e.g. unconventional myosins, Usher proteins, and some deafness-related gene products (e.g. PTPRQ, cadherin23, protocadherin15, Usherin, and VLGR1)—are expressed predominantly or exclusively in stereocilia to form a structured, interactive network that supports mechanoelectrical transduction (Fig. 5) [27].
In the normal organ of Corti, functional complexes of PTPRQ and myosin VI appear critical to maintaining the integrity of this network [28]. PTPRQ, a shaft connector at the tapered base of stereocilia, is composed of an extracellular domain containing 18 fibronectin III (FNIII) repeats, a membrane spanning domain, and a cytoplasmic domain with both phosphatidylinositol and tyrosine phosphatase activities [29,30]. Myosin VI is an actin-based motor protein that associates

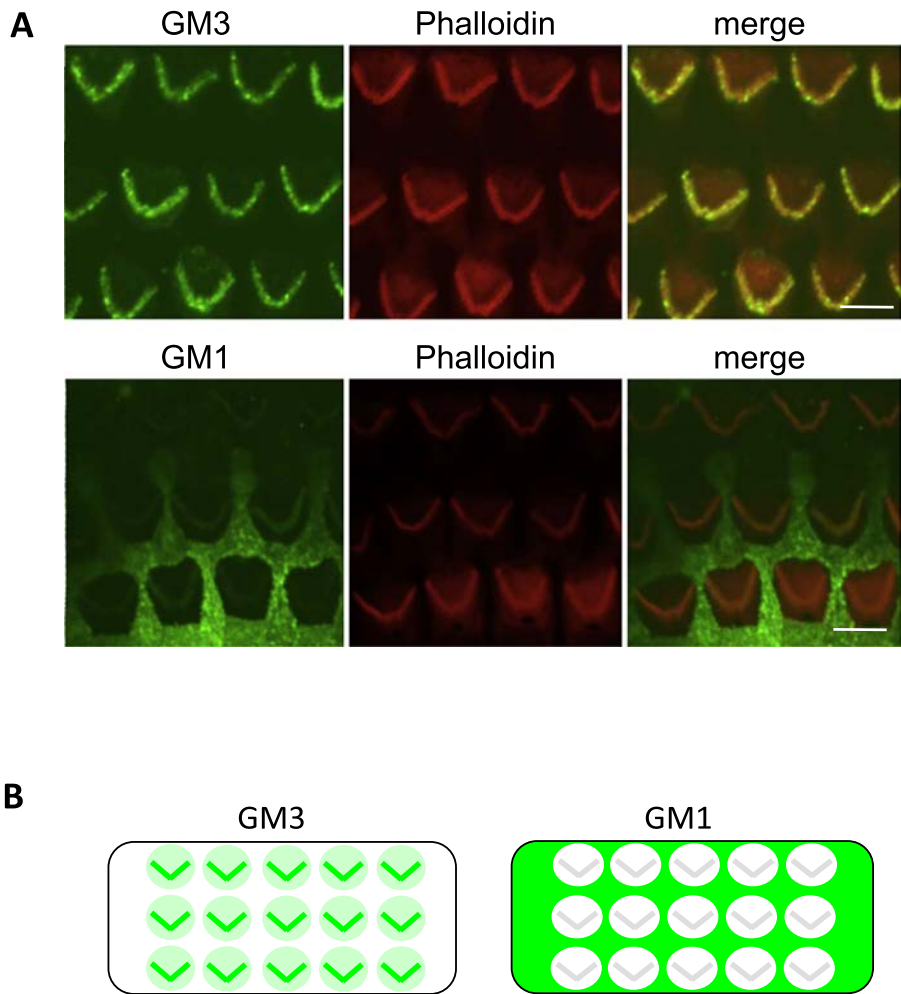


Fig. 3. Comparison of gangliosides expression in hair cells of mice aged 4 weeks. (A) Whole-mount immunostaining was performed. GM3 (upper panel, green) and GM1 (lower panel, green) of OHC stereocilia. Only GM3 was highly enriched in OHC stereocilia without staining of GM1. On the other hand, the expression levels of GM1 but not GM3 was especially high on the surface of supporting cells. (B) Schematic images of distinct expression of GM3 and GM1 in OHC.

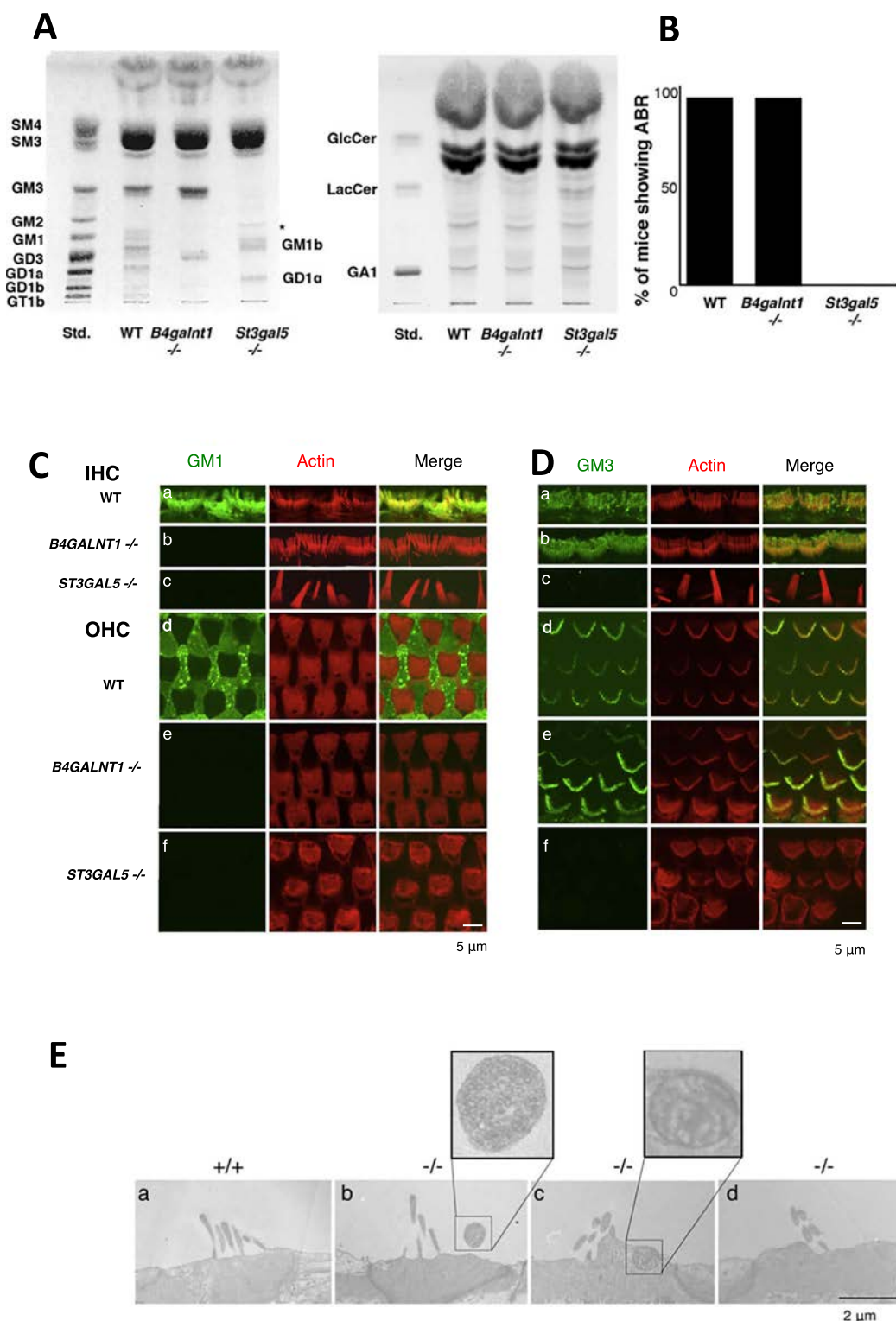


Fig. 4. Identification of GM3 as an essential molecule for hair cell function. (A) HP-TLC of acidic (left) and neutral (right) GSLs from the cochlea of 4-week-old wild-type (WT), *B4galnt1*^{-/-} and *St3gal5*^{-/-} mice. The cochlea of *B4galnt1*^{-/-} mice were mainly expressed GM3 and GD3. Each purified fraction was spotted 2 mg protein per lane. (B) Auditory-evoked brainstem response (ABR) of wild-type, *B4galnt1*^{-/-} and *St3gal5*^{-/-} mice at 4 weeks old. (C and D) Comparison of gangliosides expression in hair cells among wild-type, *B4galnt1*^{-/-} and *St3gal5*^{-/-} mice aged 4 weeks. Whole-mount immunostaining was performed. GM1 (C, green) and GM3 (D, green) of IHC (a–c) and OHC (d–f) stereocilia in wild-type (a and d), *B4galnt1*^{-/-} (b and e) and *St3gal5*^{-/-} (c and f) mice. In IHC, both GM1 and GM3 were expressed along the stereocilium from the taper region to top (Ca and Da). On the other hand, only GM3 was highly enriched in OHC stereocilia (Dd) without staining of GM1 (Cd). The stereocilia of IHC and OHC in *B4galnt1*^{-/-} mice were expressed GM3 but not GM1 (Cb and Db). In *St3gal5*^{-/-} mice, fused stereocilia was observed in IHC (Cc and Dc) and irregular phalloidin staining was observed in OHC (Cf and Df). Notably, the expression levels of GM1 but not GM3 was especially high on the surface of supporting cells (Deiters cell) (Cd and Dd). (E) TEM images of OHC in *St3gal5*^{+/+} and *St3gal5*^{-/-} mice at P17 [16].

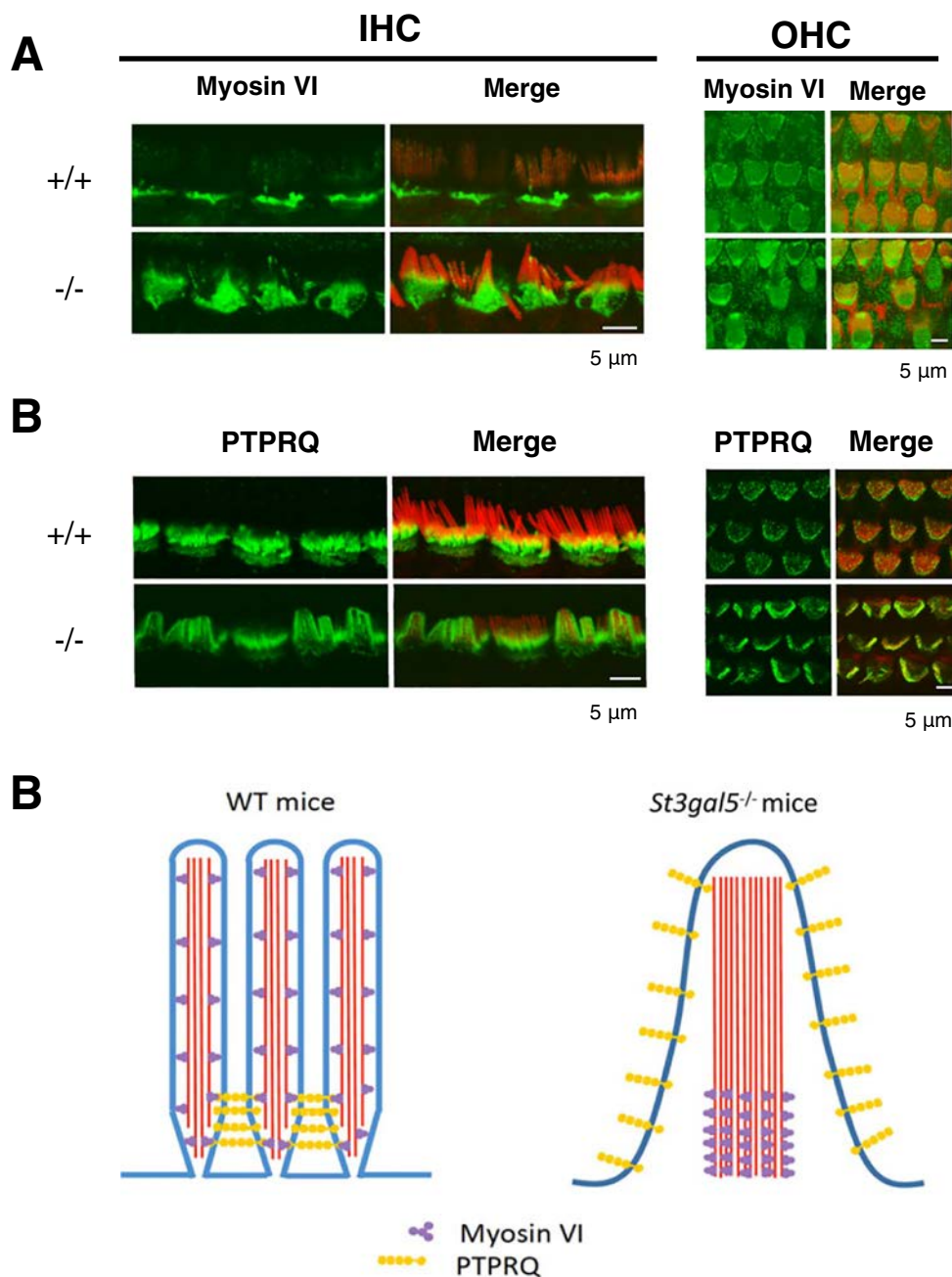


Fig. 5. Dislocalization of PTPRQ and myosin VI in the stereocilia of *St3gal5* null mice. Confocal images showing stereocilia of IHCs and OHCs of *St3gal5* +/+ and -/- mice stained for myosin VI (A) PTPRQ (B) (green) and F-actin (phalloidin, magenta). (C) Schematic images for dislocalization of PTPRQ and myosin VI in the IHC stereocilia of *St3gal5* -/- mouse [16].

with PTPRQ to form a complex mediating interaction between the plasma membrane and cytoskeleton [31]. Mice lacking PTPRQ are deaf and lack tapering at the base of stereocilia, which become fused [28]. Myosin VI-deficient mice are also deaf and have comparable structural changes of hair cells accompanied by maldistribution of PTPRQ along the length of stereocilia [28,32,33].

In bull frogs, PTPRQ colocalizes with ganglioside-rich membrane domains in basal stereocilia [34]. We used immunostaining to further investigate the relationship between gangliosides and the basal PTPRQ-myosin VI complex (Fig. 5). In wild-type murine IHCs, PTPRQ localizes exclusively to the stereocilia base, whereas PTPRQ is maldistributed along shafts of fused *St3gal5* -/- stereocilia (Fig. 5B) and myosin VI is present from base to midshaft but absent from distal regions (Fig. 5A). Such structural disturbances likely reflect loss of normal ciliary motor action. In *St3gal5* -/- OHCs, myosin VI expression is concentrated at the surface of the cuticular plate, close to vestigial kinocilia (Fig. 5A).

Together, these observations suggest that membrane microdomains

enriched with GM3 are crucial to the formation and proper localization of PTPRQ-myosin VI complexes in hair cells. In the absence of GM3, aberrant expression of PTPRQ-myosin VI complexes has important structural consequences for stereocilia and likely impairs their ability to transduce auditory signals (Fig. 5C).

4. Conclusions

Our results implicate a specific and indispensable role for GM3 in the development, function, and viability of cochlear hair cells. Although hearing is already impaired at birth in humans with GM3 synthase deficiency, the murine *St3gal5* -/- auditory phenotype indicates that ganglioside depletion might partially rescue auditory function during a critical postnatal window. These findings inform our understanding of hearing loss in humans with ST3GAL5 deficiency, but do not explain the broader neurological phenotype associated with this condition (Fig. 2). Thus future studies should more carefully delineate the role of lipid

rafts generally, and GM3 specifically, in the development and physiology of the central nervous system.

New concepts and techniques will allow us to determine novel therapies for hearing impairment. In a recent report, functional hair cell-like cells were generated from embryonic and induced pluripotent stem cells [35]. This and other strategies will give rise to new frontiers of hearing research, further advancing studies of glycoconjugate-rich microdomains and their auditory actions. We hope such research will engender new and effective therapies to restore hearing in humans.

Transparency document

The <http://dx.doi.org/10.1016/j.bbagen.2017.05.025> associated with this article can be found, in the online version.

Acknowledgements

This work was supported by research grants for a Grant-in-Aid for Scientific Research (B) (to J.-i.I.) and for Scientific Research on Innovative Areas (no. 23110002, Deciphering sugar chain-based signals regulating integrative neuronal functions) from MEXT, Japan, the Mizutani Research Foundation for Glycoscience (J.-i.I.), The Naito Foundation (J.-i.I.), the ONO Medical Research Foundation (J.-i.I.), the Uehara Memorial Foundation (J.-i.I.), and by Grant-in-Aid for Japan Society for the Promotion of Science Fellows (M.Y.). This work was also supported by MEXT-Supported Program for the Strategic Research Foundation at Private Universities. The Clinic for Special Children is supported by generous charitable contributions from the Amish and Mennonite communities it serves.

References

- [1] S. Go, M. Yoshikawa, J. Inokuchi, Glycoconjugates in the mammalian auditory system, *J. Neurochem.* 116 (2011) 756–763.
- [2] S. Hakomori, Glycosphingolipids in cellular interaction, differentiation, and oncogenesis, *Annu. Rev. Biochem.* 50 (1981) 733–764.
- [3] K. Simons, D. Toomre, Lipid rafts and signal transduction, *Nat. Rev. Mol. Cell Biol.* 1 (2000) 31–39.
- [4] S.I. Hakomori, The glycosynapse, *Proc. Natl. Acad. Sci. U. S. A.* 99 (2002) 225–232.
- [5] R.K. Yu, R.W. Ledeen, Gas-liquid chromatographic assay of lipid-bound sialic acids: measurement of gangliosides in brain of several species, *J. Lipid Res.* 11 (1970) 506–516.
- [6] A. Ishii, M. Ohta, Y. Watanabe, K. Matsuda, K. Ishiyama, K. Sakoe, M. Nakamura, J. Inokuchi, Y. Sanai, M. Saito, Expression cloning and functional characterization of human cDNA for ganglioside GM3 synthase, *J. Biol. Chem.* 273 (1998) 31652–31655.
- [7] M. Kono, S. Takashima, H. Liu, M. Inoue, N. Kojima, Y.C. Lee, T. Hamamoto, S. Tsuji, Molecular cloning and functional expression of a fifth-type alpha 2,3-sialyltransferase (mST3Gal V: GM3 synthase), *Biochem. Biophys. Res. Commun.* 253 (1998) 170–175.
- [8] S. Fukumoto, H. Miyazaki, G. Goto, T. Urano, K. Furukawa, K. Furukawa, Expression cloning of mouse cDNA of CMP-NeuAc: Lactosylceramide alpha2,3-sialyltransferase, an enzyme that initiates the synthesis of gangliosides, *J. Biol. Chem.* 274 (1999) 9271–9276.
- [9] R.L. Proia, Gangliosides help stabilize the brain, *Nat. Genet.* 36 (2004) 1147–1148.
- [10] Y. Handa, N. Ozaki, T. Honda, K. Furukawa, Y. Tomita, M. Inoue, K. Furukawa, M. Okada, Y. Sugiura, GD3 synthase gene knockout mice exhibit thermal hyperalgesia and mechanical allodynia but decreased response to formalin-induced prolonged noxious stimulation, *Pain* 117 (2005) 271–279.
- [11] K. Takamiya, A. Yamamoto, K. Furukawa, S. Yamashiro, M. Shin, M. Okada, S. Fukumoto, M. Haraguchi, N. Takeda, K. Fujimura, M. Sakae, M. Kishikawa, H. Shiku, K. Furukawa, S. Aizawa, Mice with disrupted GM2/GD2 synthase gene lack complex gangliosides but exhibit only subtle defects in their nervous system, *Proc. Natl. Acad. Sci. U. S. A.* 93 (1996) 10662–10667.
- [12] S. Chiavegatto, J. Sun, R.J. Nelson, R.L. Schnaar, A functional role for complex gangliosides: motor deficits in GM2/GD2 synthase knockout mice, *Exp. Neurol.* 166 (2000) 227–234.
- [13] M. Inoue, Y. Fujii, K. Furukawa, M. Okada, K. Okumura, T. Hayakawa, K. Furukawa, Y. Sugiura, Refractory skin injury in complex knock-out mice expressing only the GM3 ganglioside, *J. Biol. Chem.* 277 (2002) 29881–29888.
- [14] T. Yamashita, Y.P. Wu, R. Sandhoff, N. Werth, H. Mizukami, J.M. Ellis, J.L. Dupree, R. Geyer, K. Sandhoff, R.L. Proia, Interruption of ganglioside synthesis produces central nervous system degeneration and altered axon-glia interactions, *Proc. Natl. Acad. Sci. U. S. A.* 102 (2005) 2725–2730.
- [15] M. Yoshikawa, S. Go, K. Takasaki, Y. Kakazu, M. Ohashi, M. Nagafuku, K. Kabayama, J. Sekimoto, S. Suzuki, K. Takaiwa, T. Kimitsuki, N. Matsumoto, S. Komune, D. Kamei, M. Saito, M. Fujiwara, K. Iwasaki, J. Inokuchi, Mice lacking ganglioside GM3 synthase exhibit complete hearing loss due to selective degeneration of the organ of Corti, *Proc. Natl. Acad. Sci. U. S. A.* 106 (2009) 9483–9488.
- [16] M. Yoshikawa, S. Go, S. Suzuki, A. Suzuki, Y. Katori, T. Morlet, S.M. Gottlieb, M. Fujiwara, K. Iwasaki, K.A. Strauss, J. Inokuchi, Ganglioside GM3 is essential for the structural integrity and function of cochlear hair cells, *Hum. Mol. Genet.* 24 (2015) 2796–2807.
- [17] K. Hozawa, H. Wataya, T. Takasaka, B.A. Fenderson, S. Hakomori, Hearing and glycoconjugates: localization of Le(y), Le(x) and sialosyl-Le(x) in guinea pig cochlea, particularly at the tectorial membrane and sensory epithelia of the organ of Corti, *Glycobiology* 3 (1993) 47–55.
- [18] J. Rueda, R. Cantos, D.J. Lim, Distribution of glycoconjugates during cochlea development in mice: light microscopic lectin study, *Anat. Rec. A Discov. Mol. Cell. Evol. Biol.* 274 (2003) 923–933.
- [19] M.A. Simpson, H. Cross, C. Proukakis, D.A. Priestman, D.C. Neville, G. Reinkensmeier, H. Wang, M. Witznitzer, K. Gurtz, A. Verganelaki, A. Pryde, M.A. Patton, R.A. Dwek, T.D. Butters, F.M. Platt, A.H. Crosby, Infantile-onset symptomatic epilepsy syndrome caused by a homozygous loss-of-function mutation of GM3 synthase, *Nat. Genet.* 36 (2004) 1225–1229.
- [20] F. Farukhi, C. Dakkouri, H. Wang, M. Witznitzer, E.I. Traboulsi, Etiology of vision loss in ganglioside GM3 synthase deficiency, *Ophthalmic Genet.* 27 (2006) 89–91.
- [21] L. Boccuto, K. Aoki, H. Flanagan-Steet, C.F. Chen, X. Fan, F. Bartel, M. Petukh, A. Pittman, R. Saul, A. Chaubey, E. Alexov, M. Tiemeyer, R. Steet, C.E. Schwartz, A mutation in a ganglioside biosynthetic enzyme, ST3GAL5, results in salt & pepper syndrome, a neurocutaneous disorder with altered glycolipid and glycoprotein glycosylation, *Hum. Mol. Genet.* 23 (2013) 418–433.
- [22] H. Wang, A. Bright, B. Xin, J.R. Bockoven, A.S. Paller, Cutaneous dyspigmentation in patients with ganglioside GM3 synthase deficiency, *Am. J. Med. Genet. A* 161A (2013) 875–879.
- [23] K. Fragaki, S. Ait-El-Mkadem, A. Chausseuot, G. Gire, R. Mengual, L. Bonesso, M. Bénétou, J.E. Ricci, V. Desquiere-Dumas, V. Procaccio, A. Rötig, V. Paquis-Flucklinger, Refractory epilepsy and mitochondrial dysfunction due to GM3 synthase deficiency, *Eur. J. Hum. Genet.* 21 (2013) 528–534.
- [24] J.H. Luft, Ruthenium red and violet. II. Fine structural localization in animal tissues, *Anat. Rec.* 171 (1971) 369–415.
- [25] J.C. de Groot, E.G. Hendriksen, G.F. Smoorenburg, Reduced expression of sialoglycoconjugates in the outer hair cell glycocalyx after systemic aminoglycoside administration, *Hear. Res.* 205 (2005) 68–82.
- [26] M. Takumida, J. Wersäll, D. Bagger-Sjöbäck, Y. Harada, Observation of the glycocalyx of the organ of Corti: an investigation by electron microscopy in the normal and gentamicin-treated guinea pig, *J. Laryngol. Otol.* 103 (1989) 133–136.
- [27] U. Manor, B. Kachar, Dynamic length regulation of sensory stereocilia, *Semin. Cell Dev. Biol.* 19 (2008) 502–510.
- [28] H. Sakaguchi, J. Tokita, M. Naoz, D. Bowen-Pope, N.S. Gov, B. Kachar, Dynamic compartmentalization of protein tyrosine phosphatase receptor Q at the proximal end of stereocilia: implication of myosin VI-based transport, *Cell Motil. Cytoskeleton* 65 (2008) 528–538.
- [29] M.B. Wright, C. Hugo, R. Seifert, C.M. Distcheck, D.F. Bowen-Pope, Proliferating and migrating mesangial cells responding to injury express a novel receptor protein-tyrosine phosphatase in experimental mesangial proliferative glomerulonephritis, *J. Biol. Chem.* 273 (1998) 23929–23937.
- [30] A. Oganessian, M. Poot, G. Daum, S.A. Coats, M.B. Wright, R.A. Seifert, D.F. Bowen-Pope, Protein tyrosine phosphatase RQ is a phosphatidylinositol phosphatase that can regulate cell survival and proliferation, *Proc. Natl. Acad. Sci. U. S. A.* 100 (2003) 7563–7568.
- [31] R. Nambiar, R.E. McConnell, M.J. Tyska, Myosin motor function: the ins and outs of actin-based membrane protrusions, *Cell. Mol. Life Sci.* 67 (2010) 1239–1254.
- [32] T. Self, T. Sobe, N.G. Copeland, N.A. Jenkins, K.B. Avraham, K.P. Steel, Role of myosin VI in the differentiation of cochlear hair cells, *Dev. Biol.* 214 (1999) 331–341.
- [33] R. Hertzano, E. Shalit, A.K. Rzdzinska, A.A. Dror, L. Song, U. Ron, J.T. Tan, A.S. Shitrit, H. Fuchs, T. Hasson, N. Ben-Tal, H.L. Sweeney, M.H. de Angelis, K.P. Steel, K.B. Avraham, A Myo6 mutation destroys coordination between the myosin heads, revealing new functions of myosin VI in the stereocilia of mammalian inner ear hair cells, *PLoS Genet.* 4 (2008) e1000207.
- [34] H. Zhao, D.E. Williams, J.B. Shin, B. Brügger, P.G. Gillespie, Large membrane domains in hair bundles specify spatially constricted radixin activation, *J. Neurosci.* 32 (2012) 4600–4609.
- [35] K. Oshima, K. Shin, M. Diensthuber, A.W. Peng, A.J. Ricci, S. Heller, Mechanosensitive hair cell-like cells from embryonic and induced pluripotent stem cells, *Cell* 141 (2010) 704–716.
- [36] P.D. Munyer, B.A. Schulte, Developmental expression of proteoglycans in the tectorial and basilar membrane of the gerbil cochlea, *Hear. Res.* 85 (1995) 85–94.
- [37] D.J. Swartz, P.A. Santi, Immunohistochemical localization of keratan sulfate in the chinchilla inner ear, *Hear. Res.* 109 (1997) 92–101.
- [38] P. Gil-Loyzaga, Histochemistry of glycoconjugates of the auditory receptor-functional implications, *Prog. Histochem. Cytochem.* 32 (1997) 1–80.
- [39] H. Yamashita, D. Bagger-Sjöbäck, Expression of glycoconjugates in the human fetal cochlea, *Acta Otolaryngol.* 112 (1992) 628–634.
- [40] V. Tsuprun, P. Santi, Proteoglycan arrays in the cochlear basement membrane, *Hear. Res.* 157 (2001) 65–76.
- [41] H. Satoh, K. Kawasaki, I. Kihara, Y. Nakano, Importance of type IV collagen, laminin, and heparan sulfate proteoglycan in the regulation of labyrinthine fluid in the rat cochlear duct, *Eur. Arch. Otorhinolaryngol.* 255 (1998) 285–288.
- [42] K.M. Khan, N. Sarfaraz, Z. Salim, Lectin binding patterns in nonsensory regions of rat cochlea during postnatal development, *J. Anat.* 194 (1999) 497–504.

- [43] I. M. Simonneau, R. Gallego, R. Pujol, Comparative expression patterns of T-, N-, E-cadherins, beta-catenin, and polysialic acid neural cell adhesion molecule in rat cochlea during development: implications for the nature of Ko⁺ Iliker's organ, *J. Comp. Neurol.* 459 (2003) 113–126.
- [44] D.S. Whitton, X. Zhang, Polysialic acid in the cochlea of the developing mouse, *Int. J. Dev. Neurosci.* 15 (1997) 657–669.
- [45] R. Mollicone, J. Trojan, R. Oriol, Appearance of H and B antigens in primary sensory cells of the rat olfactory apparatus and inner ear, *Brain Res.* 349 (1985) 275–279.
- [46] Y. Katori, C.M. Hackney, D.N. Furness, Immunoreactivity of sensory hair bundles of the guinea-pig cochlea to antibodies against elastin and keratan sulphate, *Cell Tissue Res.* 284 (1996) 473–479.
- [47] M. Hultcrantz, D. Bagger-Sjoberg, Inner ear content of glycosaminoglycans as shown by monoclonal antibodies, *Acta Otolaryngol.* 116 (1996) 25–32.
- [48] K. Torihara, T. Morimitsu, T. Suganuma, Anionic sites on Reissner's membrane, stria vascularis, and spiral prominence, *J. Histochem. Cytochem.* 43 (1995) 299–305.
- [49] S. Maguchi, S. Gasa, J. Matsushima, Y. Saga, M. Kawano, A. Makita, Glycolipids in rat cochlea, *Auris Nasus Larynx* 18 (1991) 1–8.
- [50] P.A. Santi, P. Mancini, C. Barnes, Identification and localization of the GM1 ganglioside in the cochlea using thin-layer chromatography and cholera toxin, *J. Histochem. Cytochem.* 42 (1994) 705–716.
- [51] X. Wu, K.A. Steigelman, E. Bonten, H. Hu, W. He, T. Ren, J. Zuo, A. d'Azzo, Vacuolization and alterations of lysosomal membrane proteins in cochlear marginal cells contribute to hearing loss in neuraminidase 1-deficient mice, *Biochim. Biophys. Acta* 2010 (1802) 259–268.
- [52] R.F. Nelson, K.A. Glenn, Y. Zhang, Selective cochlear degeneration in mice lacking the F-box protein, Fbx2, a glycoprotein-specific ubiquitin ligase subunit, *J. Neurosci.* 27 (2007) 5163–5171.
- [53] M. Hedlund, P. Tangvoranuntakul, H. Takematsu, J.M. Long, G.D. Housley, Y. Kozutsumi, A. Suzuki, A. Wynshaw-Boris, A.F. Ryan, R.L. Gallo, N. Varki, A. Varki, N-Glycolylneuraminic acid deficiency in mice: implications for human biology and evolution, *Mol. Cell. Biol.* 27 (2007) 4340–4346.
- [54] K.K. Ohlemiller, A.K. Hennig, J.M. Lett, A.F. Heidbreder, M.S. Sands, Inner ear pathology in the mucopolysaccharidosis VII mouse, *Hear. Res.* 169 (2002) 69–84.
- [55] O. Akil, J. Chang, H. Hiel, J.H. Kong, E. Yi, E. Glowatzki, L.R. Lustig, Progressive deafness and altered cochlear innervation in knock-out mice lacking prosaposin, *J. Neurosci.* 26 (2006) 13076–13088.
- [56] O. Akil, Y. Sun, S. Vijayakumar, W. Zhang, T. Ku, C.K. Lee, S. Jones, G.A. Grabowski, L.R. Lustig, Spiral ganglion degeneration and hearing loss as a consequence of satellite cell death in saposin B-deficient mice, *J. Neurosci.* 35 (2015) 3263–3275.
- [57] M. Kaga, C. Azuma, T. Imamura, Auditory brainstem response (ABR) in infantile Gaucher's disease, *Neuropediatrics* 13 (1982) 207–210.
- [58] P.A. Schachern, D.A. Shea, M.M. Paparella, Otologic histopathology of Fabry's disease, *Ann. Otol. Rhinol. Laryngol.* 98 (1982) 359–363.
- [59] Y. Komura, K. Kaga, Y. Ogawa, ABR and temporal bone pathology in Hurler's disease, *Int. J. Pediatr. Otorhinolaryngol.* 43 (1998) 179–188.
- [60] C. van Capelle, A. Goedegebure, N.C. Homans, H.L.J. Hoeve, A.J. Reuser, A.T. van der Ploeg, Hearing loss in Pompe disease revisited: results from a study of 24 children, *J. Inher. Metab. Dis.* 33 (2010) 597–602.
- [61] R. Rosenberg, E. Halimi, K. Mention-Mulliez, J.M. Cuisset, M. Holder, S. Defoort-Dhellemmes, Five year follow-up of two sisters with type II sialidosis: systemic and ophthalmic findings including OCT analysis, *J. Pediatr. Ophthalmol. Strabismus* 50 (2013) e33–e36.
- [62] Y. Tanaka, K. Taguchi, T. Arayama, Auditory responses in Tay-Sachs disease, *Pract. Otorhinolaryngol.* 31 (1969) 46–53.
- [63] A.U. Ahmed, S.M. O'Halloran, N.J. Roland, M. Starkey, J.E. Wraith, Hearing loss due to mannosidosis and otitis media with effusion. A case report and review of audiological assessments in children with otitis media with effusion, *J. Laryngol. Otol.* 117 (2003) 307–309.
- [64] C. Kranz, A.A. Basinger, M. Güçsavaş-Calikoğlu, L. Sun, C.M. Powell, F.W. Henderson, A.S. Aylsworth, H.H. Freeze, Expanding spectrum of congenital disorder of glycosylation Ig (CDG-Ig): sibs with a unique skeletal dysplasia, hypogammaglobulinemia, cardiomyopathy, genital malformations, and early lethality, *Am. J. Med. Genet. A* 143 (2007) 1371–1378.
- [65] K. Dörre, M. Olczak, Y. Wada, P. Sosicka, M. Grüneberg, J. Reunert, G. Kurlmann, B. Fiedler, S. Biskup, K. Hörtnagel, S. Rust, T. Marquardt, A new case of UDP-galactose transporter deficiency (SLC35A2-CDG): molecular basis, clinical phenotype, and therapeutic approach, *J. Inher. Metab. Dis.* 38 (2015) 931–940.
- [66] J.H. Park, M. Hogrebe, M. Grüneberg, I. DuChesne, A.L. von der Heiden, J. Reunert, K.P. Schlingmann, K.M. Boycott, C.L. Beaulieu, A.A. Mhanni, A.M. Innes, K. Hörtnagel, S. Biskup, E.M. Gleixner, G. Kurlmann, B. Fiedler, H. Omran, F. Rutsch, Y. Wada, K. Tsiakas, R. Santer, D.W. Nebert, S. Rust, T. Marquardt, SLC39A8 deficiency: a disorder of manganese transport and glycosylation, *Am. J. Hum. Genet.* 97 (2015) 894–903.



Altered expression of ganglioside GM3 molecular species and a potential regulatory role during myoblast differentiation

Received for publication, December 7, 2016, and in revised form, February 27, 2017. Published, Papers in Press, March 8, 2017, DOI 10.1074/jbc.M116.771253

Shinji Go^{‡1}, Shiori Go^{‡§1}, Lucas Veillon[‡], Maria Grazia Ciampa[¶], Laura Mauri[¶], Chihiro Sato[§], Ken Kitajima[§], Alessandro Prinetti[¶], Sandro Sonnino[¶], and Jin-ichi Inokuchi^{‡2}

From the [‡]Division of Glycopathology, Institute of Molecular Biomembrane and Glycobiology, Tohoku Medical and Pharmaceutical University, Sendai 981-8558, Japan, [§]Bioscience and Biotechnology Center, Nagoya University, Nagoya 464-8601, Japan, and [¶]Department of Medical Biotechnology and Translational Medicine, University of Milan, 20090 Segrate Milano, Italy

Edited by Gerald W. Hart

Gangliosides (sialic acid-containing glycosphingolipids) help regulate many important biological processes, including cell proliferation, signal transduction, and differentiation, via formation of functional microdomains in plasma membranes. The structural diversity of gangliosides arises from both the ceramide moiety and glycan portion. Recently, differing molecular species of a given ganglioside are suggested to have distinct biological properties and regulate specific and distinct biological events. Elucidation of the function of each molecular species is important and will provide new insights into ganglioside biology. Gangliosides are also suggested to be involved in skeletal muscle differentiation; however, the differential roles of ganglioside molecular species remain unclear. Here we describe striking changes in quantity and quality of gangliosides (particularly GM3) during differentiation of mouse C2C12 myoblast cells and key roles played by distinct GM3 molecular species at each step of the process.

Glycosphingolipids (GSLs)³ are constituents of eukaryotic cell membranes located exclusively on the outer leaflet of the plasma membrane. Gangliosides, a subgroup of GSLs having one or more sialic acid residues, are involved in regulation of numerous cell biological events, including development, trafficking, signaling, and cellular interactions. Gangliosides have pathophysiological functions in diseases such as cancer, neurodegenerative disorders, and diabetes (1, 2). Sialic acid plays a

key role in the biological activities of gangliosides (3). For example, we demonstrated that localization of insulin receptor in caveolae is disrupted by elevated levels of endogenous GM3 during the state of insulin resistance. This effect is due to electrostatic interaction between the lysine residue of insulin receptor (Lys-944) and the carboxyl group of sialic acid of GM3 (4–8).

The structural diversity of GSLs arises from both the ceramide (Cer) moiety and glycan portion (Fig. 1). Cer is composed of sphingosine and a single acyl chain (Fig. 1B). Cer acyl chains vary in length of carbon backbone, degree of saturation, and the presence/absence of α -hydroxylation (9, 10).

Additional structural diversity of gangliosides arises from sialic acid (acidic sugar molecule with characteristic nine-carbon backbone) in the glycan portion. The most common sialic acid in mammals is *N*-acetylneuraminic acid (Neu5Ac). The other common sialic acid, *N*-glycolylneuraminic acid (Neu5Gc), differs from Neu5Ac by the presence of an additional oxygen atom in the acyl group at position C5 (Fig. 1B). Further structural diversity of sialic acids results from combinations of this variation at position C5 with modifications of hydroxyl groups at positions C4, C7, C8, and C9 by acetate, lactate, sulfate, phosphate esters, or methyl ethers. Sialic acid modifications greatly alter the size, hydrophobicity, net charge, and enzymatic susceptibility of the parent compound (11). Such structural divergence generated by different combinations of Cer and sialic acids in gangliosides (Fig. 1B) results in a huge numbers of “molecular species.” The identity of sialic acid species in GM3 affects its biological properties. GM3 inhibits EGFR-tyrosine kinase to differing degrees depending on its sialic acid species. Such a difference apparently results from differential carbohydrate-carbohydrate interactions between EGFR and GM3 (Neu5Ac) or GM3 (Neu5Gc) (12). We have also demonstrated relationships between various metabolic diseases and levels of serum ganglioside GM3 “acyl chain” molecular species. In particular, levels of GM3 with hydroxylated acyl chain species in human serum show strong correlations with several risk factors for metabolic diseases (13).

Taken together, the above findings indicate that differing molecular species of a given ganglioside have distinct biological properties and regulate specific and distinct biological events. Elucidation of the function of each molecular species is important and will provide new insights into ganglioside biology.

This work was supported by a Grant-in-aid for Scientific Research (B) (to J.-i. I.) and for Scientific Research on Innovative Areas (23110002, Deciphering sugar chain-based signals regulating integrative neuronal functions) from MEXT, Japan and by MEXT-Supported Program for the Strategic Research Foundation at Private Universities. The authors declare that they have no conflicts of interest with the contents of this article.

¹ Both authors contributed equally to this study.

² To whom correspondence should be addressed: Division of Glycopathology, Institute of Molecular Biomembrane and Glycobiology, Tohoku Medical and Pharmaceutical University, 4-4-1, Komatsushima, Sendai 981-8558, Japan. Tel.: 81-22-727-0117; Fax: 81-22-727-0076; E-mail: jin@tohoku-mpu.ac.jp.

³ The abbreviations used are: GSL, glycosphingolipid; Cer, ceramide; CerS, ceramide synthase; Neu5Ac, *N*-acetylneuraminic acid; Neu5Gc, *N*-glycolylneuraminic acid; EGFR, EGF receptor; MyHC, myosin heavy chain; HPTLC, high performance thin layer chromatography; CMAH, CMP-Neu5Ac hydroxylase; Elovl, expression levels of fatty acyl-CoA elongase; DM, differentiation medium; GM3, Sia α 2,3Gal β 1,4Glc-ceramide; GM2, GalNAc β 1,4(Sia α 2,3)Gal β 1,4Glc-ceramide; GM1, Gal β 1,3GalNAc β 1,4(Sia α 2,3)Gal β 1,4Glc-ceramide; GD1a, Sia α 2,3Gal β 1,3GalNAc β 1,4(Sia α 2,3)Gal β 1,4Glc-ceramide.

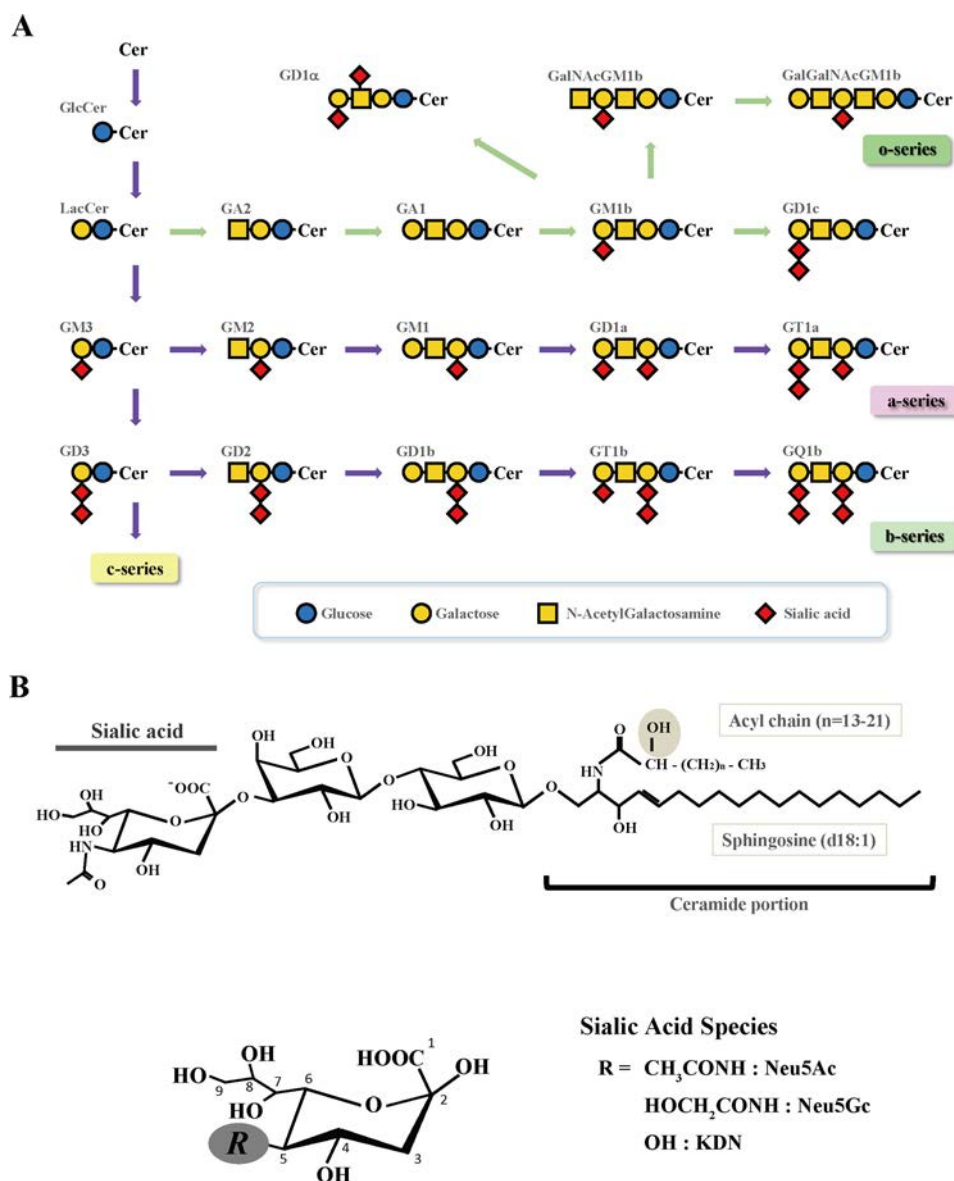


Figure 1. Structural diversity of gangliosides. A, ganglioside biosynthetic pathways. B, structures of ganglioside GM3 and sialic acid molecular species.

Regulation of skeletal muscle formation is an essential process in both normal development and repair of damaged muscle tissue. Differentiation of skeletal muscle cells (myocytes) is a multistep process; the steps include signal transduction, cell adhesion, and cell-cell fusion (14, 15). Gangliosides are known to modulate various plasma membrane functions, *e.g.* cell-cell interactions, signal transduction, and membrane ion channel activity, through formation of functional membrane microdomains termed “rafts.” Gangliosides are presumably involved in these processes in myocytes (16–19); however, direct evidence for such involvement is limited and fragmentary. In the present study we evaluated expression of gangliosides in myoblasts during differentiation. We observed striking changes in ganglioside molecular species composition during differentiation and assessed their differential functions. GM3 (Neu5Gc) and 16:0 acyl chain species, in particular, appear to play essential roles in differentiation of myoblasts to myotubes.

Results

Changes in ganglioside quantity and quality during myogenic differentiation

C2C12 is a myoblast line established from normal adult C3H mouse leg skeletal muscle and is a well established model of *in vitro* differentiation. C2C12 cells were cultured to ~90% confluence in growth medium and then cultured in differentiation medium (DM; see “Experimental procedures”). Upon differentiation stimulus, the cells gradually fused to form multinucleated fibers (myotubes) (Fig. 2A) as expected. Differentiation to myotubes was confirmed by Western blotting. Levels of differentiation marker proteins myogenin and myosin heavy chain (MyHC) increased during differentiation (Fig. 2B). HPTLC revealed the appearance of bands corresponding to GM3, GM2, GM1, and GD1a mobilities during differentiation (Fig. 2C). Amounts of all acidic GSLs increased gradually during differentiation (Fig. 2C). In particular, GM3 content increased strik-

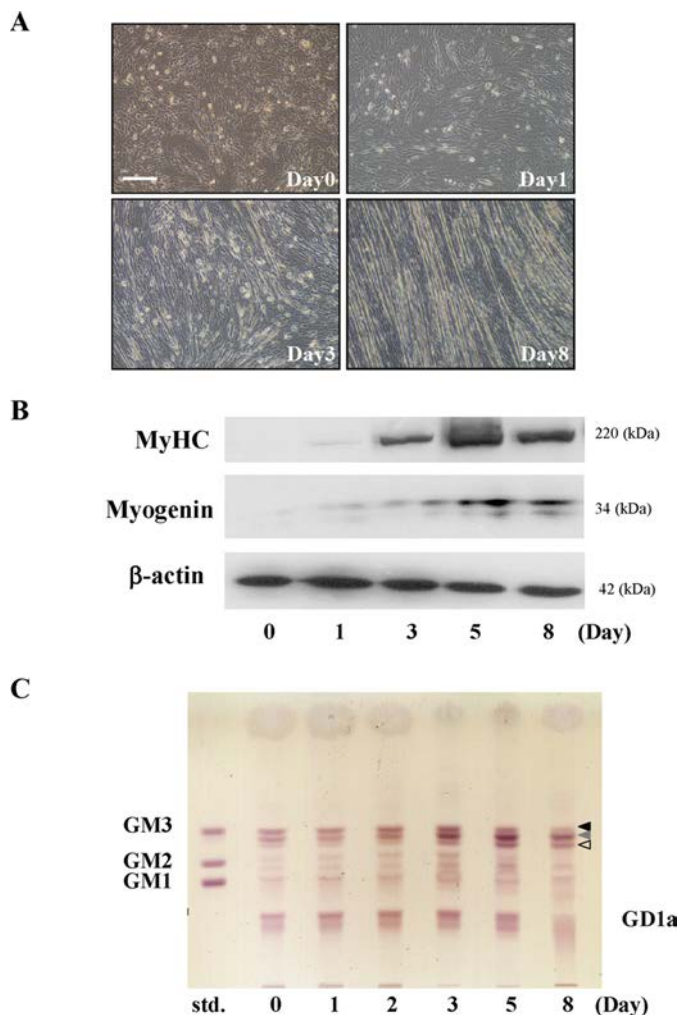


Figure 2. Changes of ganglioside expression during myoblast C2C12 differentiation. Differentiation of C2C12 cells was induced by culture in DM (see "Experimental procedures"). **A**, morphology of proliferating cells (day 0) and myotube formation on days 2–8, as revealed by phase-contrast microscopy. Scale bar, 200 μ m. **B**, expression of differentiation marker proteins myogenin and MyHC on various days, revealed by Western blotting. β -actin: loading control. Shown are representative Western blot images. **C**, GSL fraction was prepared as described under "Experimental procedures." Acidic GSLs extracted from cells (0.2 mg protein basis) were spotted and separated on HPTLC. GSLs were visualized by orcinol/sulfuric acid staining. Pointers indicate GM3 species with differing polarity (see "Changes in ganglioside quantity and quality during myogenic differentiation" under "Results"). Shown is a representative HPTLC image.

ingly, with three major bands. Through day 2, the top band (black pointer) and middle band (gray pointer) were the major GM3 bands. From day 3 onward, the top band decreased, and the middle band and bottom band (white pointer) became the major bands. These findings revealed clear changes in quantity and quality of GM3 molecular species, reflecting their importance in myogenic differentiation.

Changes of sialic acid species in gangliosides during myogenic differentiation

GM3 synthase expression increased during differentiation (Fig. 3A), consistent with the observed increase of GM3 levels (Fig. 2A). To evaluate ganglioside changes during differentiation, we used TLC immunostaining and fluorometric HPLC to assess the quantity and quality of lipid-linked sialic acids.

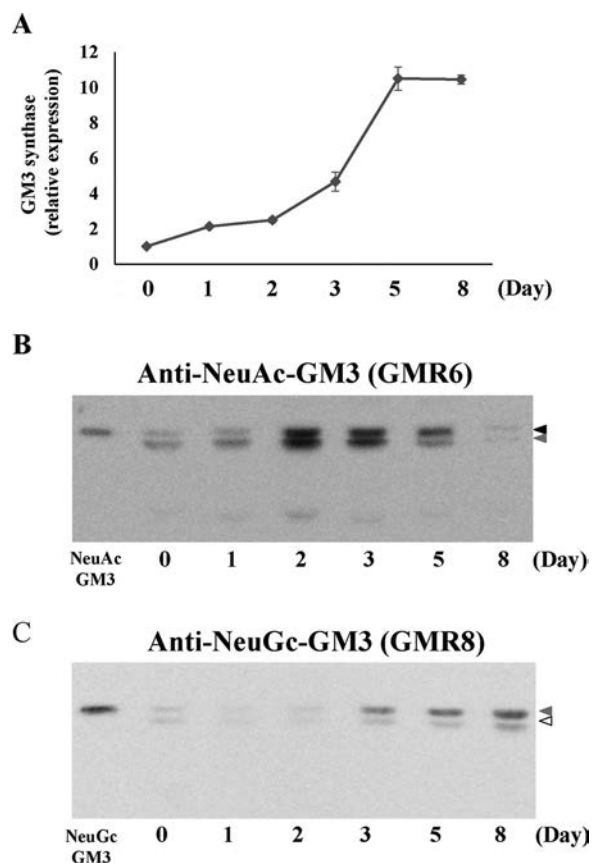


Figure 3. Alteration of sialic acid species of GM3 during C2C12 differentiation. **A**, the GM3 synthase mRNA expression levels on the indicated days, determined by quantitative RT-PCR. Data represent the relative gene expression in cells of each day compared with that in cells of day 0 (set to 1.0 separately for each target gene). Average -fold change was obtained from three experiments, shown as the means \pm S.D. **B**, GM3 (Neu5Ac) expression, detected by TLC immunostaining with specific mAb GMR6. **C**, GM3 (Neu5Gc) expression, detected by TLC immunostaining with specific mAb GMR8. Pointers indicate the position of the GM3 band on HPTLC in Fig. 2.

Changes of sialic acid species of GM3 were confirmed by TLC immunostaining using specific anti-GM3 mAbs. For anti-GM3 (Neu5Ac) mAb GMR6, positive staining was detected at day 0, and its intensity increased until day 3 and decreased thereafter (Fig. 3B). In contrast, for anti-GM3 (Neu5Gc) mAb GMR8 (20), positive bands were very weak until day 2 then increased gradually after day 3 (Fig. 3B). High GM3 (Neu5Gc) expression was maintained even on day 8.

Quantity and quality of lipid-linked sialic acids were next assessed by fluorometric HPLC. In C2C12 myoblasts before differentiation, almost all gangliosides contained Neu5Ac as sialic acid in the glycan portion (Fig. 4A, \blacksquare). After differentiation induction, the total amount of lipid-linked sialic acid increased (Fig. 4A, \blacktriangle), consistent with TLC immunostaining results (Fig. 2C). The amount of lipid-linked Neu5Ac increased gradually through day 3 and declined thereafter. In contrast, lipid-linked Neu5Gc was barely detectable until day 2, increased markedly on day 3, and by day 5 was the major sialic acid species (Fig. 4A, \blacktriangle), again consistent with TLC results (Fig. 3, B and C). Taken together, these findings demonstrate that sialic acid species of gangliosides change from Neu5Ac to Neu5Gc during myogenic differentiation of C2C12 cells.

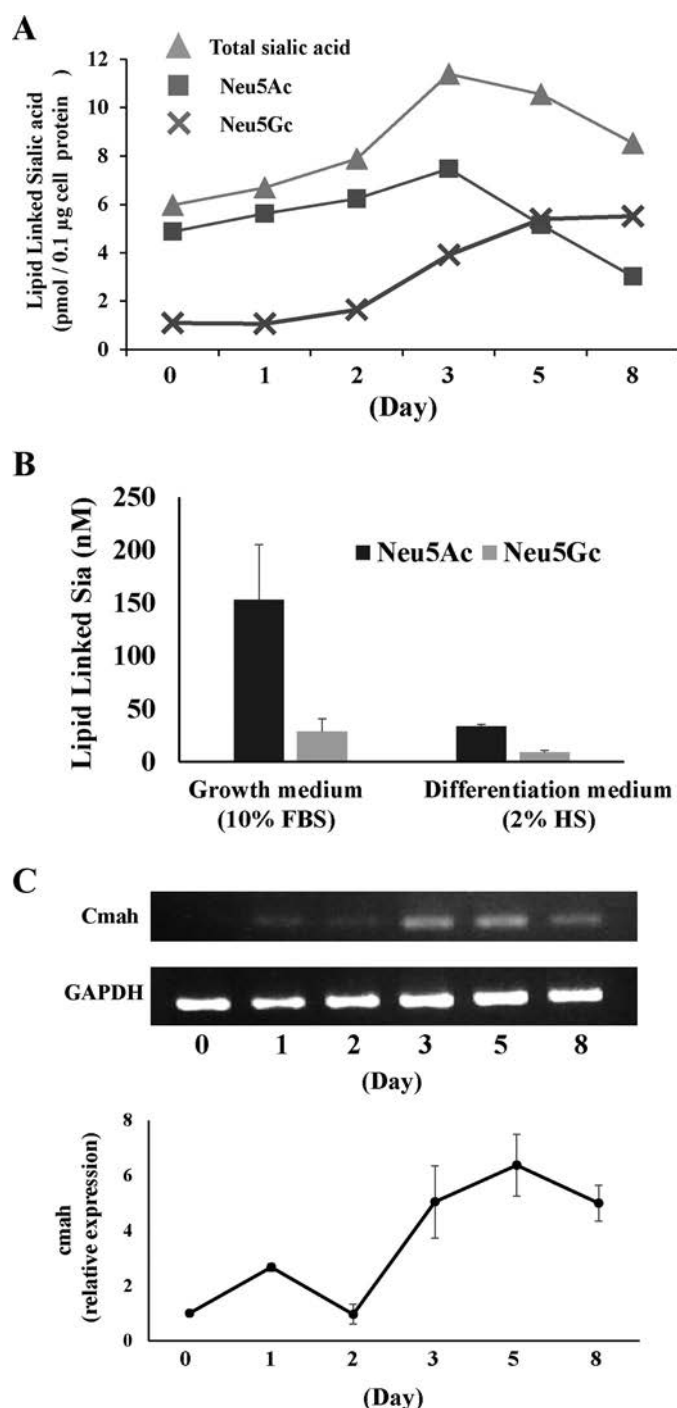


Figure 4. Quantitative and qualitative analysis of lipid-linked sialic acid species during C2C12 differentiation. A, lipid-linked sialic acid species in C2C12 were quantified and qualified by fluorometric HPLC. ▲, total lipid-linked sialic acids; ■, lipid-linked Neu5Ac; ×, lipid-linked Neu5Gc. Detected sialic acids: sum of sialic acids in GM3, GM2, GM1, and GD1a. B, lipid-linked sialic acid species in growth and differentiation medium were quantified by fluorometric HPLC. Shown is growth medium containing 10% FBS (black bar) and differentiation medium containing 2% HS (gray bar). C, expression levels of *Cmah* mRNA, determined by agarose gel electrophoresis and quantitative RT-PCR. Data represent the relative gene expression in cells of each day compared with that in cells of day 0 (set to 1.0 separately for each target gene). Average -fold change obtained from three experiments is shown as the means \pm S.D.

Neu5Gc residues on glycans are synthesized from CMP-Neu5Gc through catalytic activity of sialyltransferases. There are two CMP-Neu5Gc synthesis pathways in mammalian cells. (i) In the salvage pathway, cells take up extracellular Neu5Gc-containing glycoconjugates derived from foods such as meat, fish, and eggs (or from serum in the case of cultured cell lines). Subsequently, Neu5Gc-containing glycoconjugates are hydrolyzed to Neu5Gc monosaccharides in lysosomes. Neu5Gc monosaccharides are transported to cytosol, and Neu5Gc is activated to CMP-Neu5Gc by CMP-sialic acid synthetase in the nucleus (21–23). (ii) In the *de novo* synthesis pathway, sialic acid Neu5Ac is synthesized in cytosol and activated to CMP-Neu5Ac in the nucleus, and CMP-Neu5Ac is subsequently converted to CMP-Neu5Gc by the enzyme CMP-Neu5Ac hydroxylase (CMAH) in cytosol (24, 25). CMP-Neu5Gc is transported into the Golgi apparatus, where it undergoes transfer to glycans through catalytic activity of various sialyltransferases. Reverse-transcription polymerase chain reaction (RT-PCR) analysis of the CMAH encoding gene (*Cmah*) revealed that expression level of *Cmah* mRNA was very low during days 0–2 but increased thereafter (Fig. 4C). Expression of *Cmah* mRNA was correlated with GM3 (Neu5Gc) level during C2C12 differentiation (Figs. 3 and 4).

It is known that fetal bovine and horse serum contain Neu5Gc glycoconjugates. Therefore, we analyzed sialic acid in growth (10% FBS) and differentiation (2% HS) medium and confirmed the existence of Neu5Gc in both mediums. Lipid-linked Sia in the media is shown in Fig. 4B. Growth medium contained large amounts of sialyl glycosphingolipids compare with differentiation medium. Both mediums contained large amounts of Neu5Ac compare with Neu5Gc. Although Neu5Gc glycosphingolipids, especially Neu5Gc-GM3 in medium, may be taken up and utilized by differentiating cells, the amounts would be small. Because the expression levels of both GM3 synthase and *Cmah* increased after the induction of differentiation (Figs. 3A and 4C), we could conclude that the increase of Neu5Gc-GM3 during differentiation may be due to the increased *de novo* synthesis.

Changes of acyl chain structures in the Cer portion of GM3 during myogenic differentiation

Structural diversity of GM3 derived from acyl chain structures in C2C12 cells was evaluated by LC-MS/MS after differentiation induction. On day 0 (Fig. 5A, black bars), the three most abundant GM3 species detected were Neu5Ac-GM3 (d18:1–24:0), Neu5Ac-GM3 (d18:1–24:1), and Neu5Ac-GM3 (d18:1–16:0). Species with acyl chain carbon number 24 accounted for >50% of total GM3 (Fig. 5B, green and blue colors). Species that were abundant on day 0 contained primarily Neu5Ac as sialic acid, consistent with TLC immunostaining and HPLC results (Figs. 3 and 4).

On day 7, when differentiation was completed, Neu5Gc-GM3 (d18:1–16:0) was the most abundant GM3 molecular species, and Neu5Ac-GM3 (d18:1–16:0) was the second most abundant (Fig. 5A). GM3 species with 16:0 acyl chains accounted for ~70% of the total. Proportions of Neu5Ac species were lower, and those of Neu5Gc species were higher on day 7, but total amounts of 24:0 and 24:1 species showed little

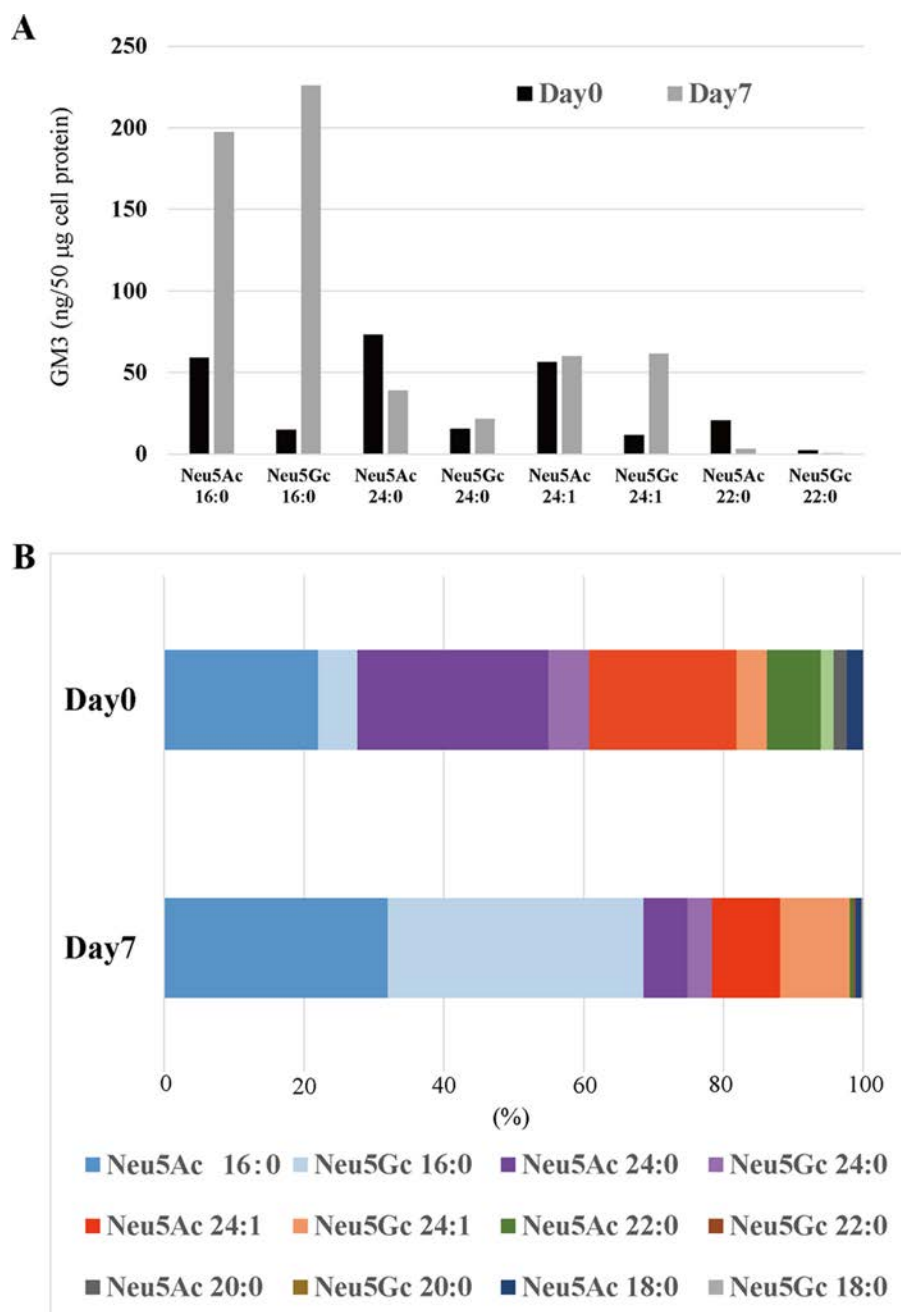


Figure 5. LC-MS/MS analysis of GM3 molecular species during C2C12 differentiation. A, levels of GM3 molecular species in C2C12 cells. The eight most abundant species on day 0 (black bars) and day 7 (gray bars) are shown. The amount of each species was quantified by LC-MS/MS using Neu5Ac GM3 (d18:1-[¹³C]16:0) as the internal standard, as described under "Experimental procedures." y axis, amount of GM3 species (ng) present per 50 µg of cell protein. B, proportions of GM3 molecular species on days 0 and 7. Amounts of individual species were determined, and their proportions were calculated.

change (Fig. 5A). The proportion of 16:0 species increased markedly during differentiation (Fig. 5, A and B).

Expression of Cer synthases

Ceramide synthase (CerS) enzymes regulate synthesis of the various Cer species. Six types of mammalian CerS have been reported. Each CerS has a preference for a unique range of acyl-CoA groups and, therefore, controls a particular subset of Cer species. We used real-time PCR to determine expression levels of CerS1 through CerS6 in C2C12 cells. The predominant forms detected in these cells were CerS1, -2, -5, and -6. CerS2,

which catalyzes synthesis of ceramide with very long acyl chains such as C24, was most abundant in C2C12. CerS2 was slightly increased after the induction of differentiation, but it was decreased sharply during the differentiation process. On the other hand the levels of CerS5 and -6, which catalyze C16-Cer synthesis, remained constant (Fig. 6A). Therefore, the increase of GM3 C16 species after differentiation (Fig. 5) could be attributed to the marked decrease of CerS2 expression during the differentiation process (Fig. 6A).

We also examined changes in mRNA expression levels of fatty acyl-CoA elongases (Elovl5) during differentiation. Levels

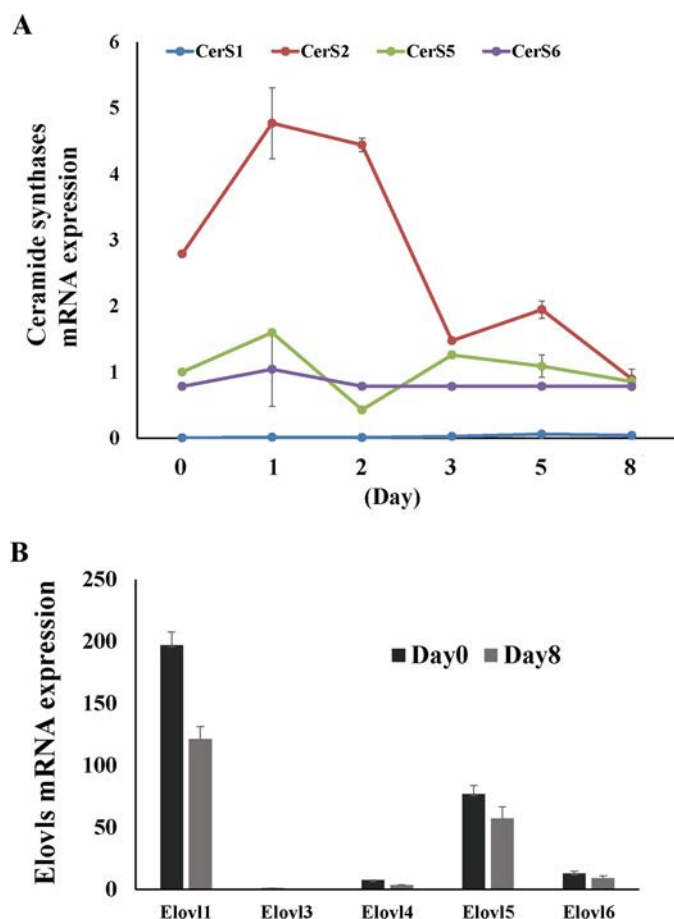


Figure 6. Changes in expression of Cer synthase mRNAs during C2C12 differentiation. A, expression levels of CerS mRNAs, determined by quantitative RT-PCR. -Fold change was calculated as $2^{-\Delta\Delta\pm CT}$ with tubulin used as the endogenous control. B, expression levels of Elovl mRNAs during differentiation, determined by quantitative RT-PCR. Data represent the relative gene expression in cells of each day compared with that in cells of day 0 (set to 1.0 separately for each target gene). Average -fold change obtained from three experiments is shown the means \pm S.D.

of all five Elovls examined were lower on day 8 than on day 0 (Fig. 6B). This trend may also explain in part the increase of shorter acyl-chain Cer species.

Effects of exogenous sialic acid and GM3 species on cell morphology

Sialic acid and acyl chain structures of GM3 showed notable changes during C2C12 cell differentiation. The potential role of such changes was investigated by adding various sialic acid and GM3 molecular species to culture medium.

Sialic acid monosaccharide (Neu5Ac or Neu5Gc) was added during medium change each day to change the sialic acid species of sialylglycoconjugates. Treatment with 2 mM Neu5Ac or Neu5Gc efficiently increased intracellular Sia monosaccharide (Fig. 7A, left panel), so exogenous sialic acids were taken up by C2C12 cells. After 2 days the amount of lipid-linked Neu5Gc exceeded that of Neu5Ac in cells treated with 2 mM Neu5Gc, although Neu5Ac was the major sialic acid in normal and Neu5Ac-treated cells (Fig. 7A, right panel). Thus, we were able to change the ratio of sialic acid species in gangliosides by treatment with Neu5Gc. Cell morphology on day 6 is shown in Fig. 7, B and C.

Sialic acid species differentially affected morphology of myoblasts and/or myofibers. The ratio of long fibers was increased by treatment with Neu5Gc (Fig. 7C, right panel). And the formed fiber width was small (Fig. 7C, left panel). Therefore, cells treated with Neu5Gc monosaccharide formed longer, narrower myofibers. Neu5Ac or Neu5Gc treatment had no effect on the expression of differentiation marker proteins myogenin and MyHC (Fig. 7D, left panel). However, phosphorylation of paxillin, which regulates adhesion state, was increased by treatment with Neu5Gc (Fig. 7D, right panel). These findings suggest that sialic acid affects cell morphology via control of cytoskeleton formation or myofiber adhesion state.

Although Neu5Ac was taken up by cells during Neu5Ac treatment, the quality and quantity of glycosphingolipids was not drastically changed (Fig. 7A). The ratio of shorter length myotubes was slightly increased by Neu5Ac treatment. These changes may not be an effect of only change in GLSs, although these results suggest that extracellular sialic acid affected myoblast differentiation.

Exogenous gangliosides can be inserted into the outer leaflet of plasma membranes and be partially taken up and metabolized (26). We confirmed the uptake and increase of GM3 in cells by TLC and fluorometric HPLC (Fig. 8A). 25 μ M exogenous GM3 efficiently increased cellular gangliosides (Fig. 8A, left panel) and lipid linked sialic acids (Fig. 8A, right panel). Therefore, we added GM3 species, shorter (16:0) species, which are the major species after differentiation, and longer (24:0 or 18:0) species, which are the major species before differentiation to evaluate their properties. In experiments with different GM3 molecular species, d18:1–16:0 species were well aligned and formed numerous myotubes, whereas cells treated with GM3 d18:1–18:0 or d18:1–24:0 species were poorly aligned and formed fewer myotubes (Fig. 8B); the ratio of cells with shorter length and larger width was increased when treated with GM3 d18:1–18:0 or d18:1–24:0 species (Fig. 8C). Although expression level of myogenin was relatively unaffected by treatment with different GM3 molecular species, the level of MyHC was notably reduced by treatment with GM3 d18:1–18:0 or d18:1–24:0 species (Fig. 8D). Cells treated with GM3 d18:1–16:0 formed relatively longer myofibers.

These findings indicate that increased longer acyl-chain GM3 species inhibit some signaling in differentiation processes such as fusion process and/or formation of myotubes, whereas shorter acyl-chain GM3 species do not inhibit, or might, enhance.

In this study we found an association of GM3 lipid species change and differentiation in myoblast. The results shown in Fig. 7 and in Fig. 8 are consistent with the hypothesis that myoblasts may regulate their differentiation by changing GLSs species.

Discussion

Skeletal muscle differentiation comprises a chain of complex processes in which cell plasma membranes play a crucial role. Cell-to-cell adhesion and recognition are essential for the differentiation process. It is necessary for progenitor cells to contact numerous similar cells and respond to inductive signals in order to undergo a coordinated process of differentiation. In

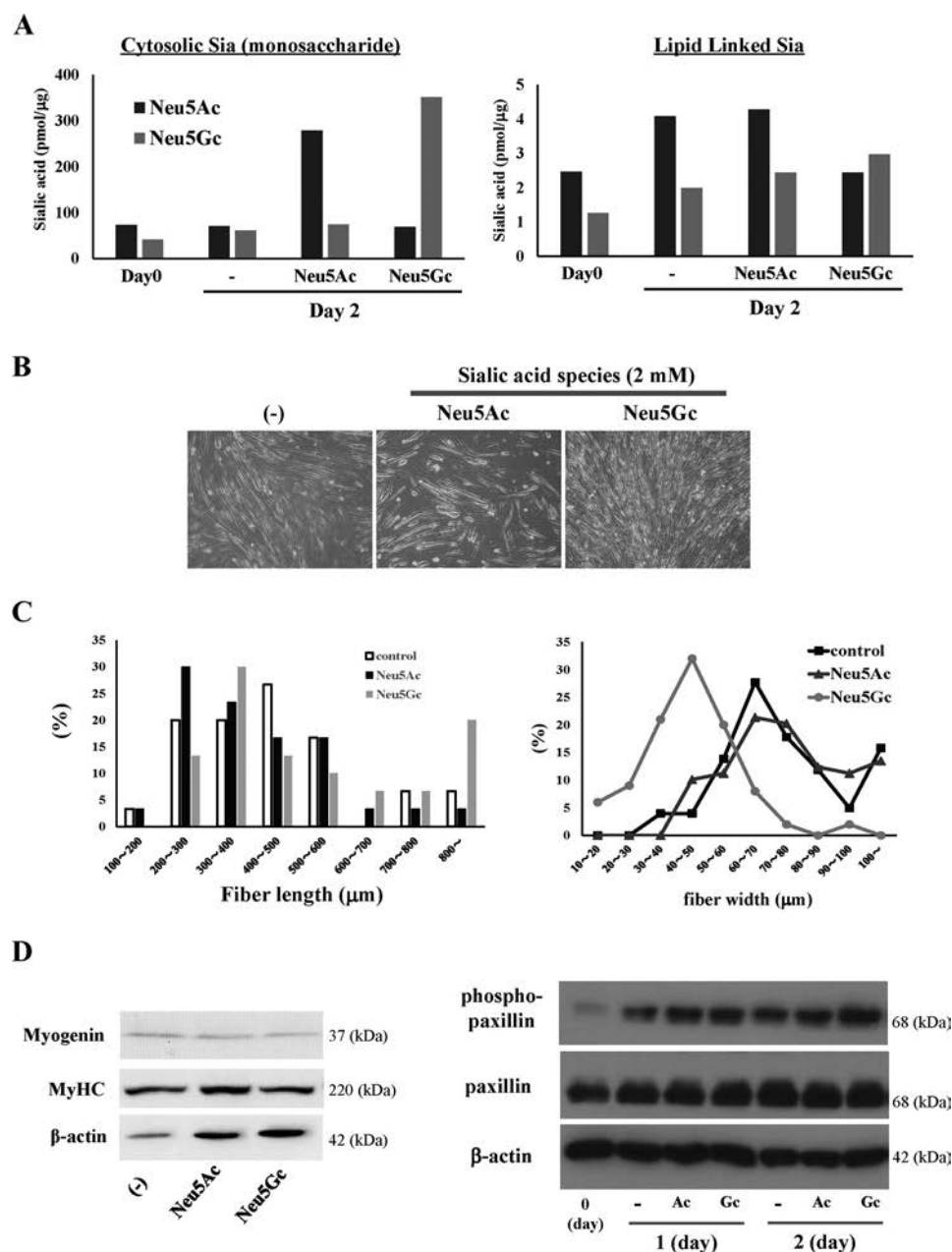


Figure 7. Effects of sialic acid monosaccharide supplementation on C2C12 differentiation. A, uptake and utilization of exogenous sialic acids in C2C12 cells. 2 mM Neu5Ac or Neu5Gc was added to the differentiation medium. After 2 days Sia monosaccharide in cytosol (left panel) and lipid-bound Sia (right panel) were measured as described under "Experimental procedures." B, phase-contrast microphotographs on day 6 of cells treated with sialic acid (2 mM) in DM. C, effects of exogenous sialic acids on morphology of myofibers. The ratio of each fiber length (right panel) and width (left panel) are shown (control and Neu5Gc; $n = 100$, Neu5Ac; $n = 89$). D, expression levels, on day 6 of differentiation, of marker proteins myogenin and MyHC in cells treated with sialic acid in DM (right panel). Shown are the effects of sialic acids on the phosphorylation state of paxillin on days 1 and 2 (left panel). Shown are representative Western blot images.

the final steps of differentiation, plasma membranes fuse with each other (14, 15, 27). Biochemical characteristics of plasma membranes thus have important effects on skeletal muscle differentiation. GSLs, particularly gangliosides, help determine plasma membrane properties and play essential roles in regulating many biological processes, including cell-cell interactions and signal transduction (1, 2). Expression of GM3, GM2, GM1, and GD1a has been reported in myoblast cell line C2C12 (16–18); however, changes in ganglioside expression and functions of specific ganglioside species during myogenic differentiation have not been studied. We analyzed changes in gangli-

oside species during myogenic differentiation using C2C12 cells as a model. We demonstrated for the first time striking changes in quantity and quality of gangliosides during the differentiation process. Alterations of molecular species of GM3, the major ganglioside in C2C12 cells, were particularly notable. Sialic acid species in GM3 were changed from Neu5Ac to Neu5Gc through elevated expression of hydroxylase CMAH. GM3 species with 16:0 acyl chains were greatly increased. To elucidate the function of this GM3 molecular species change, we added sialic acid monosaccharide or synthetic GM3 acyl chain species to culture medium. Our findings (Figs. 6 and 7)

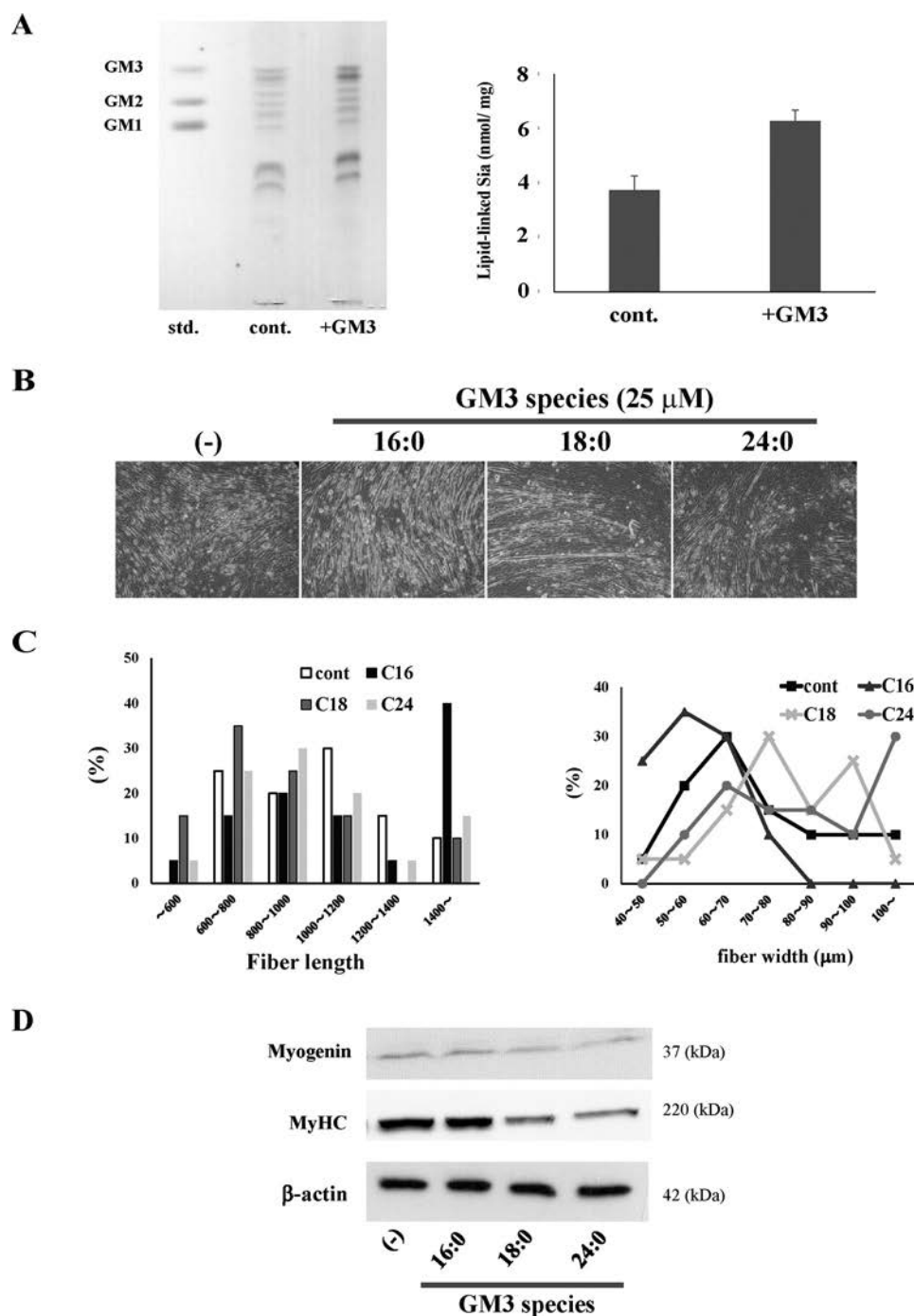


Figure 8. Effects of GM3 acyl chain structure on C2C12 differentiation. A, uptake of exogenous GM3. Shown is TLC analysis (right panel), and the amounts of lipid-linked sialic acids (left panel) of C2C12 cells treated with 25 μ M GM3 for 24 h. B, phase-contrast microphotographs on day 6 of cells treated with three GM3 species (25 μ M). C, effects of exogenous sialic acids on morphology of myofibers. The ratio of each fiber length (right panel) and width (left panel) are shown ($n = 20$). D, expression levels on day 6 of differentiation marker proteins myogenin and MyHC in cells treated with three GM3 species. Shown are representative Western blot images.

indicate that sialic acid species affect cell morphology and that GM3 acyl chain structures play key roles in regulating differentiation.

In regard to GM3 function in myogenic differentiation, previous studies indicate that sialidase (Neu3), which is localized in the plasma membrane and hydrolyzes GM3 and other gangliosides, affects differentiation of C2C12 cells. Neu3 overexpression delayed myoblast differentiation and induced hypertrophic myotube formation, whereas differentiation was

inhibited by Neu3 gene silencing (16–18). The Neu3 protein *per se* presumably modulates certain cell functions, but these studies suggest that GM3 in appropriate amounts also plays an important role in normal C2C12 differentiation, most likely via modulation of EGFR signaling. We used a GSL synthesis inhibitor to confirm that GSLs in appropriate amounts are important in myofiber formation (data not shown). Thus, proper amounts of GM3 are required at each step in the process for normal myogenic differentiation. We observed here for the first time

striking changes in GM3 quality during differentiation; *i.e.* major alterations in sialic acid species and acyl chain structures (Figs. 2–4). Our findings suggest that ganglioside quality as well as quantity is important at each step for normal myogenic differentiation.

Sialic acid species and the acyl chain structures of gangliosides are involved in maintaining cell membrane properties and lipid microdomain structures. Hashimoto and co-workers (28, 29) observed that disruption of lipid rafts by cholesterol depletion directly blocked the plasma membrane fusion that normally occurs as part of myogenic cell fusion. The molecular mechanisms that control cell fusion and other steps of myogenic differentiation remain to be elucidated; however, plasma membrane rafts clearly play an important role. A number of membrane molecules have been implicated in regulation of myogenic differentiation. Extracellular matrix receptor integrins (30) and adhesion molecules such as cadherins, NCAM, and CD9 (31–33) are involved in regulation of the recognition and adhesion steps in myoblast differentiation and maintenance of myofibers. Crucial molecules (*e.g.* BAI1, myomaker) involved in regulation of initiation signals for myogenic differentiation and plasma membrane fusion were discovered in 2013 (34, 35). Such transmembrane proteins are localized in specific regions of the plasma membrane during differentiation; it is thus possible that various GM3 molecular species interact specifically with the proteins, directly or indirectly, to regulate their functions and localization. Membrane fluidity affects myogenic differentiation, particularly the plasma membrane fusion process (36–38); thus, another possibility is that concentrations of various GSL molecular species in myoblasts help regulate membrane fluidity and are strictly controlled for this purpose.

Our knowledge of molecular mechanisms that regulate distribution and expression of GSL molecular species and other plasma membrane molecules remains fragmentary. The CerS enzymes provide one regulatory mechanism for expression of GSL acyl chain molecular species. Six mammalian CerSs have been described, each utilizing fatty acyl CoAs with differing chain lengths for *N*-acylation of the sphingoid long chain base. CerS5 and CerS6 catalyze synthesis of C16 acyl chain Cer species (9, 10). Most studies to date focused on roles of CerSs in regulation of sphingolipids have relied on CerS overexpression to increase Cer synthesis. Therefore, it remains unclear how individual CerSs contribute to a steady-state sphingolipid pool in mammalian cells, and whether maintenance of sphingolipids with specific acyl chains depends on specific CerSs (39). C16 GSL species were strikingly increased during C2C12 differentiation in the present study (Fig. 5). The increase of GM3 C16 species after differentiation could be attributed to the marked decrease of CerS2 expression during the process of differentiation (Fig. 6A). We also observed that expression levels of Elovl5 declined during myogenic differentiation, which may help account for increased levels of shorter acyl-chain species (Fig. 6B). Future studies may reveal unknown mechanisms for regulation of GSL molecular species by inter-regulation of CerSs and Elovl5.

By treatment with exogenous GM3 species, cellular gangliosides were changed (Fig. 8). We found that increased longer

acyl-chain GM3 species inhibited differentiation, whereas shorter acyl-chain GM3 did not result in inhibition (Fig. 8, B and C). These results suggest that myoblasts regulate some signaling processes during differentiation, such as fusion processes and/or formation of myotubes, by changing the metabolism of ganglioside acyl chain species.

Besides changes in acyl chains of GM3 molecular species, the present study demonstrates for the first time changes of sialic acid species from Neu5Ac to Neu5Gc during differentiation. We also observed morphological changes in myotubes after treatment with Neu5Gc (Fig. 7, B and C). This phenomenon suggests a function for Neu5Gc glycoconjugates in the process of myogenic differentiation, especially in the regulation of cell morphology. Although during the exogenous treatment we employed, the ratio of Neu5Gc was increased in both glycoproteins and glycolipids (data not shown); therefore, we cannot conclude the effects observed were the result of Neu5Gc GM3 alone. Several groups have described changes of sialic acid species on glycans during various biological processes (40–43). It appears that Neu5Gc expression can also be affected by cell activation and disease status. *Cmah* mRNA expression is altered during lymphocyte activation in mice (41, 42), and Neu5Gc treatment modifies interactions between glycans and their binding proteins. Taken together, these past and present findings indicate that the change of sialic acid species from Neu5Ac to Neu5Gc is crucial for myogenic differentiation in mice. Deletion of *Cmah* in mice increased the severity of muscular dystrophy (44, 45), suggesting that this gene is a genetic modifier of muscle homeostasis. Taken together, our results suggest that myoblasts regulate their differentiation by changing the metabolism of sialic acids, ceramide, and, consequently, gangliosides.

We want to elucidate the function of specific GM3 molecular species, which have their expression levels affected before and after myogenic differentiation, especially focusing on NeuGc GM3 with a C16 acyl chain as shown in Fig. 5A. We confirmed the change in expression of some genes related to the synthesis of this molecule. Therefore, we tried to modify the expression of these genes (such as GM3 synthase, *Cmah*, and CerSs) to show their function in myogenic differentiation. However, we could not establish gene-modified C2C12 cells while maintaining differentiation potency. Therefore, we will report further on these investigations in our next manuscript.

In conclusion, the present results demonstrate that quantity and quality of GM3 change greatly during myoblast C2C12 differentiation and suggest that these changes play a key role in regulation of the differentiation process. These findings help clarify the significance of GSL structural diversity in mammalian cells. Our ongoing studies, using genetically modified mice and cells, are focused on roles of GM3 molecular species in function and regeneration of muscle cells and tissues.

Experimental procedures

Materials

Hybridoma cells producing anti-GM3 (Neu5Gc) monoclonal antibody (mAb) GMR8 were kindly donated by Ikuo Kawashima (20), RIKEN BioResource Center. Anti-GM3 (Neu5Ac) mAb

GMR6 was from Seikagaku Co. (Tokyo, Japan). Anti-myogenin and myosin heavy chain antibodies were from e-Bioscience (Santa Clara, CA). GM3 molecular species were synthesized according to previous reports (46, 47). Neu5Ac GM3 (d18:1-[¹³C]16:0), an internal standard for quantification by LC-MS/MS, was from Tokyo Chemical Industry (Tokyo, Japan).

Cell culture

C2C12 myoblast cells were obtained from RIKEN Bio-Resource Center (Tsukuba, Japan) and cultured in Dulbecco's modified Eagle's medium (DMEM; Nacalai; Kyoto, Japan) containing 10% heat-inactivated fetal bovine serum at 37 °C in 5% CO₂ atmosphere. To induce differentiation, growth medium was replaced with DMEM containing 2% horse serum (DM) when cells reached ~90% confluency. Cells were replenished with fresh DM every 24 h. To evaluate the effects of exogenous sialic acids, Neu5Ac or Neu5Gc (2 mM) were added to DM. To evaluate the effects of exogenous GM3, synthetic GM3 acyl chain species (25 μM) were added to DM.

Analysis of GSLs

Analysis of GSLs by TLC was performed as described originally in Refs. 48 and 49 and slightly modified (50). In brief, total cell lipids were extracted using chloroform/methanol, and extracts were applied to DEAE-Sephadex A-25 column equilibrated with chloroform/methanol/water (30:60:8, v/v/v). The column was washed with the same solvent, and acidic GSL fraction was eluted with chloroform/methanol/1 M sodium acetate (30:60:8, v/v/v). Acidic and neutral lipids were subjected to mild alkaline hydrolysis and desalted using a Sep-Pak C18 cartridge. Acidic GSLs were spotted on a TLC plate and developed with chloroform/methanol/0.2% CaCl₂ (60:25:4, v/v/v). GSLs were visualized by orcinol/sulfuric acid staining.

TLC immunostaining

Acidic GSLs were spotted on a TLC plate and developed with chloroform/methanol/0.2% CaCl₂ (60:25:4, v/v/v). The dried plate was dipped in cyclohexane containing 0.1% (w/v) poly(isobutyl methacrylate) for 1 min, blocked by incubation in PBS containing 1% BSA at room temperature for 1 h, incubated with anti-GM3 mAb GMR6 (GM3(Neu5Ac) specific) or GMR8 (GM3(Neu5Gc) specific) in PBS containing 1% BSA at room temperature for 2 h, washed 5 times with PBS, and incubated with anti-mouse IgM horseradish peroxidase (HRP)-conjugated antibody at 37 °C for 1 h. HRP was detected by the addition of appropriate substrates following the manufacturer's instructions.

Sialic acid analysis by fluorometric HPLC

Sialic acids were hydrolyzed from acidic GSL fractions by trifluoroacetic acid. An aliquot of the supernatant was lyophilized and then incubated with 1,2-diamino-4,5-methylene dioxymethylene as described previously (51). 1,2-Diamino-4,5-methylene dioxymethylene-labeled sialic acids were separated and detected using an HPLC system (JASCO; Tokyo, Japan) equipped with a reversed-phase C18 column (Wakopak Handy-ODS (4.6 mm × 250 mm); Wako Pure Chemical, Osaka, Japan).

Table 1

Primers used to specifically enhance each mRNA fragment

Gene		Primer sequence
<i>CerS1</i>	Forward	5'-TGACTGGTCAGATGCGTGA-3'
	Reverse	5'-TCAGTGGCTTCTCGGCTTT-3'
<i>CerS2</i>	Forward	5'-TCATCATCACTCGGCTGGT-3'
	Reverse	5'-AGCCAA AGAAGGCAGGGTA-3'
<i>CerS3</i>	Forward	5'-ATCTCGAGCCCTTCTTCTCC-3'
	Reverse	5'-CTGGACGTTCTGCGTGAAT-3'
<i>CerS4</i>	Forward	5'-TGCGCATGCTCTACAGTTTC-3'
	Reverse	5'-CTCGAGCCATCCCATCTT-3'
<i>CerS5</i>	Forward	5'-TCCATGCCATCTGGTCTTA-3'
	Reverse	5'-TGCTGCCAGAGAGGTTGTT-3'
<i>CerS6</i>	Forward	5'-GGGTTGAAGTCTTCTGGTC-3'
	Reverse	5'-TTTCTTCCCTGGAGGCTCT-3'
<i>Cmah</i>	Forward	5'-GAAAGGCCTGTGTTTGGAA-3'
	Reverse	5'-TCATGAACCGCAGACTTTTG-3'
<i>St3gal5</i> (GM3 S)	Forward	5'-GTGGACCCCTGACCGATAAAG-3'
	Reverse	5'-AACAGAGCCATAGCCGTCTTC-3'
<i>Tubulin</i>	Forward	5'-CACTACACCATTTGGCAAGGA-3'
	Reverse	5'-TGTGGAAAACCAAGAGCC-3'
<i>Elovl 1</i>	Forward	5'-GGTGGGGGATAAAAATTGCT-3'
	Reverse	5'-CCAAGGCAGACAATCCATA-3'
<i>Elovl 2</i>	Forward	5'-GACGCTGGTCATCCTGTTCT-3'
	Reverse	5'-GCTTTGGGAAACCATTTCT-3'
<i>Elovl 3</i>	Forward	5'-TTTGCCATCTACACGGATGA-3'
	Reverse	5'-CGTGCTCCAGTTCAACAA-3'
<i>Elovl 4</i>	Forward	5'-TTTGGTGAAGCGATACCTG-3'
	Reverse	5'-ATGTCCGAGTGTAGAAGTTG-3'
<i>Elovl 5</i>	Forward	5'-CTCTCGGGTGGCTGTTCT-3'
	Reverse	5'-AGAGGCCCTTTCTGTTGT-3'
<i>Elovl 6</i>	Forward	5'-ACAATGGACCTGTGAGCAAA-3'
	Reverse	5'-GTACAGTGCAGGAAGATCAGT-3'
<i>Elovl 7</i>	Forward	5'-ATGGGACCAGCCTACCAGAA-3'
	Reverse	5'-TTGCAGTCTCCATGAAGAA-3'

RT-PCR

Total RNAs were prepared from cells using TRIzol reagent. Reverse transcription of total RNA was performed to generate first-strand cDNA. For detection of cDNA of mouse CMP-sialic acid hydroxylase, we performed RT-PCR assays using a primer set based on sequences of CMP-sialic acid hydroxylase (5'-ctgatccaggtctctctgaa-3', 5'-agcctctccaaccagtcaga-3') and GAPDH (5'-acaaaatggtgaagtcggt-3', 5'-tccagggtttcttactcctt-3'). For quantitative real-time PCR, cDNA was prepared from total RNA using a PrimeScript™ RT Reagent kit (Takara Bio). RT-PCR was performed and analyzed using SsoFast™ EvaGreen Supermix on a Real-Time PCR system (Bio-Rad). Expression values were normalized to tubulin, and relative mRNA expression was calculated as described by Livak and Schmittgen (52). Primers used are listed in Table 1.

Mass spectrometric analysis

Neu5Ac GM3 (d18:1-[¹³C]16:0) was added to acidic GSL samples as the internal standard. GM3 molecular species were quantified using HPLC coupled with electrospray ionization tandem mass spectrometry (MS/MS) in multiple reaction-monitoring negative ionization mode. The triple-stage quadrupole (TSQ) Vantage AM instrument (Thermo Fisher, Waltham, MA) was calibrated by directly infusing a mixture of GM3 species extracted from milk, and all ion source parameters and ionization conditions were optimized to improve sensitivity. GSLs were dissolved in methanol, injected onto an HPLC pump (Accela 1250, Thermo Fisher), and separated using a Develosil carbon 30 column (C30-UG-3-1 × 50 mm, Nomura Co.; Aichi, Japan). The gradient program started with 100% solvent A (20% H₂O, 50% 2-propanol, 30% methanol con-

Table 2
Mass spectrometer settings and MRM transition pairs

Q, quadrupole; CE, collision energy; S-lens, stacked-ring ion guide; RF, radio frequency.

Molecular species (Sia)	Molecular species (Cer)	Q1	Q3	CE	S-lens RF amplitude
		m/z	m/z	eV	
GM3 (Neu5Ac) [M-H] [−]	d18:1–16:1	1149.7	289.9	53	276
	d18:1–16:0	1151.7	289.9	53	276
	d18:1–h16:1	1165.7	289.9	53	276
	d18:1–[¹³ C]16:0	1167.9	289.9	53	276
	d18:1–18:1	1177.7	289.9	53	276
	d18:1–18:0	1179.7	289.9	53	276
	d18:1–h18:1	1193.7	289.9	53	276
	d18:1–h18:0	1195.7	289.9	53	276
	d18:1–20:1	1205.7	289.9	53	276
	d18:1–20:0	1207.7	289.9	53	276
	d18:1–21:1	1219.7	289.9	53	276
	d18:1–21:0	1221.7	289.9	53	276
	d18:1–h20:0	1223.7	289.9	53	276
	d18:1–22:1	1233.7	289.9	53	276
	d18:1–22:0	1235.7	289.9	53	276
	d18:1–h21:0	1237.7	289.9	53	276
	d18:1–23:1	1247.7	289.9	53	276
	d18:1–23:0	1249.7	289.9	53	276
	d18:1–h22:0	1251.7	289.9	53	276
	d18:1–24:1	1261.8	289.9	53	276
	d18:1–24:0	1263.8	289.9	53	276
GM3 (Neu5Gc) [M-H] [−]	d18:1–h23:0	1265.8	289.9	53	276
	d18:1–h24:1	1277.8	289.9	53	276
	d18:1–h24:0	1279.8	289.9	53	276
	d18:1–16:1	1165.7	305.9	53	276
	d18:1–16:0	1167.7	305.9	53	276
	d18:1–h16:1	1181.7	305.9	53	276
	d18:1–18:1	1193.7	305.9	53	276
	d18:1–18:0	1195.7	305.9	53	276
	d18:1–h18:1	1209.7	305.9	53	276
	d18:1–h18:0	1211.7	305.9	53	276
	d18:1–20:1	1221.7	305.9	53	276
	d18:1–20:0	1223.7	305.9	53	276
	d18:1–21:1	1235.7	305.9	53	276
	d18:1–21:0	1237.7	305.9	53	276
	d18:1–h20:0	1239.7	305.9	53	276
	d18:1–22:1	1249.7	305.9	53	276
	d18:1–22:0	1251.7	305.9	53	276
	d18:1–h21:0	1253.7	305.9	53	276
	d18:1–23:1	1263.7	305.9	53	276
	d18:1–23:0	1265.7	305.9	53	276
	d18:1–h22:0	1267.7	305.9	53	276
	d18:1–24:1	1277.8	305.9	53	276
	d18:1–24:0	1279.8	305.9	53	276
	d18:1–h23:0	1281.8	305.9	53	276
	d18:1–h24:1	1293.8	305.9	53	276
	d18:1–h24:0	1295.8	305.9	53	276

taining 0.1% acetic acid and 0.1% ammonia) for 5 min, then ramped to 100% solvent B (2% H₂O, 50% 2-propanol, 48% methanol containing 0.1% acetic acid, and 0.1% ammonia) over 30 min. 100% solvent B was maintained for 4 min, then the solvent was returned to 100% solvent A over 1 min and held there for 10 min. Flow was 50 μ L/min throughout the chromatographic run. –2500 V potential was applied between ion source and electrospray needle. The carrier gas was nitrogen. Relative abundances of molecular species were assessed based on relative percentage of internal standard. All GM3 molecular species may not necessarily have identical ionization efficiencies; however, because of limited availability of pure molecular species standards, we assumed that all species have ionization efficiencies comparable with that of the internal standard. Thus, in evaluating relative abundances of molecular species, detected amounts are compared that may not necessarily rep-

resent absolute amounts (13). The details for the assignment of ganglioside molecular species are shown in Table 2.

Author contributions—Shinji G. and J.-i. I. designed the study and wrote the paper. Shiori G. and Shinji G. performed and analyzed the experiments shown in Figs. 2–8. V. L. performed and analyzed the experiments shown in Fig. 5 by using LC-MS/MS. M. G. C., L. M., A. P., and S. S. synthesized GM3 molecular species. C. S. and K. K. analyzed the experiments in Figs. 3, 4, and 6. All authors analyzed the results and approved the final version of the manuscript.

Acknowledgment—We are grateful to Dr. S. Anderson for English editing of the manuscript.

References

- Jennemann, R., and Gröne, H. J. (2013) Cell-specific *in vivo* functions of glycosphingolipids: lessons from genetic deletions of enzymes involved in glycosphingolipid synthesis. *Prog. Lipid Res.* **52**, 231–248
- Regina Todeschini, A., and Hakomori, S. I. (2008) Functional role of glycosphingolipids and gangliosides in control of cell adhesion, motility, and growth, through glycosynaptic microdomains. *Biochim. Biophys. Acta* **1780**, 421–433
- Schnaar, R. L., Gerardy-Schahn, R., and Hildebrandt, H. (2014) Sialic acids in the brain: gangliosides and polysialic acid in nervous system development, stability, disease, and regeneration. *Physiol. Rev.* **94**, 461–518
- Inokuchi, J. (2010) Membrane microdomains and insulin resistance. *FEBS Lett.* **584**, 1864–1871
- Inokuchi, J. (2011) Physiopathological function of hematoside (GM3 ganglioside). *Proc. Jpn. Acad. Ser. B. Phys. Biol. Sci.* **87**, 179–198
- Inokuchi, J. (2014) GM3 and diabetes. *Glycoconj. J.* **31**, 193–197
- Kabayama, K., Sato, T., Kitamura, F., Uemura, S., Kang, B. W., Igarashi, Y., and Inokuchi, J. (2005) TNF α -induced insulin resistance in adipocytes as a membrane microdomain disorder: involvement of ganglioside GM3. *Glycobiology* **15**, 21–29
- Kabayama, K., Sato, T., Saito, K., Loberto, N., Prinetti, A., Sonnino, S., Kinjo, M., Igarashi, Y., and Inokuchi, J. (2007) Dissociation of the insulin receptor and caveolin-1 complex by ganglioside GM3 in the state of insulin resistance. *Proc. Natl. Acad. Sci. U.S.A.* **104**, 13678–13683
- Mullen, T. D., Hannun, Y. A., and Obeid, L. M. (2012) Ceramide synthases at the centre of sphingolipid metabolism and biology. *Biochem. J.* **441**, 789–802
- Park, J. W., Park, W. J., and Futerman, A. H. (2014) Ceramide synthases as potential targets for therapeutic intervention in human diseases. *Biochim. Biophys. Acta* **1841**, 671–681
- Angata, T., and Varki, A. (2002) Chemical diversity in the sialic acids and related α -keto acids: an evolutionary perspective. *Chem. Rev.* **102**, 439–469
- Hayashi, N., Chiba, H., Kuronuma, K., Go, S., Hasegawa, Y., Takahashi, M., Gasa, S., Watanabe, A., Hasegawa, T., Kuroki, Y., Inokuchi, J., and Takahashi, H. (2013) Detection of N-glycosylated gangliosides in non-small-cell lung cancer using GMR8 monoclonal antibody. *Cancer Sci.* **104**, 43–47
- Veillon, L., Go, S., Matsuyama, W., Suzuki, A., Nagasaki, M., Yatomi, Y., and Inokuchi, J. (2015) Identification of ganglioside GM3 molecular species in human serum associated with risk factors of metabolic syndrome. *PLoS ONE* **10**, e0129645
- Hindi, S. M., Tajirishi, M. M., and Kumar, A. (2013) Signaling mechanisms in mammalian myoblast fusion. *Sci. Signal.* **6**, re2
- Krauss, R. S., Cole, F., Gaio, U., Takaesu, G., Zhang, W., and Kang, J. S. (2005) Close encounters: regulation of vertebrate skeletal myogenesis by cell-cell contact. *J. Cell Sci.* **118**, 2355–2362
- Anastasia, L., Papini, N., Colazzo, F., Palazzolo, G., Tringali, C., Dileo, L., Piccoli, M., Conforti, E., Sitzia, C., Monti, E., Sampaioles, M., Tettamanti, G., and Venerando, B. (2008) NEU3 sialidase strictly modulates GM3 levels in skeletal myoblasts C2C12 thus favoring their differentiation and protecting them from apoptosis. *J. Biol. Chem.* **283**, 36265–36271

17. Papini, N., Anastasia, L., Tringali, C., Dileo, L., Carubelli, I., Sampaulesi, M., Monti, E., Tettamanti, G., and Venerando, B. (2012) MmNEU3 sialidase over-expression in C2C12 myoblasts delays differentiation and induces hypertrophic myotube formation. *J. Cell. Biochem.* **113**, 2967–2978
18. Scaringi, R., Piccoli, M., Papini, N., Cirillo, F., Conforti, E., Bergante, S., Tringali, C., Garatti, A., Gelfi, C., Venerando, B., Menicanti, L., Tettamanti, G., and Anastasia, L. (2013) NEU3 sialidase is activated under hypoxia and protects skeletal muscle cells from apoptosis through the activation of the epidermal growth factor receptor signaling pathway and the hypoxia-inducible factor (HIF)-1 α . *J. Biol. Chem.* **288**, 3153–3162
19. Singhal, N., and Martin, P. T. (2015) A role for Galgt1 in skeletal muscle regeneration. *Skelet. Muscle* **5**, 3
20. Ozawa, H., Kawashima, I., and Tai, T. (1992) Generation of murine monoclonal antibodies specific for N-glycolylneuraminic acid-containing gangliosides. *Arch. Biochem. Biophys.* **294**, 427–433
21. Samraj, A. N., Pearce, O. M., Läubli, H., Crittenden, A. N., Bergfeld, A. K., Banda, K., Gregg, C. J., Bingman, A. E., Secrest, P., Diaz, S. L., Varki, N. M., and Varki, A. (2015) A red meat-derived glycan promotes inflammation and cancer progression. *Proc. Natl. Acad. Sci. U.S.A.* **112**, 542–547
22. Varki, A. (2001) N-glycolylneuraminic acid deficiency in humans. *Biochimie* **83**, 615–622
23. Yin, J., Hashimoto, A., Izawa, M., Miyazaki, K., Chen, G. Y., Takematsu, H., Kozutsumi, Y., Suzuki, A., Furuhashi, K., Cheng, F. L., Lin, C. H., Sato, C., Kitajima, K., and Kannagi, R. (2006) Hypoxic culture induces expression of sialin, a sialic acid transporter, and cancer-associated gangliosides containing non-human sialic acid on human cancer cells. *Cancer Res.* **66**, 2937–2945
24. Kawano, T., Koyama, S., Takematsu, H., Kozutsumi, Y., Kawasaki, H., Kawashima, S., Kawasaki, T., and Suzuki, A. (1995) Molecular cloning of cytidine monophospho-N-acetylneuraminic acid hydroxylase: regulation of species- and tissue-specific expression of N-glycolylneuraminic acid. *J. Biol. Chem.* **270**, 16458–16463
25. Schlenzka, W., Shaw, L., Kelm, S., Schmidt, C. L., Bill, E., Trautwein, A. X., Lottspeich, F., and Schauer, R. (1996) CMP-N-acetylneuraminic acid hydroxylase: the first cytosolic Rieske iron-sulphur protein to be described in Eukarya. *FEBS Lett.* **385**, 197–200
26. Schwarzmann, G. (2001) Uptake and metabolism of exogenous glycosphingolipids by cultured cells. *Semin. Cell Dev. Biol.* **12**, 163–171
27. Horsley, V., and Pavlath, G. K. (2004) Forming a multinucleated cell: molecules that regulate myoblast fusion. *Cells Tissues Organs* **176**, 67–78
28. Mukai, A., Kurisaki, T., Sato, S. B., Kobayashi, T., Kondoh, G., and Hashimoto, N. (2009) Dynamic clustering and dispersion of lipid rafts contribute to fusion competence of myogenic cells. *Exp. Cell Res.* **315**, 3052–3063
29. Mukai, A., and Hashimoto, N. (2008) Localized cyclic AMP-dependent protein kinase activity is required for myogenic cell fusion. *Exp. Cell Res.* **314**, 387–397
30. Schwander, M., Leu, M., Stumm, M., Dorchie, O. M., Ruegg, U. T., Schittny, J., and Müller, U. (2003) β 1 integrins regulate myoblast fusion and sarcomere assembly. *Dev. Cell* **4**, 673–685
31. Charrin, S., Latil, M., Soave, S., Poleskaya, A., Chrétien, F., Boucheix, C., and Rubinstein, E. (2013) Normal muscle regeneration requires tight control of muscle cell fusion by tetraspanins CD9 and CD81. *Nat. Commun.* **4**, 1674
32. Ong, E., Suzuki, M., Belot, F., Yeh, J. C., Franceschini, I., Angata, K., Hinds-gaul, O., and Fukuda, M. (2002) Biosynthesis of HNK-1 glycans on O-linked oligosaccharides attached to the neural cell adhesion molecule (NCAM): the requirement for core 2- β -1,6-N-acetylglucosaminyltransferase and the muscle-specific domain in NCAM. *J. Biol. Chem.* **277**, 18182–18190
33. Suzuki, M., Angata, K., Nakayama, J., and Fukuda, M. (2003) Polysialic acid and mucin type O-glycans on the neural cell adhesion molecule differentially regulate myoblast fusion. *J. Biol. Chem.* **278**, 49459–49468
34. Hochreiter-Hufford, A. E., Lee, C. S., Kinchen, J. M., Sokolowski, J. D., Arandjelovic, S., Call, J. A., Klivanov, A. L., Yan, Z., Mandell, J. W., and Ravichandran, K. S. (2013) Phosphatidylserine receptor BAI1 and apoptotic cells as new promoters of myoblast fusion. *Nature* **497**, 263–267
35. Millay, D. P., O'Rourke, J. R., Sutherland, L. B., Bezprozvannaya, S., Shelton, J. M., Bassel-Duby, R., and Olson, E. N. (2013) Myomaker is a membrane activator of myoblast fusion and muscle formation. *Nature* **499**, 301–305
36. Cornell, R. B., Nissley, S. M., and Horwitz, A. F. (1980) Cholesterol availability modulates myoblast fusion. *J. Cell Biol.* **86**, 820–824
37. Mermelstein, C. S., Portillo, D. M., Medeiros, R. B., Matos, A. R., Einicker-Lamas, M., Tortelote, G. G., Vieyra, A., and Costa, M. L. (2005) Cholesterol depletion by methyl- β -cyclodextrin enhances myoblast fusion and induces the formation of myotubes with disorganized nuclei. *Cell Tissue Res.* **319**, 289–297
38. Sekiya, T., Takenawa, T., and Nozawa, Y. (1984) Reorganization of membrane cholesterol during membrane fusion in myogenesis *in vitro*: a study using the filipin-cholesterol complex. *Cell Struct. Funct.* **9**, 143–155
39. Mullen, T. D., Spassieva, S., Jenkins, R. W., Kitatani, K., Bielawski, J., Han-nun, Y. A., and Obeid, L. M. (2011) Selective knockdown of ceramide synthases reveals complex interregulation of sphingolipid metabolism. *J. Lipid Res.* **52**, 68–77
40. Casadesús, A. V., Fernández-Marrero, Y., Clavell, M., Gómez, J. A., Hernández, T., Moreno, E., and López-Requena, A. (2013) A shift from N-glycolyl- to N-acetylsialic acid in the GM3 ganglioside impairs tumor development in mouse lymphocytic leukemia cells. *Glycoconj. J.* **30**, 687–699
41. Naito, Y., Takematsu, H., Koyama, S., Miyake, S., Yamamoto, H., Fujinawa, R., Sugai, M., Okuno, Y., Tsujimoto, G., Yamaji, T., Hashimoto, Y., Itohara, S., Kawasaki, T., Suzuki, A., and Kozutsumi, Y. (2007) Germinal center marker GL7 probes activation-dependent repression of N-glycolylneuraminic acid, a sialic acid species involved in the negative modulation of B-cell activation. *Mol. Cell Biol.* **27**, 3008–3022
42. Naito-Matsui, Y., Takada, S., Kano, Y., Iyoda, T., Sugai, M., Shimizu, A., Inaba, K., Nitschke, L., Tsubata, T., Oka, S., Kozutsumi, Y., and Takematsu, H. (2014) Functional evaluation of activation-dependent alterations in the sialoglycan composition of T cells. *J. Biol. Chem.* **289**, 1564–1579
43. Samraj, A. N., Läubli, H., Varki, N., and Varki, A. (2014) Involvement of a non-human sialic acid in human cancer. *Front. Oncol.* **4**, 33
44. Chandrasekharan, K., Yoon, J. H., Xu, Y., deVries, S., Camboni, M., Jansen, P. M., Varki, A., and Martin, P. T. (2010) A human-specific deletion in mouse Cmah increases disease severity in the mdx model of Duchenne muscular dystrophy. *Sci. Transl. Med.* **2**, 42ra54
45. Martin, P. T., Camboni, M., Xu, R., Golden, B., Chandrasekharan, K., Wang, C. M., Varki, A., and Janssen, P. M. (2013) N-Glycolylneuraminic acid deficiency worsens cardiac and skeletal muscle pathophysiology in α -sarcoglycan-deficient mice. *Glycobiology* **23**, 833–843
46. Valiente, O., Mauri, L., Casellato, R., Fernandez, L. E., and Sonnino, S. (2001) Preparation of deacetyl-, lyso-, and deacetyl-lyso-GM3 by selective alkaline hydrolysis of GM3 ganglioside. *J. Lipid Res.* **42**, 1318–1324
47. Palestini, P., Allietta, P., Sonnino, S., Tettamanti, G., Thompson, T. E., and Tillack, T. W. (1995) Gel phase preference of ganglioside GM1 at low concentration in two-component, two-phase phosphatidylcholine bilayers depends upon the ceramide moiety. *Biochim. Biophys. Acta* **1235**, 221–230
48. Yu, R. K., and Ledeen, R. W. (1972) Gangliosides of human, bovine, and rabbit plasma. *J. Lipid Res.* **13**, 680–686
49. Ando, S., Chang, N. C., and Yu, R. K. (1978) High-performance thin-layer chromatography and densitometric determination of brain ganglioside compositions of several species. *Anal. Biochem.* **89**, 437–450
50. Chisada, S., Yoshimura, Y., Sakaguchi, K., Uemura, S., Go, S., Ikeda, K., Uchima, H., Matsunaga, N., Ogura, K., Tai, T., Okino, N., Taguchi, R., Inokuchi, J., and Ito, M. (2009) Zebrafish and mouse α 2,3-sialyltransferases responsible for synthesizing GM4 ganglioside. *J. Biol. Chem.* **284**, 30534–30546
51. Go, S., Sato, C., Yin, J., Kannagi, R., and Kitajima, K. (2007) Hypoxia-enhanced expression of free deaminoneuraminic acid in human cancer cells. *Biochem. Biophys. Res. Commun.* **357**, 537–542
52. Livak, K. J., and Schmittgen, T. D. (2001) Analysis of relative gene expression data using real-time quantitative PCR and the $2^{-\Delta\Delta CT}$ method. *Methods* **25**, 402–408



Identification of a new B4GalNacT1 (GM2/GD2/GA2 synthase) isoform, and regulation of enzyme stability and intracellular transport by arginine-based motif

Fumi Shishido ^{a,1}, Satoshi Uemura ^{b,c,*}, Madoka Kashimura ^a, Jin-ichi Inokuchi ^{a,*}

^a Division of Glycopathology, Institute of Molecular Biomembrane and Glycobiology, Tohoku Medical and Pharmaceutical University, 4-4-1, Komatsushima, Aoba-ku, Sendai, Miyagi 981-8558, Japan

^b Division of Medical Biochemistry, Faculty of Medicine, Tohoku Medical and Pharmaceutical University, 4-4-1, Komatsushima, Aoba-ku, Sendai, Miyagi 981-8558, Japan

^c Division of Chemistry and Biological Science, College of Science and Engineering, Aoyama Gakuin University, 5-10-1 Fuchinobe, Chuo-ku, Sagami-hara, Kanagawa 252-5258, Japan

ARTICLE INFO

Article history:

Received 24 February 2017

Received in revised form 17 June 2017

Accepted 10 July 2017

Available online 12 July 2017

Keywords:

Glycosyltransferase

Retrograde transport

R-based motif

mRNA transcriptional variant

ABSTRACT

Glycosphingolipids (GSLs) are abundant in plasma membranes of mammalian cells, and their synthesis is strictly regulated in the Golgi apparatus. Disruption of GSL homeostasis is the cause of numerous diseases. Hundreds of molecular species of GSLs exist, and the detailed mechanisms underlying their homeostasis remain unclear. We investigated the physiological significance of isoform production for β 1,4-*N*-acetyl-galactosaminyl transferase 1/B4GALNT1 (B4GN1), an enzyme involved in synthesis of ganglio-series GSLs GM2/GD2/GA2. We discovered a new mRNA variant (termed variant 2) of B4GN1 through EST clone search. A new isoform, M1-B4GN1, which has an NH₂-terminal cytoplasmic tail longer than that of previously-known isoform M2-B4GN1, is translated from variant 2. M1-B4GN1 has R-based motif (a retrograde transport signal) in the cytoplasmic tail. M1-B4GN1 is partially localized in the endoplasmic reticulum (ER) depending on the R-based motif, whereas M2-B4GN1 is localized in the Golgi. Stability of M1-B4GN1 is higher than that of M2-B4GN1 because of the R-based motif. M2-B4GN1 forms a homodimer via disulfide bonding. When M1-B4GN1 and M2-B4GN1 were co-expressed in CHO-K1 cells, the two isoforms formed a heterodimer. The M1/M2-B4GN1 heterodimer was more stable than the M2-B4GN1 homodimer, but the heterodimer was not transported from the Golgi to the ER. Our findings indicate that stabilization of M1-B4GN1 homodimer and M1/M2-B4GN1 heterodimer by R-based motif is related to prolongation of Golgi retention, but not to retrograde transport from the Golgi to the ER. Coexistence of several B4GN1 isoforms having distinctive characteristics presumably helps maintain overall enzyme stability and GSL homeostasis.

© 2017 Elsevier B.V. All rights reserved.

1. Introduction

Glycosphingolipids (GSLs), complex carbohydrate-based molecules comprised of hydrophilic and hydrophobic regions, are abundant in the outer leaflet of plasma membranes of mammalian cells and are involved in a variety of important physiological processes, including cell proliferation, differentiation, and adhesion [1–5]. The hydrophilic head groups of GSLs vary in terms of number and type of carbohydrate chains, resulting in the existence of several hundred molecular species of GSLs [6,7]. Certain diseases result from disruption of GSL homeostasis; e.g., GM3 level is elevated in adipose tissue of Zucker *fa/fa* rats and *ob/ob* mice, typical rodent models of obesity [8], and insulin sensitivity is en-

hanced in ST3 β -galactoside α 2,3-sialyltransferase 5/ST3GAL5 (ST3G5) knockout mice [9] (Fig. 1). In rodent obesity models, treatment with GlcCer synthase inhibitors that significantly reduce GM3 content improves insulin sensitivity and glucose homeostasis [10,11]. ST3G5 gene mutations were identified in patients with early-onset refractory epilepsy or salt-and-pepper syndrome, characterized by severe intellectual disability, epilepsy, scoliosis, choreoathetosis, dysmorphic facial features, and altered dermal pigmentation (Table 1) [12–16]. β 1,4-*N*-acetyl-galactosaminyl transferase 1/B4GALNT1 (B4GN1), a key enzyme in synthesis of complex gangliosides (GM1a, GD1a, GD1b, GT1b, GA1, GM1b), also plays important roles in GSL homeostasis (Fig. 1). B4GN1 knockout mice, which lack all complex gangliosides in the central nervous system, display subtle neurological disorders at birth and subsequent nervous system neurodegeneration, indicating that complex gangliosides are essential for maintenance of nervous system integrity [17–19]. In human native CD4⁺ T helper lymphocyte (Th), the expression level of GD2 synthesized by B4GN1 is increased by the stimulation

* Corresponding authors.

E-mail addresses: s-uemura@tohoku-mpu.ac.jp (S. Uemura), jin@tohoku-mpu.ac.jp (J. Inokuchi).

¹ These two authors contributed equally to the study.

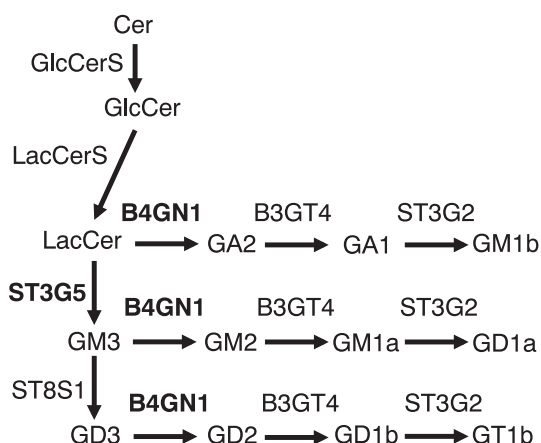


Fig. 1. Biosynthetic pathway of glycosphingolipids. Biosynthesis of ganglio-series GSLs from LacCer. ST3G5: ST3 β -galactoside α 2,3-sialyltransferase. ST8S1: ST8 α -N-acetylneuraminidase α 2,8-sialyltransferase 1. B4GN1: β 1,4-*N*-acetyl-galactosaminyl transferase 1. B3GT4: UDP-Gal: β GlcNAc β 1,3-galactosyltransferase, polypeptide 4. ST3G2: ST3 β -galactoside α 2,3-sialyltransferase 2.

of anti-CD3 and anti-CD28 antibodies [20]. The GD2 is important for efficient T cell receptor (TCR) clustering in the plasma membrane. In contrast, ST3G5 knockout mice, but not B4GN1 knockout mice, show a reduction in the proliferation of Th cells when activated with anti-CD3 and anti-CD28 antibodies and the phenotype is recovered by the supplementation of GM3, GM1a, and GD1a [21]. Therefore, GM3 is necessary for the activation of Th cell in murine. Human B4GN1 mutations have been identified in families from Kuwait, Italy, and Old Order Amish who display an unusual neurodegenerative phenotype classified as a complex form of hereditary spastic paraplegia (SPG26) (Table 1) [22–25].

We previously investigated the mechanisms whereby GSL biosynthesis is regulated by ST3G5, the primary glycosyltransferase responsible for synthesis of ganglio-series gangliosides. There are three ST3G5 isoforms, having NH₂-terminal cytoplasmic tail lengths of 69 amino acids (aa) (M1-ST3G5), 42 aa (M2-ST3G5), and 14 aa (M3-ST3G5) [26]. These isoforms are produced by leaky scanning from several mRNA variants. M1-ST3G5 is localized primarily in the endoplasmic reticulum (ER) through an arginine (R)-based motif (a retrograde

transport signal), located on its cytoplasmic tail. R-based motifs interact with COP I subunits (β -COP and δ -COP) to function as signal sequences [27]. Binding affinities to β -COP and δ -COP depend on not only R-based motif sequence but also position in a lipid bilayer [28]. We demonstrated that ER targeting of M1-ST3G5 *in vivo* leads to suppression of its GM3 synthesis activity because this synthesis occurs in the Golgi. Both M2- and M3-ST3G5 are localized in the Golgi, but the half-life of M2-ST3G5 is shorter than that of M3-ST3G5 [26].

In the present study, we investigated the biological significance of isoform production for glycosyltransferases, with focus on human and mouse B4GN1. EST clone search revealed a new isoform, M1-B4GN1, produced from new mRNA variant 2. NH₂-terminal lengths of human and mouse M1-B4GN1 (hM1- and mM1-B4GN1) are respectively 81 and 40 aa, much longer than that of previously-known isoform M2-B4GN1 (6 aa). hM1- and mM1-B4GN1 have R-based motif, a retrograde transport signal, and are partially localized in the ER, whereas hM2- and mM2-B4GN1 are localized in the Golgi. Stability of hM1-B4GN1 was higher than that of hM2-B4GN1. Co-expression of hM1- and hM2-B4GN1 resulted in enhanced stability of M2-B4GN1 through hM1-/hM2-B4GN1 dimer formation *via* a disulfide bond. These findings indicate that overall stability of B4GN1 is increased by M1-B4GN1 isoform production. Coexistence of several isoforms having distinctive membrane dynamics is presumably useful in maintenance of GSL homeostasis under varying physiological conditions.

2. Materials and methods

2.1. Plasmids

The plasmids used in this study are listed in Table 2. The open reading frame (ORF) of human M1-B4GN1 (hM1-B4GN1) was amplified using cDNA prepared from human brain tissue, and primers 5'-ATGCAGAGAGGGCGAGAAGAAAG-3' and 5'-TCACTGGGAGGTCATGC ACTGCAG-3'. Resulting fragments were cloned into pGEM-T Easy Vector (Promega; Madison, WI) to generate pFS432. pFS444 encoding hM1-B4GN1-FLAG was constructed using pFS432 and primers 5'-AGGGAGACCAAGCTTCACCATGCAGGAGAGGGCGAGAA-3' and 5'-CTTGTATCGGGATCCTGGGAGGTCATGCAGTGCAG-3'. Resulting

Table 1
Distribution of gene mutations in human *ST3GAL5* and *B4GALNT1*.

Genes	Mutations ^{a,b}	Reference
<i>ST3GAL5</i>	c.584G > C (p.Cys195Ser)	[15]
	c.601G > A (p.Gly201Arg)	
	c.862C > T (p.Arg288*)	
	c.862C > T (p.Arg288*)	[13]
	c.862C > T (p.Arg288*)	
	c.1063G > A (p.Glu355Lys)	[16]
<i>B4GALNT1</i>	c.263dupG (p.Leu89Profs*13)	[12]
	c.358C > T (p.Gln120*)	
	c.395delC (p.Pro132Glnfs*7)	[23]
	c.682C > T (p.Arg228*)	
	c.898C > T (p.Arg300Cys)	[24]
	c.917_922dupTTACCG (p.Thr307_Val308dup)	
	c.1298A > C (p.Asp433Ala)	[24]
	c.1315_1317delTTC (p.Phe439del)	
	c.852G > C (p.Lys284Asn)	[24]
	c.1458dupA (p.Leu487Thrfs*77)	
	c.1514G > A (p.Arg505His)	[25]
	c.838-2A > G (p.Gly280_Leu326del)	
	c.1458dupA (p.Leu487Thrfs*77)	[25]

^a The reference sequences of *ST3GAL5* and *B4GALNT1* are NM_003896.3 and NM_001478.4, respectively.

^b The mutations were described according to established mutation nomenclature (<http://varnomen.hgvs.org/>).

Table 2
Plasmids used.

Plasmid name	Inserted ORF	Vector
pFS 444	hM1-B4GN1-FLAG	pcDNA3-FLAG4
pFS 471	hM1-B4GN1-FLAG*	pcDNA3-FLAG4
pFS 452	hM2-B4GN1-FLAG	pcDNA3-FLAG4
pKM 6	mM1-B4GN1-FLAG	pcDNA3-FLAG4
pKM 15	mM1-B4GN1-FLAG*	pcDNA3-FLAG4
pKM 5	mM2-B4GN1-FLAG	pcDNA3-FLAG4
pFS 446	hM1-B4GN1(N)-GFP	pEGFP-N1
pFS 468	hM1-B4GN1(N)-GFP R4S	pEGFP-N1
pFS 469	hM1-B4GN1(N)-GFP R6S	pEGFP-N1
pFS 470	hM1-B4GN1(N)-GFP R7S	pEGFP-N1
pFS 460	hM1-B4GN1(N)-GFP R6/7S	pEGFP-N1
pFS 611	hM1-B4GN1(N)-GFP R4/6/7S	pEGFP-N1
pFS 453	hM2-B4GN1(N)-GFP	pEGFP-N1
pFS 222	mM1-B4GN1(N)-GFP	pEGFP-N1
pFS 398	mM1-B4GN1(N)-GFP R8S	pEGFP-N1
pFS 262	mM1-B4GN1(N)-GFP R11S	pEGFP-N1
pFS 424	mM1-B4GN1(N)-GFP R12S	pEGFP-N1
pFS 425	mM1-B4GN1(N)-GFP R13S	pEGFP-N1
pFS 426	mM1-B4GN1(N)-GFP R14S	pEGFP-N1
pFS 265	mM1-B4GN1(N)-GFP R11/12/13/14S	pEGFP-N1
pKM 9	mM2-B4GN1(N)-GFP	pEGFP-N1
pFS 473	hM1-B4GN1-FLAG	CSII-CMV-RfA
pFS 527	hM1-B4GN1-FLAG R4/6/7S	CSII-CMV-RfA
pFS 493	hM2-B4GN1-FLAG	CSII-CMV-RfA
pFS 563	hM2-B4GN1-HA	CSII-CMV-RfA
pFS 571	mM1-B4GN1-FLAG	CSII-CMV-RfA
pFS 577	mM1-B4GN1-FLAG R11/12/13/14S	CSII-CMV-RfA
pFS 573	mM2-B4GN1-HA	CSII-CMV-RfA

fragments were cloned into the *HindIII*–*Bam*HI site of pcDNA3-FLAG4 vector using the In-Fusion cloning system (Takara Bio; Shiga, Japan) to generate pFS444. Plasmids encoding hM2-B4GN1-FLAG, hM1-B4GN1-FLAG*, and hM2-B4GN1-HA were created by similar procedures.

The ORF of mouse M1-B4GN1 was amplified using cDNA prepared from mouse brain tissue, and primers 5'-ATGGCTGGCCTTGGGTA CCGCGCGAGCCTCGG-3' and 5'-TCACTCGGCGGTCATGCACTGTA-3'. Resulting fragments were cloned into pGEM-T Easy Vector to generate pKM2. To insert the Kozak sequence (GCCACC) before ATG(M1), M1-B4GN1 was amplified using pKM2 and primers 5'-GGATCCGCCACCA TGGCTGGCCTTGGGTACCTG-3' and 5'-TGGATCTCGGCGGTCATGC ACTGTAGCC-3'. Resulting fragments were cloned into pGEM-T Easy Vector to generate pKM4. The 1.7-kb *Bam*HI fragment of pKM4 was then cloned into the *Bam*HI site of pcDNA3-FLAG4 vector to generate pKM6. Plasmids encoding mM2-B4GN1-FLAG and mM1-B4GN1-FLAG* were created by similar procedures.

A pFS446 (hM1-B4GN1(N)-GFP) plasmid encoding fusion proteins of the NH₂-terminus of M1-B4GN1 and GFP was constructed using pFS432 and primers 5'-TCTCAGACTCAAGCTTCACCATGCAGGAGAG GGC-3' and 5'-GGCGACCGTGGATCAAGAGGTAGCCGGAGGCCGG-3'. Resulting fragments were cloned into the *HindIII*–*Bam*HI site of pEGFP-N1 vector using the In-Fusion system to generate pFS446. Plasmids encoding hM2-B4GN1(N)-GFP, mM1-B4GN1(N)-GFP, and mM2-B4GN1(N)-GFP were created by similar procedures.

Point mutants of hM1-B4GN1(N)-GFP, mM1-B4GN1(N)-GFP, hM1-B4GN1-FLAG, and mM1-B4GN1-FLAG were created by site-directed mutagenesis using PrimeSTAR® Mutagenesis Basal Kit (Takara) according to the manufacturer's instructions.

For lentivirus production, a pFS473 (hM1-B4GN1-FLAG/CSII-CMV-RfA) plasmid was constructed using pFS444 and primers 5'-CACCATGCAGGAGAGGGCGA-3' and 5'-TCAGATCTTATCGTCGTCATC CTGTGAATC-3'. Resulting fragments were cloned into pENTR/D-TOPO vector (Thermo Fisher; Waltham, MA) to generate pFS466. The CSII-CMV-MCS plasmid was converted to a destination vector (CSII-CMV-RfA) using the Gateway vector conversion system (Thermo Fisher). The hM1-B4GN1-FLAG gene of pFS266 was inserted into lentiviral expression vector CSII-CMV-RfA, using the LR clonase reaction to generate pFS473. Lentiviral expression plasmids encoding hM1-B4GN1-FLAG R4/6/7S mutant, hM2-B4GN1-FLAG, hM2-B4GN1-HA, mM1-B4GN1-FLAG, mM1-B4GN1-FLAG R11/12/13/14S mutant, and mM2-B4GN1-HA were created by similar procedures.

For real-time PCR assay, hM1-B4GN1 sequence containing 5'-UTR was amplified using cDNA prepared from human brain tissue, and primers 5'-GCTTGGCGAGGCCACTCATCG-3' and 5'-CCCGGGTCTCGGTACAGG-3'. Resulting fragments were cloned into pGEM-T Easy Vector to generate pFS635. The 18S rRNA sequence was amplified using cDNA prepared from human brain tissue, and primers 5'-TACCTGGTTGATCCTGCCAGTAG-3' and 5'-TAATGATCCTTCCGCAGGTTACAC-3'. Resulting fragments were cloned into pGEM-T Easy Vector to generate pFS636.

2.2. Semi-quantitative reverse transcription PCR (RT-PCR)

First-strand cDNA synthesis was performed using a First-Strand cDNA Synthesis kit for RT-PCR (AMV; Roche Diagnostics; Basel, Switzerland) and total RNA isolated from mouse tissues or human brain tissue (Takara). We designed specific primers as follows to amplify B4GN1 (all variants, or only variant 2): hB4GN1 all variants: 5'-GCTGGCAGT GCAAACCTAGC-3' and 5'-GTGAAAGCAGCCTCATGTCCT-3', hB4GN1 variant 2: 5'-ATGCAGGAGAGGGCGAGAAGA-3' and 5'-GGCTGAACCTC CACACCCTGTAGG-3', mB4GN1 all variants: 5'-CTAGTCTTGCTGCTCGC CTG-3' and 5'-GCCAGTCCAGGTGCCTAG-3', mB4GN1 variant 2: 5'-CTCAGTCTCTGAGAGCCTGG-3' and 5'-GCCAGTCCAGGTGCCTAG-3'. PCR was performed using 50 ng cDNA, specific primers as above, and KOD FX polymerase (Takara), according to the manufacturer's instructions. Cycling conditions were 94 °C for 2 min, followed by 34 cycles of 98 °C for 10 s and 68 °C for 40 s. Respective lengths of amplified fragments

of hB4GN1 all variants, hB4GN1 variant 2, mB4GN1 all variants, and mB4GN1 variant 2 were 599, 698, 539, and 618 bp.

2.3. Real-time PCR

First-strand cDNA synthesis was performed using ReverTra Ace qPCR RT Master Mix with gDNA Remover (Toyobo; Osaka, Japan) and total RNA isolated from human tissues (Takara), or human cell lines. Primers and probes specific for hB4GN1 all variants (Hs00155195_m1) were from Applied Biosystems (Foster City, CA). hB4GN1 variant 2 (primers, 5'-CATCCAAATGTCTTCAGCATTAAAGAT-3' and 5'-TCTCCCGCCTCTTCTCTCT-3'; probe, 5'-TCGGGTGTGTGAGGAAACCGAGATG-3') and 18S rRNA (Hs.PT.39a.22214856.g) were from Integrated DNA Technologies (IDT; Coralville, IA). Real-time PCR was performed with 2 × TaqMan Universal Master Mix II (Applied Biosystems) using a Step One Plus real-time PCR system (Applied Biosystems). Standard curves were constructed using pFS466 (hB4GN1 variant all), pFS635 (hB4GN1 variant 2), or pFS636 (18S rRNA), and copy numbers of tissues or cells were calculated.

2.4. Cell culture

Chinese hamster ovary CHO-K1 (CHO) cells, human kidney 293T cells, and human leukemia HAP1 cells [29] were cultured respectively in Ham's F-12 medium (Wako; Osaka, Japan), high-glucose DMEM (Nacalai Tesque; Kyoto, Japan), and low-glucose IMDM (Nacalai Tesque), each supplemented with 10% fetal bovine serum, 100 U/mL penicillin, and 100 µg/mL streptomycin. CHO-K1 cells were transiently transfected using Lipofectamine 2000 (Thermo Fisher) according to the manufacturer's instructions.

2.5. Preparation of lentiviral vectors

293 T cells (0.5×10^6) were seeded in a polylysine-coated 60-mm dish 24 h before transfection, and then transfected with 3 µg CSII-CMV-RfA cloning hM1-B4GN1-FLAG, hM2-B4GN1-FLAG, mM1-B4GN1-FLAG, mM2-B4GN1-FLAG, and hM2-B4GN1-HA, 1.5 µg pCAG-HIVgp, and 1.5 µg pCMV-VSV-G-RSV-Rev. plasmids, using Lipofectamine 2000. Cells were incubated 24 h at 37 °C, and medium was replaced with 4 mL high-glucose DMEM containing 10 µM forskolin. To maintain virus stability, culture temperature was lowered from 37 to 32 °C ~32 h after transfection. Lentivirus-containing supernatant was harvested 48 h after transfection, centrifuged at $200 \times g$ for 3 min to remove living cells, and either used immediately for experiments or snap-frozen in liquid nitrogen and stored at –80 °C for later experiments. For lentiviral transduction of CHO-K1 cells, 4 mL lentiviral supernatant was added to 0.25×10^6 cells in a 60-mm dish, cells were cultured at 32 °C for 24 h, culture temperature was raised from 32 to 37 °C, and incubation continued another 48 h.

2.6. Preparation of cell lysates

Cells were washed twice with ice-cold phosphate-buffered saline (PBS), suspended in buffer A (50 mM Tris-HCl (pH 7.5), 150 mM NaCl, 10% glycerol, 4 M urea, and 1 × Complete protease inhibitor mixture (EDTA-free; Roche Diagnostics)), and lysed by sonication. Cell debris was removed by centrifugation at $1000 \times g$ for 3 min at 4 °C, and supernatant (total cell lysates) was centrifuged at $100,000 \times g$ for 1 h at 4 °C. Precipitate (integral membrane protein fraction) was suspended in 2 × SDS sample buffer (125 mM Tris-HCl (pH 6.8), 4% SDS, 20% glycerol, and trace amount of bromophenol blue) containing 5% βMe, and incubated 5 min at 37 °C. Integral membrane protein fraction was subjected to PNGase F (New England Biolabs; Beverly, MA) digestion 1 h at 37 °C according to the manufacturer's instructions. Protein concentrations of total cell lysates were determined using a BCA protein kit (Pierce; Thermo Fisher).

2.7. Immunoblotting

Integral membrane protein fraction as above was subjected to immunoblotting. Proteins were separated by SDS-PAGE and transferred to an Immobilon PVDF membrane (Millipore; Billerica, MA). The membrane was incubated 1 h with 1:1000 dilution of anti-FLAG antibodies (Agilent Technologies; Santa Clara, CA), or anti-GFP (IgY fraction) (Aves Labs; Tigard, OR), washed, and incubated 1 h with 1:20,000 dilution of HRP-conjugated donkey anti-mouse IgG (GE Healthcare; Little Chalfont, UK) or anti-chicken IgY (Aves Labs). Labeling was detected using an ECL Select kit (GE Healthcare).

2.8. Immunofluorescence microscopy

Transfected cells were cultured on coverslips, fixed 15 min with 3.7% formaldehyde in PBS at room temperature, rinsed with PBS, permeabilized (if necessary) with 0.5% SDS or 0.5% Triton X-100 in PBS, treated with Image-iT FX Signal Enhancer (Thermo Fisher) for 30 min, incubated 1 h with anti-FLAG (monoclonal antibody: Agilent; polyclonal antibody: Sigma), anti-HA (InvivoGen; San Diego, CA), anti-KDEL (StressGen Bioreagents; Victoria, BC, Canada), or anti-GM130 (BD Bioscience; Franklin Lakes, NJ) diluted 1:100 with 1% BSA in PBS, washed three times in PBS, and incubated 30 min with Alexa 488-conjugated anti-rabbit IgG antibodies or Alexa 594-conjugated anti-mouse IgG antibodies (Thermo Fisher) diluted in 1% BSA in PBS to 5 µg/mL. Coverslips were washed three times in PBS, mounted on glass slides using ProLong Gold antifade reagent (Thermo Fisher), and analyzed by fluorescence microscopy (model FV1000, Olympus; Tokyo, Japan).

2.9. Lipid analysis

Lipids (GSLs) were analyzed as described previously [30].

2.10. Cycloheximide chase

CHO-K1 cells stably expressing hM1-B4GN1-FLAG, hM1-B4GN1-FLAG R4/6/7S mutant, or hM2-B4GN1-FLAG, or co-expressing hM1-B4GN1-FLAG and hM2-B4GN1-HA, were cultured in Ham's F-12 with or without 50 µg/mL cycloheximide for 5 h at 37 °C. Total lysates and integral membrane protein fraction were prepared as described above.

3. Results

3.1. New mRNA variant of human and mouse B4GalNAcT1 (GM2/GD2/GA2 synthase) that produces an isoform with long cytoplasmic tail

Many glycosyltransferases are type II membrane proteins that have a short cytoplasmic tail (2–17 aa) and a luminal catalytic domain. In contrast, mouse ST3G5 includes an M1-ST3G5 isoform having a long (69 aa) cytoplasmic tail. M1-ST3G5 is localized mainly in the ER, and the cytoplasmic tail contains R-based motif, a retrograde transport signal [26]. To clarify the biological significance of isoform production for lipid-glycosyltransferases, we examined B4GN1, which catalyzes GalNAc transfer to GM3, GD3, or LacCer, for possible production of isoforms having distinctive NH₂-terminal cytoplasmic tail lengths. Isoforms of ST3G5 are produced by leaky scanning from several transcriptional variants [26]. Human B4GN1 (hB4GN1) transcripts are classified into three variants (1a, 1b, 1c) according to the position of transcription initiation (Exon 1a, 1b, 1c) (Fig. 2A) [31]. Because these three exons do not contain an initiation codon, hB4GN1 is translated from a common initiation codon (M2) of Exon 2 in these transcripts, indicating that hB4GN1 expresses only one isoform. We searched for an EST clone containing the sequence upstream of M2, using the NCBI-BLAST program (<http://blast.ncbi.nlm.nih.gov/Blast.cgi>). After eliminating clones that included the same sequence as variants 1a, 1b, and 1c, we identified four EST clones (DC30908, DC341828, DC400781, DC302562) that included Exon 2 extending to

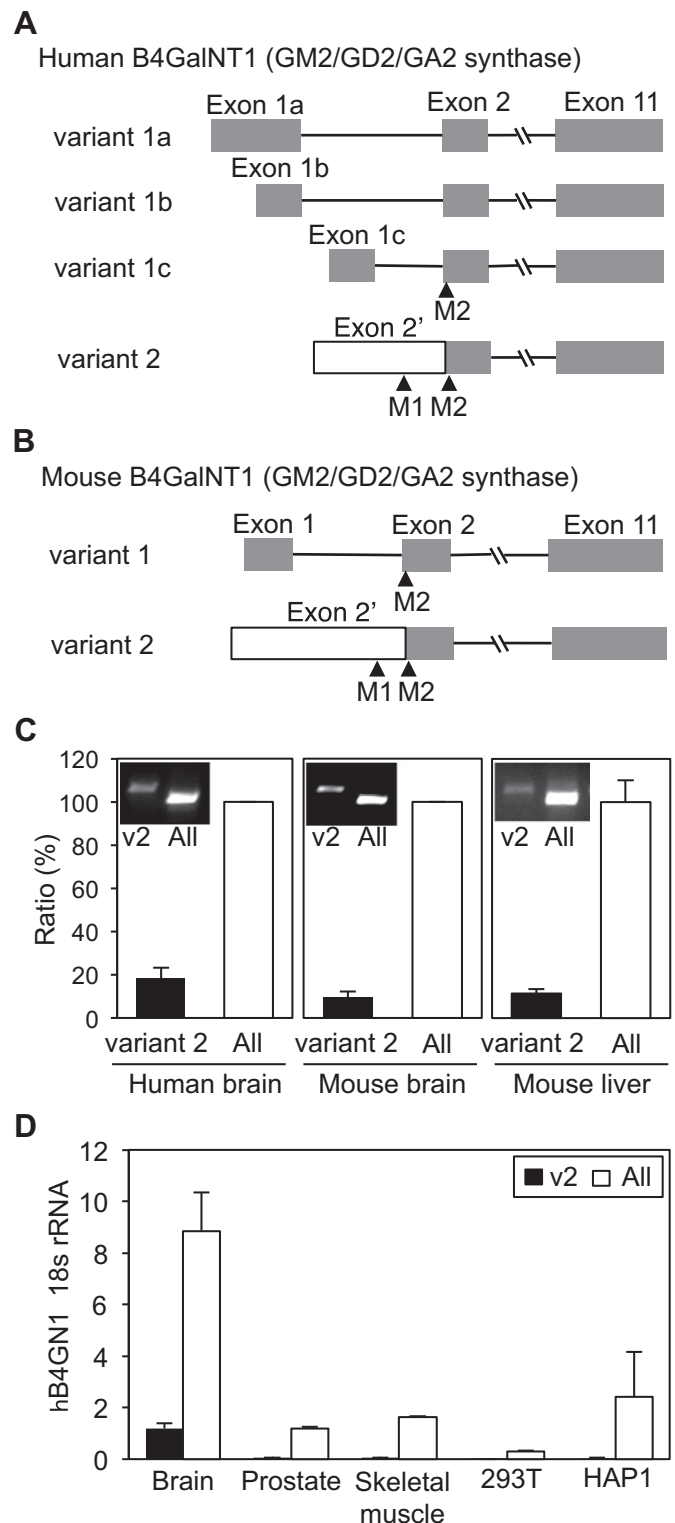


Fig. 2. New transcriptional variant and quantitation of human and mouse B4GN1. (A and B) Structures of human (A) and mouse (B) B4GN1 genes and their mRNA variants. Gray boxes: exons. Horizontal lines: introns. M1 and M2: initiation codons. The accession number of human and mouse B4GN1 variant 2 are LC273521 and LC273292, respectively. (C) mRNA expression of B4GN1 variants in human and mouse tissues. Variant 2 and total variants were amplified by semi-quantitative RT-PCR using brain (human, mouse) and liver (mouse) tissues. Expression levels of variant 2 are shown as percentage of level of total variants (defined as 100%). (D) Quantitative analyses of hB4GN1 transcripts in various tissues and cell lines by real-time PCR. Expression levels of variant 2 and total variant were normalized relative to 18S rRNA transcript.

the 5'-upstream side (termed Exon 2'; Figs. 2A and S1). These clones start from a position between Exon 1a/1b and 1c, or between 1c and 2 (dots in Fig. S1). We termed this new transcript variant 2 (Fig. 2A). Notably, the initiation codon (M1) is present in the sequence upstream of M2 in Exon 2'. These findings indicate that the new hB4GN1 isoform having a long NH₂-terminal cytoplasmic tail is translated from variant 2.

The gene structure of mouse B4GN1 (mB4GN1) was reported as variant 1 (Fig. 2B; M2 = initiation codon) [17,32]. Using the same method, we searched for new mRNA variants of mB4GN1, and extracted 25 EST clones similar to hB4GN1 variant 2 (Fig. S2). Many of these clones start in the region between Exons 1 and 2, suggesting that this region is not spliced. Again, we termed the new transcript variant 2 (Fig. 2B). Variant 2 includes a new initiation codon (M1) upstream of M2; therefore, a new isoform is presumably translated.

To determine expression levels of variant 2, we performed semi-quantitative RT-PCR using total RNAs of brain (human and mouse) and liver (mouse) tissues expressing GM2 (Fig. 2C). Forward and reverse primers were designed to amplify all variants, or only variant 2. Expression level of variant 2 as a percentage of the value for all variants was $18 \pm 5.0\%$ for human brain, $9.4 \pm 2.7\%$ for mouse brain, and $11.2 \pm 2.3\%$ for mouse liver. Variant 2 was a minor but detectable transcript in brain and liver tissues. Next, copy numbers of B4GN1 variant 2 and all variants for human brain, prostate, skeletal muscle, 293 T cells, and HAP1 cells were determined by real-time PCR. 293 T (derived from human embryonic kidney) and HAP1 cells [29] express GM2. In brain tissues, copy numbers of B4GN1 variant 2 and all variants per 10^6 copies of 18 S rRNA were 1.2 ± 0.2 and 8.9 ± 1.5 , and the ratio of variant 2 to all variants was $13.5 \pm 0.44\%$, similar to the value obtained by semi-quantitative RT-PCR. In other tissues and cell lines, gene expression levels of hB4GN1 were much lower than in brain tissue, and ratios of variant 2 to all variants were also low (prostate: $4.3 \pm 0.5\%$, skeletal muscle: $3.2 \pm 0.4\%$, 293 T: $1.0 \pm 0.2\%$, Hap1: $1.1 \pm 0.07\%$). We compared aa sequences of the isoforms translated from variant 2 of human and mouse tissues, termed hM1-B4GN1 and mM1-B4GN1 (Fig. 3). NH₂-terminal length of hM1-B4GN1 was 41 aa longer than that of mM1-B4GN1. Each of these isoforms had R-based motifs in the long cytoplasmic tail, similarly to M1-ST3G5 (Fig. 3, underlining).

We performed 5'-RACE analysis using cDNA of human and mouse brain tissues in an attempt to clarify transcriptional start sites (TSSs) of B4GN1 variant 2. Unfortunately, the sequence between Exons 1c and 2 was very similar to other genome sequences, and 5'-terminal sequences of variant 2 were therefore not amplified specifically. Use of total RNA of human cell lines 293 T and HAP1 as templates gave the same results. We were thus unable to identify TSSs of human variant 2. However, we succeeded in identifying the TSSs of mB4GN1 variants (Fig. S2). The 5'-termini of all clones analyzed in this study started

from Exon 1, and there were numerous TSSs (Fig. S2, black triangles). These findings indicate that variant 2 of mB4GN1 is a splicing variant in which the intron between Exons 1 and 2 is not removed. The result of 5'-RACE analysis of mB4GN1 transcripts suggest that hB4GN1 variant 2 is also a splicing variant in which the intron between Exons 1c and 2 is not removed.

3.2. Analysis of leaky scanning in new B4GN1 mRNA variant 2

The first AUG codon is usually recognized as an initiation codon by the ribosome. However, in some cases (known as "leaky scanning systems") the first AUG codon is skipped, and a downstream AUG codon is recognized as an initiation codon [33]. In mammals, the optimal context (motif) for recognition of an AUG start codon is GCCRCAUGG. Within this motif, the purine nucleotide (R = A or G) in position -3 is the most highly conserved and most functionally important. In mST3G5 mRNA, leaky scanning occurs even though the sequence is CCUAGCAUGC [26], and does not stop completely even when the sequence is changed to GCCACCAUGG. We investigated whether leaky scanning occurs in B4GN1 mRNA variant 2. The sequences in hB4GN1 and mB4GN1 mRNA variant 2 were ACCGAGAUGT and GCCGAGAUGG (Fig. 4A). In both these variants, the nucleotide in position -3 is G; this is presumably sufficient for recognition of AUG. To compare the molecular masses of M1-B4GN1 and M2-B4GN1, we constructed plasmids in which a Kozak sequence (ks; CACC) was inserted before M1 or M2 of



Fig. 3. Comparison of aa sequence of NH₂-terminal cytoplasmic regions of human and mouse B4GN1. Alignments were generated by the ClustalW program (DNA Data Bank of Japan). Black boxes: identical residues. Gray boxes: aa similarities. Underlining: Arginine (R)-based motif. TM: transmembrane region. M1 and M2: initiation codons.

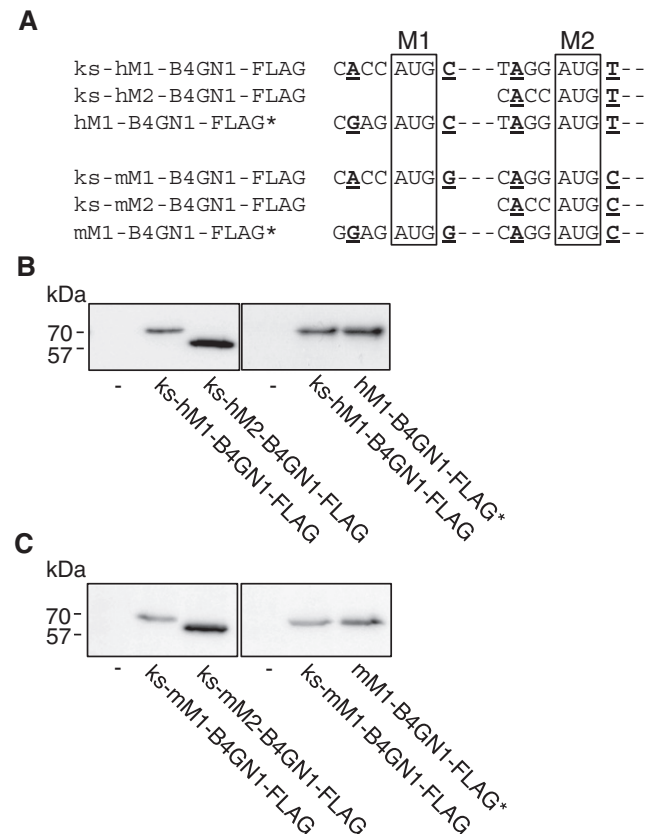


Fig. 4. Analyses of leaky scanning of human and mouse B4GN1. (A) Nucleotide sequences of human and mouse B4GN1 (hB4GN1 and mB4GN1) used. hB4GN1 or mB4GN1 was fused with FLAG tag at C-terminus. Kozak sequence (ks; CACC) was inserted before M1 or M2 (initiation codon) of B4GN1 (ks-hM1-B4GN1-FLAG, ks-hM2-B4GN1-FLAG, ks-mM1-B4GN1-FLAG, and ks-mM2-B4GN1-FLAG). hM1- and mM1-B4GN1-FLAG*: the sequence just before M1 is the mRNA sequence of variant 2. (B and C) CHO-K1 cells were transiently transfected with pcDNA3 vector (–) or a plasmid encoding hM1-B4GN1-FLAG, hM2-B4GN1-FLAG, hM1-B4GN1-FLAG*, mM1-B4GN1-FLAG, mM2-B4GN1-FLAG, or mM1-B4GN1-FLAG*. Integral membrane protein fractions were prepared, treated with PNGase F, and analyzed by immunoblotting with anti-FLAG antibodies.

B4GN1 (ks-hM1-B4GN1-FLAG, ks-hM2-B4GN1-FLAG, ks-mM1-B4GN1-FLAG, ks-mM2-B4GN1-FLAG), and transiently transfected these plasmids into CHO-K1 cells. Integral membrane protein fractions were prepared and immunoblotted with anti-FLAG antibodies. Human and mouse B4GN1s have N-glycans [34]; we therefore treated integral fraction samples with peptide: N-glycosidase F (PNGase F) to remove N-glycans before immunoblotting. hM1-, hM2-, mM1-, and mM2-B4GN1-FLAG proteins were detected respectively as 57.1, 49.6, 52.6, and 51.0 kDa bands (Fig. 4B,C). We next replaced the Kozak sequences of ks-hM1- and ks-mM1-B4GN1-FLAG with the original mRNA sequences (human: CGAG; mouse: GGAG), generated hM1- and mM1-B4GN1-FLAG* (Fig. 4A), and transiently transfected the plasmids into CHO-K1 cells. Integral membrane protein fractions were prepared, treated with PNGase F, and immunoblotted with anti-FLAG antibodies. hM1- and mM1-B4GN1-FLAG* bands migrated to the same positions as did ks-hM1- and ks-mM1-B4GN1-FLAG bands (Fig. 4B,C). Taken together, these findings indicate that human and mouse M2-B4GN1 isoforms are not produced from B4GN1 mRNA variant 2 by leaky scanning.

3.3. Retrograde transport of M1-B4GN1(N)-GFP chimeric proteins by R-based motif

Human and mouse B4GN1s have RR and RXR sequences (R-based motifs) in the NH₂-terminal cytoplasmic region (Fig. 3, underlining). To function as retrograde transport signals, R-based motifs must be positioned distally from a lipid bilayer [28]. To assess the possible function of the above sequences as R-based motifs, we transiently transfected CHO-K1 cells with fusion proteins for the NH₂-terminus of hM1-, hM2-, mM1-, or mM2-B4GN1 containing the transmembrane region and green fluorescent protein (GFP) (hM1-B4GN1(N)-GFP, hM2-B4GN1(N)-GFP, mM1-B4GN1(N)-GFP, mM2-B4GN1(N)-GFP) (Fig. 5A). Integral membrane protein fractions were prepared and immunoblotted with anti-GFP antibodies. hM1-B4GN1(N)-GFP, hM2-B4GN1(N)-GFP, mM1-B4GN1(N)-GFP, and mM2-B4GN1(N)-GFP chimeric proteins (the predicted molecular mass is 39.5 kDa, 31.5 kDa, 37.9 kDa and 33.6 kDa) were detected as 40 kDa, 28 kDa, 38 kDa, and 30 kDa bands, respectively (Fig. 5B). Some extra bands were detected under the target bands and would be degradation products in lysosome.

These chimeric proteins were observed by fluorescence microscopy (Figs. 5C, D, S3, S4, S5). Cells were fixed, permeabilized, stained with anti-GFP antibodies, and incubated with Alexa 488-conjugated anti-chicken IgY. hM1- and mM1-B4GN1(N)-GFP displayed a reticular immunofluorescence pattern in the perinuclear and cytosolic regions. This pattern was attributable to ER localization of hM1- and mM1-B4GN1(N)-GFP because it could be superimposed on the ER pattern produced by an antibody against ER retention signal KDEL (Figs. S3, S5). In contrast, hM2- and mM2-B4GN1(N)-GFP were localized in compact juxtanuclear reticulum. hM2- and mM2-B4GN1(N)-GFP were partially co-localized with GM130, a Golgi marker protein (Figs. S4, S5). These findings suggested that R-based motifs of the M1-B4GN1 NH₂-terminus function as retrograde transport signals.

To further investigate this possibility, we generated hM1-B4GN1(N)-GFP R4S, R6S, R7S, and R6/7S mutants by site-directed mutagenesis, and examined their subcellular localization (Figs. 5C, S3). These mutants were localized in both the Golgi and ER ("Golgi/ER" in Fig. 5C), or the Golgi only. We generated a hM1-B4GN1(N)-GFP R4/6/7S mutant and observed its subcellular localization. It was localized entirely in the Golgi, indicating that the ⁴R⁶R⁷R sequence is important for ER targeting in hM1-B4GN1(N)-GFP. Finally, we generated mM1-B4GN1(N)-GFP R8S, R11S, R12S, R13S, R14S, and R11/12/13/14S mutants and examined their subcellular localization (Figs. 5D, S5). The R11S, R12S, R13S, and R14S mutants were localized mainly in the Golgi, the R8S mutant was localized in the ER, and the R11/12/13/14S mutant was localized completely in the Golgi. These findings indicate that the ¹¹R¹²R¹³R¹⁴R sequence is necessary for localization of mM1-B4GN1(N)-GFP in the ER, and that the R-based motifs located on the NH₂-terminal

cytoplasmic tail of hM1- and mM1-B4GN1(N)-GFP function collectively as a retrograde transport signal.

3.4. Subcellular localization and enzyme activity of B4GN1 full-length

To examine the possibility that M1-B4GN1 full-length is also localized in the ER by R-based motifs, we used a lentivirus expression system to express hM1-B4GN1-FLAG and hM2-B4GN1-HA in CHO-K1 cells, and applied indirect immunofluorescence microscopy with anti-FLAG and anti-HA antibodies to evaluate subcellular localization (Figs. 6A, S6A). hM1-B4GN1-FLAG staining pattern was partially consistent with that of the ER (KDEL) and the Golgi (GM130). Because hM1-B4GN1-FLAG R4/6/7S mutant was localized completely in the Golgi, a part of hM1-B4GN1-FLAG was localized in the ER by R-based motif. In contrast, hM2-B4GN1-HA, which does not contain R-based motif in the cytoplasmic tail, was localized in the Golgi. M1-ST3G5, which has R-based motif, is localized mainly in the ER [26], suggesting that retrograde transport of hM1-B4GN1-FLAG does not occur efficiently. We next transfected cells with mM1-B4GN1-FLAG and mM2-B4GN1-HA, and subjected them to anti-FLAG and anti-HA antibody staining (Figs. 6B, S6B). mM1-B4GN1-FLAG was localized in both the ER and Golgi, whereas mM2-B4GN1-HA and mM1-B4GN1-FLAG R11/12/13/14S mutant were localized only in the Golgi. These findings indicate that the R-based motif of M1-B4GN1 full-length functions in part as a retrograde transport signal. In addition, we also visualized the localization of non-tagged forms of hM1-B4GN1 and mM2-B4GN1 using anti-B4GN1 antibody (9535Ex_ProteinA), which was raised against the luminal domain of mouse B4GN1 (504 aa). The localization patterns of the non-tagged forms were quite similar to those of mM1-B4GN1-FLAG and mM2-B4GN1-HA, indicating that the epitope tags do not affect the subcellular localization of B4GN1 (Fig. S7).

We compared *in vivo* enzyme activity of hM1- vs. hM2-B4GN1 in CHO-K1 cells, which express primarily GM3 ganglioside. Expression levels of hM1- and hM2-B4GN1-FLAG were nearly identical (Fig. 7A). To evaluate GSL composition, we separated acidic and neutral lipid fractions from total lipid extracts using DEAE-Sephadex A-25 column, and analyzed the fractions by TLC. Presence of hM1- or hM2-B4GN1-FLAG in the cells resulted in enhanced expression of GM2 and GD1a in acidic fraction, and reduced expression of LacCer and Gb4 in neutral fraction (Fig. 7B). No differences in lipid composition were observed, indicating that hM1- and hM2-B4GN1 display similar *in vivo* enzyme activities when overexpressed.

3.5. Effects of hM1-/hM2-B4GN1 heterodimer formation on intracellular localization and stability

The observed expression level of mRNA variant 2 in human and mouse tissues (Fig. 2C, D) suggests that M1-B4GN1 is a minor isoform. M1- and M2-B4GN1 isoforms presumably coexist in tissues and cells. M2-B4GN1 isoform was reported to form a dimer *via* disulfide bond (⁸⁰C and ⁸²C) on the luminal side [35], suggesting that B4GN1 may form not only M1/M1 or M2/M2 homodimers but also a M1/M2 heterodimer. To assess this possibility in our CHO-K1 cells, we co-expressed hM1-B4GN1-FLAG (hM1-FLAG) (predicted molecular mass 68.2 kDa) and hM2-B4GN1-HA (hM2-HA) (predicted molecular mass 60.2 kDa) using a lentivirus expression system. Integral membrane protein fractions were prepared with or without β-mercaptoethanol (βMe), treated with PNGase F, and immunoblotted with anti-FLAG and anti-HA antibodies (Fig. 8A). In CHO-K1/hM1-FLAG and CHO-K1/hM2-HA cells, M1/M1 and M2/M2 homodimers were detected respectively as ~150 kDa and ~125 kDa bands, without βMe. In cells co-expressing M1 and M2 isoforms, M1/M2 heterodimer was detected as an ~130 kDa band. A faint hM1-FLAG band was detected in the same position as M1/M2 heterodimer under βMe(–) condition when cells expressed only hM1-FLAG. hM1-FLAG was a single band under βMe(+) condition, indicating that the NH₂-terminus of M1-FLAG was

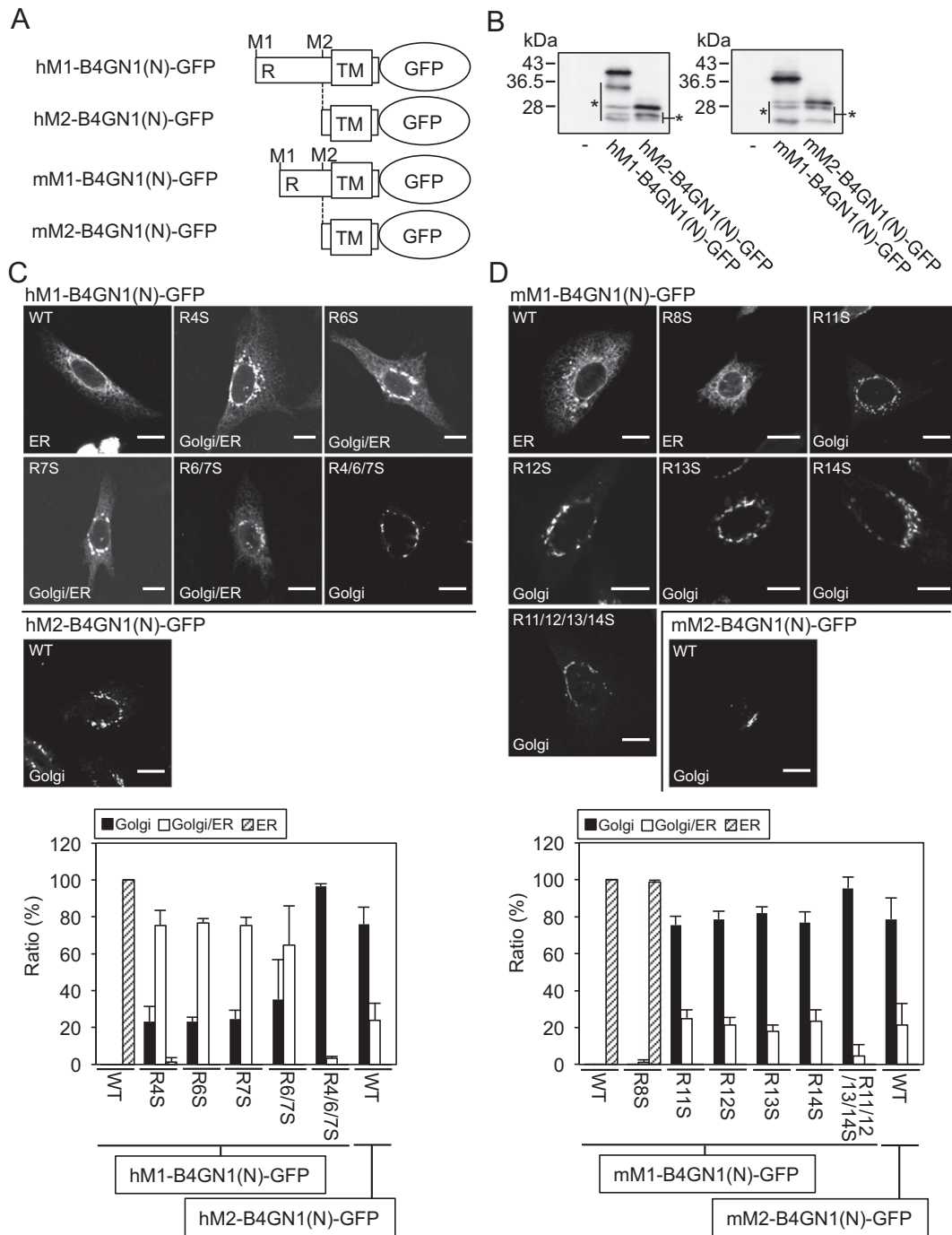


Fig. 5. ER targeting of M1-B4GN1(N)-GFP by R-based motif of cytoplasmic region. (A) Structure of cDNA constructs used. Each constructed plasmid encoded a fusion protein of the NH₂-terminus of hM1-B4GN1, hM2-B4GN1, mM1-B4GN1, or mM2-B4GN1 containing the transmembrane region, and GFP (hM1-B4GN1(N)-GFP, hM2-B4GN1(N)-GFP, mM1-B4GN1(N)-GFP, and mM2-B4GN1(N)-GFP). TM: transmembrane region. M1 and M2: initiation codons. R: Arginine (R)-based motif. (B) CHO-K1 cells were transiently transfected with pcDNA3 vector (–), hM1-B4GN1(N)-GFP, hM2-B4GN1(N)-GFP, mM1-B4GN1(N)-GFP, or mM2-B4GN1(N)-GFP. Integral membrane protein fractions were prepared and analyzed by immunoblotting with anti-GFP antibodies. The asterisk indicates the putative degraded forms of the respective proteins. (C and D) CHO-K1 cells were transiently transfected with M1-B4GN1(N)-GFP wild type (WT), M2-B4GN1(N)-GFP WT, or M1-B4GN1(N)-GFP mutants, in which the arginine (R) of the R-based motif was substituted with serine (S) (C: human; D: mouse). Cells were fixed, permeabilized with 0.5% Triton X-100 in PBS, stained for 1 h with anti-GFP antibodies, incubated with Alexa 488-conjugated anti-chicken IgY, and visualized by confocal laser-scanning microscopy. For co-localization studies, cells were incubated with antibodies against GM130 (a cis Golgi marker) or KDEL (an ER marker) for 1 h, and then with Alexa 594-conjugated anti-mouse IgG for 30 min. Localization patterns (Golgi, Golgi/ER, ER) were quantified by cell counting, and quantitative data were expressed as mean ± SD from three or more independent counts. Bar: 10 μm.

partially uncleaved. We therefore speculated that a small amount of M1/M1 homodimer was not fully denatured by SDS under βMe(–) condition, and that apparent molecular weight was less than ~150 kDa. The amount of M1/M2 heterodimer was comparable to those of M1/M1 or M2/M2 homodimers; *i.e.*, efficiency of heterodimer

formation was similar to that of homodimer formation when isoform expression levels were equal.

Subcellular localization of hM1-FLAG and hM2-HA was evaluated in cells co-expressing these isoforms (Fig. 8B). hM1-FLAG was localized in both the Golgi and ER, whereas hM2-HA was localized only in the Golgi.

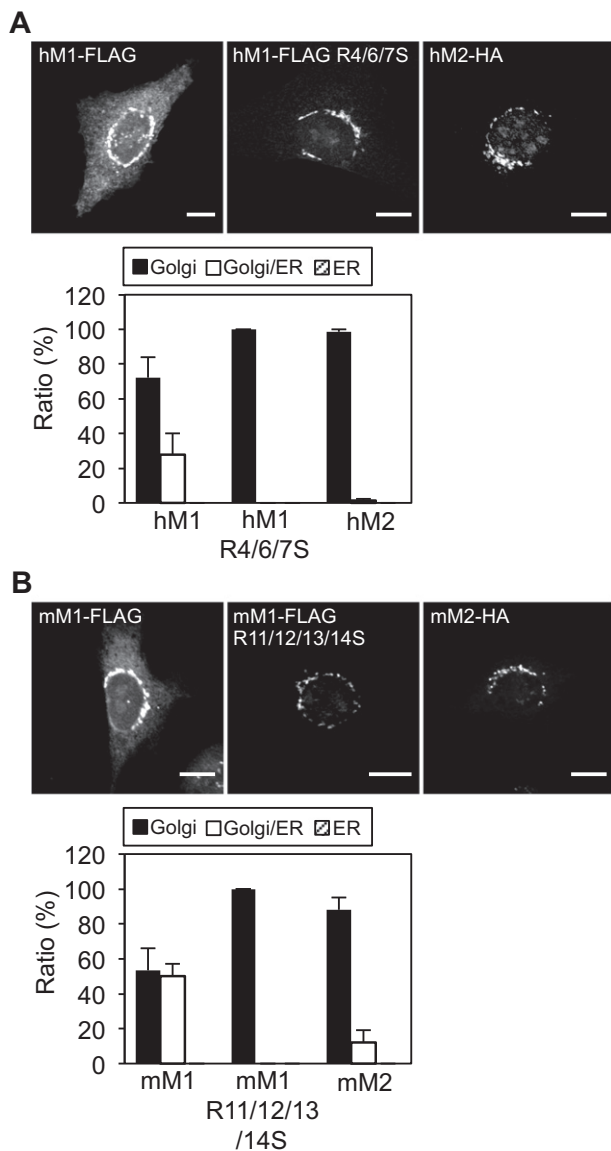


Fig. 6. Subcellular localization of M1-B4GN1 and M2-B4GN1 full-length. CHO-K1 cells were stably transfected with hM1-B4GN1-FLAG (hM1-FLAG), hM1-B4GN1-FLAG R4/6/7S mutant, hM2-B4GN1-HA (hM2-HA), mM1-B4GN1-FLAG (mM1-FLAG), mM1-B4GN1-FLAG R11/12/13/14S mutant, or mM2-B4GN1-HA (mM2-HA) using a lentivirus expression system (A: human; B: mouse). Cells were fixed, permeabilized with 0.5% SDS in PBS, stained with anti-FLAG or anti-HA antibodies and Alexa 488-conjugated anti-rabbit IgG, and visualized by confocal laser-scanning microscopy. For co-localization studies, cells were incubated with anti-GM130 or anti-KDEL antibodies for 1 h, and then with Alexa 594-conjugated anti-mouse IgG for 30 min. Localization patterns (Golgi, Golgi/ER, ER) were quantified by cell counting, and quantitative data were expressed as mean \pm SD from three or more independent counts. Bar: 10 μ m.

Similar localization patterns were observed for cells expressing only one isoform (Fig. S8), suggesting that retrograde transport of M1/M2 heterodimer did not occur. Partial ER localization of M1/M1 homodimer was not affected by appearance of M1/M2 heterodimer.

To investigate the effect of M1/M2 heterodimer formation on stability of M1- and M2-B4GN1 isoforms, cells expressing hM1-FLAG/hM2-HA, hM1-FLAG, or hM2-HA were cultured for 5 h with or without cycloheximide (CHX), an inhibitor of protein synthesis. Integral membrane protein fractions were prepared, treated with PNGase F, and immunoblotted with anti-FLAG or anti-HA antibodies (Fig. 8C, D). When a single isoform was expressed, expression levels of hM1-FLAG and hM2-HA in CHX-treated cells were respectively $58 \pm 12\%$ and $30 \pm 11\%$ of levels in untreated cells. In contrast, when the isoforms were

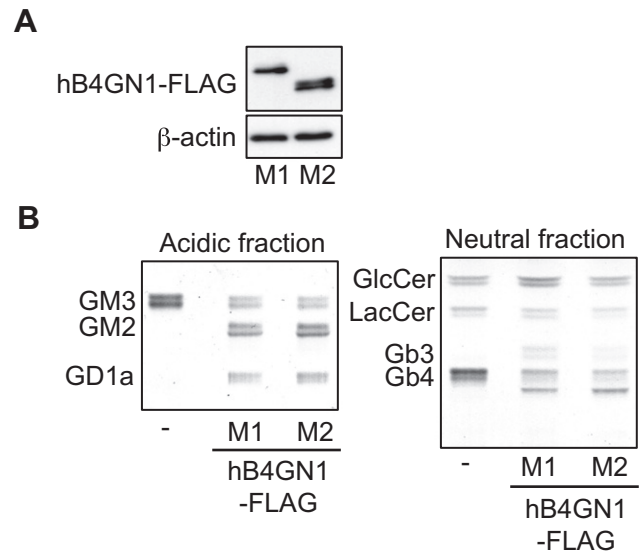


Fig. 7. *In vivo* enzyme activities of hM1- and hM2-B4GN1. (A) Total lysates and integral membrane protein fractions were prepared from CHO-K1 cells stably expressing hM1-B4GN1-FLAG (M1) and hM2-B4GN1-FLAG (M2), treated with PNGase F, and analyzed by immunoblotting with anti-FLAG antibodies (for integral membrane protein fractions) or anti- β -actin antibodies (for total lysates). (B) GSLs (acidic and neutral fractions) extracted from CHO-K1 (–), CHO-K1/hM1-B4GN1 (M1), or CHO-K1/hM2-B4GN1 (M2) cells, corresponding to 2 mg protein, were separated on TLC plates and stained with orcinol sulfuric acid reagent.

co-expressed, expression levels of hM1-FLAG and hM2-HA in treated cells were $51 \pm 17\%$ and $55 \pm 6\%$ of levels in untreated cells. These findings indicate that M2-HA stability is slightly enhanced by co-expression with M1-FLAG. Because subcellular localization of M2-HA was unaffected by M1-FLAG co-expression, the increase in M2-HA stability was most likely due to prolongation of Golgi retention.

4. Discussion

To elucidate the biological significance of lipid-glycosyltransferase isoform production, we searched for mRNA variants encoding new isoforms. An mRNA variant was found that encodes a new B4GN1 isoform (M1-B4GN1) that catalyzes synthesis of GM2, GD2, and GA2 in mice and humans (Fig. 2). The new isoform has NH₂-terminal length much longer than that of previously known isoform M2-B4GN1 (Fig. 3). Human and mouse M1-B4GN1 isoforms (hM1-B4GN1, mM1-B4GN1) have respective lengths 81 and 40 aa, whereas hM2-B4GN1 and mM2-B4GN1 both have length 6 aa (Fig. 3). NH₂-terminal aa sequences of hM1- and mM1-B4GN1 have low similarity. On the other hand, both isoforms have R-based motifs, and hM1- and mM1-B4GN1(N)-GFP chimeric proteins are localized in the ER. R-based motifs function as retrograde transport signals when positioned distally from a lipid bilayer [28]. The consensus sequences of R-based motifs in mM1-ST3G5 are RR, RXXXXR, and RXXXXXR. We use the term “functional distance” to describe the space essential for an R-based motif to function as retrograde transport signal, and define this distance as the number of aa residues from R to a lipid bilayer. Functional distances of RR, RXXXXR, and RXXXXXR in mM1-ST3G5(N)-GFP are 30, 45, and 53 aa [26]. The R11S, R12S, R13S, and R14S single mutants in mM1-B4GN1(N)-GFP are localized mainly in the Golgi, indicating that the four R residues (¹¹R¹²R¹³R¹⁴R), but not RRR, RXR, or RR sequence, are essential for function as R-based motif (Figs. 5D, S4). The distance between the ¹¹R¹²R¹³R¹⁴R sequence and a lipid bilayer is 27 aa; this is likely insufficient for RRR, RXR, or RR sequence to function. The position of ⁵¹RX⁵³R sequence in hM1-B4GN1 is homologous to that in mM1-B4GN1 (Fig. 3). Again, however, this sequence likely cannot function as a retrograde transport signal because of the short distance (29 aa). hM1-

B4GN1 has $^4\text{RX}^6\text{R}^7\text{R}$ sequence in addition to $^{51}\text{RX}^{53}\text{R}$ sequence, and the former is located 75 aa from a lipid bilayer. Because the hM1-B4GN1(N)-GFP R4/6/7S mutant is localized completely in the Golgi, the $^4\text{RX}^6\text{R}^7\text{R}$ sequence clearly functions as an ER targeting signal. The hM1-B4GN1(N)-GFP R4S, R6S, and R7S mutants are localized in both the ER and Golgi, indicating that the RR, RXR, and RXXR motifs function in part as signal sequences (Figs. 5C, S3). The hM1-B4GN1(N)-GFP R6/7S mutant is also localized in both the ER and Golgi (Figs. 5C, S3),

suggesting that only the ^4R sequence functions as signal. A single R has never been shown to be sufficient to function as a signal sequence. Another basic aa close to the R-based motif, such as ^8K or ^{12}R , may also function as a retrograde transport signal.

Expression levels of lipid-glycosyltransferases are extremely low, making it difficult to detect endogenous proteins. We previously detected endogenous ST3G5 protein by immunoprecipitation and immunoblotting, using specific anti-ST3G5 polyclonal antibody and brain tissues of *St3gal5*^{+/+} and *St3gal5*^{-/-} mice [26]. Similarly, in an attempt to detect endogenous B4GN1 protein, microsome fractions were prepared from liver or brain tissues of *B4galnt1*^{+/+} and *B4galnt1*^{-/-} mice and treated with PNGase F. The fractions were analyzed by immunoblotting using anti-B4GN1 antibody (ab135902), which can recognize overexpressed non-tagged B4GN1 proteins in CHO-K1 cells (Fig. S9A). But, we were unable to observe the bands of endogenous B4GN1 protein (Fig. S9C, E). Moreover, we concentrated B4GN1 proteins including in the microsome fraction of liver tissue by immunoprecipitation using anti-B4GN1 antibody (9535Ex_ProteinA) (Fig. S9D). Nevertheless, endogenous B4GN1 protein could not be detected. In addition, the non-tagged forms (mM1-B4GN1 and mM2-B4GN1) treated with PNGase F were detected as two bands by immunoblotting using anti-B4GN1 antibodies (9535Ex_ProteinA or ab135902) (Fig. S9A), whereas tagged forms of B4GN1 were detected as a single band by immunoblotting using anti-FLAG or anti-HA antibody (Figs. 4, 7, and 8). Since the predicted molecular masses of mM1-B4GN1 and mM2-B4GN1 are 63.4 kDa and 59.2 kDa, respectively, the upper bands in Fig. S9A are obviously high molecular masses. This may suggest that the two bands are due to the post-translational modifications, such as phosphorylations.

We examined subcellular localization, enzyme activity, and stability of overexpressed B4GN1 proteins. M1-B4GN1(N)-GFP chimeric protein was completely localized in the ER, whereas M1-B4GN1 full-length was partly localized in the Golgi. In view of the localization of M1-ST3G5 full-length and M1-ST3G5(N)-GFP chimeric protein in the ER [26], the efficiency of retrograde transport in M1-B4GN1 full-length may be lower than that in M1-ST3G5. COPI-coated vesicles including B-subcomplex (α -, β -, and ϵ -COP) and F-subcomplex (β -, δ -, γ -, and ζ -COP) are involved in retrograde transport from the Golgi to the ER [36]. R-based motif interacts with acidic aa of the pocket formed by β -COP and δ -COP in F-subcomplex [27]. Another retrograde transport signal, K(X)KXX motif, interacts with α -COP or β' -COP in B-subcomplex [37, 38]. Because F-subcomplex interacts with B-subcomplex [39], cargo proteins having R-based motifs are presumably close to those having K(X)KXX motifs when these proteins are packed into the same COPI-coated vesicle. It is therefore possible that the large luminal domains of these cargo proteins are responsible for steric hindrance between them. The molecular mass of GFPs, including M1-B4GN1(N)-GFP, is

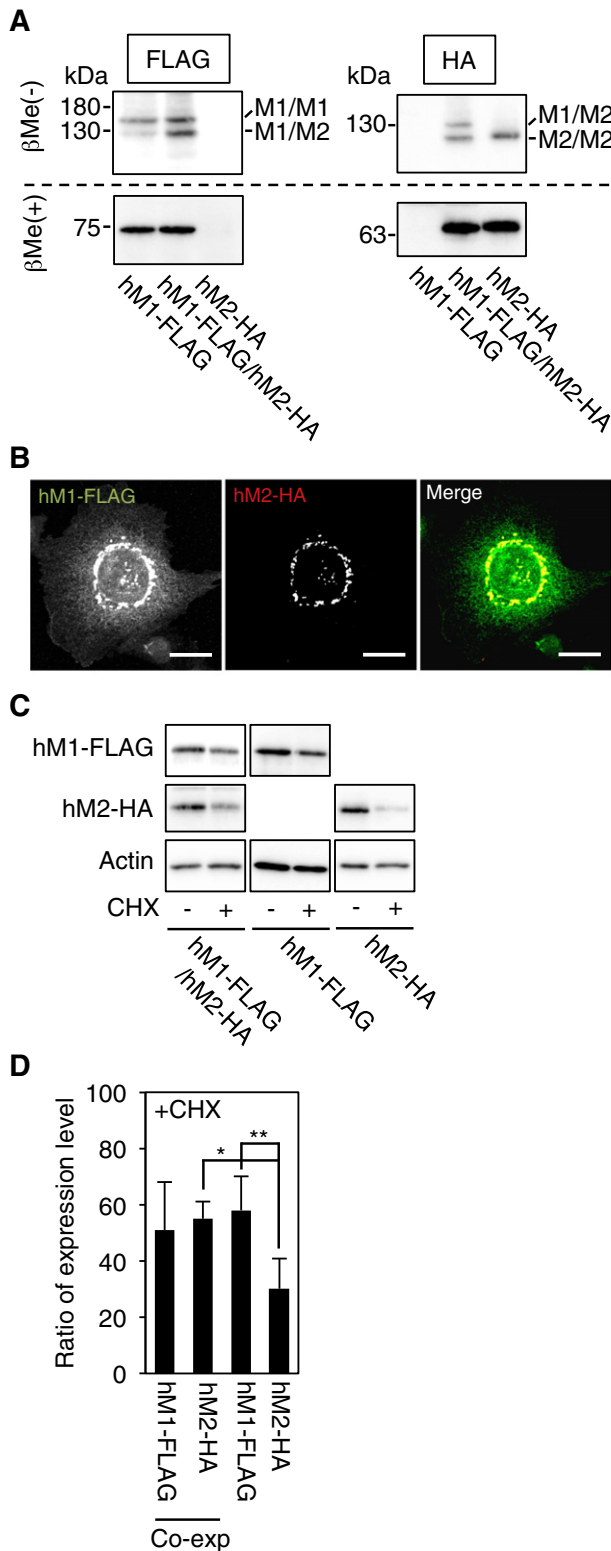


Fig. 8. Homodimer and heterodimer formation of hB4GN1 isoforms. (A) Integral membrane protein fractions were prepared from CHO-K1 cells stably expressing hM1-B4GN1-FLAG (hM1-FLAG) or hM2-B4GN1-HA (hM2-HA), or stably co-expressing hM1-B4GN1-FLAG and hM2-B4GN1-HA (CHO-K1/hM1-B4GN1-FLAG, CHO-K1/hM2-B4GN1-HA, or CHO-K1/hM1-B4GN1-FLAG/hM2-B4GN1-HA), and treated with (+) or without (−) βMe. Samples were treated with PNGase F and analyzed by immunoblotting with anti-FLAG (left panel) or anti-HA (right panel) antibodies. (B) CHO-K1/hM1-B4GN1-FLAG, CHO-K1/hM2-B4GN1-HA, and CHO-K1/hM1-B4GN1-FLAG/hM2-B4GN1-HA cells were fixed, permeabilized with 0.5% SDS in PBS, stained with anti-FLAG (rabbit polyclonal) and anti-HA (mouse monoclonal) antibodies, incubated with Alexa 488-conjugated anti-rabbit IgG and Alexa 594-conjugated anti-mouse IgG, and visualized by confocal laser-scanning microscopy. Right panel: merged images. Bar: 10 μm. (C and D) CHO-K1/hM1-B4GN1-FLAG, CHO-K1/hM2-B4GN1-HA, and CHO-K1/hM1-B4GN1-FLAG/hM2-B4GN1-HA cells were cultured with (+) or without (−) 50 μg/mL cycloheximide (CHX) for 5 h at 37 °C. C: Total lysates and integral membrane protein fractions were prepared, treated with PNGase F, and analyzed by immunoblotting with anti-FLAG (for integral membrane protein fractions), HA (for integral membrane protein fractions), or anti-β-actin antibodies (for total lysates). D: Expression levels of CHX (−) and (+) were quantified using the ImageJ software program. Expression levels of CHX (+) are expressed as ratio relative to corresponding CHX (−) level. Quantitative data are expressed as mean ± SD from three or more independent experiments. *P < 0.01; **P < 0.05. Co-exp.: co-expression with hM1-B4GN1-FLAG and hM2-B4GN1-HA.

26.8 kDa. The molecular mass of native luminal domains of M1-B4GN1 is 56.5 kDa or for practical purposes 113 kDa, because B4GN1 forms homodimers. Our findings suggest that cargo proteins having small luminal domains (e.g., GFP), in comparison with those having large luminal domains (e.g., B4GN1), are efficiently localized in the ER by R-based motif. We observed reduced retrograde transport of M1-B4GN1(N)-2GFP, which has two GFPs connected in tandem in the luminal domain (Fig. S10). The large luminal domain of B4GN1 may cause steric hindrance with other cargo proteins having K(X)KXX motif, resulting in reduced efficiency of retrograde transport.

M1-ST3G5 having R-based motif is localized mainly in the ER, leading to suppression of its GM3 synthesis activity *in vivo* [26]. M1-B4GN1 is partially localized in the ER; however, enzyme activity of hM1-B4GN1 *in vivo* was identical to that of hM2-B4GN1 (Figs. 6, 7B). To investigate *in vivo* enzyme activities of hM1- and hM2-B4GN1, we expressed these enzymes in CHO-K1 cells using a lentivirus expression system. Such systems generally lead to excessive protein expression in comparison with endogenous protein expression. If our experimental conditions resulted in saturation of hM1-B4GN1 in the Golgi, differences in subcellular localization between hM1- and hM2-B4GN1 may not have been reflected in their enzyme activity *in vivo*. In future study, we will establish knock-out cells expressing only M1- or M2-B4GN1 using CRISPR/Cas9 system, and clarify the contribution of M1- or M2-B4GN1 to ganglioside biosynthesis in the Golgi.

hM1-B4GN1 was stable relative to hM2-B4GN1 (Fig. 8C, D). hM1-B4GN1 stability was reduced by R4/6/7S mutation (data not shown), indicating that R-based motif is necessary for such stability. hM1-B4GN1 was partially localized in the ER, whereas hM2-B4GN1 was localized in the Golgi. hM1-B4GN1 stability can therefore be attributed simply to ER localization. In contrast, when hM2-B4GN1 was co-expressed with hM1-B4GN1, hM2-B4GN1 stability increased without ER localization (Fig. 8B, C, D). Under this condition, hM1-B4GN1 homodimer, hM2-B4GN1 homodimer, and hM1-B4GN1/hM2-B4GN1 heterodimer were all present, in a ratio of ~1:1:1 (Fig. 8A). Taken together, these findings suggest that hM1-B4GN1/hM2-B4GN1 heterodimer is not targeted to the ER by retrograde transport, but is more stable than hM2-B4GN1 homodimer (Fig. 9). ST3G5 and sphingomyelin synthase 2 are retained in the Golgi by retrograde transport between the Golgi cisternae during Golgi maturation [40–42]. The R-based motif (⁴RX⁶R⁷R sequence) of hM1-B4GN1 may promote retrograde transport between the Golgi cisternae or suppress export of heterodimer from the Golgi. Our findings indicate that Golgi retention, not ER localization, is a key rate-limiting step in hB4GN1 degradation.

Expression of mRNA variant 2 accounted for only 10–20% of total B4GN1 mRNA expression in human and mouse brain tissues (Fig. 2). Results of 5'-RACE analysis of mB4GN1 (Fig. 2S) suggested that hB4GN1 variant 2 may also be a splicing variant, and that expression level is regulated by a tissue-specific alternative splicing system. Because M1-B4GN1 is produced only from mRNA variant 2, expression level of M1-B4GN1 is substantially lower than that of M2-B4GN1. Most M1-B4GN1 therefore forms a heterodimer with M2-B4GN1, but not a homodimer with itself, indicating that M1-B4GN1 expression level determines overall stability of B4GN1 through prolongation of Golgi retention by R-based motif. mRNA variant 2 is more highly expressed in human brain tissue than in other tissues. Since brain tissue contains not only a-series but also b-series gangliosides, maintenance of B4GN1 protein level may be necessary to control both synthesis pathways. Results of the present and previous studies, taken together, indicate that coexistence of several B4GN1 isoforms, each with distinctive stability and subcellular localization, is essential for stable supplies and homeostasis of various GSLs.

Nomenclature

aa	amino acid(s)
B3GT4	UDP-Gal: βGlcNAc β1,3-galactosyltransferase polypeptide 4
B4GN1	B4GalNT1/β1,4 N-acetylgalactosaminyltransferase 1
Cer	ceramide

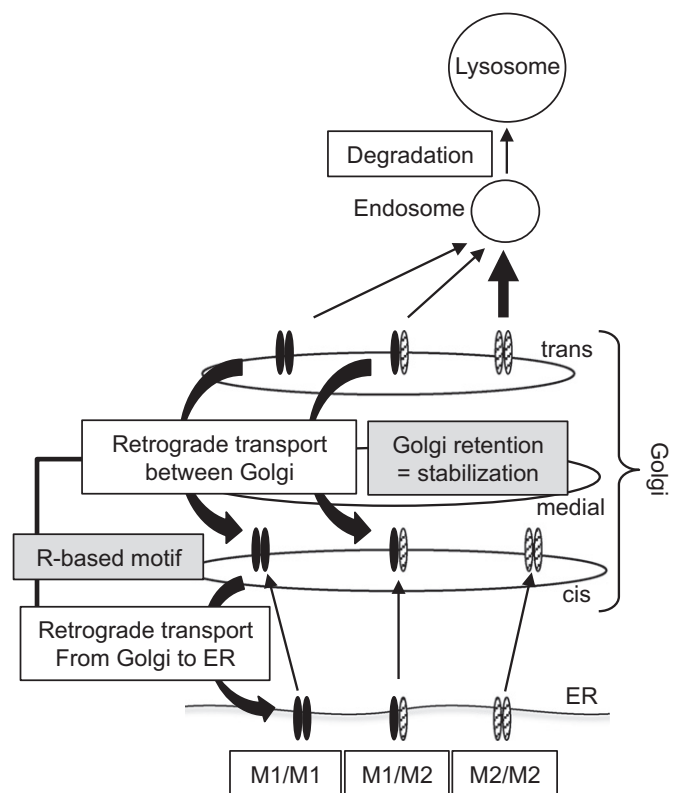


Fig. 9. Intracellular dynamics of B4GN1. M1/M1 homodimers are localized in the Golgi and partially localized in the ER. M1-B4GN1 has R-based motif in its cytoplasmic tail, which is involved in both retrograde transport from the Golgi to the ER and Golgi retention. M2/M2 homodimers without R-based motif are localized in the Golgi. M1/M2 heterodimers are also localized in the Golgi even though they have R-based motif. M1/M2 heterodimers are more stable than M2/M2 homodimers, but are not localized in the ER. This stability is due to prolongation of Golgi retention by R-based motif, as explained in Discussion.

CHX	cycloheximide
ER	endoplasmic reticulum
GalCer	galactosylceramide
GalNAc	N-acetylgalactosamine
GFP	green fluorescent protein
GalT I	β1,4-galactosyltransferase I
GlcAT-P	glucuronyl transferase
GlcCer	glucosylceramide
Golgi	Golgi apparatus
GSL	glycosphingolipid
ks	Kozak sequence
LacCer	lactosylceramide
O-FUT1	o-fucosyltransferase
	PNGase F peptide: N-glycosidase F
ST3G2	ST3 β-galactoside α2,3-sialyltransferase 2
ST3G5	ST3Gal5/ST3 β-galactoside α2,3-sialyltransferase 5
ST8S1	ST8 α-N-acetyl-neuraminide α2,8-sialyltransferase 1

Transparency document

The [Transparency document](#), associated with this article can be found, in online version.

Conflict of interest

We do not have any conflict of interest.

Acknowledgments

This study was supported by a Grant-in-Aid for Scientific Research (B) from MEXT (to J.I.) (16H04767), Mizutani Foundation for Glycoscience (J.I.), Naito Foundation (J.I.), ONO Medical Research Foundation (J.I.), Uehara Memorial Foundation (J.I.), and the MEXT-Supported Program for the Strategic Research Foundation at Private Universities (S1201031). The authors are grateful to Dr. S. Anderson for English editing of the manuscript.

Appendix A. Supplementary data

Supplementary data to this article can be found online at <http://dx.doi.org/10.1016/j.bbamem.2017.07.006>.

References

- [1] S.I. Hakomori, Glycosynaptic microdomains controlling tumor cell phenotype through alteration of cell growth, adhesion, and motility, *FEBS Lett.* 584 (2010) 1901–1906.
- [2] K. Handa, S.I. Hakomori, Carbohydrate to carbohydrate interaction in development process and cancer progression, *Glycoconj. J.* 29 (2012) 627–637.
- [3] A.R. Todeschini, S.I. Hakomori, Functional role of glycosphingolipids and gangliosides in control of cell adhesion, motility, and growth, through glycosynaptic microdomains, *Biochim. Biophys. Acta* 1780 (2008) 421–433.
- [4] J. Inokuchi, M. Nagafuku, I. Ohno, A. Suzuki, Distinct selectivity of gangliosides required for CD4(+) T and CD8(+) T cell activation, *Biochim. Biophys. Acta* 1851 (2015) 98–106.
- [5] K. Furukawa, Y. Ohmi, Y. Kondo, Y. Ohkawa, O. Tajima, K. Furukawa, Regulatory function of glycosphingolipids in the inflammation and degeneration, *Arch. Biochem. Biophys.* (2015).
- [6] M.L. Allende, R.L. Proia, Simplifying complexity: genetically rescuing glycosphingolipid synthesis pathways in mice to reveal function, *Glycoconj. J.* 31 (2014) 613–622.
- [7] S.I. Hakomori, Structure and function of glycosphingolipids and sphingolipids: recollections and future trends, *Biochim. Biophys. Acta* 1780 (2008) 325–346.
- [8] S. Tagami, J. Inokuchi, K. Kabayama, H. Yoshimura, F. Kitamura, S. Uemura, C. Ogawa, A. Ishii, M. Saito, Y. Ohtsuka, S. Sakaue, Y. Igarashi, Ganglioside GM3 participates in the pathological conditions of insulin resistance, *J. Biol. Chem.* 277 (2002) 3085–3092.
- [9] T. Yamashita, A. Hashimoto, M. Haluzik, H. Mizukami, S. Beck, A. Norton, M. Kono, S. Tsuji, J.L. Daniotti, N. Werth, R. Sandhoff, K. Sandhoff, R.L. Proia, Enhanced insulin sensitivity in mice lacking ganglioside GM3, *Proc. Natl. Acad. Sci. U. S. A.* 100 (2003) 3445–3449.
- [10] J.M. Aerts, R. Ottenhoff, A.S. Powlson, A. Grefhorst, M. van Eijk, P.F. Dubbelhuis, J. Aten, F. Kuipers, M.J. Serlie, T. Wennekes, J.K. Sethi, S. O'Rahilly, H.S. Overkleeft, Pharmacological inhibition of glucosylceramide synthase enhances insulin sensitivity, *Diabetes* 56 (2007) 1341–1349.
- [11] H. Zhao, M. Przybylska, I.H. Wu, J. Zhang, C. Siegel, S. Komarnitsky, N.S. Yew, S.H. Cheng, Inhibiting glycosphingolipid synthesis improves glycemic control and insulin sensitivity in animal models of type 2 diabetes, *Diabetes* 56 (2007) 1210–1218.
- [12] L. Boccuto, K. Aoki, H. Flanagan-Steet, C.F. Chen, X. Fan, F. Bartel, M. Petukh, A. Pittman, R. Saul, A. Chaubey, E. Alexov, M. Tiemeyer, R. Steet, C.E. Schwartz, A mutation in a ganglioside biosynthetic enzyme, ST3GAL5, results in salt and pepper syndrome, a neurocutaneous disorder with altered glycolipid and glycoprotein glycosylation, *Hum. Mol. Genet.* 23 (2014) 418–433.
- [13] K. Fragaki, S. Ait-El-Mkadem, A. Chausseuot, C. Gire, R. Mengual, L. Bonesso, M. Beneteau, J.E. Ricci, V. Desquiere-Dumas, V. Procaccio, A. Rotig, V. Paquis-Flucklinger, Refractory epilepsy and mitochondrial dysfunction due to GM3 synthase deficiency, *Eur. J. Hum. Genet.* 21 (2013) 528–534.
- [14] M.A. Simpson, H. Cross, C. Proukakis, D.A. Priestman, D.C. Neville, G. Reinkensmeier, H. Wang, M. Wiznitzer, K. Gurtz, A. Verganelaki, A. Pryde, M.A. Patton, R.A. Dwek, T.D. Butters, F.M. Platt, A.H. Crosby, Infantile-onset symptomatic epilepsy syndrome caused by a homozygous loss-of-function mutation of GM3 synthase, *Nat. Genet.* 36 (2004) 1225–1229.
- [15] J.S. Lee, Y. Yoo, B.C. Lim, K.J. Kim, J. Song, M. Choi, J.H. Chae, GM3 synthase deficiency due to ST3GAL5 variants in two Korean female siblings: masquerading as Rett syndrome-like phenotype, *Am. J. Med. Genet. A* 170 (2016) 2200–2205.
- [16] H. Wang, A. Bright, B. Xin, J.R. Bockoven, A.S. Paller, Cutaneous dyspigmentation in patients with ganglioside GM3 synthase deficiency, *Am. J. Med. Genet. A* 161a (2013) 875–879.
- [17] K. Takamiya, A. Yamamoto, K. Furukawa, S. Yamashiro, M. Shin, M. Okada, S. Fukumoto, M. Haraguchi, N. Takeda, K. Fujimura, M. Sakae, M. Kishikawa, H. Shiku, K. Furukawa, S. Aizawa, Mice with disrupted GM2/GD2 synthase gene lack complex gangliosides but exhibit only subtle defects in their nervous system, *Proc. Natl. Acad. Sci. U. S. A.* 93 (1996) 10662–10667.
- [18] K.A. Sheikh, J. Sun, Y. Liu, H. Kawai, T.O. Crawford, R.L. Proia, J.W. Griffin, R.L. Schnaar, Mice lacking complex gangliosides develop Wallerian degeneration and myelination defects, *Proc. Natl. Acad. Sci. U. S. A.* 96 (1999) 7532–7537.
- [19] S. Chiavegatto, J. Sun, R.J. Nelson, R.L. Schnaar, A functional role for complex gangliosides: motor deficits in GM2/GD2 synthase knockout mice, *Exp. Neurol.* 166 (2000) 227–234.
- [20] T.M. Villanueva-Cabello, R. Mollicone, M.E. Cruz-Munoz, D.V. Lopez-Guerrero, I. Martinez-Duncker, Activation of human naive Th cells increases surface expression of GD3 and induces neoeexpression of GD2 that colocalize with TCR clusters, *Glycobiology* 25 (2015) 1454–1464.
- [21] M. Nagafuku, K. Okuyama, Y. Onimaru, A. Suzuki, Y. Odagiri, T. Yamashita, K. Iwasaki, M. Fujiwara, M. Takayanagi, I. Ohno, J. Inokuchi, CD4 and CD8 T cells require different membrane gangliosides for activation, *Proc. Natl. Acad. Sci. U. S. A.* 109 (2012) E336–E342.
- [22] P.A. Wilkinson, M.A. Simpson, L. Bastaki, H. Patel, J.A. Reed, K. Kalidas, E. Samilchuk, R. Khan, T.T. Warner, A.H. Crosby, A new locus for autosomal recessive complicated hereditary spastic paraplegia (SPG26) maps to chromosome 12p11.1–12q14, *J. Med. Genet.* 42 (2005) 80–82.
- [23] A. Boukhris, R. Schule, J.L. Loureiro, C.M. Lourenco, E. Mundwiller, M.A. Gonzalez, P. Charles, J. Gauthier, I. Rekik, R.F. Acosta Lebrigio, M. Gausson, F. Spezziani, A. Ferbert, I. Feki, A. Caballero-Oteyza, A. Dionne-Laporte, M. Amri, A. Noreau, S. Forlani, V.T. Cruz, F. Mochel, P. Coutinho, P. Dion, C. Mhiri, L. Schols, J. Pouget, F. Darios, G.A. Rouleau, W. Marques Jr., A. Brice, A. Durr, S. Zuchner, G. Stevanin, Alteration of ganglioside biosynthesis responsible for complex hereditary spastic paraplegia, *Am. J. Hum. Genet.* 93 (2013) 118–123.
- [24] G.V. Harlalka, A. Lehman, B. Chioza, E.L. Baple, R. Maroofian, H. Cross, A. Sreekantan-Nair, D.A. Priestman, S. Al-Turki, M.E. McEntagart, C. Proukakis, L. Royle, R.P. Kozak, L. Bastaki, M. Patton, K. Wagner, R. Coblenz, J. Price, M. Mezei, K. Schlade-Bartusiak, F.M. Platt, M.E. Hurler, A.H. Crosby, Mutations in B4GALNT1 (GM2 synthase) underlie a new disorder of ganglioside biosynthesis, *Brain* 136 (2013) 3618–3624.
- [25] S.M. Wakil, D.M. Monies, K. Ramzan, S. Hagos, L. Bastaki, B.F. Meyer, S. Bohlega, Novel B4GALNT1 mutations in a complicated form of hereditary spastic paraplegia, *Clin. Genet.* 86 (2014) 500–501.
- [26] S. Uemura, S. Yoshida, F. Shishido, J. Inokuchi, The cytoplasmic tail of GM3 synthase defines its subcellular localization, stability, and in vivo activity, *Mol. Biol. Cell* 20 (2009) 3088–3100.
- [27] K. Michelsen, V. Schmid, J. Metz, K. Heusser, U. Liebel, T. Schwede, A. Spang, B. Schwappach, Novel cargo-binding site in the beta and delta subunits of coatamer, *J. Cell Biol.* 179 (2007) 209–217.
- [28] S. Shikano, M. Li, Membrane receptor trafficking: evidence of proximal and distal zones conferred by two independent endoplasmic reticulum localization signals, *Proc. Natl. Acad. Sci. U. S. A.* 100 (2003) 5783–5788.
- [29] J.E. Carette, C.P. Guimaraes, M. Varadarajan, A.S. Park, I. Wuethrich, A. Godarova, M. Kotecki, B.H. Cochran, E. Spooner, H.L. Ploegh, T.R. Brummelkamp, Haploid genetic screens in human cells identify host factors used by pathogens, *Science* (New York, N.Y.) 326 (2009) 1231–1235.
- [30] S. Uemura, S. Go, F. Shishido, J. Inokuchi, Expression machinery of GM4: the excess amounts of GM3/GM4 synthase (ST3GAL5) are necessary for GM4 synthesis in mammalian cells, *Glycoconj. J.* 31 (2014) 101–108.
- [31] K. Furukawa, H. Soejima, N. Niikawa, H. Shiku, Genomic organization and chromosomal assignment of the human beta1, 4-N-acetylgalactosaminyltransferase gene. Identification of multiple transcription units, *J. Biol. Chem.* 271 (1996) 20836–20844.
- [32] K. Sango, O.N. Johnson, C.A. Kozak, R.L. Proia, beta-1,4-N-Acetylgalactosaminyltransferase involved in ganglioside synthesis: cDNA sequence, expression, and chromosome mapping of the mouse gene, *Genomics* 27 (1995) 362–365.
- [33] M. Kozak, Pushing the limits of the scanning mechanism for initiation of translation, *Gene* 299 (2002) 1–34.
- [34] E. Jaskiewicz, G. Zhu, R. Bassi, D.S. Darling, W.W. Young Jr., Beta1,4-N-acetylgalactosaminyltransferase (GM2 synthase) is released from Golgi membranes as a neuraminidase-sensitive, disulfide-bonded dimer by a cathepsin D-like protease, *J. Biol. Chem.* 271 (1996) 26395–26403.
- [35] J. Li, T.Y. Yen, M.L. Allende, R.K. Joshi, J. Cai, W.M. Pierce, E. Jaskiewicz, D.S. Darling, B.A. Macher, W.W. Young Jr., Disulfide bonds of GM2 synthase homodimers. Antiparallel orientation of the catalytic domains, *J. Biol. Chem.* 275 (2000) 41476–41486.
- [36] L.P. Jackson, Structure and mechanism of COPI vesicle biogenesis, *Curr. Opin. Cell Biol.* 29 (2014) 67–73.
- [37] W. Ma, J. Goldberg, Rules for the recognition of dilysine retrieval motifs by coatamer, *EMBO J.* 32 (2013) 926–937.
- [38] L.P. Jackson, M. Lewis, H.M. Kent, M.A. Edeling, P.R. Evans, R. Duden, D.J. Owen, Molecular basis for recognition of dilysine trafficking motifs by COPI, *Dev. Cell* 23 (2012) 1255–1262.
- [39] C.K. Yip, T. Walz, Molecular structure and flexibility of the yeast coatamer as revealed by electron microscopy, *J. Mol. Biol.* 408 (2011) 825–831.
- [40] W. Spessott, A. Uliana, H.J. Maccioni, Defective GM3 synthesis in Cog2 null mutant CHO cells associates to mislocalization of lactosylceramide sialyltransferase in the Golgi complex, *Neurochem. Res.* 35 (2010) 2161–2167.
- [41] W. Spessott, A. Uliana, H.J. Maccioni, Cog2 null mutant CHO cells show defective sphingomyelin synthesis, *J. Biol. Chem.* 285 (2010) 41472–41482.
- [42] S. Uemura, F. Shishido, M. Kashimura, J. Inokuchi, The regulation of ER export and Golgi retention of ST3Gal5 (GM3/GM4 synthase) and B4GalNAcT1 (GM2/GD2/GA2 synthase) by arginine/lysine-based motif adjacent to the transmembrane domain, *Glycobiology* 25 (2015) 1410–1422.

Identification of a new liver-specific c-type mRNA transcriptional variant for mouse ST3GAL5 (GM3/GM4 synthase)

Fumi Shishido¹ · Satoshi Uemura² · Takahiro Nitta³ · Jin-ichi Inokuchi¹

Received: 22 June 2017 / Accepted: 26 July 2017
© Springer Science+Business Media, LLC 2017

Abstract GM3, a major lipid component of the plasma membrane outer leaflet in mammalian cells, is synthesized in the luminal side of Golgi by ST3GAL5 protein (ST3G5), a type II membrane protein. Two strains of *St3Gal5* knockout mice have been established for studies of GM3 physiological function: *St3Gal5*-Ex5-KO (lacking exon 5, which contains the catalytic domain of ST3G5), and *St3Gal5*-Ex3-KO (lacking exon 3, which contains the initiation codons). Results of the present study demonstrate that GM3 synthesis is still present, at a low level, in liver of *St3Gal5*-Ex3-KO mice. *St3Gal5* has two mRNA transcriptional variants: a-type and b-type. When exon 3 is deleted, ST3G5 is not translated from a-type or b-type, as a result of initiation codon deletion or frame shift. Through NCBI database search and real-time PCR analyses of various mouse tissues, we identified a liver-specific *St3Gal5* transcriptional variant (c-type)

capable of producing artificial ST3G5 (M*-ST3G5) having GM3 synthase activity in the absence of exon 3. *St3Gal5*-Ex3-KO mice expressed c-type mRNA without exon 3 (c-type^{-/-}) in liver. The transmembrane and catalytic domains of M*-ST3G5 translated from c-type^{-/-} were identical to those from wild-type, although the cytoplasmic regions differed. Expression of M*-ST3G5 in embryonic fibroblasts derived from *St3Gal5*-Ex3-KO mice led to GM3 synthesis; M*-ST3G5 thus displayed enzyme activity *in vivo*. Taken together, our findings indicate that expression of liver-specific c-type variant accounts for the residual GM3 synthase activity observed in liver of *St3Gal5*-Ex3-KO mice.

Keywords Sialyltransferase · mRNA transcriptional variant · Ganglioside GM3

Electronic supplementary material The online version of this article (doi:10.1007/s10719-017-9788-1) contains supplementary material, which is available to authorized users.

✉ Satoshi Uemura
s-uemura@tohoku-mpu.ac.jp

✉ Jin-ichi Inokuchi
jin@tohoku-mpu.ac.jp

¹ Division of Glycopathology, Institute of Molecular Biomembrane and Glycobiology, Tohoku Medical and Pharmaceutical University, 4-4-1, Komatsushima, Aoba-ku, Sendai, Miyagi 981-8558, Japan

² Division of Medical Biochemistry, Faculty of Medicine, Tohoku Medical and Pharmaceutical University, 4-4-1, Komatsushima, Aoba-ku, Sendai, Miyagi 981-8558, Japan

³ Division of Pathophysiology, Faculty of Pharmacy, Tohoku Medical and Pharmaceutical University, 4-4-1, Komatsushima, Aoba-ku, Sendai, Miyagi 981-8558, Japan

Abbreviations

ER	Endoplasmic reticulum
Ex	Exon
Golgi	Golgi apparatus
GSL	Glycosphingolipid
H3K4me1	Mono-methylation of residue Lys4 in histone H3
H3K4me3	Tri-methylation of residue Lys4 in histone H3
LacCer	Lactosylceramide
MEF	Mouse embryonic fibroblast
Neo	Neomycin resistance gene
ORF	Open reading frame
St3Gal5	ST3 β -galactoside α 2,3-sialyltransferase 5
ST3G5	ST3GAL5 protein
TLC	Thin-layer chromatography
TSSs	Transcriptional start sites

Introduction

GM3, one of the major gangliosides (sialic acid-containing glycosphingolipids [GSLs]) in mammalian cells, is abundant in the outer leaflet of the plasma membrane. GM3 synthesis is catalyzed by a sialyltransferase, ST3GAL5 protein (ST3G5), in the luminal side of Golgi apparatus [1]. ST3G5 possesses sialylmotifs L, S, and VS, which are conserved among sialyltransferases and are thought to function as a catalytic domain [1].

Two transcriptional variants (termed a-type and b-type) of ST3G5-encoding mRNAs have been reported in mice [2, 3]. Using a leaky scanning system, we demonstrated translation of three isoforms (M1-, M2-, and M3-ST3G5) from a-type and two isoforms (M2- and M3-ST3G5) from b-type [4]. These isoforms differ greatly in terms of stability and subcellular localization. They are all transported from endoplasmic reticulum (ER) to Golgi by an arginine (R)/lysine (K)-based motif located just above the transmembrane domain [5]. Only M1 isoform also has an R-based motif, which functions as a retrograde transport signal and is positioned distally from a lipid bilayer. Numerous M1 isoforms are localized in ER [4]. Both M2 and M3 isoforms are localized in Golgi, and the half-life of M3 isoform is longer than that of M2 isoform [4]. Based on result of our 2015 study, we proposed a mechanism in which R/K-based motif is involved in Golgi retention of M3 isoform [5]. Multiple isoforms are involved in GM3 synthesis, but the biological significance of coexistence of more than one isoform in a single cell remains unclear.

We have previously investigated expression patterns of a-type and b-type in various mouse tissues. The transcription initiation point in a-type is close to that in b-type, suggesting that transcriptional regulation is similar in the two variants. Expression patterns of a-type and b-type in various tissues were nearly identical, and both were highly expressed in brain, heart, and testis [4]. Northern blotting analysis for detection of total *St3Gal5* mRNA variants also revealed similar patterns in several tissues, except for liver [2]. Expression level of total mRNA variants in mouse liver was high, whereas those of a-type and b-type were low. These previous findings, taken together, indicate the presence in liver of other mRNA variants besides a-type and b-type.

In the present study, we investigated a *St3Gal5* knockout mouse model (*St3Gal5*-Ex3-KO) in which exon 3, which contains M2 and M3 initiation codons, is replaced by neomycin resistance gene (*Neo*). These mice displayed GM3 synthase activity in liver, but not in inner ear or lymphocytic cells. We identified a new *St3Gal5* mRNA variant (c1-type), expressed specifically in liver. The *St3Gal5*-Ex3-KO mice express artificial splicing isoforms (a-type^{-/-}, b-type^{-/-}, and c1-type^{-/-}) in which the *Neo* region is absent. ST3G5 is not translated from a-type^{-/-} and b-type^{-/-} because of initiation

codon deletion and frame shift. On the other hand, liver-specific c1-type^{-/-} can produce artificial ST3G5 that displays enzyme activity without exon 3.

Materials and methods

Mice

St3Gal5 knockout mice (termed *St3Gal5*-Ex3-KO) were produced as described previously [6]. After a sufficient number of backcross generations, mutant mice were maintained on the KK/TaJcl background.

mRNA variant-specific amplification

First-strand cDNA synthesis was performed using a First-Strand cDNA Synthesis kit for RT-PCR (AMV; Roche Diagnostics; Penzberg, Germany). Total RNA was isolated from tissues of KK/TaJcl and *St3Gal5*^{-/-} mice. Specific primers as follows were designed to amplify ST3G5 transcriptional variants (a-type, b-type, c1-type): a-type (F1-primer: 5'-TCCCTAGCATGCACACAGAGG-3'; R4-primer: 5'-TTATCCGGTCAGGGTCCACATAGTGC-3'), b-type (F2-primer: 5'-AGCCTGCGCAGGTGTGGAC-3'; R4-primer: 5'-TTATCCGGTCAGGGTCCACATAGTGC-3'), c1-type (FX-primer: 5'-GATTTCTCGACACCTCTACTCACACAG-3'; R4-primer: 5'-TTATCCGGTCAGGGTCCACATAGTGC-3'). PCR was performed using 50 ng cDNA, specific primers, and KOD FX polymerase (Takara Bio; Shiga, Japan), as per the manufacturer's instructions.

Plasmids

The open reading frame (ORF) of mouse M*-ST3GAL5 (mM*-ST3G5) was amplified using cDNA prepared from liver of *St3Gal5*-Ex3-KO mice, and primers 5'-ATGTCCTTGCTGGACACGTTC-3' and 5'-GGTTTGCCGTGTTCCGAGTTC-3'. Resulting fragments were cloned into pGEM-T Easy Vector (Promega; Madison, WI) to generate pFS615. pFS617-encoding M*-ST3G5 plasmid was constructed using pFS615 and primers 5'-CACCATGTCCTTGCTGGACACGTTC-3' and 5'-GGTTTGCCGTGTTCCGAGTTC-3'. Resulting fragments were cloned into pENTR/D-TOPO vector (Life Technologies; Carlsbad, CA) to generate pFS617. CSII-CMV-MCS plasmid was converted to Gateway® destination vector (CSII-CMV-RfA) using the Gateway® vector conversion system (Life Technologies). For lentivirus production, M*-ST3G5 of pFS617 was inserted into lentiviral expression vector CSII-CMV-RfA, using the LR clonase reaction to generate pFS620. pFS311 (M3-ST3G5/CSII-CMV-RfA) plasmid was created by similar procedures [7].

Real-time PCR

First-strand cDNA synthesis was performed as described above, and total RNA was isolated from tissues of C57BL/6 mice. Primers and probes specific for mouse *St3Gal5* c1-type (primers, 5'-ACTCAGAGGCTGTTTGAAACAGTCT-3' and 5'-GTGAGTAGAGGTGTCGAGAAATCCAT-3'; probe, 5'-ATTTAAGCCCTCATGGACGCCGCTC-3') and 18S rRNA (Hs99999901-s1) were from Applied Biosystems (Foster City, CA). Real-time PCR was performed with 2 × TaqMan universal master mix using a 7500 Real-Time PCR system (Applied Biosystems). Tissue copy numbers were calculated using appropriate standard curves.

5'-RACE analysis

5'-RACE was performed using a SMARTer RACE 5'/3' Kit (Takara) per the manufacturer's instructions with some modification. SMARTer first-strand cDNA, incorporating specific sequences at both ends, was synthesized from total RNA isolated from mouse liver tissue. 5'-RACE fragments were generated using a set of universal primer and gene-specific primer: 5'-CTAATACGACTCACTATAGGGCAAGCAGTGGTATCAACGCAGAGT-3' and 5'-GATTACGCCAAGCTTGCATTGCTGTGTGAGTAGAGGTGTCGAGAAATCC-3'. The resulting fragment was cloned into linearized pRACE vector using an In-Fusion HD Cloning Kit (Takara). Isolated plasmid DNAs were sequenced using universal primers: M13F, 5'-GTTTTCCCAGTCACGACGTT-3'; M13R, 5'-GGAAACAGCTATGACCATGA-3'.

Cell culture

Mouse embryonic fibroblasts derived from *St3Gal5*-Ex3-KO mice (MEF^{-/-}) [4] were cultured in low-glucose DMEM (Nacalai Tesque; Kyoto, Japan) supplemented with 10% fetal bovine serum, 100 U/mL penicillin, and 100 µg/mL streptomycin.

Preparation of lentiviral vectors

293 T cells (0.5×10^6) were seeded in a polylysine-coated 60-mm dish 24 h before transfection, transfected with 3 µg pFS311 (mM3-ST3G5/CSII-CMV-RfA) or pFS620 (mM*-ST3G5/CSII-CMV-RfA), 1.5 µg pCAG-HIVgp, and 1.5 µg pCMV-VSV-G-RSV-Rev. plasmids using Lipofectamine 2000, and incubated 24 h at 37 °C. *medium* was then replaced by 4 mL high-glucose DMEM containing 10 µM forskolin. Culture temperature was lowered from 37 to 32 °C ~ 32 h after transfection to maintain virus stability. Lentivirus-containing supernatant was harvested 48 h after transfection, centrifuged at $200 \times g$ for 3 min to remove living cells, and either used immediately for experiments or snap-frozen in liquid nitrogen

and stored at -80 °C for later applications. For lentiviral transduction of MEF^{-/-} cells, 2.5×10^5 cells in a 60-mm dish were added with 4 mL lentiviral supernatant, cultured at 32 °C for 24 h, temperature lowered from 32 to 37 °C, and cells incubated 48 h more.

Preparation of cell lysates

Cells were washed twice with ice-cold phosphate-buffered saline (PBS), suspended in buffer A (50 mM Tris-HCl (pH 7.5), 150 mM NaCl, 10% glycerol, 4 M urea, and 1X cOmplete Protease Inhibitor Cocktail (EDTA-free; Roche Diagnostics)), and lysed by sonication. Cell debris was removed by centrifugation at $1000 \times g$ for 3 min at 4 °C, and supernatant (total cell lysates) was centrifuged at $100,000 \times g$ for 1 h at 4 °C. Precipitate (integral membrane protein fraction) was suspended in 2X SDS sample buffer (125 mM Tris-HCl (pH 6.8), 4% SDS, 20% glycerol, and trace amount of bromophenol blue) containing 5% βMe, and incubated 5 min at 37 °C. Integral membrane protein fraction was subjected to peptide: N-glycosidase F (PNGase F) (New England Biolabs; Beverly, MA) digestion for 1 h at 37 °C as per the manufacturer's instructions. Protein concentrations of total cell lysates were determined using a BCA protein kit (Pierce/ Thermo Fisher; Waltham, MA).

Immunoblotting

Integral membrane protein fractions as above were subjected to immunoblotting. Proteins were separated by SDS-PAGE and transferred to an Immobilon PVDF membrane (Millipore; Billerica, MA), which was then incubated 1 h with anti-ST3G5 [8] or anti-β-actin antibodies (1:1000 dilution) (Sigma), washed, and incubated 1 h with HRP-conjugated donkey anti-rabbit IgG (1:20,000 dilution) or anti-mouse IgG (GE Healthcare Bio-Sciences; Piscataway, NJ). Labeling was detected using an ECL Select™ kit (GE Healthcare).

Immunofluorescence microscopy

Transfected cells were cultured on coverslips, fixed for 15 min with 3.7% formaldehyde in PBS at room temperature, rinsed with PBS, permeabilized with 0.5% SDS in PBS, treated with Image-iT FX Signal Enhancer (Thermo Fisher) for 30 min, incubated 1 h with anti-ST3G5 [4] or anti-GM130 (BD Biosciences; Franklin Lakes, NJ) diluted 1:100 with 1% BSA in PBS, washed three times in PBS, and incubated 30 min with Alexa 488-conjugated anti-rabbit IgG or Alexa 594-conjugated anti-mouse IgG antibodies (Thermo Fisher) diluted in 1% BSA in PBS to 5 µg/mL. Coverslips were washed three times in PBS, mounted on glass slides using ProLong Gold antifade reagent (Thermo Fisher), and analyzed by fluorescence microscopy (model FV1000; Olympus; Tokyo, Japan).

Lipid analysis

Lipid (GSL) analysis was performed as described previously [5].

Results

GSL composition of liver and brain tissues in *St3Gal5*-Ex3-KO mice

Proia's group originally produced *St3Gal5* knockout mice termed *St3Gal5*-Ex5-KO by replacing exon 5 (which contains sialylmotif L) with neomycin resistance gene (*Neo*) (see Fig. 1), and observed loss of GM3 synthesis in brain, skeletal muscle, and adipose tissues in these mice [9]. Kozaki's group subsequently produced *St3Gal5* knockout mice termed *St3Gal5*-Ex3-KO by replacing exon 3 (which contains two initiation codons, M2 and M3) [4, 6] with *Neo* (Fig. 1), and we found that TLC analysis did not detect GM3 in inner ear cells, thymocytes, or CD4⁺/CD8⁺ T cells [10, 11]. However, GM3 synthesis was still present at low level in liver tissue of these mice (Fig. 2). In the present study, we separated neutral and acidic GSL fractions from total lipid extracts of liver and brain tissues of wild-type (WT) and *St3Gal5*-Ex3-KO mice using a DEAE-Sephadex A-25 column, and analyzed each fraction by TLC. In WT mice, GM2 was mainly detected in the liver. Liver of *St3Gal5*-Ex3-KO mice showed much lower GM2 content (~50%) than that of WT mice, and correspondingly higher LacCer accumulation and GA2 synthesis. TLC analysis revealed two

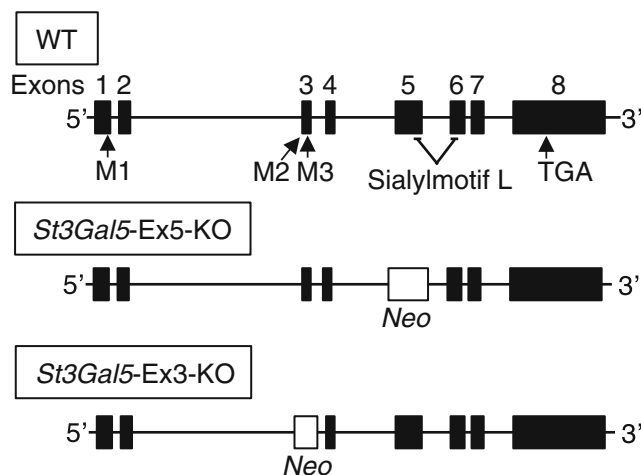


Fig. 1 Gene structures of *St3Gal5* knockout (*St3Gal5*-Ex5-KO and *St3Gal5*-Ex3-KO) mice. The *St3Gal5* gene is composed of eight exons. *St3Gal5*-Ex5-KO mice were produced by replacing exon 5 (which contains sialylmotif L) with neomycin resistance gene (*Neo*). *St3Gal5*-Ex3-KO mice were produced by replacing exon 3 (which includes initiation codons M2 and M3) with *Neo*. Black boxes: exons. Horizontal lines: introns

bands above GM3 in *St3Gal5*-Ex3-KO mice (Fig. 2a, left panel). These bands were identified by liquid chromatography-mass spectrometry (LC-MS) as sulfoglycolipids SM3 and SM2a (data not shown). These findings indicate that GM3 synthase activity is reduced but still present in liver of *St3Gal5*-Ex3-KO mice.

Brain tissues of WT mice express a-, b-, and c-series gangliosides (GM1, GD1a, GD1b, GT1b). Deletion of exon 3 results in a shift of ganglioside synthesis to the o-series ganglioside (GM1b, GD1 α) pathway (Fig. 2b). Lipid pattern changes in *St3Gal5*-Ex3-KO mice are generally similar to those in *St3Gal5*-Ex5-KO mice [9]. However, *St3Gal5*-Ex3-KO brain tissue showed two faint bands unrelated to migration of GM3 and GM2 (Fig. 2b, left panel). The upper band was identified by LC-MS as sulfoglycolipids SM1a (data not shown), but we have not yet been able to identify lower band (Fig. 2b, left panel, black dot). Our findings indicate that deletion of exon 3 abolishes GM3 synthase activity in brain.

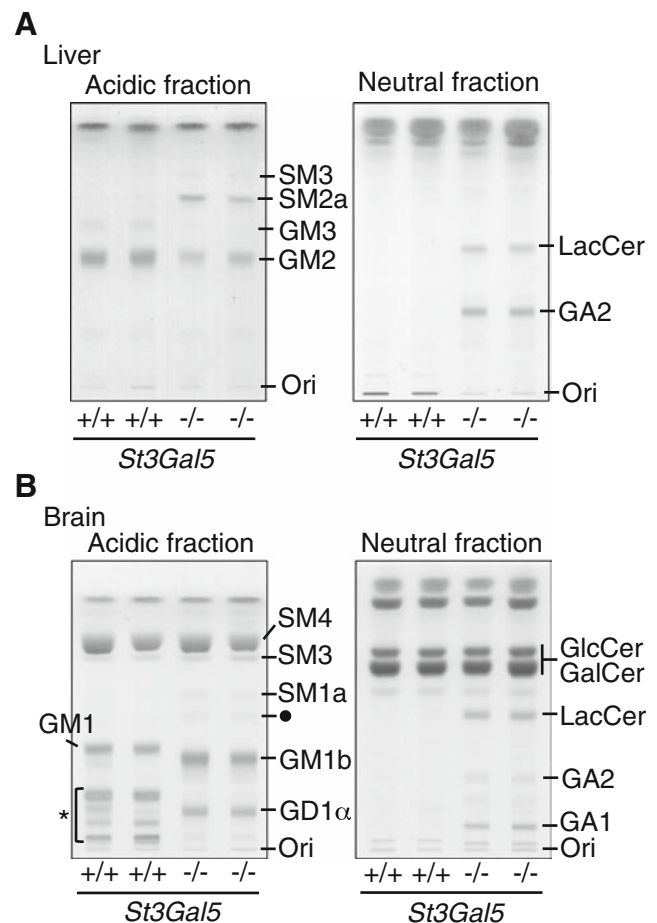


Fig. 2 GSL composition of liver and brain tissues of *St3Gal5*-Ex3-KO mice. Acidic and neutral GSL fractions were prepared from liver (a) and brain (b) tissues of WT (+/+) and *St3Gal5*-KO mice (-/-), and separated on TLC plates (amounts corresponding to 2 mg protein). GSLs were stained by orcinol/sulfuric acid. Asterisk: GD1a, GD1b, and GT1b bands. Black dot: unidentified GSL (see text)

Expression of a-type and b-type mRNA variants in *St3Gal5*-Ex3-KO mice

Mice express two transcriptional variants of *St3Gal5* mRNA: a-type and b-type [2, 3]. Transcription of a-type starts from exon 1; exon 2 is then removed by splicing, and exon 1 is connected to exon 3 (Fig. 3a). a-Type expression was detected as a 321-bp band by PCR using primers (F1/R4 primers) designed for exons 1 and 4. In contrast, transcription of b-type starts from exon 2, and exon 2 is then connected to exon 3. b-Type expression was detected as a 265-bp band by PCR using primers (F2/R4 primers) designed for exons 2 and 4. Because exon 3 is replaced by *Neo* in *St3Gal5*-Ex3-KO mice, it is possible that the *Neo* region is spliced, and exon 1 or exon 2 is directly connected to exon 4, generating a-type^{-/-} or b-type^{-/-} as a mature mRNA (Fig. 3a). If so, 197-bp (a-type^{-/-}) and 141-bp (b-type^{-/-}) bands should be amplified by PCR using F1/R4 primers and F2/R4 primers, respectively.

We examined mRNA expression of a-type and b-type in brain and liver tissues of WT (+/+) and *St3Gal5*-Ex3-KO (-/-) mice using PCR primers (Fig. 3b). In WT, both a-type and b-type bands were detected in brain, whereas only a-type band was detected in liver. Expression level of a-type in liver was much lower than in brain. These findings are consistent with real-time PCR data in our 2009 study [4]. In *St3Gal5*-Ex3-KO, we observed a-type^{-/-} and/or b-type^{-/-} bands in brain and liver. Expression levels and patterns of these mRNA variants in *St3Gal5*-Ex3-KO were generally similar to those in WT. *St3Gal5* mRNAs in *St3Gal5*-Ex3-KO were present as spliced forms a-type^{-/-} and b-type^{-/-}. However, ST3G5 protein is not translated from a-type^{-/-} or b-type^{-/-} as a result of deletion of initiation codons (M2 and M3) or frame shift. Residual GM3 synthesis activity in *St3Gal5*-Ex3-KO therefore cannot be explained by production of a-type^{-/-} or b-type^{-/-}.

Specific expression of a novel *St3Gal5* mRNA variant in liver

To account for observed GM3 synthesis in *St3Gal5*-Ex3-KO mice, we investigated the possible presence of novel mRNA variants that ST3G5 ORF even without exon 3. In the NCBI database (ncbi.nlm.nih.gov), nine transcriptional and splicing variants (including a-type and b-type) are presented as *St3Gal5* mRNA variants (Fig. 4). X¹ and X² indicate new exons of *St3Gal5*. We classified these variants into four types (a-, b-, c-, and d-types). Transcriptions of a-type (a1-a4), b-type (b1, b2), and c-type (c1, c2) start respectively from exons 1, 2, and X². Transcription of d-type starts before exon 1, and contains exons 1, 2, and X¹. Splicing variants without exon 4 (a3-, a4-, b2-, and c2-types) encode the catalytic domain involved in GM3/GM4 synthesis, but do not encode the transmembrane domain. The soluble form of ST3G5, which cannot

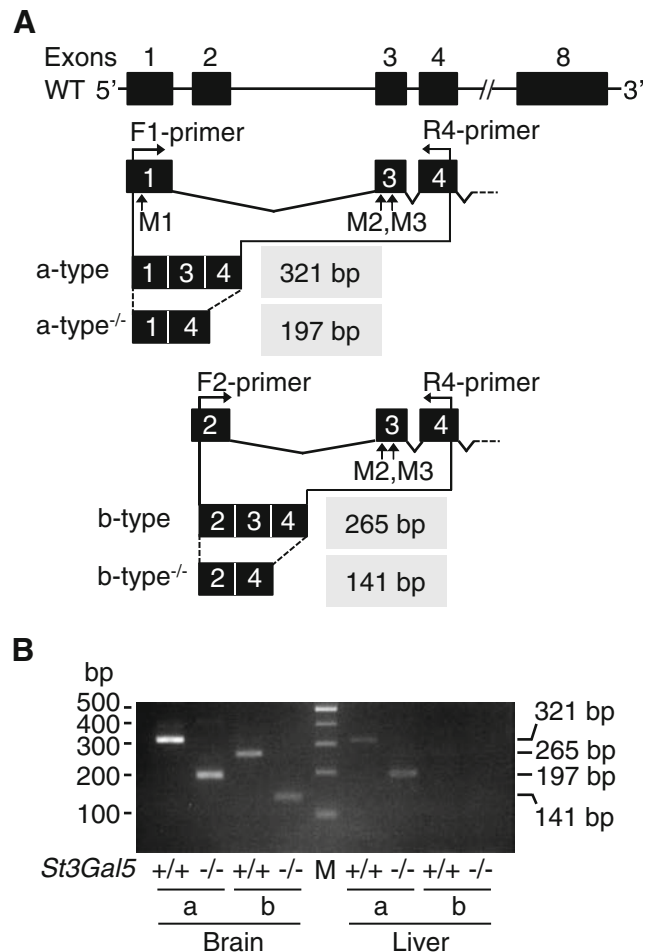


Fig. 3 Expression of mRNA transcriptional variants a-type and b-type in WT and *St3Gal5*-Ex3-KO mice. **a.** PCR products of a-type, a-type^{-/-}, b-type, and b-type^{-/-}. a-type^{-/-} and b-type^{-/-} are transcripts in which exon 3 is removed by splicing. Numbers on gray background: sizes of PCR products using F1/R4-primers or F2/R4-primers. Black boxes: exons. Horizontal lines: introns. M1, M2, M3: initiation codons. **b.** Transcripts were amplified by PCR using F1/R4-primers or F2/R4-primers, and cDNAs prepared from mouse brain and liver tissues. PCR products were separated by agarose electrophoresis and stained with ethidium bromide

produce GM3 in the luminal side of Golgi, is therefore translated from the splicing variant. Consequently, the mRNA variants that encode GM3 synthase are a1-, a2-, b1-, c1-, and d-types. We presume that, among these variants, only c1-type encodes an ORF of GM3 synthase when exon 3 is removed. In WT, M2 and M3 isoforms are most likely translated as GM3 synthases from c1-type because the initiation codons (M2 and M3) are present in exon 3 of c1-type [4]. Deletion of exon 3 in *St3Gal5*-Ex3-KO leads to generation of a novel initiation codon (M*) in exon X² of c1-type^{-/-} (Fig. 5a). M*-ST3G5 isoform, translated from M*, has a catalytic domain for GM3 synthesis, and amino acid sequence of the NH₂-terminal cytoplasmic region of this isoform is different from that of M2-ST3G5 isoform (Fig. 5b).

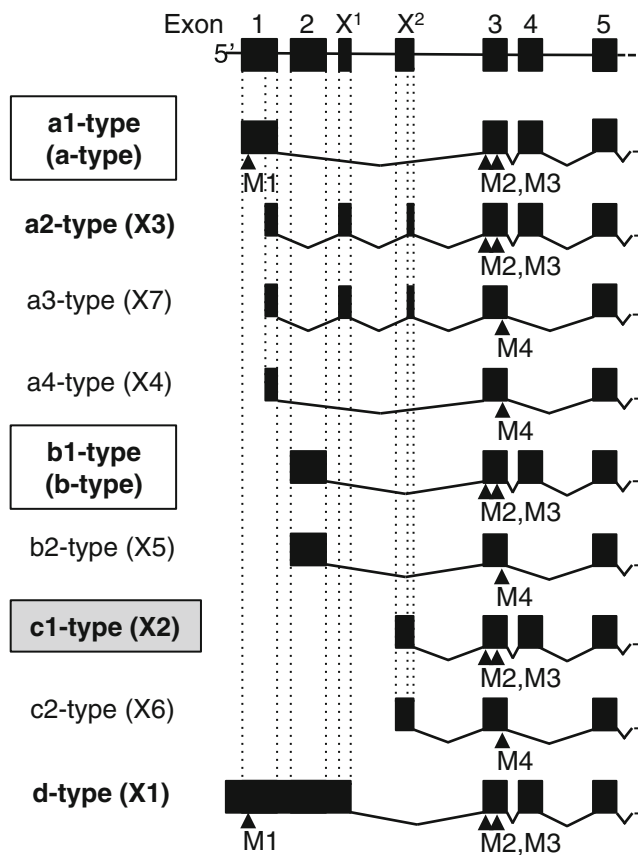


Fig. 4 Structures of mouse *St3Gal5* gene and its mRNA variants. *St3Gal5* mRNA variants (a-type, b-type, X1 through X7) in the NCBI database are shown. Transcripts are classified into four groups (a-, b-, c-, d-type) based on structure. Black boxes: exons in mouse *St3Gal5*. Exons X¹ and X² are not present in known a1-type and b1-type variants. M1, M2, M3, M4: initiation codons

To determine whether c1-type and c1-type^{-/-} are present in liver of WT and *St3Gal5*-Ex3-KO, we performed PCR using FX/R4-primers (Fig. 5a, c). 261-bp and 137-bp bands were detected in WT and *St3Gal5*-Ex3-KO, respectively. This finding indicates that mouse liver expresses c1-type, and that deletion of exon 3 in *St3Gal5*-Ex3-KO results in production of c1-type^{-/-} that encodes M*-ST3G5. We evaluated c1-type expression in various mouse tissues by real-time PCR, and found that it was highest in liver (Fig. 6).

To identify transcriptional start sites (TSSs) of c1-type, we performed 5'-RACE analysis using total RNA of mouse liver. Thirty-four clones containing 5'-end of c1-type were obtained, and their sequences were determined (Fig. 7). In this figure, black dots indicate TSSs, and numbers above the dots indicate number of clones. Only one clone starts before M* (ATG), indicating that although c1-type expression in mouse liver is high, the amount of c1-type capable of translating M*-ST3G5 is quite limited.

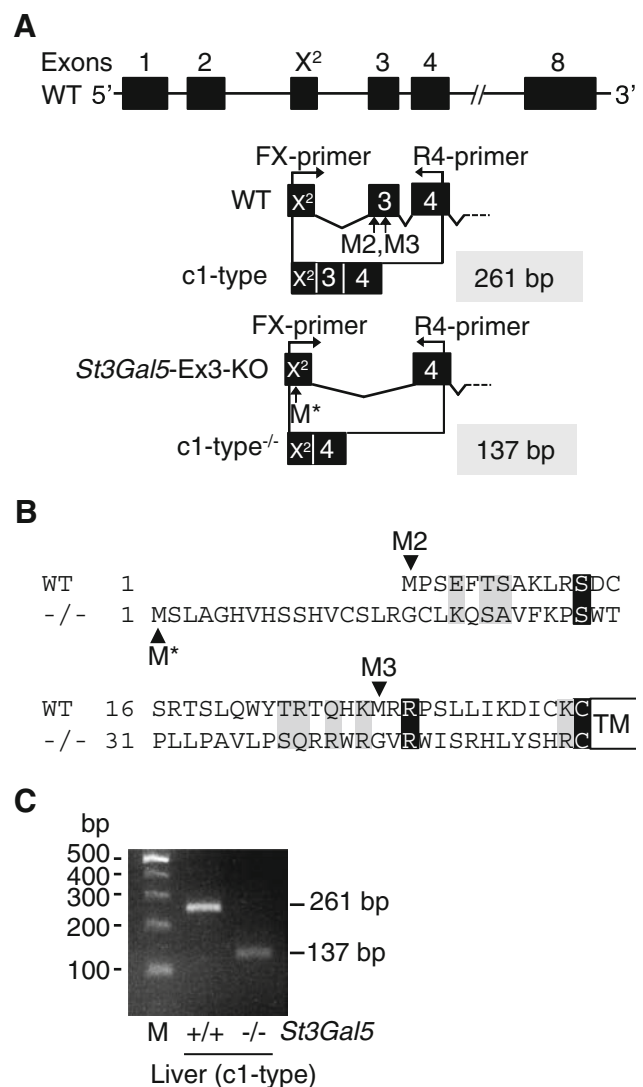


Fig. 5 Expression of c1-type in WT and *St3Gal5*-Ex3-KO mice. **a.** PCR products of c1-type and c1-type^{-/-}. c1-type^{-/-} is a transcript in which exon 3 is removed by splicing. Numbers on gray background: sizes of PCR products using FX/R4-primers. Black boxes: exons. Horizontal lines: introns. **b.** Amino acid sequences of NH₂-terminal cytoplasmic regions of WT and *St3Gal5*-Ex3-KO (-/-) mice. Alignments were generated using the ClustalW program (DNA Data Bank of Japan (DDBJ)). Black boxes: identical residues. Gray boxes: aa similarities. M2, M3, M*: initiation codons. TM: transmembrane region. **c.** Transcripts were amplified by PCR using FX/R4-primers, and cDNAs were prepared from mouse liver tissue. PCR products were separated by agarose electrophoresis and stained with ethidium bromide

Subcellular localization and *in vivo* enzyme activity of artificial M*-ST3G5 isoform

To examine GM3 synthase activity of M*-ST3G5 *in vivo*, we stably expressed mouse embryonic fibroblasts derived from *St3Gal5*-Ex3-KO mice (MEF^{-/-}) with M3- and M*-ST3G5, using a lentiviral expression system. Integral membrane protein fractions were prepared and subjected to immunoblotting with anti-ST3G5 antibodies. Expression level of M*-ST3G5

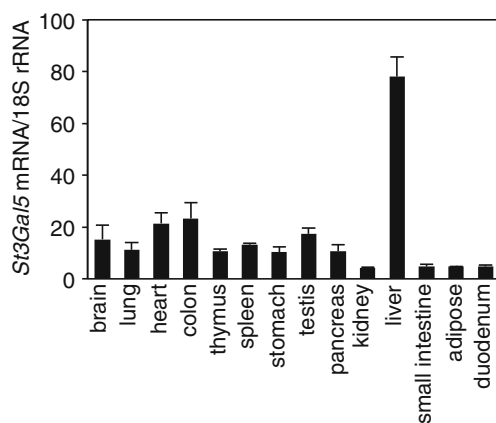


Fig. 6 *St3Gal5* c1-type transcripts from mouse tissues. Expression levels of *St3Gal5* c1-type transcripts from various tissues of C57BL/6 mice were analyzed by real-time PCR assay. Expression levels of c1-type were normalized relative to 18S rRNA transcript

was slightly lower than that of M3-ST3G5 (Fig. 8a). Acidic and neutral lipid fractions of cells were prepared and analyzed by TLC. MEF^{-/-} cells expressed only GM1b (o-series) as acidic GSL, and glucosylceramide (GlcCer), LacCer, and globosides (Gb3 and Gb4) as neutral GSLs. In MEF^{-/-}/M3-ST3G5 and M*-ST3G5 cells, GM3, GM2, GM1, and GD1a were detected in acidic fractions, while LacCer and globoside levels in neutral fractions were lower than those in MEF^{-/-}. Amounts of gangliosides in MEF^{-/-}/M*-ST3G5 cells were similar to those in MEF^{-/-}/M3-ST3G5 cells. These findings indicate that *in vivo* enzyme activities of M3- and M*-ST3G5 are nearly identical.

Our 2009 study showed that the cytoplasmic region of ST3G5 affects subcellular localization [4]. Amino acid sequences of the cytoplasmic region in M*-ST3G5 are quite different from those in M3-ST3G5. We used indirect immunofluorescence assay to examine subcellular localization of M*-ST3G5 in MEF^{-/-} cells (Fig. 8c). We confirmed that the fluorescence from anti-ST3G5 antibody

Exon X²

```

1      1      M*
1      CCCACAGATTTTATCCCCATGTCCTTGCT 30
      1 29
31     GGACACGTTCACTCCAGTCATGTTTGCTCA 60
      21
61     CTCAGAGGCTGTTTGAAACAGTCTGCAGTA 90
91     TTTAAGCCCTCATGGACGCCGCTCCTGCCT 120
121    GCTGTCCTTCCCTCGCAGCGGAGGTGGAGA 150
151    GGGGTGAGATGGATTCTCGACACCTCTAC 180
181    TCACACAG

```

Fig. 7 Transcriptional start sites (TSSs) of mouse *St3Gal5* c1-type. The nucleotide sequence shown is that of exon X² in mouse *St3Gal5*. Black dots: TSSs. Numbers above dots: number of clones obtained by 5'-RACE analysis. White letters on black background: artificial initiation codon (M*)

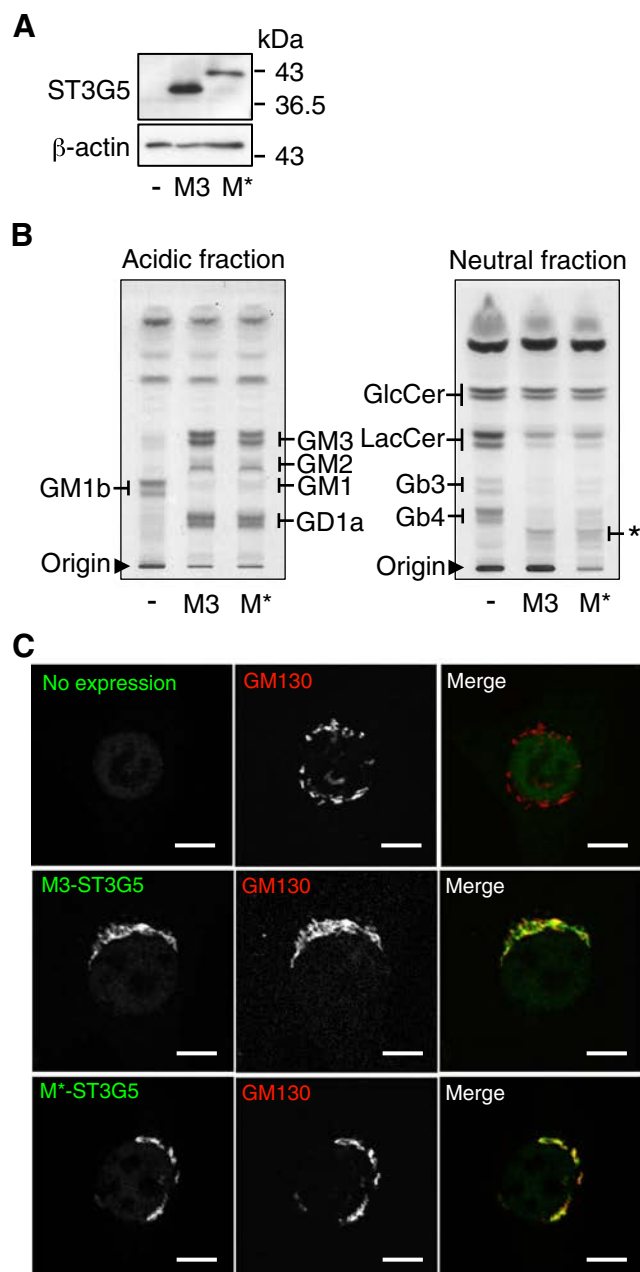


Fig. 8 *In vivo* enzyme activities and subcellular localization of M3-ST3G5 and M*-ST3G5. MEF cells derived from *St3Gal5*-Ex3-KO mice were stably expressed with M3-ST3G5 (M3) or M*-ST3G5 (M*) using a lentiviral expression system. Minus sign (-): no transfection. **a.** Total cell lysates and integral membrane protein fractions were prepared, treated with PNGase F, and analyzed by immunoblotting with anti- β -actin and anti-ST3G5 antibodies, respectively. **b.** Acidic and neutral GSL fractions were extracted from cells, separated on TLC plates (amounts corresponding to 2 mg total protein), and GSLs were stained by orcinol/sulfuric acid. **c.** Cells were fixed, permeabilized with 0.5% SDS in PBS, stained with anti-ST3G5 antibody and Alexa 488-conjugated anti-rabbit IgG, and visualized by confocal laser-scanning microscopy. For co-localization studies, cells were incubated with antibody vs. GM130 (a *cis*-Golgi marker) for 1 h, and then with Alexa594-conjugated anti-mouse IgG for 30 min. Bar: 10 μ m

was absent in MEF^{-/-} cells (no expression). Both M3- and M*-ST3G5 were partially colocalized with cis-Golgi marker GM130, indicating that M*-ST3G5 is transported from ER to Golgi as with M3-ST3G5.

Discussion

Two strains of *St3Gal5* knockout mice (*St3Gal5*-Ex5-KO and *St3Gal5*-Ex3-KO) have been established as models for studying physiological functions of ganglioside GM3. Strain *St3Gal5*-Ex5-KO, produced by deletion of exon 5 (which encodes sialylmotif L), has no GM3 synthesis activity in brain, skeletal muscle, or adipose tissues [9]. Insulin sensitivity is enhanced in this strain because insulin receptor phosphorylation is up-regulated in skeletal muscle. This finding supports the concept of type II diabetes therapy based on inhibition of ganglioside synthesis [12, 13]. Strain *St3Gal5*-Ex3-KO, which we produced by replacing exon 3 with *Neo*, has no GM3 synthesis in inner ear cells, thymocytes, or CD4⁺/CD8⁺ T-cells. The knockout mice (*St3Gal5*-Ex3-KO) display selective degeneration of the organ of Corti, and inhibition of CD4⁺ T-cell activation by treatment with anti-CD3 and anti-CD28 antibodies [10, 11]. The above findings indicate that either exon 5 or exon 3 deletion is sufficient to abolish GM3 synthase activity.

The present study showed that acidic GSL composition of liver in *St3Gal5*-Ex3-KO is similar to that in WT (Fig. 2), indicating that GM3 synthase activity is still present at low level in liver. GM3 and GM2 are not expressed in liver of *St3Gal5*-Ex5-KO (data not shown), indicating that ST3G5 is the sole GM3 synthase. We identified a liver-specific mRNA transcriptional variant (c1-type), and explained the residual synthase activity by production of artificial c1-type (c1-type^{-/-}) that lacks exon 3 (Figs. 5 and 6). In liver of *St3Gal5*-Ex3-KO, M*-ST3G5, which has GM3 synthesis activity, is presumably translated from c1-type^{-/-}.

Sulfoglycolipids (SM3, SM2a, and SM1a) were detected in livers or brains of *St3Gal5*-Ex3-KO (Fig. 2a and b) and *St3Gal5*-Ex5-KO (data not shown). The unknown band in of *St3Gal5*-Ex3-KO brain (Fig. 2b, black dot) is most likely also SB1a, but identification remains to be completed. LacCer level is strikingly increased in *St3Gal5*-Ex3-KO liver (Fig. 2a), consistent with induction of SM3 and SM2a synthesis. GAL3ST1/galactose-3-O-sulfotransferase 1 (CST) transcript encoding SM3 synthase was previously detected by PCR in WT liver, although expression level was low [14]. We detected CST transcripts by real-time PCR in WT and *St3Gal5*-Ex3-KO livers, with similar expression levels (Fig. S1). The presence of sulfoglycolipids (classified as a subset of acidic glycolipids) thus may compensate for a lack of sialic acid-containing gangliosides.

Expression of *St3Gal5* c1-type was restricted to liver. Modifications (acetylation or methylation) of histone H2A-,

H2B-, H3-, and H4-forming chromatin generally play important roles in initiation of transcription [15, 16]. One such modification known as an initiation point of transcription is trimethylation of residue Lys4 in histone H3 (H3K4me3). Data for H3K4me3 states enrolled in ENCODE (<https://www.encodeproject.org>), analyzed by Chip-seq using mouse tissues from embryonic day 14.5, adult week 8, and adult week 24 were viewed by USCS genome browser (<https://genome.ucsc.edu>) (Fig. S2). H3K4me3 peaks were consistently detected in close proximity to exons 1 and 2. Interestingly, the peaks were also detected in proximity to exon X² in liver and bone marrow in adult week 8, and to brown adipose tissue in adult week 24. These findings are in agreement with real-time PCR data (Fig. 6). The observed H3K4me3 states suggest that transcription of c1-type does not occur in embryonic liver. Switching from a1- and/or b1-type to c1-type most likely occurs at some point, because *St3Gal5* mRNAs were detected on embryonic day 15 [17]. We are currently examining possible expression of c1-type in bone marrow and brown adipose tissue by real-time PCR analysis.

Tissue-specific gene expression is controlled by enhancers located far away from TSSs. We estimated locations of enhancer regions through mono-methylation of residue Lys4 in histone H3 (H3K4me1). Data for H3K4me1 states enrolled in ENCODE were viewed by USCS genome browser similarly as H3K4me3 (Fig. S3). H3K4me1 of liver at E14.5 was observed around exons 1 and 2, which are predicted transcriptional start positions. In contrast, H3K4me1 of liver at 8w was observed around exon X² in addition to exons 1 and 2. These findings suggest that, during development, regulatory regions of transcription are altered by switching of transcriptional start positions. The roles of enhancers in liver-specific expression of c1-type will be clarified in future experimental studies.

Binding sites of transcription factors in 200-bp 5'-upstream region from TSSs were searched and predicted using the TFBIND program (tfbind.hgc.jp) (Fig. S4). Among these transcription factors, CCAAT/enhancer-binding protein (C/EBP) regulates expression of multiple hepatocyte-specific genes [18] and is involved in liver differentiation and regeneration [19–21]. We also found the sequence (5'-(A/G)TTA(C/T)GTAA(C/T)-3'), similar to the binding site of D-site of albumin promoter (DBP) expressed in adult mouse liver, although this sequence is not included in the TFBIND program list. Our ongoing studies are focused on identification of regions with promoter activity, and of transcription factors involved in c1-type expression.

Acknowledgements

This study was supported by a Grant-in-Aid for Scientific Research (B) from MEXT (to J.I.), Mizutani Foundation for Glycoscience (J.I.), Naito Foundation (J.I.), ONO Medical Research Foundation (J.I.), Uehara Memorial Foundation

(J.I.), and the MEXT-Supported Program for the Strategic Research Foundation at Private Universities. The authors are grateful to Dr. S. Anderson for English editing of the manuscript, Dr. A. Suzuki (Tohoku Medical and Pharmaceutical University), Dr. T. Moriguchi (Tohoku Medical and Pharmaceutical University), K. Toshima (Tohoku Medical and Pharmaceutical University), and Dr. A. Ishii for experimental support and useful discussion.

Compliance with ethical standards

Conflict of interest Authors declare no conflicts of interest.

Ethical approval This article does not contain any studies with human participants or animals performed by any of the authors.

References

- Ishii, A., Ohta, M., Watanabe, Y., Matsuda, K., Ishiyama, K., Sakoe, K., Nakamura, M., Inokuchi, J., Sanai, Y., Saito, M.: Expression cloning and functional characterization of human cDNA for ganglioside GM3 synthase. *J. Biol. Chem.* **273**(48), 31652–31655 (1998)
- Kono, M., Takashima, S., Liu, H., Inoue, M., Kojima, N., Lee, Y.C., Hamamoto, T., Tsuji, S.: Molecular cloning and functional expression of a fifth-type alpha 2,3-sialyltransferase (mST3Gal V: GM3 synthase). *Biochem. Biophys. Res. Commun.* **253**(1), 170–175 (1998)
- Kapitonov, D., Bieberich, E., Yu, R.K.: Combinatorial PCR approach to homology-based cloning: cloning and expression of mouse and human GM3-synthase. *Glycoconj. J.* **16**(7), 337–350 (1999)
- Uemura, S., Yoshida, S., Shishido, F., Inokuchi, J.: The cytoplasmic tail of GM3 synthase defines its subcellular localization, stability, and in vivo activity. *Mol. Biol. Cell.* **20**(13), 3088–3100 (2009)
- Uemura, S., Shishido, F., Kashimura, M., Inokuchi, J.: The regulation of ER export and Golgi retention of ST3Gal5 (GM3/GM4 synthase) and B4GalNAcT1 (GM2/GD2/GA2 synthase) by arginine/lysine-based motif adjacent to the transmembrane domain. *Glycobiology.* **25**(12), 1410–1422 (2015)
- Tsukamoto, K., Kohda, T., Mukamoto, M., Takeuchi, K., Ihara, H., Saito, M., Kozaki, S.: Binding of clostridium botulinum type C and D neurotoxins to ganglioside and phospholipid. Novel insights into the receptor for clostridial neurotoxins. *J. Biol. Chem.* **280**(42), 35164–35171 (2005)
- Uemura, S., Go, S., Shishido, F., Inokuchi, J.: Expression machinery of GM4: the excess amounts of GM3/GM4S synthase (ST3GAL5) are necessary for GM4 synthesis in mammalian cells. *Glycoconj. J.* **31**(2), 101–108 (2014)
- Uemura, S., Kurose, T., Suzuki, T., Yoshida, S., Ito, M., Saito, M., Horiuchi, M., Inagaki, F., Igarashi, Y., Inokuchi, J.: Substitution of the N-glycan function in glycosyltransferases by specific amino acids: ST3Gal-V as a model enzyme. *Glycobiology.* **16**(3), 258–270 (2006)
- Yamashita, T., Hashiramoto, A., Haluzik, M., Mizukami, H., Beck, S., Norton, A., Kono, M., Tsuji, S., Daniotti, J.L., Werth, N., Sandhoff, R., Sandhoff, K., Proia, R.L.: Enhanced insulin sensitivity in mice lacking ganglioside GM3. *Proc. Natl. Acad. Sci. U. S. A.* **100**(6), 3445–3449 (2003)
- Yoshikawa, M., Go, S., Takasaki, K., Kakazu, Y., Ohashi, M., Nagafuku, M., Kabayama, K., Sekimoto, J., Suzuki, S., Takaiwa, K., Kimitsuki, T., Matsumoto, N., Komune, S., Kamei, D., Saito, M., Fujiwara, M., Iwasaki, K., Inokuchi, J.: Mice lacking ganglioside GM3 synthase exhibit complete hearing loss due to selective degeneration of the organ of Corti. *Proc. Natl. Acad. Sci. U. S. A.* **106**(23), 9483–9488 (2009)
- Nagafuku, M., Okuyama, K., Onimaru, Y., Suzuki, A., Odagiri, Y., Yamashita, T., Iwasaki, K., Fujiwara, M., Takayanagi, M., Ohno, I., Inokuchi, J.: CD4 and CD8 T cells require different membrane gangliosides for activation. *Proc. Natl. Acad. Sci. U. S. A.* **109**(6), E336–E342 (2012)
- Aerts, J.M., Ottenhoff, R., Powlson, A.S., Grefhorst, A., van Eijk, M., Dubbelhuis, P.F., Aten, J., Kuipers, F., Serlie, M.J., Wenkes, T., Sethi, J.K., O'Rahilly, S., Overkleeft, H.S.: Pharmacological inhibition of glucosylceramide synthase enhances insulin sensitivity. *Diabetes.* **56**(5), 1341–1349 (2007)
- Zhao, H., Przybylska, M., Wu, I.H., Zhang, J., Siegel, C., Komarnitsky, S., Yew, N.S., Cheng, S.H.: Inhibiting glycosphingolipid synthesis improves glycemic control and insulin sensitivity in animal models of type 2 diabetes. *Diabetes.* **56**(5), 1210–1218 (2007)
- Hirahara, Y., Tsuda, M., Wada, Y., Honke, K.: cDNA cloning, genomic cloning, and tissue-specific regulation of mouse cerebroside sulfotransferase. *Eur. J. Biochem.* **267**(7), 1909–1917 (2000)
- Kouzarides, T.: Chromatin modifications and their function. *Cell.* **128**(4), 693–705 (2007)
- Chen, Z., Wang, L., Wang, Q., Li, W.: Histone modifications and chromatin organization in prostate cancer. *Epigenomics.* **2**(4), 551–560 (2010)
- Ji, M.Y., Lee, Y.C., Do 2nd, S., Nam, S.Y., Jung, K.Y., Kim, H.M., Park, L.K., Choo, Y.K.: Developmental patterns of mST3GalV mRNA expression in the mouse: in situ hybridization using DIG-labeled RNA probes. *Arch. Pharm. Res.* **23**(5), 525–530 (2000)
- Lekstrom-Himes, J., Xanthopoulos, K.G.: Biological role of the CCAAT/enhancer-binding protein family of transcription factors. *J. Biol. Chem.* **273**(44), 28545–28548 (1998)
- Shen, C.-N., Slack, J.M.W., Tosh, D.: Molecular basis of transdifferentiation of pancreas to liver. *Nat. Cell Biol.* **2**(12), 879–887 (2000)
- Westmacott, A., Burke, Z.D., Oliver, G., Slack, J.M., Tosh, D.: C/EBPalpha and C/EBPbeta are markers of early liver development. *Int. J. Dev. Biol.* **50**(7), 653–657 (2006)
- Greenbaum, L.E., Li, W., Cressman, D.E., Peng, Y., Ciliberto, G., Poli, V., Taub, R.: CCAAT enhancer-binding protein beta is required for normal hepatocyte proliferation in mice after partial hepatectomy. *J. Clin. Invest.* **102**(5), 996–1007 (1998)

ガングリオシドGM3合成酵素欠損症からみる スフィンゴ糖脂質機能

郷 慎司^{1,2}, 井ノ口 仁一¹

ガングリオシドはその糖鎖構造中にシアル酸を含むスフィンゴ糖脂質の総称であり、脊椎動物の多細胞社会構築と各細胞の機能（増殖、分化など）制御に重要な分子群と考えられてきた。一方で、これまで各種ガングリオシド生合成酵素欠損マウスが作製されてきたが、その症状は予想よりはるかに軽度であり驚きをもって解析が続けられてきた。近年、ガングリオシド合成酵素の変異による欠損症が多数報告された。GM3合成酵素欠損症とGM3合成酵素欠損マウスで見いだされた症状は共通した部分だけでなく大きく違う部分もあった。本稿では、GM3合成酵素欠損症からみえてきた聴覚におけるガングリオシド機能に関して概説するとともに、マウスとヒトでみられたGM3合成酵素欠損時の症状の違いを代謝の観点から新知見を交えて考察した。

1. 序説

スフィンゴ糖脂質は「セラミド」と「糖鎖」部分からなる両親媒性の分子であり、疎水性の強いセラミド部分を細胞膜の脂質二重層外層にアンカーし、親水性の糖鎖部位を外側に突出した形で発現している。スフィンゴ糖脂質の糖鎖部分は100種を超える構造多様性が存在し、その発現は細胞種ごとに厳密に制御されている。また、セラミド部分もスフィンゴシン塩基およびアシル鎖の炭素数・不飽和度の違い、水酸基の付加により多様な構造が存在する¹⁾。

スフィンゴ糖脂質は、さまざまな分子と特異的に相互作用し、生物学的機能を発揮している。糖鎖部分での相互作用には、細胞外から相手の分子が接近し作用する“トラン

ス作用”と、同じ細胞膜上に発現する分子と作用する“シス作用”の2通りが想定される。特にシス作用では細胞膜上で発現する各種受容体などの膜タンパク質に直接的に相互作用しその機能、局在、安定性を制御するほか、間接的・直接的相互作用によって多様な分子とともに細胞膜上に“機能性微小膜領域”を形成することで細胞機能を制御していると考えられている。セラミド部分の構造もまた、他の細胞膜構成脂質およびタンパク質との相互作用や、細胞膜の物理化学的性質に関与すると考えられる。このようにスフィンゴ糖脂質は多様な作用方法によって複雑に生物機能を制御していると考えられる²⁻⁴⁾。

特にシアル酸を含有するスフィンゴ糖脂質をガングリオシドと総称する。その生合成は、GM3合成酵素(ST3GAL5)によってラクトシルセラミドにシアル酸が転移されることから始まる。その後順次糖が付加されてさまざまな構造のガングリオシドが生合成される(図1)⁵⁾。これまで、ガングリオシドは各種成長因子の受容体などのタンパク質と相互作用することによって、細胞の増殖、分化、移動などを制御していることが多数報告されてきている⁶⁾。

本稿では、近年見いだされてきたヒトにおけるガングリオシド欠損症の知見とガングリオシド合成酵素欠損マウスの症状をまとめ、そこからみえてきた新しいガングリオシドの機能を概説する。

¹ 東北医科薬科大学・分子生体膜研究所・機能病態分子学(〒981-8558 宮城県仙台市青葉区小松島4-4-1)

² 川崎医科大学・病態代謝学教室(〒701-0192 岡山県倉敷市松島577)

Insights of Glycosphingolipids function from GM3 synthase deficiency

Shinji Go^{1,2} and Jin-ichi Inokuchi¹ (¹Institute of Molecular Biomembrane and Glycobiology, Division of Glycopathology, Tohoku Medical and Pharmaceutical University, 4-4-1 Komatsushima, Aoba-ku, Sendai, Miyagi 981-8558, Japan, ²Kawasaki Medical School, 577 Matsushima, Kurashiki, Okayama 701-0192, Japan)

DOI: 10.14952/SEIKAGAKU.2017.890644

© 2017 公益社団法人日本生化学会

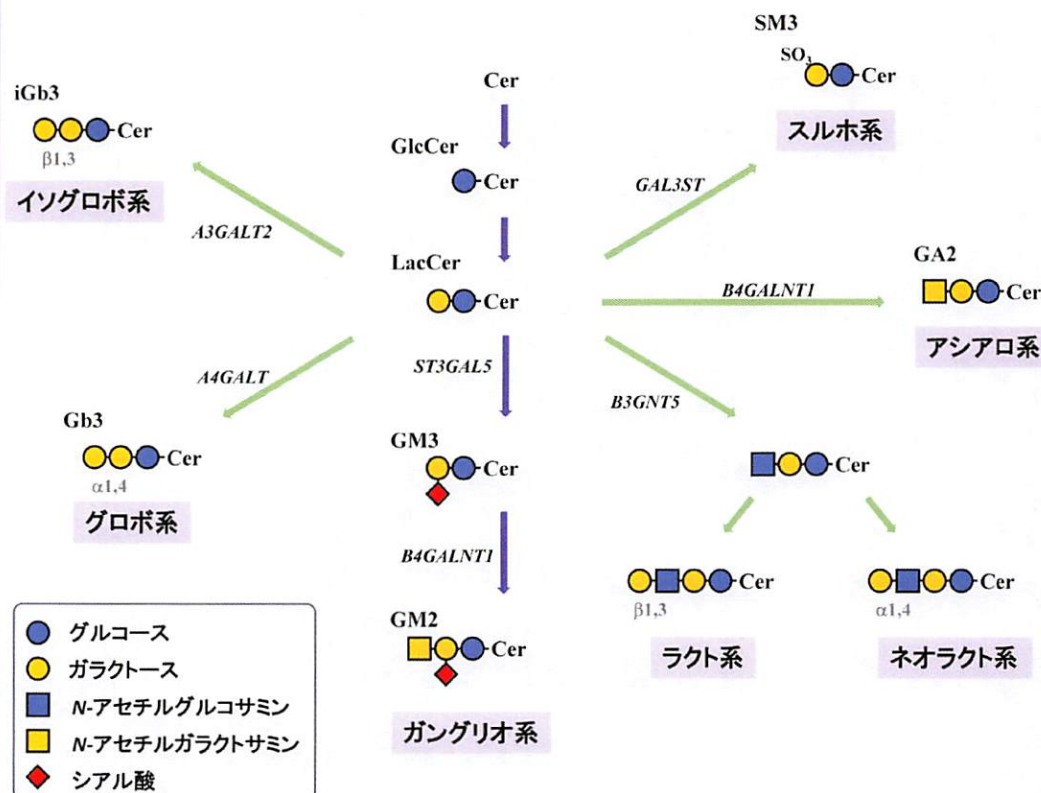


図1 スフィンゴ糖脂質生成経路

哺乳動物に発現する代表的なスフィンゴ糖脂質の生成経路を示す。セラミド (Cer) に順次、糖が付加されることにより多様な糖脂質が生成されるが、特にラクトシルセラミド (LacCer) に付加される糖の種類・結合様式によって多様性が形成される。

2. ガングリオシド欠損マウス

ガングリオシドはその糖鎖構造中にシアル酸を含む酸性スフィンゴ糖脂質の総称である (図1)。発見の経緯や、脳神経系に非常に多く存在していることから、長らく神経組織の形成や機能に必須であることが想定されてきた^{7,8)}。

1990年代に入り、スフィンゴ糖脂質、ガングリオシド生成に関わる酵素群のクローニングがなされ、各糖転移酵素遺伝子欠損マウスが作製され解析された^{5,9-13)}。ほぼすべて (ガラクトシルセラミドから合成される一部の糖脂質を除く) のスフィンゴ糖脂質を欠損するグルコシルセラミド合成酵素¹⁴⁾ およびラクトシルセラミド合成酵素の欠損マウスは胎生中期で致死となる¹⁵⁻¹⁷⁾。これらの酵素を欠損した培養細胞は生存・増殖可能であることから、多様なスフィンゴ糖脂質構造は多細胞系の発達に明らかに必須である。

しかし驚くことに、神経系に多く存在し、重要な機能を担っていると考えられてきたガングリオシドを欠損させてもマウスは生まれてくる。我々のグループも含め、GM3合成酵素欠損マウスは一見明瞭な異常がなく、正常に成長し寿命にも大きな差はないことが報告されている^{18,19)}。ただし、のちに詳細に述べる聴覚障害に加え、行動異常など

種々の神経異常は確認されている^{19,20)}。解析が進めば今後さらに一見してわからない表現型が明らかにされると考えられるが、想像以上に重篤な症状がないことに驚かされるものであった。GD3合成酵素欠損マウスも軽度の神経異常を呈するが重篤ではなく、生存にも大きな影響はない。GM2合成酵素欠損マウスも進行性の神経変性はみられるが、脳神経形成、生存に劇的な変化は確認されなかった²¹⁾。これらのマウスの詳細な解析結果は、各ガングリオシドが神経組織の恒常性維持や再生、各種臓器における機能維持に関与していることを示しているが、当初の予想ほど神経組織形成や分化自体に影響がみられなかったことは驚きであった。これらの現象に関しては、特定の代謝経路の欠損により、代償的に増加するガングリオシドもしくはスフィンゴ糖脂質分子種が、欠損したガングリオシド分子種の機能をある程度代償をしているためと考えられる (図1、図4も参照)。

これらの報告は、各ガングリオシド分子種固有の機能の存在を否定するものではない。いくつかのガングリオシドが有する非還元末端の共通構造が果たすことができる機能、厳密な特定糖鎖構造でしか果たせない機能、付加されているシアル酸の数 (電荷数) によって制御される機能など、ガングリオシドが制御する生物機能にはさまざまな

関与の形があることを示唆するものと考えられる。

これらのことから、ガングリオシド合成酵素ノックアウトマウスを用いた解析では、生体内のガングリオシド機能（消失したガングリオシドの機能）を真に反映しているのかという疑問が残ったままであった。現れた表現型は、ノックアウトによってガングリオシドが消失したことに起因するのか、代償的に増加・出現したスフィンゴ糖脂質の影響か、あるいは他の脂質とのバランスの破綻によるものか、真の答に迫るのは困難を要する問題である。

したがって単純にある特定のスフィンゴ糖脂質の糖鎖構造の合成を担う糖転移酵素のノックアウトマウスの解析だけでは、その糖脂質糖鎖構造の重要性をダイレクトに示すことは難しい。各スフィンゴ糖脂質欠損マウス（およびモデル生物）で発現する糖脂質の種類・量、表現型の詳細な解析、さまざまな種類の糖脂質改変モデル培養細胞株の作製・解析を行い、より多くの情報を集めることがますます必要となってくる。これらの情報を蓄積・統合していくことで、驚くような新たなスフィンゴ糖脂質機能の発見につながると考えられる。そのためには、各スフィンゴ糖脂質の代謝制御機構の解明、糖脂質改変技術（糖転移酵素遺伝子発現制御技術、合成酵素阻害剤開発）、糖脂質化学合成技術（可視化用ラベル糖脂質）、糖脂質検出技術（質量分析などの定性・定量法、抗体などの検出プローブ）などの技術開発、各研究分野との連携も非常に重要である。

また、近年ではエクソーム解析により原因未知の病気の原因遺伝子変異も見つけやすい環境になってきた。実際、近年これらの技術を用いて、新たなスフィンゴ糖脂質代謝関連遺伝子の変異が原因の疾患も見つかってきた。

3. ガングリオシド合成酵素欠損症

ヒトにおけるガングリオシド分解酵素の変異による「蓄積症」は1930年代のGM2ガングリオシドーシスの発見以降²²⁾、多数報告されてきたものの²³⁾、ガングリオシド「生合成酵素の欠損」による症例は報告がなかった。

そんな中、2004年、アメリカのアーミッシュの中で、てんかん症状を示す子供のなかから、「GM3合成酵素（ST3GAL5）欠損」の症例が初めて発見された²⁴⁾（図2）。2013年にも新たにフランスのグループよりミトコンドリア呼吸鎖複合体欠損症様症状患者の遺伝子解析より、GM3合成酵素の変異が見つかり症例が報告された²⁵⁾。これらの症例ではST3GAL5のナンセンス変異が確認されている（図3）。これらの報告のGM3欠損患者の血清中ではGM3以降のガングリオシドが完全に検出されなくなり、グロボ系、ネオラクト系の糖脂質が大幅に増加している。他の組織で同様のスフィンゴ糖脂質の変化が起きているか確認はとれていないが、患者から採取し培養した線維芽細胞でも同様にグロボ系スフィンゴ糖脂質の大幅な増加が確認されている。これらの患者ではてんかんの症状以外に、発達遅延、視神経萎縮および脳皮質の異常による視覚異

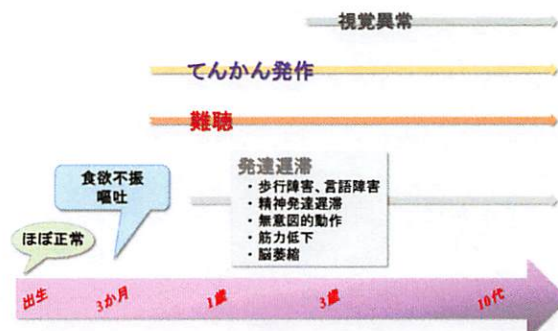


図2 GM3合成酵素欠損患者の症状の推移（アーミッシュ中心に）

GM3合成酵素欠損患者は、胎児期および生後まもなくまでは顕著な異常はみられない。生育に伴いさまざまな症状が発症する。

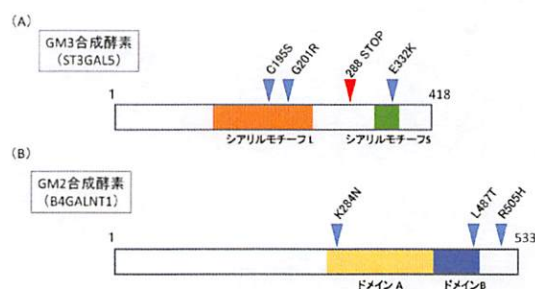


図3 これまでに報告されたヒトにおけるガングリオシド生合成酵素の変異

(A)GM3合成酵素（ST3GAL5）。アーミッシュで見つかったナンセンス変異（赤）に加え、近年、シアリルモチーフ内にミスセンス変異（青）が報告されてきた。(B)GM2合成酵素（B4GALNT1）。クウェート、イタリア、およびアーミッシュの患者からいくつかのミスセンス変異が報告された。ドメインA：glycosyl transferase, family 2 domain, ドメインB：nucleotide-diphospho-sugar transferases superfamily domain。

常、精神発達遅滞、筋力低下、食欲不振、嘔吐などさまざまな症状およびミトコンドリアの呼吸鎖の異常が報告されている²⁴⁻²⁸⁾（図2、表1）。

Boccutoらも2014年に「ソルト&ペッパー症候群」患者のSNPアレイ解析、エクソーム解析などから、アクセプター基質、ドナー基質両方との結合に関わるST3GAL5のシアリルモチーフS内のミスセンス変異[c.994G>A transition (p.E332K)]を同定した²⁹⁾。患者由来の線維芽細胞ではガングリオ系スフィンゴ糖脂質の消失、グロボ系スフィンゴ糖脂質の大幅な増加が確認されている。また、Boccutoらはこれらの線維芽細胞およびST3GAL5をノックダウンしたゼブラフィッシュにおいて、糖タンパク質N結合型およびO結合型の変化を見いだしている。特に、複合型糖鎖の増加、シアリ酸修飾の増加傾向がみられる。これらがGM3欠損の代償機構なのかは定かではないが、病態に何らかの影響を及ぼしているものと考えられる。

また、近年韓国でもST3GAL5の欠損症例が報告された³⁰⁾。この症例では「レット症候群」様の症状を呈して

表1 ガングリオシド合成酵素欠損症の発見経緯・症状

変異		発見経緯・症状	文献
ST3GAL5	C195S, G201R	レット症候群様症状	Lee ら, 2016
	E322K	ソルト&ベッパ―症候群	Buccuto ら, 2014
	R288 STOP	infantile-onset epilepsy 症候群	Simpson ら, 2004
		筋低下 視覚異常 精神発達遅滞 ミトコンドリア呼吸鎖複合体欠損症 色素異常	Fragaki ら, 2013 Wang ら, 2013
B4GALNT1	K284N	遺伝性痙性対麻痺	Harlalka ら, 2013
	L487T		
	R505H		

おり、生後まもなくの時期までは正常であるが、その後、精神遅滞やてんかん様症状などさまざまな症状が確認される。この報告の患者はST3GAL5のシアリルモチーフL内の複合ヘテロ接合性変異（p.Gly201Argとp.Cys195Ser）である。酵素活性測定は行われてはいないが、血清中のGM3, GD3は激減している。

また2013年には、遺伝性の神経変性疾患である遺伝性痙性対麻痺のエクソーム解析から、クウェート、イタリア、およびアーミッシュにおいてGM2合成酵素（B4ALNT1）の変異も報告された³¹⁾。患者由来線維芽細胞の糖脂質解析ではGM2の消失、GM3の増加が確認されている。

ST3GAL5内の変異の場所ひいては活性の残存率や地域性によって症状の違いはあるものの、多くの場合、ST3GAL5の変異によってGM3以降のガングリオシドが欠失した場合、神経系機能に大きな影響が見いだされており、またB4ALNT1の変異によりGM2以降のガングリオシドが欠損した場合も神経変性を伴うことから、ヒトにおいて神経機能の維持にやはりガングリオシドが必須であることが示唆される。

ここで生じる大きな疑問は、GM3合成酵素欠損マウスとヒトのGM3合成酵素欠損症ではその重篤度が大きく異なる点である。ここにガングリオシド、スフィンゴ糖脂質の新たな機能示唆が隠れていると考えられる。これまで筆者らを含めてGM3合成酵素欠損マウスでは各臓器でGM3以降の消失、加えて代償的にアシアロ系糖脂質が発現することを見いだしている¹⁹⁾（図4）。GM3合成酵素欠損マウスが発現するアシアロ系糖脂質にはシアル酸を含有したGM1bやGD1a, GD1cがある。これらはGM3合成酵素欠損により消失したガングリオ系ガングリオシド（GM1やGD1a, GD1bなど）の異性体であり、これらが機能代償できる生命現象が多数あるものと考えている。

これに対し、ヒトのGM3合成酵素欠損症の血清、線維芽細胞ではガングリオ系の糖脂質の消失に加え、グロボ系糖脂質の増加が認められており、アシアロ系の糖脂質の

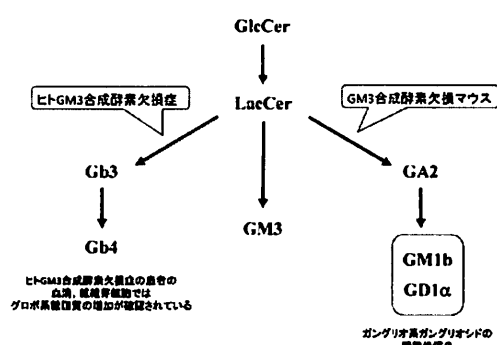


図4 GM3合成酵素欠損マウスとGM3合成酵素欠損症患者のスフィンゴ糖脂質代謝変化

GM3合成酵素欠損マウスでは大半の臓器でアシアロ系のガングリオシドGM1b, GD1aが発現が確認される。GM3合成酵素欠損症患者ではグロボ系糖脂質の増加が確認されており、マウスとヒトでGM3合成酵素欠損時の糖脂質の流れが異なる可能性がある。代償的に発現・増加する糖脂質の違いが症状の違いに関連していると考えられる。

増加は報告されていない^{24, 25, 32)}。この代償して発現するスフィンゴ糖脂質の違いがマウス、ヒト間の症状の違いに反映されている可能性が高い。

4. GM3合成酵素欠損マウスとGM3合成酵素欠損症の共通点

代償発現するスフィンゴ糖脂質分子種の違いはあるが、マウスとヒトにおいてGM3合成酵素欠損時、共通してみられる症状があれば、消失したガングリオシドの機能の本質である可能性が高いと考えた。

我々はGM3合成酵素欠損マウスが聴覚異常を有することを報告した¹⁹⁾。その後の2013年にFragakiらの報告ではフランス系のGM3合成酵素欠損症の患者で聴覚異常の記載がなされた²⁶⁾。ただし、“hearing loss”の記載のみで、詳細は不明であった。そこで我々はアメリカペンシルバニア州ランカスターのアーミッシュの人々で運営される病院で

ある Special Clinic for children との共同研究で、ST3GAL5 c.694C>T 変異を持つ複数名の GM3 合成酵素欠損患者の聴覚機能を聴性脳幹反応試験 (ABR) で詳細に評価したところ、すべてのケースにおいて内耳蝸牛有毛細胞の機能異常が示唆された³³⁾。内耳の詳細な形態的解析は不可能であるため、GM3 合成酵素欠損症の患者でどのような異常が内耳に起きているかは不明であるが、マウス、ヒト共通して GM3 合成欠損の場合には聴覚機能に影響が出ることが明らかになった (Boccuto らの報告では聴覚に関して明確な記載はない、Lee らの報告では鎮静状態の維持が難しく ABR 試験ができなかったため、聴覚機能評価ができず、これらの患者の詳細な情報が期待される)。

これらのことからガングリオシドが聴覚器官においてどのような細胞に発現しているか、GM3 欠損時にどこに障害が出るかを解析し、聴覚におけるガングリオシドの機能を明らかにすることで、ガングリオシド、特に GM3 の機能の本質がみえると考えた。

音波は外耳、中耳を経て、内耳の「蝸牛」へと伝えられる。蝸牛内の「コルチ器」が音波を神経信号に変換する。コルチ器は感覚細胞である 1 列の「内有毛細胞 (inner hair cell: IHC)」および 3~4 列の「外有毛細胞 (outer hair cell: OHC) とそれを支える支持細胞 (supporting cell) からなる。有毛細胞はその上部に「聴毛 (不動毛, stereocilia)」と呼ばれる規則正しく配列した微細な繊毛構造を有している。蝸牛内に伝わった音波によって、有毛細胞の聴毛との間で力学的ひずみが生じ、不動毛に発現するイオンチャンネルが開きイオンが流入する。流入したイオンによって有毛細胞は脱分極を起こし神経伝達物質を放出する。このシグナルを蝸牛神経が受容し、電気信号として最終的に脳の聴覚野へと伝達され音として認識される。

マウスは生後、蝸牛内の細胞の形態的・機能的成熟を経て生後約 14 日目前後から聴覚が機能し始める。蝸牛の主要なガングリオシドは GM3 である。生後まもなくのマウス蝸牛内の GM3 の発現は微量であるが、生後 14 日目前後にかけての成熟期間に大幅にその量を増加させる。加えて複雑なガングリオシドも発現してくる。このことは、生後の蝸牛の機能的・形態的成熟、および維持にガングリオシドが重要な役割をしていることを示唆する。

特に GM3 はコルチ器の内・外有毛細胞において細胞頂端側、聴毛において発現が強い (図 5)。GM3 合成酵素欠損マウスでは、生後まもなく内有毛細胞および外有毛細胞の聴毛の変性が確認された。内有毛細胞では、いったん正常な細胞が形成されるが、生後 10 日目前後から聴毛どうしの融合が確認された。この変性した聴毛では聴毛内の難聴原因遺伝子産物のタンパク質の局在の変化・異常が確認されている。また、外有毛細胞の脱落も確認された。

内耳において GM3 と GD3 のみを発現する GM2 合成酵素欠損マウスでは生後 14 日目前後でこのような聴覚異常、有毛細胞の変性はまったくみられないことから、細胞の極性形成、聴毛局在分子の輸送・局在決定にガングリオ

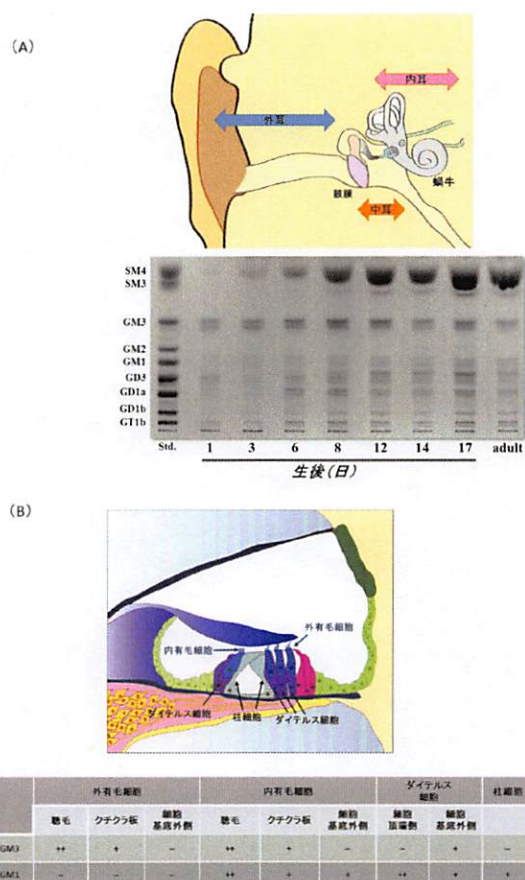


図5 マウス蝸牛内スフィンゴ糖脂質の生後の発現変化と GM3, GM1 発現部位

(A) 聴覚器の構造とマウス蝸牛内スフィンゴ糖脂質の生後の発現変化。蝸牛では GM3 が主要なガングリオシドである。生後発達とともにガングリオシド量が増加し、複雑なガングリオシドも発現してくる。(B) 蝸牛内コルチ器の構造と GM3, GM1 の発現部位。抗ガングリオシド抗体を用いた染色結果をまとめた。+ は染色性あり、- は染色性なしを示す。GM3 は特に有毛細胞聴毛に強く発現する。GM3 合成酵素欠損マウスは有毛細胞聴毛の変性を示すが、GM3 以降のガングリオシドを消失する GM2 合成酵素欠損マウスは聴覚異常を示さない。このことは GM3 が特に聴覚機能にとって重要なガングリオシドであることを示唆する。

シド GM3 が重要な役割を担っていることが強く示唆される^{33, 34)}。

ヒト GM3 合成酵素欠損症の電気生理学的聴覚機能評価でも内外有毛細胞の異常が示唆されていることから、GM3 合成酵素欠損時、マウスでみられた変化がヒトでも起きている可能性が高い。ヒト GM3 合成酵素欠損症の症状、GM3 合成酵素欠損マウス、GM2 合成酵素欠損マウスを用いた病態解析、スフィンゴ糖脂質解析、組織形態解析で、内耳における GM3 の機能にある程度迫ることはできたが、より詳細な分子機構・機能解明のため、今後モデル細胞などを用いた解析が必須になってくる。

解析手法や症例数の制限もあり、GM3 合成酵素欠損マウスと GM3 欠損症患者でみられた症状に類似した点は現

在のところ少なく、不明な点が多い。共通して聴覚異常は判明したものの、やはりそれ以外にGM3合成酵素欠損マウスでは患者でみられた重篤な症状はみられていない。今後ヒト、マウスのGM3合成酵素欠損時、代償的に発現するスフィンゴ糖脂質の種類・量を精査し、症状との関連性を見いだしていく必要がある。また、我々はこれまでGM3がインスリンシグナルの制御に関与していることや、GM3合成酵素欠損マウスにおけるCD4⁺ T細胞の機能異常を報告しており³⁵⁻³⁸⁾、現在も詳細な解析からGM3合成酵素欠損マウスにおいて新たな表現型を見いだしている。GM3欠損症患者でこれらの症状がみられるかを含め、今後、多角的な検証を行い、GM3機能の本質に迫りたい。

5. 筋分化過程におけるGM3分子種の発現変化

GM3合成酵素欠損患者では筋力の低下がみられ、車いすでの生活を余儀なくされる。この筋力低下は発育不全、栄養吸収の問題、神経機能異常などさまざまな要因が絡んだ複合的な要因であることが想定されるが、筋細胞の機能維持にGM3が重要であるとも考えられる。

筆者らは最近、C2C12細胞を用いた筋分化モデルにおいて、GM3の新たな生物機能の可能性を見いだした³⁹⁾。C2C12細胞はマウスサテライト細胞由来の筋芽細胞である。10%ウシ胎仔血清を含有する培地中では増殖するが、低血清(2%ウマ血清)にすることによって分化が誘導され、細胞融合し筋管を形成する。

C2C12細胞の分化過程のスフィンゴ糖脂質をTLC、HPLC、LC-MS/MSを用いて詳細に解析したところ、主要な糖脂質であるGM3の量的・質的变化を見いだした(図6)。GM3量は分化に伴い大幅に増加するが、それに加えシアル酸分子種がNeu5AcからNeu5Gcへと変化した。加えて、GM3のセラミドのアシル鎖構造は分化前には炭素数24のものが主要であったのに対し、分化に伴い炭素数16のアシル鎖を持ったGM3が増加し、筋管形成後は炭素数16のアシル鎖を持ったNeu5Gc-GM3が主要なものとなった。つまり、筋分化過程においてGM3の量的増加と微細構造の変化とが同時並行して起こり、同じGM3であっても分化に伴い極性が高い分子種へと変化してゆく。このGM3の量的・質的变化は筋分化および分化後の筋肉の質の制御に重要である可能性を示す結果を得ている³⁹⁾。

現在のところ、GM3合成酵素欠損マウスはほぼ正常に生まれて生育し、体重にも大きな差はないことから、筋肉の発生に関してはおおむね行われていると考えている。現在、筋損傷時の再生の面や機能的な面に関して詳細に解析を行っている。

こういった、培養モデル細胞系を用いたガングリオシドの生化学的な解析知見、分子レベルでの機能解析知見は、さまざまな報告が蓄積されている。ガングリオシド代謝遺伝子改変マウスや新たに報告されてきたヒトにおける欠損症の知見が集まり始めた現在、これらの知見を照らし合わ

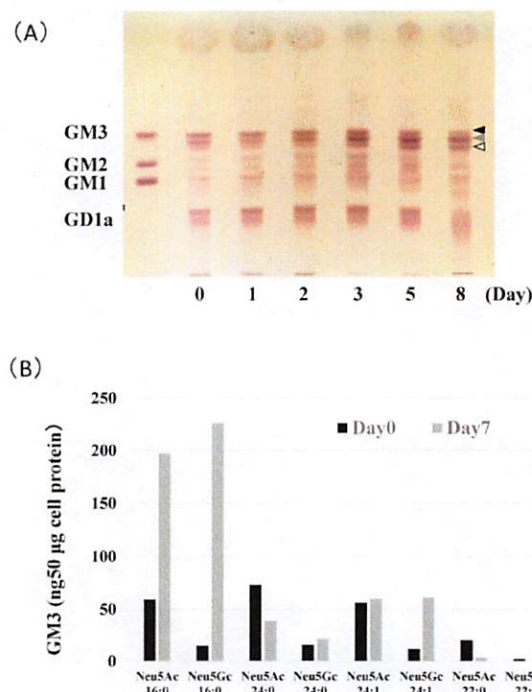


図6 マウスC2C12細胞の分化過程におけるガングリオシドの分子種変化

マウスサテライト細胞由来筋芽細胞株C2C12を低血清条件下で筋管へと分化誘導した。(A)TLCによるガングリオシド解析。分化前(Day0)では2本(黒および灰色の矢頭)が主要なGM3であるが、分化に伴い移動度が低い(極性が高い)バンドへとシフトした(灰色、白抜きの矢頭)。(B)GM3分子種のLC-MS/MS解析。シアル酸分子種(Neu5Ac, Neu5Gc)とセラミドアシル鎖構造を示す。分化前にはシアル酸構造としてNeu5Ac, アシル鎖として24:0もしくは24:1の構造を持ったGM3が主要であるが、分化後にはNeu5Gc, 16:0を持つGM3が主要となる。

せ、類似点、相違点を見つめなおし検証していく古くて新しい研究を続けることで、ガングリオシド機能の本質がみえてくるものと思われる。

このC2C12の系では、分化に伴ってGM3のシアル酸部分、セラミドのアシル鎖部分の微細構造変化が同時に起こるユニークな現象を見いだした。筋ジストロフィーのモデルマウスにおいて、ヒト(Neu5Ac)とマウス(Neu5Gc)のシアル酸構造の違いによって、症状の重症度が異なることも示唆されている⁴⁰⁾。また、近年、ガングリオシドのセラミド部分のアシル鎖構造の多様性に注目が集まりつつあり、我々のグループもこのC2C12の系以外にメタボリックシンドロームの病態にこのアシル鎖構造が重要な鍵になっていることを示唆している⁴¹⁾。

シアル酸構造、アシル鎖構造を含めたガングリオシド詳細構造とその機能に注目することでスフィンゴ糖脂質の新たなフィールドの開拓が進むかもしれない。

6. スフィンゴ糖脂質機能解明に向けて

上述のように、近年のシーケンス技術の進歩によって、これまで見つからなかったスフィンゴ糖脂質の生合成酵素の変異による疾患が新たに見つかった。もちろん、その疾患の発見、症状の解析だけではすべてがわかるわけではない。GM3合成酵素欠損マウスおよびヒト欠損症で見いだされた聴覚機能障害はGM3の新たな機能を明示するものであるが、その詳細な分子機構は未知のままである。ヒト疾患やある一つの遺伝子改変マウスの単純な表現型解析だけでは、ガングリオシドの本質を見いだすことはできない。ガングリオシド合成酵素遺伝子変異によって、どのガングリオシドが消失し、どのスフィンゴ糖脂質が出現・増加したか、やはり詳細な脂質解析が重要な鍵である。どのようなガングリオシド（スフィンゴ糖脂質）の組成の場合にどこで何が起こるか、という地道な知識の積み重ねが必要になってくると考える。ヒトにおけるスフィンゴ糖脂質の生合成酵素の変異の症例に加え、これまで蓄積されたスフィンゴ糖脂質生合成酵素欠損マウスの知見、各種培養細胞モデルを用いた膨大な知見を統合していくことで、新たなスフィンゴ糖脂質の機能の本質が見いだされると思われる。

各スフィンゴ糖脂質の機能解明には細胞膜機能性微小領域（ラフト）の実態解明が切り離せない問題である。近年、高感度のイメージング用プローブおよび技術の開発も進み、生細胞上でスフィンゴ糖脂質が膜タンパク質と相互作用する様子を観察することも可能になってきた^{42, 43)}。従来の手法を用いた知見と新たな技術による知見とを組み合わせ、これまでのラフト像もブラッシュアップしていく必要がある。また、近年注目されるエキソソームをはじめとするマイクロベシクル上のスフィンゴ糖脂質を介した細胞間情報交換も想定されてきている。また、筋分化過程で見いだされたGM3のシアル酸分子種およびセラミドのアシル鎖分子種の構造変化は、同一スフィンゴ糖脂質分子種の微細構造変化による生物機能制御を示唆する新たな知見である。こういった点に注目した研究の進展によって予想もしなかったスフィンゴ糖脂質機能の本質がみえてくると思われる。そのためには今まで以上に農学、理学、医学、工学、薬学などさまざまな分野との交流と技術・情報交換が必須である。これまでの知見を大事にし、新たな視点・技術を用いてチャレンジを続け、新たなスフィンゴ糖脂質研究が展開されることを期待する。

謝辞

本稿作成に記載されている我々の研究内容は、私立大学戦略的研究基盤形成支援事業「生体膜糖鎖異常に起因する生活習慣病発症機序の解明と臨床への応用」、新学術領域研究「統合的神経機能の制御を標的とした糖鎖の作動原理解明」の支援を受けて、主に東北医科薬科大学分子生体膜研究所で行われたものです。記載した聴覚に関する研究

は吉川弥里先生（現・就実大学薬学部）、筋分化研究に関しては郷詩織さん（現・名古屋大学大学院生命農学研究科博士後期課程）が中心になって行った仕事です。また、名古屋大学生物機能開発利用研究センター北島健先生にご指導・ご助言を賜りました。皆様に感謝申し上げます。

文 献

- 1) Jennemann, R. & Gröne, H.J. (2013) *Prog. Lipid Res.*, **52**, 231–248.
- 2) Russo, D., Parashuraman, S., & D'Angelo, G. (2016) *Int. J. Mol. Sci.*, **17**, E1732.
- 3) Kurzchalia, T.V. & Parton, R.G. (1999) *Curr. Opin. Cell Biol.*, **11**, 424–431.
- 4) Inokuchi, J. (2011) *Proc. Jpn. Acad., Ser. B, Phys. Biol. Sci.*, **87**, 179–198.
- 5) Ishii, A., Ohta, M., Watanabe, Y., Matsuda, K., Ishiyama, K., Sakoe, K., Nakamura, M., Inokuchi, J., Sanai, Y., & Saito, M. (1998) *J. Biol. Chem.*, **273**, 31652–31655.
- 6) Inokuchi, J. & Kabayama, K. (2008) *Trends Glycosci. Glycotechnol.*, **20**, 353–371.
- 7) Yu, R.K., Tsai, Y.T., & Ariga, T. (2012) *Neurochem. Res.*, **37**, 1230–1244.
- 8) Schnaar, R.L., Gerardy-Schahn, R., & Hildebrandt, H. (2014) *Physiol. Rev.*, **94**, 461–518.
- 9) Nagata, Y., Yamashiro, S., Yodoi, J., Lloyd, K.O., Shiku, H., & Furukawa, K. (1992) *J. Biol. Chem.*, **267**, 12082–12089.
- 10) Haraguchi, M., Yamashiro, S., Yamamoto, A., Furukawa, K., Takamiya, K., Lloyd, K.O., Shiku, H., & Furukawa, K. (1994) *Proc. Natl. Acad. Sci. USA*, **91**, 10455–10459.
- 11) Fukumoto, S., Miyazaki, H., Urano, T., Furukawa, K., & Furukawa, K. (1999) *J. Biol. Chem.*, **274**, 9271–9276.
- 12) Miyazaki, H., Fukumoto, S., Okada, M., Hasegawa, T., Furukawa, K., & Furukawa, K. (1997) *J. Biol. Chem.*, **272**, 24794–24799.
- 13) Kojima, Y., Fukumoto, S., Furukawa, K., Okajima, T., Wiels, J., Yokoyama, K., Suzuki, Y., Ohta, M., & Furukawa, K. (2000) *J. Biol. Chem.*, **275**, 15152–15156.
- 14) Ichikawa, S., Ozawa, K., & Hirabayashi, Y. (1998) *Biochem. Biophys. Res. Commun.*, **253**, 707–711.
- 15) Yamashita, T., Wada, R., Sasaki, T., Deng, C., Bierfreund, U., Sandhoff, K., & Proia, R.L. (1999) *Proc. Natl. Acad. Sci. USA*, **96**, 9142–9147.
- 16) Kumagai, T., Tanaka, M., Yokoyama, M., Sato, T., Shinkai, T., & Furukawa, K. (2009) *Biochem. Biophys. Res. Commun.*, **379**, 456–459.
- 17) Nishie, T., Hikimochi, Y., Zama, K., Fukusumi, Y., Ito, M., Yokoyama, H., Naruse, C., Ito, M., & Asano, M. (2010) *Glycobiology*, **20**, 1311–1322.
- 18) Yamashita, T., Hashiramoto, A., Haluzik, M., Mizukami, H., Beck, S., Norton, A., Kono, M., Tsuji, S., Danlotti, J.L., Werth, N., Sandhoff, R., Sandhoff, K., & Proia, R.L. (2003) *Proc. Natl. Acad. Sci. USA*, **100**, 3445–3449.
- 19) Yoshikawa, M., Go, S., Takasaki, K., Kakazu, Y., Ohashi, M., Nagafuku, M., Kabayama, K., Sekimoto, J., Suzuki, S., Takaiwa, K., Kimitsuki, T., Matsumoto, N., Komune, S., Kamei, D., Saito, M., Fujiwara, M., Iwasaki, K., & Inokuchi, J. (2009) *Proc. Natl. Acad. Sci. USA*, **106**, 9483–9488.
- 20) Niimi, K., Nishioka, C., Miyamoto, T., Takahashi, E., Miyoshi, I., Itakura, C., & Yamashita, T. (2011) *Biochem. Biophys. Res. Commun.*, **406**, 524–528.

- 21) Furukawa, K., Takamiya, K., Okada, M., Inoue, M., Fukumoto, S., & Furukawa, K. (2001) *Biochim. Biophys. Acta*, **1525**, 1–12.
- 22) Klenk, E., Vater, W., & Bartsch, G. (1957) *J. Neurochem.*, **1**, 203–206.
- 23) Sandhoff, K. & Harzer, K. (2013) *J. Neurosci.*, **33**, 10195–10208.
- 24) Simpson, M.A., Cross, H., Proukakis, C., Priestman, D.A., Neville, D.C., Reinkensmeier, G., Wang, H., Wiznitzer, M., Gurtz, K., Verganelaki, A., Pryde, A., Patton, M.A., Dwek, R.A., Butters, T.D., Platt, F.M., & Crosby, A.H. (2004) *Nat. Genet.*, **36**, 1225–1229.
- 25) Fragaki, K., Ait-El-Mkadem, S., Chaussonot, A., Gire, C., Mengual, R., Bonesso, L., Beneteau, M., Ricci, J.E., Desquiere-Dumas, V., Procaccio, V., Rötig, A., & Paquis-Flucklinger, V. (2013) *Eur. J. Hum. Genet.*, **21**, 528–534.
- 26) Farukhi, F., Dakkouri, C., Wang, H., Wiznitzer, M., & Traboulsi, E.I. (2006) *Ophthalmic Genet.*, **27**, 89–91.
- 27) Wang, H., Bright, A., Xin, B., Bockoven, J.R., & Paller, A.S. (2013) *Am. J. Med. Genet. A*, **161**, 875–879.
- 28) Wang, H., Wang, A., Wang, D., Bright, A., Sency, V., Zhou, A., & Xin, B. (2016) *Clin. Genet.*, **89**, 625–629.
- 29) Boccuto, L., Aoki, K., Flanagan-Steet, H., Chen, C.F., Fan, X., Bartel, F., Petukh, M., Pittman, A., Saul, R., Chaubey, A., Alexov, E., Tiemeyer, M., Steet, R., & Schwartz, C.E. (2014) *Hum. Mol. Genet.*, **23**, 418–433.
- 30) Lee, J.S., Yoo, Y., Lim, B.C., Kim, K.J., Song, J., Choi, M., & Chae, J.H. (2016) *Am. J. Med. Genet. A*, **170**, 2200–2205.
- 31) Harlalka, G.V., Lehman, A., Chioza, B., Baple, E.L., Maroofian, R., Cross, H., Sreekantan-Nair, A., Priestman, D.A., Al-Turki, S., McEntagart, M.E., Proukakis, C., Royle, L., Kozak, R.P., Bastaki, L., Patton, M., Wagner, K., Coblenz, R., Price, J., Mezei, M., Schlade-Bartusiak, K., Platt, F.M., Hurler, M.E., & Crosby, A.H. (2013) *Brain*, **136**, 3618–3624.
- 32) Liu, Y., Su, Y., Wiznitzer, M., Epifano, O., & Ladisch, S. (2008) *Glycobiology*, **18**, 593–601.
- 33) Yoshikawa, M., Go, S., Suzuki, S., Suzuki, A., Katori, Y., Morlet, T., Gottlieb, S.M., Fujiwara, M., Iwasaki, K., Strauss, K.A., & Inokuchi, J. (2015) *Hum. Mol. Genet.*, **24**, 2796–2807.
- 34) 井ノ口仁一 (2015) *生化学* **87**, 560–572.
- 35) Tagami, S., Inokuchi, J., Kabayama, K., Yoshimura, H., Kitamura, F., Uemura, S., Ogawa, C., Ishii, A., Saito, M., Ohtsuka, Y., Sakaue, S., & Igarashi, Y. (2002) *J. Biol. Chem.*, **277**, 3085–3092.
- 36) Kabayama, K., Sato, T., Kitamura, F., Uemura, S., Kang, B.W., Igarashi, Y., & Inokuchi, J. (2005) *Glycobiology*, **15**, 21–29.
- 37) Kabayama, K., Sato, T., Saito, K., Loberto, N., Prinetti, A., Sonnino, S., Kinjo, M., Igarashi, Y., & Inokuchi, J. (2007) *Proc. Natl. Acad. Sci. USA*, **104**, 13678–13683.
- 38) Nagafuku, M., Okuyama, K., Onimaru, Y., Suzuki, A., Odagiri, Y., Yamashita, T., Iwasaki, K., Fujiwara, M., Takayanagi, M., Ohno, I., & Inokuchi, J. (2012) *Proc. Natl. Acad. Sci. USA*, **109**, 336–342.
- 39) Go, S., Go, S., Veillon, L., Ciampa, M.G., Mauri, L., Sato, C., Kitajima, K., Prinetti, A., Sonnino, S., & Inokuchi, J. (2017) *J. Biol. Chem.*, **292**, 7040–7051.
- 40) Martin, P.T., Camboni, M., Xu, R., Golden, B., Chandrasekharan, K., Wang, C.M., Varki, A., & Janssen, P.M. (2013) *Glycobiology*, **23**, 833–843.
- 41) Veillon, L., Go, S., Matsuyama, W., Suzuki, A., Nagasaki, M., Yatom, Y., & Inokuchi, J. (2015) *PLoS One*, **10**, e0129645.
- 42) Suzuki, K.G., Kasai, R.S., Fujiwara, T.K., & Kusumi, A. (2013) *Methods Cell Biol.*, **117**, 373–390.
- 43) Suzuki, K.G., Kasai, R.S., Hirosawa, K.M., Nemoto, Y.L., Ishibashi, M., Miwa, Y., Fujiwara, T.K., & Kusumi, A. (2012) *Nat. Chem. Biol.*, **8**, 774–783.

著者寸描

●郷 慎司 (ごう しんじ)

川崎医科大学病態代謝学講師。博士 (農学)。

■略歴 岐阜県生まれ。名古屋大学農学部卒業。同大学院生命農学研究科博士課程修了。東北薬科大学 (現・東北医科薬科大学) 分子生体膜研究所学術フロンティア研究員。助教を経て、2017年より現職。

■研究テーマと抱負 糖鎖の代謝制御機構と機能の解明。特に糖スクレオチドとシアル酸代謝に注目した研究。

■ウェブサイト <https://www.kawasaki-m.ac.jp/med/study/info.php?id=211>

■趣味 HPLC。

●井ノ口 仁一 (いのくち じんいち)



東北医科薬科大学分子生体膜研究所所長。薬学部機能病態分子学教室教授。薬学博士。

■略歴 福岡県に生まれる。福岡大学薬学部を卒業。同大学院、生化学教室助手を経て、1985年ミシガン大学医学部神経化学研究所博士研究員。91年生化学工業東京研究所主任研究員を経て、98年北海道大学大学院薬学研究科助教授。2006年

より現職。

■研究テーマと抱負 生体恒常性維持機構におけるスフィンゴ糖脂質の分子種特異的な作動原理を解明し、生理活性糖脂質としての位置付けを明確にすることが、使命であると考えている。

■ウェブサイト http://www.tohoku-mpu.ac.jp/pharmacy/about/lp_d04/

■趣味 音楽鑑賞、ウォーキング、ガーデニング。



N-glycan-dependent cell-surface expression of the P2Y₂ receptor and N-glycan-independent distribution to lipid rafts



Tetsuto Nakagawa, Chihiro Takahashi, Hitomi Matsuzaki, Shohei Takeyama, Shinpei Sato, Ayaka Sato, Yoshiyuki Kuroda, Hideyoshi Higashi*

Division of Glyco-Signal Research, Institute of Molecular Biomembrane and Glycobiology, Tohoku Medical and Pharmaceutical University, Sendai, Miyagi 981-8558, Japan

ARTICLE INFO

Article history:

Received 3 February 2017

Accepted 10 February 2017

Available online 14 February 2017

Keywords:

Cell surface expression

ER-associated protein degradation

Lipid raft

N-linked glycosylation

P2Y₂ receptor

ABSTRACT

P2Y₂ receptor (P2Y₂R) is a G-protein-coupled receptor (GPCR) that couples with Gαq/11 and is stimulated by ATP and UTP. P2Y₂R is involved in pain, proinflammatory changes, and blood pressure control. Some GPCRs are localized in lipid rafts for interaction with other signaling molecules. In this study, we prepared N-glycan-deficient mutants by mutating the two consensus Asn residues for N-glycosylation to Gln to examine intracellular localization and association with lipid rafts. Western blotting of the wild type (WT) protein and mutants (N9Q, N13Q, N9Q/N13Q) in COS-7 cells showed that both Asn residues were glycosylated in the WT. Fluorescent microscopy analysis showed that WT, N9Q and N13Q were expressed in the endoplasmic reticulum (ER), Golgi body, and cell membrane, but N9Q/N13Q was only found in the ER. WT, N9Q and N13Q moved from the cell surface to endosomes within 15 min after UTP stimulation. WT and the N9Q/N13Q glycosylation-deficient mutant appeared in the detergent insoluble membrane fraction, lipid raft. These findings suggest that P2Y₂R is localized in lipid rafts in the ER during biosynthesis, and that N-glycosylation is required for subsequent expression in the cell membrane. In the presence of epoxomicin, a proteasome inhibitor, there was a significant increase in the level of N9Q/N13Q, which suggests that N-glycan-deficient P2Y₂R undergoes proteasomal degradation.

© 2017 Elsevier Inc. All rights reserved.

1. Introduction

The P2Y receptor family consists of G-protein-coupled receptors (GPCRs) that are activated by nucleotides such as adenosine triphosphate (ATP) and uridine triphosphate (UTP) and have various physiological functions. P2Y₂ receptor (P2Y₂R) is a Gαq/11-coupled receptor that has ATP and UTP as ligands and is expressed in mammalian tissues as a mediator of pain and inflammation. P2Y₂R is associated with chloride secretion upon damage to respiratory tract epithelial cells [1], neuronal protection upon development of inflammation [2], phagocytosis of apoptotic cells by macrophages [3,4], and axonal elongation and differentiation of neurocytes [5]. There are an increasing number of reports on cross talk of signals via ATP and bradykinin upon development of inflammation [6–9], and we recently suggested that P2Y₂R may be associated with the bradykinin receptor, B2R [10]. We also showed

that sugar chains of B2R in Western blotting have a wide range of sizes, while the sizes of the sugar chains of P2Y₂R are uniformly small.

Glycosylation promotes expression of proteins in the cell membrane [11] and some GPCRs are localized in membrane microdomains such as rafts for interaction with other signaling molecules and regulation of their activity [12–14]. In this study, the cellular localization and distribution to lipid rafts of WT P2Y₂R and its mutants with loss of N-glycosylation sites were examined. The results showed that most of WT P2Y₂R localized in lipid rafts and was expressed on the cell surface. Besides, a glycosylation-deficient P2Y₂R mutant remained localized in lipid rafts, was not transferred beyond the ER, and was degraded by proteasomes. These results show that P2Y₂R requires N-glycosylation for expression on the cell surface.

2. Materials and methods

Preparation of Plasmids. Human P2Y₂R genes with a C-terminal c-Myc epitope tag (EQKLISEEDL) were prepared by PCR and

* Corresponding author.

E-mail address: hhigashi@tohoku-mpu.ac.jp (H. Higashi).

inserted into the pIRES2-EGFP plasmid (Clontech) with *EcoRI* and *BamHI* sites. The IRES and EGFP gene sequences were removed using *BamHI* and *NotI*, followed by blunting and ligation. Phusion High-Fidelity DNA Polymerase, restriction enzymes and a Quick Ligation kit were purchased from New England Biolabs. A DNA blunting kit was obtained from Takara Bio.

Cell culture. COS-7 cells were grown in D-MEM supplemented with 10% fetal calf serum and kept in a humidified 5% CO₂ atmosphere at 37 °C. COS-7 cells were transiently transfected using Viafect transfection reagent (Promega). In some experiments, epoxomicin (Peptide Institute Inc.) and bafilomycin A1 (LC Labs) were added at final concentrations of 1 and 0.1 μM, respectively, 12 h before harvesting.

Preparation of membrane fractions. COS-7 cells cultured on a 6-well plate were washed once with PBS and harvested using a cell scraper. After centrifugation at 3000 rpm for 5 min at 4 °C, precipitated cells were suspended in ice-cold TBS and homogenized in 500 μL of TBS containing Protease Inhibitor Cocktail (Nacalai Tesque) with 15 strokes using a teflon homogenizer on ice. The homogenate was centrifuged at 700 g for 5 min at 4 °C, and supernatant was centrifuged at 21,900 g for 90 min at 4 °C. This pellet was used as the total membrane fraction. In some experiment, the pellet was first treated with Peptide-N-Glycosidase F (PNGase F, New England Biolabs). The pellet was resuspended in 100 μL of ice-cold TBS containing 0.1% Triton X-100, and the tube was inverted using a rotator for 1 h at 4 °C. The supernatant and pellet from centrifugation at 21,900 g for 90 min at 4 °C were used as the detergent-soluble and detergent-insoluble membrane fractions, respectively.

Chloroform-methanol precipitation of protein. Methanol (400 μL) was added to 100 μL of detergent soluble membrane fraction, followed by 100 μL of CHCl₃, and then 300 μL of water. The mixture was vortexed well after each addition. After centrifugation at 17,400 g for 1 min at room temperature, the upper layer was removed while leaving the intermediate protein layer. To eliminate layer separation, 400 μL of methanol was added and the tube was inverted a few times to mix gently. After centrifugation at 17,400 g for 2 min, supernatant was removed and the dried pellet was used as a protein sample for SDS-PAGE.

SDS-PAGE and Western blotting. SDS-PAGE was performed using a Novex NuPAGE SDS-Gel system with 4–12% Bis-Tris gels (Thermo Fisher Scientific). Proteins were electrophoretically transferred to an Immobilon PVDF membrane (Merck Millipore) using a semi-dry

blotting system. After blocking with 5% skim milk in PBS, P2Y₂R was detected using *anti-Myc* mouse mAb (9B11; Cell Signaling Technology) followed by Horseradish Peroxidase conjugated anti-mouse IgG goat pAb (Jackson ImmunoResearch Lab.), and a Lumina Forte Western HRP Substrate (Merck Millipore).

Immunocytochemistry. COS-7 cells were cultured on Millicell EZ 8 well slides (Merck Millipore) for 1 day, stimulated with 0.1 mM UTP 15 min before fixation, and fixed by 3% paraformaldehyde after removal of the medium. After blocking with 5% skim milk in PBS, P2Y₂R was detected using *anti-Myc* monoclonal antibodies (9B11 mouse mAb and 71D10 rabbit mAb; Cell Signaling Technology) followed by Alexa Fluor 546 conjugated secondary antibodies (Thermo Fisher Scientific), and observed using an Olympus FV1000 confocal laser scanning microscope. The following antibodies were used to detect organelles: *anti-KDEL* mouse mAb (10C3; Enzo Life Science) for the ER, *anti-RCAS1* rabbit mAb (D2B6N; Cell Signaling Technology) for Golgi bodies, *anti-Na⁺-K⁺ ATPase* rabbit mAb (D2B6N; abcam) for plasma membrane, *anti-hTransferin receptor* mouse mAb (H68.4; Thermo Fisher Scientific) for recycling endosomes, *anti-EEA1* mouse mAb (4/EEA1; BD Biosciences) for early endosomes, and Alexa Fluor 546 conjugated secondary antibodies (Thermo Fisher Scientific).

3. Results

3.1. Preparation of N-glycan-deficient mutants of P2Y₂ receptor

P2Y₂R has N-glycosylation consensus sequences (Asn-X-Ser/Thr) at three sites, including two (Asn9 and Asn13) in the N-terminal extracellular region and a third (Asn66) located in an intracellular region. For deletion of N-glycans, N9Q and N13Q point mutants and the N9Q/N13Q double mutant were made by replacing Asn9, Asn13 or both with Gln residues (Fig. S1). Each P2Y₂R construct had a c-Myc epitope tag attached to the C-terminal region for detection in Western blotting and immunostaining. After expressing WT or glycosylation-deficient P2Y₂R in COS-7 cells, Western blotting was performed with *anti-Myc* antibody. Bands were detected at 46 kDa for the WT protein, 42 kDa for N9Q and N13Q, and 38 kDa for the glycosylation-deficient N9Q/N13Q protein, indicating that both Asn9 and Asn13 are glycosylated in P2Y₂R (Fig. 1A). The apparent absence of glycosylation in WT, N9Q and N13Q P2Y₂R (38 kDa bands) may have been due to transient expression. Membrane fractions prepared from COS-7 cells

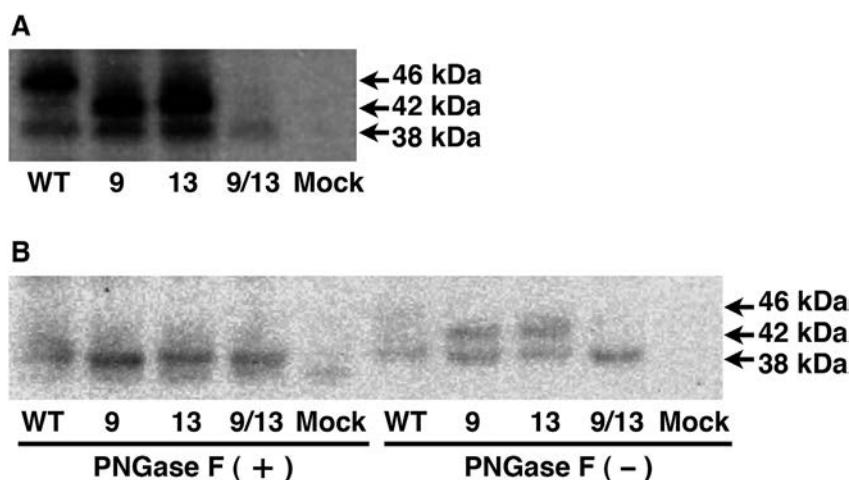


Fig. 1. Confirmation of N-linked glycosylation of P2Y₂R. (A) Membrane fractions of COS-7 cells expressing P2Y₂R wild-type (WT) and mutants (N9Q, N13Q, N9Q/N13Q) analyzed by Western blotting using *anti-Myc* antibody. (B) Membrane fractions treated with PNGase F and examined by Western blotting.

expressing WT or mutant P2Y₂R were treated with PNGase F and then subjected to Western blotting. The bands at 46 kDa for WT and 42 kDa for N9Q and N13Q were eliminated by PNGase F and only the 38 kDa band remained, thus confirming that both Asn9 and Asn13 in P2Y₂R undergo *N*-glycosylation (Fig. 1B).

3.2. Subcellular localization of *N*-glycan deficient P2Y₂ receptor

WT and mutant P2Y₂R were expressed in COS-7 cells to observe the distribution using confocal fluorescent microscopy. Except glycosylation-deficient mutant N9Q/N13Q, P2Y₂R appeared to distribute on cell membrane and the distribution disappeared by UTP stimulation (Fig. 2A). Furthermore, WT and N9Q/N13Q were expressed in COS-7 cells for fluorescent double staining of marker proteins for the ER, Golgi body, late endosome, and recycling endosome, and observation by confocal microscopy. The distribution

of WT P2Y₂R was consistent with staining of the ER, Golgi body, and cell membrane (Fig. 2B). When the cells expressed WT P2Y₂R were stimulated with UTP, distribution to the cell membrane decreased, and a granulated distribution overlapping early endosomes and recycling endosomes was observed (Fig. 2B). N9Q/N13Q P2Y₂R was distributed only in the ER, and not in the cell membrane or Golgi body (Fig. 2B), and showed no changes in distribution upon stimulation with UTP (Fig. 2A). We examined localization of P2Y₂R in lipid rafts, based on resistance to detergent. Almost all N9Q/N13Q proteins were found in the detergent insoluble membrane fraction, lipid raft (Fig. 3A). While N9Q/N13Q P2Y₂R was not transferred to the Golgi body due to the absence of *N*-glycan, this mutant remained in the detergent insoluble membrane fraction. These results show that P2Y₂R is distributed to lipid rafts in the ER membrane prior to *N*-glycosylation in ER.

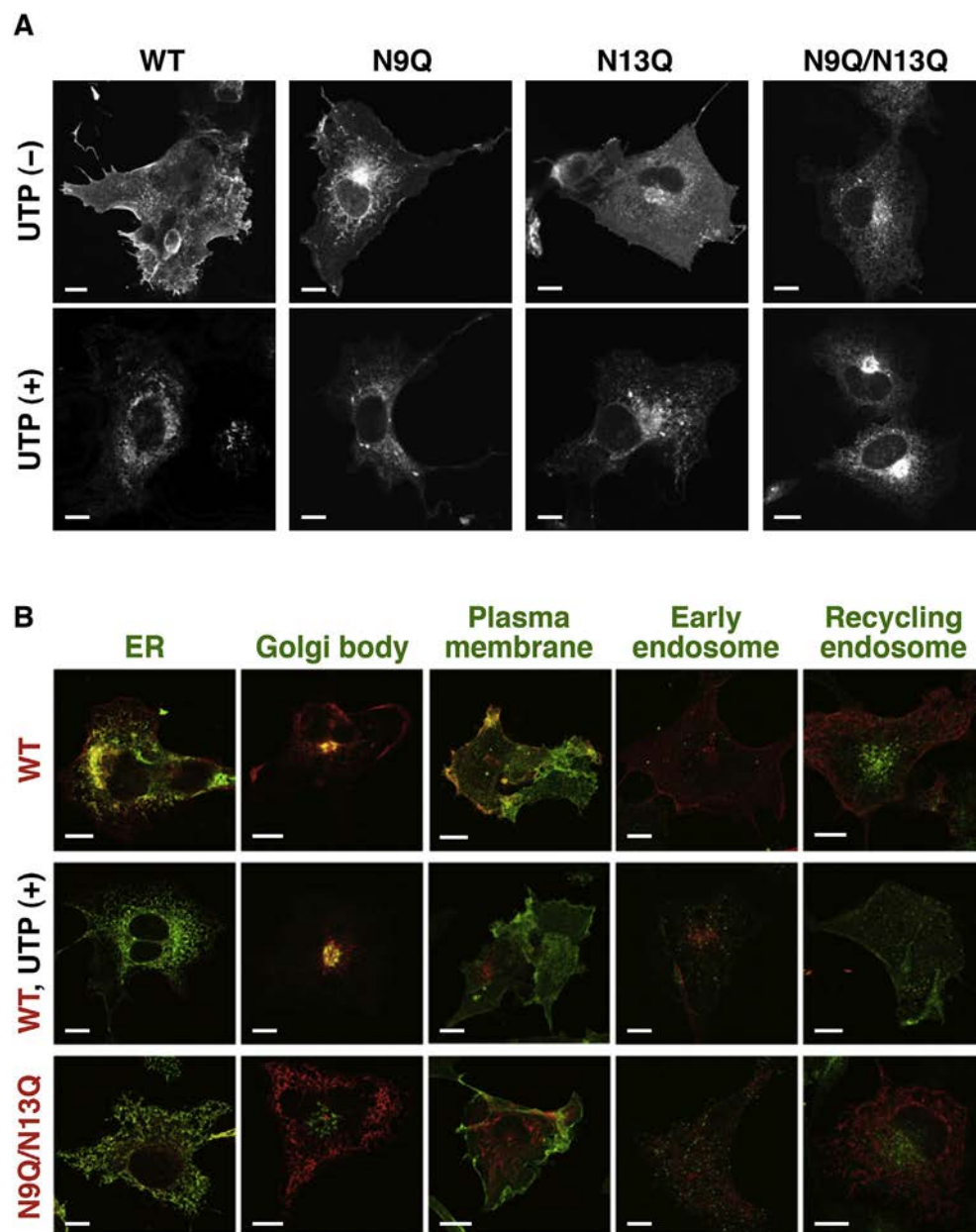


Fig. 2. Localization of P2Y₂R WT and N9Q/N13Q mutant. (A) Intracellular localization in COS-7 cells observed by confocal laser scanning microscopy. In some experiments, cells were treated with 0.1 mM UTP (UTP (+)). (B) Colocalization of P2Y₂R (red) and organelles (green) examined by double staining. Scale bars indicate 10 μm.

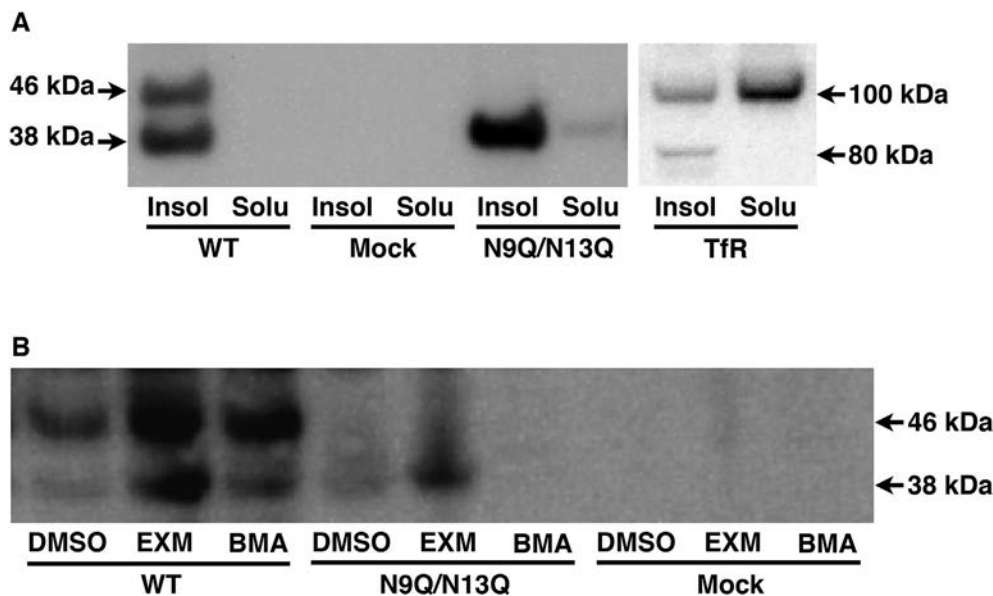


Fig. 3. Distribution to lipid rafts and proteolysis of P2Y₂R mutants. (A) Detergent insoluble (Insol) and soluble (Solu) membrane fractions analyzed by Western blotting using anti-Myc antibody. To ensure separation of lipid raft and non-raft proteins, the distribution of transferrin receptor (TfR) in the same sample was examined. (B) COS-7 cells expressing P2Y₂R WT or N9Q/N13Q were treated with the proteasome inhibitor epoxomicin (EXM) or the lysosome inhibitor bafilomycin A1 (BMA) 12 h before harvesting, and total membrane fractions were analyzed by Western blotting.

3.3. ER-associated degradation of *N*-glycan-deficient P2Y₂ receptor

Epoxomicin, a proteasome inhibitor, or bafilomycin A1, a lysosome-autophagy inhibitor, was added 12 h after transfection of WT or N9Q/N13Q P2Y₂R in COS-7 cells. Culture was then performed for an additional 12 h. Western blotting and immunostaining with anti-Myc antibody showed significantly increased levels of WT and N9Q/N13Q P2Y₂R in cells treated with epoxomicin (Fig. 3B). This result suggests that P2Y₂R (38 kDa) without glycosylation is degraded by proteasomes. Glycosylated WT P2Y₂R (46 kDa) also significantly increased because of degradation of proteins that were folded or glycosylated incorrectly due to excess expression. The level of WT P2Y₂R was also increased by bafilomycin A1 (Fig. 3B). There was also an increased level of receptors without glycosylation, which were not transferred to the cell membrane, and such receptors may be degraded by autophagy. Collectively, these findings show that *N*-glycan modification at either of the two consensus sequences in the N-terminal domain of P2Y₂R is required for transfer of the receptor to the cell membrane, and that non-glycosylated P2Y₂R is degraded by proteasomes.

4. Discussion

Many GPCRs have *N*-glycosylation consensus sequences in the extracellular region, and most membrane proteins are likely to be glycosylated. Most of the roles of *N*-glycosylation in GPCRs are unclear, but glycosylation is known to be required for expression of angiotensin II receptor (AT₁R) and follicle-stimulating hormone receptor (FSHR) in cell membranes [15–17], and for maintaining a higher level of β_2 -adrenaline receptor in the cell membrane, although glycosylation is not essential for this receptor [18]. In contrast, there are many receptors, including α_2 -adrenaline receptor, H₂ histamine receptor, and muscarinic receptor, for which loss of *N*-glycosylation has almost no impact on cell surface expression [18–20].

Expression of membrane proteins at a designated site requires formation of the native fold, and misfolded proteins are excluded

from transport vesicles by a quality control mechanism in the ER [21,22]. In this mechanism, non-native folds are detected to facilitate refolding or degradation. The mechanism involves molecular chaperones and lectin-like chaperones, which recognize the hydrophobic surface of non-native proteins, unbridged Cys residues, and immature *N*-glycosylation. Calnexin, calreticulin, and BiP are molecular chaperones related to GPCRs [23–28]. Calnexin and calreticulin are homologous lectin-like molecular chaperones that facilitate maturation of glycoproteins by recognizing *N*-glycosylation in an early phase of modification of membrane proteins and secreted proteins during folding [29]. BiP binds to the hydrophobic region on the surface of a protein during folding or to a misfolded protein, and is involved in retrograde trafficking to the ER or membrane transport to the cytoplasm in ER-associated degradation (ERAD) [30,31].

The results of this study show that both *N*-glycosylation consensus sequences in the extracellular region of P2Y₂R are modified, and that the N9Q/N13Q double mutant with complete loss of glycosylation was not transferred to the cell surface and had an extremely low expression level. Since N9Q/N13Q P2Y₂R cannot remain in the ER with lectin-like chaperones such as calnexin and calreticulin, molecular chaperones such as BiP that recognize hydrophobic surfaces may be involved. The expression level of N9Q/N13Q P2Y₂R was low because the absence of *N*-glycosylation may prevent proper folding and quality control by calnexin and calreticulin, causing lower folding efficiency. Thus, the expressed protein is degraded by proteasomes as a misfolded protein, rather than remaining in the ER.

Lipid rafts mature in the Golgi body through synthesis of glycolipid and sphingomyelin structural components, and signaling proteins associate with the rafts during the course of maturation. However, the *N*-glycan-deficient P2Y₂R existed in the detergent insoluble membrane fraction when the lipid raft was fractionated, while P2Y₂R remained in the ER. Since the detergent insoluble membrane fraction is product in the experiment, these results may be an artifact, but it is possible that P2Y₂R may associate with lipid rafts in the ER because glucosylceramide synthases are also present

in the ER, and retrograde traffic of vesicles can be observed from the *cis* Golgi. Previously, we demonstrated that B2 bradykinin receptor is closely associated with P2Y₂R and has heterogeneous glycans differ from P2Y₂R [10]. If localization of P2Y₂R in lipid rafts occurs before glycosylation, this may lead to uniform and short sugar chains. P2Y₂R forms hetero-oligomers with various GPCRs [10,32,33], and P2Y₂R localized in lipid rafts may recruit interacting GPCRs.

This study shows that *N*-glycosylation of P2Y₂R is involved in receptor cell surface expression, and that P2Y₂R is distributed to lipid rafts before *N*-glycosylation. P2Y₂R lacking *N*-glycosylation at one site was transferred to the cell surface but the effect of partial loss of *N*-glycosylation on the receptor function of P2Y₂R and association with other GPCRs are unclear.

Acknowledgements

Funding: This study was supported by the Strategic Study Base Formation Support Project for Private Universities, Japan.

Appendix A. Supplementary data

Supplementary data related to this article can be found at <http://dx.doi.org/10.1016/j.bbrc.2017.02.061>.

Transparency document

Transparency document related to this article can be found online at <http://dx.doi.org/10.1016/j.bbrc.2017.02.061>.

References

- [1] V.L. Cressman, E. Lazarowski, L. Homolya, R.C. Boucher, B.H. Koller, B.R. Grubb, Effect of loss of P2Y₂ receptor gene expression on nucleotide regulation of murine epithelial Cl⁻ transport, *J. Biol. Chem.* 274 (1999) 26461–26468.
- [2] G.A. Weisman, D. Ajit, R. Garrad, T.S. Peterson, L.T. Woods, C. Thebeau, J.M. Camden, L. Erb, Neuroprotective roles of the P2Y₂ receptor, *Purinergic Signal* 8 (2012) 559–578.
- [3] M.R. Elliott, F.B. Chekeni, P.C. Trampont, E.R. Lazarowski, A. Kadl, S.F. Walk, D. Park, R.I. Woodson, M. Ostankovich, P. Sharma, J.J. Lysiak, T.K. Harden, N. Leitinger, K.S. Ravichandran, Nucleotides released by apoptotic cells act as a find-me signal to promote phagocytic clearance, *Nature* 461 (2009) 282–286.
- [4] M. Kronlage, J. Song, L. Sorokin, K. Isfort, T. Schwerdtle, J. Leipziger, B. Robaye, P.B. Conley, H.C. Kim, S. Sargin, P. Schon, A. Schwab, P.J. Hanley, Autocrine purinergic receptor signaling is essential for macrophage chemotaxis, *Sci. Signal* 3 (2010) ra55.
- [5] D.B. Arthur, K. Akassoglou, P.A. Insel, P2Y₂ receptor activates nerve growth factor/TrkA signaling to enhance neuronal differentiation, *Proc. Natl. Acad. Sci. U. S. A.* 102 (2005) 19138–19143.
- [6] A. Luckhoff, R. Zeh, R. Busse, Desensitization of the bradykinin-induced rise in intracellular free calcium in cultured endothelial cells, *Pflügers Arch.* 412 (1988) 654–658.
- [7] G. Reetz, G. Reiser, Cross-talk of the receptors for bradykinin, serotonin, and ATP shown by single cell Ca²⁺ responses indicating different modes of Ca²⁺ activation in a neuroblastoma x glioma hybrid cell line, *J. Neurochem.* 62 (1994) 890–897.
- [8] U. Czubayko, G. Reiser, Desensitization of P2U receptor in neuronal cell line. Different control by the agonists ATP and UTP, as demonstrated by single-cell Ca²⁺ responses, *Biochem. J.* 320 (Pt 1) (1996) 215–219.
- [9] H.E. Lopez-Valdes, L. Beltran-Parral, K.C. Brennan, A.C. Charles, Bradykinin increases resensitization of purinergic receptor signaling in glioma cells, *Cancer Cell Int.* 10 (2010) 35.
- [10] S. Yashima, A. Shimazaki, J. Mitoma, T. Nakagawa, M. Abe, H. Yamada, H. Higashi, Close association of B2 bradykinin receptors with P2Y₂ ATP receptors, *J. Biochem.* 158 (2015) 155–163.
- [11] K. Ohtsubo, S. Takamatsu, C. Gao, H. Korekane, T.M. Kurosawa, N. Taniguchi, N-Glycosylation modulates the membrane sub-domain distribution and activity of glucose transporter 2 in pancreatic beta cells, *Biochem. Biophys. Res. Commun.* 434 (2013) 346–351.
- [12] R. Shamri, V. Grabovsky, S.W. Feigelson, O. Dwir, Y. Van Kooyk, R. Alon, Chemokine stimulation of lymphocyte alpha 4 integrin avidity but not of leukocyte function-associated antigen-1 avidity to endothelial ligands under shear flow requires cholesterol membrane rafts, *J. Biol. Chem.* 277 (2002) 40027–40035.
- [13] A.M. Navratil, S.P. Bliss, K.A. Berghorn, J.M. Haughian, T.A. Farmerie, J.K. Graham, C.M. Clay, M.S. Roberson, Constitutive localization of the gonadotropin-releasing hormone (GnRH) receptor to low density membrane microdomains is necessary for GnRH signaling to ERK, *J. Biol. Chem.* 278 (2003) 31593–31602.
- [14] E.M. Hur, Y.S. Park, B.D. Lee, I.H. Jang, H.S. Kim, T.D. Kim, P.G. Suh, S.H. Ryu, K.T. Kim, Sensitization of epidermal growth factor-induced signaling by bradykinin is mediated by c-Src. Implications for a role of lipid microdomains, *J. Biol. Chem.* 279 (2004) 5852–5860.
- [15] S. Jayadev, R.D. Smith, G. Jagadeesh, A.J. Baukal, L. Hunyady, K.J. Catt, N-linked glycosylation is required for optimal AT_{1a} angiotensin receptor expression in COS-7 cells, *Endocrinology* 140 (1999) 2010–2017.
- [16] B. Deslauniers, C. Ponce, C. Lombard, R. Languier, J.C. Bonnafous, J. Marie, N-glycosylation requirements for the AT_{1a} angiotensin II receptor delivery to the plasma membrane, *Biochem. J.* 339 (Pt 2) (1999) 397–405.
- [17] D. Davis, X. Liu, D.L. Segaloff, Identification of the sites of N-linked glycosylation on the follicle-stimulating hormone (FSH) receptor and assessment of their role in FSH receptor function, *Mol. Endocrinol.* 9 (1995) 159–170.
- [18] D.G. Sawutz, S.M. Lanier, C.D. Warren, R.M. Graham, Glycosylation of the mammalian alpha 1-adrenergic receptor by complex type N-linked oligosaccharides, *Mol. Pharmacol.* 32 (1987) 565–571.
- [19] Y. Fukushima, Y. Oka, T. Saitoh, H. Katagiri, T. Asano, N. Matsushashi, K. Takata, E. van Breda, Y. Yazaki, K. Sugano, Structural and functional analysis of the canine histamine H2 receptor by site-directed mutagenesis: N-glycosylation is not vital for its action, *Biochem. J.* 310 (Pt 2) (1995) 553–558.
- [20] C.J. van Koppen, N.M. Nathanson, Site-directed mutagenesis of the m2 muscarinic acetylcholine receptor. Analysis of the role of N-glycosylation in receptor expression and function, *J. Biol. Chem.* 265 (1990) 20887–20892.
- [21] L. Ellgaard, A. Helenius, Quality control in the endoplasmic reticulum, *Nat. Rev. Mol. Cell Biol.* 4 (2003) 181–191.
- [22] B. Kleizen, I. Braakman, Protein folding and quality control in the endoplasmic reticulum, *Curr. Opin. Cell Biol.* 16 (2004) 343–349.
- [23] J.P. Morello, A. Salahpour, U.E. Petaja-Repo, A. Laperriere, M. Loneragan, M.F. Arthus, I.R. Nabi, D.G. Bichet, M. Bouvier, Association of calnexin with wild type and mutant AVPR2 that causes nephrogenic diabetes insipidus, *Biochemistry* 40 (2001) 6766–6775.
- [24] P.M. Lancot, P.C. Leclerc, E. Escher, G. Guillemette, R. Leduc, Role of N-glycan-dependent quality control in the cell-surface expression of the AT₁ receptor, *Biochem. Biophys. Res. Commun.* 340 (2006) 395–402.
- [25] D. Mizrahi, D.L. Segaloff, Intracellularly located misfolded glycoprotein hormone receptors associate with different chaperone proteins than their cognate wild-type receptors, *Mol. Endocrinol.* 18 (2004) 1768–1777.
- [26] S. Siffroi-Fernandez, A. Giraud, J. Lanet, J.L. Franc, Association of the thyrotropin receptor with calnexin, calreticulin and BiP. Effects on the maturation of the receptor, *Eur. J. Biochem.* 269 (2002) 4930–4937.
- [27] P.M. Lancot, P.C. Leclerc, M. Clement, M. Auger-Messier, E. Escher, R. Leduc, G. Guillemette, Importance of N-glycosylation positioning for cell-surface expression, targeting, affinity and quality control of the human AT₁ receptor, *Biochem. J.* 390 (2005) 367–376.
- [28] A. Anukanth, H.G. Khorana, Structure and function in rhodopsin. Requirements of a specific structure for the intradiscal domain, *J. Biol. Chem.* 269 (1994) 19738–19744.
- [29] D.B. Williams, Beyond lectins: the calnexin/calreticulin chaperone system of the endoplasmic reticulum, *J. Cell. Sci.* 119 (2006) 615–623.
- [30] B.D. Hamman, L.M. Hendershot, A.E. Johnson, BiP maintains the permeability barrier of the ER membrane by sealing the luminal end of the translocon pore before and early in translocation, *Cell* 92 (1998) 747–758.
- [31] B. Meusser, C. Hirsch, E. Jarosch, T. Sommer, ERAD: the long road to destruction, *Nat. Cell Biol.* 7 (2005) 766–772.
- [32] K. Yoshioka, O. Saitoh, H. Nakata, Heteromeric association creates a P2Y₂-like adenosine receptor, *Proc. Natl. Acad. Sci. U. S. A.* 98 (2001) 7617–7622.
- [33] T. Suzuki, K. Namba, H. Tsuga, H. Nakata, Regulation of pharmacology by hetero-oligomerization between A₁ adenosine receptor and P2Y₂ receptor, *Biochem. Biophys. Res. Commun.* 351 (2006) 559–565.



A Key Regulator of Cell Adhesion: Identification and Characterization of Important *N*-Glycosylation Sites on Integrin $\alpha 5$ for Cell Migration

Qinglei Hang,^a Tomoya Isaji,^a Sicong Hou,^a Yuqin Wang,^{a,b} Tomohiko Fukuda,^a Jianguo Gu^{a,b}

Division of Regulatory Glycobiology, Institute of Molecular Biomembrane and Glycobiology, Tohoku Medical and Pharmaceutical University, Sendai, Miyagi, Japan^a; Department of Pharmacology, Pharmacy College, Nantong University, Nantong, Jiangsu, China^b

ABSTRACT The *N*-glycosylation of integrin $\alpha 5 \beta 1$ is thought to control many fundamental aspects of cell behavior, including cell adhesion and migration. However, the mechanism of how *N*-glycans function remains largely obscure. Here, we used a loss-of-function approach. Wild-type (WT) integrin $\alpha 5$ and *N*-glycosylation mutant S3-5 (sites 3 to 5) integrin $\alpha 5$, which contains fewer *N*-glycans, were stably reconstituted in $\alpha 5$ knockout cancer cells. We found that the migration ability of S3-5 cells was decreased in comparison with that of the WT. Interestingly, the levels of phosphorylated focal adhesion kinase and actin stress fiber formation were greatly enhanced in the S3-5 mutant. In a mechanistic manner, the internalization of active but not total integrin $\alpha 5 \beta 1$ was inhibited in S3-5 cells, which is a process that is related to the enhanced expression of active integrin $\alpha 5 \beta 1$ on the cell surface. Importantly, restoration of *N*-glycosylation on the β -propeller domain of $\alpha 5$ reinstated the cell migration ability, active $\alpha 5 \beta 1$ expression, and internalization. Moreover, these *N*-glycans are critical for $\alpha 5$ -syndecan-4 complex formation. These findings indicate that *N*-glycosylation on the β -propeller domain functions as a molecular switch to control the dynamics of $\alpha 5 \beta 1$ on the cell surface that in turn is required for optimum adhesion for cell migration.

KEYWORDS *N*-glycan, activation, complex formation, internalization

Cell migration is essential not only for normal physiological processes such as embryonic development and wound healing but also for pathological changes such as inflammatory disease and cancer (1). Integrin, the $\alpha \beta$ heterodimeric transmembrane receptor, plays a central role in cell migration by connecting an extracellular matrix (ECM) to the cytoskeleton as well as functioning as a bidirectional signaling molecule that transmits information across the cell membrane (2). Due to its importance, integrin has been highly implicated in the development of tumor malignancy. Therefore, a detailed molecular understanding of the mechanisms involved in integrin-mediated tumor cell migration is very important for our ability to intervene in the procession of cancer.

In mammals, different α and β subunit combinations make up a total of 24 integrins. Integrins are found in either active or inactive conformations with respect to their high or low affinity for their ECM ligands (3), and an allosteric change that favors high affinity can be induced by either cytoplasmic events ("inside-out" activation) or extracellular factors ("outside-in" activation) (4), which triggers integrin clustering, cytoskeletal remodeling, and the assembly of cell adhesion complexes, including focal adhesion (FA) and fibrillary adhesion (5). Indeed, cell migration is a highly dynamic process that

Received 11 October 2016 Returned for modification 3 November 2016 Accepted 29 January 2017

Accepted manuscript posted online 6 February 2017

Citation Hang Q, Isaji T, Hou S, Wang Y, Fukuda T, Gu J. 2017. A key regulator of cell adhesion: identification and characterization of important *N*-glycosylation sites on integrin $\alpha 5$ for cell migration. *Mol Cell Biol* 37:e00558-16. <https://doi.org/10.1128/MCB.00558-16>.

Copyright © 2017 American Society for Microbiology. All Rights Reserved.

Address correspondence to Jianguo Gu, jgu@tohoku-mpu.ac.jp.

is regulated by FA turnover in a coordinated manner, which requires the upregulation of cell matrix attachment at the leading edge of the cell and downregulation at its trailing edge. An appropriate balance in the adhesion and de-adhesion of the integrins is important for cell migration. The disassembly of FA requires the internalization of integrins that are either then recycled back to the cell membrane at the leading edge of migrating cells or degraded in the lysosome (6, 7). Thus, elucidating the precise mechanisms that control the internalization of integrins is fundamental to understanding coordinated cell migration.

Current insight into this regulation is derived largely from studies focused on the inner membrane, particularly cytoplasmic tails. For example, NPxY motif-binding proteins such as talin and kindlin (8), different small GTPases such as Rab and Rho families and their regulators, as well as serine/threonine kinases have been implicated in the internalization of integrins (9). However, little is known about the function of the outer membrane of integrins in this process.

Of note, integrins are known to be major glycan-carrying proteins. In fact, the functions of integrins are also dependent on their complex *N*-glycosylation modifications (10). Among the different types of integrins, $\alpha 5 \beta 1$, a major fibronectin (FN) receptor, is believed to be a relatively well-characterized example, and *N*-glycosylation is important for its mediated many biological functions such as cell adhesion and migration (11, 12). Although the importance of the *N*-glycosylation of $\alpha 5 \beta 1$ for cell migration has been highlighted, most studies have examined only total changes by displaying or masking specific glycan epitopes via the overexpression and knockdown, or knockout, of glycosyltransferase genes. For instance, alterations in the oligosaccharide portion of integrin $\alpha 5 \beta 1$ from the enhanced expression of some glycosyltransferase genes such as *N*-acetylglucosaminyltransferase V (GnT-V), GnT-III, or $\alpha 2,6$ -galactoside sialyltransferase 1 (ST6GAL1) can be used to regulate cell spreading and migration onto FN (10, 13, 14). However, the use of these approaches makes it quite difficult to clarify the details of the underlying mechanisms involved in the importance of *N*-glycosylation on $\alpha 5 \beta 1$.

To resolve these issues using the *N*-glycosylation mutants of integrin $\alpha 5$, we first identified the individual *N*-glycosylation of $\alpha 5$ as a key regulator for cell migration. We found that the *N*-glycosylation of the β -propeller domain on $\alpha 5$ was essential for the internalization of active integrin $\alpha 5 \beta 1$ and membrane complex formation (e.g., syndecan-4), which in turn was important for its expression on the cell surface, which may result in a form of cell adhesion that is more appropriate for migration.

RESULTS

***N*-Glycosylation on integrin $\alpha 5$ is required for $\alpha 5 \beta 1$ -mediated cell migration.**

Given the importance of $\alpha 5$ for cell migration, we hypothesized the involvement of *N*-glycosylation. To test this idea, we chose MDA-MB-231, HeLa, and U-251MG cells as the cell models, which relatively express higher levels of endogenous integrins on the cell surface, including integrins $\alpha 3$, $\alpha 5$, $\alpha 6$, αV , $\beta 1$, and $\beta 4$, than do 293T cells (see Fig. S1A in the supplemental material). First, we transfected either green fluorescent protein (GFP)-tagged wild-type (WT) or S3-5 mutant integrin $\alpha 5$ into $\alpha 5$ knockout ($\alpha 5$ -KO)-MDA-MB-231, $\alpha 5$ -KO-HeLa, and $\alpha 5$ -KO-U-251MG cells, which was established previously (15), because *N*-glycosylation on sites 3 to 5 (Fig. 1A) from among the 14 potential *N*-glycosylation sites in integrin $\alpha 5$ is necessary for its dimer formation with $\beta 1$ and total cell surface expression in CHO-B2 cells (12). Consistently, in immunoprecipitation (IP) and flow cytometric analyses, WT-MDA-MB-231 and S3-5-MDA-MB-231 cells exhibited comparable $\alpha 5 \beta 1$ heterodimeric formation abilities (Fig. 1B) and the same expression levels of $\alpha 5 \beta 1$ (Fig. 1C) or $\alpha 5$ (Fig. S1B) on the cell surface, as did HeLa and U-251MG cells (Fig. S1C and D). It is noteworthy that due to the heterogeneity of glycans, WT $\alpha 5$ on SDS-PAGE gels usually shows a diffuse band, as shown in Fig. 1B, which seems to have a relatively higher intensity than that of the S3-5 mutant. However, after the removal of heterogeneity by treatment with the peptide:*N*-glycosidase F (PNGase F) for deglycosylation, WT cells exhibited an expression level of $\alpha 5$ similar to that of S3-5 mutant cells (Fig. S1E). Together, these results suggested that S3-5 mutant $\alpha 5$ can also

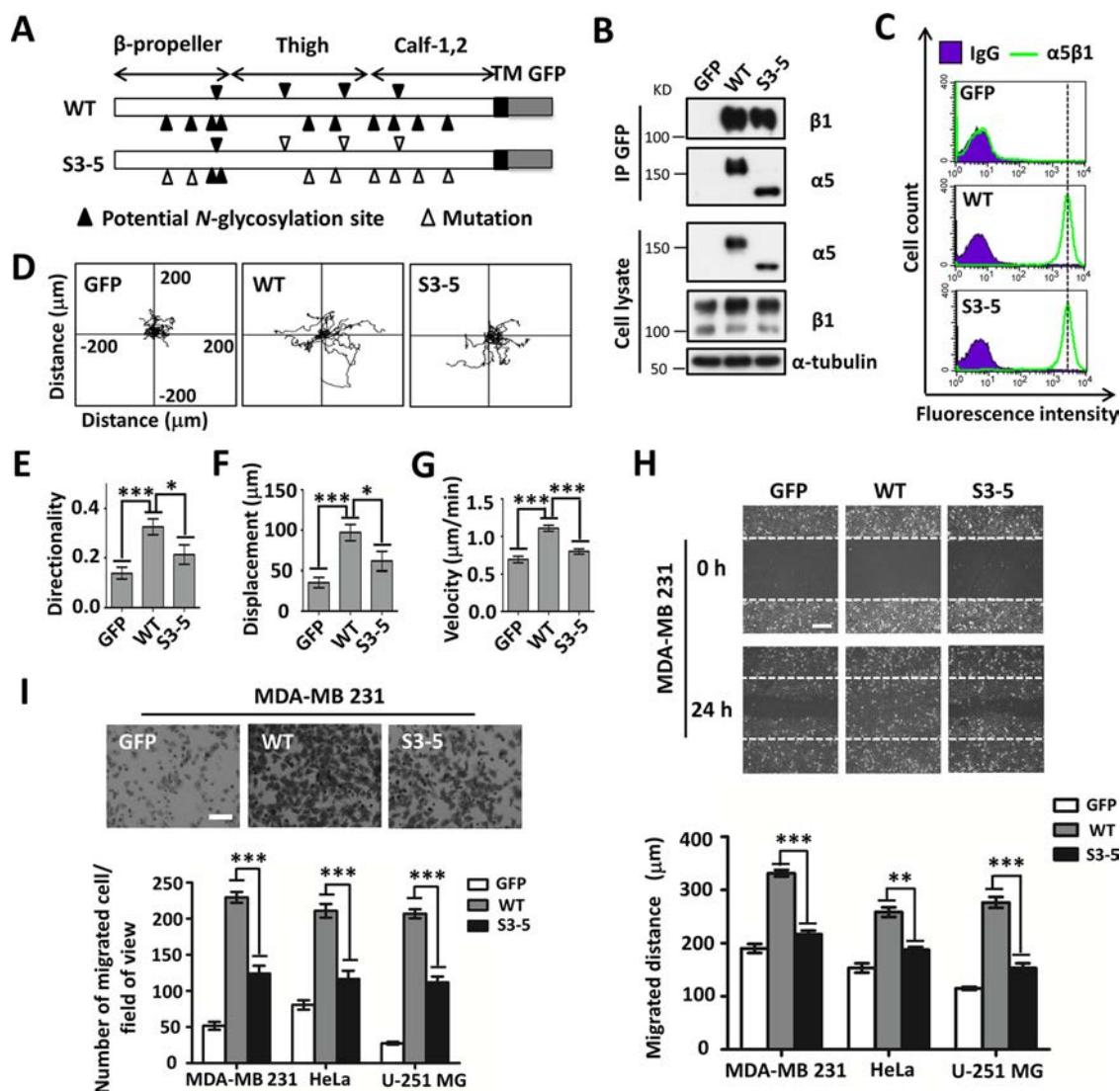


FIG 1 Comparison of FN-mediated cell migration in cell lines expressed with WT or S3-5 mutant $\alpha 5$. (A) Schematic diagram of potential N-glycosylation sites on the WT and S3-5 integrin $\alpha 5$ subunits. Putative N-glycosylation sites (N84Q, N182Q, N297Q, N307Q, N316Q, N524Q, N530Q, N593Q, N609Q, N675Q, N712Q, N724Q, N773Q, and N868Q) and point mutations are indicated. TM, transmembrane. (B and C) WT- and S3-5-MDA-MB-231 cells exhibit comparable $\alpha 5\beta 1$ heterodimer formation abilities (B) and the same expression levels of total integrin $\alpha 5\beta 1$ on the cell surface (C). (B, top) The stable cell lines were established as described in Materials and Methods. The indicated cell extracts were immunoprecipitated (IP) with anti-GFP-agarose, followed by anti- $\beta 1$ and $\alpha 5$ antibodies for Western blotting. (Bottom) Whole-cell extracts were also subjected to Western blotting (as an input). (C) The expression levels of $\alpha 5\beta 1$ were analyzed by flow cytometry. IgG was used as a control. (D to G) Individual migration tracks, persistence values, and mean speeds of GFP-, WT-, and S3-5-MDA-MB-231 cells migrating on FN. (E) Movements of the indicated cells were observed by time-lapse video microscopy ($n = 12$, from triplicate experiments). (E to G) The directionality (E), displacement (F), and speed (G) of migration were extracted from the track plots. (H and I) Cell wound closure (H) and abilities of migration toward FN (I) were determined by using wound healing and Transwell assays. Representative images of MDA-MB-231 cells appear at the top. The migrated distances relative to 0 h (H) and the numbers of migrated cells (I) of the MDA-MB-231, HeLa, and U-251MG cell lines were measured and statistically analyzed, respectively (bottom, $n = 3$ individual experiments). All values are reported as the means \pm SE (error bars), as determined by Student's t test. *, $P < 0.05$; **, $P < 0.01$; ***, $P < 0.001$. Bars, 250 μ m (H) and 350 μ m (I).

serve as a successful loss-of-function model to identify the roles of the remaining N-glycosylation on $\alpha 5$ in MDA-MB-231, HeLa, and U-251MG cells.

Next, we compared cell movement on FN between GFP-, WT-, and S3-5-MDA-MB-231 cells via time-lapse imaging for 12 h (Fig. 1D). As shown in Fig. 1D to G, GFP control cells still exhibited some cell motilities, which might be due to the function of other FN receptors such as integrin $\alpha \beta 1$, but these motilities were much weaker than those of WT cells, as reflected by the directionality (Fig. 1E), displacement (Fig. 1F), and mean migration speed (Fig. 1G). Interestingly, although the cell motility of S3-5 cells was

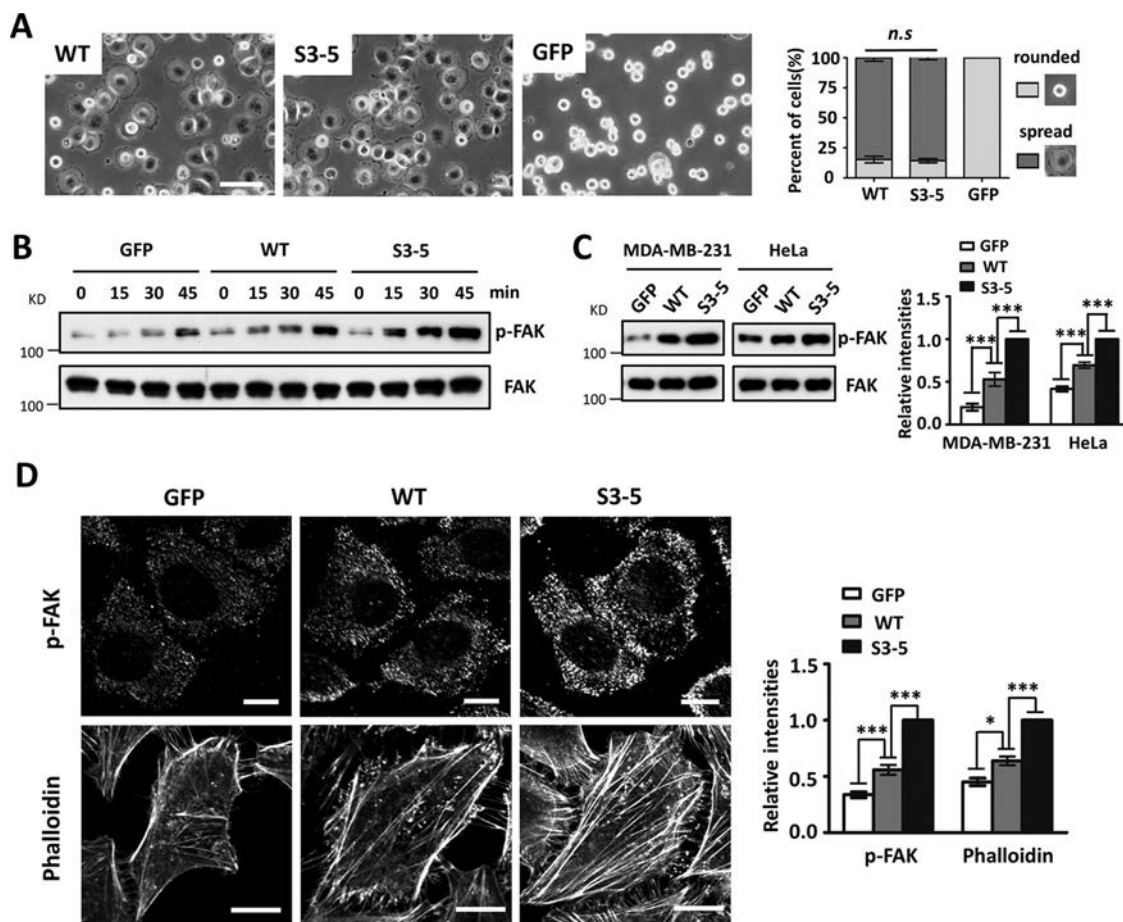


FIG 2 Changes in cell spreading, phosphorylation of FAK, and actin filament formation in S3-5 cells. (A) MDA-MB-231 cells were detached, blocked, and then replated onto FN-coated plates. After incubation for 20 min, cells were fixed, and representative images were taken. The percentages of rounded and spread cells were statistically analyzed (right) ($n = 9$, from 3 individual experiments). (B) MDA-MB-231 cells were detached, suspended in assay medium for 40 min, and then replated onto an FN-coated plate for the indicated times. Western blotting was performed with the indicated antibodies. (C, left) After culture on FN-coated dishes for 2 days, the indicated MDA-MB-231 and HeLa cells were lysed and immunoblotted with the indicated antibodies. (Right) Relative ratios (p-FAK versus FAK) ($n = 3$ individual experiments); the relative ratio was 1.0 for S3-5 mutant cells. (D) Immunofluorescence labeling and confocal microscopy of p-FAK (top) and actin stress fibers (bottom) in GFP, WT, and S3-5 mutant cells. MDA-MB-231 and HeLa cells were cultured on FN-coated coverslips, and cells were fixed, permeabilized, and then visualized with p-FAK and phalloidin-Alexa Fluor 549 (actin), respectively. The relative fluorescence intensities of p-FAK and phalloidin were quantified by using ImageJ software ($n = 6$, from 3 individual experiments); relative fluorescence intensity was 1.0 for S3-5 mutant cells. All values are reported as the means \pm SE (error bars), as determined by Student's t test. n.s., not significant ($P > 0.05$); *, $P < 0.05$; ***, $P < 0.001$. Bars, 120 μ m (A) and 20 μ m (D).

stronger than that of control GFP cells, it was significantly weaker than that of WT cells (Fig. 1D to G). These phenomena were also confirmed via wound healing (Fig. 1H) and Transwell (Fig. 1I) assays. In addition, decreased wound closure (Fig. 1H, bottom) and migration abilities (Fig. 1I, bottom) were also observed for both S3-5-HeLa and S3-5-U-251MG cells. Of note, we previously showed that *N*-glycosylation on the calf domain of $\alpha 5$ exhibited an inhibitory effect on cell proliferation via complex formation with epidermal growth factor receptor (EGFR) (15). Taken together, these results strongly suggest that the remaining *N*-glycosylation, other than that on sites 3 to 5 of $\alpha 5$, plays a crucial role in the mediation of cell migration.

Deletion of *N*-glycosylation on integrin $\alpha 5$ increases cell matrix adhesion. In order to explore the underlying mechanisms involved in the *N*-glycosylation of $\alpha 5$ -mediated cell migration, we compared the cell spreading abilities of WT and S3-5 cells. As shown in Fig. 2A, both WT- and S3-5-MDA-MB-231 cells exhibited comparable abilities for cell spreading on FN. A similar result was also observed for HeLa or U-251MG cells (data not shown), indicating that the remaining *N*-glycosylation on integrin $\alpha 5$ had no significant effect on cell spreading.

It is well known that integrin $\alpha 5 \beta 1$ facilitates cell migration, which in turn requires a dynamic turnover of cell matrix associations, during which the activation of focal adhesion kinase (FAK) is an important step (16). To determine whether *N*-glycosylation on $\alpha 5$ affected the FN-mediated activation of FAK, serum-starved cells were replated onto FN-coated plates and then harvested at the indicated times. The phosphorylation levels of FAK (p-FAK) in the cell lysates were detected. As expected, Western blot (WB) analysis revealed that the levels of p-FAK upon FN stimulation at each time point in GFP-MDA-MB-231 cells were lower than those in WT cells (Fig. 2B). However, intriguingly, S3-5-MDA-MB-231 cells exhibited increased expression levels of p-FAK compared with the WT ones (Fig. 2B). In addition, when cells were grown on FN-coated dishes for 2 days, p-FAK levels were still significantly higher in S3-5 cells than those in WT cells, in both MDA-MB-231 and HeLa cells (Fig. 2C). Immunofluorescence staining clearly showed that p-FAK containing cell matrix adhesion in S3-5 cells was consistently more prominent in both size and staining intensity than that in WT-MDA-MB-231 cells (Fig. 2D, top). Furthermore, the actin stress fibers detected by phalloidin were more abundant in S3-5-HeLa cells than in WT cells (Fig. 2D, bottom). Considering the decreased cell migration ability of S3-5 cells, these findings indicate that integrin $\alpha 5$ *N*-glycosylation can regulate a modest level of cell-FN adhesion for migration.

Removal of *N*-glycosylation on integrin $\alpha 5$ increases the active form of $\beta 1$ on the cell surface. Next, we investigated the cause of increased cell-FN adhesion in S3-5 cells. Considering that the efficiency of cell adhesion on the ECM is generally thought to be proportional to the amount of either active or total (i.e., active and inactive) integrin on the cell surface (17), we compared the expression levels of both active and total integrin $\beta 1$ in WT and S3-5 cells. The active form of $\beta 1$ was detected with the antibody HUTS-4-recognizing epitopes in the region spanning positions 355 to 425 (hybrid domain) of the common $\beta 1$ subunit, the expressions of which are reported to parallel the activity of integrin $\beta 1$ (18), and the level of active integrin $\beta 1$ recognized by this antibody but not total $\beta 1$ was clearly increased upon Mn^{2+} stimulation during Western blot analysis (see Fig. S1F in the supplemental material). Flow cytometric analysis clearly showed that approximately 10% of cell surface integrin $\beta 1$ is in the active conformation (Fig. 3A), which is consistent with data from a previous report (19), and that levels of the active form of $\beta 1$ but not the total form on the cell surface were significantly increased in S3-5-MDA-MB-231, S3-5-HeLa, and S3-5-U-251MG cells compared with those in WT cells (Fig. 3A).

Given the increased expression levels of active $\beta 1$ on the cell surface of S3-5 mutant cells, we wondered whether the expression of total active $\beta 1$ was also increased. Interestingly, as shown in Fig. 3B (middle), both WT and S3-5 mutant cells exhibited expression levels of both active $\beta 1$ and total $\beta 1$ similar to those in the whole-cell lysates. However, increased expression levels of active $\beta 1$ on the cell surface in S3-5 cells, as described above, were observed in the biotinylation experiment (Fig. 3B, top). Furthermore, the increased cell surface expression of active integrin $\beta 1$ (Fig. 3C, middle), but not that of the total version (Fig. 3C, top), in mutant MDA-MB-231 cells was consistently confirmed by immunostaining. Taken together, these results indicate that the *N*-glycosylation of $\alpha 5$ can regulate the localization of the active form of $\beta 1$ on the cell surface, which might explain the enhancement of cell-FN adhesion in S3-5 mutant cells.

***N*-Glycosylation on integrin $\alpha 5$ plays important roles in the internalization of active $\alpha 5 \beta 1$.** Because the loss of *N*-glycosylation on $\alpha 5$ increased the expression levels of active $\beta 1$ on the cell surface, we sought to investigate the underlying mechanism. Given that the endocytic trafficking of integrins, which involves their internalization from the cell surface and recycling back to the plasma membrane, is important for cell migration (20) and expression levels on the cell surface (21), we wondered whether *N*-glycosylation on $\alpha 5$ regulates its internalization. To address this, biotin pulse-chase experiments were performed. After biotin labeling of cell surface proteins at 4°C, cells were incubated at 37°C for different times to induce internalization, and the biotin remaining in the form of cell surface proteins was then stripped at 4°C, leaving only

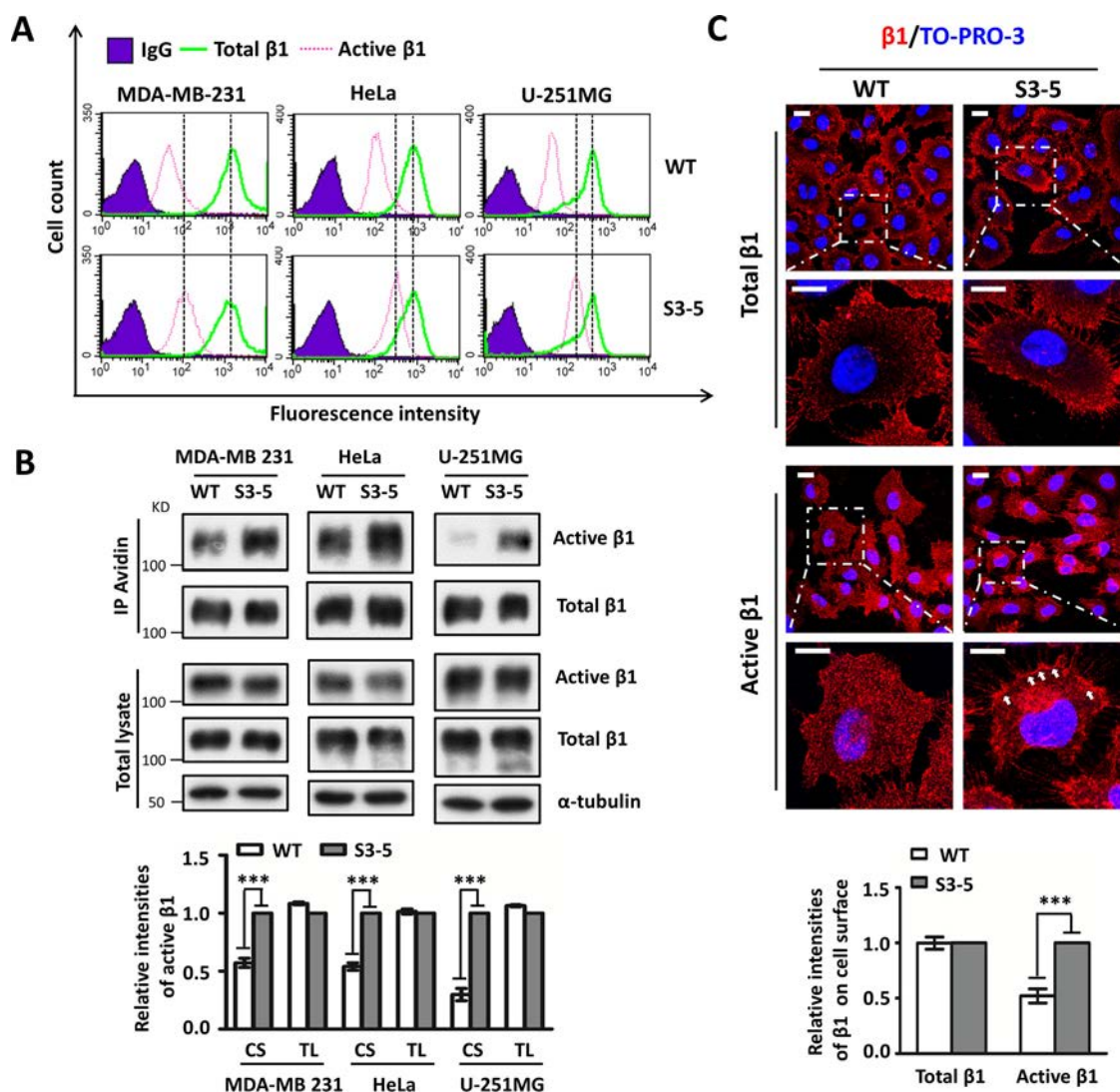


FIG 3 Increased expression levels of active integrin $\beta 1$ in S3-5 mutant cells. (A and B) The expression levels of active and total integrin $\beta 1$ on the cell surface (CS) or in total cell lysates (TL) were analyzed by flow cytometry (A) or biotinylation (B), and immunoblotting was performed with the indicated antibodies. The relative ratio (active $\beta 1$ versus total $\beta 1$) is shown at the bottom ($n = 3$ individual experiments), which was 1.0 for S3-5 mutant cells. (C) Comparison of the localization patterns of active integrin $\beta 1$ in WT- and S3-5-MDA-MB-231 cells. Cells were cultured on FN-coated coverslips and then subjected to immunostaining analyses. The images were merged with total (top) or active (middle) integrin $\beta 1$ (red) and To-Pro-3 staining (blue). The relative fluorescence intensities of total $\beta 1$ and active $\beta 1$ on cell surface were quantified by using ImageJ software ($n = 6$, from 3 individual experiments); relative fluorescence intensity was 1.0 for S3-5 mutant cells (bottom). All values are reported as the means \pm SE (error bars), as determined by Student's t test. ***, $P < 0.001$. Bars, 20 μ m (C).

internalized proteins biotinylated. Internalization of integrin $\alpha 5\beta 1$ was quantified by the immunoprecipitation of streptavidin-agarose, followed by Western blot analysis. As shown in Fig. 4A and B, the internalization of active $\beta 1$ in WT cells was increased within 5 min and then decreased at 10 min, while it continued to increase even at 15 min in S3-5 mutant cells, indicating delayed internalization in mutant cells. However, there were no significant differences in the internalizations of total $\alpha 5$ or $\beta 1$ subunits between WT and mutant cells. Consistently, the delayed internalization of active $\beta 1$ in S3-5 mutant cells was also confirmed by a biotinylation-based capture enzyme-linked immunosorbent assay (ELISA) (Fig. 4C). Taken together, these data indicate that N -glycosylation serves as a switch to control the internalization of active, but not inactive, integrin $\alpha 5\beta 1$.

Site 1 and site 2 N -glycosylation of the β -propeller domain on $\alpha 5$ mediates the regulation of cell migration. The data described above led us to investigate which

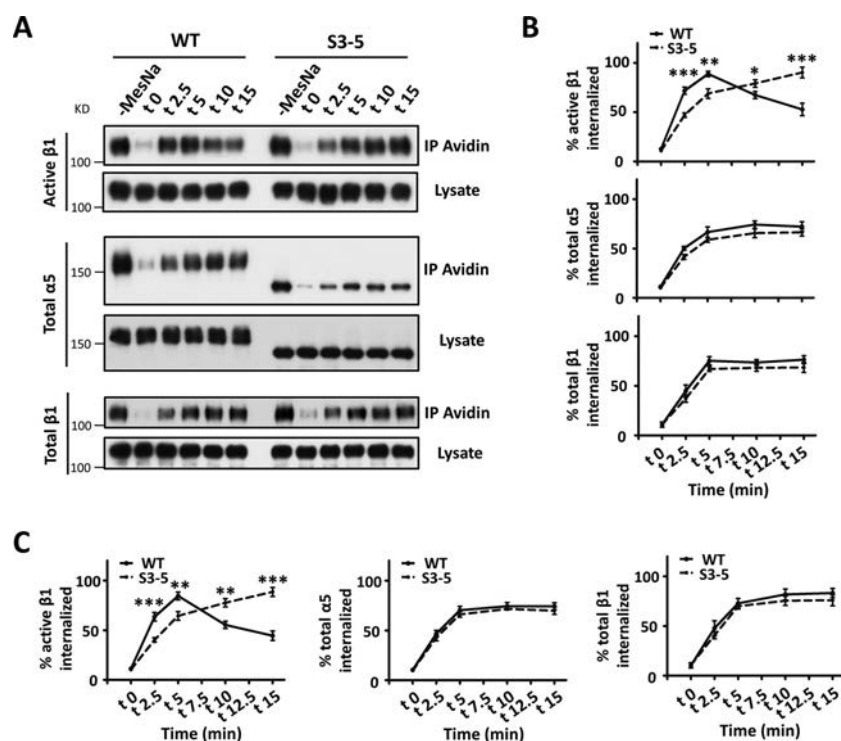


FIG 4 Delayed internalization of active integrin $\beta 1$ in S3-5 mutant MDA-MB-231 cells. (A) A biochemical internalization assay of active integrin $\beta 1$, total integrin $\alpha 5$, and total integrin $\beta 1$ was performed. The indicated internalized integrins at the indicated times were immunoprecipitated by avidin-agarose and then subjected to Western blotting for detection. The cell lysates were used as controls to show similar expression levels of the indicated integrins between WT and S3-5 cells. (B) The percentages of internalized integrins were statistically calculated from the signal intensity of MesNa-resistant integrin at each time point relative to the value for the control groups (without MesNa), which was the total integrin on the cell surface ($n = 3$ individual experiments). (C) The proportions of internalized integrins of WT and S3-5 mutant cells during the internalization period were also determined by a capture ELISA using microtiter wells coated with anti-active integrin $\beta 1$, anti-integrin $\alpha 5$, or anti-integrin $\beta 1$ antibodies, as described in Materials and Methods. The proportions of internalized integrins were statistically calculated ($n = 3$ individual experiments). All values are reported as the means \pm SE (error bars), as determined by Student's t test. *, $P < 0.05$; **, $P < 0.01$; ***, $P < 0.001$.

N-glycosylation site(s) of integrin $\alpha 5$ was essential for regulation. We recently demonstrated that N-glycosylation of the calf domain on $\alpha 5$ (sites 10 to 14) (Fig. 5A) was essential for its association with EGFR (15). This represented the first restoration of N-glycosylation in both the calf and the remaining domains in S3-5 mutant cells. However, as shown in Fig. 5B and C, restoration of N-glycosylation on the calf domain (sites 3 to 5 and 10 to 14) affected neither cell migration nor the expression of active $\beta 1$ on the cell surface. Furthermore, deletion of the N-glycosylation sites on the calf domain (sites 1 to 9) enhanced cell migration (Fig. 5B) and decreased the expression level of active $\beta 1$ on the cell surface (Fig. 5C), which was similar to the reaction in WT cells and highlighted the importance of N-glycosylation on the β -propeller and thigh domains (sites 1 to 9) of integrin $\alpha 5$. Furthermore, the restoration of N-glycosylation on the β -propeller domain (sites 1 to 5), but not that on the thigh domain (sites 3 to 9), largely rescued the cell migration ability (Fig. 5B). Consistently, the increased expression levels of active $\beta 1$ on the cell surface of S3-5 cells was almost normalized in S1-5 mutant cells compared with that in WT or S1-9 mutant cells (Fig. 5C). Moreover, importantly, the delayed internalization of active $\beta 1$ (Fig. 5D) and the enhanced expression levels of p-FAK in S3-5 cells were also reversed in S1-5 but not S3-9 cells (Fig. 5E), indicating that site 1 and site 2 N-glycosylation on $\alpha 5$ was most important for active $\beta 1$ -mediated appropriate cell adhesion for migration. Of note, as shown in Fig. S1B in the supplemental material, all the mutant cells exhibited almost the same expression levels of integrin $\alpha 5$ on the cell surface compared with the WT ones, further suggesting that the

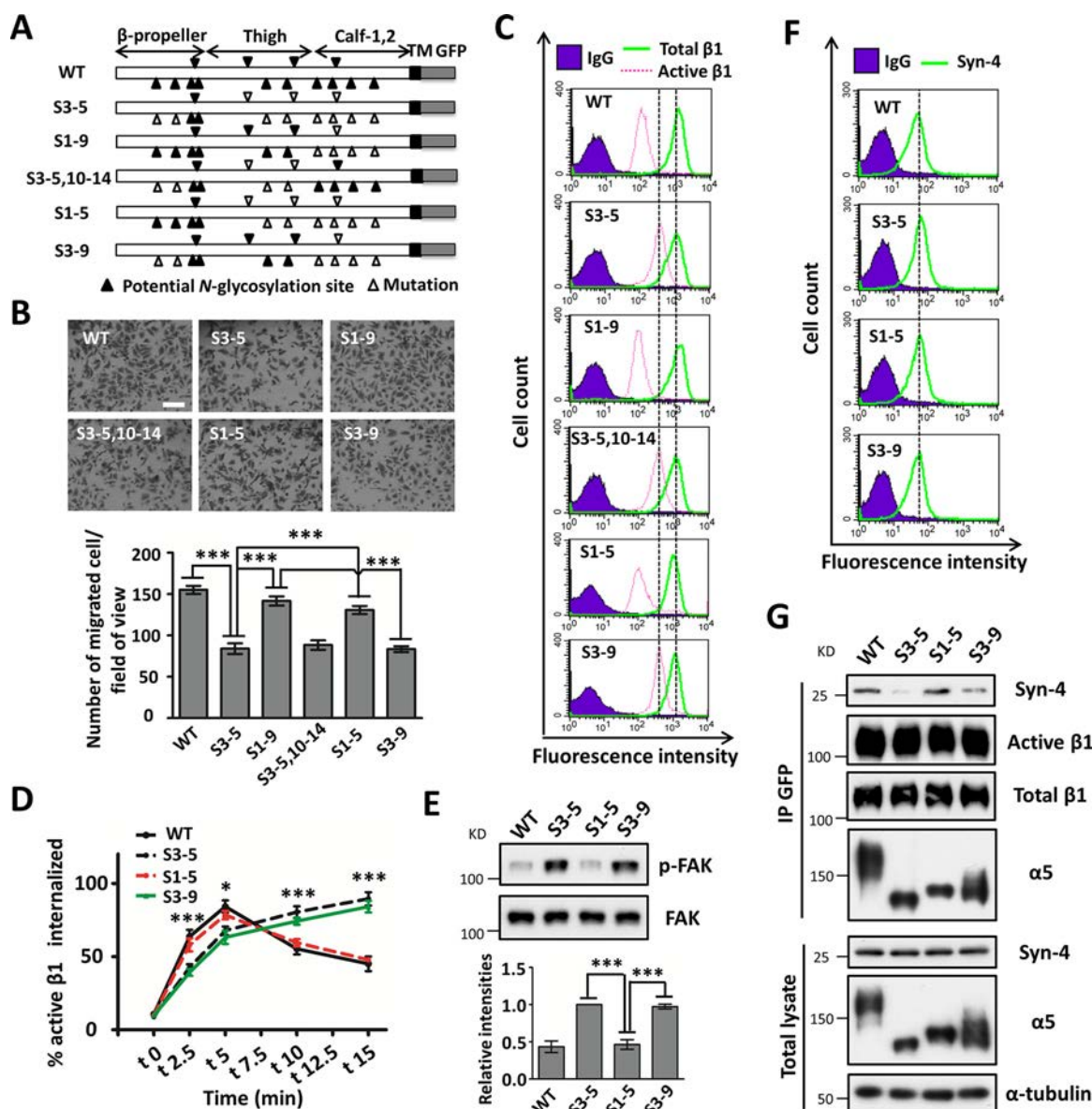


FIG 5 Importance of *N*-glycosylation on the β -propeller domain of $\alpha 5$ for cell migration and $\alpha 5$ -syndecan-4 complex formation. (A) Schematic diagram of potential *N*-glycosylation sites on the WT and mutational $\alpha 5$ subunits (S3-5; S1-9; S3-5,10-14; S1-5; and S3-9). (B) Comparison of the cell migration abilities among WT and mutant cells with restored S1-9; S3-5,10-14; S1-5; or S3-9 $\alpha 5$. The stable cell lines were established as described in Materials and Methods. The cell migration abilities were analyzed ($n = 3$ individual experiments). (C) The expression levels of active and total $\beta 1$ were analyzed by flow cytometry. (D) The internalization of active integrin $\beta 1$ in WT, S3-5, S1-5, and S3-9 mutant cells was determined by a capture ELISA. The proportions of internalized active $\beta 1$ were statistically calculated ($n = 3$ individual experiments). (E, top) After culture on FN-coated dishes for 2 days, the indicated MDA-MB-231 cells were lysed and immunoblotted with the indicated antibodies. (Bottom) Relative ratios (p-FAK versus FAK) ($n = 3$ individual experiments); the relative ratio was 1.0 for S3-5 mutant cells. (F) The surface expression levels of syndecan-4 on WT and S3-5, S1-5, and S3-9 mutant cells were analyzed by flow cytometry. (G, top) The indicated MDA-MB-231 cell extracts were immunoprecipitated with anti-GFP-agarose followed by anti-syndecan-4 (Syn-4), active $\beta 1$, total $\beta 1$, and $\alpha 5$ antibodies for Western blotting. (Bottom) Whole-cell extracts were also immunoblotted with the indicated antibodies. All values are reported as the means \pm SE (error bars), as determined by Student's *t* test; *, $P < 0.05$; ***, $P < 0.001$. Bar, 350 μ m (B).

remaining *N*-glycosylation sites, with the noted exception of sites 3 to 5 of integrin $\alpha 5$, had no effect on its expression.

Next, we explored the underlying mechanisms of the *N*-glycosylation of integrin $\alpha 5$ -mediated activation and migration. Considering that integrin-mediated cellular events are thought to be regulated not only by a conformational change caused by their activations but also by their cross talk with other membrane proteins (22), we further investigated $\alpha 5\beta 1$ -mediated complex formation. Here, we chose one representative membrane protein, syndecan-4, a transmembrane heparan sulfate proteoglycan

that can interact with integrin $\alpha 5\beta 1$ (23) and has been reported to be a control protein for $\alpha 5\beta 1$ trafficking (24). As shown in Fig. 5F, WT and S3-5, S1-5, and S3-9 mutant cells exhibited same expression levels of syndecan-4 on the cell surface as determined by flow cytometry, suggesting that N-glycosylation on $\alpha 5$ had no effect on the expression of syndecan-4. However, immunoprecipitates with anti-GFP-agarose showed that the interaction between syndecan-4 and $\alpha 5$ was significantly decreased in S3-5 cells (Fig. 5G). Importantly, the decreased association between $\alpha 5$ and syndecan-4 could be reversed in S1-5 but not S3-9 cells (Fig. 5G), which indicated that site 1 and site 2 N-glycosylation on $\alpha 5$ was required for its cooperation with syndecan-4. In addition, these four cell lines exhibited almost the same association abilities between $\alpha 5$ and active or total $\beta 1$ (Fig. 5G), which further suggested that N-glycosylation on $\alpha 5$ had no significant effect on the heterodimerization of $\alpha 5\beta 1$. It is notable that the expression levels of active $\beta 1$ on the cell surface were significantly different among these mutants (Fig. 5C), but the total expression levels of active $\beta 1$ were almost the same, as shown in Fig. 3B and 5G. In fact, based on data from previous reports, the active $\beta 1$ integrins were predominantly cytoplasmic (19, 25), as also shown in Fig. 3C. Taken together, these results clearly showed that site 1 and site 2 N-glycosylation on the β -propeller domain of $\alpha 5$ plays a crucial role in regulating appropriate cell adhesion for migration by controlling the internalization of its active form and complex formation (e.g., syndecan-4), which demonstrates a novel mechanism for integrin $\alpha 5$ -mediated cell migration.

DISCUSSION

Previously, our group identified specific N-glycosylation on integrin $\alpha 5$ that plays crucial roles in several biological functions. In detail, we first underscored the importance of three N-glycosylation sites (sites 3 to 5 and particularly site 5) on the β -propeller domain of $\alpha 5$ in its heterodimeric formation with $\beta 1$ (12). Also, we recently identified that N-glycosylation on the calf domain, at sites 10 to 14, was essential for the $\alpha 5$ -mediated inhibitory effect on EGFR signaling and cell proliferation (15). Here, we expanded our understanding of the N-glycosylation of $\alpha 5$ and found that site 1 and site 2 N-glycosylation on the β -propeller domain plays a key role in driving integrin $\alpha 5\beta 1$ dynamics and cell migration, which is a central role for integrin. Mechanistically, site 1 and site 2 N-glycosylation regulates complex formation with syndecan-4, which probably enhances active integrin $\alpha 5\beta 1$ internalization and promotes FA disassembly to provide modest cell-substrate adhesiveness for cell migration (Fig. 6). Taken together, these findings support the idea that individual integrin $\alpha 5$ N-glycosylation differentially functions as a molecular switch to regulate the biological functions of $\alpha 5\beta 1$.

The N-glycosylation of $\alpha 5$ is widely believed to play important roles in cell migration through several experimental methods, including the remodeling of N-glycans by treatment with N-glycanase F or an N-linked oligosaccharide-processing inhibitor and manipulation of the expression levels of some important glycosyltransferases (14). Apparently, the use of these models to comprehensively explore the functions of $\alpha 5$ N-glycosylation and its underlying mechanisms is insufficient, because those studies lacked strict control. In the present study, we clearly demonstrated that the removal of the majority of $\alpha 5$ N-glycosylation, except for that on sites 3 to 5, affected neither $\alpha 5\beta 1$ heterodimer formation nor cell surface expression or cell spreading, but it dramatically suppressed cell migration in several cancer cell lines, including MDA-MB-231, HeLa, and U-251MG cells. These data suggest that $\alpha 5$ N-glycosylation, with the exception of sites 3 to 5, is important for cell migration. These results seem contradictory compared to those of our previous study, in which CHO-B2-S3-5 mutant cells exhibited cell spreading and migration abilities on FN comparable to those of the WT (12). These differences could be explained at least in part by the lack of $\alpha 2,6$ -sialylation expression in the CHO-B2 cell line (26), since $\alpha 2,6$ -sialylation plays very important roles in integrin $\alpha 5\beta 1$ -mediated cell migration and other functions (27).

FAK is a key molecule in integrin-mediated cell adhesion and migration, and the autophosphorylation of FAK at tyrosine 397 plays important roles not only in intracellular signaling but also in cell motility (28). Unexpectedly, the phosphorylated levels of

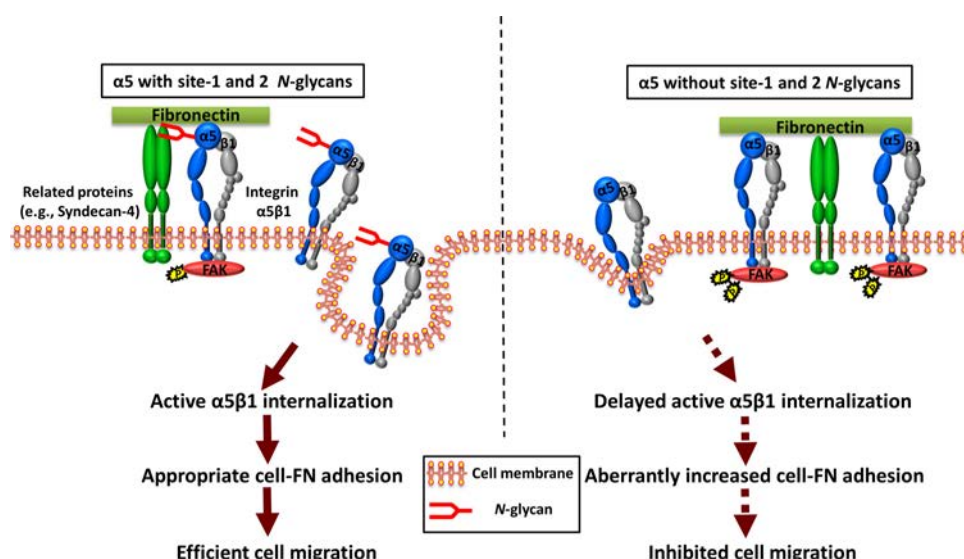


FIG 6 Proposed model for the regulation of integrin $\alpha 5\beta 1$ -mediated cell migration by *N*-glycosylation. (Left) Integrin $\alpha 5\beta 1$ may form a complex with several receptors (e.g., syndecan-4), which may trigger active $\alpha 5\beta 1$ internalization and the turnover of FA to provide the appropriate cell-substrate adhesiveness for efficient cell migration. (Right) However, in the case of the $\alpha 5$ mutant lacking *N*-glycosylation on sites 1 and 2, the cells exhibit increased active $\alpha 5\beta 1$ expression on the cell surface and enhanced cell adhesion signaling as a result of its decreased ability to associate with related proteins, which results in the suppression of cell migration. The present study provides new insights into the concept that modest cell adhesion is best for cell migration (40). The solid arrows indicate a normal signal pathway in integrin $\alpha 5\beta 1$ -mediated cell migration, while the dotted arrows indicate that these events are aberrant.

FAK upon FN stimulation in S3-5 mutant cells were higher than those in WT cells. Furthermore, actin stress fiber formation was also greatly enhanced in the mutant cells. These data further support the notion that more cell-substrate adhesiveness, less cell migration, and a modest amount of cell adhesion are important for cell migration (29). In fact, cell migration is a strictly controlled dynamic process, which requires regulated cycles of polarized cell-substrate attachment to form focal contact at the leading edge of the cell with corresponding detachment at its trailing edge (30). Therefore, an imbalance of attachment and detachment in this process may result in abnormal adhesion (31). Such a cell adhesion phenotype is compatible with data from a previous study in which a loss of the protein annexin A2 inhibited intestinal epithelial cell migration while promoting enhanced cell matrix adhesion (21). Given that the conformational activation of integrins on the cell surface supports cell adhesion and spreading, whereas the transition of integrins toward an inactive bent conformation causes cell detachment and rounding (32, 33), it is possible that the increased cell adhesion ability is due to an aberrant activation of integrin. In agreement with this hypothesis, our flow cytometric and biotinylation analyses showed that S3-5 mutant cells highly expressed the active form of $\alpha 5\beta 1$ on the cell surface. Similarly, Park et al. previously reported that aberrant activation of integrin $\alpha 4\beta 7$ suppressed lymphocyte migration and underscored the importance of a proper balance in the adhesion and de-adhesion of integrin (34). The enhanced expression of active $\beta 1$ on the cell surface might have been due to different trafficking events, since the internalization of the active form of $\alpha 5\beta 1$ but not the total version was significantly delayed in S3-5 cells compared with that in WT cells. These results suggested that $\alpha 5$ *N*-glycosylation may have a significant effect on the expression and internalization of active $\alpha 5\beta 1$. Our finding is analogous to those of a previous report indicating that the downregulation of the protein neuropilin-1 (Nrp1) resulted in a delay in active integrin $\alpha 5\beta 1$ internalization but not that of the total version (35). Therefore, it is reasonable to consider that the internalization of active and inactive integrins may occur through distinct molecular mechanisms. Actually, inactive and active integrins $\alpha 5\beta 1$ undergo different trafficking path-

ways: the Rab4-dependent short loop for inactive integrin $\beta 1$ (19) and the Rab11-dependent long loop used by active $\alpha 5\beta 1$ (20). Thus, further studies elucidating the functions of $\alpha 5$ N-glycosylation in regulating its degradation and recycling are required for a comprehensive understanding of how N-glycosylation coordinates the trafficking of integrin $\alpha 5\beta 1$ during cell migration.

Integrin $\alpha 5\beta 1$ internalization is the first step in its trafficking. It is required for the disassembly regulation of FA and plays a key role in efficient cell migration (34). However, the current mechanism for integrin $\alpha 5\beta 1$ internalization remains largely unclear, since most studies focus mainly on intracellular trafficking regulation without extracellular information (7, 9). Here, we found the site 1 and site 2 N-glycosylation on $\alpha 5$ could regulate active $\alpha 5\beta 1$ internalization, which may broaden our understanding of the functions of the extracellular domains in $\alpha 5\beta 1$ trafficking. In addition, the internalization of $\alpha 5\beta 1$ is also related to the assistance of other transmembrane proteins such as the FN receptor syndecan-4 (24, 36), myelin-associated glycoprotein (37), EGFR (38), and Nrp1 (35). As a model, here we focused on syndecan-4 and found that its associative ability with $\alpha 5\beta 1$ was dependent on $\alpha 5$ N-glycosylation. In particular, site 1 and site 2 N-glycosylation of $\alpha 5$ was most important for interactions and cell migration. Of course, we could not exclude the effects of cell migration on the remaining N-glycosylation sites. In fact, the restoration of site 1 and site 2 N-glycosylation in the S3-5 mutant efficiently rescued the expression of the active form of $\beta 1$ to a level similar to that in WT cells, whereas the cell migration ability was only partially rescued. This is a possible reason why N-glycosylation on the calf domain (sites 10 to 14) of $\alpha 5$ is necessary for EGFR- $\alpha 5$ complex formation, as previously reported (15), which may also play important roles in $\alpha 5\beta 1$ trafficking and cell migration, as discussed above. Moreover, it is of note that the internalization ratio of active $\beta 1$ in S3-9 cells was slightly higher than that in S3-5 cells to some extent but was not significant (Fig. 5E), and also, there was a weak interaction between $\alpha 5$ and syndecan-4 in S3-9 mutant cells (Fig. 5G), which may indicate that N-glycosylation on the thigh domain of $\alpha 5$ also has some effects on the internalization of active $\beta 1$. Considering the roles of the bulky glycocalyx of the ECM in integrin-mediated tumor phenotypes (39), it is tempting to speculate that individual N-glycosylation on integrin may exhibit a suitable physical or specific structure that functions as a nexus for integrin-mediated complex formation to integrate both the ECM and cytokines in the microenvironment surrounding tumors.

In summary, we have delineated the mechanism for N-glycosylation on the β -propeller domain of $\alpha 5$ as a controller that coordinates cell-FN adhesion and internalization dynamics of $\alpha 5\beta 1$ for cell migration. These findings will improve our understanding of how cell-substrate adhesiveness is regulated and the importance of a modest level of cell adhesion for cell migration.

MATERIALS AND METHODS

Antibodies and reagents. The experiments were performed by using the following antibodies: monoclonal antibodies (MAbs) against integrin $\alpha 5$, integrin $\beta 1$, integrin $\alpha 6$, p-FAK, and FAK (BD Biosciences, San Jose, CA); MAbs against human $\alpha 5\beta 1$ (HA5), active integrin $\beta 1$ (HUTS-4), integrin $\alpha 3$, and integrin $\beta 4$ and rabbit polyclonal antibody against integrin $\alpha 5$ (Millipore, Billerica, MA); mouse MAb to syndecan-4 (Santa Cruz Biotechnology, Santa Cruz, CA); antibody against integrin αV (BioLegend, San Diego, CA); MAb against the human integrin $\beta 1$ subunit (P5D2) (Developmental Studies Hybridoma Bank, University of Iowa, IA); MAb against α -tubulin (Sigma-Aldrich, St. Louis, MO); and Alexa Fluor 647- or 546-goat anti-mouse IgG and Alexa Fluor 546-phalloidin (Thermo Fisher Scientific, Waltham, MA). The peroxidase-conjugated goat antibodies against mouse and rabbit IgG were obtained from Chemicon and Cell Signaling Technology (Danvers, MA), respectively. 2-Mercaptoethanesulfonic acid sodium salt (MesNa), iodoacetamide, *o*-Phenylenediamine dihydrochloride (OPD), and FN were obtained from Sigma; control mouse IgG1 was obtained from Tonbo Biosciences (San Diego, CA); and sulfo-NHS-SS biotin (sulfosuccinimidyl-2-[biotinamido]ethyl-1,3-dithiopropionate), streptavidin-conjugated horseradish peroxidase, and To-Pro-3 were obtained from Thermo Fisher Scientific. PNGase F, agarose-conjugated anti-GFP antibody (RQ2), streptavidin-conjugated agarose, and Ab-Capture Extra beads were obtained from New England BioLabs, Medical & Biological Laboratories Co. Ltd. (Nagoya, Japan), Millipore, and ProteNova Co. Ltd. (Kagawa, Japan), respectively.

Cell lines and cell culture. The 293T and HeLa cell lines were provided by the RIKEN cell bank (Tokyo, Japan). The MDA-MB-231 cell lines were purchased from the American Type Culture Collection (Manassas, VA). The U-251MG cell line was a gift from Jun Nakayama (Shinshu University Graduate School

of Medicine, Japan). Integrin $\alpha 5$ -KO-MDA-MB-231, $\alpha 5$ -KO-HeLa, and $\alpha 5$ -KO-U-251MG cells were previously established in our laboratory (15). The stable cell lines used in this study were established as mentioned below. All cell lines were maintained at 37°C in Dulbecco's modified Eagle's medium (DMEM) supplemented with 10% fetal bovine serum (FBS) under a humidified atmosphere containing 5% CO₂, except for virus production.

Integrin $\alpha 5$ expression vectors. The pENTR-D-Topo vectors of GFP and GFP-tagged integrin $\alpha 5$ with altered N-glycosylation sites (the WT and the S3-5; S1-9; S3-5,10-14; and S1-5 mutants) were previously established in our laboratory (12, 15). The mutation vector S3-9 was constructed by using an in-fusion kit (TaKaRa Bio) according to the manufacturer's instructions and then cloned into the CSII-EF-Rfa vector by using a Gateway cloning system kit (Thermo Fisher Scientific) to acquire all lentivirus expression vectors.

Virus production, infection, and stable cell line construction. Virus production and infection were performed as described previously (15). In brief, CSII-EF-Rfa-based lentivirus vectors were cotransfected with pCAG-HIVgp and pCMV-VSV-G-RSV-Rev into 293T cells. After transfection for 48 h, the lentivirus supernatants were collected. The indicated integrin $\alpha 5$ KO cells were infected with the resultant viral supernatant for 72 h, and GFP-positive cells were then sorted 3 times by using a FACSAria II instrument. Stable cell lines were used in subsequent studies.

Cell spreading and cell adhesion response assays. Six-well plates were coated with FN (10 μ g/ml) in phosphate-buffered saline (PBS) overnight at 4°C and then blocked with 1% bovine serum albumin (BSA) in DMEM for 1 h at 37°C. The indicated cells were detached and suspended in assay medium (50 mM HEPES and 0.1% BSA in serum-free DMEM [pH 7.4]) for 40 min at 3×10^4 cells/ml. After a 20-min incubation, nonadherent cells were gently removed by washing with PBS, attached cells were fixed with 4% paraformaldehyde (PFA) in PBS, and photos were then taken by phase-contrast microscopy.

To assay the cell adhesion response upon FN treatment, the indicated cells were also detached and suspended in the assay medium for 40 min at 1×10^6 cells/ml. After replating onto FN-coated 6-well plates for 0, 15, 30, and 45 min, nonadherent cells were gently removed by washing with PBS, and the attached cells were collected, lysed, and then analyzed by WB, as described below.

Video microscope. A glass-bottom dish (Asahi Techno Glass, Japan) was precoated with 10 μ g/ml FN at 4°C overnight and then blocked with 1% BSA in DMEM for 1 h at 37°C. A 2-ml aliquot of the cell suspension (2.5×10^4 cells/ml) in serum-free DMEM was added to each glass-bottom dish. After incubation for 1 h to allow cells to adhere to FN, the serum-free medium was gently replaced with 2 ml growth medium, followed by mounting with 1 ml glycerol. The cells were then monitored, and the images and videos were acquired by using inverted microscopes (Axio Observer.D1; Carl Zeiss) every 10 min at 37°C with 5% CO₂ in a heated chamber with temperature and CO₂ control (Onpu-4 & CO₂; Air Brown, Japan). Cell motility was analyzed in roughly 12 cells by measuring the x and y coordinates of tracked cells over 12 h. The directionality (ratio of the Euclidean distance versus accumulated distance, $0 \leq \text{values} \leq 1$) parameters, displacement (micrometers), and the manual tracking plug-in velocity (micrometers per minute) were analyzed by using Chemotaxis and Migration Tool software (version 2.0).

Wound healing assay. A confluent layer of cells cultured on an FN-coated (10 μ g/ml) 6-well plate was starved in serum-free medium for 12 h and then scraped by using a p200 pipette tip. Serum-free medium was replaced with 3% FBS-containing DMEM. Wounded areas were photographed under a light microscope at 0 and 24 h for MDA-MB-231 cells, at 36 h for HeLa cells, and at 48 h for U-251MG cells. Wound closure was measured by observing the distances between the sides of the wound at the indicated times.

Cell migration assay. Each Transwell (BD BioCoat control 8.0- μ m-pore-size inserts) was coated only on the bottom side with 10 μ g/ml FN at 4°C overnight. Cells were prestarved in serum-free medium for 12 h, trypsinized, and suspended in complete DMEM. The suspended cells were centrifuged, and the supernatants were removed. The resultant cell pellets were resuspended with assay medium (0.1% BSA in DMEM containing 3% FBS) and diluted to 1×10^5 cells/ml, and the cell viabilities were confirmed by trypan blue staining. Aliquots of 500 μ l of the cell suspension were added to each FN-coated Transwell, followed by incubation at 37°C for 5 h for HeLa cells and for 4 h for MDA-MB-231 or U-251MG cells. After incubation, cells on the upper side were gently removed by scraping with a cotton swab. The membranes in the Transwells were fixed with 4% PFA for 30 min, followed by staining with 0.5% crystal violet for 4 h. Cells that had migrated to the lower side were counted by using a phase-contrast microscope.

Western blot and immunoprecipitation analyses. For WB, the indicated cells were washed with ice-cold PBS and then lysed in the cell lysate (20 mM Tris-HCl [pH 7.4], 150 mM NaCl, 1% Triton X-100) with protease and phosphatase inhibitors (Nacalai Tesque, Kyoto, Japan) for 30 min. After centrifugation, the supernatant was collected, and protein concentrations were determined by using a bicinchoninic acid (BCA) protein assay kit (Pierce, Rockford, IL). The protein samples were resolved by nonreducing SDS-PAGE for $\alpha 5$ and active $\beta 1$ or reducing SDS-PAGE for other proteins. After electrophoresis, the proteins were transferred onto a polyvinylidene difluoride (PVDF) membrane (Millipore) and detected with the indicated primary and secondary antibodies by using the Immobilon Western chemiluminescent horseradish peroxidase (HRP) substrate (Millipore), according to the manufacturer's instructions. For IP, cells were lysed in 0.1% Triton-Tris-buffered saline (TBS) buffer (20 mM Tris-HCl [pH 7.4], 150 mM NaCl) with a protease inhibitor and then centrifuged. The supernatants were immunoprecipitated with anti-GFP-agarose for 1 h at 4°C with rotation, and the immunoprecipitates were subjected to SDS-PAGE.

PNGase F treatment. The indicated cell lysates were treated with PNGase F at 37°C for 1 h according to the manufacturer's instructions or not treated and then subjected to SDS-PAGE with the indicated antibodies.

Flow cytometric analysis. The indicated semiconfluent cells were detached from 10-cm culture dishes and subsequently stained with either mouse IgG or primary antibodies for 1 h on ice, followed by

incubation with Alexa Fluor 647–goat anti-mouse IgG for 1 h. During incubation, the cells were mixed gently every 10 min by flicking. After incubation, cells were washed and then analyzed by using a FACSCalibur flow cytometer (BD Biosciences).

Cell surface biotinylation. Cells were gently washed twice with PBS and then incubated with ice-cold PBS containing 0.2 mg/ml sulfo-NHS-SS biotin for 1 h at 4°C. After incubation, cells were washed 3 times with ice-cold PBS, and the cells were harvested by using lysis buffer. A total of 200 μ g of the biotinylated protein was precipitated with streptavidin-conjugated agarose (20 μ l) for another 1 h at 4°C with rotation and then subjected to SDS-PAGE as described above.

Immunofluorescence. Cells were plated onto FN-coated glass coverslips (MatTek Corporation, Ashland, MA) for 48 h, washed with PBS, fixed with 4% PFA, and blocked with PBS–0.1% Triton X-100–10% BSA. Antibodies against p-FAK, active $\beta 1$, or P5D2 were used, followed by incubation with anti-mouse Alexa Fluor 546-conjugated secondary antibodies and Alexa Fluor 546-phalloidin. Finally, the cells were incubated with To-Pro-3 for 30 min. The confocal images were also acquired by using a 60 \times /1.35-numerical-aperture (NA) oil immersion objective lens (FV1000; Olympus, Tokyo, Japan). The fluorescence intensities were quantified by using ImageJ software.

Capture ELISA. Corning (Corning, NY) 96-well enzyme immunoassay (EIA)/radioimmunoassay (RIA) plates were coated with 5 μ g/ml the appropriate anti-integrin antibodies in 0.05 M Na₂CO₃ (pH 9.6) at 4°C overnight and then blocked in PBS containing 0.05% Tween 20 (PBS-T) with 5% BSA for 1 h at room temperature. The indicated integrins were captured by incubation of 50 μ l (about 80 μ g) of the cell lysate overnight at 4°C. Unbound material was removed by extensive washing with PBS-T, and wells were incubated with streptavidin-conjugated horseradish peroxidase in PBS-T containing 1% BSA for 1 h at 4°C. Following further washing, biotinylated integrins were detected by a chromogenic reaction with OPD for 20 min, and the absorbances at 450 nm were measured.

Biotinylation-based integrin internalization assay. Cells grown on FN-coated 10-cm dishes were serum starved for 1 h prior to the assay and washed with ice-cold PBS, and surface proteins were biotinylated with 0.2 mg/ml sulfo-NHS-SS biotin in PBS for 1 h, followed by washing in TBS and placement in a cold room. For internalization, cells were then incubated in prewarmed complete DMEM at 37°C for 0, 2.5, 5, 10, and 15 min, whereas the control groups (without MesNa) remained on ice. Surface biotin was then stripped from the cells with 10 min of incubation in 50 mM MesNa–TBS (pH 8.6) twice, followed by washing and quenching of MesNa with 20 mM iodoacetamide in TBS for 10 min. Cells of the control group were not subjected to surface reduction (without MesNa) in order to obtain total surface-labeled integrin. After quenching, the cells were lysed, precipitated with streptavidin-conjugated agarose, and subjected to WB or a capture ELISA.

Statistical analysis. Results are reported as the means \pm standard errors (SE). Statistical analyses were performed by using Student's *t* test and GraphPad Prism version 5. Statistical significance was defined as a *P* value of <0.05.

SUPPLEMENTAL MATERIAL

Supplemental material for this article may be found at <https://doi.org/10.1128/MCB.00558-16>.

SUPPLEMENTAL FILE 1, PDF file, 0.8 MB.

ACKNOWLEDGMENTS

Q.H. performed all the experiments with the help of T.I., S.H., Y.W., and T.F. Q.H. and T.I. constructed the virus expression and the $\alpha 5$ knockout vectors. Q.H., T.F., and S.H. did the cell sorting experiments and constructed the related stable cell lines. J.G. designed the experiment. Q.H. and J.G. analyzed the data, prepared the figures, and wrote the manuscript. All authors discussed the results and commented on the manuscript.

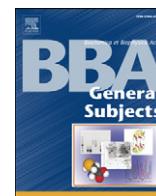
We declare no competing financial interests.

This work was partially supported by grants-in-aid for scientific research (15H04354 to J.G. and 24570169 to T.I.) and for Challenging Exploratory Research (15K14408 to J.G.) from the Japan Society for the Promotion of Science, a grant from the National Natural Science Foundation of China (no. 31670807), and a Strategic Research Foundation grant-aided project for private universities from the Ministry of Education, Culture, Sports, Science, and Technology of Japan.

REFERENCES

1. Franz CM, Jones GE, Ridley AJ. 2002. Cell migration in development and disease. *Dev Cell* 2:153–158. [https://doi.org/10.1016/S1534-5807\(02\)00120-X](https://doi.org/10.1016/S1534-5807(02)00120-X).
2. Hynes RO. 2002. Integrins: bidirectional, allosteric signaling machines. *Cell* 110:673–687. [https://doi.org/10.1016/S0092-8674\(02\)00971-6](https://doi.org/10.1016/S0092-8674(02)00971-6).
3. Wolfenson H, Lavelin I, Geiger B. 2013. Dynamic regulation of the structure and functions of integrin adhesions. *Dev Cell* 24:447–458. <https://doi.org/10.1016/j.devcel.2013.02.012>.
4. Kim C, Ye F, Ginsberg MH. 2011. Regulation of integrin activation. *Annu Rev Cell Dev Biol* 27:321–345. <https://doi.org/10.1146/annurev-cellbio-100109-104104>.
5. Shattil SJ, Kim C, Ginsberg MH. 2010. The final steps of integrin activation:

- the end game. *Nat Rev Mol Cell Biol* 11:288–300. <https://doi.org/10.1038/nrm2871>.
6. Margadant C, Monsuur HN, Norman JC, Sonnenberg A. 2011. Mechanisms of integrin activation and trafficking. *Curr Opin Cell Biol* 23: 607–614. <https://doi.org/10.1016/j.ceb.2011.08.005>.
 7. Caswell PT, Vadvre S, Norman JC. 2009. Integrins: masters and slaves of endocytic transport. *Nat Rev Mol Cell Biol* 10:843–853. <https://doi.org/10.1038/nrm2799>.
 8. Margadant C, Kreft M, de Groot DJ, Norman JC, Sonnenberg A. 2012. Distinct roles of talin and kindlin in regulating integrin $\alpha 5 \beta 1$ function and trafficking. *Curr Biol* 22:1554–1563. <https://doi.org/10.1016/j.cub.2012.06.060>.
 9. Bridgewater RE, Norman JC, Caswell PT. 2012. Integrin trafficking at a glance. *J Cell Sci* 125:3695–3701. <https://doi.org/10.1242/jcs.095810>.
 10. Gu J, Taniguchi N. 2004. Regulation of integrin functions by N-glycans. *Glycoconj J* 21:9–15. <https://doi.org/10.1023/B:GLYC.0000043741.47559.30>.
 11. Isaji T, Sato Y, Fukuda T, Gu J. 2009. N-Glycosylation of the I-like domain of $\beta 1$ integrin is essential for $\beta 1$ integrin expression and biological function: identification of the minimal N-glycosylation requirement for $\alpha 5 \beta 1$. *J Biol Chem* 284:12207–12216. <https://doi.org/10.1074/jbc.M807920200>.
 12. Isaji T, Sato Y, Zhao Y, Miyoshi E, Wada Y, Taniguchi N, Gu J. 2006. N-Glycosylation of the beta-propeller domain of the integrin $\alpha 5$ subunit is essential for $\alpha 5 \beta 1$ heterodimerization, expression on the cell surface, and its biological function. *J Biol Chem* 281:33258–33267. <https://doi.org/10.1074/jbc.M607771200>.
 13. Takahashi M, Kizuka Y, Ohtsubo K, Gu J, Taniguchi N. 27 April 2016. Disease-associated glycans on cell surface proteins. *Mol Aspects Med* <https://doi.org/10.1016/j.mam.2016.04.008>.
 14. Janik ME, Litynska A, Vereecken P. 2010. Cell migration—the role of integrin glycosylation. *Biochim Biophys Acta* 1800:545–555. <https://doi.org/10.1016/j.bbagen.2010.03.013>.
 15. Hang Q, Isaji T, Hou S, Im S, Fukuda T, Gu J. 2015. Integrin $\alpha 5$ suppresses the phosphorylation of epidermal growth factor receptor and its cellular signaling of cell proliferation via N-glycosylation. *J Biol Chem* 290:29345–29360. <https://doi.org/10.1074/jbc.M115.682229>.
 16. Mitra SK, Schlaepfer DD. 2006. Integrin-regulated FAK-Src signaling in normal and cancer cells. *Curr Opin Cell Biol* 18:516–523. <https://doi.org/10.1016/j.ceb.2006.08.011>.
 17. Ginsberg MH, Partridge A, Shattil SJ. 2005. Integrin regulation. *Curr Opin Cell Biol* 17:509–516. <https://doi.org/10.1016/j.ceb.2005.08.010>.
 18. Luque A, Gomez M, Puzon W, Takada Y, Sanchez-Madrid F, Cabanas C. 1996. Activated conformations of very late activation integrins detected by a group of antibodies (HUTS) specific for a novel regulatory region (355–425) of the common $\beta 1$ chain. *J Biol Chem* 271:11067–11075. <https://doi.org/10.1074/jbc.271.19.11067>.
 19. Arjonen A, Alanko J, Veltel S, Ivaska J. 2012. Distinct recycling of active and inactive $\beta 1$ integrins. *Traffic* 13:610–625. <https://doi.org/10.1111/j.1600-0854.2012.01327.x>.
 20. Caswell PT, Norman JC. 2006. Integrin trafficking and the control of cell migration. *Traffic* 7:14–21. <https://doi.org/10.1111/j.1600-0854.2005.00362.x>.
 21. Rankin CR, Hilgarth RS, Leoni G, Kwon M, Den Beste KA, Parkos CA, Nusrat A. 2013. Annexin A2 regulates $\beta 1$ integrin internalization and intestinal epithelial cell migration. *J Biol Chem* 288:15229–15239. <https://doi.org/10.1074/jbc.M112.440909>.
 22. Streuli CH, Akhtar N. 2009. Signal co-operation between integrins and other receptor systems. *Biochem J* 418:491–506. <https://doi.org/10.1042/BJ20081948>.
 23. Fiore VF, Ju L, Chen Y, Zhu C, Barker TH. 2014. Dynamic catch of a Thy-1- $\alpha 5 \beta 1$ +syndecan-4 trimolecular complex. *Nat Commun* 5:4886. <https://doi.org/10.1038/ncomms5886>.
 24. Morgan MR, Hamidi H, Bass MD, Warwood S, Ballestrem C, Humphries MJ. 2013. Syndecan-4 phosphorylation is a control point for integrin recycling. *Dev Cell* 24:472–485. <https://doi.org/10.1016/j.devcel.2013.01.027>.
 25. Tiwari S, Askari JA, Humphries MJ, Bulleid NJ. 2011. Divalent cations regulate the folding and activation status of integrins during their intracellular trafficking. *J Cell Sci* 124:1672–1680. <https://doi.org/10.1242/jcs.084483>.
 26. Xu X, Nagarajan H, Lewis NE, Pan S, Cai Z, Liu X, Chen W, Xie M, Wang W, Hammond S, Andersen MR, Neff N, Passarelli B, Koh W, Fan HC, Wang J, Gui Y, Lee KH, Betenbaugh MJ, Quake SR, Famili I, Palsson BO, Wang J. 2011. The genomic sequence of the Chinese hamster ovary (CHO)-K1 cell line. *Nat Biotechnol* 29:735–741. <https://doi.org/10.1038/nbt.1932>.
 27. Lu J, Gu J. 2015. Significance of beta-galactoside $\alpha 2,6$ sialyltransferase [sic] 1 in cancers. *Molecules* 20:7509–7527. <https://doi.org/10.3390/molecules20057509>.
 28. Hood JD, Cheresch DA. 2002. Role of integrins in cell invasion and migration. *Nat Rev Cancer* 2:91–100. <https://doi.org/10.1038/nrc727>.
 29. Wolfman T, Spatz JP, Burgess RW. 2008. Cell adhesion to agrin presented as a nanopatterned substrate is consistent with an interaction with the extracellular matrix and not transmembrane adhesion molecules. *BMC Cell Biol* 9:64. <https://doi.org/10.1186/1471-2121-9-64>.
 30. DiMilla PA, Stone JA, Quinn JA, Albelda SM, Lauffenburger DA. 1993. Maximal migration of human smooth muscle cells on fibronectin and type IV collagen occurs at an intermediate attachment strength. *J Cell Biol* 122:729–737. <https://doi.org/10.1083/jcb.122.3.729>.
 31. Parsons JT, Horwitz AR, Schwartz MA. 2010. Cell adhesion: integrating cytoskeletal dynamics and cellular tension. *Nat Rev Mol Cell Biol* 11:633–643. <https://doi.org/10.1038/nrm2957>.
 32. Kinbara K, Goldfinger LE, Hansen M, Chou FL, Ginsberg MH. 2003. Ras GTPases: integrins' friends or foes? *Nat Rev Mol Cell Biol* 4:767–776. <https://doi.org/10.1038/nrm1229>.
 33. Sheetz MP. 2001. Cell control by membrane-cytoskeleton adhesion. *Nat Rev Mol Cell Biol* 2:392–396. <https://doi.org/10.1038/35073095>.
 34. Park EJ, Mora JR, Carman CV, Chen J, Sasaki Y, Cheng G, von Andrian UH, Shimaoka M. 2007. Aberrant activation of integrin $\alpha 4 \beta 7$ suppresses lymphocyte migration to the gut. *J Clin Invest* 117:2526–2538. <https://doi.org/10.1172/JCI31570>.
 35. Valdembré D, Caswell PT, Anderson KI, Schwarz JP, König I, Astanina E, Caccavari F, Norman JC, Humphries MJ, Bussolino F, Serini G. 2009. Neuropilin-1/GIPC1 signaling regulates $\alpha 5 \beta 1$ integrin traffic and function in endothelial cells. *PLoS Biol* 7:e25. <https://doi.org/10.1371/journal.pbio.1000025>.
 36. Bass MD, Williamson RC, Nunan RD, Humphries JD, Byron A, Morgan MR, Martin P, Humphries MJ. 2011. A syndecan-4 hair trigger initiates wound healing through caveolin- and RhoG-regulated integrin endocytosis. *Dev Cell* 21:681–693. <https://doi.org/10.1016/j.devcel.2011.08.007>.
 37. Hines JH, Abu-Rub M, Henley JR. 2010. Asymmetric endocytosis and remodeling of $\beta 1$ -integrin adhesions during growth cone chemorepulsion by MAG. *Nat Neurosci* 13:829–837. <https://doi.org/10.1038/nn.2554>.
 38. Caswell PT, Chan M, Lindsay AJ, McCaffrey MW, Boettiger D, Norman JC. 2008. Rab-coupling protein coordinates recycling of $\alpha 5 \beta 1$ integrin and EGFR1 to promote cell migration in 3D microenvironments. *J Cell Biol* 183:143–155. <https://doi.org/10.1083/jcb.200804140>.
 39. Paszek MJ, DuFort CC, Rossier O, Bainer R, Mouw JK, Godula K, Hudak JE, Lakins JN, Wijekoon AC, Cassereau L, Rubashkin MG, Magbanua MJ, Thorn KS, Davidson MW, Rugo HS, Park JW, Hammer DA, Giannone G, Bertozzi CR, Weaver VM. 2014. The cancer glycocalyx mechanically primes integrin-mediated growth and survival. *Nature* 511:319–325. <https://doi.org/10.1038/nature13535>.
 40. Palecek SP, Loftus JC, Ginsberg MH, Lauffenburger DA, Horwitz AF. 1997. Integrin-ligand binding properties govern cell migration speed through cell-substratum adhesiveness. *Nature* 385:537–540. <https://doi.org/10.1038/385537a0>.



Alteration of *N*-glycan expression profile and glycan pattern of glycoproteins in human hepatoma cells after HCV infection

Tian Xiang^a, Ganglong Yang^b, Xiaoyu Liu^a, Yidan Zhou^c, Zhongxiao Fu^a, Fangfang Lu^a, Jianguo Gu^d, Naoyuki Taniguchi^e, Zengqi Tan^b, Xi Chen^f, Yan Xie^a, Feng Guan^{b,*}, Xiao-Lian Zhang^{a,*}

^a State Key Laboratory of Virology, Hubei province Key Laboratory of Allergy and Immune-related diseases, Medical Research Institute, Department of Immunology of Wuhan University School of Basic Medical Sciences, Wuhan 430071, China

^b The Key Laboratory of Carbohydrate Chemistry & Biotechnology, Ministry of Education, School of Biotechnology, Jiangnan University, Wuxi 214122, China

^c University of Illinois at Urbana-Champaign, School of Molecular and Cellular Biology, Department of Microbiology, IL 61801, USA

^d Division of Regulatory Glycobiology, Tohoku Medical and Pharmaceutical University, 4-4-1 Komatsushima, Aobaku, Sendai, Miyagi 981-8558, Japan

^e Systems Glycobiology Group, Global Research Cluster, RIKEN and RIKEN-Max Planck Joint Research Center, 2-1 Hirosawa, Wako, Saitama 351-0198, Japan

^f Wuhan Institute of Biotechnology, Medical Research Institute of Wuhan University, Wuhan 430071, China

ARTICLE INFO

Article history:

Received 10 November 2016

Received in revised form 9 February 2017

Accepted 11 February 2017

Available online 14 February 2017

Keywords:

Glycosyltransferase expression analysis

Hepatitis C virus (HCV)

Lectin microarray

Mass spectrometry

N-glycan

α1,6-fucosyltransferase 8 (FUT8)

ABSTRACT

Background: Hepatitis C virus (HCV) infection causes chronic liver diseases, liver fibrosis and even hepatocellular carcinoma (HCC). However little is known about any information of *N*-glycan pattern in human liver cell after HCV infection.

Methods: The altered profiles of *N*-glycans in HCV-infected Huh7.5.1 cell were analyzed by using mass spectrometry. Then, lectin microarray, lectin pull-down assay, reverse transcription-quantitative real time PCR (RT-qPCR) and western-blotting were used to identify the altered *N*-glycosylated proteins and glycosyltransferases.

Results: Compared to uninfected cells, significantly elevated levels of fucosylated, sialylated and complex *N*-glycans were found in HCV infected cells. Furthermore, *Lens culinaris* agglutinin (LCA)-binding glycoconjugates were increased most. Then, the LCA-agarose was used to precipitate the specific glycosylated proteins and identify that fucosylated modified annexin A2 (ANXA2) and heat shock protein 90 beta family member 1 (HSP90B1) was greatly increased in HCV-infected cells. However, the total ANXA2 and HSP90B1 protein levels remained unchanged. Additionally, we screened the mRNA expressions of 47 types of different glycosyltransferases and found that α1,6-fucosyltransferase 8 (FUT8) was the most up-regulated and contributed to strengthen the LCA binding capability to fucosylated modified ANXA2 and HSP90B1 after HCV infection.

Conclusions: HCV infection caused the altered *N*-glycans profiles, increased expressions of FUT8, fucosylated ANXA2 and HSP90B1 as well as enhanced LCA binding to Huh7.5.1.

General significance: Our results may lay the foundation for clarifying the role of *N*-glycans and facilitate the development of novel diagnostic biomarkers and therapeutic targets based on the increased FUT8, fucosylated ANXA2 and HSP90B1 after HCV infection.

© 2017 Elsevier B.V. All rights reserved.

1. Introduction

Hepatitis C virus (HCV) is an enveloped, positive-sense RNA virus that is a major cause of chronic liver disease and infects nearly 185 million people worldwide. Approximately 350,000 to 500,000 people die

each year from hepatitis C-related liver diseases, according to the 2014 WHO report [1,2]. In the case of HCV infection, pathological mechanisms have generally been well characterized from a biochemical and biophysical perspective. However, little is known about the *N*-glycan expression profile and glycan pattern of glycoproteins of host cell proteins after HCV infection [3–6].

N-linked glycosylation is one of the most common types of post-translational protein modification [7]. The sugar composition of oligosaccharides and the number and size of branches in the sugar tree vary widely [8,9]. As of yet, alterations of protein *N*-linked glycosylation have been identified as biomarkers for the development of many diseases, including cancer [10–14]. Several studies have shown that changes in the β-1, 6-branched and bisected *N*-glycan expression were associated with replicative immortality, tissue invasion and metastasis

Abbreviations: ACA, *Amaranthus caudatus* agglutinin; AFP, alpha-fetoprotein; ANXA2, annexin A2; ECA, *Erythrina cristagalli* agglutinin; FUT8, α1,6-fucosyltransferase 8; HCC, hepatocellular carcinoma; HCV, Hepatitis C virus; HCVcc, HCV cell culture; HSP90B1, heat shock protein 90 beta family member 1; LCA, *Lens culinaris* agglutinin; NS3, nonstructural protein 3; PFN-1, Profilin-1; POFUT1, Protein O-fucosyltransferase1.

* Corresponding authors at: Department of Immunology, Wuhan University School of Medicine, 115 Donghu Road, Wuhan, 430071, China.

E-mail addresses: fengguan@jiangnan.edu.cn (F. Guan), zhangxiaolian@whu.edu.cn (X.-L. Zhang).

of cancer cells [15,16]. The enzyme activities of glycosyltransferases and their gene expressions showed distinct differences between normal cells and cancer cells, and certain glycosyltransferases were involved in signal transduction processes related to epithelial–mesenchymal transition (EMT), metastasis and therapeutics in cancer cells [17,18]. Sialyl Lewis X epitope with α 1,3 Fuc was markedly increased in advanced breast cancer patients [19]. Furthermore, increased α -1-3 fucosylation of α -1-acid glycoprotein (AGP) and fucosylated haptoglobin were reported as novel biomarkers for pancreatic cancer [20,21].

In many cases of viral infected host cells, *N*-linked glycans are viral receptors and/or co-receptors thought to be involved in cellular surface attachment and entry of viruses [22]. The surface proteins of many enveloped as well as non-enveloped human viruses recognize terminal sugar chain moieties of glycan and select glycans for binding to specific tissues and hosts [23–25]. For example, human influenza A virus infection is restricted at the level of virus entry in Lec1 cells, which lack complex *N*-linked glycosylation by a mutation in the *N*-acetylglucosaminyltransferase I (GnT1) gene, and thus cannot initiate infection [26]. All viruses studied to date use host (specific cellular subtype)-encoded glycosyltransferases and glycosidases to add and remove sugar residues from their glycoproteins cotranslationally or shortly after translation of the protein [27–29]. Thus, detection of the glycopattern of host cells and the profiling of *N*-linked glycans from isolated glycoproteins can reflect the progression of viral infection and are beneficial for the rapid identification of abnormal protein glycosylation [26,30,31].

Human hepatoma cell line Huh7.5.1 is the only available cell line for HCV infection *in vitro* currently. In this study, the alteration of *N*-linked glycans after HCV infection of Huh7.5.1 was examined by Matrix-Assisted Laser Desorption/Ionization Time of Flight Mass Spectrometry (MALDI-TOF-MS). The altered glycoproteins were analyzed by lectin microarrays and lectin pull-down analysis, which were further confirmed by confocal microscopy and western blotting. The mRNA levels of glycan-related glycosyltransferase genes were analyzed using multiple reverse transcription-quantitative real time PCR (RT-qPCR). The integrated strategy described here may provides valuable information to reveal the molecular mechanisms of HCV infection and facilitate the discovery of new diagnostic biomarkers and therapeutic targets.

2. Materials and methods

2.1. Cell culture and viral infection

Huh7.5.1 cells were cultured in complete Dulbecco's modified Eagle's medium (DMEM) with 10% fetal bovine serum (FBS) (HyClone Laboratories, Logan, UT, USA). The HCV cell culture (HCVcc) infection was performed according to our previous publications [32,33]. In brief, Huh7.5.1 cells in 24-well plates were infected with HCVcc (MOI of ~ 1 ; 0.8×10^6 copies/ml) at 37 °C for 4 h. The supernatants were discarded, and the infected cells were washed twice with phosphate buffered saline (PBS) and incubated in DMEM containing 10% FBS for 72 h.

2.2. Total cellular protein extraction

Huh7.5.1 cells and HCVcc infected Huh7.5.1 cells (2×10^7 , respectively) were lysed with Tissue Protein Extraction Reagent (T-PER) (Thermo Scientific; San Jose, CA) according to the manufacturer's instructions. The solution was centrifuged at 12000 g for 20 min. The supernatant of the total protein was stored at -80 °C. The concentration of the protein was measured by a BCA kit (Beyotime, Shanghai, China).

2.3. *N*-linked glycans separation and derivation

The total proteins from Huh7.5.1 and HCV-infected cells were concentrated and desalted using a size-exclusion spin ultrafiltration unit (Amicon Ultra-0.5 10 KD, Millipore; Billerica, MA). The total proteins

were then denatured with 8 M urea, 10 mM DTT, and 10 mM IAM and centrifuged at 14,000 g for 15 min. The denatured protein was modified with sialic acid as previously described [18,34]. In brief, the denatured proteins were desalted with water for three times and reconstituted with 100 μ l of 1 M acetohydrazide, 20 μ l of 1 N HCl, and 20 μ l of 2 M EDC and incubated at room temperature (RT) for 4 h (every sialic acid residue will obtain additional 56.0676 mass). Next, the proteins were incubated with PNGase F (New England BioLabs; Ipswich, MA) at 37 °C overnight to release *N*-glycans. The effluents were collected and lyophilized.

2.4. Desalting of *N*-glycans

Desalting was performed as previously described using Sepharose 4B (Sigma-Aldrich) [35]. Sepharose 4B was washed with MW (methanol/H₂O (1:1 v/v)) and BMW (1-butanol/methanol/H₂O (5:1:1 v/v/v)) under centrifugation. Glycans were dissolved in 500 μ l of BMW and added to the microtube. After incubation for 45 min, *N*-glycans were washed three times with BMW, eluted with MW and lyophilized.

2.5. Mass spectrometry

Alteration of *N*-glycans in total proteins was characterized by MALDI-TOF/TOF-MS (UltrafleXtreme, Bruker Daltonics; Bremen, Germany). Lyophilized *N*-glycans were dissolved in 10 μ l of MW, spotted onto a MTP AnchorChip sample target and air-dried. Then 1 μ l of 20 mg/ml DHB in MW was added to recrystallize the glycans. Samples were evaluated on mass spectrometry (MS) in positive reflectron mode (ion source 1 voltage: 25 kV; ion source 2 voltage: 22.5 kV; lens voltage: 7.5 kV; reflector voltage: 26.4 kV; reflector 2 voltage: 13.4 kV) across the *m/z* range of 700 to 3500, with gating of ions below *m/z* 400. For these studies, each spot was measured using 5000 laser shots in groups of 500 shots per sampling area of the spot. MS was calibrated before being run, using a Peptide Calibration Standard II (external standard) from Bruker Daltonics (Part NO. 222570). The *m/z* data were analyzed and annotated using GlycoWorkbench software [36].

2.6. Lectin microarray analysis

Lectin microarray analysis was performed as previously described [17,18]. In brief, 40 commercial lectins from Vector Laboratories (Burlingame, CA) and Sigma-Aldrich were immobilized onto a microplate. Total proteins (2 mg) from Huh7.5.1 cells and HCVcc infected Huh7.5.1 cells were labelled with fluorescent dye Cy3 (GE Healthcare; Buckinghamshire, UK) and about 10–15 μ g protein was spotted for each individual spot on the lectin microplate. The Mean Fluorescence Intensity (MFI) at 570 nm was determined on a SpectraMax® i3x microplate reader (Molecular Devices, Sunnyvale, CA), and average backgrounds were removed. The lectin microarray data were normalized as described previously [37], and the change of protein glycosylation during HCV infection was evaluated by comparison of the data from HCV infected cells versus Huh7.5.1 cells and then presented by using MeV software (Version 4.6.0) [38].

2.7. Confocal microscopy

Huh7.5.1 cells were plated in confocal dishes (NEST Biological Technology Co., Ltd., Shanghai, China) at a density of 5×10^4 cells/ml. After 24 h, HCVcc (MOI of 1) was added to the Huh7.5.1 cells and incubated at 37 °C for 4 h. The supernatants were discarded, and the cells were washed twice with PBS and incubated in DMEM containing 10% FBS for 72 h. Cells were then fixed with Intracellular (IC) Fixation Buffer (eBioscience) for 30 min at 4 °C and then permeabilized with Permeabilization Buffer (1 \times , eBioscience) for 30 min at RT (25 °C). Biotin-labelled LCA, *Erythrina cristagalli* agglutinin (ECA) and *Amaranthus caudatus* agglutinin (ACA) were incubated with permeabilized cells for

1 h at RT. FITC-streptavidin was then used to detect the binding ability of biotin-lectin with cells and nuclei were stained with DAPI (100×, Ribobio, Guangzhou, China) in $1 \times$ PBS for 10 min at RT. The stained cells were observed and analyzed using a Leica-LCS-SP8-STED confocal microscope (Heidelberg, Germany).

2.8. Lectin pull-down assay

Lectin pull-down assays were performed according to previous publications [39,40]. Total cell lysates (2 mg of protein) were incubated with LCA-agarose (Vector Laboratories, Burlingame, CA) (40 μ l) at 4 °C for 16 h. The precipitated samples were washed with Glycoprotein Eluting Solution (Vector Laboratories, Burlingame, CA) and analyzed with SDS-PAGE. The bands of proteins that were differently expressed between Huh7.5.1 cells and HCV-infected cells were extracted from the SDS gel and prepared for identification with LC-MS (TripleTOF5600+, SCIEX, USA).

2.9. In-gel digestion and LC-MS/MS analysis

Gel processing and in-gel digestion were performed as described in the previous study [41]. In brief, gel slices were destained, then DTT (10 mM DTT/50 mM NH_4HCO_3), iodoacetamide and trypsin (0.025 μ g/ μ l trypsin/10 mM NH_4HCO_3) solution were used to reduce, alkylate and digest respectively. After digestion, peptides were extracted from the gel cubes with 150 μ l extraction buffer (60% acetonitrile/5% formic acid) and incubated for 15 min at RT in a shaker. Supernatant was transferred to a new tube and gel pieces were further extracted with 100 μ l extraction buffer. Prior to LC-MS, extracts were concentrated in a vacuum centrifuge and desalted with Millipore ZipTip C18.

Peptides were detected by RPLC-ESI-MS/MS which was carried out on a hybrid quadrupole-TOF LC/MS/MS mass spectrometer (TripleTOF 5600+, AB Sciex) equipped with a nanospray source. Peptides were first loaded onto a C18 trap column (5 μ m, 5×0.3 mm, Agilent Technologies) and then eluted into a C18 analytical column (75 μ m \times 150 mm, 3 μ m particle size, 100 Å pore size, Eksigent). Mobile phase A (3% DMSO, 97% H_2O , 0.1% formic acid) and mobile phase B (3% DMSO, 97% ACN, 0.1% formic acid) were used to establish a 30-min gradient, which comprised of: 0 min in 5% B, 15 min of 5–35% B, 1 min of 35–80% B, the gradient was maintained in 80% B for 5 min, followed by 0.1 min of 80–5% B, and a final step in 5% B for 8.9 min. A constant flow rate was set at 300 nl/min. MS scans were conducted from 350 to 1500 amu, with a 250 ms time span. For MS/MS analysis, each scan cycle consisted of one full-scan mass spectrum (with m/z ranging from 350 to 1500 and charge states from 2 to 5) followed by 40 MS/MS events. The threshold count was set to 120 to activate MS/MS accumulation and former target ion exclusion was set for 18 s.

Raw data from TripleTOF 5600+ were analyzed with ProteinPilot Software. Data were searched against the UniProt human reference proteome database using the following parameters: Sample Type, Identification; Cys Alkylation, Iodoacetamide; Digestion, Trypsin. Search Effort was set to Rapid ID.

2.10. Quantification of HCV and glycosyltransferase mRNA expressions by reverse transcription-quantitative real time PCR (RT-qPCR)

The total RNA from HCV-infected cells and Huh7.5.1 cells was extracted using the TRIzol reagent (Invitrogen, Carlsbad, CA). First-strand cDNA was synthesized from the total RNA using ReverTra Ace- α First-strand cDNA Synthesis Kit (Toyobo, Osaka, Japan). The primers of HCV and 47 glycosyltransferases genes are listed in Supplementary Table S1. The relative mRNA expression of HCV and each of the 47 glycosyltransferases was quantified using real-time RT-PCR with the SYBR Green real-time PCR Master Mix kit (Toyobo, Osaka, Japan). GAPDH was used as the endogenous control [33].

2.11. Transfection

The siRNA (small interfering RNA) oligonucleotides against FUT8 (GenBank accession no: NM_178155.2) were designed by Invitrogen BLOCK-iTTM RNAi Designer and synthesized by Invitrogen (Shanghai, China). The siRNA sequence of FUT8 (si-FUT8) was 5'-GGACUGCACAUCGAUACATT-3' (target position: 2606–2624), and si-NC (5'-CAGCCTAACGTGTTGTCCATTCGCT-3') was used as a negative control. Huh7.5.1 (5×10^4) cells were plated in six-well plates overnight and then transiently transfected with siRNA after the cells reached 70–90% confluence using INTERFERin[®] *in vitro* siRNA transfection (Invitrogen, CA, USA) according to the manufacturer's protocol.

2.12. Flow cytometry (FCM)

Huh7.5.1 (5×10^4) cells were plated in six-well plates overnight and then transiently transfected with siRNA. After 24 h, HCVcc (MOI of 1) was added to the Huh7.5.1 cells and incubated at 37 °C for 4 h. The supernatants were discarded, and the infected cells were washed twice with PBS and incubated in DMEM containing 10% FBS for 72 h. Cells were then fixed with Intracellular (IC) Fixation Buffer (eBioscience) for 30 min at 4 °C and then permeabilized with Permeabilization Buffer (1 \times , eBioscience) for 30 min at RT (25 °C). Biotin-labelled LCA was incubated with permeabilized cells for 1 h at RT. FITC-streptavidin (1:500; Abcam; UK) was then used to detect the binding ability of lectin with cells and analyzed on a BD Accuri C6 Flow cytometer (BD Biosciences).

2.13. Western blotting analysis

HCVcc-infected cells and Huh7.5.1 cells (2×10^7 , respectively) were pre-transfected with or without FUT8-siRNA. Total proteins were extracted with T-PER Regent and then pulled down by LCA-agarose. Protein concentrations were quantified using the BCA Protein Assay Kit (Beyotime, China), after which 30 μ g of each of the protein lysates was loaded onto the SDS-PAGE gel. The electrophoresed proteins were transferred to PVDF membranes (Millipore, USA). The membranes were blocked in 5% nonfat milk and incubated with diluted nonstructural protein 3 (NS3), ANXA2, HSP90B1 and PFN-1 antibodies (1:3000; Abcam; UK), followed by incubation with a horseradish peroxidase (HRP)-conjugated secondary antibody (1:5000; Santa Cruz; USA). β -actin was used as a control (1:10,000; Abcam; UK).

2.14. Statistical analysis

Data are presented as the mean \pm SD and were analyzed by GraphPad Prism V.5.00 software (GraphPad Software, San Diego CA, USA). Differences between groups were tested by one-way ANOVA followed by the Newman-Keuls post hoc test. Two-sided p -values under 0.05 were considered statistically significant (*, $p < 0.05$, **, $p < 0.01$, ***, $p < 0.001$).

3. Results

3.1. Altered N-glycan profile in HCV infected Huh7.5.1 cells

QRT-PCR and western blotting were used to detect HCV RNA and NS3 protein levels in Huh7.5.1 cells (Fig. 1A). MALDI-TOF/TOF-MS profiles of total N-glycans in HCVcc-infected Huh7.5.1 cells and Huh7.5.1 cells were then compared to reveal abnormal N-glycosylation. Representative MALDI-TOF-MS spectra of N-glycans with signal-to-noise ratios >5 from total glycoproteins were annotated using GlycoWorkbench software. MS profiles of N-glycans and proposed structures are shown in Fig. 1B and C (Magnified figures for Fig. 1B and C are presented in supplementary materials as Figs. S2 and S3 respectively). In total, 23 N-glycans structures were proposed from the HCVcc-infected Huh7.5.1 cells and Huh7.5.1 cells, of which 21 N-glycans

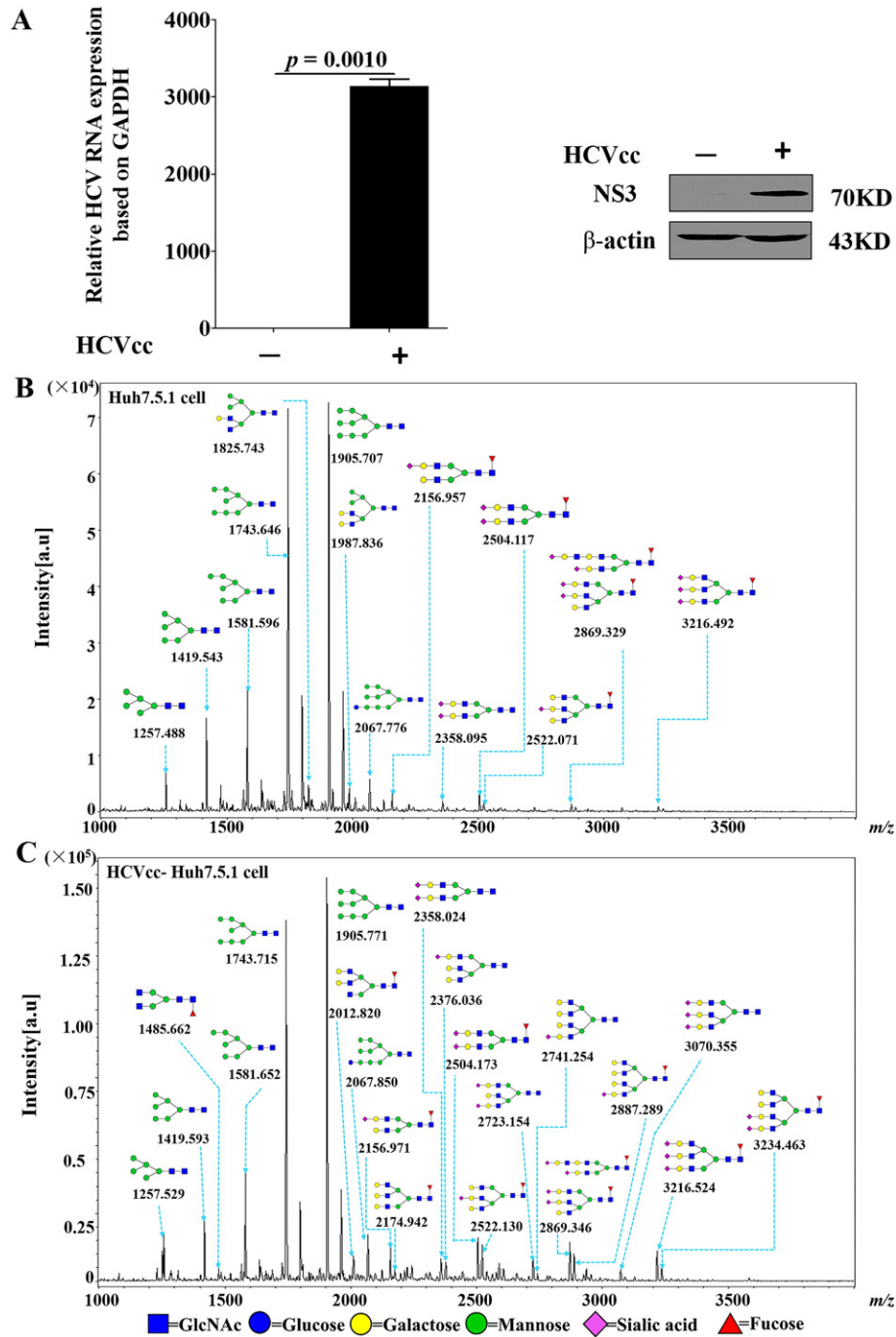


Fig. 1. MALDI-TOF-MS spectra of *N*-glycans. (A) qRT-PCR and western blotting analysis were used to detect the relative HCV RNA expression and NS3 protein level post 72 h of HCV infection in Huh7.5.1 cells. The *N*-glycans from the control Huh7.5.1 cells (B) and HCVcc-infected Huh7.5.1 (C) samples were separated, as described in M&M. The lyophilized *N*-glycans were resuspended in MW, and the mixture was spotted on a MTP Anchor Chip sample target and air-dried. MALDI-TOF-MS was performed in positive-ion mode. Peaks (signal-to-noise ratio > 5) were selected for relative proportion analysis, and m/z data were analyzed and annotated using GlycoWorkbench software. All analyses were performed at least three times.














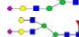



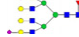





and 14 *N*-glycans were derived from HCVcc-infected Huh7.5.1 cells and Huh7.5.1 cells, respectively (Table 1). There were 12 common *N*-glycan structures in both uninfected Huh7.5.1 cells and HCVcc-infected cells, but they displayed different intensities. Two structures (Nos. 6 and 8) were found only in Huh7.5.1 control cells, and 9 structures (Nos. 3, 9, 12, 14, 17, 18, 20, 21, and 23) were unique to HCVcc-infected cells (Table 1). The structures of identified glycans were annotated by the MS/MS data and partial results are shown in the supplementary information (Fig. S1). Changes in the relative variation of *N*-glycans in HCV infection are summarized in Table 2. The proportions of fucosylated

(47.6% vs. 28.6%) and sialylated (57.1% vs. 42.9%) and complex glycan type (71.4% vs. 42.9%) were higher in HCVcc-infected cells than in the Huh7.5.1 control (Table 2). However, the proportions of oligomannose and hybrid-type *N*-glycans were down-regulated in HCVcc-infected Huh7.5.1 cells (Table 2).

3.2. Glycan patterns of glycoproteins in HCVcc-infected cells

Lectins are carbohydrate-binding proteins that recognize specific glycans based on subtle differences in structure. In our study, the glycan

Table 1Proposed structures and their molecular ions in MALDI spectra of *N*-glycans from Huh7.5.1 and HCVcc infected cell.^a

No.	Experimental <i>m/z</i>		Calculated <i>m/z</i>	Glycan structure	Relative intensity			
	Huh 7.5.1	HCVcc-Huh7.5.1			Huh 7.5.1		HCVcc-Huh7.5.1	
					Average	CV%	Average	CV%
1	1257.488	1257.529	1257.423		0.052	18	0.125	7
2	1419.543	1419.593	1419.476		0.122	3	0.148	9
3		1485.662	1485.534		ND	ND	0.024	9
4	1581.596	1581.652	1581.528		0.158	5	0.273	13
5	1743.646	1743.715	1743.581		0.490	17	0.892	16
6	1825.743		1825.634		0.028	54	ND	ND
7	1905.707	1905.771	1905.634		1.000	0	1.000	0
8	1987.836		1987.687		0.024	38	ND	ND
9		2012.820	2012.719		ND	ND	0.046	31
10	2067.776	2067.850	2067.687		0.040	6	0.111	5
11	2156.957	2156.971	2156.802		0.023	10	0.089	46
12		2174.942	2174.772		ND	ND	0.025	34
13	2358.095	2358.024	2357.907		0.072	29	0.041	26
14		2376.036	2375.877		ND	ND	0.036	11
15	2504.117	2504.173	2503.965		0.128	26	0.088	8
16	2522.071	2522.130	2521.935		0.009	22	0.073	26
17		2723.154	2723.040		ND	ND	0.023	13
18		2741.254	2741.009		ND	ND	0.015	42
19	2869.329	2869.346	2869.098		0.006	25	0.071	15
20		2887.289	2887.067		ND	ND	0.045	39
21		3070.355	3070.203		ND	ND	0.009	30
22	3216.492	3216.524	3216.261		0.003	4	0.042	11
23		3234.463	3234.230		ND	ND	0.019	33

^a CV, coefficient of variation. ND, not detected in the samples.

pattern of glycoproteins in HCVcc-infected Huh7.5.1 cells was further confirmed using lectin microarray, which consisted of 40 types of different lectins. Hierarchical clustering analysis (HCA) of all 40 lectins was performed by MeV 4.6.0 (Fig. 2A). According to the results, 5 of 40 lectins (Table 3, shown in blue) in HCVcc-infected cells showed a statistically significant MFI exceeding 1.5 times over control Huh7.5.1 cells. Among these, Fuc α 1-6GlcNAc, Gal β 1-4GlcNAc and Gal β 1-3GalNAc α -Ser/Thr (T) were binding ligands for LCA, ECA and ACA, respectively, with >1.6 times stronger binding signals than the control MFI (Fig. 2A, B). In accordance with the results from MALDI-TOF/TOF-MS/MS analysis, lectin microarrays also identified that fucosylated glycans (LCA binding) were elevated in HCVcc-infected Huh7.5.1 cells. We further confirmed the glycan profiles using FITC-LCA, -ECA and -ACA lectin binding assays by confocal microscopy (Fig. 2C). These findings showed that HCVcc-infected Huh7.5.1 cells had greatly increased fluorescence

signal intensities of these three lectins and were in line with the results of lectin microarray analysis (Figs. 2A, B).

3.3. Validation of glycoproteins immunoprecipitated with LCA

Since fucosylated glycans were the most elevated in HCVcc-infected Huh7.5.1 cells, we performed fucosylated glycan-binding lectin LCA-agarose pull-down and extracted LCA-binding proteins for SDS-PAGE analysis as indicated in Fig. 3A. Four differently expressed protein bands between Huh7.5.1 cells and HCVcc-infected cells (Fig. 3A, indicated by the red arrow) underwent LC-MS/MS analysis. The data of identification of each band by LC-MS/MS analysis are shown in the Supplementary Table S2. In this Table S2, numbers 1 to 3 are HSP90B1, ANXA2 and Profilin-1 (PFN-1), respectively. These three proteins (HSP90B1, ANXA2 and PFN-1) have high protein score according to LC-MS/MS analysis and their molecular weights (MWs) are also similar to the sizes of the corresponding bands which we cut and analyzed from Fig. 3A. In addition, HSP90B1, ANXA2 and PFN-1 are pivotal oncogenic proteins involved in HBV/HCV infection and the progression of HCC, thus having the potential to be used as diagnostic or prognostic biomarkers [42–45]. Therefore, these three proteins were chosen to evaluate the LC-MS/MS results by western blotting. We observed that the total levels of these three proteins were not increased in HCVcc-infected cells compared to Huh7.5.1 cells (Fig. 3B), however the LCA-precipitated protein levels of HSP90B1 and ANXA2, but not PFN-1, were increased in HCVcc-infected cells (Fig. 3B). Thus, our results further

Table 2Different types of *N*-glycans in Huh7.5.1 and HCV infected Huh7.5.1 cells.

<i>N</i> -glycan types	Huh7.5.1	HCVcc-Huh7.5.1
Oligomannose-type	42.9%	28.6%
Hybrid-type	14.2%	0%
Complex-type	42.9%	71.4%
Biantennary	28.5%	23.8%
Tri- and tetra-antennary	21.4%	52.3%
Fucosylated	28.6%	47.6%
Sialylated	42.9%	57.1%

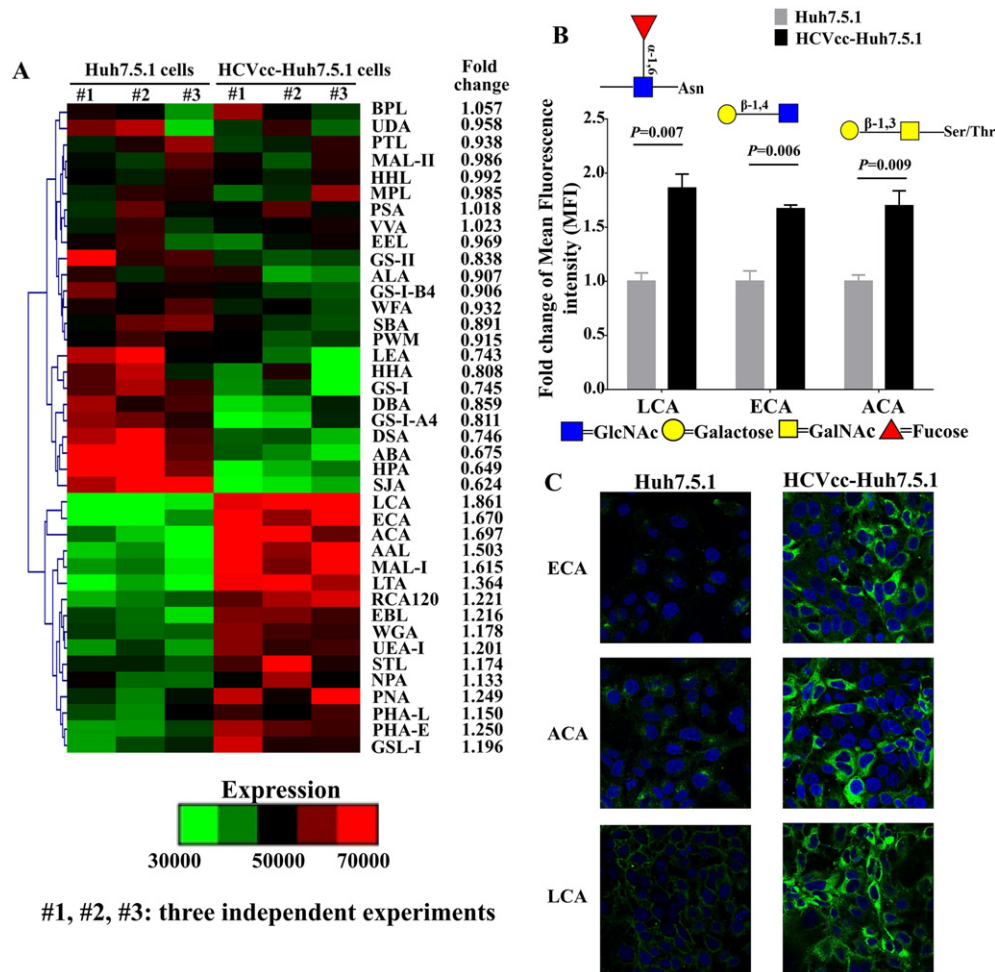


Fig. 2. Variation in glycans recognized by lectin microarrays in Huh7.5.1 and HCVcc-infected Huh7.5.1 cells. (A) Variations in the expression of glycans was recognized by 40 different lectins presented as a heatmap. (B) Representative fold changed histogram of glycans recognized by LCA, ECA and ACA between HCVcc-infected Huh7.5.1 cells and Huh7.5.1. Data are presented as the mean \pm SD. (C) Analysis of the altered expression of glycans evaluated by lectins using confocal microscopy. Signals from a merge image of FITC-conjugated lectins (green) and DAPI staining of nucleus (blue) in control samples (left) and HCVcc-infected samples (right) are shown (objective magnification 40 \times). All analyses were performed at least three times.

support the notion that HCV infection enhances α 1,6 fucosylation observed in the specific glycoproteins.

3.4. Variation of glycosyltransferase expression patterns in HCV-infected Huh7.5.1 cells

To further identify which glycosyltransferases were changed after HCV infection in Huh7.5.1 cells, the differences in the expression of glycosyltransferases between Huh7.5.1 control cells and HCVcc-infected cells were investigated using RT-qPCR. 47 glycosyltransferases gene (Table S1) belonging to 4 different families, including sialyltransferases (STs), galactosyltransferases (GalTs), N-acetylglucosaminyltransferases (GnTs) and fucosyltransferases (FUTs) were studied [46–48]. The fucosylation-related gene Fut8 in HCVcc-infected cells reached the highest level expression in comparison to the other 46 glycosyltransferase genes, and was 4 times higher than that of control cells (the data in Fig. 3C represents the FUT glycosyltransferase families). FUT8 is the only enzyme responsible for the α 1,6-fucosylation of N-glycans, catalyzing the transfer of fucose from GDP-L-fucose to the asparagine-linked N-acetylglucosamine [49]. Significant changes of the FUT8 mRNA expression by RT-qPCR were consistent with results from mass spectrometry (Table 2), lectin microarray analysis (Fig. 2A and B), confocal microscopy (Fig. 2C), western blotting analysis (Fig. 3D) and FCM (Fig. 3E), which indicated that the α 1,6-fucosylation of N-glycans was enhanced in Huh7.5.1 cells after HCV infection.

Next, we evaluated whether fucosylation modifications of ANXA2 and HSP90B1 were mediated by FUT8. We determined that FUT8 siRNA significantly suppressed α 1,6 fucosylation in HCVcc-infected cells compared with control siRNA from 90.6% to 72.4%, as evaluated by LCA staining shown in Fig. 3E. Western blotting also showed that FUT8 siRNA significantly decreased LCA-precipitated protein levels of ANXA2 and HSP90B1 in HCVcc-infected cells (Fig. 3F). These results confirmed that the elevated FUT8 expression in HCVcc-infected cells led to increased fucosylation of ANXA2 and HSP90B1, which changed the glycoconjugate and glycan pattern of liver cells during HCV infection.

4. Discussion

In the present study, we analyzed the changes of N-linked glycan expression profiles after HCV infection in Huh7.5.1 cells using MALDI-TOF/TOF-MS. We found that the levels of fucosylated, sialylated and complex N-glycans were greatly enhanced (Table 2). Combined with the increased fucosylated glycans (LCA binding) of lectin array, our present data suggest that increased fucosylated N-glycans might be, at least, one of important factors involved in HCV infection of liver cells. In Table 3, Gal β -GlcNAc/GalNAc-reactive lectin (ECA, MAL-I, ACA) signals were also enhanced significantly. The increase of these lectin signals means the increase of asialo-glycans [50]. Elevated levels of both sialo- and asialo-glycans suggest that branched N-glycans might be increased

Table 3

Differences in glycan patterns between control and HCVcc-infected cells by lectin microarray analysis.

Lectin	Abbreviation	Carbohydrate specificity	Fold changed between HCVcc-Huh7.5.1 and Huh7.5.1
<i>Lens culinaris</i> agglutinin	LCA	Fuc α 1-6GlcNAc, α -D-Man	1.861**
<i>Amaranthus caudatus</i> agglutinin	ACA	Gal β 1-3GalNAc	1.697**
<i>Erythrina cristagalli</i> agglutinin	ECA	Gal β 1-4GlcNAc	1.670**
<i>Maackia amurensis</i> I	MAL-I	Gal β 1-4GlcNAc	1.615*
<i>Aleuria aurantia</i>	AAL	Fuc α 1-6GlcNAc, Fuc α 1-3(Gal β 1-4)GlcNAc	1.503*
<i>Lotus tetragonolobus</i> agglutinin	LTA	Fuc α 1-3(Gal β 1-4)GlcNAc, Fuc α 1-2 Gal β 1-4GlcNAc	1.364
<i>Phaseolus vulgaris</i>	PHA-E	complex-type N-glycan	1.250
<i>Arachis hypogaea</i>	PNA	Gal β 1-4 GalNAc	1.249
<i>Ricinus communis</i>	RCA 120	Gal β 1-4GlcNAc, Gal	1.221
Elderberry	EBL	Neu5Ac α 6Gal/GalNAc	1.216
<i>Ulex europaeus</i> agglutinin I	UEA-I	Fuc α 1-2 Gal β 1-4 GlcNAc	1.201
<i>Galanthus nivalis</i>	GSL-I	α Man	1.196
<i>Triticum aestivum</i>	WGA	Chitin oligomers, NeuAc	1.178
<i>Solanum tuberosum</i>	STL	GlcNAc β 1-4 GlcNAc, Mixture Man5 to Man9	1.174
<i>Phaseolus vulgaris</i>	PHA-L	Tri/tetra-antennary complex-type N-glycan	1.150
<i>Narcissus pseudonarcissus</i>	NPA	Non-substituted α -1,6Man	1.133
<i>Bauhinia purpurea</i>	BPL	Gal β 1-3 GalNAc, GalNAc	1.057
<i>Vicia villosa</i>	VVA	GalNAc	1.023
<i>Pisum sativum</i>	PSA	α Man, α Glc	1.018
<i>Hippeastrum hybrid</i>	HHL	High-Man, Mana1-3Man, Mana1-6Man	0.992
<i>Maackia amurensis</i> II	MAL-II	Neu5Ac α (2-3)	0.986
<i>Maclura pomifera</i>	MPL	Gal β 3GalNAc	0.985
<i>Eunoymus europaeus</i>	EEL	Gal α 3Gal	0.969
<i>Urtica dioica</i>	UDA	GlcNAc	0.958
<i>Psophocarpus tetragonolobus</i>	PTL	GalNAc, Gal	0.938
<i>Wisteria floribunda</i>	WFA	GalNAc β 1-4 GlcNAc, Gal β 1-3(-6)GalNAc	0.932
<i>Phytolacca americana</i>	PWM	Branched (LacNAc) _n	0.915
<i>Artocarpus integrifolia</i>	ALA	Gal β 1-3GalNAc, GalNAc	0.907
<i>G. simplicifolia</i>	GSL-I-B4	α -Linked Gal	0.906
Soybean agglutinin	SBA	α -or β -terminal terminal GalNAc, GalNAc α 1-3GalNAc	0.891
<i>Dolichos biflorus</i>	DBA	Blood group A antigen, GalNAc α 1-3 GalNAc	0.859
<i>Griffonia simplicifolia</i>	GSL-II	Agalactosylated Tri/tetra-antennary glycans	0.838
<i>Griffonia simplicifolia</i>	GSL-I-A4	α -Linked GalNAc	0.811
<i>Hippeastrum hybrid amaryllis</i>	HHA	α -1,6Man	0.808
<i>Datura stramonium</i>	DSA	(GlcNAc β 1-4) _n , Gal β 1-4GlcNAc	0.746
<i>Griffonia simplicifolia</i>	GS-I	Melibio, α -D-Galactose	0.745
<i>Lycopersicon esculentum</i>	LEA	GlcNAc trimmers/tetramers	0.743
<i>Agaricus bisporus</i>	ABA	Gal β 1-4 GalNAc	0.675
<i>Helix pomatia</i>	HPA	α -Linked terminal GalNAc	0.649
<i>Sophora japonica</i>	SJA	β GalNAc	0.624

* $p < 0.05$.** $p < 0.01$.

after HCV infection, which actually was supported by mass spectrometry analysis (increased ratios of Tri- and tetra-antennary N-glycans in Table 2). Roles of those branching N-glycans in HCV pathology remain further study.

It has been reported that α 1,6 fucosylation plays an important role in TGF- β , EGF, HGF and T-cell receptor-mediated signaling in many physiological and pathological functions, including cancers and inflammatory bowel disease [51–53]. In addition, an enhanced degree of α 1,6 fucosylation has also been observed in many viral infections, including hepatitis B virus (HBV) [41], herpes simplex virus (HSV) [54] and human T-cell leukemia virus [55]. For example, high FUT8 expression was reported to be a good indicator of poor prognosis in HBV-related HCC [41]. However, the relationship between FUT8 and HCV has not been reported. In our study, we demonstrated that FUT8 mRNA exhibited the highest induced expression among 47 types of different glycosyltransferase mRNAs after HCV infection. Knockdown of FUT8 significantly decreased the enrichment of ANXA2 and HSP90B1 in LCA-precipitated proteins (Fig. 3F). FUT8 expression is elevated in HCC and is also critical for the regeneration of the liver by increasing the phosphorylation levels of AKT in response to epidermal growth factor (EGF) and hepatocyte growth factor (HGF) [56,57]. The interactions between FUT8 and ANXA2 or HSP90B1 might play important roles in HCV-promoted HCC progression.

ANXA2 and HSP90B1 were previously reported to be involved in HBV-related HCC and may serve as biomarkers to predict HCC metastasis [42,58–60]. In particular, core fucosylation of ANXA2 has been

observed in a study on hepatic cancer cells and was observed to be related to the metastatic potential of hepatic cancer [61]. Combining the detection of serum ANXA2 and alpha-fetoprotein (AFP) substantially improved the diagnostic efficiency (96.52%) and the negative predictive value (96.61%) for HCC [58,59]. ANXA2 can form a tetrameric complex with the S100A10 subunit and, in this manner, regulates the cell membrane cytoarchitecture, dynamics of endosomal membranes and structural organization in physiological conditions [62,63]. During HIV-1 infection, ANXA2 served as a cellular cofactor that supports viral infection of macrophage by binding with phosphatidylserine in the human cell membrane [64], or enhanced cytomegalovirus plaque formation in human foreskin fibroblast [65]. Furthermore, the knockdown of ANXA2 or treatment with ANXA2 antibodies significantly increased drug sensitivity and decreased proliferation and migration of cancer cells by inhibiting the EGFR-dependent PI3K-AKT downstream pathways [66–68]. HCV NS5A protein activated PI3K-AKT signaling by enhancing sterol regulatory element-binding protein (SREBPs) expression and facilitating the entry and replication of HCV in liver cells [69–72]. Thus, we assume that HCV-induced FUT8 expression might activate AKT signaling and enhance ANXA2 fucosylation to promote HCC progression or mediate drug-resistance. These will be needed to further confirm in our future study.

HSP90B1 is an endoplasmic reticulum (ER) heat shock protein 90 paralog that acts as a protein chaperone and plays an important role in maintaining liver development and hepatocyte function [43]. Increased expression of HSP90B1 by HBx-induced NF- κ B activation feedback

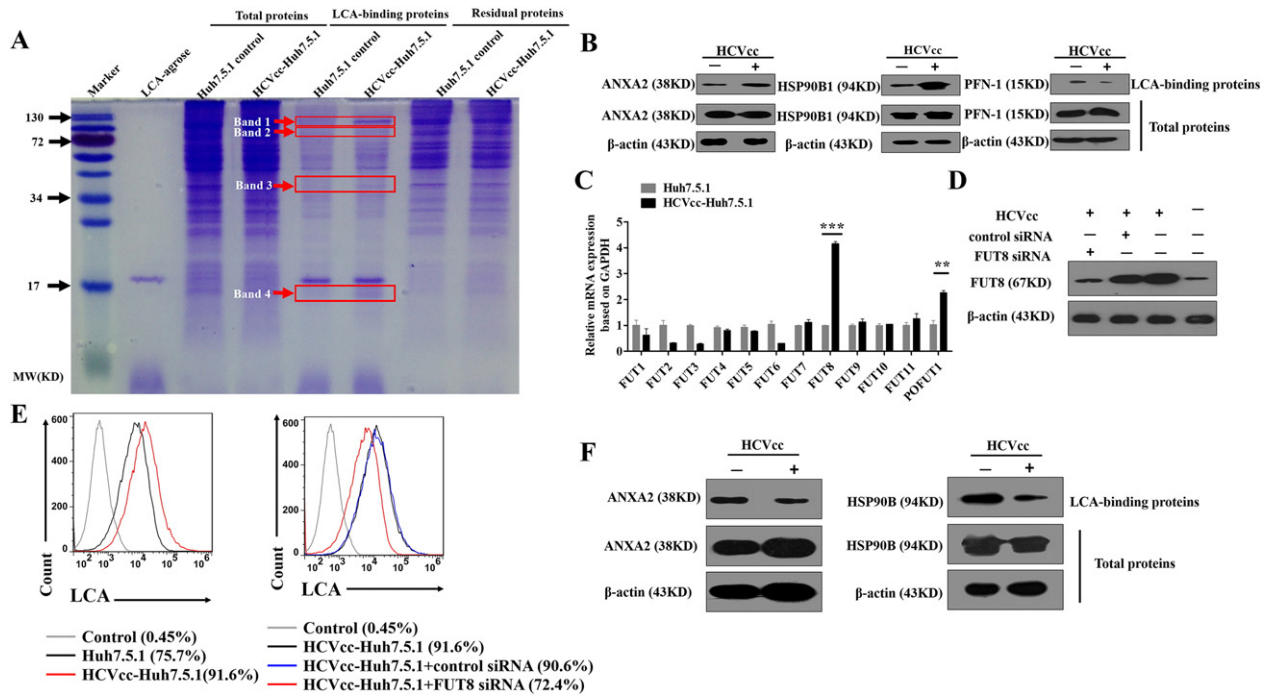


Fig. 3. FUT8 modified ANXA2 and HSP90B1 in HCVcc-infected Huh7.5.1 cells. (A) LCA-agarose pull-down and SDS-PAGE analysis. Four protein bands differently expressed in LCA-precipitated samples (indicated by red arrow) were cut and extracted for MS analysis. (B) The protein levels of ANXA2, HSP90B1 and PFN-1 in total cells or LCA-precipitated proteins were analyzed with western blotting. β -actin was used as endogenous control. (C) The mRNA expression of FUT glycosyltransferases families was analyzed with RT-qPCR in control cells or HCVcc-infected cells. Data are presented as the mean \pm SD. **, $p < 0.01$, ***, $p < 0.001$. (D) Huh7.5.1 cells and HCVcc-infected cells were pre-transfected with or without FUT8-siRNAs. The protein expression of FUT8 was evaluated by western blotting analysis. (E) The relative glycosylated activity of FUT8 of the cells was evaluated by FITC-LCA staining and analyzed by FCM. (F) Huh7.5.1 cells were pre-transfected with FUT8-siRNA and then either were or were not infected with HCVcc. The total proteins were extracted from control or HCVcc-infected cells and then incubated with or without LCA-conjugated agarose. The protein levels of ANXA2 and HSP90B1 in total cells or LCA-precipitated proteins were analyzed by western blotting. All analyses were performed at least three times.

enhances HBV production in HBV-transfected cells and a mouse model [60]. Moreover, the up-regulated HSP90B1 expression was observed in HBV-infected patients and is associated with poor outcomes of HBV-related HCC [42,60]. In this study, we found that HCV infection induced an increase of fucosylated ANXA2 and HSP90B1, as demonstrated by LCA-pulldown and western blot analysis (Figs. 3A–E), but it did not have an effect on total protein expression of ANXA2 and HSP90B1. Kim et al. reported that HCV E2 protein increased surface expression of HSP90B1 in liver cells, which resulted in inhibition of apoptosis and a maintenance of prolonged infection states [73]. This phenomenon likely occurred because various components of HCV virus are involved in regulating host cell function at different levels. However, we still need to further study which component of HCV regulates FUT8 expression. Nonetheless, these results indicate that in HCV infection, ANXA2 and HSP90B1 are fucosylated and thus are promising glycoprotein biomarkers that may predict HCV infection and HCV-associated HCC. In addition, increased binding ability of LCA to HCVcc-infected HCC cells (Fig. 3E) could possibly be used to monitor HCV infection in HCC.

Our results in Fig. 3C showed that protein O-fucosyltransferase 1 (POFUT1) was also increased after HCV infection. POFUT1 can boost the activation of Notch signaling through adding O-fucose to conserved threonine or serine residues in the epidermal growth factor-like repeats of Notch receptors and ligands [74]. POFUT1 overexpression in HCC was correlated with aggressive tumor behaviors and associated with poor prognosis. It promoted cell proliferation, migration and invasion in hepatoma cells [75] and oral squamous cell carcinoma (OSCC)-derived cell lines [76]. These indicate that POFUT1 may serve as a diagnostic marker and a therapeutic target for some tumor. But the relationship between POFUT1 and viral infection has not been reported, and molecular details underlying this HCV-infection induced POFUT1 expression change and the roles that this regulatory mechanism plays in HCV pathology need further research.

In summary, the information of *N*-glycan pattern and their glycosyltransferases which were simultaneously obtained in our study provide insight into the relation between *N*-glycans and their glycoproteins in the context of HCV infection. Furthermore, we identified that HCV enhances FUT8 expression and thus promotes the fucosylation of ANXA2 and HSP90B1 in Huh7.5.1 cells. This observation may provide valuable information for the discovery of new diagnostic biomarkers and therapeutic targets based on the increased FUT8, fucosylated ANXA2 and HSP90B1 after HCV infection, and may lay the foundation for clarifying the role of *N*-glycans in HCV infection and hepatitis C-related liver diseases.

Supplementary data to this article can be found online at <http://dx.doi.org/10.1016/j.bbagen.2017.02.014>.

Conflict of interest

None.

Author contributions

Conceived and designed the experiments: XLZ. Performed the experiments: TX, GLY, XYL, YDZ, ZXF, FFL. Analyzed the data: TX, FG, XLZ. Wrote the manuscript: TX, XLZ. Revised the manuscript: XLZ, TX, JGG, NT, ZQT, XC, YX.

Transparency document

The Transparency document associated with this article can be found, in online version.

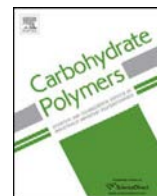
Acknowledgements

This work was supported by grants from the National Natural Science Foundation of China (21572173, 31370197 and 31221061), National Outstanding Youth Foundation of China (81025008), the Hubei Province's Outstanding Medical Academic Leader Program (523-276003), and Hubei Province Major Knowledge Innovation Project (Natural Science Foundation) (2016CFA062, 2016ACA150).

References

- [1] H. Pantua, J. Diao, M. Ultsch, M. Hazen, M. Mathieu, K. McCutcheon, K. Takeda, S. Date, T.K. Cheung, Q. Phung, P. Hass, D. Arnett, J.A. Hongo, D.J. Matthews, A. Brown, A.H. Patel, R.F. Kelley, C. Eigenbrot, S.B. Kapadia, Glycan shifting on hepatitis C virus (HCV) E2 glycoprotein is a mechanism for escape from broadly neutralizing antibodies, *J. Mol. Biol.* 425 (2013) 1899–1914.
- [2] D.J. Edwards, D.G. Coppens, T.L. Prasad, L.A. Rook, J.K. Iyer, Access to hepatitis C medicines, *Bull. World Health Organ.* 93 (2015) 799–805.
- [3] R.E. Jacob, I. Perdivara, M. Przybylski, K.B. Tomer, Mass spectrometric characterization of glycosylation of hepatitis C virus E2 envelope glycoprotein reveals extended microheterogeneity of *N*-glycans, *J. Am. Soc. Mass Spectrom.* 19 (2008) 428–444.
- [4] F. Helle, G. Duverlie, J. Dubuisson, The hepatitis C virus glycan shield and evasion of the humoral immune response, *Viruses* 3 (2011) 1909–1932.
- [5] Y. Li, B.G. Pierce, Q. Wang, Z.Y. Keck, T.R. Fuerst, S.K. Fount, R.A. Mariuzza, Structural basis for penetration of the glycan shield of hepatitis C virus E2 glycoprotein by a broadly neutralizing human antibody, *J. Biol. Chem.* 290 (2015) 10117–10125.
- [6] X. Qu, X. Pan, J. Weidner, W. Yu, D. Alonzi, X. Xu, T. Butters, T. Block, J.T. Guo, J. Chang, Inhibitors of endoplasmic reticulum alpha-glucosidases potentially suppress hepatitis C virus virion assembly and release, *Antimicrob. Agents Chemother.* 55 (2011) 1036–1044.
- [7] L.X. Xie, S.Y. Liu, Y.S. Chen, K. Liu, F. Xue, An animal experiment about early pulmonary candidiasis in immunosuppressive rabbits: thin-section CT images dynamically observed and proved by histopathological results, *Acta Radiol.* 52 (2011) (1987) 743–749 Stockholm, Sweden.
- [8] C. De Castro, A. Molinaro, F. Piacente, J.R. Gurnon, L. Sturiale, A. Palmigiano, R. Lanzetta, M. Parrilli, D. Garozzo, M.G. Tonetti, J.L. Van Etten, Structure of *N*-linked oligosaccharides attached to chlorovirus PBCV-1 major capsid protein reveals unusual class of complex *N*-glycans, *Proc. Natl. Acad. Sci. U. S. A.* 110 (2013) 13956–13960.
- [9] J. Breitling, M. Aebi, *N*-linked protein glycosylation in the endoplasmic reticulum, *Cold Spring Harb. Perspect. Biol.* 5 (2013) a013359.
- [10] H.H. Freeze, V. Westphal, Balancing *N*-linked glycosylation to avoid disease, *Biochimie* 83 (2001) 791–799.
- [11] H. Schachter, H.H. Freeze, Glycosylation diseases: quo vadis? *Biochim. Biophys. Acta* 1792 (2009) 925–930.
- [12] J.G. Leroy, Congenital disorders of *N*-glycosylation including diseases associated with O- as well as N-glycosylation defects, *Pediatr. Res.* 60 (2006) 643–656.
- [13] S. Hakomori, Glycosylation defining cancer malignancy: new wine in an old bottle, *Proc. Natl. Acad. Sci. U. S. A.* 99 (2002) 10231–10233.
- [14] A. Vasconcelos-Dos-Santos, I.A. Oliveira, M.C. Lucena, N.R. Mantuano, S.A. Whelan, W.B. Dias, A.R. Todeschini, Biosynthetic machinery involved in aberrant glycosylation: promising targets for developing of drugs against cancer, *Front. Oncol.* 5 (2015) 138.
- [15] T. Lange, S. Ullrich, I. Muller, M.F. Nentwich, K. Stubke, S. Feldhaus, C. Knies, O.J. Hellwinkel, R.L. Vessella, C. Abramjuk, M. Anders, J. Schroder-Schwarz, T. Schlomm, H. Huland, G. Sauter, U. Schumacher, Human prostate cancer in a clinically relevant xenograft mouse model: identification of beta(1,6)-branched oligosaccharides as a marker of tumor progression, *Clin. Cancer Res.* 18 (2012) 1364–1373.
- [16] Y. Song, J.A. Aglipay, J.D. Bernstein, S. Goswami, P. Stanley, The bisecting GlcNAc on *N*-glycans inhibits growth factor signaling and retards mammary tumor progression, *Cancer Res.* 70 (2010) 3361–3371.
- [17] Y. Qin, Y. Zhong, M. Zhu, L. Dang, H. Yu, Z. Chen, W. Chen, X. Wang, H. Zhang, Z. Li, Age- and sex-associated differences in the glycoproteins of human salivary glycoproteins and their roles against influenza A virus, *J. Proteome Res.* 12 (2013) 2742–2754.
- [18] Z. Tan, W. Lu, X. Li, G. Yang, J. Guo, H. Yu, Z. Li, F. Guan, Altered *N*-glycan expression profile in epithelial-to-mesenchymal transition of NMuMG cells revealed by an integrated strategy using mass spectrometry and glycogene and lectin microarray analysis, *J. Proteome Res.* 13 (2014) 2783–2795.
- [19] U.M. Abd Hamid, L. Royle, R. Saldova, C.M. Radcliffe, D.J. Harvey, S.J. Storr, M. Pardo, R. Antrobus, C.J. Chapman, N. Zitzmann, J.F. Robertson, R.A. Dwek, P.M. Rudd, A strategy to reveal potential glycan markers from serum glycoproteins associated with breast cancer progression, *Glycobiology* 18 (2008) 1105–1118.
- [20] M. Balmana, E. Gimenez, A. Puerta, E. Llop, J. Figueras, E. Fort, V. Sanz-Nebot, C. de Bolos, A. Rizzi, S. Barrabes, M. de Frutos, R. Peracaula, Increased alpha1-3 fucosylation of alpha-1-acid glycoprotein (AGP) in pancreatic cancer, *J. Proteome* 132 (2016) 144–154.
- [21] N. Okuyama, Y. Ide, M. Nakano, T. Nakagawa, K. Yamanaka, K. Moriwaki, K. Murata, H. Ohigashi, S. Yokoyama, H. Eguchi, O. Ishikawa, T. Ito, M. Kato, A. Kasahara, S. Kawano, J. Gu, N. Taniguchi, E. Miyoshi, Fucosylated haptoglobin is a novel marker for pancreatic cancer: a detailed analysis of the oligosaccharide structure and a possible mechanism for fucosylation, *Int. J. Cancer* 118 (2006) 2803–2808.
- [22] T. Takahashi, T. Suzuki, Role of glycans in viral infection, in: T. Suzuki, K. Ohtsubo, N. Taniguchi (Eds.), *Sugar Chains: Decoding the Functions of Glycans*, Springer Japan, Tokyo 2015, pp. 71–93.
- [23] K. Viswanathan, A. Chandrasekaran, A. Srinivasan, R. Raman, V. Sasisekharan, R. Sasisekharan, Glycans as receptors for influenza pathogenesis, *Glycoconj. J.* 27 (2010) 561–570.
- [24] K.I. Hidari, M. Yamaguchi, F. Ueno, T. Abe, K. Yoshida, T. Suzuki, Influenza virus utilizes *N*-linked sialoglycans as receptors in A549 cells, *Biochem. Biophys. Res. Commun.* 436 (2013) 394–399.
- [25] G. Herrler, J. Hausmann, H.-D. Klenk, Sialic acid as receptor determinant of ortho- and paramyxoviruses, in: A. Rosenberg (Ed.), *Biology of the Sialic Acids*, Springer US, Boston, MA 1995, pp. 315–336.
- [26] V.C. Chu, G.R. Whittaker, Influenza virus entry and infection require host cell *N*-linked glycoprotein, *Proc. Natl. Acad. Sci. U. S. A.* 101 (2004) 18153–18158.
- [27] R.W. Doms, R.A. Lamb, J.K. Rose, A. Helenius, Folding and assembly of viral membrane proteins, *Virology* 193 (1993) 545–562.
- [28] S. Olofsson, J.E. Hansen, Host cell glycosylation of viral glycoproteins—a battlefield for host defence and viral resistance, *Scand. J. Infect. Dis.* 30 (1998) 435–440.
- [29] D.J. Vigerust, V.L. Shepherd, Virus glycosylation: role in virulence and immune interactions, *Trends Microbiol.* 15 (2007) 211–218.
- [30] J. Gu, T. Isaji, Q. Xu, Y. Kariya, W. Gu, T. Fukuda, Y. Du, Potential roles of *N*-glycosylation in cell adhesion, *Glycoconj. J.* 29 (2012) 599–607.
- [31] M.N. Fukuda, H. Sasaki, L. Lopez, M. Fukuda, Survival of recombinant erythropoietin in the circulation: the role of carbohydrates, *Blood* 73 (1989) 84–89.
- [32] F. Chen, Y. Zhao, M. Liu, D. Li, H. Wu, H. Chen, Y. Zhu, F. Luo, J. Zhong, Y. Zhou, Z. Qi, X.L. Zhang, Functional selection of hepatitis C virus envelope E2-binding peptide ligands by using ribosome display, *Antimicrob. Agents Chemother.* 54 (2010) 3355–3364.
- [33] Y. Zhao, Y. Ren, X. Zhang, P. Zhao, W. Tao, J. Zhong, Q. Li, X.L. Zhang, Ficolin-2 inhibits hepatitis C virus infection, whereas apolipoprotein E3 mediates viral immune escape, *J. Immunol.* 193 (2014) 783–796.
- [34] G.C. Gil, B. Iliff, R. Cerny, W.H. Velander, K.E. Van Cott, High throughput quantification of *N*-glycans using one-pot sialic acid modification and matrix assisted laser desorption/ionization time-of-flight mass spectrometry, *Anal. Chem.* 82 (2010) 6613–6620.
- [35] G. Yang, T. Cui, Y. Wang, S. Sun, T. Ma, T. Wang, Q. Chen, Z. Li, Selective isolation and analysis of glycoprotein fractions and their glycomes from hepatocellular carcinoma sera, *Proteomics* 13 (2013) 1481–1498.
- [36] A. Ceroni, K. Maass, H. Geyer, R. Geyer, A. Dell, S.M. Haslam, GlycoWorkbench: a tool for the computer-assisted annotation of mass spectra of glycans, *J. Proteome Res.* 7 (2008) 1650–1659.
- [37] B.M. Bolstad, R.A. Irizarry, M. Astrand, T.P. Speed, A comparison of normalization methods for high density oligonucleotide array data based on variance and bias, *Bioinformatics* 19 (2003) 185–193.
- [38] V.T. Chu, R. Gottardo, A.E. Raftery, R.E. Bumgarner, K.Y. Yeung, MeV + R: using MeV as a graphical user interface for bioconductor applications in microarray analysis, *Genome Biol.* 9 (2008) R118.
- [39] S. Kitazume, Y. Tachida, M. Kato, Y. Yamaguchi, T. Honda, Y. Hashimoto, Y. Wada, T. Saito, N. Iwata, T. Saido, N. Taniguchi, Brain endothelial cells produce amyloid (beta) from amyloid precursor protein 770 and preferentially secrete the O-glycosylated form, *J. Biol. Chem.* 285 (2010) 40097–40103.
- [40] H.M. Ikonen, S. Minner, I.J. Guldvik, M.J. Sandmann, M.C. Tsourlakis, V. Berge, A. Svindland, T. Schlomm, I.G. Mills, O-GlcNAc transferase integrates metabolic pathways to regulate the stability of c-MYC in human prostate cancer cells, *Cancer Res.* 73 (2013) 5277–5287.
- [41] S.R. Piersma, M.O. Warmoes, M. de Wit, I. de Reus, J.C. Knol, C.R. Jimenez, Whole gel processing procedure for GeLC-MS/MS based proteomics, *Proteome Sci.* 11 (2013) 17.
- [42] Z. Yang, L. Zhuang, P. Szatmary, L. Wen, H. Sun, Y. Lu, Q. Xu, X. Chen, Upregulation of heat shock proteins (HSPA12A, HSP90B1, HSPA4, HSPA5 and HSPA6) in tumour tissues is associated with poor outcomes from HBV-related early-stage hepatocellular carcinoma, *Int. J. Med. Sci.* 12 (2015) 256–263.
- [43] S. Rachidi, S. Sun, B.X. Wu, E. Jones, R.R. Drake, B. Ogretmen, L.A. Cowart, C.J. Clarke, Y.A. Hannun, G. Chiosis, B. Liu, Z. Li, Endoplasmic reticulum heat shock protein gp96 maintains liver homeostasis and promotes hepatocellular carcinogenesis, *J. Hepatol.* 62 (2015) 879–888.
- [44] W. Zhang, P. Zhao, X.L. Xu, L. Cai, Z.S. Song, D.Y. Cao, K.S. Tao, W.P. Zhou, Z.N. Chen, K.F. Dou, Annexin A2 promotes the migration and invasion of human hepatocellular carcinoma cells in vitro by regulating the shedding of CD147-harboring microvesicles from tumor cells, *PLoS One* 8 (2013), e67268.
- [45] N.M. Boukdi, V. Shetty, L. Cubano, M. Ricaurte, J. Coelho-Dos-Reis, Z. Nickens, P. Shah, A.H. Talal, R. Philip, P. Jain, Unique and differential protein signatures within the mononuclear cells of HIV-1 and HCV mono-infected and co-infected patients, *Clin. Proteomics* 9 (2012) 11.
- [46] R. Saldova, H. Piccard, M. Perez-Garay, D.J. Harvey, W.B. Struwe, M.C. Galligan, N. Berghmans, S.F. Madden, R. Peracaula, G. Opdenakker, P.M. Rudd, Increase in sialylation and branching in the mouse serum *N*-glycome correlates with inflammation and ovarian tumour progression, *PLoS One* 8 (2013), e71159.
- [47] U.M. Unligil, J.M. Rini, Glycosyltransferase structure and mechanism, *Curr. Opin. Struct. Biol.* 10 (2000) 510–517.
- [48] M. Bubka, P. Link-Lenczowski, M. Janik, E. Poheć, A. Litynska, Overexpression of *N*-acetylglucosaminyltransferases III and V in human melanoma cells. Implications for MCAM *N*-glycosylation, *Biochimie* 103 (2014) 37–49.
- [49] E. Miyoshi, K. Noda, Y. Yamaguchi, S. Inoue, Y. Ikeda, W. Wang, J.H. Ko, N. Uozumi, W. Li, N. Taniguchi, The alpha1-6-fucosyltransferase gene and its biological significance, *Biochim. Biophys. Acta* 1473 (1999) 9–20.
- [50] M.H. Wilbrink, G.A. ten Kate, S.S. van Leeuwen, P. Sanders, E. Sallomons, J.A. Hage, L. Dijkhuizen, J.P. Kamerling, Galactosyl-lactose sialylation using *Trypanosoma cruzi* trans-sialidase as the biocatalyst and bovine kappa-casein-derived

- glycomacropeptide as the donor substrate, *Appl. Environ. Microbiol.* 80 (2014) 5984–5991.
- [51] X. Wang, S. Inoue, J. Gu, E. Miyoshi, K. Noda, W. Li, Y. Mizuno-Horikawa, M. Nakano, M. Asahi, M. Takahashi, N. Uozumi, S. Ihara, S.H. Lee, Y. Ikeda, Y. Yamaguchi, Y. Aze, Y. Tomiyama, J. Fujii, K. Suzuki, A. Kondo, S.D. Shapiro, C. Lopez-Otin, T. Kuwaki, M. Okabe, K. Honke, N. Taniguchi, Dysregulation of TGF- β 1 receptor activation leads to abnormal lung development and emphysema-like phenotype in core fucose-deficient mice, *Proc. Natl. Acad. Sci. U. S. A.* 102 (2005) 15791–15796.
- [52] X. Wang, J. Gu, H. Ihara, E. Miyoshi, K. Honke, N. Taniguchi, Core fucosylation regulates epidermal growth factor receptor-mediated intracellular signaling, *J. Biol. Chem.* 281 (2006) 2572–2577.
- [53] H. Fujii, S. Shinzaki, H. Iijima, K. Wakamatsu, C. Iwamoto, T. Sobajima, R. Kuwahara, S. Hiwama, Y. Hayashi, S. Takamatsu, N. Uozumi, Y. Kamada, M. Tsujii, N. Taniguchi, T. Takehara, E. Miyoshi, Core fucosylation on T cells, Required for activation of T-cell receptor signaling and induction of colitis in mice, is increased in patients with inflammatory bowel disease, *Gastroenterology* 150 (2016) 1620–1632.
- [54] R. Norden, K. Nystrom, S. Olofsson, Inhibition of protein deacetylation augments herpes simplex virus type 1-activated transcription of host fucosyltransferase genes associated with virus-induced sLex expression, *Arch. Virol.* 155 (2010) 305–313.
- [55] N. Hiraiwa, M. Hiraiwa, R. Kannagi, Human T-cell leukemia virus-1 encoded tax protein transactivates alpha 1 \rightarrow 3 fucosyltransferase Fuc-T VII, which synthesizes sialyl Lewis X, a selectin ligand expressed on adult T-cell leukemia cells, *Biochem. Biophys. Res. Commun.* 231 (1997) 183–186.
- [56] Y. Wang, T. Fukuda, T. Isaji, J. Lu, W. Gu, H.H. Lee, Y. Ohkubo, Y. Kamada, N. Taniguchi, E. Miyoshi, J. Gu, Loss of alpha1,6-fucosyltransferase suppressed liver regeneration: implication of core fucose in the regulation of growth factor receptor-mediated cellular signaling, *Sci. Report.* 5 (2015) 8264.
- [57] Y. Wang, T. Fukuda, T. Isaji, J. Lu, S. Im, Q. Hang, W. Gu, S. Hou, K. Ohtsubo, J. Gu, Loss of alpha1,6-fucosyltransferase inhibits chemical-induced hepatocellular carcinoma and tumorigenesis by down-regulating several cell signaling pathways, *FASEB J.* 29 (2015) 3217–3227.
- [58] H.J. Zhang, D.F. Yao, M. Yao, H. Huang, W. Wu, M.J. Yan, X.D. Yan, J. Chen, Expression characteristics and diagnostic value of annexin A2 in hepatocellular carcinoma, *World J. Gastroenterol.* 18 (2012) 5897–5904.
- [59] Z. Dong, M. Yao, H. Zhang, L. Wang, H. Huang, M. Yan, W. Wu, D. Yao, Inhibition of annexin A2 gene transcription is a promising molecular target for hepatoma cell proliferation and metastasis, *Oncol. Lett.* 7 (2014) 28–34.
- [60] H. Fan, X. Yan, Y. Zhang, X. Zhang, Y. Gao, Y. Xu, F. Wang, S. Meng, Increased expression of Gp96 by HBx-induced NF-kappaB activation feedback enhances hepatitis B virus production, *PLoS One* 8 (2013), e65588.
- [61] Z. Dai, Y.K. Liu, J.F. Cui, H.L. Shen, J. Chen, R.X. Sun, Y. Zhang, X.W. Zhou, P.Y. Yang, Z.Y. Tang, Identification and analysis of altered alpha1,6-fucosylated glycoproteins associated with hepatocellular carcinoma metastasis, *Proteomics* 6 (2006) 5857–5867.
- [62] A.G. Banerjee, J. Liu, Y. Yuan, V.K. Gopalakrishnan, S.L. Johansson, A.K. Dinda, N.P. Gupta, L. Trevino, J.K. Vishwanatha, Expression of biomarkers modulating prostate cancer angiogenesis: differential expression of annexin II in prostate carcinomas from India and USA, *Mol. Cancer* 2 (2003) 34.
- [63] Y. Shiozawa, A.M. Havens, Y. Jung, A.M. Ziegler, E.A. Pedersen, J. Wang, J. Wang, G. Lu, G.D. Roodman, R.D. Loberg, K.J. Pienta, R.S. Taichman, Annexin II/annexin II receptor axis regulates adhesion, migration, homing, and growth of prostate cancer, *J. Cell. Biochem.* 105 (2008) 370–380.
- [64] G. Ma, T. Greenwell-Wild, K. Lei, W. Jin, J. Swisher, N. Hardegen, C.T. Wild, S.M. Wahl, Secretory leukocyte protease inhibitor binds to annexin II, a cofactor for macrophage HIV-1 infection, *J. Exp. Med.* 200 (2004) 1337–1346.
- [65] J.F. Wright, A. Kurosky, E.L. Prydzial, S. Wasi, Host cellular annexin II is associated with cytomegalovirus particles isolated from cultured human fibroblasts, *J. Virol.* 69 (1995) 4784–4791.
- [66] P.K. Shetty, S.I. Thamake, S. Biswas, S.L. Johansson, J.K. Vishwanatha, Reciprocal regulation of annexin A2 and EGFR with Her-2 in Her-2 negative and herceptin-resistant breast cancer, *PLoS One* 7 (2012), e44299.
- [67] P. Chaudhary, S.I. Thamake, P. Shetty, J.K. Vishwanatha, Inhibition of triple-negative and herceptin-resistant breast cancer cell proliferation and migration by annexin A2 antibodies, *Br. J. Cancer* 111 (2014) 2328–2341.
- [68] Z.D. Zhang, Y. Li, Q. Fan, B. Zhao, B. Tan, X.F. Zhao, Annexin A2 is implicated in multi-drug-resistance in gastric cancer through p38MAPK and AKT pathway, *Neoplasma* 61 (2014) 627–637.
- [69] D. Cheng, L. Zhang, G. Yang, L. Zhao, F. Peng, Y. Tian, X. Xiao, R.T. Chung, G. Gong, Hepatitis C virus NS5A drives a PTEN-PI3K/Akt feedback loop to support cell survival, *Liver Int.* 35 (2015) 1682–1691.
- [70] Z. Liu, Y. Tian, K. Machida, M.M. Lai, G. Luo, S.K. Fong, J.H. Ou, Transient activation of the PI3K-AKT pathway by hepatitis C virus to enhance viral entry, *J. Biol. Chem.* 287 (2012) 41922–41930.
- [71] Q. Shi, B. Hoffman, Q. Liu, PI3K-Akt signaling pathway upregulates hepatitis C virus RNA translation through the activation of SREBPs, *Virology* 490 (2016) 99–108.
- [72] K. Kim, K.H. Kim, H.Y. Kim, H.K. Cho, N. Sakamoto, J. Cheong, Curcumin inhibits hepatitis C virus replication via suppressing the Akt-SREBP-1 pathway, *FEBS Lett.* 584 (2010) 707–712.
- [73] M.S. Kim, S. Kim, H. Myung, Degradation of AIMP1/p43 induced by hepatitis C virus E2 leads to upregulation of TGF- β signaling and increase in surface expression of gp96, *PLoS One* 9 (2014), e96302.
- [74] T. Okajima, A. Xu, L. Lei, K.D. Irvine, Chaperone activity of protein O-fucosyltransferase 1 promotes notch receptor folding, *Science* 307 (2005) 1599–1603.
- [75] L. Ma, P. Dong, L. Liu, Q. Gao, M. Duan, S. Zhang, S. Chen, R. Xue, X. Wang, Overexpression of protein O-fucosyltransferase 1 accelerates hepatocellular carcinoma progression via the Notch signaling pathway, *Biochem. Biophys. Res. Commun.* 473 (2016) 503–510.
- [76] S. Yokota, K. Ogawara, R. Kimura, F. Shimizu, T. Baba, Y. Minakawa, M. Higo, A. Kasamatsu, Y. Endo-Sakamoto, M. Shiiba, H. Tanzawa, K. Uzawa, Protein O-fucosyltransferase 1: a potential diagnostic marker and therapeutic target for human oral cancer, *Int. J. Oncol.* 43 (2013) 1864–1870.



Chitosan oligosaccharides inhibit epithelial cell migration through blockade of *N*-acetylglucosaminyltransferase V and branched GlcNAc structure

Qingsong Xu^{a,c,*}, Wenjing Wang^b, Chen Qu^a, Jianguo Gu^c, Heng Yin^d, Zhihao Jia^a, Linsheng Song^a, Yuguang Du^{e,**}

^a College of Fisheries and Life Science, Dalian Ocean University, Dalian 116023, China

^b Dalian Elite Analytical Instruments Company Limited, Dalian 116023, China

^c Tohoku Medical and Pharmaceutical University, Sendai, Miyagi, 981-8558, Japan

^d Dalian Institute of Chemical Physics, Chinese Academy of Sciences, Dalian 116023, China

^e Institute of Process Engineering, Chinese Academy of Sciences, Beijing 100190, China

ARTICLE INFO

Article history:

Received 9 November 2016

Received in revised form 10 March 2017

Accepted 24 April 2017

Available online 25 April 2017

Keywords:

Chitosan oligosaccharides

N-Acetylglucosaminyltransferase V

Branched *N*-glycan

Cell migration

ABSTRACT

Chitosan oligosaccharides (COS) have been shown to regulate various cellular and biological functions. The aim of this study was to investigate the antimetastatic potency of COS and the underlying mechanism. Here, we established a stably *N*-acetylglucosaminyltransferase V (GnT-V)-overexpressed MCF10A cell line. As expected, GnT-V overexpression greatly promoted cell migration in the transfectants by using wound healing assay. However, the induction in the cell migration was significantly suppressed by an addition of COS. Curiously, COS inhibited the protein expression of GnT-V in a dose dependent manner. Consistent with that, the reactivities with datura stramonium (DSA) and leuco-agglutinating phytohemagglutinin (L4-PHA) lectins, which specifically recognize branched *N*-acetylglucosamine (GlcNAc) structure, were also suppressed by COS. Taken together, these results demonstrated COS inhibited breast epithelial cell migration through down-regulation of GnT-V and its products, branched *N*-glycans, indicating that COS may serve as a potential novel therapeutic candidate for the treatment of metastatic breast cancer.

© 2017 Elsevier Ltd. All rights reserved.

1. Introduction

Chitin, a linear biopolymer comprising *N*-acetylglucosamine residues, is the second most abundant polysaccharide in nature. Nevertheless, its high molecular weight and low solubility seriously limited its practical application (Sayari et al., 2016). As the

degradation and deacetylation product of chitin, chitosan oligosaccharides (COS) have attracted more and more attentions recently, because the latter are not only easily soluble in water (generally, the molecular weight of COS is 10 kDa or less) and free amino groups in *D*-glucosamine units, but also readily absorbed through the intestine, quickly getting into the bloodstream (Chae, Jang, & Nah, 2005). Therefore, COS have many important biological activities, such as immuno-stimulation, antimicrobial effect and antitumor activity (Zou et al., 2016). The antitumor activity of COS has been known since 1986. Suzuki et al. demonstrated hexa-*N*-acetylchitoheptaose and chitoheptaose had antitumor activity against sarcoma 180 solid tumor (Suzuki et al., 1986). Zou et al. found that the antitumor effects on S180 tumor-bearing mice could be observed in both oral and intraperitoneal administration of COS (Zou et al., 2016), which strongly suggest COS might be considered promising candidate as antitumor functional food or pharmaceutical adjuvant in oncotherapy. Also, our previous studies showed that COS could induce apoptosis of human hepatocellular carcinoma cells via up-regulation of Bax (Xu et al., 2008), and inhibit breast cancer cellular

Abbreviations: COS, chitosan oligosaccharides; GnT-V, *N*-acetylglucosaminyltransferase V; DSA, datura stramonium; L4-PHA, leuco-agglutinating phytohemagglutinin; GlcNAc, *N*-acetylglucosamine; GalT, galactosyltransferase; GlcNAcT, *N*-acetylglucosaminyltransferase; DP, degree of polymerization; ATCC, American Tissue Culture Collection; SDS-PAGE, sodium dodecyl sulfate polyacrylamide gel electrophoresis; FN, fibronectin; BSA, bovine serum albumin; LLC, Lewis lung carcinoma; MMP-2, matrix metalloproteinase-2; MMP-9, matrix metalloproteinase-9; MT1-MMP, membrane-type matrix metalloproteinase-1.

* Corresponding author at: College of Fisheries and Life Science, Dalian Ocean University, 52. Heishijiao Street, Shahekou District, Dalian 116023, China.

** Corresponding author.

E-mail addresses: xuqingsong@dlou.edu.cn (Q. Xu), ygdu@ipe.ac.cn (Y. Du).

transplantation tumor angiogenesis through interference with the nitric oxide signaling pathway (Wu, Yao, Bai, Du, & Ma, 2010).

Recently, tumor metastasis and invasion has become a hot research field attracting much attention. Metastasis is a sequential process whereby cancer cells penetrate the basement membrane, invade blood/lymphatic vessels, survive in the vasculature before extravasation to next sites, and finally adapt to new host environments to proliferate and form metastases (Langley & Fidler, 2007). Alterations in glycan structures are associated with many physiological and pathological processes, including cell migration, differentiation and tumor invasion (Zhao et al., 2008). *N*-Acetylglucosaminyltransferase V (GnT-V) catalyzes the attachment of a UDP-GlcNAc to a mannose of *N*-glycan by a β 1,6-linkage to form a branched GlcNAc structure. β 1,6 GlcNAc-branched *N*-glycans can be subsequently modified by β 1,4 galactosyltransferase (GalT) and β 1,3 *N*-Acetylglucosaminyltransferase (GlcNAcT) to form poly-*N*-acetylglucosamine for the elongation of *N*-glycans, which are further processed to form other sugar motifs such as sialyl Lewis X, which contributes to increasing cancer invasion and metastasis (Taniguchi & Korekane, 2011). It has also been reported that GnT-V activity and β 1,6 GlcNAc branched *N*-glycan levels are increased in highly metastatic tumor cell lines (Pochec et al., 2013). Consistently, cancer metastasis is greatly suppressed in GnT-V knockout mice (Granovsky et al., 2000). Meanwhile, elevated expression and activity of GnT-V in hepatocellular carcinoma is a common early event involved in tumor invasion during hepatocarcinogenesis (Liu et al., 2013). These results strongly demonstrated that glycosyltransferase-modified *N*-glycan structures could modulate cell migration and thereby cancer metastasis as well.

As a non-toxic natural product, COS has very important research significances on physiological and pathological conditions, especially on the antitumor activity. However, the effect of COS on cancer metastasis still remains elusive. In this study, we investigated the effect of COS on cell migration induced by GnT-V, and found COS could suppress GnT-V expression and its products, which may give a hint for developing a novel therapeutic candidate for some metastatic cancers.

2. Materials and methods

2.1. Preparation of the COS

COS were prepared by the enzymatic hydrolysis of chitosan according to the method we reported previously (Li, Liu, Xu, Du, & Xu, 2014). The products of the enzymolysis were a mixture of several oligosaccharides with a degree of deacetylation over 95% and an average molecular weight ≤ 1000 Da. The percentage composition of COS was 3.7%, 16.1%, 28.8%, 37.2% and 14.2%, with a degree of polymerization (DP) of 2–6.

2.2. Cell line and cell culture

Human immortalized MCF-10A breast epithelial cell line, sharing many features of mesenchymal cancer cell lines (Sarrío et al., 2008), was obtained from American Tissue Culture Collection (ATCC) and cultured according to ATCC recommendations. Briefly, MCF10A was cultured in DMEM/F12 medium, supplemented with 5% horse serum, 20 ng/ml EGF, 100 ng/ml cholera toxin, 10 μ g/ml insulin, and 0.5 μ g/ml hydrocortisone, under a humidified atmosphere of 5% CO₂ and 95% O₂ at 37 °C.

2.3. GnT-V overexpression and retroviral infection

The cDNA of human GnT-V was amplified using pENTR-D-Topo for the Gateway Conversion System (Invitrogen), according to the recommended protocol. The cloned genes were integrated into the

virus expression vector, pBABE-puro (Addgene, Inc. Cambridge, MA), and inserted into the Gateway Conversion System utilizing an LR Clonase reaction. The GnT-V construct was transfected into Phoenix-Ampho cells with Lipofectamine 2000 (Invitrogen) for the preparation of viral supernatants. After virus infection, the infected cells were selected with 5 μ g/ml puromycin to get the GnT-V stably transfected MCF10A cells (GnT-V transfectants). For mock treatment, the same protocol was performed with the empty virus expression vector.

2.4. RT-PCR for GnT-V mRNA expression analysis

GnT-V transfectants were incubated with COS (0, 50, 100 and 200 μ g/ml) for 24 h, then cellular total RNA was extracted using cold TRIZOL reagent (Takara, Dalian, China) according to the manufacturer's protocol. RNA samples (2.0 μ g) were used as templates to perform the RT-PCR assay. PCR primers were as follows: GnT-V: forward sequence: GACCTGCAGTTCCTTCTTCG and reverse sequence: CCATGGCAGAAGTCCTGTTT; and β -actin: forward sequence: GGGTCAGAAGGATTCTATG and reverse sequence: GGTCTCAAACATGATCTGGG. The β -actin mRNA was used as a control in PCR runs and the reaction products were visualized by electrophoresis in 1.5% agarose gels containing ethidium bromide.

2.5. Western blot and lectin blot analysis

GnT-V transfectants were incubated with COS (0, 50, 100 and 200 μ g/ml) for 72 h, then equal amounts of proteins were separated by 7.5% sodium dodecyl sulfate polyacrylamide gel electrophoresis (SDS-PAGE), and transferred to polyvinylidene fluoride (PVDF) membranes. The membranes were blocked with 5% skim milk in PBS containing 0.1% Tween 20 (PBST) at room temperature for 2 h. After incubation, the membranes were probed with the appropriate antibodies, or with biotinylated DSA and biotinylated L4-PHA lectin (Seikagaku kogyo Inc., Japan). Immunoreactive bands were visualized utilizing a Vectastain ABC kit (Vector Laboratories, CA) and an ECL kit (Amersham, UK). Antibody against GnT-V (24B11) was obtained from FUJIREBIO Inc. (Tokyo, Japan), and the anti- α -tubulin antibody was from Sigma.

2.6. An *in vitro* assay of 2-D cell migration across an artificial gap

An *in vitro* cell migration assay was performed to investigate the ability of cell motility as previously described (Xu et al., 2011). Briefly, the GnT-V transfectants were incubated with COS (200 μ g/ml) for 48 h, then a confluent layer of cells was scraped/wounded using a yellow tip. The open gap was then observed microscopically over time when the cells moved in and filled the damaged area. Micrographs were taken at 0, 12 and 24 h after wounding under an inverted microscope (Leica, German). The pictures showed the cells as they began to migrate toward the center of the wound. Wound closure was measured by showing the distances between the sides of the wound at the indicated times.

2.7. Cell adhesion evaluation

Cell adhesion assay was performed as previously described (Xu et al., 2011). Briefly, the GnT-V transfectants were incubated with COS (100 and 200 μ g/ml) for 72 h, then 3 μ g/ml of fibronectin (FN) were coated in 96-well plates (Corning Inc., PA) at 37 °C for 1 h, and then blocked with 1% bovine serum albumin (BSA) in DMEM/F12 for 1 h. The cells in suspension were added to each well (5×10^4 per well) and the plates were incubated at 37 °C for 30 min. After incubation, attached cells were fixed with 25% glutaraldehyde, and stained with 0.5% crystal violet. The absorbance at 590 nm was

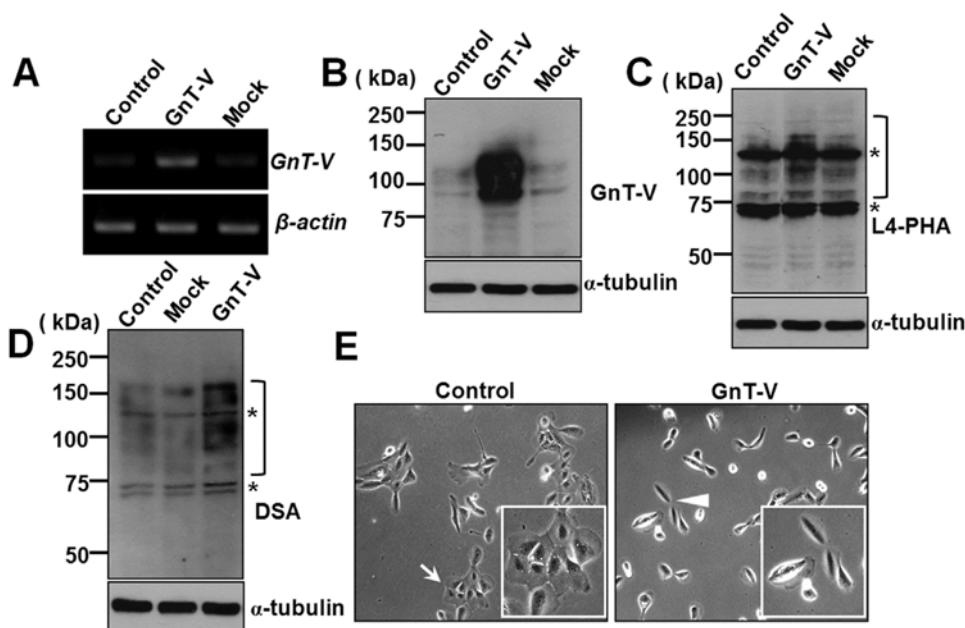


Fig. 1. Effects of GnT-V overexpression on *N*-glycan expression and cell morphology in MCF10A cells. Stable GnT-V-expressed cells were harvested for RT-PCR (A) and immunoblotting analysis (B) to confirm GnT-V expression. Equal amounts of protein (20 μ g) were separated on 7.5% SDS-PAGE under reducing conditions, and the membranes were probed with antibody against GnT-V (B), L4-PHA lectin (C), and DSA lectin (D). α -tubulin was used as a loading control. Square brackets indicated the L4-PHA and DSA specific reactive bands, and asterisks indicated nonspecific staining of L4-PHA and DSA, since those bands did not disappear after treatment with 100 mM acetic acid. The morphological changes of the GnT-V transfectants were photographed under a phase-contrast microscope (E). Photographs were taken of living cells using a 20 \times objective. Insets, representative amplified cell morphology. The arrow indicates aggregated cells, while the arrowhead shows scattering cell with a spindle shape.

detected on an automated micro-titer plate spectrometer (Biotech Instruments Inc., USA).

2.8. Expression of the branched *N*-glycans were analyzed by flow cytometry

To examine the branched *N*-glycans on the cell surface, a flow cytometry analysis was performed as previously described (Xu et al., 2011). Briefly, the GnT-V transfectants were incubated with COS (200 μ g/ml) for 72 h, then the cells were suspended and incubated with biotinylated DSA or L4-PHA lectin for 30 min, followed by streptavidin Alexa Fluor 488 conjugate (Invitrogen). Negative controls were performed the same treatment without biotinylated lectins. A FACSCalibur instrument (BD Biosciences), equipped with CELL QuestPro software was used to analyze the fluorescence intensity of cells.

2.9. Statistical analysis

Student's *t*-test was executed for comparison of two groups. $P < 0.05$ was defined as statistically significant.

3. Results

3.1. Overexpression of GnT-V increased expression levels of branched *N*-glycans and cell migration

GnT-V, a glycosyltransferase encoded by the *Mgat5* gene which catalyzes the formation of β 1,6 GlcNAc branches on *N*-glycans, is believed to be associated with cancer growth and metastasis (Miyoshi, Terao, & Kamada, 2012). To investigate effects of COS on breast epithelial cell migration, we established a GnT-V stable expression cell line. The expression levels of GnT-V were verified by RT-PCR and immunoblot analysis, and both gene and protein levels of GnT-V were dramatically increased in GnT-V-transfected MCF10A cells (Fig. 1A/B). In addition, the reactivity with DSA or

L4-PHA lectin, which specifically recognizes branched GlcNAc, was also up-regulated in the GnT-V transfectants (Fig. 1C/D). The wild type MCF10A cells formed a typical compact cobblestone epithelial morphology indicated by arrow, while the GnT-V transfectants exhibited obvious mesenchymal morphological changes including loss of cell-cell contact and spindle shape indicated by arrowhead (Fig. 1E), which indicates that cells have more migratory ability.

3.2. COS suppressed cell migration and cell adhesion induced by GnT-V

Previously, Gu et al. reported that GnT-V influenced cell migration and FN-mediated cell adhesion (Gu & Taniguchi, 2008). In this study, an *in vitro* assay of cell migration and FN-dependent cell adhesion was performed. Comparing with control cells, the GnT-V transfectants efficiently moved in and filled the open gap at 12 and 24 h after wounding. However, the increased wound closure was greatly suppressed in the presence of COS at 200 μ g/ml final concentration (Fig. 2A/B). Cell adhesion on fibronectin was significantly increased in the GnT-V transfectants compared with control cells. Similarly, COS significantly suppressed FN-dependent cell adhesion induced in the GnT-V transfectants (Fig. 2C). These results demonstrate that COS could functionally affect cell behavior.

3.3. COS inhibited GnT-V protein expression

To further verify the nature of COS as a potential antagonist of cancer metastasis, we evaluated the gene and protein expression of GnT-V, which was critically responsible for aforementioned cell behavior. As shown in Fig. 3A, the gene expression levels of GnT-V in the transfectants were around 10-fold higher than those in the control or mock cells, and COS did not obviously affect its expression. However, although the underlying mechanisms remain unclear, COS significantly inhibited the protein expression of GnT-V at 100 and 200 μ g/ml concentrations (Fig. 3B). These results sug-

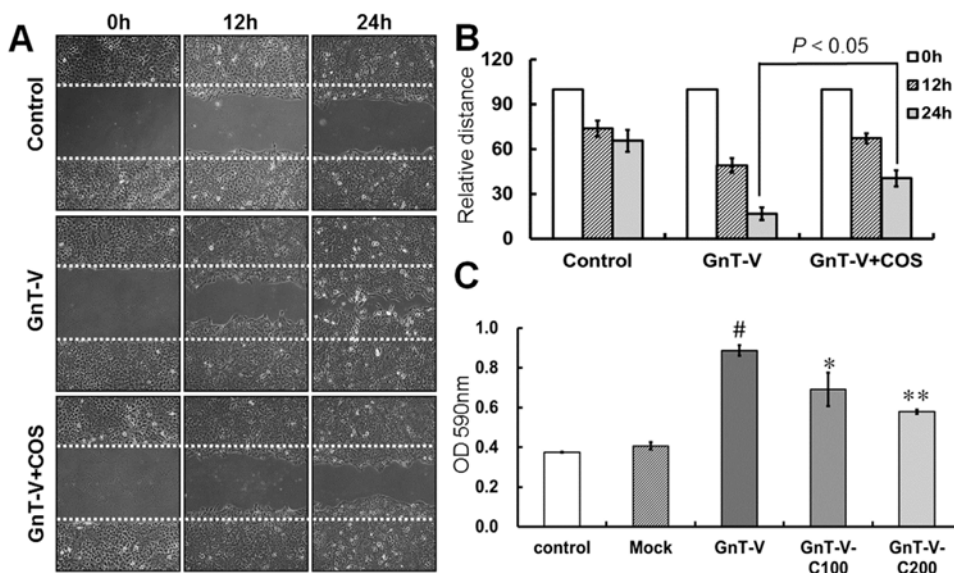


Fig. 2. Effects of COS on cell migration and cell adhesion induced by GnT-V. (A) The scraped gap was detected using a microscope, and the distances between the two sides were recorded at the indicated times. (B) Quantitative data of the cell migration distance were obtained from three independent experiments. The distance between the two sides immediately after scraping (0h) was set as 100. The relative migratory distance was defined as the width of the wound relative to the distance at 0h. (C) Different cells were spread on FN-coating plates in the presence or absence of COS for 30 min. The attached cells were detected as described in "Materials and methods". # $P < 0.05$ compared to the mock control group, * $P < 0.05$, ** $P < 0.01$ compared to the GnT-V transfectant group without COS treatment.

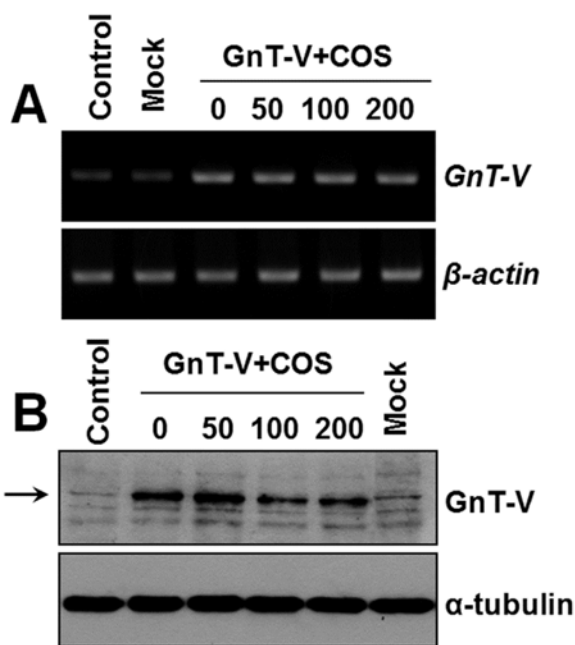


Fig. 3. Effects of COS on GnT-V expression. (A) The gene expression of GnT-V was analyzed by RT-PCR, and β -actin was used as a loading control. (B) The protein expression of GnT-V was analyzed by Western blot, and α -tubulin was used as a loading control. The arrow indicated the protein expression of GnT-V.

gest COS may be related with protein translation, post-translational processing and stability of GnT-V.

3.4. COS suppressed branched GlcNAc structures

The branched *N*-glycans modified by GnT-V were evaluated by lectin blot analysis. As shown in Fig. 1, the reactivities with DSA or L4-PHA lectin, which specifically recognizes branched *N*-glycans were clearly increased in the GnT-V transfectants compared to the control cells. Interestingly, these enhancements were suppressed

by COS in a dose dependent manner (Fig. 4A/B). It is well known that branched GlcNAc *N*-glycans, which enhance the formation of complexes on the cell surface such as integrins, galectins and growth factor receptors, lead to an increase in cell motility and cellular signaling (Dennis, Lau, Demetriou, & Nabi, 2009; Kariya & Gu, 2011). The flow cytometry analysis indicated that branched GlcNAc *N*-glycans expressed on the cell surface were also significantly suppressed by COS in GnT-V transfectant cells (Fig. 4C/D).

4. Discussion

More and more attentions have been given to the development of chitosan or its derivatives as antitumor agents in the past decades (Mattaveewong et al., 2016). Although the antitumor activity of COS has been studied *in vivo* and *in vitro* (Park, Chung, Choi, & Park, 2011), the molecular mechanisms of the antitumor activity are still obscure. Our previous studies indicated that COS could induce hepatoma cell apoptosis (Xu et al., 2008) and inhibit tumor angiogenesis (Wu et al., 2010). In this study, we focused on the antimetastatic potency of COS and the underlying mechanism. In a GnT-V stable expression cell line, COS successfully inhibited GnT-V induced cell migration and FN-mediated cell adhesion. In line with these results, Shen et al. found COS administered significantly inhibited lung metastasis in Lewis lung carcinoma (LLC) bearing mice. A roughly 80% reduction in metastatic lung tumors was observed in LLC-bearing mice treated with 500 mg/kg of COS (Shen, Chen, Chan, Jeng, & Wang, 2009). Nam et al. investigated the antimetastatic property of COS by evaluating motility and invasion in MDA-MB-231 human breast carcinoma cells. COS led to a concentration-dependent decrease in cell migration and inhibited the invasion of MDA-MB-231 cells through a matrigel-coated membrane (Nam & Shon, 2009). Meanwhile, our new study demonstrated that COS (200 μ g/ml) could significantly suppressed the EGF-induced mouse epithelial GE11 cells motility (Xu, Wang, Yang, Du, & Song, 2017). In this study, our results indicated that antimetastatic potency of COS was involved in alterations of GnT-V expression and branched GlcNAc *N*-glycans.

GnT-V is one of the important glycosyltransferases involved in tumor metastasis and carcinogenesis. Three different pathways

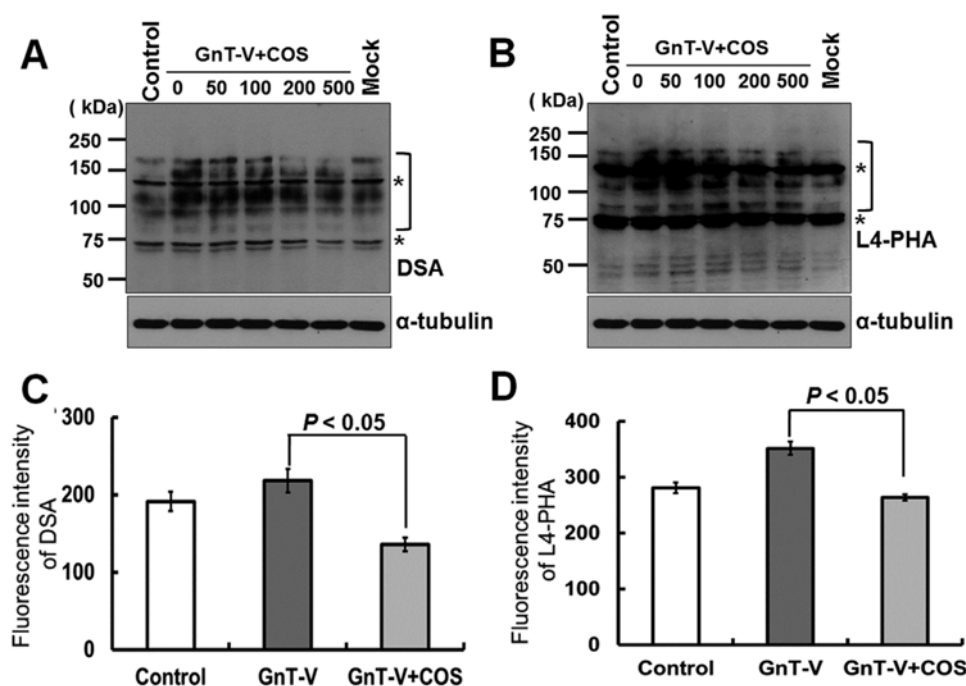


Fig. 4. Effects of COS on the expression levels of branched GlcNAc *N*-glycans. Equal amounts of protein (20 μ g) were used for lectin blot analysis. After separation on 7.5% SDS-PAGE and the proteins were probed with DSA lectin (A) and L4-PHA lectin (B), α -tubulin was used as a loading control. Square brackets indicated the DSA and L4-PHA specific reactive bands, and asterisks indicated nonspecific staining of DSA and L4-PHA, since those bands did not disappear after treatment with 100 mM acetic acid. Expression levels of branched GlcNAc *N*-glycans on the cell surface were detected by FACS analysis. Prior to detection, cells were incubated with biotinylated DSA lectin (C) and L4-PHA lectin (D), followed by treatment with streptavidin Alexa Fluor 488 conjugate.

were identified to be related to the facilitation of cancer metastasis by GnT-V. The first pathway was the promotion of epidermal growth factor receptor signaling by lattice formation between polylactosamine on β 1,6 GlcNAc branches and galectin-3, resulting in the blockage of receptor endocytosis (Partridge et al., 2004). The second pathway involved in the up-regulation metastasis by repressing protease degradation through the addition of β 1,6 GlcNAc branches (Ihara et al., 2002). In the third pathway, GnT-V inhibited E-cadherin/ β -catenin complex function, which led to the release of cancer cells from the original tissue (Pinho et al., 2013). Therefore, suppression of GnT-V could be a promising anti-cancer way. In this study, we clearly showed COS inhibited GnT-V expression and its products to block cell migration. Similar to our findings, Sato et al. demonstrated staurosporine could suppress the expression of GnT-V by 30–40% and alter the *N*-glycosylation of cell surface proteins to affect the metastasis of colorectal adenocarcinoma cells (Sato, Takahashi, Kawado, Takayama, & Furukawa, 2005). GnT-V is present in the Golgi apparatus in a membrane-bound form and is released from cells after cleavage by certain proteases. Secretase is an important protease for GnT-V secretion processing, which can increase the secretion rate of endogenous GnT-V (Nakahara et al., 2006). There have been some studies on secretase inhibition activities of COS and its derivatives. An investigation of β -secretase inhibitory activity of COS was performed by Byun et al. They demonstrated that the inhibition pattern of COS was a noncompetitive by Dixon plot, and the inhibition constant (K_i) of COS was 3.87–6.47 μ M (Byun, Kim, Park, Lin, & Kim, 2005). Phenolic acid conjugated COS also exhibited significant β -secretase inhibitory activity (Eom et al., 2013). Thus, we proposed that the effects of COS on GnT-V expression might be related with secretase activity.

Furthermore, Ko's group reported that tissue inhibitor of metalloproteinase-1 (MMP-1) was aberrantly glycosylated by GnT-V showing a weaker inhibition with respect to both MMP-2 and MMP-9, and this aberrancy was closely associated with cancer cell

invasion and metastasis *in vivo* as well as *in vitro* (Kim et al., 2008). Furthermore, GnT-V modulated the transcriptional activation of membrane-type matrix metalloproteinase-1 (MT1-MMP) in cancer cells. It not only promoted proteolytic activity for cancer cells, but also led to the activation of MMP-2. Consequently, the activation of the two MMPs triggered by GnT-V intensified the cancer invasive potential (Lee et al., 2013). On the other hand, Kim et al. reported that COS suppressed activation and expression of MMP-2 in human dermal fibroblasts (Kim & Kim, 2006). Nam et al. proved that COS inhibited the metastasis of MDA-MB-231 human breast carcinoma cells by blockage of MMP-9 (Nam & Shon, 2009). Based on those observations, we speculated that COS regulate GnT-V expression to influence metalloproteinase activities, and finally affect cell migration.

5. Conclusions

In summary, this study demonstrated that COS could be a potential therapeutic candidate for the metastatic breast cancer. The antimetastatic potency of COS involves in the suppression of GnT-V expression and branched *N*-glycans. Further research and development of COS might provide an effective, inexpensive and safe antitumor agent.

Conflict of interest

The authors declared that they have no conflict of interest.

Acknowledgement

This work was supported by grants from the National Natural Science Foundation of China (31372347), and National Natural Science Foundation of China (31670807).

References

- Byun, H. G., Kim, Y. T., Park, P. J., Lin, X., & Kim, S. K. (2005). Chitoooligosaccharides as a novel β -secretase inhibitor. *Carbohydrate Polymers*, 61(2), 198–202.
- Chae, S. Y., Jang, M. K., & Nah, J. W. (2005). Influence of molecular weight on oral absorption of water soluble chitosans. *Journal of Controlled Release*, 102(2), 383–394.
- Dennis, J. W., Lau, K. S., Demetriou, M., & Nabi, I. R. (2009). Adaptive regulation at the cell surface by N-glycosylation. *Traffic*, 10(11), 1569–1578.
- Eom, T. K., Ryu, B., Lee, J. K., Byun, H. G., Park, S. J., & Kim, S. K. (2013). Beta-secretase inhibitory activity of phenolic acid conjugated chitoooligosaccharides. *Journal of Enzyme Inhibition and Medicinal Chemistry*, 28(1), 214–217.
- Granovsky, M., Fata, J., Pawling, J., Muller, W. J., Khokha, R., & Dennis, J. W. (2000). Suppression of tumor growth and metastasis in Mgat5-deficient mice. *Nature Medicine*, 6(3), 306–312.
- Gu, J., & Taniguchi, N. (2008). Potential of N-glycan in cell adhesion and migration as either a positive or negative regulator. *Cell Adhesion & Migration*, 2(4), 243–245.
- Ihara, S., Miyoshi, E., Ko, J. H., Murata, K., Nakahara, S., Honke, K., et al. (2002). Prometastatic effect of N-acetylglucosaminyltransferase V is due to modification and stabilization of active matriptase by adding beta 1–6 GlcNAc branching. *Journal of Biological Chemistry*, 277(19), 16960–16967.
- Kariya, Y., & Gu, J. G. (2011). N-Glycosylation of beta 4 integrin controls the adhesion and motility of keratinocytes. *PLoS One*, 6(11), e27084.
- Kim, M. M., & Kim, S. K. (2006). Chitoooligosaccharides inhibit activation and expression of matrix metalloproteinase-2 in human dermal fibroblasts. *FEBS Letters*, 580(11), 2661–2666.
- Kim, Y. S., Hwang, S. Y., Kang, H. Y., Sohn, H., Oh, S., Kim, J. Y., et al. (2008). Functional proteomics study reveals that N-acetylglucosaminyltransferase V reinforces the invasive/metastatic potential of colon cancer through aberrant glycosylation on tissue inhibitor of metalloproteinase-1. *Molecular & Cellular Proteomics*, 7(1), 1–14.
- Langley, R. R., & Fidler, I. J. (2007). Tumor cell-organ microenvironment interactions in the pathogenesis of cancer metastasis. *Endocrine Reviews*, 28(3), 297–321.
- Lee, J. H., Kang, J. G., Song, K. J., Jeon, S. K., Oh, S., Kim, Y. S., et al. (2013). N-Acetylglucosaminyltransferase V triggers overexpression of MT1-MMP and reinforces the invasive/metastatic potential of cancer cells. *Biochemical and Biophysical Research Communications*, 431(4), 658–663.
- Li, Y., Liu, H., Xu, Q. S., Du, Y. G., & Xu, J. (2014). Chitosan oligosaccharides block LPS-induced O-GlcNAcylation of NF-kappaB and endothelial inflammatory response. *Carbohydrate Polymers*, 99, 568–578.
- Liu, J., Liu, H., Zhang, W. J., Wu, Q., Liu, W. S., Liu, Y. D., et al. (2013). N-acetylglucosaminyltransferase V confers hepatoma cells with resistance to anoikis through EGFR/PAK1 activation. *Glycobiology*, 23(9), 1097–1109.
- Mattaveewong, T., Wongkrasant, P., Chanchai, S., Pichyangkura, R., Chatsudthipong, V., & Muanprasat, C. (2016). Chitosan oligosaccharide suppresses tumor progression in a mouse model of colitis-associated colorectal cancer through AMPK activation and suppression of NF-kappaB and mTOR signaling. *Carbohydrate Polymers*, 145, 30–36.
- Miyoshi, E., Terao, M., & Kamada, Y. (2012). Physiological roles of N-acetylglucosaminyltransferase V (GnT-V) in mice. *BMB Reports*, 45(10), 554–559.
- Nakahara, S., Saito, T., Kondo, N., Moriwaki, K., Noda, K., Ihara, S., et al. (2006). A secreted type of beta1,6 N-acetylglucosaminyltransferase V (GnT-V), a novel angiogenesis inducer, is regulated by gamma-secretase. *FASEB Journal*, 20(14), 2451–2459.
- Nam, K. S., & Shon, Y. H. (2009). Suppression of metastasis of human breast cancer cells by chitosan oligosaccharides. *Journal of Microbiology and Biotechnology*, 19(6), 629–633.
- Park, J. K., Chung, M. J., Choi, H. N., & Park, Y. I. (2011). Effects of the molecular weight and the degree of deacetylation of chitosan oligosaccharides on antitumor activity. *International Journal of Molecular Sciences*, 12(1), 266–277.
- Partridge, E. A., Le Roy, C., Di Guglielmo, G. M., Pawling, J., Cheung, P., Granovsky, M., et al. (2004). Regulation of cytokine receptors by Golgi N-glycan processing and endocytosis. *Science*, 306(5693), 120–124.
- Pinho, S. S., Figueiredo, J., Cabral, J., Carvalho, S., Dourado, J., Magalhaes, A., et al. (2013). E-cadherin and adherens-junctions stability in gastric carcinoma: Functional implications of glycosyltransferases involving N-glycan branching biosynthesis, N-acetylglucosaminyltransferases III and V. *Biochimica Et Biophysica Acta*, 1830(3), 2690–2700.
- Pochee, E., Janik, M., Hoja-Lukowicz, D., Link-Lenczowski, P., Przybylo, M., & Litynska, A. (2013). Expression of integrins alpha3beta1 and alpha5beta1 and GlcNAc beta1,6 glycan branching influences metastatic melanoma cell migration on fibronectin. *European Journal of Cell Biology*, 92(12), 355–362.
- Sarrio, D., Rodriguez-Pinilla, S. M., Hardisson, D., Cano, A., Moreno-Bueno, G., & Palacios, J. (2008). Epithelial-mesenchymal transition in breast cancer relates to the basal-like phenotype. *Cancer Research*, 68(4), 989–997.
- Sato, T., Takahashi, M., Kawado, T., Takayama, E., & Furukawa, K. (2005). Effect of staurosporine on N-glycosylation and cell adhesion to fibronectin of SW480 human colorectal adenocarcinoma cells. *European Journal of Pharmaceutical Sciences*, 25(2–3), 221.
- Sayari, N., Sila, A., Abdelmalek, B. E., Abdallah, R. B., Ellouz-Chaabouni, S., Bougatef, A., et al. (2016). Chitin and chitosan from the Norway lobster by-products: Antimicrobial and anti-proliferative activities. *International Journal of Biological Macromolecules*, 87, 163–171.
- Shen, K. T., Chen, M. H., Chan, H. Y., Jeng, J. H., & Wang, Y. J. (2009). Inhibitory effects of chitoooligosaccharides on tumor growth and metastasis. *Food and Chemical Toxicology*, 47(8), 1864–1871.
- Suzuki, K., Mikami, T., Okawa, Y., Tokoro, A., Suzuki, S., & Suzuki, M. (1986). Antitumor effect of hexa-N-acetylchitohexaose and chitohexaose. *Carbohydrate Research*, 151, 403–408.
- Taniguchi, N., & Korekane, H. (2011). Branched N-glycans and their implications for cell adhesion, signaling and clinical applications for cancer biomarkers and in therapeutics. *BMB Reports*, 44(12), 772–781.
- Wu, H. G., Yao, Z. A., Bai, X. F., Du, Y. G., & Ma, X. J. (2010). Chitoooligosaccharides inhibit nitric oxide mediated migration of endothelial cells in vitro and tumor angiogenesis in vivo. *Carbohydrate Polymers*, 82, 927–932.
- Xu, Q. S., Dou, J. L., Wei, P., Tan, C. Y., Yun, X. J., Wu, Y. H., et al. (2008). Chitoooligosaccharides induce apoptosis of human hepatocellular carcinoma cells via up-regulation of Bax. *Carbohydrate Polymers*, 71, 509–514.
- Xu, Q., Akama, R., Isaji, T., Lu, Y., Hashimoto, H., Kariya, Y., et al. (2011). Wnt/beta-catenin signaling down-regulates N-acetylglucosaminyltransferase III expression: The implications of two mutually exclusive pathways for regulation. *Journal of Biological Chemistry*, 286(6), 4310–4318.
- Xu, Q., Wang, W., Yang, W., Du, Y., & Song, L. (2017). Chitosan oligosaccharide inhibits EGF-induced cell growth possibly through blockade of epidermal growth factor receptor/mitogen-activated protein kinase pathway. *International Journal of Biological Macromolecules*, 98, 502–505.
- Zhao, Y. Y., Takahashi, M., Gu, J. G., Miyoshi, E., Matsumoto, A., Kitazume, S., et al. (2008). Functional roles of N-glycans in cell signaling and cell adhesion in cancer. *Cancer Science*, 99(7), 1304–1310.
- Zou, P., Yang, X., Zhang, Y., Du, P., Yuan, S., Yang, D., et al. (2016). Antitumor effects of orally and intraperitoneally administered chitosan oligosaccharides (COSs) on S180-bearing/residual mouse. *Journal of Food Science*, 81(12), H3035–H3042.



Contents lists available at ScienceDirect

Biochemical and Biophysical Research Communications

journal homepage: www.elsevier.com/locate/ybbrc



Differential expression of ST6GAL1 in the tumor progression of colorectal cancer



Sen Zhang^{a,1}, Jishun Lu^{b,c,1}, Zhijue Xu^b, Xia Zou^{a,b}, Xue Sun^d, Yingjiao Xu^b, Aidong Shan^b, Jiaoyang Lu^a, Xialin Yan^a, Yalu Cui^b, Wei Yan^b, Yuguo Du^d, Jianguo Gu^{c,e}, Minhua Zheng^a, Bo Feng^{a,**}, Yan Zhang^{b,*}

^a Department of General Surgery, Shanghai Minimally Invasive Surgery Center, Ruijin Hospital, Shanghai Jiao Tong University School of Medicine, 197, Ruijin Er Road, Shanghai 200025, China

^b Key Laboratory of Systems Biomedicine (Ministry of Education), and Collaborative Innovation Center of Systems Biomedicine, Shanghai Center for Systems Biomedicine (SCSB), Shanghai Jiao Tong University, 800 Dongchuan Road, Shanghai 200240, China

^c Division of Regulatory Glycobiology, Institute of Molecular Biomembrane and Glycobiology, Tohoku Medical and Pharmaceutical University, 4-4-1 Komatsushima, Aobaku, Sendai 981-8558, Miyagi, Japan

^d State Key Lab of Environmental Chemistry and Ecotoxicology, Research Center for Eco-Environmental Sciences, Chinese Academy of Sciences, Beijing 100085, China

^e Department of Pharmacology, Pharmacy College, Nantong University, Nantong 226001, Jiangsu, China

ARTICLE INFO

Article history:

Received 16 March 2017

Accepted 31 March 2017

Available online 1 April 2017

Keywords:

Metabolic labeling

Sialylation

ST6GAL1

Colorectal cancer

ABSTRACT

Elevated expression of β -galactoside α 2,6-sialyltransferase 1 (ST6GAL1) has been observed in colorectal cancer (CRC) and demonstrated to be important for its tumorigenesis. Here, we found that ST6GAL1 expression was significantly higher in non-metastatic tumors (stage I and II) than that in metastatic tumors (stage III and IV) using 62 pair-matched tumor/normal tissues. To elucidate the molecular mechanisms of how ST6GAL1 affected the CRC progression, we performed a global identification of the substrates of ST6GAL1 in the colon adenocarcinoma cell line SW480. A total of 318 membrane proteins were identified differentially affected by ST6GAL1 overexpression using metabolic labeling and proteomic analysis. Subsequent bioinformatic analysis revealed a list of potential substrates that might mediate the different functions of ST6GAL1 in CRC including cell movement, cell death and survival. Taken together, these results indicate a dynamic change in the expression of ST6GAL1 during the CRC progression and provide a list of sialylated proteins potentially relevant to the different functions of ST6GAL1 in CRC.

© 2017 Elsevier Inc. All rights reserved.

1. Introduction

Sialic acid is the most abundant terminal monosaccharide of glycoconjugates on the eukaryotic cell surface. It is known to be linked via an α 2,3 or α 2,6 bond to Gal/GalNAc, or α 2,8 bond to sialic acid in proteins. Given the relatively strong electronegative charge

of sialic acids and their location at the outmost reaches of the cell surface, sialic acids may regulate numerous cell-cell and cell-matrix interactions. Not surprisingly, altered sialylation has been long associated with tumorigenesis and tumor progression and it is usually driven by the dysregulated expression of certain sialyltransferases and sialidases responsible for the addition and removal of sugars [1–3].

Among these, β -galactoside α 2,6-sialyltransferase 1 (ST6GAL1), which primarily produces α 2,6 linked sialic acids on N-glycans, has received much attention in recent years as elevated expression of this sialyltransferase was observed in multiple types of carcinomas including colorectal, ovarian, breast, prostate, ovarian, and pancreatic carcinomas [4]. The selective enrichment of ST6GAL1-mediated α 2,6 sialic acids on tumor cells is significant in that it may elicit various biologic outcomes. It has been also reportedly

Abbreviations: CRC, colorectal cancer; EGFR, EGF receptor; OE, overexpression; qPCR, quantitative RT-PCR; ST6GAL1, β -galactoside α 2,6-sialyltransferase 1; WT, wild-type.

* Corresponding author.

** Corresponding author.

E-mail addresses: yanzhang2006@sjtu.edu.cn (Y. Zhang), fengbo2022@163.com (B. Feng).

¹ Both authors contributed equally to this work.

<http://dx.doi.org/10.1016/j.bbrc.2017.03.167>

0006-291X/© 2017 Elsevier Inc. All rights reserved.

involved in tumorigenesis, epithelial mesenchymal transition, cell adhesion, migration and invasion, apoptosis, drug resistance, immune evasion and maintenance of cancer stem cell property [4–10]. In contrast to these important roles, there is limited information regarding the molecular details of how ST6GAL1-catalyzed α 2,6 sialylated proteins mediate these functions [11]. ST6GAL1 could regulate the cell migration and invasion partly by increasing the α 2,6 sialylation of β 1 integrin [12–14]. Sialylation of the Fas death receptor by ST6GAL1 provides protection against Fas-mediated apoptosis in colon carcinoma cells [15]. In addition, there are also several other reported proteins whose activities are regulated by sialylation which includes CD45, EGFR, and PECAM [12–19]. Clearly, these limited proteins could not provide the comprehensive explanation for its diverse roles in tumors. To obtain a better understanding of the mechanistic roles of this sialyltransferase, identification of its additional function-related sialylated proteins is of critical importance.

The up-regulated expression of ST6GAL1 was first described in colorectal cancer (CRC) [20]. Increasing evidence has indicated that ST6GAL1 may serve as a major inhibitor of several cell death pathways and contribute to the colorectal tumorigenesis [6,15,21]. However, the mechanistic roles of ST6GAL1 in the tumor progression are still obscure. In the current study, interestingly, we found that ST6GAL1 was significantly induced in tumors at stage I and II but not in those at stage III and IV when compared with their paired normal tissues. Subsequent metabolic labeling and proteomics analysis in the colon cancer cell line SW480 revealed a list of proteins that may mediate the effects of ST6GAL1 on tumor development and progression. These results indicate a dynamic change in ST6GAL1 expression in human CRC progression and suggest the distinct roles of ST6GAL1 at different stages.

2. Materials and methods

Tissue Specimens — From May 2009 to Jun 2012, a total of 62 CRC cases with pathological stage I (n = 19), II (n = 20), III (n = 17) and IV (n = 6) were recruited from Ruijin Hospital (Shanghai, China) in accordance with the guidelines set by the Ethical Committee of Ruijin Hospital. All participants gave the written, informed consent and no participants had received any medication prior to sample collection. Staging of CRC was performed according to the Union Internationale Contre Le Cancer (UICC). Tumor tissues and paired normal colonic tissues, located approximately 10 cm from the distal edge of the tumor were snap frozen in liquid nitrogen 30 min after vessel ligation and stored in the liquid nitrogen prior to analysis. The inclusion and exclusion criteria of patients, and protein extraction were performed as described in Ref. [22].

Cell Lines and Cell Culture — The HEK 293T and SW480 cell lines were purchased from ATCC (Manassas, VA, USA). The HEK 293T cells were cultured as described previously [10]. SW480 and ST6GAL1-overexpressing cells were maintained in Leibovitz's L15 Medium (HyClone, Logan, Utah, USA) with 10% FBS under a humidified atmosphere at 37 °C without CO₂ addition. The ST6GAL1-overexpressing cells were established by virus transfection and cell-sorting using FACS Aria II (BD Bioscience, Bedford, Massachusetts, USA).

Western Blot Analysis and Immunoprecipitation — Western blot analysis and immunoprecipitation were performed as described previously [10]. For details, please refer to our [supplementary materials](#).

Flow Cytometry Analysis of Cells — Cell cytometry was performed as reported in Ref. [23]. Cells were grown to about 90% confluency and detached using trypsin containing 1 mM EDTA at 37 °C, and washed three times with cold PBS. Then, cells were stained with 1 μ g/ml Alkyne 555 (Invitrogen, Eugene, Oregon, USA)

for 30 min at RT temperature or with 10 μ g/ml SNA-FITC (Vector, Burlingame, California, USA) or 10 μ g/ml MAA-FITC (EY Laboratories, San Mateo, California, USA) for 60 min on ice. Finally, cells were washed three times with PBS and analyzed by flow cytometry (BD Biosciences, San Jose, California, USA).

qPCR for mRNA Expression Analysis — The qPCR analysis was performed as described previously [24]. The sequences of primers used for quantitative RT-PCR (qPCR) analysis are as follows: *GAPDH* (5'-TTCAACAGCAACTCCACTCTT-3' and 5'-TGGTCCAGGGTTCT-TACTCC-3'), *EGFR* (5'-ACCTGCGTGAAGAAGTGTCC-3' and 5'-CGTCTTCTCCATCTCATAGC-3'), *ABCB1* (5'-GCCAAGCCAAAA-TATCAGC-3' and 5'-TTCCAATGTGTTCGGCAT-3').

Cell Migration Assay — Cell migratory ability was examined with Transwell (BD BioCoat™ control inserts, 8.0-mm inserts; BD Biosciences, Bedford, Massachusetts, USA) as described previously [23]. Transwells were coated only on the bottom side with 10 μ g/ml fibronectin or collagen I at 4 °C overnight.

Metabolite Labeling and Fluorescence Detection — cells (4.0×10^6) were cultured with 100 μ M of the Ac₄ManNAz or ManNAc for 60 h. After metabolic labeling, the cells were incubated with Alkyne 555, catalyst (CuSO₄, NaVc, TBTA) for click chemistry [25]. The obtained cells were then detected with a laser-scanning confocal microscope (Nikon, Tokyo, Japan) or flow cytometry (BD Biosciences, San Jose, California, USA) for the check of the labeling efficiency. For details, please refer to [26].

Protein Enrichment and Mass Spectrometry Analysis — After washing with PBS, 1×10^7 metabolic labeled cells were used to perform the subsequent click reaction with biotinylated alkyne and glycoprotein enrichment by streptavidin-agarose resin as described previously [25]. The beads were pelleted by centrifugation and washed, reduced and alkylated followed by on bead trypsin digestion as shown in Ref. [27]. The released peptides were analyzed on a Q Exactive Plus mass spectrometer equipped with an Easy-nLC 1000 (Thermo Fisher Scientific, Odense, Denmark). Spectra was searched against a human proteins database (Uniprot Complete Proteome – taxonomy Homo sapiens, release 2016.08) using the Andromeda module of MaxQuant software v. 1.5.5.1. For details, please refer to our [supplementary materials](#).

Bioinformatic Annotation and Analysis — N- and O-glycoprotein prediction analysis using the NetNGlyc 1.0 and the NetOGlyc 4.0 servers was performed. Gene ontology (GO) enrichment analysis was carried out using DAVID Bioinformatics Resources 6.8. Functional analysis was generated using the Ingenuity Pathways Analysis (IPA) software v7.1 (Ingenuity Systems).

3. Results

To explore the roles of ST6GAL1 in the CRC progression, we first evaluated its expression in the tissue specimens at different stages by western blot analysis (Fig. 1A and S1). 62 patients were randomly selected based only on the criteria of matched age and gender (Table 1). Interestingly, the expression of ST6GAL1 was significantly increased in tumors at the stage I and II as compared with their pair-matched normal tissues, while no statistical difference was observed when the tumors were developed to the stage III and IV (Fig. 1B). Furthermore, the expression of ST6GAL1 in tumors at stage I and II was significantly higher than that at stage III and IV (Fig. 1C). These results clearly indicate a dynamic change in ST6GAL1 expression in the colorectal tumors at different stages, suggesting important roles of ST6GAL1 in CRC progression.

Next, to explore molecular mechanisms of how ST6GAL1 affected the CRC progression, we first overexpressed this sialyltransferase in SW480, a human colon adenocarcinoma cell line with the low expression of ST6GAL1. Western blot, lectin blot, cell cytometry and qPCR results demonstrated the high expression of

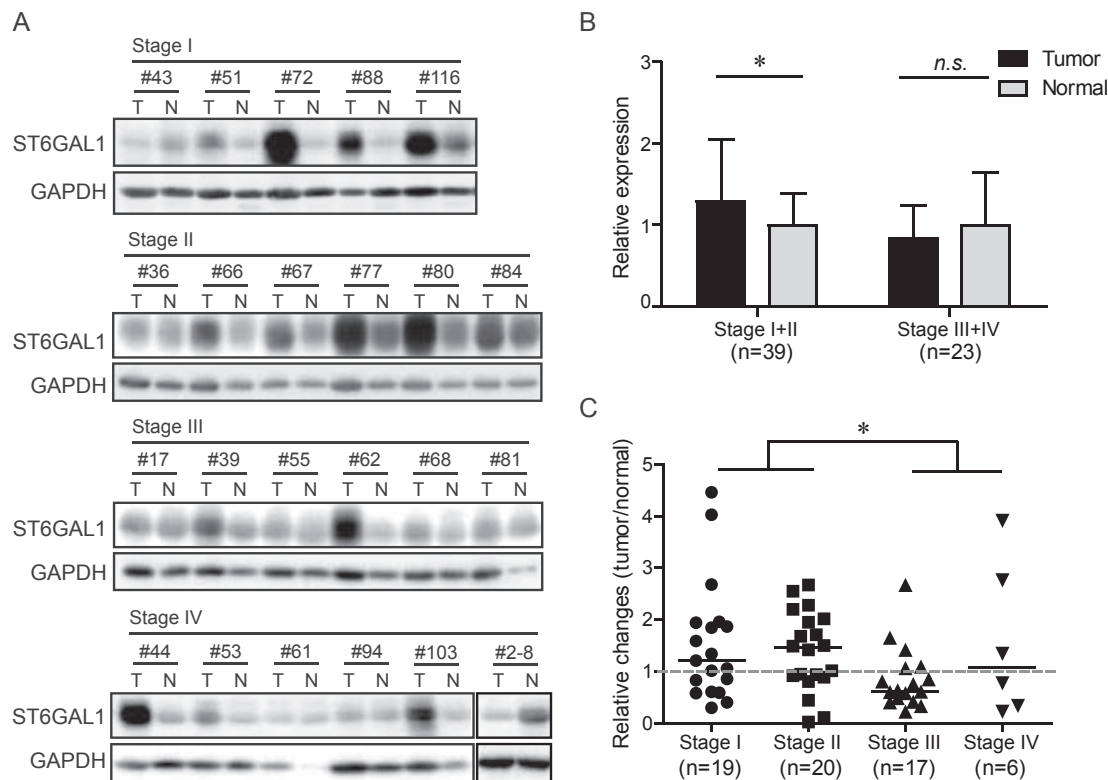


Fig. 1. ST6GAL1 was significantly higher in colorectal tumors at stage I and II but not in those at stage III and IV compared with their pair-matched normal tissues. A) Representative images of the immunoblot for ST6GAL1 in primary colorectal tumors at different stages. For the rest of our immunoblot images, please refer to our supplementary materials. B) ST6GAL1 bands detected from the immunoblot were quantified by densitometric scanning and protein intensity values were normalized by GAPDH. The normalized ST6GAL1 intensity in tumors was compared with that in its pair-matched normal tissues. Error bars indicate standard derivation. C) The ratio (tumor/normal) for each sample pair was calculated. Middle lines indicate Median values (n.s.: no significance; *, $p < 0.05$ by paired t -test or Mann-Whitney U test).

Table 1
Clinical features of samples used in this study.

UICC Stage	Stage I	Stage II	Stage III	Stage IV
Number	19	20	17	6
Age (year) median/range	59/47–76	60/50–78	59/40–77	61/35–74
Gender				
Male	11	13	10	3
Female	8	7	7	3
Location ^a				
AC	4	4	3	—
TC	1	—	—	—
DC	2	4	—	2
SC	4	2	1	1
RC	8	10	13	3
CEA (ng/ml) median/range	2.62/1.36–8.90	4.19/0.94–376.43	2.86/0.7–891.16	10.43/4.43–303.24
CA19-9 (ng/ml) median/range	6.53/2.00–42.70	11.42/0.80–91.70	18.9/2.00–1554.6	185.35/51.60–3770.46
CA125 (ng/ml) median/range	10.00/3.9–32.6	14.80/7.40–34.90	13.60/7.20–62.30	84.55/14.80–238.80
AFP (ng/ml) median/range	2.96/1.48–4.39	3.15/1.57–6.14	3.19/1.89–8.40	5.42/4.88–5.88

^a AC, ascending colon; TC, transverse colon; DC, descending colon; SC, sigmoid colon; RC, rectum.

ST6GAL1 in the ST6GAL1-overexpressing SW480 cells (Fig. 2A–D). Then, to identify the sialylated proteins differentially affected by ST6GAL1, SW480 and ST6GAL1-overexpressing cells were separately labeled with Ac₄ManNAz and ManNAc followed by the enrichment and identification of the sialylated membrane proteins. Fig. 3A showed the schematic representation of our strategy.

Ac₄ManNAz is intracellularly deacetylated and used to incorporate azidos to tag the sialic acid linked glycans and the sialylated proteins [26]. The azido-tagged proteins on the cell surface were then reacted with biotin-alkyne and enriched with streptavidin-beads. The sialylated proteins were efficiently and specifically labeled by azido sugars, as shown by the strong signals in the glycoproteins

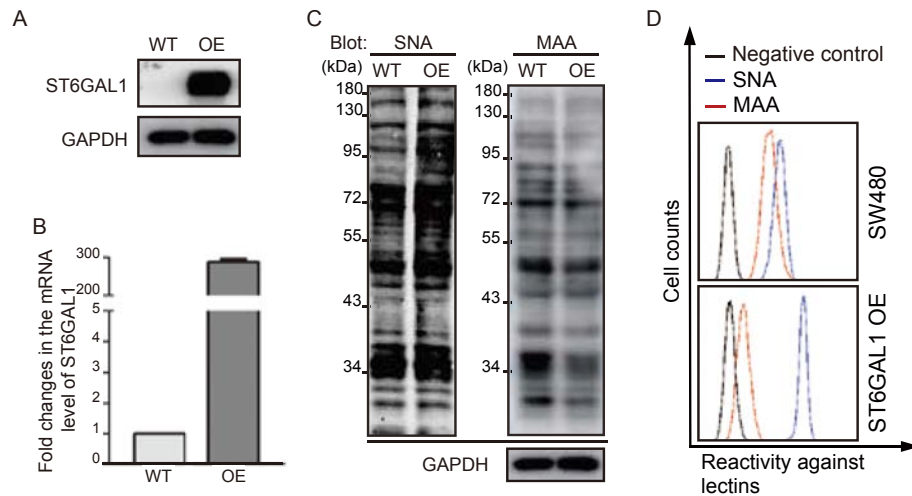


Fig. 2. ST6GAL1 were efficiently overexpressed in colon cancer cells SW480. A-D) The efficiency of the ST6GAL1 overexpression in SW480 was confirmed by the analyses of western blot, qPCR, lectin blot and cell cytometry. GAPDH was used as an internal control.

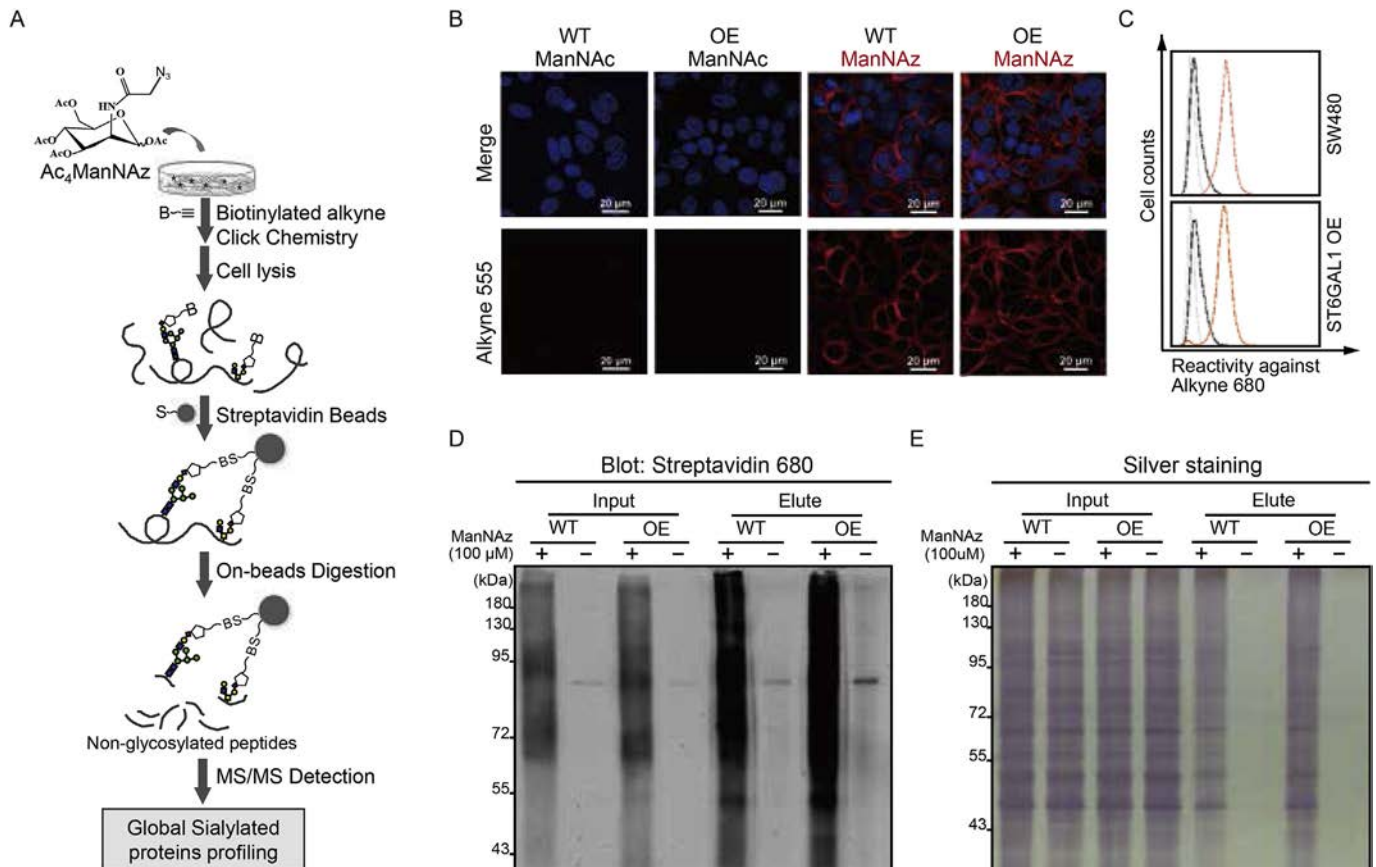


Fig. 3. Sialylated proteins in SW480 and ST6GAL1-overexpressing cells were efficiently labeled and enriched. A) Schematic representation of the cell surface sialylated protein labeling, enrichment and identification. B-C) The labeling efficiency of cell surface sialylated proteins with Ac₄ManNAz was checked by the analyses of immunostaining and cytometry. D-E) The selectivity and efficiency of the enrichment of these proteins were examined by the analyses of silver staining and western blot with streptavidin 680.

from the cells incubated with Ac₄ManNAz but not from those pretreated with ManNAc according to the fluorescence-staining and FACS analyses (Fig. 3B and C). We also checked the efficiency of sialylated protein enrichment by silver staining and western blot analyses. The amount of proteins as well as the signals against

streptavidin 680 in the elute fraction of Ac₄ManNAz treated cells were markedly higher as compared with those incubated with ManNAc (Fig. 3D and E), indicating the efficient and selective enrichment of the azido sugar modified proteins.

The MS analysis of the elute fractions collected from the cells

cultured with Ac₄ManNAz led to the identification of a total of 709 membrane proteins by searching the data against the Uniprot Complete Proteome Human Database and GO analysis (Cellular Component). Prediction analysis of these proteins indicated that 567 of them could be *N*-glycosylated and 625 of them could be *O*-glycosylated (Fig. 4A). Considering sialic acids mainly exist as the terminal sugars on the *N*-glycans, *O*-glycans and glycolipids, these results suggest that most of the labeled glycoproteins arising from the Ac₄ManNAz treatment might be sialylated.

Next, we examined the differential regulation of glycoproteins upon ST6GAL1 overexpression in SW480 cells based on our identified set of 709 membrane proteins. Proteins were considered as differentially expressed between the wild-type SW480 and ST6GAL1-overexpressing cells if their fold change in relative expression ≥ 2 (47–49). Based on these selection criteria, we found a total of 318 glycoproteins were differentially affected (up-regulated or down-regulated or specifically expressed in either cells) after

ST6GAL1 overexpression in SW480. Volcano plot-log₁₀ (intensity of the protein in ST6GAL1 overexpression) vs. log₂ (fold change of ST6GAL1 overexpression/wild-type) was constructed to graphically display the quantitative data using the overlapped proteins between control and ST6GAL1-overexpressing cells (Fig. 4B). To evaluate the potential roles of ST6GAL1 in CRC, these proteins were used for the functional analysis by the IPA software. Fig. 4C showed the top 15 most significantly perturbed functions upon the overexpression of ST6GAL1 in SW480. The first three were cell movement, cell death and survival, and cell growth and proliferation, which are in good agreement with numerous reports on the functions of ST6GAL1 under pathological conditions [4]. Table S1 listed the proteins that are related with these functions.

To experimentally confirm these changes, two proteins ABCB1 (~10 folds up) and EGFR (~2 folds up), which showed big difference in the extent of their changes, were selected to perform the qPCR, immunoprecipitation and western blot analyses (Fig. 4D–F). ABCB1

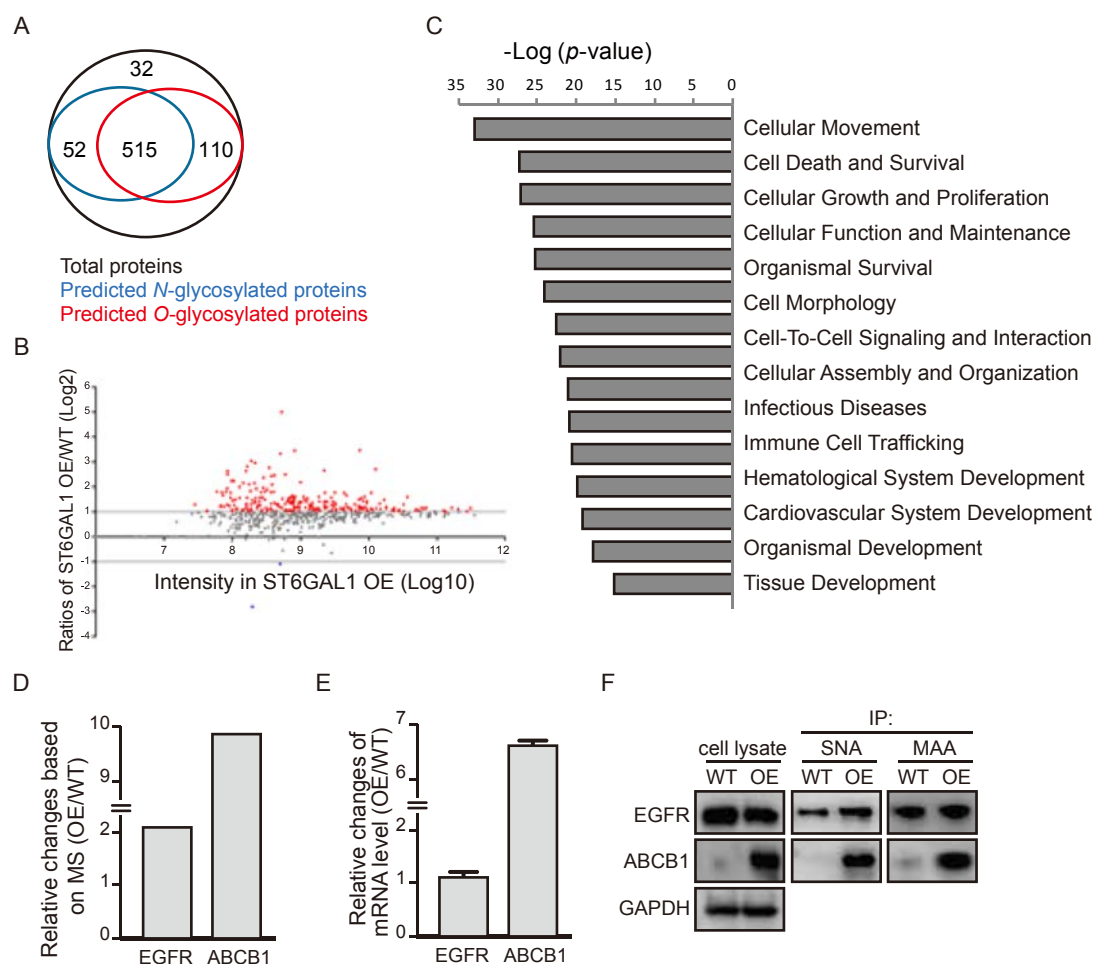


Fig. 4. Identification of the sialylated proteins and functional analysis by IPA. A) Comparative analysis of *N*-glycoprotein and *O*-glycoprotein predictions using the NetNGlyc 1.0 and NetOGlyc 4.0 servers. B) Volcano plot illustrates differentially regulated membrane proteins. The x-axis represented the log₁₀ (intensity in ST6GAL1-overexpressing cells). The y-axis represented the log₂ (ratio) where 'ratio' was the ratio of the averages of LFQ Intensities of ST6GAL1-overexpression over control. The non-axial horizontal lines denoted ± 2 -fold change. The colored dots showed proteins considered as up- (red) or down- (blue) regulated, while the non-regulated proteins were displayed as gray dots. C) ST6GAL1 overexpression significantly perturbed many functional pathways including cellular movement, cell death and survival. IPA analysis of the differentially regulated proteins on the plasma membrane (≥ 2 -fold) revealed the top 15 most significantly perturbed functions upon the overexpression of ST6GAL1 in SW480. The functional pathways included in this analysis were shown along the y-axis of the bar chart. The x-axis indicates the statistical significance on the left. Calculated using the right-tailed Fisher exact test, the p-value indicated which biological annotations were significantly associated with the input molecules relative to all functionally characterized mammalian molecules. D) The intensity ratio (ST6GAL1 overexpression/WT) of ABCB1 or EGFR was shown based on the MS analysis. E) The transcriptional levels of EGFR and ABCB1 in WT and ST6GAL1 overexpressing cells were checked by qPCR analysis. F) The sialylation pattern of EGFR and ABCB1 after ST6GAL1 overexpression was investigated by immunoprecipitation analysis with SNA and MAA beads and its protein level in whole cell lysate was analyzed by western blot. (For interpretation of the references to colour in this figure legend, the reader is referred to the web version of this article.)

were significantly upregulated at both mRNA and protein levels, indicating the different expression of this protein observed in our MS data is mainly due to its increased mRNA level. In contrast, there was little change in either mRNA or protein level of EGFR after ST6GAL1 overexpression. Since immunoprecipitation analysis showed a significant increase in the α 2,6 sialylation level, it is highly likely that ~2 folds upregulation of EGFR observed in our MS data is attributed to its enhanced sialylation.

4. Discussion

Elevated expression of ST6GAL1 has been observed in multiple types of carcinomas, among which colorectal cancer was the first reported [20]. Although it has been well documented that ST6GAL1 expression contributes to the colorectal tumorigenesis [6], the mechanistic roles of this protein in tumor progression are still obscure. Interestingly, we found that as compared with their pair-matched normal tissues, the expression of ST6GAL1 was significantly increased in tumors at stage I and II (non-metastatic), but not at stage III and IV (metastatic). Meanwhile, ST6GAL1 expression in the tumors at stage I and II was statistically higher than that at stage III and IV, suggesting a dynamic change of ST6GAL1 expression in CRC progression. Metabolic labeling revealed 318 sialylated membrane proteins differentially affected by ST6GAL1 overexpression. Considering the distinct roles of different linkages of sialylation in cell biology, these results suggest important roles of the dynamic change in ST6GAL1 expression during the CRC progression.

We showed that high expression of ST6GAL1 was decreased at the advanced stage of CRC. Consistent with our observation, there is evidence that the mRNA level of ST6GAL1 is significantly increased in colorectal carcinoma specimens, but not in highly invasive tumors and tumors exhibiting distant metastases when compared with their pair-matched normal tissues [28]. These results suggest that high expression of this enzyme may not benefit the CRC progression to the advanced/metastatic stage. Supporting this hypothesis, a very recent work showed that knockdown of ST6GAL1 dramatically enhances the migration and invasion of the colon cancer cell line SW620, and also promotes its liver metastasis *in vivo* [29]. Furthermore, our MS data showed that ST6GAL1 overexpression increased the expression of ICAM-1, a liver metastasis suppressor of colon cancer (data not shown). It is well-known that sialyl Lewis structure serves as a key mechanism for directing tumor cell adhesion to the endothelium and the α 2,3 linked sialic acid on sialyl Lewis structure is critical for this function. A previous report showed that α 2,3 sialylated type 2 chain structures is predominantly expressed in colorectal tissues associated with the malignant transformation, in particular, with the lymphatic spread of distal colorectal adenocarcinoma [30]. Therefore, it is possible that decreased expression of ST6GAL1 and α 2,6 sialylation may benefit the tumor metastasis by increasing the α 2,3 sialylated structures on cell surface because α 2,3 and α 2,6 sialyltransferases share the common glycan substrates.

Our IPA analysis revealed a list of novel glycoproteins that could mediate these functions above. Among the list, we found that overexpression of ST6GAL1 resulted in an increased transcription of ABCB1 by more than ~6 folds. Consistent with this, it has been previously reported that ST6GAL1 expression could induce the expression of ABCB1 in human leukemia cells [31]. In addition, a recent study showed that KAI1 is significantly decreased after ST6GAL1 knockdown in SW620 cells. This protein could also be found in our list, which was increased by ~2-fold after ST6GAL1 overexpression. These results partially suggest the reliability of the list we obtained, which may contribute to the identification of additional molecules linking the functions of ST6GAL1 in tumor.

5. Declaration

We declare that this manuscript is original, has not been published before and is not currently being considered for publication elsewhere. There is no conflict of interest concerning this manuscript.

Acknowledgement

This work was supported by The National Natural Science Foundation of China (31370806, 31170771, 31600643, 31670807), The National Basic Research Program of China (2012CB822103, 2011CB910603), Shanghai Municipal Commission of Health and Family Planning Program (201640030), Shanghai Jiao Tong University Interdiscipline with Medicine Program (YG2013MS26), China Postdoctoral Science Foundation (2016M600310).

Appendix A. Supplementary data

Supplementary data related to this article can be found at <http://dx.doi.org/10.1016/j.bbrc.2017.03.167>.

References

- [1] A. Harduin-Lepers, M.-A. Krzewinski-Recchi, F. Colomb, F. Foulquier, S. Groux-Degroote, P. Delannoy, Sialyltransferases functions in cancers (Elite edition), *Front. Biosci.* 4 (2011) 499–515.
- [2] F. Dall'Olio, N. Malagolini, M. Trinchera, M. Chiricolo, Sialosignaling: sialyltransferases as engines of self-fueling loops in cancer progression, *Biochimica Biophysica Acta (BBA) - General Subj.* 1840 (2014) 2752–2764.
- [3] S.S. Pinho, C.A. Reis, Glycosylation in cancer: mechanisms and clinical implications, *Nat. Rev. Cancer* 15 (2015) 540–555.
- [4] J. Lu, J. Gu, Significance of beta-galactoside α 2,6 sialyltransferase 1 in cancers, *Molecules* 20 (2015) 7509–7527.
- [5] X. Chen, L. Wang, Y. Zhao, S. Yuan, Q. Wu, X. Zhu, B. Niang, S. Wang, J. Zhang, ST6Gal-I modulates docetaxel sensitivity in human hepatocarcinoma cells via the p38 MAPK/caspase pathway, *Oncotarget* 7 (2016) 51955–51964.
- [6] M.J. Schultz, A.T. Holdbrooks, A. Chakraborty, W.E. Grizzle, C.N. Landen, D.J. Buchsbaum, M.G. Conner, R.C. Arend, K.J. Yoon, C.A. Klug, D.C. Bullard, R.A. Kesterson, P.G. Oliver, A.K. O'Connor, B.K. Yoder, S.L. Bellis, The tumor-associated glycosyltransferase ST6Gal-I regulates stem cell transcription factors and confers a cancer stem cell phenotype, *Cancer Res.* 76 (2016) 3978–3988.
- [7] Z. Liu, A.F. Swindall, R.A. Kesterson, T.R. Schoeb, D.C. Bullard, S.L. Bellis, ST6Gal-I regulates macrophage apoptosis via α 2-6 sialylation of the TNFR1 death receptor, *J. Biol. Chem.* 286 (2011) 39654–39662.
- [8] M. Perdicchio, J.M. Ilarregui, M.I. Verstege, L.A. Cornelissen, S.T. Schetters, S. Engels, M. Ambrosini, H. Kalay, H. Veninga, J.M. den Haan, L.A. van Berkel, J.N. Samsom, P.R. Crocker, T. Sparwasser, L. Berod, J.J. Garcia-Vallejo, Y. van Kooyk, W.W. Unger, Sialic acid-modified antigens impose tolerance via inhibition of T-cell proliferation and de novo induction of regulatory T cells, *Proc. Natl. Acad. Sci. U. S. A.* 113 (2016) 3329–3334.
- [9] C.M. Brittain, K.A. Dorsett, S.L. Bellis, The glycosyltransferase ST6Gal-I protects tumor cells against serum growth factor withdrawal by enhancing survival signaling and proliferative potential, *J. Biol. Chem.* 292 (2017) 4663–4673.
- [10] J. Lu, T. Isaji, S. Im, T. Fukuda, N. Hashii, D. Takakura, N. Kawasaki, J. Gu, beta-Galactoside α 2,6-sialyltransferase 1 promotes transforming growth factor-beta-mediated epithelial-mesenchymal transition, *J. Biol. Chem.* 289 (2014) 34627–34641.
- [11] M.J. Schultz, A.F. Swindall, S.L. Bellis, Regulation of the metastatic cell phenotype by sialylated glycans, *Cancer Metastasis Rev.* 31 (2012) 501–518.
- [12] E.C. Seales, G.A. Jurado, B.A. Brunson, J.K. Wakefield, A.R. Frost, S.L. Bellis, Hypersialylation of beta1 integrins, observed in colon adenocarcinoma, may contribute to cancer progression by up-regulating cell motility, *Cancer Res.* 65 (2005) 4645–4652.
- [13] F.M. Shaikh, E.C. Seales, W.C. Clem, K.M. Hennessy, Y. Zhuo, S.L. Bellis, Tumor cell migration and invasion are regulated by expression of variant integrin glycoforms, *Exp. Cell Res.* 314 (2008) 2941–2950.
- [14] D.R. Christie, F.M. Shaikh, J.A.T. Lucas, J.A. Lucas 3rd, S.L. Bellis, ST6Gal-I expression in ovarian cancer cells promotes an invasive phenotype by altering integrin glycosylation and function, *J. Ovarian Res.* 1 (2008) 3.
- [15] A.F. Swindall, S.L. Bellis, Sialylation of the Fas death receptor by ST6Gal-I provides protection against Fas-mediated apoptosis in colon carcinoma cells, *J. Biol. Chem.* 286 (2011) 22982–22990.
- [16] M. Amano, M. Galvan, J. He, L.G. Baum, The ST6Gal I sialyltransferase selectively modifies N-glycans on CD45 to negatively regulate galectin-1-induced CD45 clustering, phosphatase modulation, and T cell death, *J. Biol. Chem.*

- 278 (2003) 7469–7475.
- [17] H.Y. Yen, Y.C. Liu, N.Y. Chen, C.F. Tsai, Y.T. Wang, Y.J. Chen, T.L. Hsu, P.C. Yang, C.H. Wong, Effect of sialylation on EGFR phosphorylation and resistance to tyrosine kinase inhibition, *Proc. Natl. Acad. Sci. U. S. A.* 112 (2015) 6955–6960.
- [18] J.J. Park, J.Y. Yi, Y.B. Jin, Y.J. Lee, J.S. Lee, Y.S. Lee, Y.G. Ko, M. Lee, Sialylation of epidermal growth factor receptor regulates receptor activity and chemosensitivity to gefitinib in colon cancer cells, *Biochem. Pharmacol.* 83 (2012) 849–857.
- [19] S. Kitazume, R. Imamaki, K. Ogawa, Y. Komi, S. Futakawa, S. Kojima, Y. Hashimoto, J.D. Marth, J.C. Paulson, N. Taniguchi, Alpha2,6-sialic acid on platelet endothelial cell adhesion molecule (PECAM) regulates its homophilic interactions and downstream antiapoptotic signaling, *J. Biol. Chem.* 285 (2010) 6515–6521.
- [20] F. Dall'Olio, N. Malagolini, G. di Stefano, F. Minni, D. Marrano, F. Serafini-Cessi, Increased CMP-NeuAc:Gal beta 1,4GlcNAc-R alpha 2,6 sialyltransferase activity in human colorectal cancer tissues, *Int. J. Cancer* 44 (1989) 434–439.
- [21] Y. Zhuo, S.L. Bellis, Emerging role of α 2,6-sialic acid as a negative regulator of galectin binding and function, *J. Biol. Chem.* 286 (2011) 5935–5941.
- [22] X. Zou, B. Feng, T. Dong, G. Yan, B. Tan, H. Shen, A. Huang, X. Zhang, M. Zhang, P. Yang, M. Zheng, Y. Zhang, Up-regulation of type I collagen during tumorigenesis of colorectal cancer revealed by quantitative proteomic analysis, *J. Proteomics* 94 (2013) 473–485.
- [23] J. Lu, T. Isaji, S. Im, T. Fukuda, A. Kameyama, J. Gu, Expression of N-Acetylglucosaminyltransferase III suppresses alpha2,3-sialylation, and its distinctive functions in cell migration are attributed to alpha2,6-sialylation levels, *J. Biol. Chem.* 291 (2016) 5708–5720.
- [24] Y. Xu, W. Pang, J. Lu, A. Shan, Y. Zhang, Polypeptide N-Acetylgalactosaminyltransferase 13 contributes to neurogenesis via stabilizing the mucin-type O-Glycoprotein podoplanin, *J. Biol. Chem.* 291 (2016) 23477–23488.
- [25] S. Wang, W. Xie, X. Zhang, X. Zou, Y. Zhang, Disulfide- and terminal alkyne-functionalized magnetic silica particles for enrichment of azido glycopeptides, *Chem. Commun. (Camb)* 48 (2012) 5907–5909.
- [26] J. Du, S. Hong, L. Dong, B. Cheng, L. Lin, B. Zhao, Y.G. Chen, X. Chen, Dynamic sialylation in transforming growth factor-beta (TGF-beta)-induced epithelial to mesenchymal transition, *J. Biol. Chem.* 290 (2015) 12000–12013.
- [27] R. Sheta, F. Roux-Dalvai, C.M. Woo, F. Fournier, S. Bourassa, C.R. Bertozzi, A. Droit, D. Bachvarov, Proteomic dataset for altered glycoprotein expression upon GALNT3 knockdown in ovarian cancer cells, *Data Brief.* 8 (2016) 342–349.
- [28] T. Petretti, W. Kemmner, B. Schulze, P.M. Schlag, Altered mRNA expression of glycosyltransferases in human colorectal carcinomas and liver metastases, *Gut* 46 (2000) 359–366.
- [29] Y.R. Jung, J.J. Park, Y.B. Jin, Y.J. Cao, M.J. Park, E.J. Kim, M. Lee, Silencing of ST6Gal I enhances colorectal cancer metastasis by down-regulating KAI1 via exosome-mediated exportation and thereby rescues integrin signaling, *Carcinogenesis* 37 (2016) 1089–1097.
- [30] T. Fukasawa, T. Asao, H. Yamauchi, M. Ide, Y. Tabe, T. Fujii, S. Yamaguchi, S. Tsutsumi, S. Yazawa, H. Kuwano, Associated expression of α 2,3sialylated type 2 chain structures with lymph node metastasis in distal colorectal cancer, *Surg. Today* 43 (2013) 155–162.
- [31] H. Ma, L. Cheng, K. Hao, Y. Li, X. Song, H. Zhou, L. Jia, Reversal effect of ST6GAL 1 on multidrug resistance in human leukemia by regulating the PI3K/Akt pathway and the expression of P-gp and MRP1, *PLoS One* 9 (2014) e85113.

Specific *N*-glycan alterations are coupled in EMT induced by different density cultivation of MCF 10A epithelial cells

Qingsong Xu^{1,2} · Xueming Niu¹ · Wenjing Wang³ · Wen Yang¹ ·
Yuguang Du⁴ · Jianguo Gu² · Linsheng Song¹

Received: 11 August 2016 / Revised: 22 November 2016 / Accepted: 28 November 2016 / Published online: 29 December 2016
© Springer Science+Business Media New York 2016

Abstract Epithelial-mesenchymal transition (EMT) is a process in tumor progression during which cancer cells undergo dramatic changes acquiring highly invasive properties. In a widespread adoption of TGF- β -induced EMT model, we have previously observed that expression of bisecting GlcNAc on *N*-glycans was dramatically decreased. Herein, we performed *in vitro* studies with the MCF10A cell line. In response to low cell density, MCF10A cells suffered spontaneously morphologic and phenotypic EMT-like changes, including elongated spindle shape, extended out from edge of the cell sheet, cytoskeleton reorganization, vimentin and fibronectin up-regulation, catenins redistribution, and cadherin switching. Moreover, these phenotypic changes were associated with specific *N*-glycan alterations. Interestingly, the amounts of bisecting GlcNAc structure were declined, by contrast, the formation of β 1-6 GlcNAc branches were obviously up-regulated during the EMT induced by sparse cell conditions. We further investigated *N*-glycans on the β 1-integrin, which is a good target of some glycosyltransferases. The reactivity with E4-PHA lectin decreased, whereas the staining for L4-

PHA lectin, which recognizes branched GlcNAc, increased in sparse cell conditions compared with dense cell conditions. Taken together, these results demonstrated that specific *N*-glycan alterations are coupled in EMT process and promoted cells migration at a low cell density.

Keywords Epithelial-mesenchymal transition · Cell density · *N*-glycan · Migration · Tumor

Introduction

Metastasis is a sequential process whereby cancer cells penetrate the basement membrane, invade blood/lymphatic vessels, survive in the vasculature before extravasating to secondary sites, and finally adapt to new host environments to proliferate and form metastases [1]. This process is mediated by the epithelial-mesenchymal transition (EMT) whereby tightly connected epithelial cells convert to disorganized motile mesenchymal cells with defined morphology, gene characteristic and protein expression. Therefore, EMT is regarded as a differentiated or morphogenetic process, which contributes to the pathogenesis of diseases, such as cancer metastasis and tissue fibrosis [2]. A growing body of evidences indicates that EMT is stimulated by signals from the tumor microenvironment, including a variety of growth factors and cytokines (such as transforming growth factor- β and epidermal growth factor) [3]. In addition, EMT is regulated by a series of intracellular signaling networks, including ERK1/2, PI3K/Akt, Smads, RhoB, β -catenin, and so forth [4]. These factors alter the epithelial profile by repressing genes encoding epithelial junction complexes and cytokeratins, and induce the expression of their mesenchymal counterparts, N-cadherin and vimentin. A defined feature of EMT is a reduction in E-cadherin levels and a concomitant induction of N-cadherin [5]. However, the

✉ Qingsong Xu
xuqingsong@dlou.edu.cn

✉ Jianguo Gu
jgu@tohoku-mpu.ac.jp

¹ College of Fisheries and Life Science, Dalian Ocean University, 52. Heishijiao Street, Shahekou District, Dalian 116023, China

² Tohoku Medical and Pharmaceutical University, Sendai, Miyagi 981-8558, Japan

³ Dalian Elite Analytical Instruments Company Limited, Dalian 116023, China

⁴ Institute of Process Engineering, Chinese Academy of Sciences, Beijing 100190, China

significance of EMT during cancer progression and even its relevance in human tumor remain a matter for debate.

It is widely known that the tumor microenvironment has a profound impact on determining the gene expression patterns [6]. Kim and his collaborators suggested that the gene expression patterns of cancer cells could vary significantly according to the conditions under which they were cultured. Culture media formulations and cell density could modulate the cancer cell transcriptome [7]. Indeed, some researchers found that lowered cell density, conditions under which cell contact was reduced, lead to reducing expression of genes associated with mammary epithelial cell differentiation and increasing expression of genes associated with breast cancer [8]. Other researchers proposed that limiting cell spreading, either by increasing cell density or by culturing cells on precisely defined micro-patterned substrata, blocked expression of characteristic markers of EMT in cells [9]. MCF10A mammary epithelial cells have been used to investigate EMT pathways in premalignant cells, because they readily undergo EMT when exposed to some stimulus, such as transforming growth factor β (TGF- β) [10]. Moreover, MCF10A cells have been found to exhibit many EMT-like changes when grown at different density: cells grown under sparse conditions express higher levels of mesenchymal markers, while cells grown under confluent conditions express higher levels of epithelial markers [11]. However, the extent to what density-dependent alterations in MCF10A cells fully recapitulate the EMT program and how this process occurs remain unknown.

Glycans, for instance glycosphingolipids (GSLs), *N*-glycans, and *O*-glycans are related to numerous of biological phenomena that include virus/bacteria-host interactions, inflammation, morphogenesis, cell-cell interactions, and cancer progression [12]. Some research data indicated that aberrant formation of glycans was detected in different EMT models. Guan et al. [13] reported the function of GSLs in phenotypic alteration of cell growth, motility, and adhesion during EMT, and the expression of GM2 and Gg4 were found to be dramatically decreased or depleted after TGF- β treatment. Overexpression of the fucosyltransferase 8, which is related to enhance core fucosylation of E-cadherin, decreased Src phosphorylation and suppressed cell migration in giant lung carcinoma cell line 95C, but low core fucosylation of E-cadherin activated Src and promoted an EMT-like phenomenon [14]. The expression of β -galactoside α 2, 6-sialyltransferase 1 (ST6GAL1), which modifies *N*-glycans with terminal α 2, 6-sialylation, was up-regulated in different carcinomas and in an EMT model induced by TGF- β [15]. Our previous results showed that expression of *N*-acetylglucosaminyltransferase III (GnT-III) and bisecting GlcNAc on *N*-glycans were obviously decreased in an EMT model induced by TGF- β . GnT-III prolonged E-cadherin turnover and prevented β -catenin translocation into the cell nucleus from E-cadherin/catenin complex [10]. *N*-acetylgalactosaminyltransferase 6 (GALNT6), which participates the primary step of *O*-glycosylation, could stabilize *O*-

glycosylated fibronectin, promote the acinar disruption, and further stimulate cellular alteration similar to those of EMT in normal mammary epithelial cells [16]. Above-mentioned results strongly indicated that remodeling of glycan structures by glycosyltransferases could modulate cell migration and thereby tumor metastasis as well. It is therefore very important to clarify the mechanisms for the alteration of glycans under physiological and pathological conditions.

In this study, we performed new experiments in which we assessed the effect of differential density on cellular morphology and phenotype in human MCF10A mammary epithelial cells. Interestingly, the alterations of bisecting GlcNAc and β 1-6 GlcNAc branched *N*-glycan were coupled with cells spontaneous EMT-like changes at a sparse condition, which might be contributed to diagnosis and therapy of breast cancer.

Materials and methods

Cell line and cell culture

MCF10A, a human non-tumorigenic immortalized mammary epithelial cell line, was cultured in DMEM/F12 medium, supplemented with 5% horse serum, 20 ng/ml EGF, 10 μ g/ml insulin, 0.5 μ g/ml hydrocortisone, and 100 ng/ml cholera toxin, under a humidified atmosphere containing 5% CO₂ at 37 °C. Cells were plated at 5×10^6 , 1×10^6 , 5×10^5 and 1×10^5 on 15-cm dishes for density gradient culture, followed by incubation for 3 days. Cells at 5×10^6 and 1×10^5 were defined as a dense culture and a sparse culture, respectively.

PCR for mRNA expression analysis

Total RNA was prepared with Trizol (Invitrogen), and 2.0 μ g of total RNA was reverse transcribed using the Superscript III RNase H Reverse Transcriptase kit (Invitrogen) according to the manufacturer's instructions. The sequences of the primers used for the PCR amplification were shown in Table 1. The *GAPDH* mRNA was used as a control in PCR runs and the reaction products obtained were submitted to electrophoresis in 1.5% agarose gels containing ethidium bromide.

Western blot and lectin blot analyses

Cells cultured under different conditions, as indicated, were washed with PBS and then lysed with lysis buffer (10 mM Tris-HCl, 1% Triton-X100, 150 mM NaCl, aprotinin, leupeptin and 1 mM phenylmethylsulfonyl fluoride). Insoluble materials were removed by centrifugation at 15,000 rpm for 10 min at 4 °C. Equal amounts of protein were separated using 7.5% sodium dodecyl sulfate polyacrylamide gel electrophoresis (SDS-PAGE), transferred to nitrocellulose and probed with the appropriate antibodies, as indicated, or with biotinylated erythro-

Table 1 Primers used for RT-PCR experiments

Gene	Primer sequence (5'-3')	
<i>E-cadherin</i>	Forward	ACGCATTGCCACATACA
	Reverse	CGTTAGCCTCGTTCTCA
<i>P-cadherin</i>	Forward	GGTGGTTCTCCGCAATG
	Reverse	GCCGCCTTCAGGTTCTC
<i>N-cadherin</i>	Forward	GAAAGACCCATCCACG
	Reverse	CCTGCTCACCACCACTA
<i>Vimentin</i>	Forward	ATGGCTCGTCACCTTCG
	Reverse	AGTTTCGTTGATAACCTGTCC
<i>GnT-III</i>	Forward	GCCGCGTCATCAACGCCATCAA
	Reverse	CAGGTAGTCGTCGGCGATCCA
<i>GnT-V</i>	Forward	GACCTGCAGTTCCTTCTCG
	Reverse	CCATGGCAGAAGTCCTGTTT
<i>GAPDH</i>	Forward	AGCCACATCGCTCAGACA
	Reverse	TGGACTCCACGACGTACT

agglutinating phytohemagglutinin (E4-PHA) lectin, biotinylated leuco-agglutinating phytohemagglutinin (L4-PHA), and biotinylated *Datura stramonium* (DSA) lectin (Seikagaku kogyo Inc., Japan). Immunoreactive bands were visualized using a Vectastain ABC kit (Vector Laboratories, CA) and an ECL kit (Amersham, UK). Monoclonal antibodies against E-cadherin, P-cadherin N-cadherin, β -catenin, p120-catenin, γ -catenin, and α -catenin were purchased from BD Biosciences, and the anti- α -tubulin antibody was from Sigma. Monoclonal antibodies against Fibronectin and HRP-labeled anti-mouse IgG were obtained from Cell Signaling.

Microscopy and cell image

Cellular morphology was confirmed using phase-contrast observations. For immunofluorescence assay, cells were seeded on glass-bottom dishes before fixation. After washing twice with PBS, the cells were fixed for 30 min in 4% paraformaldehyde solution at 37 °C. For permeabilization, the cells were treated with 0.2% (v/v) Triton X-100 in PBS. The fixed cells were blocked with 2% BSA in PBS for 1 h and then incubated with monoclonal antibodies against E-cadherin, N-cadherin and β -catenin in blocking buffer for 1 h at room temperature. Following three washes in PBS, the cells were incubated with a 1:500 dilution of Alexa Fluor® secondary antibody or with a 1:300 dilution of Alexa Fluor® 488 phalloidin for actin (Invitrogen) for 1 h at room temperature. After washing three times with PBS, the cells were observed using an Olympus fluorescence microscope (FV1000 system).

Flow cytometry

Flow cytometry was performed as previously described [17]. Briefly, cells were detached by trypsinizing and incubated with

biotinylated L4-PHA lectin, followed by streptavidin Alexa Fluor 488 conjugate (Invitrogen). Negative controls underwent the same procedure without biotinylated lectin. The analyses were performed using a FACS Calibur instrument (BD Biosciences), equipped with CELL QuestPro software.

Immunoprecipitation

For immunoprecipitation, the supernatant (2 mg of protein) was incubated with anti- β 1 integrin (P5D2) antibody (3 μ g/ml), which was obtained from the Developmental Studies Hybridoma Bank, University of Iowa, for 1 h at 4 °C. Protein G beads (30 μ l in 50% slurry) were then added, followed by incubation overnight at 4 °C with a rotator. After washing 3 times with lysis buffer, the immunoprecipitates were subjected to 7.5% SDS-PAGE, and the separated proteins were transferred to a nitrocellulose membrane. The membrane was incubated with E4-PHA or L4-PHA lectin for lectin blot analysis, or with an antibody for immunoblot analysis.

Statistical analysis

Statistical analysis was performed with SPSS 13.0 software. Student's t-test was performed for comparisons between two groups. $P < 0.05$ was considered to be statistically significant.

Results

The MCF10A cells suffered spontaneous EMT-like phenotypic changes at low cell density

To determine how gradual differences in MCF10A cell density affected patterns of phenotypic changes, cells were plated at 5×10^6 , 1×10^6 , 5×10^5 and 1×10^5 on 15-cm dishes for density gradient culture, followed by incubation for 3 days. Cells at 5×10^6 and 1×10^5 were defined as a dense culture and a sparse culture, respectively. As shown in Fig. 1, cells cultured under sparse conditions had adequate space available for cell spreading. In contrast, cells cultured under dense conditions had not enough space for full spreading, resulting in a reduction in cell size. Furthermore, image analysis of cell morphology for different densities revealed that MCF10A suffered spontaneous morphologic changes depending on cell confluence, showing “fibroblast like” spindle morphology in sparse culture conditions and epithelial-like compact morphology in dense cultures, suggesting that they might be susceptible to EMT at a low cell density.

Effects of spontaneous EMT-like phenotypic changes on expression of EMT marker molecules in MCF10A cells

We next investigated whether the expression of some important genes identified as EMT markers may correlate with these

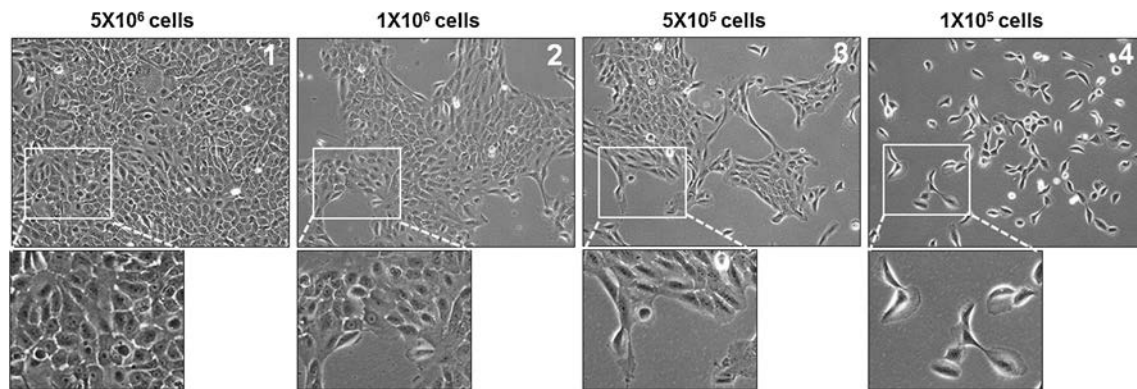


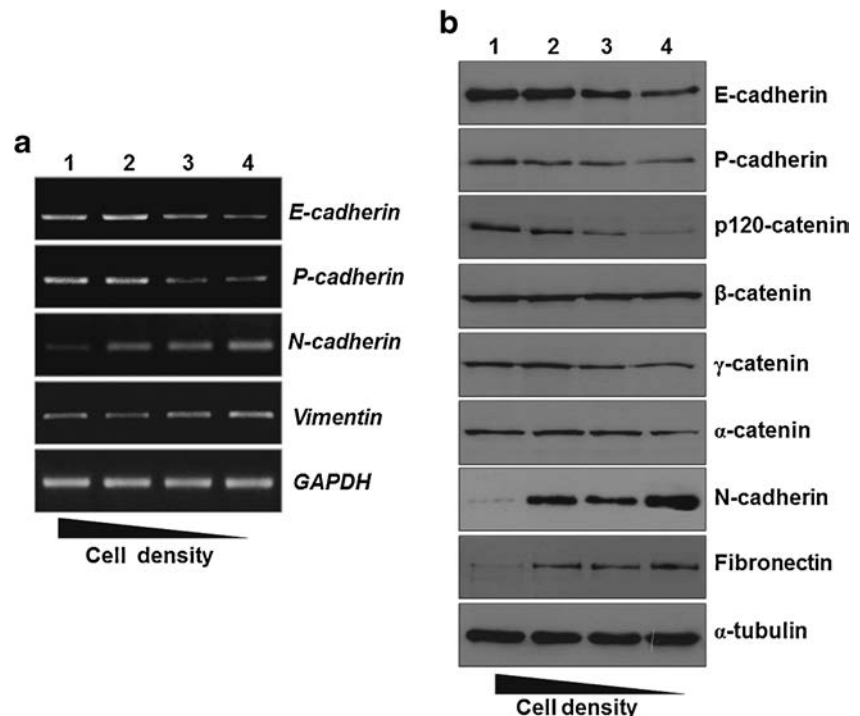
Fig. 1 MCF10A cells suffer spontaneous, morphologic- EMT-like changes in response to different cell densities. Cells were plated at 5×10^6 , 1×10^6 , 5×10^5 and 1×10^5 on 15-cm dishes for density gradient

culture, followed by incubation for 3 days. The cell densities were photographed by phase-contrast microscopy at $200 \times$ magnification

phenotypic changes. By RT-PCR, we observed significant decrease in *E-cadherin* and *P-cadherin* expression in sparse cultured cells, whereas the *N-cadherin* and *vimentin* genes were increased (Fig. 2a). To further confirm the molecular events associated with the plasticity of MCF10A cells, we characterized the relative proteins modulated during the phenotypic changes by Western blot. As expected, the total level of E-cadherin and P-cadherin expression were greatly down-regulated in sparse condition, while the mesenchymal N-cadherin and fibronectin were obviously up-regulated. In addition, the downstream elements of E-cadherin, the p120-catenin, β -catenin, γ -catenin and α -catenin, were evaluated in different cell densities. The expression levels of β -catenin were nearly no changes, however, the

expression levels of p120-catenin, γ -catenin and α -catenin were effectively decreased in a density-dependent manner (Fig. 2b). Furthermore, we found that cadherin switching also occurred during the morphologic changes (Fig. 3). The immunofluorescence data indicated that E-cadherin expression in cell-cell junctions became jagged and faint in the sparse condition, whereas, N-cadherin expression became enhanced at cell borders. β -catenin staining was decreased in cell-cell contacts and accumulated significantly in the cytosol and nuclei during sparse culture. F-actin distribution also dramatically changed from cell-cell borders to the stress fiber at low cell density. These results suggested that MCF10A cells suffered spontaneous, EMT-like phenotypic and intrinsic properties alteration in a sparse condition.

Fig. 2 Effects of cell density on expression of EMT marker molecules in MCF10A cells. **a** RT-PCR was carried out to examine the expression levels of *E-cadherin*, *P-cadherin*, *N-cadherin*, and *vimentin* in different density cells. The expression level of *GAPDH* was used as a load control. **b** Cell lysates from different density cells were immunoblotted (IB) with anti-E-cadherin, P-cadherin, N-cadherin, fibronectin, p120-catenin, β -catenin, γ -catenin and α -catenin antibodies. α -tubulin was used as a load control. Cells inoculated at 5×10^6 , 1×10^6 , 5×10^5 and 1×10^5 on 15-cm dishes were defined as 1, 2, 3, and 4 density gradient culture



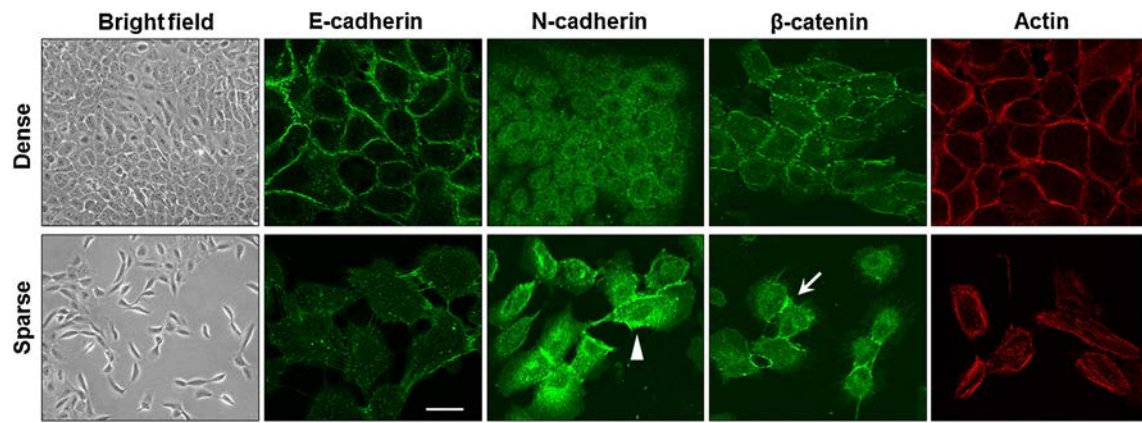


Fig. 3 The distributions of E-cadherin, N-cadherin and β -catenin were evaluated by immunofluorescence assay. Dense and sparse cultured cells were stained with monoclonal antibodies against E-cadherin, N-cadherin and β -catenin respectively, followed by incubation with Alexa Fluor-conjugated secondary antibody. Localization of F-actin was examined

by staining with Alexa Fluor 488 phalloidin. The small triangle showed N-cadherin expression, and the arrow indicated β -catenin expression. Cells inoculated at 5×10^6 , and 1×10^5 on 15-cm dishes were defined as Dense and Sparse culture. Scale bar, 50 μ m

Spontaneous EMT-like phenotypic changes induced specific N-glycan alterations

Aberrant expression of glycans has been observed in cancer development and progression [18]. In a TGF- β -induced EMT model, we have previously observed that expression of bisecting GlcNAc was dramatically down-regulated. To confirm whether the phenomenon described above would be also observed in another EMT model, MCF10A epithelial cells

were evaluated in a spontaneous EMT process. As shown in Fig. 4a/b, the expression of *Gnt-III* gene was greatly declined, and the relative ratio was decreased 2.4 fold in sparse condition compared to dense condition. Meanwhile, the products of Gnt-III detected by E4-PHA lectin, which preferentially recognizes bisecting GlcNAc, were declined in a cellular density dependent manner (Fig. 4c). Normally, introduction of the bisecting GlcNAc suppresses further processing and elongation of N-glycans catalyzed by other branching enzymes such

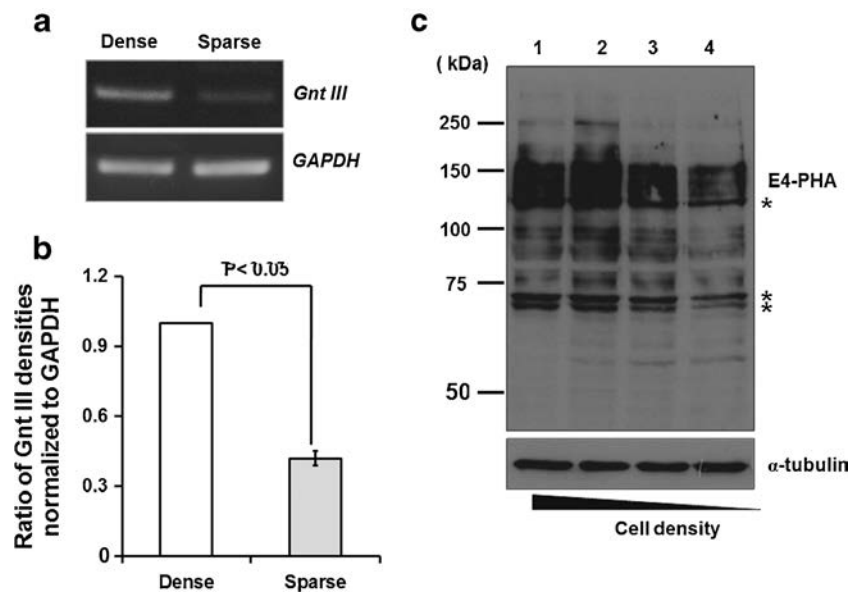


Fig. 4 Effects of spontaneous, EMT-like phenotypic changes on *Gnt-III* and bisecting GlcNAc. **a** RT-PCR was carried out to examine the expression levels of *Gnt-III* gene, and the expression level of *GAPDH* was used as a load control. **b** The relative ratio of *Gnt III* densities normalized to *GAPDH* was shown. The quantitative data were obtained from three independent experiments, and the *p* value was calculated using Student's two-tailed *t* test. Error bars indicate SD. **c** Equal amounts of protein (20 μ g) were separated on 7.5% SDS-PAGE, and the membranes

were probed with E4-PHA lectin, and α -tubulin was used as a load control. The asterisks indicated nonspecific staining of E4-PHA, since those bands did not disappear after treatment with 100 mM acetic acid. Cells inoculated at 5×10^6 , and 1×10^5 on 15-cm dishes were defined as Dense and Sparse culture. Cells inoculated at 5×10^6 , 1×10^6 , 5×10^5 and 1×10^5 on 15-cm dishes were defined as 1, 2, 3, and 4 density gradient culture

as *N*-acetylglucosaminyltransferase V (*GnT-V*), which is strongly associated with cancer metastasis, because neither of them can utilize the bisected oligosaccharide as a substrate [19]. Indeed, the expression of *GnT-III* gene was reduced in low cell density, while the expression of *GnT-V* gene was increased in sparse cultured cells (Fig. 5a). As the result of up-regulated *GnT-V*, the cell surface $\beta 1, 6$ GlcNAc branching structure, which is recognized by L4-PHA lectin in a FACS analysis, increased 1.3-fold in sparse culture compared to dense culture (Fig. 5b/c). Meanwhile, the reactivity with DSA and L4-PHA lectin (Fig. 5d/e), which preferentially recognizes whole cellular branched GlcNAc, were dramatically enhanced in low cell density culture. These results indicated that spontaneous EMT induced by low cell density specifically down-regulated bisecting GlcNAc and up-regulated GlcNAc branched *N*-glycan.

EMT influence composition of *N*-glycans on $\beta 1$ integrin protein

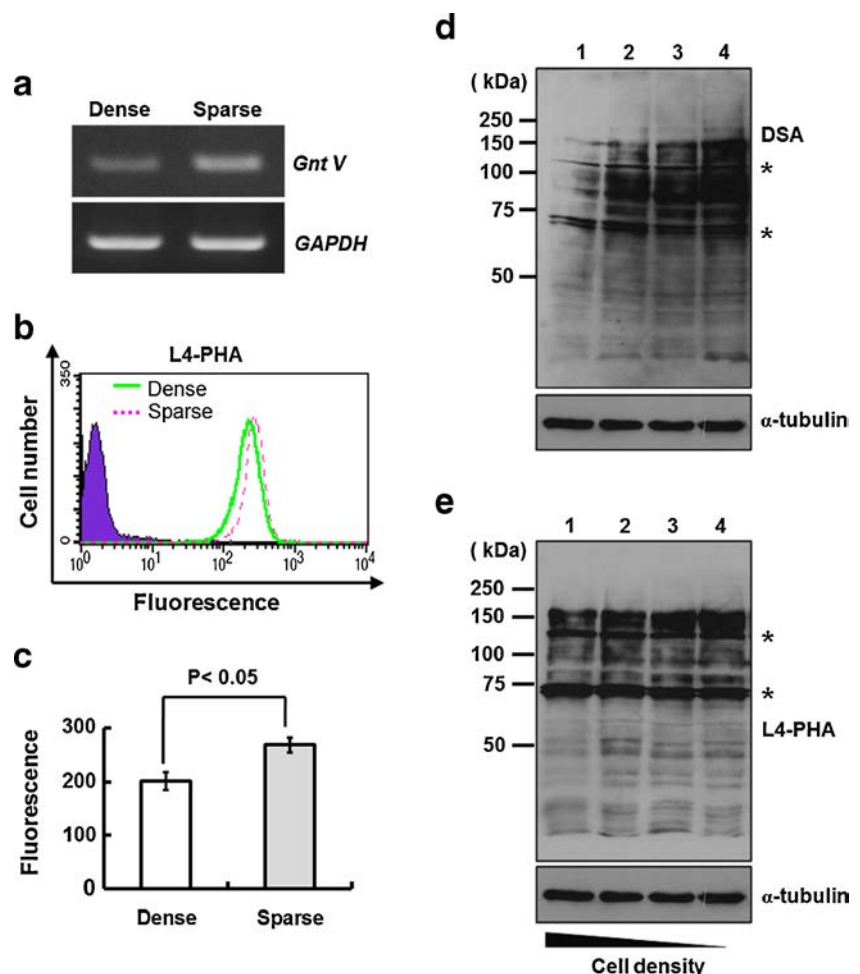
There is a certain set of glycoproteins on cell surface, such as cadherin, EGFR, galectin and integrins family, and the

glycosylation of integrins is related to tumor metastasis [17]. To examine whether the alteration of *N*-glycans on the cell surface was correlated with special glycans changes on glycoprotein, we further investigated *N*-glycans on the $\beta 1$ integrin, which is a good target of some glycosyltransferases. As shown in Fig. 6 a/b/c, the reactivity with L4-PHA lectin, which recognizes $\beta 1$ -6 GlcNAc branched structures, increased 1.3-fold on $\beta 1$ integrin subunit in sparse cells compared to dense cells. In contrast, the reactivity with E4-PHA lectin, which recognizes bisecting GlcNAc, decreased obviously on $\beta 1$ integrin in low cell density culture. These results suggested that spontaneous, EMT-like phenotypic changes can influence composition of *N*-glycans on some important glycoproteins.

Discussion

Intercellular communication is dependent on a dynamic and complex network of cytokines, growth factors, chemokines, and matrix remodeling enzymes [20]. Cellular confluent condition has an important influence on cell communication, and then affects the cell normal physiological function. EMT is

Fig. 5 Effects of spontaneous EMT-like phenotypic changes on GlcNAc-branched *N*-glycan. **a** The expression of *GnT-V* gene was determined by RT-PCR. **b** Cell surface expression levels of *N*-glycans were examined by FACS analysis. Prior to analysis, cells were incubated with biotinylated L4-PHA lectin, followed by incubation with streptavidin Alexa Fluor 488 conjugate. **c** The quantitative data were obtained from three independent experiments, and the *p* value was calculated using Student's two-tailed *t* test. Error bars indicate SD. Equal amounts of protein (20 μ g) were separated on 7.5% SDS-PAGE, and the membranes were probed with DSA lectin **d** or L4-PHA lectin **e**, and α -tubulin was used as a load control. The asterisks indicated nonspecific staining of DSA and L4-PHA, since those bands did not disappear after treatment with 100 mM acetic acid. Cells inoculated at 5×10^6 , and 1×10^5 on 15-cm dishes were defined as Dense and Sparse culture. Cells inoculated at 5×10^6 , 1×10^6 , 5×10^5 and 1×10^5 on 15-cm dishes were defined as 1, 2, 3, and 4 density gradient culture



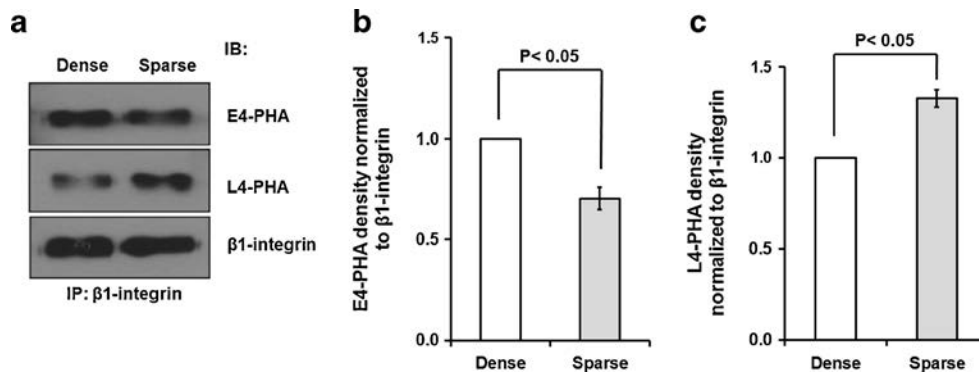


Fig. 6 Effects of EMT on composition of *N*-glycans on $\beta 1$ integrin. **a** Cell lysates from different density cells were immunoprecipitated (IP) using anti- $\beta 1$ integrin antibody. Immunoprecipitates were run on a 7.5% SDS-polyacrylamide gel and probed with the biotinylated E4-PHA and L4-PHA lectins. **b** Bar graphs, quantification of bisecting GlcNAc structures (E4-PHA reactivity) that are modifying $\beta 1$ integrin. **c** Bar graphs, quantification of $\beta 1$ -6 GlcNAc-branched *N*-glycan structures (L4-PHA reactivity) that are modifying $\beta 1$ integrin. Amounts

of *N*-glycan structures were determined from the ratios of densities of E4-PHA or L4-PHA reactivity after normalization to $\beta 1$ integrin. The modification of *N*-glycan structures in sparse cultured cells were expressed as the fold decrease or increase, compared with the density cultured cells, which was taken as 1. The *p* value was calculated using Student's two-tailed *t* test. Error bars indicate SD. Cells inoculated at 5×10^6 , and 1×10^5 on 15-cm dishes were defined as Dense and Sparse culture

known to be closely related to enhancement of cell motility. In the EMT process, the phenotype conversion from less mobile epithelial cells to fibroblastic mesenchymal cells with higher motility is accompanied by declining expression of epithelial cell molecules and enhancing expression of mesenchymal molecules. This process is implicated in the promotion of tumor invasion and metastasis [21]. A growing body of evidences indicated that cellular microenvironments are closely linked to EMT, such as growth factors [22], cytokines [23], cell density [11], and growth matrix [9] etc. However, the relationship between cellular microenvironments and EMT is a little bit complicated. In this study, we clearly observed spontaneous EMT process in a low cell density condition. The E-cadherin expression in cell-cell contacts, or the total level, was greatly down-regulated, meanwhile, the N-cadherin expression was distinctly up-regulated in sparse culture. Cadherin switching usually refers to a switch from the expression of E-cadherin to that of N-cadherin. N-cadherin promotes motility when expressed in epithelial cells, and cells that express more E-cadherin remain less motile. Cadherin switching is an important event in EMT process. Previous studies implicated that EGF could induce EMT in breast cancer cells, while EGFR activation disturbed cell-cell adhesion by destabilizing the E-cadherin/catenin complex, promoted EMT and contributed to the acquisition of a motile phenotype [24]. The newly synthesized E-cadherin and catenin complex move together to the cell surface. Our results indicated that the expression of p120-catenin and α -catenin were declined in a cellular density dependent manner, which would destabilize the E-cadherin/catenin complex and facilitate EMT process. The similar notion was proposed by David Sarrio and his collaborators [11].

Cell surface glycan characteristics can vary during cell-cell interactions, growth regulation and differentiation. Altered glycan signatures are also observed in tumor cells, and play a critical

role in the escape of tumor cells from immune surveillance as well as metastasis [19]. *N*-Acetylglucosaminyltransferase III (GnT-III) transfers *N*-acetylglucosamine (GlcNAc) from UDP-GlcNAc to a $\beta 1,4$ mannose in *N*-glycans to form a “bisecting” GlcNAc linkage. Bisecting GlcNAc alters not only the composition, but also the conformation of the *N*-glycan [25]. GnT-III is generally regarded as a key glycosyltransferase in *N*-glycan biosynthetic pathways. Introduction of the bisecting GlcNAc suppresses further processing and elongation of *N*-glycans catalyzed by *N*-acetylglucosaminyltransferase V (GnT-V) [26]. GnT-III has been proposed as an antagonist of GnT-V, thereby contributing to the suppression of cancer metastasis. In fact, overexpression of GnT-III in highly metastatic melanoma cells reduced $\beta 1$ -6 branching in cell-surface *N*-glycans and increased bisected *N*-glycans [27]. Furthermore, it is known that the $\beta 1$ -6 GlcNAc-branched *N*-glycans, which may enhance the complex formation such as integrins and galectins on cell surface, resulting in an increase in cell motility and cell signaling [28, 29]. It has also been reported that $\beta 1$ -6 GlcNAc-branched *N*-glycans levels are increased in highly metastatic tumor cell lines [30]. Consistently, cancer metastasis is greatly suppressed in GnT-V knockout mice [31]. Our recent research indicated that bisecting GlcNAc *N*-glycans structure catalyzed by GnT-III was dramatically declined in TGF- β -induced EMT model [10]. In this study, it was an interesting notion that bisecting GlcNAc *N*-glycans structure was also down-regulated in cellular density-dependent EMT model. Moreover, when epithelial cells converted into fibroblastic mesenchymal cells, the $\beta 1$ -6 GlcNAc-branched *N*-glycan structure was obviously enhanced, which might increase cell migration and contribute to EMT process. Based on the discussion above, we speculated that there are bidirectional regulation mechanisms. Cell-cell contact can modulate *N*-glycan alteration, whereas specific *N*-glycan alterations facilitated EMT process. A detailed characterization of the bidirectional regulation

mechanisms between specific *N*-glycan and EMT are required for further studies.

A series of glycoproteins on cell surface were modified by special glycans structure, such as cadherin, EGFR, galectin and integrins family. Our FACS analysis results indicated that *N*-glycans expressed on the cell surface were altered in sparse condition, which might influence the function of some important glycoproteins and cell migration. It has been reported that β 1-4-bisecting GlcNAc on E-cadherin glycosylation is a mechanism involved in TGF- β -induced EMT [32]. Janik et al. also proposed that an increase in β 1-6-GlcNAc sugar chains of the integrin resulted in the stimulation of cell migration [33]. Our results indicated that the β 1-6 GlcNAc-branched *N*-glycan structure were obviously increased on β 1-integrin, which might be related to the EMT. In this study, the mechanism of EMT induced by sparse cell culture could be ascribed to two aspects. One was that sparse condition promoted the breakdown of cell-cell junctions, as described above; the other was that alteration of *N*-glycans might influence some important surface glycoproteins stability and function, which mediated cell migration, as reported previously [34, 35].

In conclusion, we successfully constructed an EMT model utilizing different cellular density culture in MCF10A epithelial cells, and demonstrated that density-dependent specific *N*-glycan alterations were coupled in EMT process and promoted cells migration. Our results provided a new insight into the mechanism of epithelial-mesenchymal transition.

Acknowledgements This work was supported by grants from the National High Technology Research and Development Program of China (863 Program, No. 2014AA093604), The Technology Foundation for Selected Overseas Chinese Scholar, Ministry of Personnel of China (Q.S. Xu), and the Ocean Public Welfare Scientific Research Project, State Oceanic Administration of China (Grant No. 201405003).

Compliance with ethical standards

Conflicts of interest The authors declared that they have no conflict of interest.

Ethical approval This article does not contain any studies with human participants or animals performed by any of the authors.

References

- Langley, R.R., Fidler, I.J.: Tumor cell-organ microenvironment interactions in the pathogenesis of cancer metastasis. *Endocr. Rev.* **28**(3), 297–321 (2007). doi:[10.1210/er.2006-0027](https://doi.org/10.1210/er.2006-0027)
- Smith, B.N., Bhowmick, N.A.: Role of EMT in Metastasis and Therapy Resistance. *J. Clin. Med.* **5**(2) (2016). doi:[10.3390/jcm5020017](https://doi.org/10.3390/jcm5020017)
- Raghavan, C.T., Nagaraj, R.H.: AGE-RAGE interaction in the TGFbeta2-mediated epithelial to mesenchymal transition of human lens epithelial cells. *Glycoconj. J.* **33**(4), 631–643 (2016). doi:[10.1007/s10719-016-9686-y](https://doi.org/10.1007/s10719-016-9686-y)
- Zhang, J., Tian, X.J., Xing, J.: Signal Transduction Pathways of EMT Induced by TGF-beta, SHH, and WNT and Their Crosstalks. *J. Clin. Med.* **5**(4) (2016). doi:[10.3390/jcm5040041](https://doi.org/10.3390/jcm5040041)
- Iskender, B., Izgi, K., Canatan, H.: Novel anti-cancer agent myrtucommulone-a and thymoquinone abrogate epithelial-mesenchymal transition in cancer cells mainly through the inhibition of PI3K/AKT signalling axis. *Mol. Cell. Biochem.* (2016). doi:[10.1007/s11010-016-2697-y](https://doi.org/10.1007/s11010-016-2697-y)
- Yuan, Y., Jiang, Y.C., Sun, C.K., Chen, Q.M.: Role of the tumor microenvironment in tumor progression and the clinical applications (review). *Oncol. Rep.* **35**(5), 2499–2515 (2016). doi:[10.3892/or.2016.4660](https://doi.org/10.3892/or.2016.4660)
- Kim, S.W., Kim, S.J., Langley, R.R., Fidler, I.J.: Modulation of the cancer cell transcriptome by culture media formulations and cell density. *Int. J. Oncol.* **46**(5), 2067–2075 (2015). doi:[10.3892/ijco.2015.2930](https://doi.org/10.3892/ijco.2015.2930)
- Cichon, M.A., Nelson, C.M., Radisky, D.C.: Regulation of epithelial-mesenchymal transition in breast cancer cells by cell contact and adhesion. *Cancer Informat.* **14**(Suppl 3), 1–13 (2015). doi:[10.4137/CIN.S18965](https://doi.org/10.4137/CIN.S18965)
- Nelson, C.M., Khauv, D., Bissell, M.J., Radisky, D.C.: Change in cell shape is required for matrix metalloproteinase-induced epithelial-mesenchymal transition of mammary epithelial cells. *J. Cell. Biochem.* **105**(1), 25–33 (2008). doi:[10.1002/jcb.21821](https://doi.org/10.1002/jcb.21821)
- Xu, Q., Isaji, T., Lu, Y., Gu, W., Kondo, M., Fukuda, T., Du, Y., Gu, J.: Roles of N-acetylglucosaminyltransferase III in epithelial-to-mesenchymal transition induced by transforming growth factor beta1 (TGF-beta1) in epithelial cell lines. *J. Biol. Chem.* **287**(20), 16563–16574 (2012). doi:[10.1074/jbc.M111.262154](https://doi.org/10.1074/jbc.M111.262154)
- Sarrio, D., Rodriguez-Pinilla, S.M., Hardisson, D., Cano, A., Moreno-Bueno, G., Palacios, J.: Epithelial-mesenchymal transition in breast cancer relates to the basal-like phenotype. *Cancer Res.* **68**(4), 989–997 (2008). doi:[10.1158/0008-5472.CAN-07-2017](https://doi.org/10.1158/0008-5472.CAN-07-2017)
- Li, X., Wang, X., Tan, Z., Chen, S., Guan, F.: Role of glycans in cancer cells undergoing epithelial-mesenchymal transition. *Front. Oncol.* **6**, 33 (2016). doi:[10.3389/fonc.2016.00033](https://doi.org/10.3389/fonc.2016.00033)
- Guan, F., Handa, K., Hakomori, S.I.: Specific glycosphingolipids mediate epithelial-to-mesenchymal transition of human and mouse epithelial cell lines. *Proc. Natl. Acad. Sci. U. S. A.* **106**(18), 7461–7466 (2009). doi:[10.1073/pnas.0902368106](https://doi.org/10.1073/pnas.0902368106)
- Shao, K., Chen, Z.Y., Gautam, S., Deng, N.H., Zhou, Y., Wu, X.Z.: Posttranslational modification of E-cadherin by core fucosylation regulates Src activation and induces epithelial-mesenchymal transition-like process in lung cancer cells. *Glycobiology.* **26**(2), 142–154 (2016). doi:[10.1093/glycob/cwv089](https://doi.org/10.1093/glycob/cwv089)
- Lu, J., Isaji, T., Im, S., Fukuda, T., Hashii, N., Takakura, D., Kawasaki, N., Gu, J.: Beta-galactoside alpha2,6-sialyltransferase 1 promotes transforming growth factor-beta-mediated epithelial-mesenchymal transition. *J. Biol. Chem.* **289**(50), 34627–34641 (2014). doi:[10.1074/jbc.M114.593392](https://doi.org/10.1074/jbc.M114.593392)
- Park, J.H., Katagiri, T., Chung, S., Kijima, K., Nakamura, Y.: Polypeptide N-acetylgalactosaminyltransferase 6 disrupts mammary acinar morphogenesis through O-glycosylation of fibronectin. *Neoplasia.* **13**(4), 320–326 (2011). doi:[10.1593/neo.101440](https://doi.org/10.1593/neo.101440)
- Xu, Q., Akama, R., Isaji, T., Lu, Y., Hashimoto, H., Kariya, Y., Fukuda, T., Du, Y., Gu, J.: Wnt/beta-catenin signaling down-regulates N-acetylglucosaminyltransferase III expression: the implications of two mutually exclusive pathways for regulation. *J. Biol. Chem.* **286**(6), 4310–4318 (2011). doi:[10.1074/jbc.M110.182576](https://doi.org/10.1074/jbc.M110.182576)

18. Takahashi, M., Kizuka, Y., Ohtsubo, K., Gu, J., Taniguchi, N.: Disease-associated glycans on cell surface proteins. *Mol. Asp. Med.* (2016). doi:[10.1016/j.mam.2016.04.008](https://doi.org/10.1016/j.mam.2016.04.008)
19. Takahashi, M., Kuroki, Y., Ohtsubo, K., Taniguchi, N.: Core fucose and bisecting GlcNAc, the direct modifiers of the N-glycan core: their functions and target proteins. *Carbohydr. Res.* **344**(12), 1387–1390 (2009). doi:[10.1016/j.carres.2009.04.031](https://doi.org/10.1016/j.carres.2009.04.031)
20. Balkwill, F.R., Capasso, M., Hagemann, T.: The tumor microenvironment at a glance. *J. Cell Sci.* **125**(Pt 23), 5591–5596 (2012). doi:[10.1242/jcs.116392](https://doi.org/10.1242/jcs.116392)
21. Cai, Z., Wang, Q., Zhou, Y., Zheng, L., Chiu, J.F., He, Q.Y.: Epidermal growth factor-induced epithelial-mesenchymal transition in human esophageal carcinoma cells—a model for the study of metastasis. *Cancer Lett.* **296**(1), 88–95 (2010). doi:[10.1016/j.canlet.2010.03.020](https://doi.org/10.1016/j.canlet.2010.03.020)
22. Buonato, J.M., Lan, I.S., Lazzara, M.J.: EGF augments TGFbeta-induced epithelial-mesenchymal transition by promoting SHP2 binding to GAB1. *J. Cell Sci.* **128**(21), 3898–3909 (2015). doi:[10.1242/jcs.169599](https://doi.org/10.1242/jcs.169599)
23. Matthaei, M., Gillessen, J., Muether, P.S., Hoerster, R., Bachmann, B.O., Hueber, A., Cursiefen, C., Heindl, L.M.: Epithelial-mesenchymal transition (EMT)-related cytokines in the aqueous humor of Phakic and Pseudophakic Fuchs' dystrophy eyes. *Invest. Ophthalmol. Vis. Sci.* **56**(4), 2749–2754 (2015). doi:[10.1167/iovs.15-16395](https://doi.org/10.1167/iovs.15-16395)
24. Hardy, K.M., Booth, B.W., Hendrix, M.J., Salomon, D.S., Strizzi, L.: ErbB/EGF signaling and EMT in mammary development and breast cancer. *J. Mammary Gland Biol. Neoplasia.* **15**(2), 191–199 (2010). doi:[10.1007/s10911-010-9172-2](https://doi.org/10.1007/s10911-010-9172-2)
25. Gu, J., Sato, Y., Kariya, Y., Isaji, T., Taniguchi, N., Fukuda, T.: A mutual regulation between cell-cell adhesion and N-glycosylation: implication of the bisecting GlcNAc for biological functions. *J. Proteome Res.* **8**(2), 431–435 (2009). doi:[10.1021/pr800674g](https://doi.org/10.1021/pr800674g)
26. Pinho, S.S., Figueiredo, J., Cabral, J., Carvalho, S., Dourado, J., Magalhaes, A., Gartner, F., Mendonfa, A.M., Isaji, T., Gu, J., Carneiro, F., Seruca, R., Taniguchi, N., Reis, C.A.: E-cadherin and adherens-junctions stability in gastric carcinoma: functional implications of glycosyltransferases involving N-glycan branching biosynthesis, N-acetylglucosaminyltransferases III and V. *Biochim. Biophys. Acta.* **1830**(3), 2690–2700 (2013). doi:[10.1016/j.bbagen.2012.10.021](https://doi.org/10.1016/j.bbagen.2012.10.021)
27. Yoshimura, M., Nishikawa, A., Ihara, Y., Taniguchi, S., Taniguchi, N.: Suppression of lung metastasis of B16 mouse melanoma by N-acetylglucosaminyltransferase III gene transfection. *Proc. Natl. Acad. Sci. U. S. A.* **92**(19), 8754–8758 (1995)
28. Kariya, Y., Gu, J.G.: N-glycosylation of beta 4 integrin controls the adhesion and motility of keratinocytes. *PLoS One.* **6**(11), e27084 (2011). doi:[10.1371/journal.pone.0027084](https://doi.org/10.1371/journal.pone.0027084)
29. Dennis, J.W., Lau, K.S., Demetriou, M., Nabi, I.R.: Adaptive regulation at the cell surface by N-glycosylation. *Traffic.* **10**(11), 1569–1578 (2009). doi:[10.1111/j.1600-0854.2009.00981.x](https://doi.org/10.1111/j.1600-0854.2009.00981.x)
30. Pochech, E., Litynska, A., Amoresano, A., Casbarra, A.: Glycosylation profile of integrin alpha(3)beta(1) changes with melanoma progression. *Biochim. Biophys. Acta.* **1643**(1–3), 113–123 (2003). doi:[10.1016/j.bbamcr.2003.10.004](https://doi.org/10.1016/j.bbamcr.2003.10.004)
31. Granovsky, M., Fata, J., Pawling, J., Muller, W.J., Khokha, R., Dennis, J.W.: Suppression of tumor growth and metastasis in Mgat5-deficient mice. *Nat. Med.* **6**(3), 306–312 (2000). doi:[10.1038/73163](https://doi.org/10.1038/73163)
32. Pinho, S.S., Oliveira, P., Cabral, J., Carvalho, S., Huntsman, D., Gartner, F., Seruca, R., Reis, C.A., Oliveira, C.: Loss and recovery of Mgat3 and GnT-III mediated E-cadherin N-glycosylation is a mechanism involved in epithelial-mesenchymal-epithelial transitions. *PLoS One.* **7**(3), e33191 (2012). doi:[10.1371/journal.pone.0033191](https://doi.org/10.1371/journal.pone.0033191)
33. Janik, M.E., Litynska, A., Vereecken, P.: Cell migration-the role of integrin glycosylation. *Biochim. Biophys. Acta.* **1800**(6), 545–555 (2010). doi:[10.1016/j.bbagen.2010.03.013](https://doi.org/10.1016/j.bbagen.2010.03.013)
34. Isaji, T., Gu, J., Nishiuchi, R., Zhao, Y., Takahashi, M., Miyoshi, E., Honke, K., Sekiguchi, K., Taniguchi, N.: Introduction of bisecting GlcNAc into integrin alpha5beta1 reduces ligand binding and down-regulates cell adhesion and cell migration. *J. Biol. Chem.* **279**(19), 19747–19754 (2004). doi:[10.1074/jbc.M311627200](https://doi.org/10.1074/jbc.M311627200)
35. Zhao, Y., Nakagawa, T., Itoh, S., Inamori, K., Isaji, T., Kariya, Y., Kondo, A., Miyoshi, E., Miyazaki, K., Kawasaki, N., Taniguchi, N., Gu, J.: N-acetylglucosaminyltransferase III antagonizes the effect of N-acetylglucosaminyltransferase V on alpha3beta1 integrin-mediated cell migration. *J. Biol. Chem.* **281**(43), 32122–32130 (2006). doi:[10.1074/jbc.M607274200](https://doi.org/10.1074/jbc.M607274200)

SCIENTIFIC REPORTS

OPEN

Inhibition of fucosylation by 2-fluorofucose suppresses human liver cancer HepG2 cell proliferation and migration as well as tumor formation

Ying Zhou¹, Tomohiko Fukuda¹, Qinglei Hang¹, Sicong Hou¹, Tomoya Isaji¹, Akihiko Kameyama² & Jianguo Gu¹

Core fucosylation is one of the most important glycosylation events in the progression of liver cancer. For this study, we used an easily handled L-fucose analog, 2-fluoro-L-fucose (2FF), which interferes with the normal synthesis of GDP-fucose, and verified its potential roles in regulating core fucosylation and cell behavior in the HepG2 liver cancer cell line. Results obtained from lectin blot and flow cytometry analysis clearly showed that 2FF treatment dramatically inhibited core fucosylation, which was also confirmed via mass spectrometry analysis. Cell proliferation and integrin-mediated cell migration were significantly suppressed in cells treated with 2FF. We further analyzed cell colony formation in soft agar and tumor xenograft efficacy, and found that both were greatly suppressed in the 2FF-treated cells, compared with the control cells. Moreover, the treatment with 2FF decreased the core fucosylation levels of membrane glycoproteins such as EGF receptor and integrin $\beta 1$, which in turn suppressed downstream signals that included phospho-EGFR, -AKT, -ERK, and -FAK. These results clearly described the roles of 2FF and the importance of core fucosylation in liver cancer progression, suggesting 2FF shows promise for use in the treatment of hepatoma.

Glycosylation is by far the most prolific form of protein modification in mammalian cells. Accumulating data have made it clear that glycan structures expressed on glycoproteins have essential roles in various biological processes such as inflammation, growth, differentiation, carcinogenesis, and cancer metastasis^{1,2}. Alteration during glycosylation is now regarded as a feature event in the progression of cancer. Among all forms of carbohydrate modification involved with the progression of cancer, fucosylation is considered one of the most important^{3,4}.

In regards to liver cancer, core fucosylation is a pre-eminent factor. Core fucosylation, also known as $\alpha 1,6$ -fucosylation, is catalyzed by $\alpha 1,6$ -fucosyltransferase (Fut8) to transfer fucose residue from guanosine 5'-diphosphate (GDP)-fucose to the innermost asparagine-linked GlcNAc via an $\alpha 1,6$ link, which is a process that has been implicated in the progression of liver cancer⁵. Early work by Breborowicz, J. *et al.* suggested that core fucosylated alpha-fetoprotein (AFP) was a reliable marker that could be used to distinguish hepatocellular carcinoma (HCC) from chronic hepatitis and liver cirrhosis⁶.

Recent studies have shown that core fucosylation is up-regulated both in the serum and on the cell surface of liver cancer cells^{7,8}, although contradictory results were also reported whereby an increased level of tetra-antennary N-glycan, rather than core fucosylation, was associated with hepatocellular carcinoma⁹. Consistently, Yamashita, F. *et al.* associated a high expression of core fucosylation with a poor prognosis¹⁰. Furthermore, our previous studies indicated that loss of Fut8 gene significantly suppressed liver regeneration¹¹ and chemical-induced HCC¹² via the down-regulation of several cell-signaling pathways. Taken together, these

¹Division of Regulatory Glycobiology, Institute of Molecular Biomembrane and Glycobiology, Tohoku Medical and Pharmaceutical University, 4-4-1 Komatsushima, Aoba-ku, Sendai, Miyagi, 981-8558, Japan. ²Department of Life Science and Biotechnology, National Institute of Advanced Industrial Science and Technology (AIST), 1-1-1 Umezono, Tsukuba, Ibaraki, 305-8568, Japan. Correspondence and requests for materials should be addressed to J.G. (email: jgu@tohoku-mpu.ac.jp)

studies clearly show that core fucosylation plays crucial roles in liver cancer, which enabled us to predict that the inhibition of core fucosylation could provide a novel strategy for liver cancer therapy⁹.

How to inhibit core fucosylation in HCC? As described above, biosynthesis of core fucosylated *N*-glycans requires donor substrate GDP-fucose, *N*-glycans and Fut8. Fut8 is localized in the inner lumen of Golgi bodies, thus, conventional wisdom holds that an inhibitor of Fut8 cannot be efficiently delivered to a Golgi apparatus. On the other hand, GDP-fucose in the cytoplasm is known to be synthesized by two distinct pathways^{13,14}. One is called the *de novo* pathway, and this pathway converts GDP-mannose into GDP-fucose *via* enzymatic reactions catalyzed by GDP-mannose 4,6-dehydratase (GMD) and GDP-keto-6-deoxymannose 3, and 5-epimerase 4-reductase (FX)^{15–17}. Blocking this pathway forces cells to make use of another pathway, which is called the salvage pathway. This pathway uses fucose kinases to convert L-fucose into GDP-fucose^{18,19}. GDP-fucose is then delivered into the Golgi apparatus via GDP-fucose transporters. Finally, GDP-fucose serves as a donor substrate and is transferred into the oligosaccharides of protein to synthesize core fucose by the action of Fut8²⁰. Thus, the inhibition of GDP-fucose production is desirable in order to block fucosylation. Previous efforts to delete core fucosylation have focused mostly on the manipulation of Fut8 by knockout or knockdown of its gene. Additionally, there have been efforts to knockout the key enzymes for GDP-fucose production such as GMD and FX and impair the Golgi GDP-fucose transporter^{21–25}. The methods described above, however, are not suitable for pharmacological application.

A variety of glycosyltransferase inhibitors have been developed, and mainly based on donor or accept substrates mimics²⁶. Several GDP-fucose analogs have been reported to be inhibitors of FUTs^{27,28}. However, those charged groups (GDP portion) prevent uptake into cells, which limits their use in biological systems. On the other hand, a specific fluorinated analog of fucose, 2-fluoro-L-fucose (2FF), has been reported to easily enter cells via passive diffusion wherein it is metabolized into a corresponding donor substrate analog of GDP-fucose, GDP-2FF, via the salvage pathway^{29–31}. Since GDP-2FF accumulates in cells, it will also lead to a shutdown of the *de novo* pathway that synthesizes natural GDP-fucose²⁹. In fact, the addition of 2FF has efficiently suppressed the endogenous production of GDP-fucose, which dramatically inhibited the formation of fucosylation in both cancer and plant cells^{31–33}. Therefore, 2FF has been used to reduce cell-surface fucosylated glycans such as Lewis antigens for E-selectin binding in colon carcinoma cells³¹, and has blocked core fucosylation in HL-60 cells²⁹. However, the effect that 2FF exerts on liver cancer cells remains unclear.

In this study, we examined the effects of 2FF in live cancer HepG2 cells and further clarified the underlying molecular mechanisms. We found that treatment with 2FF greatly decreased core fucosylation levels and both suppressed downstream signaling and tumor formation, which suggested that 2FF might be a novel candidate for liver cancer therapy.

Results

2FF suppressed fucosylation in HepG2 cells. Several analogues of L-fucose have shown inhibitory effects on fucosylation. One such analogue is 2FF, as shown in Fig. 1A. To investigate whether 2FF also inhibits fucosylation levels in HepG2 hepatoma cells, we first carried out lectin blot testing to detect fucosylation levels by probing with *aleuria aurantia lectin* (AAL), a specific lectin that preferentially binds to Fuc α 1-6GlcNAc³⁴. The fucosylation levels were inhibited by 2FF in a dose-dependent manner. The inhibitory effects of 2FF were observed even at a final concentration at 10 μ M, and remarkably appeared at 100 μ M (Fig. 1B). In addition, time course studies have indicated that the effect of 2FF persisted for more than 7 days without further adding 2FF (Fig. 1C). After the removal of 2FF, its effect at least lasted for another 3 days (Fig. 1D). These alterations in the fucosylation expression on the cell surface were further confirmed by flow cytometric analysis using AAL lectin. The reactive abilities of AAL lectin were persistently decreased in the HepG2 cells during 7-day culture in the presence of 2FF, compared with the control cells cultured without 2FF (Fig. 1E). To explore whether the decreased fucosylation was due to a suppression of fucosyltransferase gene expression by 2FF, we performed semi-quantitative RT-PCR to detect typical fucosylation related genes such as α 1,3-fucosyltransferase 4 (Fut4), α 1,3-fucosyltransferase 7 (Fut7), and Fut8 because 2FF was known to inhibit not only the products of Fut8 but also the products of Fut4 and Fut7 in HL-60 cells²⁹. As shown in Fig. 1F, the treatment with 2FF did not significantly affect gene expression level. These data again indicated that 2FF strongly down-regulates fucosylation levels via an interruption of intracellular GDP-fucose synthesis, and/or that GDP-2FF may inhibit fucosyltransferases, which includes Fut8, in HepG2 cells.

Alteration of the N-linked glycans of HepG2 cells treated with 2FF. To further verify the effects of 2FF in regulating carbohydrate structures, the *N*-glycan profiles of those cells were analyzed by mass spectrometry. MALDI-TOF mass spectrometry of *N*-glycans clearly supported the suppression of core fucosylation by treating HepG2 cells with 2FF (Fig. 2A). Without 2FF, fucosylated complex *N*-glycans were accompanied by large signals from high mannose-type glycans (Fig. 2A upper). These fucosylated glycans, mostly core fucosylated glycans, were considerably displaced by corresponding afucosylated glycans in 2FF-treated HepG2 cells (Fig. 2A lower). The percentages of fucosylated complex glycans among all complex glycans in an *m/z* range of from 1,500 to 3,500 were reduced from 75 to 8% by treatment with 2FF (Fig. 2B). Curiously, sialylated complex glycans were observed in an *m/z* of more than 3,500 in both measurements of the MS spectra. Afucosylated sialylated glycans were also significantly increased by treatment with 2FF. In fact, upon 2FF treatment, reactivity against both *concanavalin A* (ConA) and *wheat germ agglutinin* (WGA) showed no change. An SNA lectin blot showed a tendency whereby sialylation was up-regulated upon 2FF treatment in a dose-dependent manner (Fig. 2C). That phenomenon could be interpreted as sialylation is up-regulated by a lack of terminal fucosylation, which was blocked by 2FF, since fucosyltransferase and sialyltransferase can compete for the same terminal structure as an accepted substrate²⁹. These results clearly demonstrated that fucosylation, particularly core fucosylation, is down-regulated via 2FF treatment to HepG2 cells.

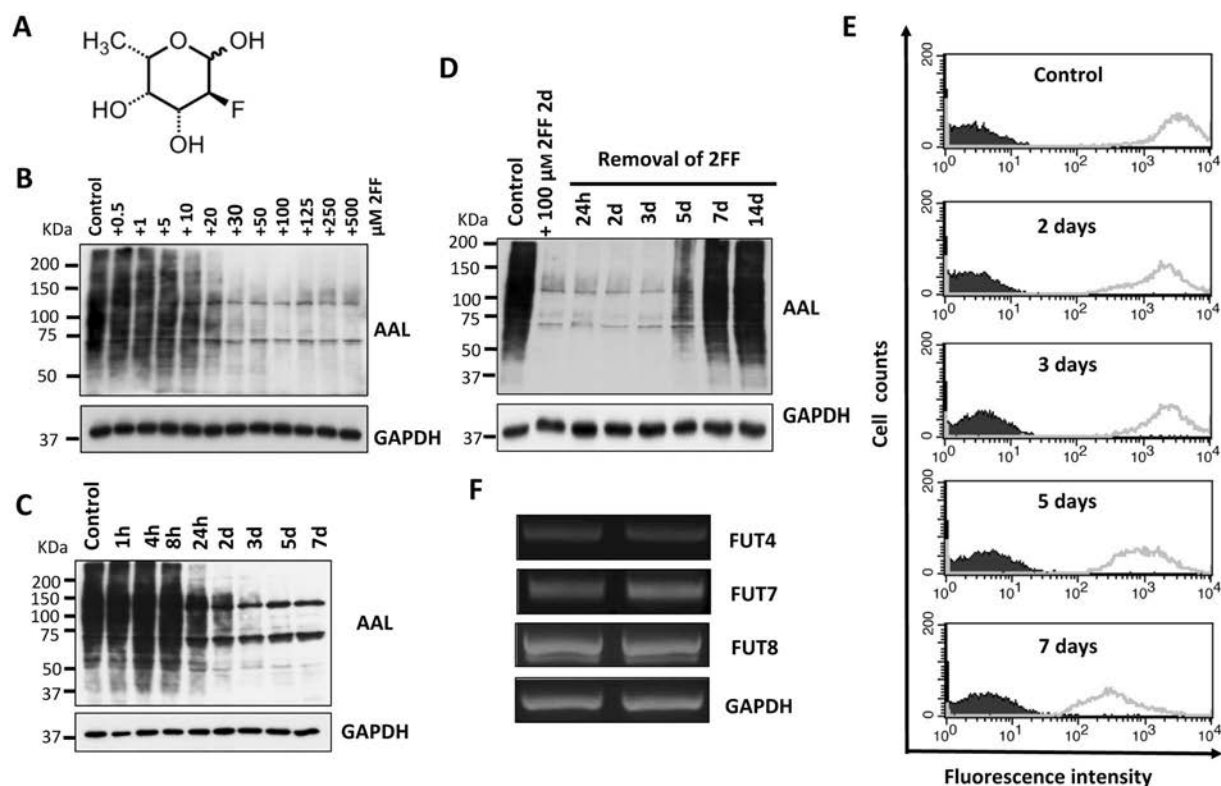


Figure 1. Treatment with 2FF suppressed fucosylation on glycoproteins. (A) The structure of 2FF as previously described²⁹. (B) HepG2 cells were cultured with 2FF for 3 days at different concentrations, as indicated. Cell lysates were prepared, and then subjected to lectin blot analysis using AAL, which preferentially recognizes core fucose, as described in “Methods”. GAPDH was used as a loading control. Control refers to cells treated with the same amount of DMSO. (C) HepG2 cells were cultured in the presence of 100 μ M 2FF for different time points (0 h–7 days). Equal amounts of proteins were probed with AAL lectin as described above. (D) HepG2 cells were cultured in the presence of 100 μ M 2FF for 2 days, then the culture medium containing 2FF was removed and change into normal culture medium for different time points (24 h, 2d, 3d, 5d, 7d). (E) HepG2 cells were incubated with 100 μ M 2FF at different time points, and then stained with (grey line) or without (dark line) biotin-conjugated AAL followed by streptavidin-conjugate Alexa Fluor 647 and subjected to flow cytometry analysis. (F) RT-PCR was carried out using total RNA extracted from HepG2 cells treated with or without 2FF to detect the expression level of representative genes involved in fucosylation. The expression level of GAPDH was examined as a loading control. The relative mRNA levels were normalized with the GAPDH control gene.

Treatment with 2FF inhibited cell proliferation and colony formation. In consideration of the importance of core fucosylation in physiological and pathological functions^{11, 12, 35}, we speculated a potential role for 2FF in the regulation of cell proliferation. To test this hypothesis, we investigated the proliferation of HepG2 cells, which were pre-treated with or without 2FF for 3 days followed by 24 h serum-starvation. As shown in Fig. 3A, cell proliferation was significantly suppressed following treatment with 2FF, compared with control cells without 2FF treatment (Fig. 3A). There was no significant difference in cell viabilities between the control and 2FF-treated cells (data not shown). This phenomenon was also observed in Hela cells (Fig. 3D). The ability to grow in an anchorage-independent manner has always been regarded as one of the hallmarks of cancer, and this ability is believed closely related to cell proliferation and cell-survival signals. Therefore, we performed a clonogenicity study using a soft agar assay. Colony formation abilities were significantly suppressed in the HepG2 cells treated with 2FF, compared with control cells (Fig. 3B). Each colony size treated with 2FF was much smaller than the control without 2FF (Fig. 3C). In contrast, Rillahan, C.D. *et al.*, reported that inhibition of fucosylation in HL-60, Ramos, or CHO-K1 cells did not significantly affect cell proliferation²⁹. These contradictory data could be speculated that the different phenotypes could be due to cell types. Since different cell types differentially express growth factor receptors to control cell proliferation, for example, HepG2 cells highly express EGFR and c-Met, while HL-60 cells and CHO-K1 cells do not express EGFR^{36, 37}. In fact, HL-60 cells abundantly express insulin-like growth factor I receptor (IGF-IR), which may be modified by different glycans compared with those on EGFR, to contribute to the cell growth^{38, 39}. Furthermore, even same receptor may also be modified by different glycans in different cells.

2FF suppressed integrin-mediated cell migration. As described above, 2FF treatment had a major impact on cell growth. Then, we used a transwell assay to examine the migratory ability of HepG2 cells following 2FF treatment. As shown in Fig. 4A, the integrin-mediated cell migration was significantly inhibited in

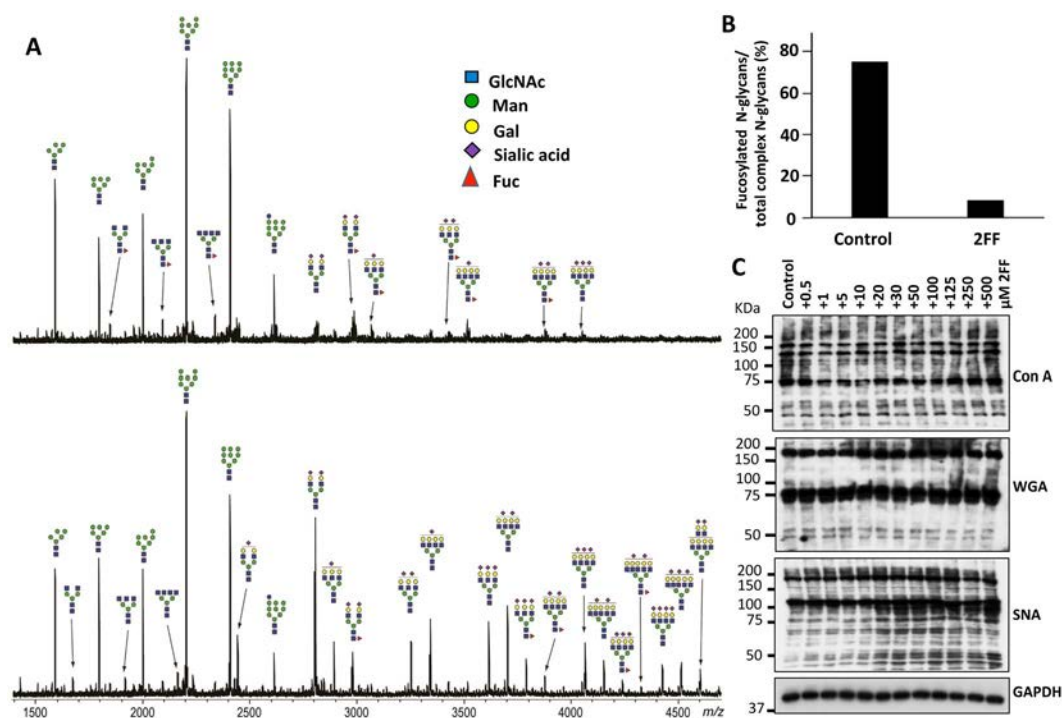


Figure 2. Comparison of N-glycan profiles in HepG2 cells treated with and without 2FF. (A) MS spectrum of the permethylated glycans from the cells treated with DMSO only (upper) and DMSO containing 2FF (lower). (B) Percentages of fucosylated complex glycans in total complex glycans from HepG2 cells. The values were calculated from peak areas in the range of m/z 1,500–3,500 of the MS spectra. (C) HepG2 cells were cultured with 2FF for 3 days at different concentrations as indicated, and then equal amounts of cell lysates were probed with Con A, which specifically recognizes alpha-linked mannose and glucose; WGA, which selectively binds to N-Acetyl glucosamine (GlcNAc) and SNA, which specifically recognizes α 2, 6 sialylation. GAPDH was used as a loading control.

2FF-treated cells compared with control cells. In a similar manner, the migratory ability that was suppressed by 2FF was also observed in Hela cells (Fig. 4B). Collectively, these data strongly suggested that 2FF could effectively inhibit cell proliferation and cell migration *in vitro*.

2FF inhibited core fucosylation of EGFR and integrin β 1 and the related intracellular signaling. N-Glycosylation is known to be essential for the functional expression of membrane glycoproteins such as EGFR and integrins, and regulates several functions: cell-surface expression, dimerization, endocytosis and specific ligand binding^{40, 41}. Recently, we showed that a loss of core fucosylation via knockout of the Fut8 gene decreased the interaction between EGFR and its ligand, including downstream signaling, which in turn suppressed cell proliferation^{11, 12}. In addition, the deletion of core fucosylation significantly suppressed integrin α 3 β 1-mediated cell migration⁴². Therefore, issues having to do with the down-regulation of cell proliferation and migration were related in these molecules.

First, we performed a pull down assay using the biotinylated PhoSL, which preferentially recognizes core fucosylated N-glycans, to examine the effect of 2FF on the core fucosylation of EGFR and integrin β 1⁴³. As shown in Fig. 5A, core fucosylation was expressed on EGFR (upper panel) and integrin β 1 (lower panel) in the control cells, but not in the 2FF-treated HepG2 cells, suggesting that 2FF efficiently blocked core fucosylation in these membrane proteins. Then, we asked whether 2FF affected intracellular signaling. To address this point, we examined the expression levels of phospho-EGFR and its downstream signaling such as phospho-AKT and phospho-ERK, as well as integrin's downstream signal phospho-FAK. Interestingly, all of these signals were suppressed in the 2FF-treated HepG2 cells, compared with the control cells (Fig. 5B). Based on these observations, it is not difficult to conclude that the decreased core fucosylation by 2FF might impair the biological functions of some important membrane receptors such as EGFR and integrin β 1, which subsequently inhibits intracellular signaling.

Inhibitory effects of 2FF on tumorigenesis and core fucosylation *in vivo*. Based on the inhibitory effects of 2FF on malignant phenotypes observed *in vitro*, we used a well-established xenograft tumor model to further examine the tumorigenicity of HepG2 cells *in vivo*. The same amounts of control and 2FF pre-treated HepG2 cells (4×10^6) were injected subcutaneously into the left and right flanks of each mouse, respectively. Based on the inhibitory effect of 2FF on fucosylation that lasted for 7 days at least (Fig. 1C); 100 μ l of the DMEM solution containing with 2FF at 100 μ M were directly injected into each tumor tissue from three directions after the inoculation for 7 days, and once a week for 3 weeks. All the mice were euthanized at 25 days after the first injection of 2FF. Tumor tissues were isolated, photographed and then weighed. Interestingly, significant decreases

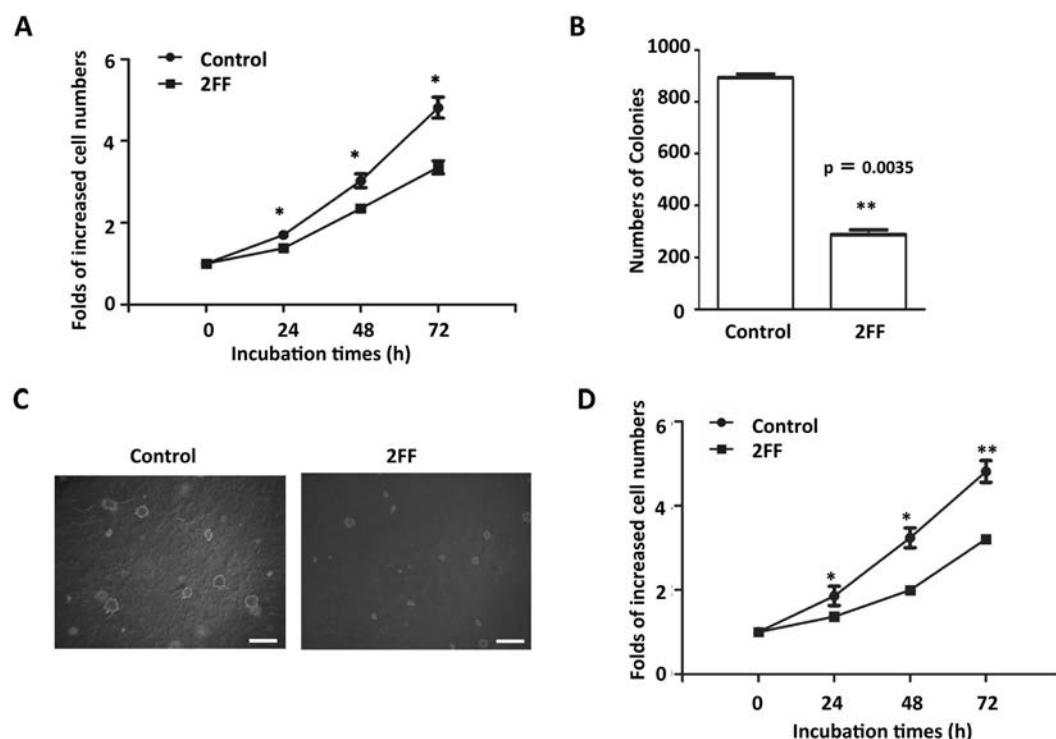


Figure 3. Effects of 2FF treatment on cell proliferation. HepG2 and Hela cells were pre-treated with or without 100 μ M 2FF for 3 days and then starved for 24 h and replaced with DMEM containing 3% FBS to assay cell proliferation. **(A)** The pre-treated cells were incubated in 2FF containing medium for another 4 days. The time point at the replacement was deemed as 0 h. Cells at the same areas were photographed and counted every 24 h. The results are shown as fold changes relative to the numbers of those at 0 h, and presented as the mean \pm s.e.m. (* p < 0.05 by t-test). **(B)** Soft agars were prepared as described in the “Methods”. Controls and 2FF-treated HepG2 cells (5,000 per/well) were cultured on the soft agar for 3 weeks. The colonies that formed were stained with crystal violet. The stained colonies were counted (** p < 0.01 by t-test). Three independent experiments were performed. **(C)** Representative images showed different sizes of colonies treated with or without 2FF. Scale bars indicate 500 μ m. **(D)** Pre-treated Hela cells were incubated in 2FF containing medium for another 4 days. The time point at the replacement was deemed as 0 h. Cells were photographed at the same areas and counted every 24 h. The results are shown as fold changes relative to the numbers of those at 0 h, and presented as the mean \pm s.e.m. (* p < 0.05 by t-test, ** p < 0.01 by t-test).

were noted in both the size (Fig. 6A,B) and weight (Fig. 6C) of tumor tissues in the 2FF-treated side, compared with the control side 25 days after inoculation. The time course of tumor growth also clearly showed the inhibitory effects of 2FF on tumor formation (Fig. 6D). Furthermore, AAL lectin blot showed that the levels of core fucosylation were apparently decreased in the tumor tissues that grew from the HepG2 cells treated with 2FF, compared with the controls (Fig. 6E). Importantly, in accordance with the results *in vitro* (Fig. 5), the cellular signals including p-EGFR, p-AKT, p-ERK and p-FAK in the 2FF-treated tumor tissues were decreased compared with those in the controls treated without 2FF (Fig. 6F). These results addressed the efficient effects of 2FF *in vivo*.

Discussion

Liver cancer ranks as the second leading cause of death from cancer⁴⁴. Effective therapy for liver cancer remains one of the biggest challenges for public health⁴⁵. Increased levels of core fucosylation, usually higher expressions of either Fut8 or GDP-fucose, have lately been recognized as reliable indicators for liver cancer³. Therefore, regulation of the core fucosylation of *N*-glycans can serve as an essential strategy for liver cancer therapy. For example, knockout of the Fut8 gene in mice strongly suppressed a chemical-induced hepatocellular carcinoma¹². Also, down regulation of the Fut8 expression by miRNAs inhibited the progression of liver cancer³⁵. In addition, an abrogation of ability to form or transport GDP-fucose was also worked⁹. Those findings prompted us to investigate whether there is a pharmacological approach that could block core fucosylation in liver cancer cells.

In this study, we used the easily handled 2FF, an analog of fucose, to inhibit GDP-fucose formation. Considered a universal inhibitor of fucosylation, 2FF is used to reduce cell-surface fucosylated glycans such as Lewis antigens and core fucosylated *N*-glycans²⁹. Our results, as determined by western blot and flow cytometry in liver cancer cells, also confirmed this conclusion (Fig. 1B–E). The inhibitory effects on fucosylated glycans did not seem to be due to an inhibition of the expression levels of fucosyltransferases, since there were no significant changes between cells treated with or without 2FF in the mRNA levels of typical fucosylation-related genes such as Fut4, Fut7 and Fut8, which produce Lewis X (Le^x) or sialyl Lewis X (SLe^x) and core fucosylated *N*-glycans, respectively (Fig. 1F). Surprisingly, changes in the *N*-glycan structures analyzed by mass spectrometry have shown that the

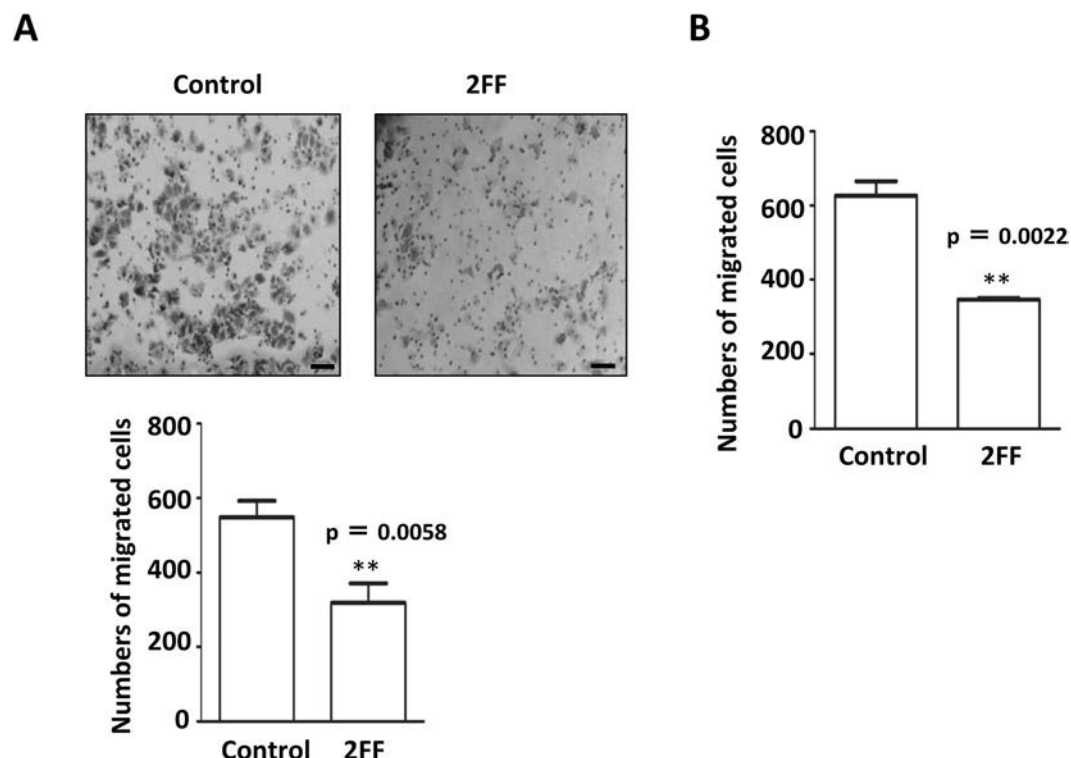


Figure 4. Effects of 2FF treatment on integrin-mediated cell migration. **(A)** The migration abilities of HepG2 cells toward FN were detected by transwell assay as described in “Methods”. HepG2 cells pre-treated with and without 2FF for 3 days were seeded into the top chambers of a transwell. After incubation for 24 h, the migrated cells were fixed and stained with 0.5% crystal violet. Representative images of the bottom surface were captured using phase-contrast microscopy (upper). The numbers of migrated cells in nine random microscopic fields ($\times 200$) were counted and averaged. Data represent the mean \pm s.e.m. of three independent experiments (lower) (** $p < 0.01$ by t-test). Scale bars indicate 50 μ m. **(B)** The migration abilities of Hela cells toward FN were detected. Hela cells pre-treated with or without 2FF for 3 days were seeded into the top chambers of the transwell, and incubated for 4 h. The migrated cells were calculated as described above. Data represented the mean \pm s.e.m. of three independent experiments (** $p < 0.01$ by t-test).

majority of fucosylation in HepG2 cells is core fucosylation, while $\alpha 1,2$; $\alpha 1,3$ or $\alpha 1,4$ fucosylated *N*-glycans were at undetectable levels (Fig. 2). However, unexpectedly, sialylation levels seemed to be enhanced in the 2FF-treated cells (Fig. 2). It could be partly explained by that fucosyltransferases and sialyltransferases may compete for the same terminal glycan structures as an accepted substrate²⁹. In fact, Rillahan, *et al.* reported that a treatment with the sialylation inhibitor resulted in a complete loss of sialic acids and a notable increase in overall fucosylation. Conversely, knockout of Fut9, a key enzyme for the synthesis of Le^x or SLe^x, resulted in an increase in sialylation⁴⁶. The detailed molecular mechanisms are required for further study. Thus, it is not difficult to speculate that the effects of 2FF in HepG2 cells share similar phenomena as observed in Fut8 deficient liver cells. As expected, the treatment with 2FF significantly suppressed cell proliferation and colony formation (Fig. 3)^{11,12}. Alterations of glycans can have a significant impact on cell proliferation, migration and invasion, all of which contribute to the transformation progress and subsequent metastasis of malignancy^{47–49}. In order to further understand the link between 2FF-induced core fucosylation deficiency and cellular progression, we examined cell migration, and found that 2FF inhibits integrin-mediated cell migration (Fig. 4). These results clearly indicated that 2FF effectively suppresses both cell proliferation and cell migration.

Previously, we reported that core fucosylation was required for the binding of EGF to a receptor and for the regulation of EGFR-mediated intracellular signaling in embryonic fibroblast cells⁵⁰. In addition, the attenuated EGFR-mediated signaling was confirmed in Fut8 knockout HepG2 cells¹². Conversely, the incorporation of core fucose by Fut8 promoted EGFR dimerization and phosphorylation in lung cancer cells⁵¹. Furthermore, *N*-glycosylation is now known as a critical determinant of EGFR conformation, and specifically the orientation of the EGFR ectodomain relative to the membrane⁵². In agreement with these observations, this study showed that treatment with 2FF also decreased the levels of phospho-EGFR and downstream signaling such as phospho-ERK and phospho-AKT (Fig. 5B). It is reasonable to conclude that the inhibitory effect of 2FF on cell proliferation can at least be partially mediated via attenuated EGFR-mediated signaling. On the other hand, integrins are known to associate with EGFR in order to cooperatively regulate cell proliferation, migration, differentiation and survival in fibroblasts and epithelial cells⁵³. Also, with EGFR they share some of the elements in signal pathways such as AKT and ERK⁵⁴. Among the various types of integrins, integrin $\beta 1$ plays crucial roles in cell migration and adhesion^{55–57}. A knockout of $\beta 1$ has sufficiently inhibited cell migration and affected the EGFR-mediated cell

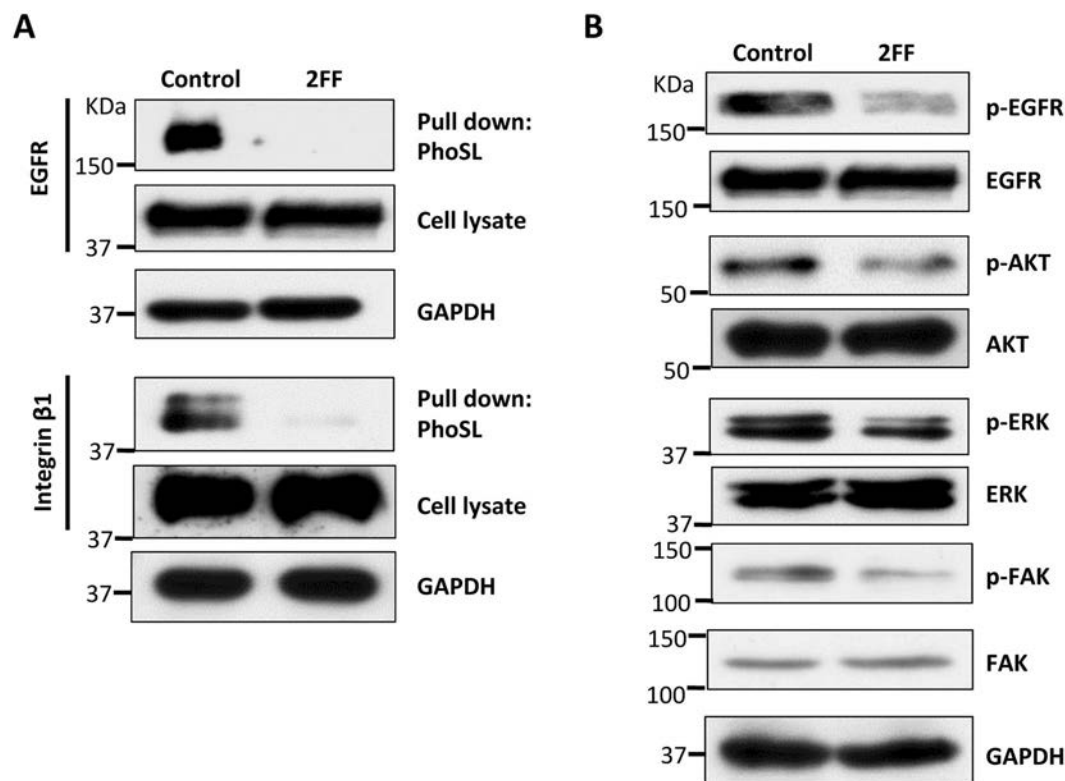


Figure 5. Treatment with 2FF suppressed core fucosylation on EGFR and integrin $\beta 1$, as well as down stream signaling. HepG2 cells were cultured with and without (control) 2FF for 3 days, and harvested for lectin pull down assay or immunoblotting as described in “Methods”. (A) The cell lysates were pooled and incubated with 10 μ l of indicated bead-bound PhoSL, which specifically recognizes core fucose. The lectin precipitated samples and equal amounts of cell lysates were then subjected to SDS-PAGE, and probed with anti-EGFR (upper panel) and anti-integrin $\beta 1$ (lower panel) antibodies. GAPDH were used as a loading control. (B) Cell lysates were immunoblotted with anti-phospho-EGFR, anti-EGFR, anti-phospho-AKT, anti-AKT, anti-phospho-ERK1/2, anti-ERK1/2, anti-phospho-FAK, and anti-FAK antibodies, respectively. GAPDH was used as a loading control.

proliferation in a cell density-dependent manner in MDA-MB231 breast cancer cells⁵⁸. In the present study, 2FF suppressed cell migration and the attenuated integrin-mediated specific downstream signaling of phospho-FAK (Fig. 5B), which is responsible for integrin-mediated cell migration^{59,60}. In fact, we previously reported that deletion of Fut8 significantly suppressed integrin $\alpha 3\beta 1$ -mediated cell migration⁴². Nonetheless, we cannot exclude the possibility that 2FF may influence the functions of other glycoproteins, since core fucose widely exists on the surfaces of cells.

It was also worth noting that although we addressed the importance of core fucosylation in cell behaviors since 2FF mainly inhibited core fucosylation in HepG2 cells, we could not conclude that other fucosylations expressed at marginal levels were unimportant. Previous studies have shown that oral administration of 2FF inhibits neutrophil extravasation *via* the suppression of Lewis antigen expression and delays tumor growth in immune deficient mice³¹. In order to further address the effects of 2FF *in vivo*, we subcutaneously inoculated HepG2 cells pretreated with 2FF (intratumoral administration before treatment) into nude mice. After tumors were formed, 2FF solutions were directly injected into each tumor tissue. Consistently, treatment with 2FF prevented tumorigenesis as well as core fucosylation *in vivo* (Fig. 6). These data strongly suggested that the chemical compound 2FF is easy to handle and exerts a potential inhibitory effect on tumor growth.

In addition, we also cannot exclude the potential effects on sialylation. As described above, sialylation and fucosylation can be regulated mutually. However, the phenomenon, an increase in sialylation in the 2FF-treated cells, observed in the present study could not be simply explained by mutual regulation. The increased sialylation may associate with some unknown mechanisms, and could also influences cell biological functions, which requires further study. In fact, an aberrant expression of sialylation has long been associated with metastatic cell behaviors such as invasion and enhanced cell survival, and the increased $\alpha 2,6$ sialylation on *N*-glycans catalyzed by β -galactoside $\alpha 2,6$ sialyltransferase 1 (ST6Gal I) is frequently observed in many types of the cancers^{61,62}.

In summary, our study provided evidence that 2FF inhibited core fucosylation in the HepG2 cells of cell-surface glycoproteins, which in turn inhibited cellular signaling for cell proliferation and migration as well as for tumor growth. We believe that 2FF shows promise as a therapeutic compound for hepatoma and other cancers.

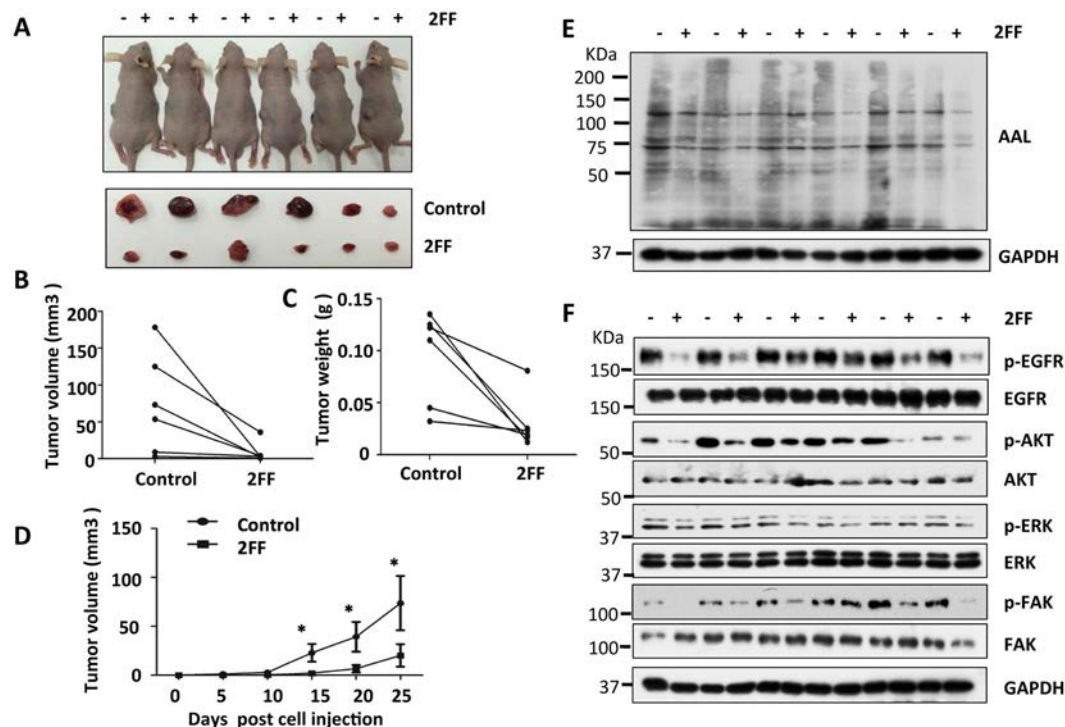


Figure 6. Effects of 2FF on tumor growth and fucosylation *in vivo*. HepG2 cells (4×10^6) were inoculated into both the left (control cells, -) and right posterior flanks (2FF-treated cells, +) of nude BALB/c-nu mice as described in “Methods”. (A) Photographs illustrate the representative features of tumor growth 25 days after injection (upper panel), and each corresponding pair of dissected tumor tissues (lower panel). Changes in each of the corresponding pair of tumor volumes (B) and weights (C) were also measured. (D) Tumor growth curves were measured every 5 days ($n = 6$, $*p < 0.05$ by t-test). (E) Tumor tissues were homogenized and lysates were blotted with AAL lectin. GAPDH was used as a loading control. (F) The lysates from tumor tissues were immunoblotted with anti-phospho-EGFR, anti-EGFR, anti-phospho-AKT, anti-AKT, anti-phospho-ERK1/2, anti-ERK1/2, anti-phospho-FAK, and anti-FAK antibodies, respectively. GAPDH was used as a loading control.

Methods

Antibodies and reagents. Experiments were performed using the following antibodies: Rabbit antibodies against EGFR, p-EGFR, AKT, p-AKT, ERK1/2, and p-ERK1/2 were purchased from Cell Signaling Technology (Danvers, MA, USA); Mouse antibodies against integrin $\beta 1$, FAK and p-FAK were purchased from BD Biosciences (Franklin Lakes, NJ, USA); Rabbit antibody against glyceraldehyde-3-phosphate dehydrogenase (GAPDH) was purchased from Santa Cruz Biotechnology (Santa Cruz, CA, USA). Peroxidase-conjugated goat antibodies against rabbit and mouse IgG were obtained from Cell Signaling Technology and Promega, respectively. Biotinylated *aleuria aurantia lectin* (AAL), *concanavalin A* (ConA) and *wheat germ agglutinin* (WGA) were purchased from Seikagaku Crop (Tokyo, Japan). Biotinylated Pholiota Squarrosa lectin (PhoSL), which specifically recognizes core fucosylated N-glycans, was a generous gift from Dr. Yuka Kobayashi (J-oil Mills, Tokyo, Japan). Alexa Fluor® 647 goat anti-mouse secondary antibody and fetal bovine serum (FBS) were purchased from Invitrogen (Life Technologies). 2FF was purchased from Synchem, Inc., IL, USA. Fibronectin (FN) and dimethyl sulfoxide (DMSO) were obtained from sigma (St. Louis, MO, USA); and, Dulbecco's modified Eagle's medium (DMEM) was purchased from Gibco (Grand Island, NY, USA).

Cell culture and treatment. Human hepatoma HepG2 and Hela cell lines were purchased from the RIKEN cell bank (Japan). Cells were cultured in DMEM containing 10% FBS and incubated at 37°C in a humidified atmosphere with 5% CO_2 . The cells were incubated with and without 2FF dissolved in DMSO for indicated times. The final concentrations of 2FF were diluted with culture media at $0.5\sim 500\mu\text{M}$. The same amounts of DMSO were used as controls.

Western blot and lectin blot assay. Cells cultured in the presence or absence of 2FF under different conditions, as indicated, were harvested, washed by cold PBS and then scraped off culture plates with lysis buffer containing 20 mM Tris-HCl (pH = 7.4), 1% Triton X-100, 150 mM NaCl, and protease and phosphatase inhibitors (Nacalai Tesque). After incubation for 15 min at 4°C , cell debris were removed by centrifugation for 10 min at 13,000 g. Protein concentrations were measured using a BCA protein assay kit (Pierce). Equal amounts for each sample were run on 6, 7.5 or 10% SDS-PAGE gels, as indicated.

For the pull-down assay, $500\mu\text{g}$ of cell lysates were collected and incubated with $10\mu\text{L}$ FG streptavidin beads (Tamagawa Seiki Co., Tokyo, Japan) and $2\mu\text{g}$ biotinylated PhoSL for 2 h at 4°C . The precipitates were then washed

by cold lysis buffer and boiled in SDS loading buffer. Resolved proteins were then transferred onto a PVDF membrane (Millipore) for detection.

For Western blot assay, the membranes were blocked with 5% skim milk in TBS containing 0.1% Tween-20 (TBST) for 1 h at room temperature (RT) and then probed with specific antibodies at 4 °C overnight. Detection was achieved using secondary HRP-conjugated IgG against rabbit or mouse IgG and finally visualized using the ECL system (Amersham).

For lectin blot assay, the membranes were blocked with 3% bovine serum albumin (BSA) in TBST followed by specific lectins. The bands were finally visualized using a Vectastain ABC Kit (Vector Laboratories).

RT-PCR. Total RNAs of HepG2 cells treated with and without 2FF were extracted by Trizol reagent (Invitrogen). 1 µg of total RNAs were reverse-transcribed using a Prime Script RT Reagent kit with gDNA Eraser (Takara, Japan). The specific primers used for the PCR amplification were as follows: Fut4, forward, 5'-ACTACCACCAACTGAGCCAACATGTGA-3', reverse, 5'-AAGGAGGTGATGTGGACAGCGTAG-3';

Fut7, forward, 5'-AGTACCGCTTCTACCTGTCCTTTGAGAA-3', reverse, 5'-AGCCTGTCACGCCAGGCAAAGAA-3'; and, Fut8, forward, 5'-CACTTGGTACGAGATAATGAC-3', reverse, 5'-CACATGATGGAGCTGACAGCC-3'. The GAPDH mRNA served as the control. The obtained reaction products were then placed into 2% agarose gels containing ethidium bromide for electrophoresis.

Flow cytometry analysis. Cells were harvested and adjusted to a concentration of $1-5 \times 10^6$ cells/mL in cold PBS. Then cells were stained with biotinylated AAL for 1 h on ice, followed by streptavidin-conjugate Alexa Fluor 647 for 1 h in the dark on ice. A negative control was prepared without AAL. After incubation, cells were washed 3 times with ice-cold PBS, and then analyzed using a FACSCalibur flow cytometer (BD Biosciences).

Mass spectrometry. Membrane fractions of cells were prepared as described previously⁶³. Pellets were dissolved in 100 µL of 0.1 M Tris-HCl (pH = 8.6), then 20 µL of 200 mM DTT in 1 M Tris-HCl (pH = 8.6) containing 1% SDS was added with heating to 80 °C for 10 min. After cooling to RT, 40 µL of 5% Nonidet P-40 and 15 µL of distilled water were added to the mixture. Glycopeptidase F (16 mU, Takara Bio Inc.), an amidohydrolase that removes intact N-glycans from glycoproteins, was added to the solution, which was then incubated at 37 °C for 16 h. After the addition of 234 µL of ethanol to the solution, the mixtures were cooled to −20 °C and kept in a freezer for 20 min followed by centrifugation at 15,000 rpm for 20 min. Supernatants were transferred into new microtubes and dried via a centrifuge evaporator. The residues were dissolved in 200 µL of water, and then loaded onto a solid-phase extraction cartridge (Sep-Pak C18, 50 mg, Waters Corp) and washed with 1 mL water. The flow-through and washings were combined and applied to a HyperSep Hypercarb SPE cartridge (25 mg). After washing with 1 mL water and then with 1 mL 0.1% TFA, glycans were eluted with 1 mL of 50% acetonitrile containing 0.1% TFA. The eluted solution was dried *in vacuo*, and then permethylated as described previously⁶³. Mass spectrometry was performed using a MALDI-TOF mass spectrometer (Ultraflex). Ions were generated using a 337-nm nitrogen laser and were accelerated to 20 kV. All spectra were obtained with a delayed extraction of 140 ns in a reflectron mode, and were the result of a signal averaging of 300 laser shots. For sample preparation, 2, 5-dihydroxybenzoic acid was used as a matrix.

Cell growth assay. HepG2 and Hela cells were pre-treated with or without 2FF at a final concentration of 100 µM for 3 days followed by 24 h serum-starvation. Then, 3×10^3 cells were then seeded into 6-cm dishes and cultured under 3% FBS media with or without 100 µM 2FF. Cells were photographed in the same area when the indicated times were reached. Cell numbers at each time point were counted and normalized to those at 0 h when the cell culture media were replaced with 3% FBS.

Soft agar assay. A total of 1 mL 0.5% base agar in complete culture medium was added into each 6-cm dish and set aside for 5 min to allow the agars to solidify. The pre-treated cells described above were then mixed with the 0.33% agarose (5,000 cells/mL) and layered onto the base agar. Agar dishes were incubated at 37 °C and fed with complete culture medium. Culture media were changed every 4–5 days. Three weeks later, agar dishes were stained with 0.005% crystal violet overnight. The colony numbers were counted from three independent plates. Representative photographs were taken.

Transwell cell migration assays. Cell migration assays were performed using a transwell chamber (BD BioCoat™ control inserts, 8.0-mm inserts; BD Biosciences) according to the manufacturer's instructions. Briefly, the bottom sides of transwells were coated with 10 µg/mL fibronectin (FN) and let stand at 4 °C overnight. Cells were harvested by trypsin containing 1 mM EDTA and re-suspended in the serum-free DMEM medium at a concentration of 1×10^5 cells/mL for HepG2 and 4×10^4 cells/mL for Hela. Then, 500 µL of suspension was added to the upper chamber and cells were allowed to migrate to the lower chamber containing 500 µL complete medium at 37 °C. At the end of the cell migration, the filter side of the upper chamber was cleaned using cotton swabs and the migrated cells located at the reverse side of the chamber were fixed in 4% paraformaldehyde. After being washed with PBS, cells were stained with crystal violet and let stand overnight. Cells that migrated across the filters were counted using a phase-contrast microscope, and the values were averaged.

Xenograft assay. Four-week old male BALB/c-nu mice were obtained from Charles River Laboratories, Japan, and acclimated for one week. Mice were raised in 22 ± 3 °C with saturated humidity and a standard light/dark cycle. Plenty of food and water was guaranteed.

The same amounts of control and 2FF pre-treated HepG2 cells (4×10^6) were injected subcutaneously into the left and right flanks of each mouse, respectively. Based on the inhibitory effect of 2FF on fucosylation lasted for 7 days at least (Fig. 1C), 100 µL of the DMEM solution containing with 2FF at 100 µM were directly injected into

each tumor tissue from three directions after the inoculation for 7 days, and once a week for 3 weeks. All the mice were euthanized at 25 days after the first injection of 2FF. Tumor tissues were isolated, photographed and then weighed. And the same amounts of tumor tissues were homogenized for lectin blot with AAL and Western blot with several indicated antibodies. Measurement of tumor sizes began on the fifth day, and sizes were monitored every 5 days by measuring the tumor length and width with a vernier caliper. Tumor volumes were estimated according to the following formula: volume (mm^3) = $(L \times W^2)/2$, where L and W are the length and width of the tumor tissues. All experiments were performed according to protocols approved by the Tohoku Medical and Pharmaceutical University Research Ethics Board.

Statistical analysis. Statistical analyses were performed using a student's t-test with GraphPad Prism5 software. Results were presented as the mean \pm s.e.m. Statistical significance was accepted at $p < 0.05$. All experiments were repeated at least three times.

References

- Agard, N. J. & Bertozzi, C. R. Chemical approaches to perturb, profile, and perceive glycans. *Acc Chem Res* **42**, 788–797, <https://doi.org/10.1021/ar800267j> (2009).
- Kiessling, L. L. & Splain, R. A. Chemical approaches to glycobiology. *Annu Rev Biochem* **79**, 619–653, <https://doi.org/10.1146/annurev.biochem.77.070606.100917> (2010).
- Miyoshi, E. *et al.* Fucosylation is a promising target for cancer diagnosis and therapy. *Biomolecules* **2**, 34–45, <https://doi.org/10.3390/biom2010034> (2012).
- Vajaria, B. N. & Patel, P. S. Glycosylation: a hallmark of cancer? *Glycoconjugate journal* **34**, 147–156, <https://doi.org/10.1007/s10719-016-9755-2> (2017).
- Miyoshi, E. *et al.* The alpha1-6-fucosyltransferase gene and its biological significance. *Biochim Biophys Acta* **1473**, 9–20 (1999).
- Breborowicz, J., Mackiewicz, A. & Breborowicz, D. Microheterogeneity of alpha-fetoprotein in patient serum as demonstrated by lectin affinity-electrophoresis. *Scand J Immunol* **14**, 15–20 (1981).
- Zhang, Y. *et al.* ESI-LC-MS Method for Haptoglobin Fucosylation Analysis in Hepatocellular Carcinoma and Liver Cirrhosis. *Journal of proteome research* **14**, 5388–5395, <https://doi.org/10.1021/acs.jproteome.5b00792> (2015).
- Nie, H. *et al.* Specific N-glycans of Hepatocellular Carcinoma Cell Surface and the Abnormal Increase of Core-alpha-1, 6-fucosylated Triantennary Glycan via N-acetylglucosaminyltransferases-IVa Regulation. *Sci Rep* **5**, 16007, <https://doi.org/10.1038/srep16007> (2015).
- Mehta, A., Herrera, H. & Block, T. Glycosylation and liver cancer. *Advances in cancer research* **126**, 257–279, <https://doi.org/10.1016/b.sacr.2014.11.005> (2015).
- Yamashita, F., Tanaka, M., Satomura, S. & Tanikawa, K. Prognostic significance of Lens culinaris agglutinin A-reactive alpha-fetoprotein in small hepatocellular carcinomas. *Gastroenterology* **111**, 996–1001 (1996).
- Wang, Y. *et al.* Loss of alpha1,6-fucosyltransferase suppressed liver regeneration: implication of core fucose in the regulation of growth factor receptor-mediated cellular signaling. *Sci Rep* **5**, 8264, <https://doi.org/10.1038/srep08264> (2015).
- Wang, Y. *et al.* Loss of alpha1,6-fucosyltransferase inhibits chemical-induced hepatocellular carcinoma and tumorigenesis by down-regulating several cell signaling pathways. *FASEB J* **29**, 3217–3227, <https://doi.org/10.1096/fj.15-270710> (2015).
- Tonetti, M. *et al.* The metabolism of 6-deoxyhexoses in bacterial and animal cells. *Biochimie* **80**, 923–931 (1998).
- Miyoshi, E., Moriwaki, K. & Nakagawa, T. Biological function of fucosylation in cancer biology. *J Biochem* **143**, 725–729, <https://doi.org/10.1093/jb/mvn011> (2008).
- Tonetti, M., Sturla, L., Bisso, A., Benatti, U. & De Flora, A. Synthesis of GDP-L-fucose by the human FX protein. *The Journal of biological chemistry* **271**, 27274–27279 (1996).
- Ohshima, C. *et al.* Molecular cloning and expression of GDP-D-mannose-4,6-dehydratase, a key enzyme for fucose metabolism defective in Lec13 cells. *The Journal of biological chemistry* **273**, 14582–14587 (1998).
- Sullivan, F. X. *et al.* Molecular cloning of human GDP-mannose 4,6-dehydratase and reconstitution of GDP-fucose biosynthesis *in vitro*. *The Journal of biological chemistry* **273**, 8193–8202 (1998).
- Coffey, J. W., Miller, O. N. & Sellinger, O. Z. The Metabolism of L-Fucose in the Rat. *The Journal of biological chemistry* **239**, 4011–4017 (1964).
- Kaufman, R. L. & Ginsburg, V. The metabolism of L-fucose by HeLa cells. *Exp Cell Res* **50**, 127–132 (1968).
- Becker, D. J. & Lowe, J. B. Fucose: biosynthesis and biological function in mammals. *Glycobiology* **13**, 41R–53R, <https://doi.org/10.1093/glycob/cwg054> (2003).
- Nakayama, K. *et al.* Mutation of GDP-mannose-4,6-dehydratase in colorectal cancer metastasis. *PLoS One* **8**, e70298, <https://doi.org/10.1371/journal.pone.0070298> (2013).
- Louie, S. *et al.* FX knockout CHO hosts can express desired ratios of fucosylated or afucosylated antibodies with high titers and comparable product quality. *Biotechnol Bioeng* **114**, 632–644, <https://doi.org/10.1002/bit.26188> (2017).
- Moriwaki, K. *et al.* Deficiency of GMDS leads to escape from NK cell-mediated tumor surveillance through modulation of TRAIL signaling. *Gastroenterology* **137**(188–198), 198 e181–182, <https://doi.org/10.1053/j.gastro.2009.04.002> (2009).
- Moriwaki, K., Shinzaki, S. & Miyoshi, E. GDP-mannose-4,6-dehydratase (GMDS) deficiency renders colon cancer cells resistant to tumor necrosis factor-related apoptosis-inducing ligand (TRAIL) receptor- and CD95-mediated apoptosis by inhibiting complex II formation. *The Journal of biological chemistry* **286**, 43123–43133, <https://doi.org/10.1074/jbc.M111.262741> (2011).
- Sturla, L. *et al.* Impairment of the Golgi GDP-L-fucose transport and unresponsiveness to fucose replacement therapy in LAD II patients. *Pediatr Res* **49**, 537–542, <https://doi.org/10.1203/00006450-200104000-00016> (2001).
- Gloster, T. M. & Vocadlo, D. J. Developing inhibitors of glycan processing enzymes as tools for enabling glycobiology. *Nature chemical biology* **8**, 683–694, <https://doi.org/10.1038/nchembio.1029> (2012).
- Manabe, Y. *et al.* Development of alpha1,6-fucosyltransferase inhibitors through the diversity-oriented syntheses of GDP-fucose mimics using the coupling between alkyne and sulfonyl azide. *Bioorganic & medicinal chemistry* **25**, 2844–2850, <https://doi.org/10.1016/j.bmc.2017.02.036> (2017).
- Tu, Z., Lin, Y. N. & Lin, C. H. Development of fucosyltransferase and fucosidase inhibitors. *Chemical Society reviews* **42**, 4459–4475, <https://doi.org/10.1039/c3cs60056d> (2013).
- Rillahan, C. D. *et al.* Global metabolic inhibitors of sialyl- and fucosyltransferases remodel the glycome. *Nature chemical biology* **8**, 661–668, <https://doi.org/10.1038/nchembio.999> (2012).
- Okeley, N. M. *et al.* Development of orally active inhibitors of protein and cellular fucosylation. *Proc Natl Acad Sci USA* **110**, 5404–5409, <https://doi.org/10.1073/pnas.1222263110> (2013).
- Belcher, J. D. *et al.* The fucosylation inhibitor, 2-fluorofucose, inhibits vaso-occlusion, leukocyte-endothelium interactions and NF-kB activation in transgenic sickle mice. *PLoS One* **10**, e0117772, <https://doi.org/10.1371/journal.pone.0117772> (2015).
- Villalobos, J. A., Yi, B. R. & Wallace, I. S. 2-Fluoro-L-Fucose Is a Metabolically Incorporated Inhibitor of Plant Cell Wall Polysaccharide Fucosylation. *PLoS One* **10**, e0139091, <https://doi.org/10.1371/journal.pone.0139091> (2015).

33. Dumont, M. *et al.* Inhibition of fucosylation of cell wall components by 2-fluoro-2-deoxy-L-fucose induces defects in root cell elongation. *Plant J* **84**, 1137–1151, <https://doi.org/10.1111/tpj.13071> (2015).
34. Matsumura, K. *et al.* Carbohydrate binding specificity of a fucose-specific lectin from *Aspergillus oryzae*: a novel probe for core fucose. *The Journal of biological chemistry* **282**, 15700–15708, <https://doi.org/10.1074/jbc.M701195200> (2007).
35. Cheng, L. *et al.* Comprehensive N-glycan profiles of hepatocellular carcinoma reveal association of fucosylation with tumor progression and regulation of FUT8 by microRNAs. *Oncotarget* **7**, 61199–61214, <https://doi.org/10.18632/oncotarget.11284> (2016).
36. Chen, L. L. *et al.* Retroviral gene transfer of epidermal growth factor receptor into HL60 cells results in a partial block of retinoic acid-induced granulocytic differentiation. *Cell growth & differentiation: the molecular biology journal of the American Association for Cancer Research* **4**, 769–776 (1993).
37. Jo, M., Thomas, K. S., O'Donnell, D. M. & Gonias, S. L. Epidermal growth factor receptor-dependent and -independent cell-signaling pathways originating from the urokinase receptor. *The Journal of biological chemistry* **278**, 1642–1646, <https://doi.org/10.1074/jbc.M210877200> (2003).
38. Li, Y. M. *et al.* Regulation of myeloid growth and differentiation by the insulin-like growth factor I receptor. *Endocrinology* **138**, 362–368, <https://doi.org/10.1210/endo.138.1.4847> (1997).
39. Sinclair, J., McClain, D. & Taetle, R. Effects of insulin and insulin-like growth factor I on growth of human leukemia cells in serum-free and protein-free medium. *Blood* **72**, 66–72 (1988).
40. Lau, K. S. *et al.* Complex N-glycan number and degree of branching cooperate to regulate cell proliferation and differentiation. *Cell* **129**, 123–134, <https://doi.org/10.1016/j.cell.2007.01.049> (2007).
41. Fernandes, H., Cohen, S. & Bishayee, S. Glycosylation-induced conformational modification positively regulates receptor-receptor association: a study with an aberrant epidermal growth factor receptor (EGFRvIII/DeltaEGFR) expressed in cancer cells. *The Journal of biological chemistry* **276**, 5375–5383, <https://doi.org/10.1074/jbc.M005599200> (2001).
42. Zhao, Y. *et al.* Deletion of core fucosylation on alpha3beta1 integrin down-regulates its functions. *The Journal of biological chemistry* **281**, 38343–38350, <https://doi.org/10.1074/jbc.M608764200> (2006).
43. Kobayashi, Y. *et al.* A novel core fucose-specific lectin from the mushroom *Pholiota squarrosa*. *The Journal of biological chemistry* **287**, 33973–33982, <https://doi.org/10.1074/jbc.M111.327692> (2012).
44. Bosch, F. X., Ribes, J. & Borrás, J. Epidemiology of primary liver cancer. *Seminars in liver disease* **19**, 271–285, <https://doi.org/10.1055/s-2007-1007117> (1999).
45. Sia, D., Villanueva, A., Friedman, S. L. & Llovet, J. M. Liver Cancer Cell of Origin, Molecular Class, and Effects on Patient Prognosis. *Gastroenterology*, doi:<https://doi.org/10.1053/j.gastro.2016.11.048> (2016).
46. Noro, E. *et al.* Large-Scale Identification of N-Glycan Glycoproteins Carrying Lewis x and Site-Specific N-Glycan Alterations in Fut9 Knockout Mice. *Journal of proteome research* **14**, 3823–3834, <https://doi.org/10.1021/acs.jproteome.5b00178> (2015).
47. Vajaria, B. N. & Patel, P. S. Glycosylation: a hallmark of cancer? *Glycoconjugate journal*, doi:<https://doi.org/10.1007/s10719-016-9755-2> (2016).
48. Padler-Karavani, V. Aiming at the sweet side of cancer: aberrant glycosylation as possible target for personalized-medicine. *Cancer Lett* **352**, 102–112, <https://doi.org/10.1016/j.canlet.2013.10.005> (2014).
49. Reis, C. A., Osorio, H., Silva, L., Gomes, C. & David, L. Alterations in glycosylation as biomarkers for cancer detection. *J Clin Pathol* **63**, 322–329, <https://doi.org/10.1136/jcp.2009.071035> (2010).
50. Wang, X. *et al.* Core fucosylation regulates epidermal growth factor receptor-mediated intracellular signaling. *The Journal of biological chemistry* **281**, 2572–2577, <https://doi.org/10.1074/jbc.M510893200> (2006).
51. Liu, Y. C. *et al.* Sialylation and fucosylation of epidermal growth factor receptor suppress its dimerization and activation in lung cancer cells. *Proc Natl Acad Sci USA* **108**, 11332–11337, <https://doi.org/10.1073/pnas.1107385108> (2011).
52. Kaszuba, K. *et al.* N-Glycosylation as determinant of epidermal growth factor receptor conformation in membranes. *Proc Natl Acad Sci USA* **112**, 4334–4339, <https://doi.org/10.1073/pnas.1503262112> (2015).
53. Schwartz, M. A. & Ginsberg, M. H. Networks and crosstalk: integrin signalling spreads. *Nature cell biology* **4**, E65–68, <https://doi.org/10.1038/ncb0402-e65> (2002).
54. Cabodi, S. *et al.* Integrin regulation of epidermal growth factor (EGF) receptor and of EGF-dependent responses. *Biochemical Society transactions* **32**, 438–442, <https://doi.org/10.1042/BST0320438> (2004).
55. Guo, H. B., Lee, I., Kamar, M., Akiyama, S. K. & Pierce, M. Aberrant N-glycosylation of beta1 integrin causes reduced alpha5beta1 integrin clustering and stimulates cell migration. *Cancer research* **62**, 6837–6845 (2002).
56. Seales, E. C. *et al.* Hypersialylation of beta1 integrins, observed in colon adenocarcinoma, may contribute to cancer progression by up-regulating cell motility. *Cancer research* **65**, 4645–4652, <https://doi.org/10.1158/0008-5472.CAN-04-3117> (2005).
57. Isaji, T. *et al.* Introduction of bisecting GlcNAc into integrin alpha5beta1 reduces ligand binding and down-regulates cell adhesion and cell migration. *The Journal of biological chemistry* **279**, 19747–19754, <https://doi.org/10.1074/jbc.M311627200> (2004).
58. Hou, S. *et al.* Distinct effects of beta1 integrin on cell proliferation and cellular signaling in MDA-MB-231 breast cancer cells. *Sci Rep* **6**, 18430, <https://doi.org/10.1038/srep18430> (2016).
59. Sieg, D. J. *et al.* FAK integrates growth-factor and integrin signals to promote cell migration. *Nature cell biology* **2**, 249–256, <https://doi.org/10.1038/35010517> (2000).
60. Mitra, S. K. & Schlaepfer, D. D. Integrin-regulated FAK-Src signaling in normal and cancer cells. *Current opinion in cell biology* **18**, 516–523, <https://doi.org/10.1016/j.ceb.2006.08.011> (2006).
61. Schultz, M. J., Swindall, A. F. & Bellis, S. L. Regulation of the metastatic cell phenotype by sialylated glycans. *Cancer metastasis reviews* **31**, 501–518, <https://doi.org/10.1007/s10555-012-9359-7> (2012).
62. Lu, J. & Gu, J. Significance of beta-Galactoside alpha2,6 Sialyltransferase 1 in Cancers. *Molecules* **20**, 7509–7527, <https://doi.org/10.3390/molecules20057509> (2015).
63. Dong, W., Matsuno, Y. K. & Kameyama, A. A procedure for Alcian blue staining of mucins on polyvinylidene difluoride membranes. *Anal Chem* **84**, 8461–8466, <https://doi.org/10.1021/ac301678z> (2012).

Acknowledgements

This work was partially supported by a Grant-in-Aid for Scientific Research (15H04354 to JG), for Challenging Exploratory Research (15K14408 to JG) from the Japan Society for the Promotion of Science, and by a Strategic Research Foundation Grant-aided Project for Private Universities from the Ministry of Education, Culture, Sports, Science and Technology of Japan.

Author Contributions

Y.Z. performed all the experiments with the help of T.F., Q.H., S.H. and T.I. A.K. performed the mass spectrometry analysis. Y.Z. and T.F. performed the animal experiments. T.F., Q.H., S.H. and J.G. designed the experiment. Y.Z., T.F. and J.G. analyzed the data, prepared the figures and wrote the manuscript. All authors discussed the results and commented on the manuscript.

Additional Information

Supplementary information accompanies this paper at <https://doi.org/10.1038/s41598-017-11911-9>.

Competing Interests: The authors declare that they have no competing interests.

Publisher's note: Springer Nature remains neutral with regard to jurisdictional claims in published maps and institutional affiliations.



Open Access This article is licensed under a Creative Commons Attribution 4.0 International License, which permits use, sharing, adaptation, distribution and reproduction in any medium or format, as long as you give appropriate credit to the original author(s) and the source, provide a link to the Creative Commons license, and indicate if changes were made. The images or other third party material in this article are included in the article's Creative Commons license, unless indicated otherwise in a credit line to the material. If material is not included in the article's Creative Commons license and your intended use is not permitted by statutory regulation or exceeds the permitted use, you will need to obtain permission directly from the copyright holder. To view a copy of this license, visit <http://creativecommons.org/licenses/by/4.0/>.

© The Author(s) 2017

Review

Roles of Integrin $\alpha 6 \beta 4$ Glycosylation in Cancer

Yoshinobu Kariya ^{1,*}, Yukiko Kariya ¹ and Jianguo Gu ^{2,*}

¹ Department of Biochemistry, Fukushima Medical University School of Medicine, 1 Hikarigaoka, Fukushima City, Fukushima 960-1295, Japan; ykk-kari@fmu.ac.jp

² Division of Regulatory Glycobiology, Institute of Molecular Biomembrane and Glycobiology, Tohoku Medical and Pharmaceutical University, 4-4-1 Komatsushima, Aoba-ku, Sendai, Miyagi 981-8558, Japan

* Correspondence: kariya@fmu.ac.jp (Y.K.); jgu@tohoku-mpu.ac.jp (J.G.); Tel.: +81-24-547-1144 (Y.K.); +81-22-727-0216 (J.G.); Fax: +81-24-548-8641 (Y.K.); +81-22-727-0078 (J.G.)

Academic Editor: Helen M. Sheldrake

Received: 30 May 2017; Accepted: 30 June 2017; Published: 5 July 2017

Abstract: Malignant transformation is accompanied with aberrant glycosylation of proteins. Such changes in glycan structure also occur in the integrins, which are a large family of cell surface receptors for the extracellular matrix and play key roles in tumor progression. There is now increasing evidence that glycosylation of integrins affects cellular signaling and interaction with the extracellular matrix, receptor tyrosine kinases, and galectins, thereby regulating cell adhesion, motility, growth, and survival. Integrin $\alpha 6 \beta 4$ is a receptor for laminin-332 and the increased expression level is correlated with malignant progression and poor survival in various types of cancers. Recent studies have revealed that integrin $\alpha 6 \beta 4$ plays central roles in tumorigenesis and the metastatic process. In this review, we summarize our current understanding of the molecular mechanisms of tumor progression driven by integrin $\alpha 6 \beta 4$ and also discuss the modification of glycans on integrin $\beta 4$ subunit to address the important roles of glycan in integrin-mediated tumor progression.

Keywords: integrin; glycosylation; cancer; *N*-acetylglucosaminyltransferase-V (GnT-V); epithelial to mesenchymal transition (EMT); galectin-3

1. Introduction

Integrins are a large family of heterodimeric transmembrane receptors comprising α and β subunits. In mammals, 18 α and 8 β subunits have been characterized, and the combination of them forms 24 distinct integrins. Integrins bind to extracellular matrix proteins including collagen, fibronectin, laminin, osteopontin, and tenascin in the extracellular domain, which leads to the assembly of signaling complexes including focal adhesion kinase, paxillin, and Src in the cytoplasmic domain and the rearrangement of actin cytoskeleton. The transducing signals from integrin receptors to cytoskeletal and adhesive machinery regulate cell adhesion, migration, proliferation, differentiation, and tumor progression.

Of note, integrins are known to be major glycan-carrying proteins. In fact, the functions of integrins are also dependent on their complex *N*-glycosylation modifications [1]. Among the different types of integrins, $\alpha 5 \beta 1$, a major fibronectin receptor, is believed to be a relatively well-characterized example, and *N*-glycosylation is important for its mediated many biological functions such as cell adhesion and migration [2,3]. Alterations in the oligosaccharide portion of integrin $\alpha 5 \beta 1$ from the enhanced expression of some glycosyltransferase genes—such as *N*-acetylglucosaminyltransferase-V (GnT-V), *N*-acetylglucosaminyltransferase-III (GnT-III), or $\alpha 2,6$ -galactoside sialyltransferase 1—can be used to regulate the cell spreading and migration onto fibronectin [1,4,5]. Furthermore, we recently found that *N*-glycosylation on the calf domain of $\alpha 5$, putative sites 10–14, was essential

for the $\alpha 5$ -mediated inhibitory effect on epidermal growth factor receptor (EGFR) signaling and cell proliferation [6], while *N*-glycosylation on sites 1–2 on the β -propeller domain of $\alpha 5$ played a key role in driving integrin $\alpha 5\beta 1$ dynamics and cell migration [7]. Taken together, these findings support the idea that individual integrin $\alpha 5$ *N*-glycosylation differentially functions as a molecular switch to regulate the biological functions of $\alpha 5\beta 1$. Similarly, recent studies have revealed that glycosylation of the integrin $\beta 4$ subunit is important for integrin $\alpha 6\beta 4$ functions, the expression of which is associated with cancer progression. In this review, we summarize our current understanding of integrin $\alpha 6\beta 4$ in cancer and also discuss function of glycans on integrin $\beta 4$ subunit.

2. Structure and Functions of Integrin $\alpha 6\beta 4$

Integrin $\alpha 6\beta 4$ is an essential component of the hemidesmosome that provides stable adhesion of basal epithelial cells to the underlying basement membrane [8–10]. The integrin $\beta 4$ can form heterodimer only with the $\alpha 6$ integrin. Patients with genetic mutations in either integrin $\alpha 6$ or $\beta 4$ subunit suffer from the junctional epidermolysis bullosa with pyloric atresia (JEB-PA), which is an autosomal-recessive disorder clinically characterized by mucocutaneous fragility and gastrointestinal atresia [11–13]. The extracellular domain of integrin $\beta 4$ associates with extracellular matrix, laminin-332, which is a major component of the hemidesmosome [14,15] (Figure 1). The cytoplasmic domain of integrin $\beta 4$ is much longer (>1000 amino acid) than that of other integrin β subunits (<50 amino acid) [16], and the large cytoplasmic domain of integrin $\beta 4$ interacts with other hemidesmosome component, plectin, collagen XVII (BP180/BPAG2), and BP230 (BPAG1) [9,10] (Figure 1). The adhesion complex consisting of those hemidesmosome proteins plays an important role in maintaining the hemidesmosome structure. Mice carrying a target deletion of the integrin $\beta 4$ cytoplasmic domain display extensive epidermal detachment at birth and die shortly thereafter from a syndrome resembling the human JEB-PA [17]. The integrin $\beta 4$ cytoplasmic domain contains several serine, threonine, and tyrosine phosphorylation sites (Figure 1), and the phosphorylation of integrin $\beta 4$ cytoplasmic domain is caused by activation of receptor tyrosine kinases (RTKs) [18], and directly by protein kinase [19].

3. Integrin $\alpha 6\beta 4$ in Cancer

Integrin $\alpha 6\beta 4$ was first discovered as a tumor-specific antigen [20,21]. Subsequent studies demonstrated that increased expression level of integrin $\alpha 6\beta 4$ was correlated with malignant progression and poor survival in squamous cell carcinoma (SCC) of the skin [21,22], lung [23], head and neck [24], and cervix [25]. Further studies have reported that high expression levels of integrin $\alpha 6\beta 4$ were found in several types of cancer—including breast, bladder, colon, ovarian, pancreatic, prostate, and thyroid—and linked to poor prognosis [26]. In a mouse model of active H-Ras and I κ B α -driven human cutaneous SCC, integrin $\beta 4$ -negative keratinocytes (derived from JEB-PA patients with null ITGB4 gene mutations) failed tumor formation but reintroduction of integrin $\beta 4$ gene into the cells restored it [27], suggesting that integrin $\beta 4$ plays an essential role in human SCC development.

Association of integrin $\alpha 6\beta 4$ with laminin substrates significantly promotes cancer cell adhesion, migration, invasion, proliferation, and tumorigenesis through the activation of Rac1, PKC, PI3K, and ERK signaling pathways [10,14,26,28–32] (Figure 1). The PI3K activation response to integrin $\alpha 6\beta 4$ ligation is involved in invasive potential of carcinoma cells, and Tyr¹⁴⁹⁴ in the cytoplasmic domain of the integrin $\beta 4$ is required for the activation [33]. Ligand binding to the extracellular domain of integrin $\alpha 6\beta 4$ induced phosphorylation at serine and tyrosine residues in integrin $\beta 4$ cytoplasmic domain, which were associated with a metastatic phenotype of cancer cells [34]. Phosphorylation of Tyr¹⁴⁹⁴ and Tyr¹⁵²⁶ in integrin $\beta 4$ leads to recruitment of tyrosine phosphatase Shp2 and Shc to the $\beta 4$ cytoplasmic domain, respectively, followed by activation of Ras-MAP kinase pathways, and promotes cell cycle progression [31,35–37] (Figure 1). However, crystallographic studies have been shown that the structural environment of Tyr¹⁴⁹⁴ and Tyr¹⁵²⁶ are not compatible with binding to the SH2 and PTB binding domains of Shp2 and Shc, respectively [38]. Furthermore, both Tyr residues are not well solvent-exposed. It is therefore questionable whether these residues are involved in the

recruitment of SHP2 and Shc, and the subsequent coupling of the integrin $\alpha 6\beta 4$ to the MAPK signaling pathways [39].

During cancer progression, integrin $\alpha 6\beta 4$ is released from hemidesmosomes and the number of hemidesmosomes is decreased, which facilitates the cancer cell migration and invasion [26,39]. Serine phosphorylation of integrin $\beta 4$ cytoplasmic domain by PKC induces relocation of integrin $\alpha 6\beta 4$ from hemidesmosomes to cell protrusions in cancer cells [40]. Compared with carcinoma in situ or normal tissue, increased phosphorylation at Ser¹³⁵⁶ in the integrin $\beta 4$ cytoplasmic domain was found in around 60% of invasive cutaneous SCC. Triple mutation at Ser¹³⁵⁶, Ser¹³⁶⁰, and Ser¹³⁶⁴ to non-phosphorylatable alanines in the integrin $\beta 4$ cytoplasmic domain stabilized hemidesmosome-like structures and reduced cell migration in SCC cells [41]. Thus, the phosphorylation at specific sites in the integrin $\beta 4$ cytoplasmic domain leads to the disruption of stable adhesion structure, hemidesmosomes [19,37,42,43], thereby facilitating the migration of cancer cells (Figure 1). Integrin $\beta 4$ is also phosphorylated by the associations with several RTKs—including EGFR, ErbB2, and Met [18,32]—which are often mutated or amplified in tumors. RTKs activate Src-family kinases, and thereby phosphorylates integrin $\beta 4$ cytoplasmic domain. Tyrosine phosphorylation of integrin $\beta 4$ through Src family kinase, Fyn, which is activated by EGFR, causes disruption of hemidesmosomes, thereby promoting squamous carcinoma invasion [44]. Conversely, integrin $\alpha 6\beta 4$ regulates the expression of ErbB2 and the subsequent Src-family kinase-dependent phosphorylation of RTKs and activation of Ras, STAT-3, and c-Jun [45]. These findings suggest that cooperative signaling between integrin $\beta 4$ and RTKs promotes cancer progression.

Metastasis of cancer cells is a major cause of death in patients with cancer. A first step in metastasis of cancer cells is to move from the primary site and invade into the stroma. In the process of metastasis, some cancer cells undergo epithelial to mesenchymal transition (EMT), which is characterized by loss of epithelial phenotype with cell-cell adhesion and cell polarity, and gain of fibroblast-like morphology [46]. EMT induces cell motility, and stem cell-like properties, thereby enhancing cancer invasion, metastasis, and chemoresistance [47]. A cDNA microarray analysis using clinical samples of pancreatic ductal adenocarcinoma revealed that high levels of integrin $\beta 4$ expression were significantly correlated with the hallmarks of EMT, with high tumor grade, and with the presence of lymph node metastasis [48]. Overexpression of integrin $\beta 4$ promoted cell motility of pancreatic ductal adenocarcinoma cell lines in combination with down-regulation of E-cadherin and up-regulation of vimentin expression [48]. Integrin $\alpha 6\beta 4$ also promotes EMT in hepatocellular carcinoma by upregulating the expression of transcription factor Slug that inhibits the transcription of E-cadherin gene [49]. A recent report has demonstrated that cells with an intermediate level of integrin $\beta 4$ expression exhibited a hybrid epithelial/mesenchymal phenotype and contained cancer stem cell-enriched populations in triple-negative breast cancer cells. Therefore, integrin $\beta 4$ can be a mechanistically driven prognostic biomarker for identifying the more aggressive subtypes of mesenchymal carcinoma cells in triple-negative breast cancer cells [50]. A subpopulation of the PC-3 prostate cancer cell line, TEM4-18, displayed the hallmarks of EMT, including frank loss of E-cadherin expression and upregulation of E-cadherin repressor ZEB1 compared to parent cells [51]. Surprisingly, the ZEB1-mediated EMT in TEM4-18 cells repressed integrin $\beta 4$ and laminin-332 expression by the binding of ZEB1 to the promoter elements of integrin $\beta 4$ and laminin $\gamma 2$ (one of the subunit of laminin-332) genes. The ZEB1 expression exhibited enhanced trans-endothelial migration but decreased transwell migration and invasion of cancer cells [51]. These results suggest that integrin $\alpha 6\beta 4$ is associated with EMT, but the regulatory mechanism of EMT by integrin $\alpha 6\beta 4$ might depend on cancer types.

Exosomes are cell-derived small membrane vesicles (30–100 nm) containing proteins, lipids, RNA, and DNA that can be horizontally transferred to recipient cells [52]. Recent evidence suggests that exosomes play a critical role in the development of cancers, such as activation of fibroblasts, promoting angiogenesis, enhancing invasiveness and chemoresistance [52]. Hoshino et al. have reported that exosomes containing integrin $\alpha 6\beta 4$ and $\alpha v\beta 5$ derived from tumor cells were associated with lung

and liver metastasis, respectively [53]. Furthermore, exosomal integrin $\alpha 6 \beta 4$ uptake activated Src and upregulated pro-migratory and pro-inflammatory S100 molecules in resident cells. These results suggest that exosomal integrin $\alpha 6 \beta 4$ determines metastatic organotropism and could be a biomarker for lung-specific metastasis.

4. Roles of Glycans in Integrin $\beta 4$ Function

N-glycosylation is a common protein post-transcriptional modification occurring on asparagine in the asparagine-X-serine/threonine motif, where X can be any amino acid except proline. Integrins $\alpha 6$ and $\beta 4$ have nine (Asn⁷⁸, Asn²²³, Asn²⁸⁴, Asn³⁷⁰, Asn⁷³¹, Asn⁷⁴⁸, Asn⁸⁹¹, Asn⁹²⁷, Asn⁹⁵⁸) [54] and five (Asn³²⁷, Asn⁴⁹¹, Asn⁵⁷⁹, Asn⁶¹⁷, and Asn⁶⁹⁵) *N*-glycosylation potential sites in each extracellular domain, respectively [55] (Figure 1). Although the *N*-glycans on integrin $\beta 1$ is required for the heterodimer formation with integrin $\alpha 5$ [56], the presence of *N*-glycans on integrin $\beta 4$ is not essential for integrin $\alpha 6 \beta 4$ heterodimer formation [55]. In contrast, a defect of *N*-glycosylation in integrin $\beta 4$ decreases its function such as cell spreading, adhesion, and migration on its substrate, laminin-332, as well as localization to lipid rafts [55].

Overexpression of $\beta 1,6$ -*N*-acetylglucosamine (GlcNAc)-branched *N*-glycans is often found in tumor tissues, and the increase in $\beta 1,6$ -GlcNAc-branched *N*-glycans is directly associated with malignancy and poor prognosis [57]. The addition of the $\beta 1,6$ -GlcNAc-branched *N*-glycans is catalyzed by GnT-V, a member of the family glycosyltransferase [58] (Figure 2). GnT-V knockout mice showed reduced $\beta 1,6$ -GlcNAc-branched *N*-glycans, resulting in suppression of mammary tumor growth and metastasis induced by the polyomavirus middle T oncogene [59]. In vitro, $\beta 1,6$ -GlcNAc-branched *N*-glycans-modified integrins $\alpha 3 \beta 1$ and $\alpha 5 \beta 1$, and laminin-332 strongly promoted cancer cell motility [60–62]. In contrast, introduction of bisecting GlcNAc by GnT-III expression suppresses $\beta 1,6$ -GlcNAc branching formation catalyzed by GnT-V [58], resulting in suppression of cancer metastasis (Figure 2). These findings indicate that $\beta 1,6$ -GlcNAc-branched *N*-glycans catalyzed by GnT-V play important roles in tumor malignancy and progression.

Galectins are a family of soluble lectins that bind β -galactoside-containing glycans such as *N*-acetylglucosamine (Gal $\beta 1,4$ -GlcNAc $\beta 1,3$). The most studied member of the galectin family, galectin-3 is known to be associated with cancer aggressiveness and metastasis [63,64]. The binding of galectin-3 to β -galactoside sugars on glycoproteins crosslinks between the glycoproteins and regulates diverse cellular functions in cancer cells. $\beta 1,6$ -GlcNAc-branched *N*-glycans catalyzed by GnT-V can be elongated with *N*-acetylglucosamine repeats (polylactosamine), which acts as a high-affinity ligand for galectin-3 (Figure 2). Previously, we found the molecular complex consisting of integrin $\alpha 6 \beta 4$, EGFR, and galectin-3 in gastric cancer cell line MKN45 cells, which highly express GnT-V [65,66]. The formation of integrin $\alpha 6 \beta 4$ /EGFR/galectin-3 complex was inhibited by either the presence of a competitive inhibitor of galectin-binding to β -galactoside structure, β -lactose or GnT-III expression [66]. In addition, the breakdown of the tri-molecular complex by an anti-galectin-3 antibody inhibited integrin $\alpha 6 \beta 4$ clustering and cell migration [66]. Similar effect was also observed on the laminin-332/integrin $\alpha 6 \beta 4$ association. In GnT-III-overexpressing MKN45 cells, the modification of laminin-332 increased bisecting GlcNAc, thereby decreasing $\beta 1,6$ -GlcNAc branched *N*-glycans, as well as integrin $\alpha 6 \beta 4$ clustering and cell motility [61]. These findings indicate that galectin-3 cross-links among integrin $\alpha 6 \beta 4$, EGFR, and laminin-332, thereby inducing efficient signaling and the following cellular function.

Mucin type *O*-glycosylation (hereafter referred to as *O*-glycosylation) is one of the most abundant forms of post-translational modification of secreted and membrane-bound proteins that contains a range of *N*-acetylglucosamine (GalNAc)-Serine/Threonine *O*-linked oligosaccharides (*O*-glycans) [67]. Sialic acids occupy terminal positions of *N*-glycans and *O*-glycans in glycoproteins, and altered sialylation has long been associated with the cancer progression. Desialylation of *O*-glycans on integrin $\beta 4$ by sialidase NEU1 suppressed colon cancer cell adhesion to laminin-332, tyrosine phosphorylation of integrin $\beta 4$, and metastasis of human colon cancer cells [68]. In contrast, sialylation

of integrin $\beta 4$ was downregulated during EMT but then reverted and upregulated in the mesenchymal state after EMT [69]. These results indicate that sialylation of integrin $\beta 4$ is dynamically regulated and contributes to cancer progression. Although there are some data using lectin suggesting that O-glycosylation may occur on the integrin $\beta 4$ [55,68], direct evidence for the O-glycan structure and O-glycosylation site in the molecule has not been presented. Further studies including mass spectrometry analysis are required for the study about O-glycosylation on the integrin $\beta 4$.

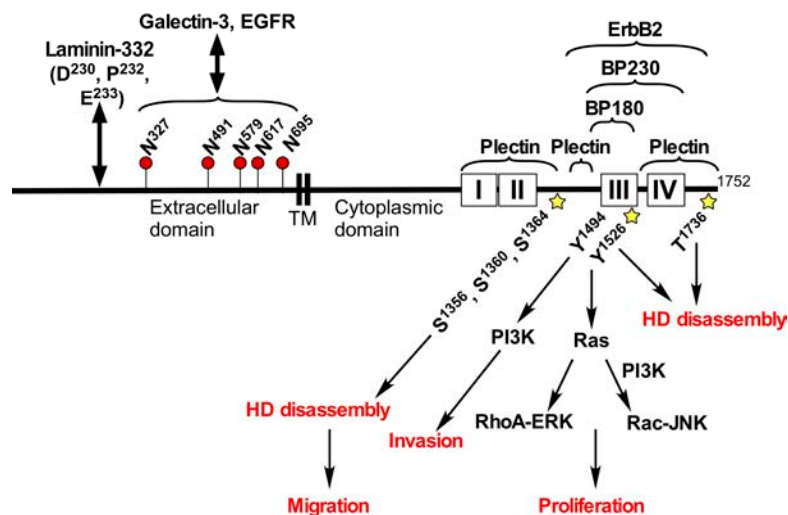


Figure 1. Structure and functions of integrin $\beta 4$. Integrin $\beta 4$ contains laminin-332 binding sites [14] and five N-glycosylation sites (Asn³²⁷, Asn⁴⁹¹, Asn⁵⁷⁹, Asn⁶¹⁷, Asn⁶⁹⁵) in its extracellular domain [55], and the binding sites for Plectin [70], BP180, BP230 [71,72], and ErbB2 [45] in its cytoplasmic domain. Phosphorylation of Ser¹³⁵⁶, Ser¹³⁶⁰, Ser¹³⁶⁴, Tyr¹⁵²⁶, and Thr¹⁷³⁶ induces hemidesmosome disassembly [19,37,42,43]. Phosphorylation of Tyr¹⁵²⁶ promotes recruitment of Shc, which in turn activates Ras, Raf-ERK and Rac-JNK signaling [31,37]. Tyr¹⁴⁹⁴ is associated with PI3K activation [33]. N-Glycosylation sites are shown by flags. Numbers and boxes indicate the number of amino acid residue and the four fibronectin type III repeats, respectively. Star shape indicates phosphorylation site. TM, transmembrane region. HD, hemidesmosome. EGFR, epidermal growth factor receptor.

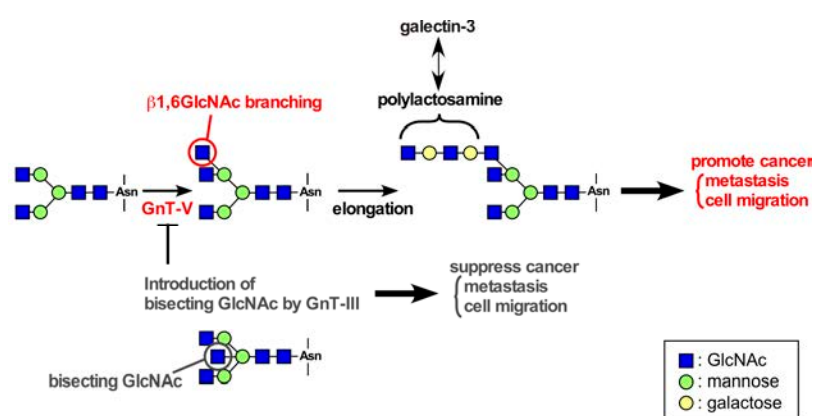


Figure 2. Glycosylation reactions catalyzed by GnT-V. GnT-V catalyzes the formation of $\beta 1,6$ -GlcNAc-branched structures. $\beta 1,6$ -GlcNAc-branching can be elongated with N-acetylglucosamine repeats (polyglucosamine), which acts as a high-affinity ligand for galectin-3. Enhanced expression of GnT-V results in increased migration and metastasis of cancer cells. GnT-III adds GlcNAc to the core mannose to form bisecting N-acetylglucosamine (GlcNAc) in N-glycans, which inhibit the $\beta 1,6$ -GlcNAc branching formation catalyzed by GnT-V and the resultant increase in cancer migration and metastasis.

5. Conclusions and Perspective

In normal stratified and complex epithelial tissues, integrin $\alpha 6 \beta 4$ is an essential component of the hemidesmosomes. However, integrin $\alpha 6 \beta 4$ also overexpresses in several types of cancers and the expression level is correlated with malignant progression and poor survival in cancer patients. Integrin $\alpha 6 \beta 4$ significantly promotes cancer cell adhesion, migration, invasion, proliferation, and tumorigenesis through the activation of Rac1, PKC, PI3K, and ERK signaling pathways, which are induced by the interaction with other molecules including RTKs and laminin-332. Phosphorylation of the cytoplasmic domain in integrin $\beta 4$ also contributes to the cancer progression by activation of Ras-MAP kinase pathways and hemidesmosome disassembly. In addition, the expression levels of integrin $\beta 4$ are closely correlated with the hallmarks of EMT, and also exosomal integrin $\alpha 6 \beta 4$ determines metastatic organotropism.

The biosynthesis of glycan is primarily determined by the glycosyltransferases, the expression level of which is controlled at the level of gene transcription, and by enzymatic activity and chaperone. Since the expression profile of glycosyltransferases in cancer cells is quite different from that of normal cells, the resultant glycan structure is aberrant and specific to cancer. Therefore, alteration of glycan structures is one of the hallmarks of cancer. Recent studies have revealed that integrin $\alpha 6 \beta 4$ functions are regulated by glycosylation of integrin $\beta 4$. The formation of integrin $\alpha 6 \beta 4$ /EGFR/galectin-3 complex through *N*-glycans induces integrin $\alpha 6 \beta 4$ clustering and cell migration. Specifically, sialylation of integrin $\beta 4$ seems to be associated with cancer progression. Therefore, glycosylation on integrin $\beta 4$ may be a useful biomarker and a novel therapeutic target for cancer.

Acknowledgments: This work was partially supported by the Japan Society for Promotion of Science KAKENHI Grant Number JP25860243 to Yoshinobu Kariya; JP15H04354 to Jianguo Gu.

Conflicts of Interest: The authors declare no conflict of interest.

References

- Gu, J.; Taniguchi, N. Regulation of integrin functions by *N*-glycans. *Glycoconj. J.* **2004**, *21*, 9–15. [[CrossRef](#)] [[PubMed](#)]
- Isaji, T.; Gu, J.; Nishiuchi, R.; Zhao, Y.; Takahashi, M.; Miyoshi, E.; Honke, K.; Sekiguchi, K.; Taniguchi, N. Introduction of bisecting GlcNAc into integrin $\alpha 5 \beta 1$ reduces ligand binding and downregulates cell adhesion and cell migration. *J. Biol. Chem.* **2004**, *279*, 19747–19754. [[CrossRef](#)] [[PubMed](#)]
- Isaji, T.; Sato, Y.; Fukuda, T.; Gu, J. *N*-glycosylation of the I-like domain of $\beta 1$ integrin is essential for $\beta 1$ integrin expression and biological function: Identification of the minimal *N*-glycosylation requirement for $\alpha 5 \beta 1$. *J. Biol. Chem.* **2009**, *284*, 12207–12216. [[CrossRef](#)] [[PubMed](#)]
- Takahashi, M.; Kizuka, Y.; Ohtsubo, K.; Gu, J.; Taniguchi, N. Disease-associated glycans on cell surface proteins. *Mol. Asp. Med.* **2016**, *51*, 56–70. [[CrossRef](#)] [[PubMed](#)]
- Janik, M.E.; Litynska, A.; Vereecken, P. Cell migration—the role of integrin glycosylation. *Biochim. Biophys. Acta* **2010**, *1800*, 545–555. [[CrossRef](#)] [[PubMed](#)]
- Hang, Q.; Isaji, T.; Hou, S.; Im, S.; Fukuda, T.; Gu, J. Integrin $\alpha 5$ suppresses the phosphorylation of epidermal growth factor receptor and its cellular signaling of cell proliferation via *N*-Glycosylation. *J. Biol. Chem.* **2015**, *290*, 29345–29360. [[CrossRef](#)] [[PubMed](#)]
- Hang, Q.; Isaji, T.; Hou, S.; Wang, Y.; Fukuda, T.; Gu, J. A key regulator of cell adhesion: Identification and characterization of important *N*-Glycosylation Sites on Integrin $\alpha 5$ for Cell Migration. *Mol. Cell Biol.* **2017**, *37*. [[CrossRef](#)] [[PubMed](#)]
- Sonnenberg, A.; Calafat, J.; Janssen, H.; Daams, H.; van der Raaij-Helmer, L.M.; Falcioni, R.; Kennel, S.J.; Aplin, J.D.; Baker, J.; Loizidou, M.; et al. Integrin $\alpha 6 / \beta 4$ complex is located in hemidesmosomes, suggesting a major role in epidermal cell-basement membrane adhesion. *J. Cell Biol.* **1991**, *113*, 907–917. [[CrossRef](#)] [[PubMed](#)]
- Litjens, S.H.; de Pereda, J.M.; Sonnenberg, A. Current insights into the formation and breakdown of hemidesmosomes. *Trends Cell Biol.* **2006**, *16*, 376–383. [[CrossRef](#)] [[PubMed](#)]

10. Kariya, Y.; Kariya, Y.; Gu, J. Laminin-332 and integrins: Signaling platform for cell adhesion and migration and its regulation by N-glycosylation. In *Laminins: Structure, Biological Activity and Role in Disease*; Nova Science Publishers, Inc.: Hauppauge, NY, USA, 2013; pp. 29–51.
11. Takizawa, Y.; Shimizu, H.; Nishikawa, T.; Hatta, N.; Pulkkinen, L.; Uitto, J. Novel ITGB4 mutations in a patient with junctional epidermolysis bullosa-pyloric atresia syndrome and altered basement membrane zone immunofluorescence for the $\alpha 6\beta 4$ integrin. *J. Investig. Dermatol.* **1997**, *108*, 943–946. [[CrossRef](#)] [[PubMed](#)]
12. Ko, M.S.; Marinkovich, M.P. Role of dermal-epidermal basement membrane zone in skin, cancer, and developmental disorders. *Dermatol. Clin.* **2010**, *28*, 1–16. [[CrossRef](#)] [[PubMed](#)]
13. Pulkkinen, L.; Rouan, F.; Bruckner-Tuderman, L.; Wallerstein, R.; Garzon, M.; Brown, T.; Smith, L.; Carter, W.; Uitto, J. Novel ITGB4 mutations in lethal and nonlethal variants of epidermolysis bullosa with pyloric atresia: Missense versus nonsense. *Am. J. Hum. Genet.* **1998**, *63*, 1376–1387. [[CrossRef](#)] [[PubMed](#)]
14. Russell, A.J.; Fincher, E.F.; Millman, L.; Smith, R.; Vela, V.; Waterman, E.A.; Dey, C.N.; Guide, S.; Weaver, V.M.; Marinkovich, M.P. $\alpha 6\beta 4$ integrin regulates keratinocyte chemotaxis through differential GTPase activation and antagonism of $\alpha 3\beta 1$ integrin. *J. Cell Sci.* **2003**, *116*, 3543–3556. [[CrossRef](#)] [[PubMed](#)]
15. Kariya, Y.; Tsubota, Y.; Hirosaki, T.; Mizushima, H.; Puzon-McLaughlin, W.; Takada, Y.; Miyazaki, K. Differential regulation of cellular adhesion and migration by recombinant laminin-5 forms with partial deletion or mutation within the G3 domain of $\alpha 3$ chain. *J. Cell Biochem.* **2003**, *88*, 506–520. [[CrossRef](#)] [[PubMed](#)]
16. Hogervorst, F.; Kuikman, I.; von dem Borne, A.E.; Sonnenberg, A. Cloning and sequence analysis of $\beta 4$ cDNA: An integrin subunit that contains a unique 118 kd cytoplasmic domain. *EMBO J.* **1990**, *9*, 765–770. [[PubMed](#)]
17. Murgia, C.; Blaikie, P.; Kim, N.; Dans, M.; Petrie, H.T.; Giancotti, F.G. Cell cycle and adhesion defects in mice carrying a targeted deletion of the integrin $\beta 4$ cytoplasmic domain. *EMBO J.* **1998**, *17*, 3940–3951. [[CrossRef](#)] [[PubMed](#)]
18. Mainiero, F.; Pepe, A.; Yeon, M.; Ren, Y.; Giancotti, F.G. The intracellular functions of $\alpha 6\beta 4$ integrin are regulated by EGF. *J. Cell Biol.* **1996**, *134*, 241–253. [[CrossRef](#)] [[PubMed](#)]
19. Rabinovitz, I.; Tsomo, L.; Mercurio, A.M. Protein kinase C- α phosphorylation of specific serines in the connecting segment of the $\beta 4$ integrin regulates the dynamics of type II hemidesmosomes. *Mol. Cell Biol.* **2004**, *24*, 4351–4360. [[CrossRef](#)] [[PubMed](#)]
20. Falcioni, R.; Kennel, S.J.; Giacomini, P.; Zupi, G.; Sacchi, A. Expression of tumor antigen correlated with metastatic potential of Lewis lung carcinoma and B16 melanoma clones in mice. *Cancer Res.* **1986**, *46*, 5772–5778. [[PubMed](#)]
21. Kimmel, K.A.; Carey, T.E. Altered expression in squamous carcinoma cells of an orientation restricted epithelial antigen detected by monoclonal antibody A9. *Cancer Res.* **1986**, *46*, 3614–3623. [[PubMed](#)]
22. Savoia, P.; Trusolino, L.; Pepino, E.; Cremona, O.; Marchisio, P.C. Expression and topography of integrins and basement membrane proteins in epidermal carcinomas: Basal but not squamous cell carcinomas display loss of $\alpha 6\beta 4$ and BM-600/nicein. *J. Investig. Dermatol.* **1993**, *101*, 352–358. [[CrossRef](#)] [[PubMed](#)]
23. Mariani Costantini, R.; Falcioni, R.; Battista, P.; Zupi, G.; Kennel, S.J.; Colasante, A.; Venturo, I.; Curio, C.G.; Sacchi, A. Integrin ($\alpha 6/\beta 4$) expression in human lung cancer as monitored by specific monoclonal antibodies. *Cancer Res.* **1990**, *50*, 6107–6112. [[PubMed](#)]
24. Wolf, G.T.; Carey, T.E.; Schmaltz, S.P.; McClatchey, K.D.; Poore, J.; Glaser, L.; Hayashida, D.J.; Hsu, S. Altered antigen expression predicts outcome in squamous cell carcinoma of the head and neck. *J. Natl. Cancer Inst.* **1990**, *82*, 1566–1572. [[CrossRef](#)] [[PubMed](#)]
25. Carico, E.; French, D.; Bucci, B.; Falcioni, R.; Vecchione, A.; Mariani-Costantini, R. Integrin $\beta 4$ expression in the neoplastic progression of cervical epithelium. *Gynecol. Oncol.* **1993**, *49*, 61–66. [[CrossRef](#)] [[PubMed](#)]
26. Stewart, R.L.; O'Connor, K.L. Clinical significance of the integrin $\alpha 6\beta 4$ in human malignancies. *Lab. Investig.* **2015**, *95*, 976–986. [[CrossRef](#)] [[PubMed](#)]
27. Dajee, M.; Lazarov, M.; Zhang, J.Y.; Cai, T.; Green, C.L.; Russell, A.J.; Marinkovich, M.P.; Tao, S.; Lin, Q.; Kubo, Y.; et al. NF- κ B blockade and oncogenic Ras trigger invasive human epidermal neoplasia. *Nature* **2003**, *421*, 639–643. [[CrossRef](#)] [[PubMed](#)]
28. Kariya, Y.; Miyazaki, K. The basement membrane protein laminin-5 acts as a soluble cell motility factor. *Exp. Cell Res.* **2004**, *297*, 508–520. [[CrossRef](#)] [[PubMed](#)]

29. Nikolopoulos, S.N.; Blaikie, P.; Yoshioka, T.; Guo, W.; Puri, C.; Tacchetti, C.; Giancotti, F.G. Targeted deletion of the integrin $\beta 4$ signaling domain suppresses laminin-5-dependent nuclear entry of mitogen-activated protein kinases and NF- κ B, causing defects in epidermal growth and migration. *Mol. Cell Biol.* **2005**, *25*, 6090–6102. [[CrossRef](#)] [[PubMed](#)]
30. Shaw, L.M.; Rabinovitz, I.; Wang, H.H.; Toker, A.; Mercurio, A.M. Activation of phosphoinositide 3-OH kinase by the $\alpha 6\beta 4$ integrin promotes carcinoma invasion. *Cell* **1997**, *91*, 949–960. [[CrossRef](#)]
31. Mainiero, F.; Murgia, C.; Wary, K.K.; Curatola, A.M.; Pepe, A.; Blumemberg, M.; Westwick, J.K.; Der, C.J.; Giancotti, F.G. The coupling of $\alpha 6\beta 4$ integrin to Ras-MAP kinase pathways mediated by Shc controls keratinocyte proliferation. *EMBO J.* **1997**, *16*, 2365–2375. [[CrossRef](#)] [[PubMed](#)]
32. Kariya, Y.; Kariya, Y.; Gu, J. Roles of laminin-332 and $\alpha 6\beta 4$ integrin in tumor progression. *Mini Rev. Med. Chem.* **2009**, *9*, 1284–1291. [[CrossRef](#)] [[PubMed](#)]
33. Shaw, L.M. Identification of insulin receptor substrate 1 (IRS-1) and IRS-2 as signaling intermediates in the $\alpha 6\beta 4$ integrin-dependent activation of phosphoinositide 3-OH kinase and promotion of invasion. *Mol. Cell Biol.* **2001**, *21*, 5082–5093. [[CrossRef](#)] [[PubMed](#)]
34. Sacchi, A.; Falcioni, R.; Piaggio, G.; Gianfelice, M.A.; Perrotti, N.; Kennel, S.J. Ligand-induced phosphorylation of a murine tumor surface protein (TSP-180) associated with metastatic phenotype. *Cancer Res.* **1989**, *49*, 2615–2620. [[PubMed](#)]
35. Trusolino, L.; Bertotti, A.; Comoglio, P.M. A signaling adapter function for $\alpha 6\beta 4$ integrin in the control of HGF-dependent invasive growth. *Cell* **2001**, *107*, 643–654. [[CrossRef](#)]
36. Bertotti, A.; Comoglio, P.M.; Trusolino, L. $\beta 4$ integrin activates a Shp2-Src signaling pathway that sustains HGF-induced anchorage-independent growth. *J. Cell Biol.* **2006**, *175*, 993–1003. [[CrossRef](#)] [[PubMed](#)]
37. Dans, M.; Gagnoux-Palacios, L.; Blaikie, P.; Klein, S.; Mariotti, A.; Giancotti, F.G. Tyrosine phosphorylation of the $\beta 4$ integrin cytoplasmic domain mediates Shc signaling to extracellular signal-regulated kinase and antagonizes formation of hemidesmosomes. *J. Biol. Chem.* **2001**, *276*, 1494–1502. [[CrossRef](#)] [[PubMed](#)]
38. Alosnso-Garcia, N.; Garcia-Rubio, I.; Manso, J.A.; Buey, R.M.; Urien, H.; Sonnenberg, A.; Jeschke, G.; de Pereda, J.M. Combination of X-ray crystallography, SAXS and DEER to obtain the structure of the FnIII-3,4 domains of integrin $\alpha 6\beta 4$. *Acta Crystallogr. D Biol. Crystallogr.* **2015**, *71*, 969–985. [[CrossRef](#)] [[PubMed](#)]
39. Ramovs, V.; Molder, L.T.; Sonnenberg, A. The opposing roles of laminin-binding integrins in cancer. *Matrix Biol.* **2017**, *57–58*, 213–243. [[CrossRef](#)] [[PubMed](#)]
40. Rabinovitz, I.; Toker, A.; Mercurio, A.M. Protein kinase C-dependent mobilization of the $\alpha 6\beta 4$ integrin from hemidesmosomes and its association with actin-rich cell protrusions drive the chemotactic migration of carcinoma cells. *J. Cell Biol.* **1999**, *146*, 1147–1160. [[CrossRef](#)] [[PubMed](#)]
41. Kashyap, T.; Germain, E.; Roche, M.; Lyle, S.; Rabinovitz, I. Role of $\beta 4$ integrin phosphorylation in human invasive squamous cell carcinoma: Regulation of hemidesmosome stability modulates cell migration. *Lab. Invest.* **2011**, *91*, 1414–1426. [[CrossRef](#)] [[PubMed](#)]
42. Wilhelmsen, K.; Litjens, S.H.; Kuikman, I.; Margadant, C.; van Rheenen, J.; Sonnenberg, A. Serine phosphorylation of the integrin $\beta 4$ subunit is necessary for epidermal growth factor receptor induced hemidesmosome disruption. *Mol. Biol. Cell* **2007**, *18*, 3512–3522. [[CrossRef](#)] [[PubMed](#)]
43. Frijns, E.; Kuikman, I.; Litjens, S.; Raspe, M.; Jalink, K.; Ports, M.; Wilhelmsen, K.; Sonnenberg, A. Phosphorylation of threonine 1736 in the C-terminal tail of integrin $\beta 4$ contributes to hemidesmosome disassembly. *Mol. Biol. Cell* **2012**, *23*, 1475–1485. [[CrossRef](#)] [[PubMed](#)]
44. Mariotti, A.; Kedeshian, P.A.; Dans, M.; Curatola, A.M.; Gagnoux-Palacios, L.; Giancotti, F.G. EGF-R signaling through Fyn kinase disrupts the function of integrin $\alpha 6\beta 4$ at hemidesmosomes: Role in epithelial cell migration and carcinoma invasion. *J. Cell Biol.* **2001**, *155*, 447–458. [[CrossRef](#)] [[PubMed](#)]
45. Guo, W.; Pylayeva, Y.; Pepe, A.; Yoshioka, T.; Muller, W.J.; Inghirami, G.; Giancotti, F.G. $\beta 4$ integrin amplifies ErbB2 signaling to promote mammary tumorigenesis. *Cell* **2006**, *126*, 489–502. [[CrossRef](#)] [[PubMed](#)]
46. Kalluri, R.; Weinberg, R.A. The basics of epithelial-mesenchymal transition. *J. Clin. Invest.* **2009**, *119*, 1420–1428. [[CrossRef](#)] [[PubMed](#)]
47. Shibue, T.; Weinberg, R.A. EMT, CSCs, and drug resistance: The mechanistic link and clinical implications. *Nat. Rev. Clin. Oncol.* **2017**. [[CrossRef](#)] [[PubMed](#)]

48. Masugi, Y.; Yamazaki, K.; Emoto, K.; Effendi, K.; Tsujikawa, H.; Kitago, M.; Itano, O.; Kitagawa, Y.; Sakamoto, M. Upregulation of integrin $\beta 4$ promotes epithelial-mesenchymal transition and is a novel prognostic marker in pancreatic ductal adenocarcinoma. *Lab. Investig.* **2015**, *95*, 308–319. [[CrossRef](#)] [[PubMed](#)]
49. Li, X.L.; Liu, L.; Li, D.D.; He, Y.P.; Guo, L.H.; Sun, L.P.; Liu, L.N.; Xu, H.X.; Zhang, X.P. Integrin $\beta 4$ promotes cell invasion and epithelial-mesenchymal transition through the modulation of Slug expression in hepatocellular carcinoma. *Sci. Rep.* **2017**, *7*, 40464. [[CrossRef](#)] [[PubMed](#)]
50. Bierie, B.; Pierce, S.E.; Kroeger, C.; Stover, D.G.; Pattabiraman, D.R.; Thiru, P.; Liu Donaher, J.; Reinhardt, F.; Chaffer, C.L.; Keckesova, Z.; et al. Integrin $\beta 4$ identifies cancer stem cell-enriched populations of partially mesenchymal carcinoma cells. *Proc. Natl. Acad. Sci. USA* **2017**, *114*, E2337–E2346. [[CrossRef](#)] [[PubMed](#)]
51. Drake, J.M.; Barnes, J.M.; Madsen, J.M.; Domann, F.E.; Stipp, C.S.; Henry, M.D. ZEB1 coordinately regulates laminin-332 and $\beta 4$ integrin expression altering the invasive phenotype of prostate cancer cells. *J. Biol. Chem.* **2010**, *285*, 33940–33948. [[CrossRef](#)] [[PubMed](#)]
52. Soung, Y.H.; Nguyen, T.; Cao, H.; Lee, J.; Chung, J. Emerging roles of exosomes in cancer invasion and metastasis. *BMB Rep.* **2016**, *49*, 18–25. [[CrossRef](#)] [[PubMed](#)]
53. Hoshino, A.; Costa-Silva, B.; Shen, T.L.; Rodrigues, G.; Hashimoto, A.; Tesic Mark, M.; Molina, H.; Kohsaka, S.; Di Giannatale, A.; Ceder, S.; et al. Tumour exosome integrins determine organotropic metastasis. *Nature* **2015**, *527*, 329–335. [[CrossRef](#)] [[PubMed](#)]
54. Tamura, R.N.; Rozzo, C.; Starr, L.; Chambers, J.; Reichardt, L.F.; Cooper, H.M.; Quaranta, V. Epithelial integrin $\alpha 6 \beta 4$: Complete primary structure of $\alpha 6$ and variant forms of $\beta 4$. *J. Cell Biol.* **1990**, *111*, 1593–1604. [[CrossRef](#)] [[PubMed](#)]
55. Kariya, Y.; Gu, J. N-glycosylation of $\beta 4$ integrin controls the adhesion and motility of keratinocytes. *PLoS ONE* **2011**, *6*, e27084. [[CrossRef](#)] [[PubMed](#)]
56. Isaji, T.; Sato, Y.; Zhao, Y.; Miyoshi, E.; Wada, Y.; Taniguchi, N.; Gu, J. N-glycosylation of the beta-propeller domain of the integrin $\alpha 5$ subunit is essential for $\alpha 5 \beta 1$ heterodimerization, expression on the cell surface, and its biological function. *J. Biol. Chem.* **2006**, *281*, 33258–33267. [[CrossRef](#)] [[PubMed](#)]
57. Dennis, J.W.; Laferte, S. Oncodevelopmental expression of—GlcNAc beta 1-6Man alpha 1-6Man beta 1—Branched asparagine-linked oligosaccharides in murine tissues and human breast carcinomas. *Cancer Res.* **1989**, *49*, 945–950. [[PubMed](#)]
58. Gu, J.; Isaji, T.; Sato, Y.; Kariya, Y.; Fukuda, T. Importance of N-glycosylation on $\alpha 5 \beta 1$ integrin for its biological functions. *Biol. Pharm. Bull.* **2009**, *32*, 780–785. [[CrossRef](#)] [[PubMed](#)]
59. Granovsky, M.; Fata, J.; Pawling, J.; Muller, W.J.; Khokha, R.; Dennis, J.W. Suppression of tumor growth and metastasis in Mgat5-deficient mice. *Nat. Med.* **2000**, *6*, 306–312. [[PubMed](#)]
60. Zhao, Y.; Nakagawa, T.; Itoh, S.; Inamori, K.; Isaji, T.; Kariya, Y.; Kondo, A.; Miyoshi, E.; Miyazaki, K.; Kawasaki, N.; et al. N-acetylglucosaminyltransferase III antagonizes the effect of N-acetylglucosaminyltransferase V on $\alpha 3 \beta 1$ integrin-mediated cell migration. *J. Biol. Chem.* **2006**, *281*, 32122–32130. [[CrossRef](#)] [[PubMed](#)]
61. Kariya, Y.; Kato, R.; Itoh, S.; Fukuda, T.; Shibukawa, Y.; Sanzen, N.; Sekiguchi, K.; Wada, Y.; Kawasaki, N.; Gu, J. N-Glycosylation of laminin-332 regulates its biological functions: A novel function of the bisecting GlcNAc. *J. Biol. Chem.* **2008**, *283*, 33036–33045. [[CrossRef](#)] [[PubMed](#)]
62. Guo, H.B.; Lee, I.; Kamar, M.; Akiyama, S.K.; Pierce, M. Aberrant N-glycosylation of $\beta 1$ integrin causes reduced $\alpha 5 \beta 1$ integrin clustering and stimulates cell migration. *Cancer Res.* **2002**, *62*, 6837–6845. [[PubMed](#)]
63. Takenaka, Y.; Fukumori, T.; Raz, A. Galectin-3 and metastasis. *Glycoconj. J.* **2004**, *19*, 543–549. [[CrossRef](#)] [[PubMed](#)]
64. Liu, F.T.; Rabinovich, G.A. Galectins as modulators of tumour progression. *Nat. Rev. Cancer* **2005**, *5*, 29–41. [[CrossRef](#)] [[PubMed](#)]
65. Huang, B.; Wu, Q.; Ge, Y.; Zhang, J.; Sun, L.; Zhang, Y.; Fu, L.; Fan, J.; Wang, Z. Expression of N-acetylglucosaminyltransferase V in gastric cancer correlates with metastasis and prognosis. *Int. J. Oncol.* **2014**, *44*, 849–857. [[PubMed](#)]
66. Kariya, Y.; Kawamura, C.; Tabei, T.; Gu, J. Bisecting GlcNAc residues on laminin-332 downregulate galectin-3-dependent keratinocyte motility. *J. Biol. Chem.* **2010**, *285*, 3330–3340. [[CrossRef](#)] [[PubMed](#)]
67. Brockhausen, I. Mucin-type O-glycans in human colon and breast cancer: Glycodynamics and functions. *EMBO Rep.* **2006**, *7*, 599–604. [[CrossRef](#)] [[PubMed](#)]

68. Uemura, T.; Shiozaki, K.; Yamaguchi, K.; Miyazaki, S.; Satomi, S.; Kato, K.; Sakuraba, H.; Miyagi, T. Contribution of sialidase NEU1 to suppression of metastasis of human colon cancer cells through desialylation of integrin β 4. *Oncogene* **2009**, *28*, 1218–1229. [[CrossRef](#)] [[PubMed](#)]
69. Du, J.; Hong, S.; Dong, L.; Cheng, B.; Lin, L.; Zhao, B.; Chen, Y.G.; Chen, X. Dynamic Sialylation in Transforming Growth Factor- β (TGF- β)-induced Epithelial to Mesenchymal Transition. *J. Biol. Chem.* **2015**, *290*, 12000–12013. [[CrossRef](#)] [[PubMed](#)]
70. Wilhelmsen, K.; Litjens, S.H.; Sonnenberg, A. Multiple functions of the integrin α 6 β 4 in epidermal homeostasis and tumorigenesis. *Mol. Cell Biol.* **2006**, *26*, 2877–2886. [[CrossRef](#)] [[PubMed](#)]
71. Koster, J.; Geerts, D.; Favre, B.; Borradori, L.; Sonnenberg, A. Analysis of the interactions between BP180, BP230, plectin and the integrin α 6 β 4 important for hemidesmosome assembly. *J. Cell Sci.* **2003**, *116*, 387–399. [[CrossRef](#)] [[PubMed](#)]
72. Schaapveld, R.Q.; Borradori, L.; Geerts, D.; van Leusden, M.R.; Kuikman, I.; Nievers, M.G.; Niessen, C.M.; Steenbergen, R.D.; Snijders, P.J.; Sonnenberg, A. Hemidesmosome formation is initiated by the β 4 integrin subunit, requires complex formation of β 4 and HD1/plectin, and involves a direct interaction between β 4 and the bullous pemphigoid antigen 180. *J. Cell Biol.* **1998**, *142*, 271–284. [[CrossRef](#)] [[PubMed](#)]



© 2017 by the authors. Licensee MDPI, Basel, Switzerland. This article is an open access article distributed under the terms and conditions of the Creative Commons Attribution (CC BY) license (<http://creativecommons.org/licenses/by/4.0/>).



Core Fucosylation of the T Cell Receptor Is Required for T Cell Activation

Wei Liang^{1†}, Shanshan Mao^{1†}, Shijie Sun^{1†}, Ming Li¹, Zhi Li², Rui Yu¹, Tonghui Ma¹, Jianguo Gu³, Jianing Zhang⁴, Naoyuki Taniguchi⁵ and Wenzhe Li^{1*}

¹ College of Basic Medical Sciences, Dalian Medical University, Dalian, China, ² Clinical Laboratory, Dalian Municipal Central Hospital, Dalian, China, ³ Division of Regulatory Glycobiology, Institute of Molecular Biomembrane and Glycobiology, Tohoku Medical and Pharmaceutical University, Sendai, Japan, ⁴ School of Life Science and Medicine, Dalian University of Technology, Panjin, China, ⁵ Systems Glycobiology Research Group, Advanced Science Institute, RIKEN, Saitama, Japan

OPEN ACCESS

Edited by:

Michael Loran Dustin,
Harvard University, United States

Reviewed by:

Balbino Alarcon,
Consejo Superior de Investigaciones
Científicas (CSIC), Spain
Christoph Wülfing,
University of Bristol, United Kingdom

*Correspondence:

Wenzhe Li
liwenzhe@dlmedu.edu.cn

[†]These authors have contributed
equally to this work.

Specialty section:

This article was submitted
to T Cell Biology,
a section of the journal
Frontiers in Immunology

Received: 30 September 2017

Accepted: 11 January 2018

Published: 29 January 2018

Citation:

Liang W, Mao S, Sun S, Li M, Li Z,
Yu R, Ma T, Gu J, Zhang J,
Taniguchi N and Li W (2018) Core
Fucosylation of the T Cell Receptor
Is Required for T Cell Activation.
Front. Immunol. 9:78.
doi: 10.3389/fimmu.2018.00078

CD4⁺ T cell activation promotes the pathogenic process of systemic lupus erythematosus (SLE). T cell receptor (TCR) complex are highly core fucosylated glycoproteins, which play important roles in T cell activation. In this study, we found that the core fucosylation of CD4⁺ T cells was significantly increased in SLE patients. Loss of core fucosyltransferase (Fut8), the sole enzyme for catalyzing the core fucosylation of N-glycan, significantly reduced CD4⁺ T cell activation and ameliorated the experimental autoimmune encephalomyelitis-induced syndrome in Fut8^{-/-} mice. T cell activation with OVA₃₂₃₋₃₃₉ loaded major histocompatibility complex II (pMHC-II) on B cell was dramatically attenuated in Fut8^{-/-}OT-II CD4⁺ T cells compared with Fut8^{+/+}OT-II CD4⁺ T cells. Moreover, the phosphorylation of ZAP-70 was significantly reduced in Fut8^{+/+}OT-II CD4⁺ T cells by the treatment of fucosidase. Our results suggest that core fucosylation is required for efficient TCR-pMHC-II contacts in CD4⁺ T cell activation, and hyper core fucosylation may serve as a potential novel biomarker in the sera from SLE patients.

Keywords: core fucosylation, T cell receptor, T cell activation, systemic lupus erythematosus, T-B cell interaction

INTRODUCTION

Systemic lupus erythematosus (SLE) is a severe autoimmune disease that characterized by the production of autoantibodies and the subsequent inflammatory disorders (1). Although the pathogenesis is not completely understood, the activation of CD4⁺ T cells seems plays an essential role in the onset and development of SLE (2). Appropriate CD4⁺ T cell activation is crucially important for adaptive immune responses and autoimmunity, but hyper-activation of these cells results in autoimmune diseases. T cell recognition of peptide-loaded major histocompatibility complex II (pMHC-II) on the antigen-presenting cells (APCs) by T cell receptors (TCRs) is the most important checkpoint for CD4⁺ T cell activation (3). During antigen recognition, the CD4 coreceptor binds to the non-polymorphic surfaces of the membrane-proximal domains of the same pMHCs, which results in a marked increase in the sensitivity of T cells to pMHCs on APC. When adequate agonistic TCR signaling creates a favorable microenvironment for binding, CD28-B7 molecules provide costimulatory lower the thresholds for TCRs triggering and activation. The signaling through TCR induces a conformational change in leukocyte function-associated antigen-1, which greatly

increases its affinity for intercellular adhesion molecule 1 and contributes to immune synapse formation T cells and APC (4, 5).

Glycosylation plays a regulatory and often pivotal role in T cell activation (6–10). Several studies have reported that glycosylation could contribute to higher activation thresholds of T cells. For instance, β 1,6N-acetylglucosaminyltransferase V (Mgat5) deficiency mediates lower T lymphocyte activation thresholds, and subsequently improves T cell activity *in vitro* and results in autoimmune disease *in vivo* (11, 12). Deletion of sialyltransferase ST3Gal-1 increase the sensitivity of TCRs to low-affinity ligands in CD8⁺ T cells (13). Fucosyltransferase 1 transgenic mice show increased TCR signaling and apoptosis that results in thymocyte maturation arrest (14). Notably, reduced N-glycosylation of TCR chains can improve functional avidity and recognition by T cells (15) suggesting that the glycosylation of TCR has a unique role in the regulation of T cell activation.

T cell receptors are heavily core-fucosylated glycoproteins. The core fucosylation of protein is catalyzed by core fucosyltransferase (Fut8), which transfers fucose residue from GDP-fucose to the innermost N-acetylglucosamine (GlcNAc) residue of N-linked glycans *via* an α 1,6 linkage in the Golgi apparatus of mammals (Figure S1 in Supplementary Material). Fut8-mediated core fucosylation is an important post-translational process (16), which regulates protein conformation, stability, and functional expression. Studies have shown that the N-glycans at Asn⁷⁰ [GlcNAc(α 1,6Fuc)- β 1,4GlcNAc: (A2G2F)], Asn¹⁸⁵ (A2G2F), and Asn²⁰³ in the α chain (C α) and Asn²³⁶ in the β chain (C β) extend from the surface of TCR on *Drosophila melanogaster* cells (6, 17). Interestingly, they found that the C α and C β of TCR were connected by the hydrogen bonds of the core fucose residue from Asn¹⁸⁵ (A2G2F) to side chains of Glu¹⁸¹ β and Ser¹⁸² β (6, 17), suggesting a crucial role of core fucosylation on the conformation of TCR. However, to the best of our knowledge, none of the previous studies had addressed the regulatory role of TCR core fucosylation on CD4⁺ T cell activation.

B cells play a role in evoking T cell responses by functioning as APCs, and the presentation of peptide by MHC-II on the B cells initiates T cell activation (18). Therefore, it is reasonable to anticipate that the core fucosylation has significant functional implications in T–B cell interaction, and thus affect the CD4⁺ T cell activation. In this study, we provide the first confirmation that SLE patients exhibited hyper core fucosylation on CD4⁺ T cells, which significantly enhanced the activation of their CD4⁺ T cells. Knockout of Fut8 gene resulted in attenuated T–B cell interaction *via* TCR–pMHC and the consequential reduced CD4⁺ T cell activation. Our data suggest that the core fucosylation may serve as a potential novel biomarker with promising clinical and therapeutic implications in SLE patients.

MATERIALS AND METHODS

Mice

Fut8^{−/−} mice were generated as previously described (19), and homozygous wild-type (Fut8^{+/+}) and Fut8^{−/−} mice on the C57BL/6 background were obtained by crossing heterozygous

Fut8^{+/−} mice (C57BL/6). OT-II (Jackson Laboratory) is a C57BL/6 TCR transgenic strain, expressing a receptor specific for peptide OVA_{323–339}. Fut8^{+/+}OT-II mice and Fut8^{−/−}OT-II mice were generated by crossing heterozygous Fut8^{+/−}OT-II mice. Mice were maintained in the specific pathogen-free laboratory animal facility of Dalian Medical University. All animal work was approved by the Ethics Committee at the Dalian Medical University.

Patients

Serum samples were collected from a total of 17 SLE patients (14 women, 3 men; mean age, 49 years; range, 18–67 years) with and healthy controls (12 women, 12 men; mean age, 18–48 years) (Table S1 in Supplementary Material). The diagnosis of underlying disease was made based on clinical manifestation, serology, imaging, and/or histopathology. These participants were Chinese, recruited at Dalian municipal central hospital. The anti-nuclear antibodies (ANA) titers of AD patients were detected with using Anti-nuclear Antibodies IgG Kit (EUROIMMUN, Germany). The Ethics Committee at the hospital approved the study protocol.

Antibodies

Anti-CD16/32 (2.4G2), anti-CD3(145-2c11), anti-CD28 (37.51), FITC-anti-MHC II (M5/114.15.2), FITC-anti-CD69 (H1.2F3), PE-labeled anti-CD4 (GK1.5), APC-labeled anti-CD8 (53-6.7), biotin-labeled anti-TCR β (H57-597), and PE-Cy5-labeled anti-TCR β (H57-597) were obtained from e-Bioscience; anti-GAPDH, horseradish peroxidase (HRP)-conjugated goat anti-mouse IgG and HRP-conjugated donkey anti-human IgG were obtained from proteintech; additional biotin-conjugated lens culinaris agglutinin (LCA) were purchased from Vector; anti-TCR $\alpha\beta$ (ab25336), anti-pZAP70 (ab194800), anti-ZAP70 (ab32410), Natural streptavidin protein (FITC) (ab136201), and streptavidin (HRP) (ab7403) were purchased from Abcam.

Histological Analysis

Formalin-fixed tissue samples were paraffin-embedded and sections were analyzed by hematoxylin–eosin (H&E) staining. The sections were stained with biotin-conjugated LCA. Briefly, sections were deparaffinized three times in xylene and hydrated through a 100, 90, 80, and 70% ethanol to phosphate-buffered saline (PBS). To quench the endogenous peroxidase activity, slides were incubated with 3% H₂O₂ for 30 min. Then, the slides were incubated with biotin-conjugated LCA, and washed three times with PBS. The slides probed with HRP–streptavidin for 30 min, and visualized with 3,3′-diaminobenzidine. The intensity of LCA-positive staining in the spleen was analyzed by integrated optical density using Image-Pro® Plus software (version 6.0; Media Cybernetics, USA).

Cell Lysate

Cells were solubilized in lysis buffer [Tris–HCl (50 mM), 1% Triton X-100, 10% glycerol, phenylmethylsulfonyl fluoride (100 μ M), leupeptin (5 μ g/mL), aprotinin (1 μ g/mL), NaF (100 mM), 150 mM NaCl, 2 mM EDTA, and sodium orthovanadate (1 mM)] for 15 min at 4°C. Cell lysate was centrifuged at

20,000 $\times g$ for 10 min at 4°C, and the supernatant was subjected to immunoprecipitation or Western blot, as indicated below.

Fut8 Enzyme Activity Assay

The Fut8 enzyme activity was measured by using the previous method (20). Five micrograms cell lysates as the enzyme source were added to the assay buffer (200 mM MES, 1% Triton X-100) supplemented with donor (500 μ M GDP-L-fucose) and substrate [50 μ M GnGn-Asn-4-(2-pyridylamine) butylamine (PABA)]. The mixture was incubated at 37°C for 8 h, and the reaction was stopped by heating at 100°C for 5 min. The reactive solution was then centrifuged at 12,000 $\times g$ for 10 min, and 10 μ L of the reaction products were subjected to high-performance liquid chromatography (HPLC) with a Fluorescent detector (Waters Corporation, USA). The excitation and emission wavelengths are 320 and 400 nm, respectively.

PCR Array

Total RNAs were extracted from Fut8^{+/+} SPLs and Fut8^{-/-} SPLs with TRIzol reagent (Takara Bio). Mouse T Cell and B Cell Activation PCR Array (SA Biosciences) was carried out according to the protocol of the manufacturer. The difference of gene expression between Fut8^{+/+} SPLs and Fut8^{-/-} SPLs was calculated.

Animal Immunization

Mouse was immunized by subcutaneous injection with 200 μ g OVA mixed with an equal volume of complete Freund's adjuvant (CFA) (Sigma). Two weeks later, mice were immunized with 200 μ g OVA by subcutaneous injection. Mice sera were collected at 0, 7, and 14 days post-immunization.

Enzyme-Linked Immunosorbent Assay (ELISA)

The concentrations of IL-2 analyzed using mouse IL-2 ELISA kits (Boster Biological Engineering, Wuhan, China), according to the manufacturer's instructions. The concentrations of IL-2 were calculated according to a standard curve prepared using samples of known concentration. The absorbance was measured at a test wavelength of 450 nm with a microplate reader.

The immunoglobulin isotypes were measured by mouse mAb isotyping reagents (Sigma).

Cell Proliferation Assay

The growth rate of cells was measured using MTT assay. CD4⁺ T cells (1×10^6) were cultured in 96-well culture plate with anti-CD3 ϵ (2 μ g/mL) and anti-CD28 mAbs (1 μ g/mL). After 48 h of incubation, each well was added 10 μ L of MTT solution, and then the absorbance was analyzed by a microplate reader (Thermo Multiskan Ascent, Finland) at 570 nm.

In addition, T cell proliferation with the OVA₃₂₃₋₃₃₉-loaded B cells was analyzed by carboxyfluorescein diacetatesuccinimidyl ester (CFSE, Sigma) dilution methods. CD4⁺ T cells (1×10^6) were purified, and then labeled with 5 μ M CFSE in PBS for 8 min at room temperature and coinubate with OVA₃₂₃₋₃₃₉ loaded Fut8^{+/+} OT-II B cells (1×10^6) for 48 h, and then analyzed by flow cytometric analysis.

Western Blot and Lectin Blot Analysis

Protein samples were electrophoresed on 10% polyacrylamide gels. After electrophoresis at 240 mA for 30 min, proteins were transferred to PVDF membranes. Membranes were blocked in 5% BSA in TBS-T (10 mM Tris-HCl, 150 mM NaCl, and 0.1% Tween 20) at room temperature for 1 h, and then incubated with the biotin-labeled LCA, which preferentially recognizes the core fucose, or primary Abs in 1% BSA in TBS-T overnight at 4°C. After washing, the membranes were covered with the HRP-conjugated streptavidin or HRP-labeled secondary Abs at room temperature for 1 h, and visualized with an ECL system (Amersham).

Immunoprecipitation

Cell extracts (500 μ g) were mixed with 20 μ L of Protein G-Sepharose (50%) and corresponding Abs, and then incubated at 4°C overnight with continuous rotation. After washing three times in lysis buffer, the pull down samples were boiled for 5 min in Laemmli sample buffer with or without 2-mercaptoethanol.

T-B Cell Conjugate Formation

Conjugate formation between T cells and B cells were carried out as described previously with slight modification (21). T cells and 1 μ g/mL OVA₃₂₃₋₃₃₉ (NH₂-ISQAVHAAHAEINEAGR-COOH)-pulsed B cells were mixed at a 1:1 ratio and a quick centrifugation to initiate cell-cell contact. To observe conjugate formation, B cells and T cells were labeled with MHC-II-FITC and TCR β -PE-Cy5 before mixing. T-B cell conjugates were then analyzed by flow cytometry to determine the percentage of T-B cells that had both TCR β -PE-Cy5 and MHC-II-FITC positive staining.

Remove of Core Fucose on Surface of T Cells

Purified CD4⁺ T cells (4×10^6) were treated with 100 mU Glyko[®] α (1-2,3,4,6) Bovine Kidney Fucosidase (GKX-5006, Prozyme), incubate 3 h at 37°C in the reaction buffer. The enzyme reaction was terminated by centrifuging at 2,500 $\times g$ for 5 min and the cells were collected.

Confocal Microscopy

Conjugate formation between T cells and B cells were carried out as described previously with slight modification (21). T cells and 1 μ g/mL OVA₃₂₃₋₃₃₉ pulsed B cells were mixed at a 1:1 ratio and a quick centrifugation to initiate cell-cell contact. Cell-cell conjugates were subsequently transferred to poly-D-lysine coated coverslips and incubated at 37°C for 30 min. Cells were fixed with 4% PFA for 20 min, and then blocked with 5% BSA and anti-CD16/CD32 (2.4G2) mAb for 30 min. After washing, cells were stained with anti-MHC-II Ab for 1 h. All images were taken using a spinning disk confocal microscope (Leica).

MACS Magnetic Cell Sorting

Single splenic cell suspensions were prepared by first grinding the tissues and then by passage through 30- μ m nylon mesh. Red blood cells were lysed by incubation with 0.14 M NH₄Cl and 20 mM Tris (pH7.4) for 3 min at room temperature.

After the lysis of red blood cells, CD4⁺ T cells and B cells were positively isolated with anti-CD4 Ab and anti-CD45R Ab-conjugated magnetic beads (Miltenyi Biotec). The purified cell populations were detected by fluorescence activated cell sorting analysis.

Flow Cytometric Analysis (FACS)

Cells were isolated from tissue and incubated with an anti-CD16/CD32 (2.4G2) mAb to block Fcγ receptors. The cells were stained on ice for 15 min with several combinations of mAbs, as indicated in the figure legends. Flow cytometry was performed on a FACS-Calibur (Becton Dickinson, Mountain View, CA, USA) and analyzed using FlowJo software (Tree Star).

Induction of Experimental Autoimmune Encephalomyelitis (EAE)

For EAE induction, Fut8^{+/+} and Fut8^{-/-} mice were subcutaneously injected with 100 μg of myelin oligodendrocyte glycoprotein peptides (MOG₃₅₋₅₅) emulsified in CFA. Then, mice were injected intraperitoneally with 200 μg pertussis toxin (PTX) (List Biological Laboratories) on 0, 1, and 2 days. Clinical assessment of EAE was performed according to the following scale: 0, no disease; 1, limp tail; 2, hind-limb weakness; 3, partial hind-limb paralysis; 4, complete paralysis of hind-limbs; and 5, moribund state.

Statistical Analysis

Student's *t*-test was used for statistical analysis. Data are presented as mean values ± SEM, or as mean values ± SD. A probability value of *p* < 0.05 was considered significant. **p* < 0.05, ***p* < 0.01, ****p* < 0.001.

RESULTS

Core Fucosylation Is Significantly Upregulated in the Sera and CD4⁺ T Cells of SLE Patients

Higher circulating levels of ANA were detected in sera from SLE patients. In this study, we found that core fucosylation was dramatically increased in the sera from patients with SLE, as evidenced by LCA, which preferentially recognizes the core fucose structure (22) (*p* < 0.001) (Figures 1A,B). The expression of IgGs was also upregulated in sera of the SLE patients (*p* < 0.05) (Figure 1B). These observations pinpoint the contribution of hyper core fucosylation to SLE severity and pathogenesis.

The hyperactivity of B cells in SLE is T cell dependent, and CD4⁺ T cell activation plays a crucial role in SLE pathogenesis (23). We found that the percentage of CD4⁺ T cells in the peripheral blood of SLE patients is similar to those of healthy control (Figure 1C). However, the percentage of CD4⁺CD69⁺ T cells was significantly increased in the SLE (*n* = 17) (Figure 1D). Moreover, the enzyme activity of Fut8 was dramatically increased in the CD4⁺ T cells isolated from the SLE patients (Figures 1E,F), indicated that increased core fucosylation in SLE patients correlates with CD4⁺ T cell activation.

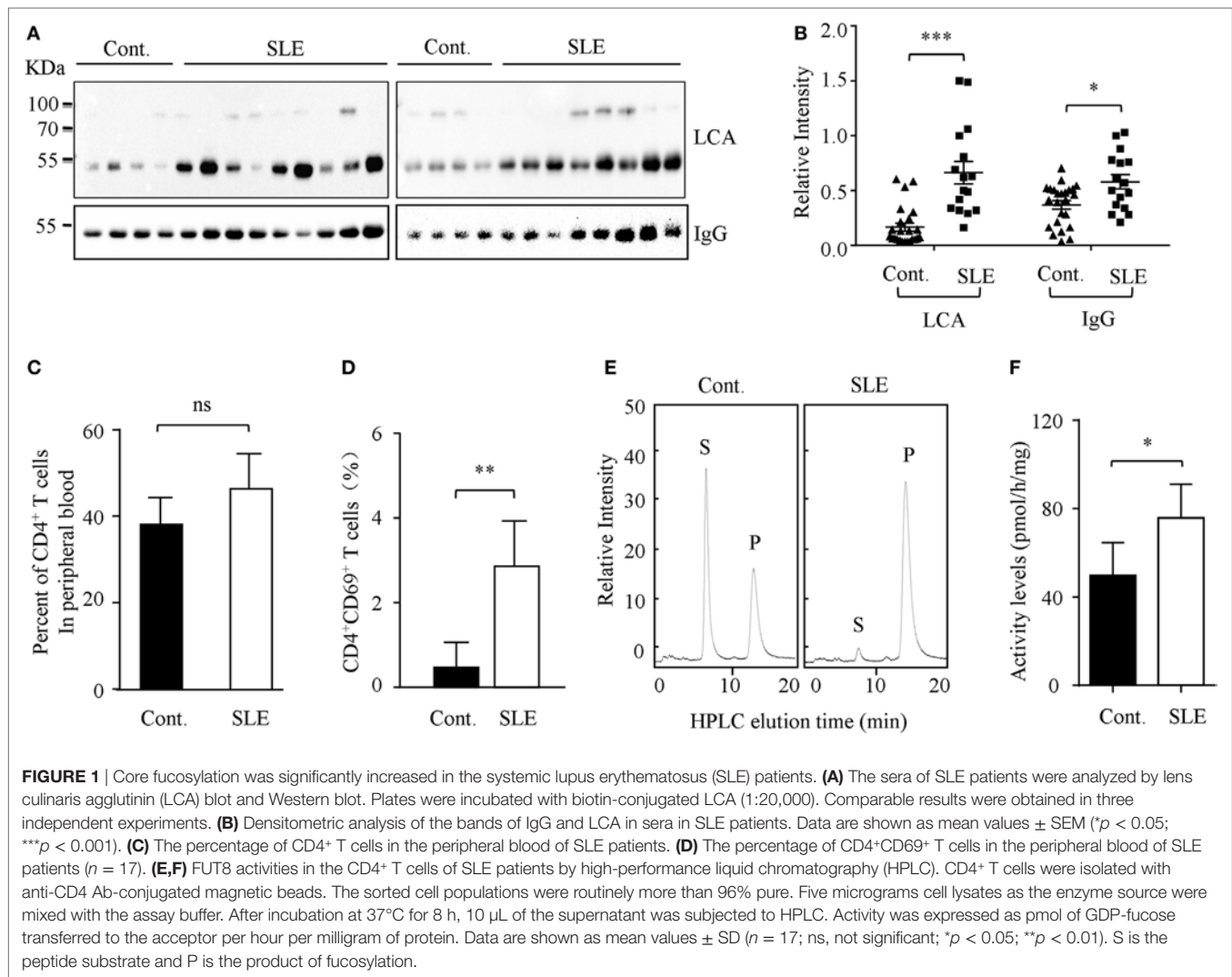
Lack of Core Fucosylation Ameliorated EAE Symptoms with Reduced CD4⁺ T Cell Activation

Wild-type (Fut8^{+/+}) and Fut8^{-/-} mice were generated previously (19). Histological analyses of the splenic architecture of Fut8^{+/+} and Fut8^{-/-} mice were unremarkable in H&E staining. The Fut8 products, core-fucosylated N-glycans, are ubiquitously expressed in the Fut8^{+/+} spleen, as confirmed by LCA (Figure 2A), while those were abolished in Fut8^{-/-} spleens. LCA blot analysis also confirmed the knockout of Fut8 expression in the whole cell lysates of Fut8^{-/-} SPLs (Figure 2B). The FUT8 enzymatic activity was not detected in the Fut8^{-/-} SPLs using HPLC analysis (Figure 2C).

Experimental autoimmune encephalomyelitis is an activated CD4⁺ T cell-mediated autoimmune disease model. Peptides (MOG₃₅₋₅₅) and PTX could induce the migration of activated T cells through the blood-brain barrier and caused several neurologic symptoms. To determine the association between core fucosylation and the activation of CD4⁺ T cells, EAE models were established using Fut8^{+/+} and Fut8^{-/-} mice. EAE is actively induced but appear more quickly upon adoptive transfer of activated MOG₃₅₋₅₅-specific T cells in Fut8^{+/+} mice (Figure 2D; Video S1 in Supplementary Material), while Fut8^{-/-} mice showed slight EAE symptoms (Figure 2D; Video S2 in Supplementary Material). The body weights of Fut8^{+/+} mice were significantly reduced, but no change was found in Fut8^{-/-} mice during EAE induction (Figure 2D). In addition, the proliferation of CD4⁺ T cells was significantly decreased in Fut8^{-/-} EAE mice. Moreover, the proliferation of CD4⁺ T cells with MOG₃₅₋₅₅-loaded B cells was remarkably reduced by de-core fucosylation (Figure 2E).

Lack of Core Fucosylation Suppressed the IgG Class-Switching by Impaired CD4⁺ T Cell Activation

Flow cytometry analysis revealed that, although Fut8^{-/-} mice contained normal proportions of CD4⁺ and CD8⁺ T cell populations in the spleen (Figures 3A,B), they were markedly reduced after OVA immunization contrast with the Fut8^{+/+} mice (Figures 3A,B). Immunoglobulin class-switching is a biological mechanism that changes a mature B cell's production of antibody *via* its B cell receptor from one class to another. For example, from an isotype called IgM to an isotype called IgGs. To illustrate the effects of Fut8 in the class-switching of immunoglobulin, we measured the class-switched (IgGs of different subclasses) and non-switched (IgM) in the sera of Fut8^{+/+} and Fut8^{-/-} mice using mouse mAb isotyping reagents. In 4-week-old Fut8^{-/-} mice, the amounts of IgG₁, IgG_{2a}, IgG_{2b}, and IgG₃ were significantly lower than those in Fut8^{+/+} mice after OVA immunization, while those of IgM were relatively normal (Figure 3C). The cytokines, such as IL-4, IL-5, IL-6, and IFNγ secreted by CD4⁺ T cells, contribute to the different IgG class-switching in the mice and human. It is reasonable to consider that the reduced IgG class-switching attributed to the low levels of cytokines secreted by CD4⁺ T cells in Fut8^{-/-} mice (Table 1). In addition, since the TGF receptor signaling was attenuated in the Fut8^{-/-} mice (19), the IgG₃



class-switching regulated by TGF signaling was also suppressed in the *Fut8*^{-/-} mice.

Loss of Core Fucosylation Impaired the Signal Transduction via TCR

T cell receptor signaling is very important for T cell activation. As illustrated in **Figure 4A**, no different expression of TCR was found in the *Fut8*^{+/+}CD4⁺ T and *Fut8*^{-/-}CD4⁺ T cells. Nonetheless, the core fucose of the N-glycans in the molecules was eliminated by a disruption of the *Fut8* (**Figure 4B**). Moreover, the MS spectra of N-glycans released from TCRs were analyzed. It is notable that the high levels of signals were corresponded to the core-fucosylated glycans bearing non-, mono-, or di-galactose in the *Fut8*^{+/+}CD4⁺ T cells, while those were completely disappeared in *Fut8*^{-/-}CD4⁺ T cells (Figure S2 in Supplementary Material). These results further confirmed in mice that TCRs are highly core-fucosylated proteins and contributes to its activities.

In order to examine the role of core fucosylation in the activation of CD4⁺ T cells, we isolated CD4⁺ T cells from *Fut8*^{+/+} and *Fut8*^{-/-} mice, and checked the level of core fucosylation.

FACS analysis showed that core fucosylation on the cellular surfaces was abolished in *Fut8*^{-/-} CD4⁺ T cells (**Figure 4C**). We compared the phosphorylation levels of *Fut8*^{+/+}CD4⁺ T cells with *Fut8*^{-/-}CD4⁺ T cells in response to costimulations with anti-CD3/CD28 Abs. In those comparisons, the levels of pZAP-70 in *Fut8*^{-/-}CD4⁺ T cells were significantly lower than those in *Fut8*^{+/+}CD4⁺ T cells (**Figure 4D**). Moreover, the populations of CD69⁺ cells (activated T cells) in *Fut8*^{-/-}CD4⁺ T cells were lower than those in *Fut8*^{+/+}CD4⁺ T cells following OVA immunization, while these were similar before immunization (**Figure 4E**). Furthermore, cell proliferation of *Fut8*^{-/-}CD4⁺ T cells was significantly reduced in response to the stimulation of anti-CD3/CD28 Abs (**Figure 4F**).

Core Fucosylation Is Essential for TCR-pMHC Conjugates in CD4⁺ T Cell Activation

B cells present antigenic peptide with MHC-II molecule as APCs, and CD4⁺ T cells physiologically recognize a complex of a peptide-loaded MHC-II in T-B cell interaction (18).

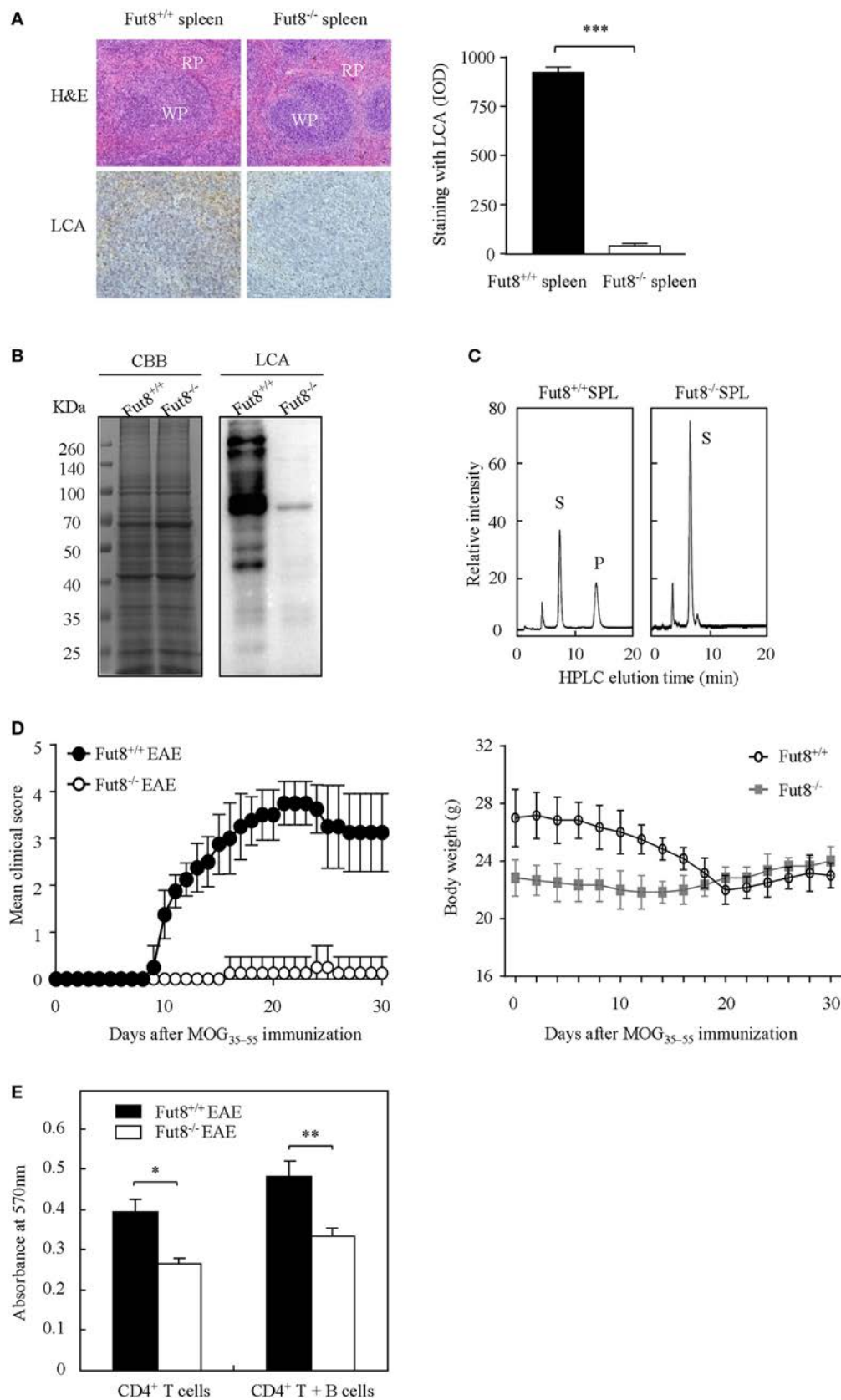
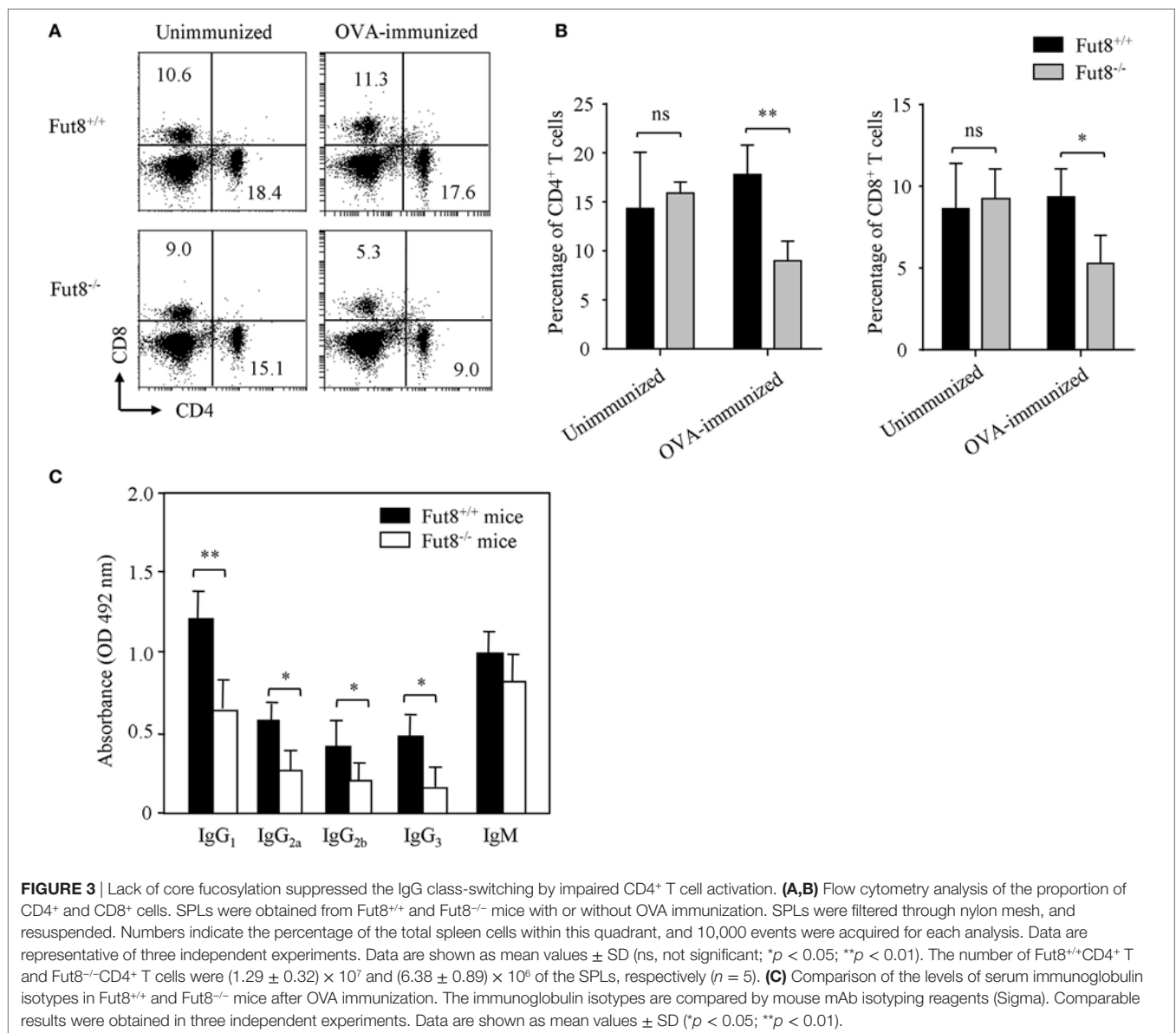


FIGURE 2 | Continued

FIGURE 2 | The experimental autoimmune encephalomyelitis (EAE) model was slightly induced in *Fut8*^{-/-} mice. **(A)** Immunohistochemical analysis of *Fut8*^{+/+} spleen and *Fut8*^{-/-} spleen. The paraffin sections of spleens were deparaffinized and hydrated through a graded series of ethanol to phosphate-buffered saline. One section was assessed by hematoxylin–eosin staining (magnification ×200). RP, red pulp; WP, white pulp. Another section was incubated with biotin-conjugated lens culinaris agglutinin (LCA) (1:200) for 1 h. Finally, the slides were visualized with 3,3'-diaminobenzidine. The staining with LCA was showed by integrated optical density analysis. Data are shown as mean values ± SD (***p* < 0.001). **(B)** Lectin blot of *Fut8*^{+/+} SPL and *Fut8*^{-/-} SPL. The SPL lysates were run on 10% SDS-PAGE gel and stained with Coomassie blue staining and LCA (1:5,000). **(C)** High-performance liquid chromatography (HPLC) analysis of *Fut8* activity. *Fut8* activities were examined using fluorescence-labeled sugar chain, GnGn-Asn-PABA, as an acceptor substrate, as described in Section “Materials and Methods.” The substrate (S) and *Fut8* product (P) were eluted at 8 and 15 min, respectively. **(D)** Disease score of mice in *Fut8*^{+/+} and *Fut8*^{-/-} mice EAE model. EAE induction of *Fut8*^{+/+} and *Fut8*^{-/-} mice (*n* = 7). Mice were immunized with 100 μg MOG_{35–55} peptide in complete Freund's adjuvant and injected with 200 μg pertussis toxin, and detected the signs of EAE daily for 30 days. Comparable results were obtained in four independent experiments. Body weights of mice were measured every 2 days after EAE induction of *Fut8*^{+/+} and *Fut8*^{-/-} mice (*n* = 7). **(E)** Cell proliferation from EAE mice. Purified splenic CD4⁺ T cells and/or MOG_{35–55} peptide-loaded B cells from EAE models were incubated for 48 h at 37°C, and then the cell proliferation was detected by MTT assay. Comparable results were obtained in four independent experiments. Data are shown as mean values ± SD (**p* < 0.05; ***p* < 0.01).



Therefore, we were interested in determining whether core fucosylation is involved in the TCR sensitivity to pMHC-II. To explore the role of core fucosylation on the TCR interaction

with pMHC-II ligands, we crossed *Fut8*^{+/-} mice with OT-II TCR transgenic mice (expressing CD4⁺ TCR specific for OVA_{323–339}), and obtained *Fut8*^{+/+}OT-II and *Fut8*^{-/-}OT-II mice. LCA blots

TABLE 1 | Gene expression of Fut8^{-/-} SPLs after OVA immunization.

Gene name	Gene access number	Fold change (Fut8 ^{+/+} /Fut8 ^{-/-})
T-cell activation		
CD3e	NM-007648	2.15
CD4	NM-013488	3.16
CD8	NM-009858	2.51
Cd40L	NM-011616	2.17
IL-2R α	NM-008367	3.04
IL-4	NM-021283	2.18
IL-6	NM-031168	2.14
IL-10	NM-010548	2.25
IL-12	NM-008352	3.89
IFN γ	NM-008337	3.08
CXCR4	NM-009911	2.04
CXCL12	NM-001012477	2.07
B-cell activation		
CD79a	NM-007655	3.35
CD81	NM-133655	2.82
Cell signaling		
MAPKKK	NM_009316	2.41
Vav1	NM-011691	3.28
PIK3	NM-001077495	2.36
PKC	NM-008859	2.00
Cyclin D3	NM-001081636	3.84

analysis showed that the core fucosylation level of T and B cells in Fut8^{-/-}OT-II mice (Figure S3 in Supplementary Material). Since MHC-II on the B cell surface can present peptides for recognition and activation of T cells, in this study, B cells were isolated from Fut8^{+/+}OT-II and Fut8^{-/-}OT-II spleen and incubated with monobiotin-labeled OVA₃₂₃₋₃₃₉. Although electron density was seen for the structures of I-A^d covalently linked to an OVA₃₂₃₋₃₃₉, with a single N-glycan (24), the core fucosylation did not affect the peptide presentation abilities of the MHCs between Fut8^{+/+}OT-II and Fut8^{-/-}OT-II B cells (Figure S4 in Supplementary Material). The CD4⁺ T cells were then stimulated with OVA₃₂₃₋₃₃₉ loaded B cells and subsequent T cell priming was investigated. The freshly purified *ex vivo* CD4⁺ T cells were stimulated with the OVA₃₂₃₋₃₃₉-loaded B cells. As shown in **Figure 5A**, compared with Fut8^{+/+}OT-II CD4⁺ T cells, the phosphorylation level of ZAP-70 was dramatically decreased in Fut8^{-/-}OT-II CD4⁺ T cells with stimulation of OVA₃₂₃₋₃₃₉-loaded B cells. Moreover, to remove the cell-surface fucosylation, the Fut8^{+/+}OT-II CD4⁺ T cells were treated with 100 mU Glyko[®] α (1-2,3,4,6) Fucosidase, which can cleaves α 1,6-linked fucose more efficiently than other α -fucose linkages (25). The signaling *via* TCR was significantly suppressed in OT-II CD4⁺ T cells treated with this fucosidase, when the T cells were stimulated with OVA₃₂₃₋₃₃₉-loaded B cells (**Figure 5B**), indicated that the Fut8 inactivation results in the less responsive for TCR stimulation with pMHC-II, despite similar TCR expression levels (**Figure 4A**). Moreover, the population of TCR⁺CD69⁺ cells was significantly reduced in Fut8^{-/-}OT-II CD4⁺ T/OVA₃₂₃₋₃₃₉-loaded B cells compared with Fut8^{+/+}OT-II CD4⁺ T/OVA₃₂₃₋₃₃₉-loaded B cells (**Figure 5C**).

To further determine how Fut8 deficiency affects the T-B cell interactions, the communication of CD4⁺ T cells and B cells was observed by confocal microscopy. OVA₃₂₃₋₃₃₉-loaded MHC-II was

markedly increased at the site of T-B cell contact in Fut8^{+/+}OT-II T cells for 30 min and was ubiquitous on the Fut8^{-/-}OT-II T cell surface (**Figures 5D,E**). Next, T-B cell conjugates were quantitatively analyzed *via* flow cytometry analysis. Few conjugates of T-B cells were observed in the absence of OVA₃₂₃₋₃₃₉ peptide, whereas peptide-pulsed B cells effectively interacted with CD4⁺ T cells. The percentages of T-B cell conjugates in Fut8^{+/+}OT-II and Fut8^{-/-}OT-II MHC-II⁺ TCR β ⁺ cells were 29.4 and 7.4%, respectively (**Figures 5F,G**), indicated that core fucosylation affected the T-B cell interaction. Moreover, the secretion of IL-2 was reduced in the culture media of Fut8^{-/-}OT-II T-B cells compared with Fut8^{+/+}OT-II T-B cells (**Figure 5H**). Furthermore, the T cell proliferation with OVA₃₂₃₋₃₃₉-loaded B cells was analyzed by CFSE dilution methods. Compared to the proliferation of Fut8^{+/+}OT-II CD4⁺ T cells, those of Fut8^{-/-}OT-II CD4⁺ T cells was significantly reduced with the cocultivation of OVA₃₂₃₋₃₃₉-loaded Fut8^{+/+}OT-II B cells (**Figure 5I**). These results indicated that Fut8 deficiency contributes to attenuated T-B cell communication, and follows attenuated T cell activation.

To further elucidate the underlying mechanism of the reduced T-B cell interaction caused by the disruption of Fut8, T and B cell Activation PCR Array was used to compare mRNA expression in Fut8^{+/+} SPLs with that in Fut8^{-/-} SPLs following OVA immunization. As illustrated in **Table 1**, the expression levels of four genes (CD3e, CD4, CD8, and CD40L) associated with TCR complex formation, eight genes (IL-2R α , IL-4, IL-6, IL-10, IL-12, IFN γ , CXCL12, and CXCR4) involved in T cell activation, and two genes (CD79a and CD81) associated with B cell activation, were downregulated in Fut8^{-/-} SPLs. Moreover, the gene expressions of signal molecules such as MAPKKK, Vav1, PIK3, PKC, and Cyclin D3 were downregulated in Fut8^{-/-} SPLs. Since core fucosylation of proteins is an important post-translational process, it is not surprising that many molecules involved in T and B cell activation were downregulated in Fut8^{-/-} SPLs.

DISCUSSION

The glycosylation and Golgi processing pathways have coevolved with the larger regulatory network that controls T cell activation. It is not surprising that changes of glycosylation are linked to AD pathogenesis, such as galactosylation (26, 27) and sialylation (28, 29). The lower levels of sialylated IgG were found in rheumatoid arthritis (RA) and Wegener's granulomatosis patients, and the sialylated IgG was increased in the sera of patients during remission (28, 29). Moreover, loss of galactose residues on IgG₁ is showed in the sera of RA patients (26, 27). The significant differences of O-glycan on T helper cells were detected in active SLE patients (30). Core-fucosylated glycans that contain bisecting GlcNAc was increased on the IgG of SLE (31). In this study, core fucosylations were associated with SLE severities, and significantly increased in the CD4⁺ T cells of SLE patients. Coincidentally, previous study by Fujii et al. found that the core fucosylation on T cells, required for activation of TCR signaling with anti-CD3/CD28 Abs and induction in colitis, is significantly increased in patients with inflammatory bowel disease (32). Hence, one possible consequence of hyper core

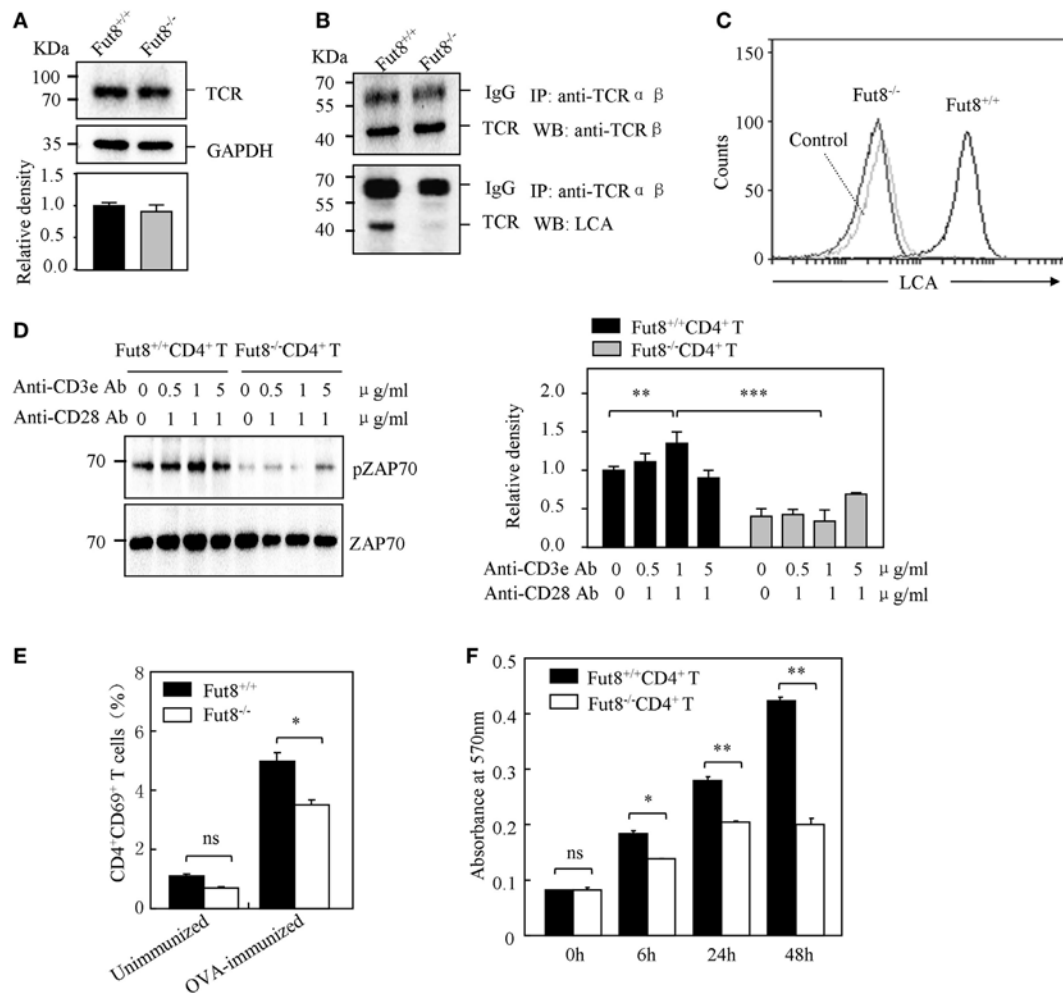


FIGURE 4 | Core fucosylation is required for the activation of CD4⁺ T cells. **(A)** Western blots analysis of T cell receptor (TCR). Whole cell lysates were resolved by SDS-PAGE on a 8% gel, transferred to a PVDF membrane, and probed with anti-TCRβ Ab. Densitometric analysis of the bands of TCRβ normalized against GAPDH. **(B)** Core fucose of N-glycan on TCRβ in *Fut8*^{-/-} CD4⁺ T cells was detected by LCA blot. Whole cell lysates were immunoprecipitated with an anti-TCRαβ antibody. The immunoprecipitates were resolved by SDS-PAGE on a 8% gel, and probed with the LCA and anti-TCRβ Ab. **(C)** Histograms of binding capacity with LCA. Core fucosylation level on the surface proteins of *Fut8*^{+/+} CD4⁺ T and *Fut8*^{-/-} CD4⁺ T cells investigated by FACS analysis. **(D)** Downregulation of phosphorylated Zap70 in *Fut8*^{-/-} CD4⁺ T cells. Purified CD4⁺ T cells were serum-starved and were stimulated with anti-CD3/CD28 Abs for 5 min at 37°C. Cells were lysated in lysis buffer for 15 min on ice. Whole cell lysates were subjected to 10% SDS-PAGE. The blots were probed by anti-pZAP70 Ab and anti-ZAP70 Ab. Densitometric analysis of the bands of pZAP70 normalized against ZAP70. Data are reported as the mean ± SD from three independent experiments (***p* < 0.01; ****p* < 0.001). **(E)** Loss of *Fut8* reduced the CD4⁺CD69⁺ cells populations in the SPL after OVA immunization. SPLs were isolated from OVA-immunized and unimmunized mice (*n* = 5). Cells were stained with anti-CD69 and anti-CD4 Abs, and then detected by FACS. Data are reported as the mean ± SD from three independent experiments (**p* < 0.05; ns, not significant). **(F)** Loss of *Fut8* decreased the proliferation of CD4⁺ T cells. Purified CD4⁺ T cells were stimulated with anti-CD3e Ab-coated microbeads and anti-CD28 Ab for 0, 6, 24, and 48 h at 37°C. The growth rates of CD4⁺ T cell were detected by MTT assay. Data are reported as the mean ± SD from three replicate cultures (**p* < 0.05; ***p* < 0.01). The absorbance related to the formazan dye level was measured with a microplate reader at 570 nm.

fucosylation-induced T cell activation could be the development of SLE. However, the underlying mechanisms of how core fucosylation regulate T cell activation with TCR–pMHC interaction remain unclear.

T cell recognition of pMHC-II ligands on B cells is thought to be carefully coordinated in CD4⁺ T cells. Conformational flexibility is likely responsible for the high degree of promiscuity or cross-reactivity that is evident in the TCR recognition of pMHCs (33–35). There are two models to explain how TCR–pMHC interactions result in T cell activation (36, 37). One

model involves an activation threshold based on the occupancy time of the TCR clustering with pMHCs. The alternative model is that pMHC could induce a specific conformational change of TCR complex and influence the quality of signal transductions *via* TCRs. Since the core fucose of N-glycan is located on the cellular surface of T and B cells, and the core fucosylation could affect the flexibility of N-glycan antenna (38) as well as the conformational stability of proteins (39), it is reasonable to assume that core fucosylation of TCR would affect the geometry and conformation of any TCR–pMHC clusters in the T–B cell

interactions. Based on a previous study in *D. melanogaster* cells, the closeness of the interaction of C α with C β is shown by the hydrogen bonds of the core fucose residue (6, 17), suggested

core fucose possibly strengthens association of C α with C β . A water molecule also bridges the fucose exocyclic oxygen and the side chain of Arg^{150 β} (17). In this scenario, core fucosylation

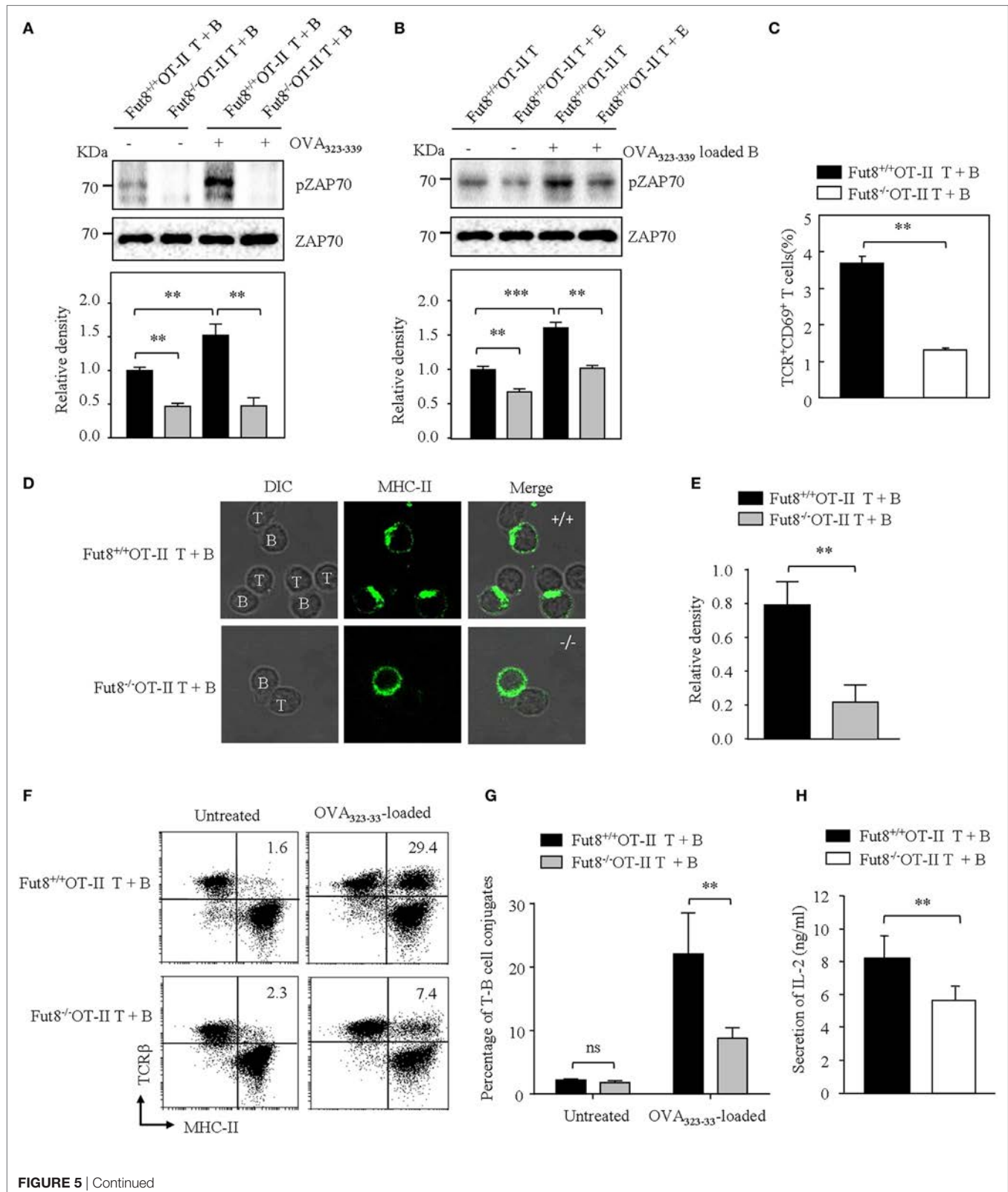
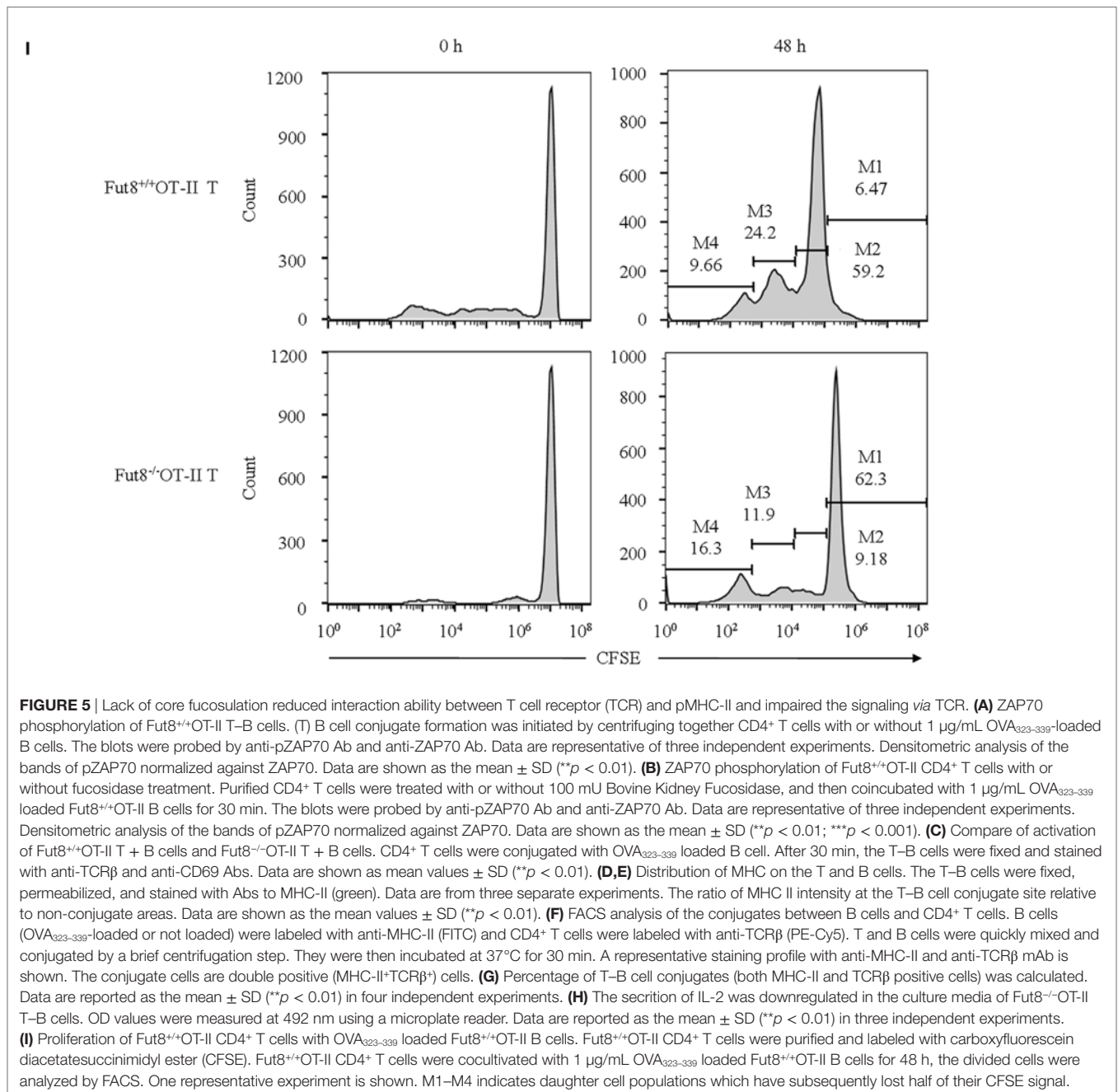


FIGURE 5 | Continued



is expected to provide exciting opportunities to control the TCR function. In the present study, the percentage of T-B cell conjugates (TCR⁺MHC-II⁺) was reduced by a factor of 3.97 (29.4/7.4%) in Fut8^{-/-}OT-II cells, indicated that the core fucosylation has significant functional implications in TCR-pMHC interaction.

Given the intimate relationship between pMHC recognition and TCR signaling, the signaling via TCR is also regulated by glycosylation. It has long been appreciated that Mgat5 deficiency could enhance TCR recruitment to the synapse and results in greater TCR internalization/endocytosis (11). Physiologically,

TCR recognition of pMHC-II ligands on APCs such as dendritic cells and B cells are the most important checkpoint for CD4⁺ T cell activation (40). Engagement of the TCR complexes leads to a signaling cascade of protein tyrosine kinases, such as ZAP70. To explore the role of core fucosylation on the T cell activation, we generated Fut8^{+/+}OT-II and Fut8^{-/-}OT-II mice. Fut8 deficiency results in the attenuated phosphorylation of ZAP70 in Fut8^{-/-}OT-II CD4⁺ T cells with OVA₃₂₃₋₃₃₉-loaded B cells. Also, the phosphorylation of ZAP-70 was significantly reduced in Fut8^{+/+}OT-II CD4⁺ T cells by the treatment of fucosidase. Moreover, in Fut8^{-/-}OT-II cells, the number of CD4⁺ T cells activation (CD69⁺) was decreased

by a factor of 3.5. The proliferation of the Fut8^{-/-}OT-II CD4⁺ T cells cocultivated with OVA_{323–339}-loaded B cells was decreased compared with the Fut8^{+/+}OT-II CD4⁺ T cells. It is conceivable that low T–B cell conjugates was proportional to the decreased T cell activation and proliferation in Fut8^{-/-} CD4⁺ T cells. Core fucosylation is likely to be important in all three proposed stages involved in the T cell activation. First, core fucosylation is essential for the TCR structural formation. Second, core fucosylation of TCR could regulate the recognition of pMHC and affect T cell activation threshold. Third, fucose-specific lectins (41) might participate the events in the T–B cell interaction.

Systemic lupus erythematosus is characterized by the overproduction of auto antibodies, mainly IgG. However, B lymphocyte hyperactivity in SLE is T cell dependent. T cells from SLE patients are activated with a decreased activation threshold and regulated abnormally (32). Indeed, overactive CD4⁺ T cells had been implicated in the pathogenesis of SLE (42). Although we know that CD4⁺ T cell deregulation contributes to SLE pathogenesis, but the mechanism is still largely unknown. Studies in SLE patients and murine models of lupus have shown enhanced level of IL-4 (43), IFN γ (44), and IL-6 (45, 46). Compared to Fut8^{+/+} mice, the IgG class-switching was significantly reduced in the sera of Fut8^{-/-} mice after OVA immunization due to low levels of IL-4, IL-5, IL-6, IFN γ , and TGF secreted by Fut8^{-/-}CD4⁺ T cells. Development of SLE is associated with genetic, hormonal, environmental, and immunological factors, mainly those related to the helper T cell activation. To investigate the mechanisms of the CD4⁺ T cell activation that is important for SLE pathogenesis, we induced the EAE model using Fut8^{+/+} and Fut8^{-/-} mice. Loss of Fut8 reduced CD4⁺ T cell activation and ameliorated the EAE in Fut8^{-/-} mice. Fut8^{-/-} mice are resistant to the induction of EAE, whereas Mgat5^{-/-} mice are hypersensitive to it (47). In this regard, Fut8 and Mgat5 function as opposing regulators of T cell activation thresholds and susceptibility to AD. The hyper core fucosylations are associated with SLE severities, however, whether altered core fucosylation is a consequence or an underlying cause of the SLE cascade remains unclear.

FUT8 is able to modify multiple proteins, followed by the change of their functions. Because the most of immune response molecules are glycoproteins, FUT8 knockdown/knock out affected their function associated with immune response. Okada et al. (10) showed that loss of core fucosylation caused an inhibitory receptor PD-1 deprivation on the cellular surface and augmented T cell activation, when Fut8^{-/-}CD4⁺ T cells transferred

into Rag2^{-/-} mice. Although we did not measure the cell-surface PD-1 expression in the T cell activation and T–B cell interaction, the core fucosylation could regulate the PD-1 expression by modulating TCR signaling strength. Physiologically, there may be some equilibria of the core fucosylation on the TCR and PD-1 to regulate T cell activation. The complexity of *in vivo* condition made us cannot conclude the inability for TCR signaling pathway is the sole reason for the T cell activation, but our study first revealed that Fut8 is essential for TCR–pMHC contact and the following CD4⁺ T cell activation. The balance between specific and degenerate T cell recognition of pMHC-II holds important implications for protective immunity versus autoimmunity. With a better understanding of how core fucosylation regulates of the adaptive immune system, its use in therapy for SLE may prove to be a useful intervention.

ETHICS STATEMENT

All animal work was approved by the Ethics Committee at the Dalian Medical University. The Ethics Committee at the hospital approved the study protocol.

AUTHOR CONTRIBUTIONS

WL, SM, and SS designed research and performed experiment; ML, ZL, and RY analyzed the experimental data; TM, JG, JZ, and NT corrected paper; WL designed research and wrote paper. All authors reviewed the results and approved the final version of the manuscript.

FUNDING

This work was supported by the National Nature Science Foundation of China (31570797, 31270864, 30972675), and Natural Science Foundation of Liaoning Province (2015020253), China.

SUPPLEMENTARY MATERIAL

The Supplementary Material for this article can be found online at <http://www.frontiersin.org/articles/10.3389/fimmu.2018.00078/full#supplementary-material>.

VIDEO S1 | Experimental autoimmune encephalomyelitis symptoms in Fut8^{+/+} mice.

VIDEO S2 | Experimental autoimmune encephalomyelitis symptoms in Fut8^{-/-} mice.

REFERENCES

- Yin Y, Choi SC, Xu Z, Perry DJ, Seay H, Croker BP, et al. Normalization of CD4⁺ T cell metabolism reverses lupus. *Sci Transl Med* (2015) 7(274):274ra18. doi:10.1126/scitranslmed.aaa0835
- Rupanagudi KV, Kulkarni OP, Lichtnekert J, Darisipudi MN, Mulay SR, Schott B, et al. Cathepsin S inhibition suppresses systemic lupus erythematosus and lupus nephritis because cathepsin S is essential for MHC class II-mediated CD4⁺ T cell and B cell priming. *Ann Rheum Dis* (2015) 74(2):452–63. doi:10.1136/annrheumdis-2013-203717
- Reinherz EL, Tan K, Tang L, Kern P, Liu J, Xiong Y, et al. The crystal structure of a T cell receptor in complex with peptide and MHC class II. *Science* (1999) 286(5446):1913–21. doi:10.1126/science.286.5446.1913
- Lee KH, Holdorf AD, Dustin ML, Chan AC, Allen PM, Shaw AS. T cell receptor signaling precedes immunological synapse formation. *Science* (2002) 295(5559):1539–42. doi:10.1126/science.1067710
- Johnson JL, Jones MB, Ryan SO, Cobb BA. The regulatory power of glycans and their binding partners in immunity. *Trends Immunol* (2013) 34(6):290–8. doi:10.1016/j.it.2013.01.006
- Rudd PM, Wormald MR, Stanfield RL, Huang M, Mattsson N, Speir JA, et al. Roles for glycosylation of cell surface receptors involved in cellular immune recognition. *J Mol Biol* (1999) 293(2):351–66. doi:10.1006/jmbi.1999.3104
- Daniels MA, Hogquist KA, Jameson SC. Sweet 'n' sour: the impact of differential glycosylation on T cell responses. *Nat Immunol* (2002) 3(10):903–10. doi:10.1038/ni1002-903


8. Lowe JB. Glycosylation, immunity, and autoimmunity. *Cell* (2001) 104(6): 809–12. doi:10.1016/S0092-8674(01)00277-X
9. Rudd PM, Elliott T, Cresswell P, Wilson IA, Dwek RA. Glycosylation and the immune system. *Science* (2001) 291(5512):2370–6. doi:10.1126/science.291.5512.2370
10. Okada M, Chikuma S, Kondo T, Hibino S, Machiyama H, Yokosuka T, et al. Blockage of core fucosylation reduces cell-surface expression of PD-1 and promotes anti-tumor immune responses of T cells. *Cell Rep* (2017) 20(5):1017–28. doi:10.1016/j.celrep.2017.07.027
11. Demetriou M, Granovsky M, Quaggin S, Dennis JW. Negative regulation of T-cell activation and autoimmunity by Mgat5 N-glycosylation. *Nature* (2001) 409(6821):733–9. doi:10.1038/35055582
12. Lau KS, Partridge EA, Grigorian A, Silvescu CI, Reinhold VN, Demetriou M, et al. Complex N-glycan number and degree of branching cooperate to regulate cell proliferation and differentiation. *Cell* (2007) 129(1):123–34. doi:10.1016/j.cell.2007.01.049
13. Starr TK, Daniels MA, Lucido MM, Jameson SC, Hogquist KA. Thymocyte sensitivity and supramolecular activation cluster formation are developmentally regulated: a partial role for sialylation. *J Immunol* (2003) 171(9):4512–20. doi:10.4049/jimmunol.171.9.4512
14. Moore GT, Brown SJ, Winterhalter AC, Lust M, Salvaris EJ, Selan C, et al. Glycosylation changes in hFUT1 transgenic mice increase TCR signaling and apoptosis resulting in thymocyte maturation arrest. *Mol Immunol* (2008) 45(8):2401–10. doi:10.1016/j.molimm.2007.11.006
15. Kuball J, Hauptrock B, Malina V, Antunes E, Voss RH, Wolfl M, et al. Increasing functional avidity of TCR-redirectioned T cells by removing defined N-glycosylation sites in the TCR constant domain. *J Exp Med* (2009) 206(2):463–75. doi:10.1084/jem.20082487
16. Calderon AD, Liu Y, Li X, Wang X, Chen X, Li L, et al. Substrate specificity of FUT8 and chemoenzymatic synthesis of core-fucosylated asymmetric N-glycans. *Org Biomol Chem* (2016) 14(17):4027–31. doi:10.1039/c6ob00586a
17. Garcia KC, Degano M, Stanfield RL, Brunmark A, Jackson MR, Peterson PA, et al. An alphabeta T cell receptor structure at 2.5 Å and its orientation in the TCR-MHC complex. *Science* (1996) 274(5285):209–19. doi:10.1126/science.274.5285.209
18. Batista FD, Harwood NE. The who, how and where of antigen presentation to B cells. *Nat Rev Immunol* (2009) 9(1):15–27. doi:10.1038/nri2454
19. Wang X, Inoue S, Gu J, Miyoshi E, Noda K, Li W, et al. Dysregulation of TGF-beta1 receptor activation leads to abnormal lung development and emphysema-like phenotype in core fucose-deficient mice. *Proc Natl Acad Sci U S A* (2005) 102(44):15791–6. doi:10.1073/pnas.0507375102
20. Uozumi N, Teshima T, Yamamoto T, Nishikawa A, Gao YE, Miyoshi E, et al. A fluorescent assay method for GDP-L-Fuc:N-acetyl-beta-D-glucosaminide alpha 1-6fucosyltransferase activity, involving high performance liquid chromatography. *J Biochem* (1996) 120(2):385–92. doi:10.1093/oxfordjournals.jbchem.a021424
21. Watson AR, Lee WT. Differences in signaling molecule organization between naive and memory CD4+ T lymphocytes. *J Immunol* (2004) 173(1):33–41. doi:10.4049/jimmunol.173.1.33
22. Tateno H, Nakamura-Tsuruta S, Hirabayashi J. Comparative analysis of core-fucose-binding lectins from *Lens culinaris* and *Pisum sativum* using frontal affinity chromatography. *Glycobiology* (2009) 19(5):527–36. doi:10.1093/glycob/cwp016
23. Mao L, Hou H, Wu S, Zhou Y, Wang J, Yu J, et al. TIGIT signalling pathway negatively regulates CD4+ T-cell responses in systemic lupus erythematosus. *Immunology* (2017) 151(3):280–90. doi:10.1111/imm.12715
24. Scott CA, Peterson PA, Teyton L, Wilson IA. Crystal structures of two I-Ad-peptide complexes reveal that high affinity can be achieved without large anchor residues. *Immunity* (1998) 8(3):319–29. doi:10.1016/S1074-7613(00)80537-3
25. O'Flaherty R, Harbison AM, Hanley PJ, Taron CH, Fadda E, Rudd PM. Aminoquinoline fluorescent labels obstruct efficient removal of N-glycan core alpha(1-6) fucose by bovine kidney alpha-L-fucosidase (BKF). *J Proteome Res* (2017) 16(11):4237–43. doi:10.1021/acs.jproteome.7b00580
26. Parekh RB, Roitt IM, Isenberg DA, Dwek RA, Ansell BM, Rademacher TW. Galactosylation of IgG associated oligosaccharides: reduction in patients with adult and juvenile onset rheumatoid arthritis and relation to disease activity. *Lancet* (1988) 1(8592):966–9. doi:10.1016/S0140-6736(88)91781-3
27. Ercan A, Cui J, Chatterton DE, Deane KD, Hazen MM, Brintnell W, et al. Aberrant IgG galactosylation precedes disease onset, correlates with disease activity, and is prevalent in autoantibodies in rheumatoid arthritis. *Arthritis Rheum* (2010) 62(8):2239–48. doi:10.1002/art.27533
28. Matsumoto A, Shikata K, Takeuchi F, Kojima N, Mizuochi T. Autoantibody activity of IgG rheumatoid factor increases with decreasing levels of galactosylation and sialylation. *J Biochem* (2000) 128(4):621–8. doi:10.1093/oxfordjournals.jbchem.a022794
29. Espy C, Morelle W, Kavian N, Grange P, Goulvestre C, Viallon V, et al. Sialylation levels of anti-proteinase 3 antibodies are associated with the activity of granulomatosis with polyangiitis (Wegener's). *Arthritis Rheum* (2011) 63(7):2105–15. doi:10.1002/art.30362
30. Ramos-Martinez E, Lascuain R, Tenorio EP, Sanchez-Gonzalez A, Chavez-Rueda K, Chavez-Sanchez L, et al. Differential expression of O-glycans in CD4(+) T lymphocytes from patients with systemic lupus erythematosus. *Tohoku J Exp Med* (2016) 240(1):79–89. doi:10.1620/tjem.240.79
31. Vuckovic F, Kristic J, Gudelj I, Teruel M, Keser T, Pezer M, et al. Association of systemic lupus erythematosus with decreased immunosuppressive potential of the IgG glycome. *Arthritis Rheumatol* (2015) 67(11):2978–89. doi:10.1002/art.39273
32. Fujii H, Shinzaki S, Iijima H, Wakamatsu K, Iwamoto C, Sobajima T, et al. Core fucosylation on T cells, required for activation of T-cell receptor signaling and induction of colitis in mice, is increased in patients with inflammatory bowel disease. *Gastroenterology* (2016) 150(7):1620–32. doi:10.1053/j.gastro.2016.03.002
33. Alarcon B, Gil D, Delgado P, Schamel WW. Initiation of TCR signaling: regulation within CD3 dimers. *Immunol Rev* (2003) 191:38–46. doi:10.1034/j.1600-065X.2003.00017.x
34. Mason D. A very high level of crossreactivity is an essential feature of the T-cell receptor. *Immunol Today* (1998) 19(9):395–404. doi:10.1016/S0167-5699(98)01299-7
35. Kass I, Buckle AM, Borg NA. Understanding the structural dynamics of TCR-pMHC complex interactions. *Trends Immunol* (2014) 35(12):604–12. doi:10.1016/j.it.2014.10.005
36. Alam SM, Davies GM, Lin CM, Zal T, Nasholds W, Jameson SC, et al. Qualitative and quantitative differences in T cell receptor binding of agonist and antagonist ligands. *Immunity* (1999) 10(2):227–37. doi:10.1016/S1074-7613(00)80023-0
37. Schamel WW, Arechaga I, Risueno RM, van Santen HM, Cabezas P, Risco C, et al. Coexistence of multivalent and monovalent TCRs explains high sensitivity and wide range of response. *J Exp Med* (2005) 202(4):493–503. doi:10.1084/jem.20042155
38. Stubbs HJ, Lih JJ, Gustafson TL, Rice KG. Influence of core fucosylation on the flexibility of a biantennary N-linked oligosaccharide. *Biochemistry* (1996) 35(3):937–47. doi:10.1021/bi9513719
39. Wormald MR, Dwek RA. Glycoproteins: glycan presentation and protein-fold stability. *Structure* (1999) 7(7):R155–60. doi:10.1016/S0969-2126(99)80095-1
40. Wolfert MA, Boons GJ. Adaptive immune activation: glycosylation does matter. *Nat Chem Biol* (2013) 9(12):776–84. doi:10.1038/nchembio.1403
41. Lehrman MA, Hill RL. The binding of fucose-containing glycoproteins by hepatic lectins. Purification of a fucose-binding lectin from rat liver. *J Biol Chem* (1986) 261(16):7419–25.
42. Moulton VR, Tsokos GC. T cell signaling abnormalities contribute to aberrant immune cell function and autoimmunity. *J Clin Invest* (2015) 125(6):2220–7. doi:10.1172/jci78087
43. Mi XB, Zeng FQ. Hypomethylation of interleukin-4 and -6 promoters in T cells from systemic lupus erythematosus patients. *Acta Pharmacol Sin* (2008) 29(1):105–12. doi:10.1111/j.1745-7254.2008.00739.x
44. Gereiz L, Shkolnik T, Hirschmann O, Lorber M, Arad G, Kaempfer R. Hyperinducible expression of the interferon-gamma (IFN-gamma) gene and its suppression in systemic lupus erythematosus (SLE). *Clin Exp Immunol* (1997) 109(2):296–303. doi:10.1046/j.1365-2249.1997.4471345.x
45. Linker-Israeli M, Deans RJ, Wallace DJ, Prehn J, Ozeri-Chen T, Klinenberg JR. Elevated levels of endogenous IL-6 in systemic lupus erythematosus. A putative role in pathogenesis. *J Immunol* (1991) 147(1):117–23.
46. Grondal G, Gunnarsson I, Ronnelid J, Rogberg S, Klareskog L, Lundberg I. Cytokine production, serum levels and disease activity in systemic lupus erythematosus. *Clin Exp Rheumatol* (2000) 18(5):565–70.

47. Grigorian A, Lee SU, Tian W, Chen IJ, Gao G, Mendelsohn R, et al. Control of T cell-mediated autoimmunity by metabolite flux to N-glycan biosynthesis. *J Biol Chem* (2007) 282(27):20027–35. doi:10.1074/jbc.M701890200

Conflict of Interest Statement: The authors declare that the research was conducted in the absence of any commercial or financial relationships that could be construed as a potential conflict of interest.

Copyright © 2018 Liang, Mao, Sun, Li, Li, Yu, Ma, Gu, Zhang, Taniguchi and Li. This is an open-access article distributed under the terms of the Creative Commons Attribution License (CC BY). The use, distribution or reproduction in other forums is permitted, provided the original author(s) and the copyright owner are credited and that the original publication in this journal is cited, in accordance with accepted academic practice. No use, distribution or reproduction is permitted which does not comply with these terms.

Catfish rhamnose-binding lectin induces G_{0/1} cell cycle arrest in Burkitt's lymphoma cells via membrane surface Gb3

Shigeki Sugawara¹ · Changhun Im¹ · Tasuku Kawano¹ · Takeo Tatsuta¹ ·
Yasuhiro Koide² · Daiki Yamamoto² · Yasuhiro Ozeki² · Kazuo Nitta¹ ·
Masahiro Hosono¹ 

Received: 15 June 2016 / Revised: 24 August 2016 / Accepted: 3 October 2016 / Published online: 28 October 2016
© Springer Science+Business Media New York 2016

Abstract *Silurus asotus* egg lectin (SAL), an α -galactoside-binding protein isolated from the eggs of catfish, is a member of the rhamnose-binding lectin family that binds to Gb3 glycan (Gal α 1–4Gal β 1–4Glc). We have previously demonstrated that SAL reduces the proliferation of Gb3-expressing Burkitt's lymphoma Raji cells and confirm here that it does not reduce their viability, indicating that unlike other lectins, it is not cytotoxic. The aim of this study was to determine the signal transduction mechanism(s) underlying this novel SAL/Gb3 binding-mediated effect profile. SAL/Gb3 interaction arrested the cell cycle through increasing the G_{0/1} phase population of Raji cells. SAL suppressed the transcription of cell cycle-related factors such as c-MYC, cyclin D3, and cyclin-dependent protein kinase (CDK)-4. Conversely, the CDK inhibitors p21 and p27 were elevated by treatment with SAL. In particular, the production of p27 in response to SAL treatment increased steadily, whereas p21 production was maximal at 12 h and lower at 24 h. Activation of Ras-MEK-ERK pathway led to an increase in expression of p21. Notably, treatment of Raji cells with anti-Gb3 mAb alone did not produce the above

effects. Taken together, our findings suggest that Gb3 on the Raji cell surface interacts with SAL to trigger sequential GDP-Ras phosphorylation, Ras-MEK-ERK pathway activation, p21 production, and cell cycle arrest at the G_{0/1} phase.

Keywords Cell cycle arrest · Extracellular signal-regulated kinase · Globotriaosylceramide · p21 · SUEL/ rhamnose-binding lectin

Abbreviations

BrdU	Bromodeoxy uridine
CCND3	Cyclin D3
CDK	Cyclin-dependent protein kinase
ERK	Extracellular signal-regulated kinase
FBS	Fetal bovine serum
FITC	Fluorescein isothiocyanate
Gb3	Gal α 1–4Gal β 1–4Glc-Cer
GDP	Guanosine diphosphate
GEM	Glycosphingolipid-enriched microdomains
GTP	Guanosine triphosphate
GSL	Glycosphingolipid
mAb	Monoclonal antibody
JNK	c-Jun N-terminal kinase
MAPK	Mitogen-activated protein kinase
MEK	MAPK/ERK kinase
PVDF	Polyvinylidene difluoride
qRT-PCR	Quantitative reverse transcription-polymerase chain reaction
SAL	<i>Silurus asotus</i> egg lectin
SDS-PAGE	Sodium dodecyl sulfate-polyacrylamide gel electrophoresis
SUEL	Sea urchin egg lectin

Electronic supplementary material The online version of this article (doi:10.1007/s10719-016-9739-2) contains supplementary material, which is available to authorized users.

✉ Masahiro Hosono
mhosono@tohoku-mpu.ac.jp

¹ Division of Cell Recognition Study, Institute of Molecular Biomembrane and Glycobiology, Tohoku Medical and Pharmaceutical University, 4-4-1 Komatsushima, Aoba-ku, Sendai 981-8558, Japan

² Laboratory of Glycobiology and Marine Biochemistry, Department of Life and Environmental System Science, Graduate School of NanoBio Sciences, Yokohama City University, 22-2 Seto, Kanazawa-ku, Yokohama 236-0027, Japan

Introduction

Rhamnose-binding lectins (RBLs) have been found in the eggs (oocytes) of various fish species [1–3] and are capable of binding to L-rhamnose and α -D-galactosides. The primary structure of rhamnose-binding lectins is similar to that of a D-galactose-binding lectin termed SUEL that was purified from sea urchin (*Anthocidaris crassispina*) eggs and is composed of 105 amino acid residues [4]. The symbolic term “RBLs” is named after their carbohydrate-binding specificity against L-rhamnose. Indeed, it shows the highest affinity among common saccharides, however, actual ligands of RBL are thought to be α -galactosyl sugar chains such as human type B oligosaccharide and globotriaosylceramide (Gb3) being on the cell surface. *Silurus asotus* egg lectin (SAL) is a 32-kDa protein comprised of three tandem repeats of 95 amino acid residues [5]. Previously, we demonstrated that SAL agglutinated Raji Burkitt's lymphoma cells (which express glycosphingolipids [GSLs] containing Gb3 (or CD77; Gal α 1–4Gal β 1–4Glc) in GSL-enriched microdomains on the cell surface) but does not agglutinate erythroleukemia K562 cells (which do not express Gb3 on the cell surface) [6]. Additionally, SAL caused a reduction in cell size and increased annexin-V binding to and propidium iodide incorporation into Raji cells. Although this effect on Raji cells might represent damage at the late apoptosis or necrosis stage, the SAL-treated Raji cells remained viable [7]. In contrast, the lectin CSL3 purified from the eggs of the chum salmon (*Oncorhynchus keta*) was found to induce cell death of Gb3-displaying Caco-2 cells via an apoptotic pathway [8]. Watanabe *et al.* reported that Gb3-expressing HeLa cells were killed by pierisin, a toxic lectin isolated from cabbage butterfly (*Pieris rapae*) wings [9]. Pierisin contains a triple tandem repeat of ricin B-like domains and an ADP-ribosyltransferase domain in the polypeptide [10]. Treatment of HeLa cells with pierisin caused a delay in the cell cycle as well as apoptosis [11]. Therefore, SAL appears to have a different biological function as compared to CSL3 and pierisin.

Much research has focused on Gb3 because it comprises one of the components of glycosphingolipid-enriched microdomains (GEMs) on the cell surface, which has been shown to function as trigger of signal transduction. The glycosphingolipids including Gb3 in GEM were reported to associate with signal transducers such as Src family kinases and small G-proteins localized in the cytosol through the lipid bilayer [12]. Therefore, in this study we focused on identifying the signal transduction pathways stimulated by the SAL-Gb3 interaction. We found that the interaction between SAL and Gb3 enhanced the expression level of cyclin-dependent protein kinase inhibitors. This enhancement promoted Raji cell cycle arrest at the G_{0/1} phase through phosphorylation of GDP-Ras, mitogen-activated protein kinase (MAPK)/extracellular signal-regulated kinase (ERK) kinase (MEK), and ERK. Taken together, these findings suggest that Gb3 plays an important role in cell signal regulation through its ability to bind to lectins. Elucidation of the mechanism of cell cycle arrest by SAL

and Gb3 might lead to the discovery of novel lectin-based cell regulatory systems.

Materials and methods

Materials SAL was purified by sequential chromatography on DE23 (Whatman, Little Chalfont, UK) anion exchange and D-galactose-Sepharose 6B columns as described previously [13].

Cell lines Burkitt's lymphoma Raji cells from the Cell Resource Center of Biomedical Research, Institute of Development, Aging and Cancer, Tohoku University (Sendai, Japan) were cultured in RPMI-1640 medium (Nissui Pharmaceutical Co., Tokyo, Japan) supplemented with 10 % v/v fetal bovine serum (FBS) and antibiotic-antimycotic solution (penicillin [100 IU/ml], streptomycin [100 μ g/ml], and amphotericin B [0.25 μ g/ml], Life Technologies, Carlsbad, CA, USA) and maintained at 37 °C in a 95 % air/5 % CO₂ atmosphere.

Cytotoxicity and cell viability assays Raji cells (1×10^6 /ml) were seeded in 6-well plates and incubated with various concentrations of SAL (0–100 μ g/ml) for 24, 36, 48, 72, 96, or 120 h. Cytotoxic activity and cell growth were determined by trypan blue (0.5 % w/v) exclusion assay [14]. Cell proliferation was determined by WST-8 assay using a Cell Counting Kit-8 (Dojindo Laboratories; Kumamoto, Japan). After plating the cells into a 96-well flat-bottom plate at 5×10^4 cells/well (90 μ l), the cells were treated with 100 μ g/ml SAL (final concentration) for 24 or 48 h. Then, 10 μ l WST-8 solution was added into each well and the cells were incubated for 4 h at 37 °C. The absorbance was measured at a wavelength of 450 nm using the GloMax Multi Detection System (Promega, Madison, WI, USA). Cells were treated with rat anti-Gb3 monoclonal antibody (mAb) (clone 38.13; Beckman Coulter, Miami, FL, USA) in flat-bottom plastic plates for 24, 48, 72, 96, or 120 h at 37 °C. Cytotoxic activity and cell growth were determined as described above. Bright-field images were acquired using an inverted microscope (model IX71; Olympus Co., Tokyo, Japan) with a 10 \times objective lens.

Detection of cell cycle arrest by SAL Cell cycle arrest was assayed using a fluorescein isothiocyanate (FITC) bromodeoxy uridine (BrdU) flow kit (BD Biosciences, San Jose, CA, USA) according to the manufacturer's protocol. In brief, cells (5×10^5) were treated with SAL (100 μ g/l) for 24 h, fixed with 4 % paraformaldehyde, and permeabilized by saponin for 1 h at 37 °C in the presence of 1 U DNase. Cell division was estimated as the ratio of BrdU incorporation into cells (detected using a FITC-conjugated anti-BrdU antibody after incubation for 20 min at room temperature) to total

DNA amount in the cells (detected with 7-aminoactinomycin D) using a FACSCalibur (BD Biosciences) with single laser emitting excitation at 488 nm and analyzed with Cell Quest pro software (BD Biosciences).

Expression levels of mRNA encoding cell cycle-related molecules Raji cells (5×10^5) were cultured for 12 or 24 h in RPMI-1640 medium containing SAL (100 µg/ml), SAL (100 µg/ml)/saccharide (20 mM), or without SAL at 37 °C in 95 % air/5 % CO₂. Total RNA was extracted from cells using an AllPrep RNA/Protein Kit (Qiagen, Valencia, CA, USA). cDNA was synthesized from the total RNA (1 µg) using a SuperScript VILO cDNA Synthesis Kit (Invitrogen, San Diego, CA, USA). Quantitative reverse transcription-polymerase chain reaction (qRT-PCR) assays were performed using a LightCycler 480 system with the LightCycler 480 Probes Master Kit (Roche Diagnostics, Indianapolis, IN, USA). PCR primers for amplification of *CDK4*, *c-MYC*, cyclin D3 (*CCND3*), *p21*, and *p27* using a TaqMan/probe library assay were designed by the Universal Probe Library Assay Design Center (<https://www.roche-applied-science.com/sis/rtpcr/upl/center.jsp>). The expression levels of these genes were standardized relative to the mRNA expression level of *GAPDH* (as a housekeeping gene) based on their average crossing point values.

Protein expression of signal transduction molecules, their phosphorylated forms, and cell cycle-related molecules Raji cells (5×10^5) were cultured for 12 or 24 h in RPMI-1640 with or without SAL (100 µg/ml) at 37 °C in 95 % air/5 % CO₂. Cell lysate was prepared using an AllPrep RNA/Protein Kit (Qiagen), subjected to sodium dodecyl sulfate-polyacrylamide gel electrophoresis (SDS-PAGE) (10 % separation gel), and electrotransferred onto a polyvinylidene difluoride (PVDF) membrane (pore size 0.45 µm) (Hybond-P; GE Healthcare Bio-Sciences AB, Uppsala, Sweden) according to the manufacturer's protocol [15–17]. The membrane was treated with blocking buffer (Blocking One; Nacalai Tesque Inc., Kyoto, Japan) for 1 h at room temperature and washed with Tris-buffered saline (TBS) containing 0.05 % Tween-20. The primary antibodies used were directed to p21^{Waf1/Cip1} (1:1000, rabbit mAb, clone 12D1; Cell Signaling Technology Inc., Danvers, MA, USA [CST]), p27^{Kip1} (1:1000, rabbit mAb; clone D69C12; CST), c-MYC (1:1000, rabbit polyclonal antibody; CST), CDK4 (1:2000, mouse mAb; clone DCS156; CST), cyclin D3 (1:2000, mouse mAb; clone DCS22; CST), phospho-MEK_{1/2} (1:1000, rabbit mAb; CST), MEK1 (1:1000, rabbit mAb; CST), phospho-ERK_{1/2} (1:1000, mouse mAb; BD Biosciences), ERK1 (1:5000, mouse mAb; BD Biosciences), phospho-p38 MAPK (1:2500, mouse mAb; BD Biosciences), p38 MAPK (1:5000, mouse mAb; BD Biosciences), phospho-JNK (1:250, mouse mAb; BD Biosciences), JNK (1:250, mouse

mAb; BD Biosciences), and GAPDH (1:20,000, mouse mAb; clone 6C5; Ambion/Invitrogen, Carlsbad, CA, USA). These antibodies were applied in immunoreaction enhancer solution (Can Get Signal Solution 1; Toyobo Co., Osaka, Japan). The membrane was incubated for 16 h at 4 °C. The secondary antibody, horseradish peroxidase (HRP)-conjugated anti-mouse or anti-rabbit IgG (Chemicon International Inc., Temecula, CA, USA), was diluted 1:20,000 in immunoreaction enhancer solution. The membrane was incubated for 1 h at room temperature and then exposed to X-ray film (Fuji Film Co., Tokyo, Japan) using enhanced chemical luminescence and western blotting with ECL Prime detection reagent (GE Healthcare Bio-Sciences AB). A synthetic inhibitor of MEK_{1/2}, 1,4-diamino-2,3-dicyano-1,4-bis (2-aminophenylthio) butadiene (U0126) (1 µg) (Calbiochem; San Diego, CA, USA) was dissolved in 247 µl dimethylsulfoxide to create a 10 mM stock solution. Cells were incubated with U0126 (10 µM) in RPMI-1640 with FBS for 2 h, supplemented with SAL (100 µg/ml), and incubated for another 12 h. Whole cell extracts were separated by SDS-PAGE on a 10 % gel and blotted onto PVDF membranes. Phosphorylated kinases were identified by western blotting with anti-phospho-MEK_{1/2}, anti-MEK_{1/2}, anti-phospho-ERK_{1/2}, anti-ERK₁, and HRP-conjugated anti-mouse IgG antibodies. Signals were detected by X-ray film exposure and western blotting as described above. Proteins were quantified by densitometry using NIH ImageJ software (version 1.440, Bethesda, MD, USA). The optical densities of phosphorylated MEK_{1/2} (P-MEK_{1/2}) and phosphorylated ERK_{1/2} (P-ERK_{1/2}) were measured and normalized to the optical densities of MEK_{1/2} and ERK₁, respectively.

Detection of GTP-Ras The active form of Ras exchanged through GDP to GTP as a result of SAL stimulation was assayed by affinity precipitation using a Ras activation assay kit (Upstate Biotechnology; Lake Placid, NY, USA). Raji cells (1×10^6) were cultured for 0.5, 3, 6, 12, or 24 h in RPMI-1640 containing SAL (100 µg/ml) at 37 °C in 95 % air/5 % CO₂, lysed with Mg²⁺ lysis buffer (125 mM 4-(2-hydroxyethyl)-1-piperazineethanesulfonic acid [HEPES], pH 7.5, 750 mM NaCl, 5 % Igepal® CA-630, 50 mM MgCl₂, 5 mM ethylenediaminetetraacetic acid, and 10 % glycerol), and incubated with the agarose-conjugated Ras-binding domain of Raf-1 (5 µl) for 30 min at 4 °C. The agarose-coated beads were boiled in sample buffer and the cell lysate was then subjected to SDS-PAGE on a 10 % separation gel and transferred onto a PVDF membrane. The GTP-Ras formed following SAL stimulation was detected by anti-Ras mAb (0.05 µg/ml) and HRP-conjugated polyclonal antibodies (1:1000) [18, 19]. Activated Ras was detected using ECL Prime (GE Healthcare Bio-Sciences AB).

RNA interference-mediated knockdown of alpha-1,4-galactosyltransferase (A4GALT) Raji cells (1.2×10^6) cells were centrifuged and resuspended in 100 μ l nucleofection V solution (Lonza, Basel, Switzerland) containing 20 μ M A4GALT siRNA (Dharmacon, Lafayette, CO, USA) and electroporated with a Nucleofector (Lonza) using the M-13 program. After nucleofection, the cells were transferred to a 12-well plate containing 1 ml fresh complete medium (RPMI 1640 containing 10 % FBS and antibiotic-antimycotic solution) and incubated at 37 °C for 120 h. After incubation, the expression of Gb3 was detected by flow cytometry.

Flow cytometric analysis of Gb3 expression Cells (2×10^5) were treated with or without anti-Gb3 mAb (BGR23, mouse IgG2b; Tokyo Kasei Co. Ltd., Tokyo, Japan) at a dilution of 1:1000 in PBS (100 μ l) at 4 °C for 30 min and washed three times with PBS. The cells were then treated with Alexa Fluor (AF) 488-conjugated goat anti-mouse IgG (H + L) (Molecular Probes, Invitrogen AG, Basel, Switzerland) at a dilution of

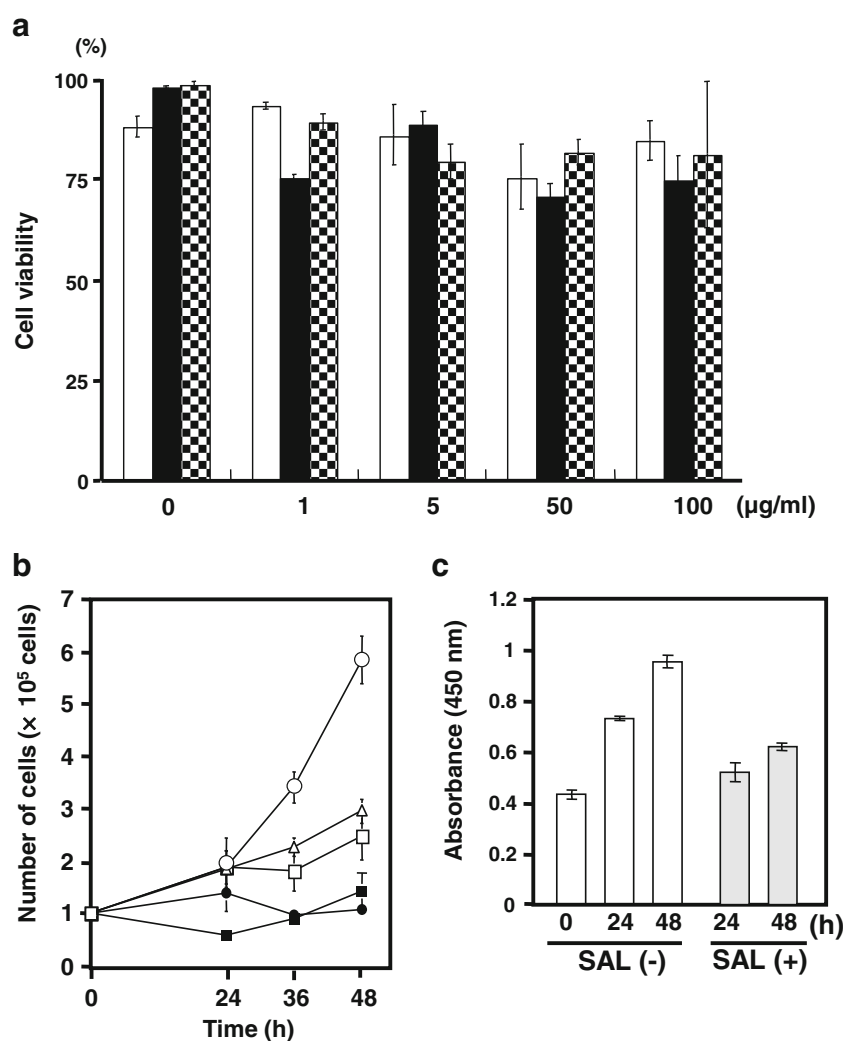
1:2500 in PBS (100 μ l) at 4 °C for 30 min. The degree of Gb3 expression on the cell surface was analyzed using the FACSCalibur as described above.

Statistical analysis Experimental results are presented as the means \pm standard error (SE). Differences in means were evaluated using the two-tailed Student's *t*-test with *P* values <0.05 considered to be statistically significant.

Results

Effects of SAL on cell proliferation and viability In the current study, we further expand upon our previous findings following exposure of Raji cells to SAL (100 μ g/ml) for 24 h by examining the concentration- and time-dependent effect of SAL. According to the trypan blue exclusion assay, SAL did not reduce the viability of Raji cells even at the concentration of 100 μ g/ml for 120 h (Fig. 1a and S1). Proliferation was

Fig. 1 SAL reduces the proliferation but has no effect on the viability of Raji cells. **a.** Time- and dose-dependent effects of SAL treatment on cell viability. Cells were treated with SAL (0, 1, 5, 50, or 100 μ g/ml) for 24 h (white columns), 36 h (black columns), or 48 h (gray columns) at 37 °C. Cell viability was evaluated by trypan blue exclusion assay. The values shown are the means of triplicate experiments. Error bars: standard error (SE). **b.** Cells were treated with SAL (0, 1, 5, 50, or 100 μ g/ml) for 24, 36, or 48 h at 37 °C. The number of living cells was assessed by trypan blue exclusion assay. \circ : 0 μ g/ml (control). Δ : 1 μ g/ml. \square : 5 μ g/ml. \blacksquare : 50 μ g/ml. \bullet : 100 μ g/ml. **c.** Cells were treated with (+) or without (–) SAL (100 μ g/ml) for 24 or 48 h at 37 °C. Proliferation was evaluated by the WST-8 assay. The values shown are the means of triplicate experiments. Error bars: SE



reduced further at higher concentrations and was abolished completely at 50 $\mu\text{g/ml}$ (Fig. 1b). The WST-8 assay showed that SAL reduced cell proliferation in a time-dependent manner (Fig. 1c). On the other hand, Gb3-binding monoclonal antibody, anti-Gb3, had no such effects to Raji cells including cell-agglutination (Fig. 2a–c, S2 and S3). Stimulation with SAL (100 $\mu\text{g/ml}$) for 72 h caused a 6-fold decrease in the number of cells compared with control cells (Fig. 3). When the medium was replaced by SAL-free medium, the cells completely recovered their proliferation activity after 48 h (Fig. 3, column “SAL free”). These results suggest that SAL reduced the proliferation of Raji cells but was not cytotoxic.

G₁ cell cycle arrest by SAL To gain insight into the mechanism of SAL-induced growth inhibition in Raji cells, we analyzed the SAL-dependent changes in cell cycle distribution. Flow cytometric analysis showed that stimulation with SAL (100 $\mu\text{g/ml}$) for 24 h caused a substantial increase of the ratio of the G_{0/1} phase to the whole Raji cell population of 20 % with a consequent decrease of the proportion of cells in S phase by 20 % (Fig. 4 and Table 1). The G_{0/1} cell cycle arrest no longer occurred when SAL was removed from the medium. In contrast, the G_{2/M}

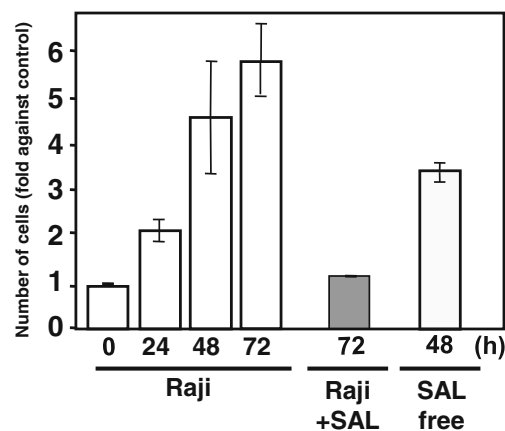


Fig. 3 Removal of SAL restores cell proliferation. Cells were cultured without SAL at 37 °C for 0, 24, 48, or 72 h (Raji). Other cells were treated with SAL (100 $\mu\text{g/ml}$) for 72 h (Raji + SAL) or with SAL followed by SAL-free medium for 48 h (SAL free). The number of living cells was assessed by trypan blue exclusion assay. The values shown are the means of triplicate experiments. Error bars: SE

phase was not shifted by SAL treatment (Table 1). These findings suggest that SAL arrests the G_{0/1} phase of the cell cycle by binding to Gb3, followed by the loss of cell proliferation.

Fig. 2 Anti-Gb3 mAb does not induce apoptosis or inhibit cell proliferation. Cells were treated with anti-Gb3 mAb (100 or 200 $\mu\text{g/ml}$) or SAL (100 $\mu\text{g/ml}$) for 24 h at 37 °C. Cell viability (a) and proliferation (b) were evaluated by trypan blue exclusion and WST-8 assays, respectively. The values shown are the means of triplicate experiments. Error bars: SE. **c.** Cell agglutination induced by treatment with anti-Gb3 mAb (100 or 200 $\mu\text{g/ml}$) or SAL (20 $\mu\text{g/ml}$). Negative control (Cont): addition of PBS instead of lectin or antibody. The images are from bright-field microscopy at 100 \times magnification

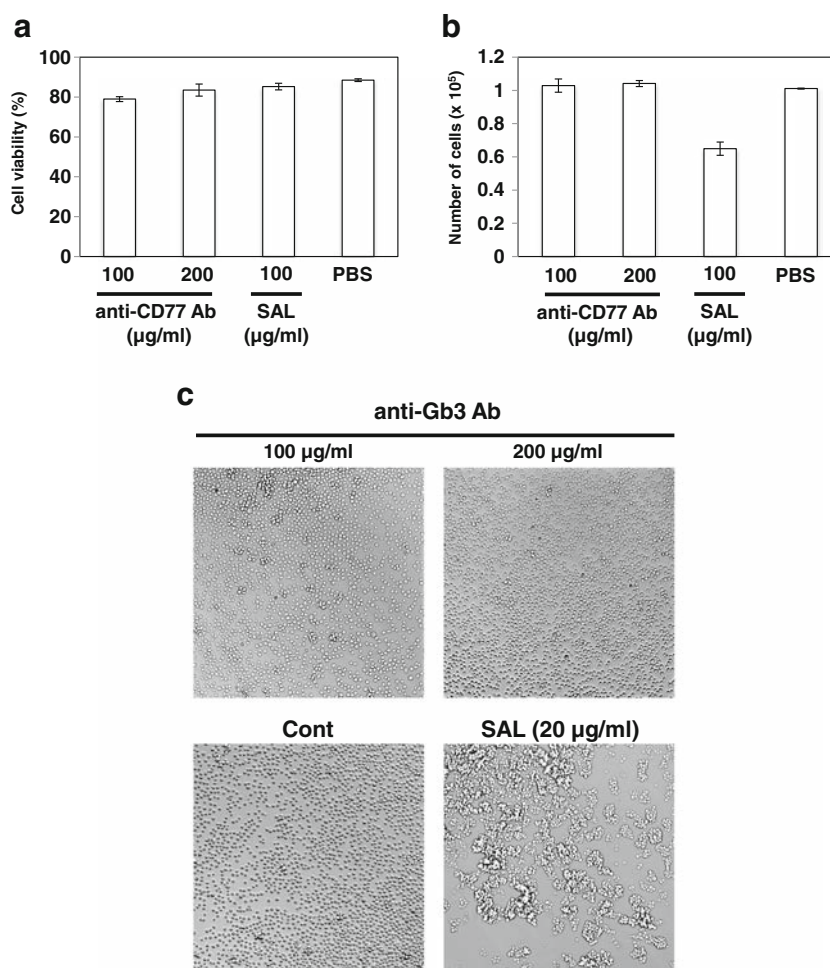
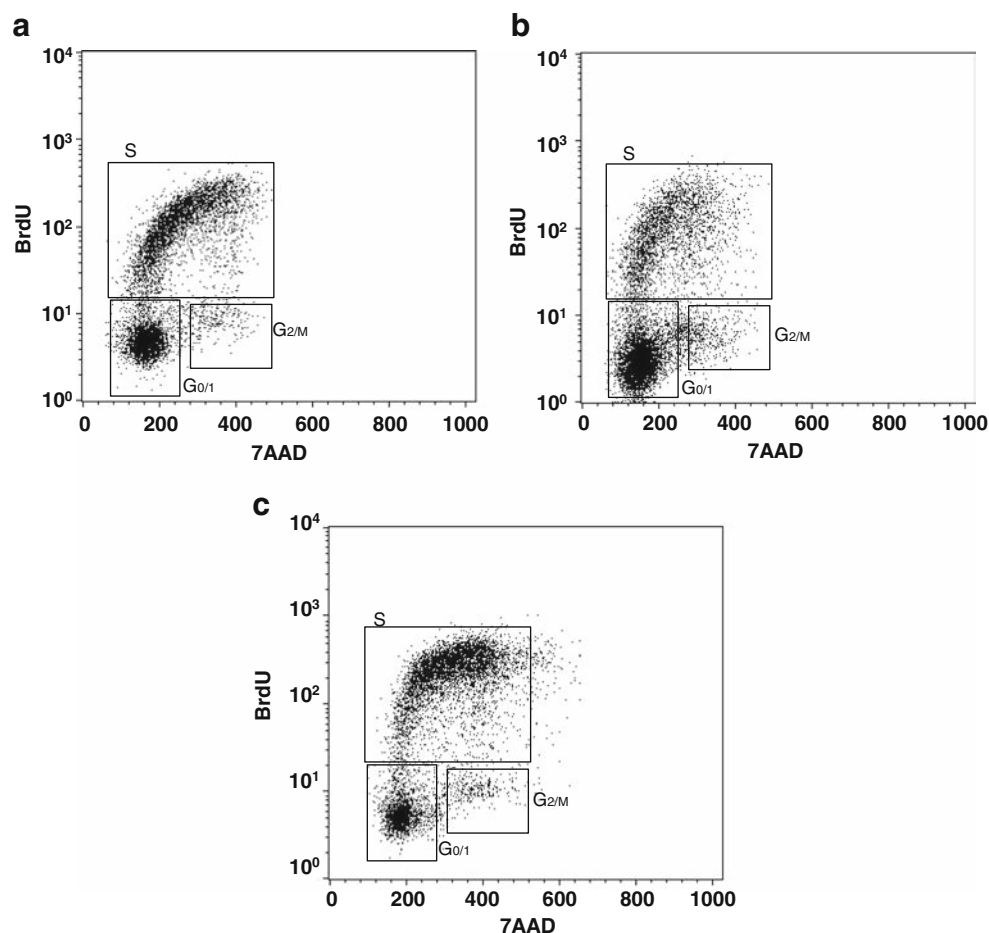


Fig. 4 Alteration of cell cycle distribution in SAL-treated Raji cells. Cells were cultured without SAL at 37 °C for 72 h (SAL-untreated) (**a**). Other cells were treated with SAL (100 µg/ml) for 72 h (SAL-treated) (**b**) or subsequently with SAL-free medium for 48 h (SAL-removed) (**c**). The distribution of cells in each cell cycle phase ($G_{0/1}$, S, and $G_{2/M}$) was determined by FACSCalibur analysis



Down-regulation of *c-MYC*, *CDK4*, and *CCND3* gene expression levels and the induction of mRNA and protein expression levels of the CDK inhibitors p21 and p27 by SAL Numerous studies have shown that CDK acts as an accelerating factor of the cell cycle [20, 21]. In Raji cells treated with SAL for 24 h, *CDK4* mRNA levels were down-regulated in comparison with those of untreated cells (Fig. 5a). However, SAL had no effect on the mRNA expression levels of *CDK2* (data not shown). The expression of *CDK4* is regulated by *c-Myc*. In addition, mammalian cyclin D3 is a member of the G_1/S cyclin family and functions as a key protein to transition the cell cycle to the next phase [22–24]. Therefore,

the alteration of protein expression levels of *c-MYC* and cyclin D3 in Raji cells were examined following SAL treatment. As shown Fig. 5a, SAL treatment for 24 h reduced the expression level of *c-MYC* by 40 % and that of *CCND3* by 30 %. Western blotting confirmed the coordinate decreased expression levels of the *c-Myc*, *CDK4*, and cyclin D3 proteins (Fig. 5b). In addition, the inhibitory effects of SAL on gene expression were partially eliminated in the presence of 10 mM melibiose or rhamnose (Fig. 5c). These findings indicate that the interaction between SAL and Gb3 reduced the expression of *CDK4*, *c-MYC*, and *CCND3* mRNAs.

p21 and p27 have been shown to inhibit CDK activity and cell cycle progression [25–27]. We therefore examined whether the expression of p21 and p27 was changed by treatment with SAL. qRT-PCR analysis showed increases of 130 % and 70 % in the mRNA expression levels of *p21* and *p27*, respectively, in SAL-treated Raji cells (Fig. 5a). In addition, western blotting analysis showed corresponding increases of p21 and p27 protein expression levels (Fig. 5b). Furthermore, up-regulation of *p21* was specifically inhibited in the presence of rhamnose or melibiose (10 mM) but not by glucose and lactose. Notably, however, elevation of *p27* was not blocked by these saccharides (Fig. 5c).

Table 1 Effect of SAL on cell cycle distribution. The percentages of cells in each cell cycle phase ($G_{0/1}$, S, or $G_{2/M}$) were determined by FACSCalibur analysis. The values shown are the means \pm SE from two or more independent experiments

	$G_{0/1}$	S	$G_{2/M}$ (%)
SAL-untreated	34.3 \pm 2.5	62.0 \pm 2.9	2.7 \pm 0.4
SAL-treated	53.5 \pm 3.2	35.1 \pm 2.5	7.5 \pm 1.7
SAL-removed	27.0 \pm 0.7	67.5 \pm 1.1	3.7 \pm 0.5

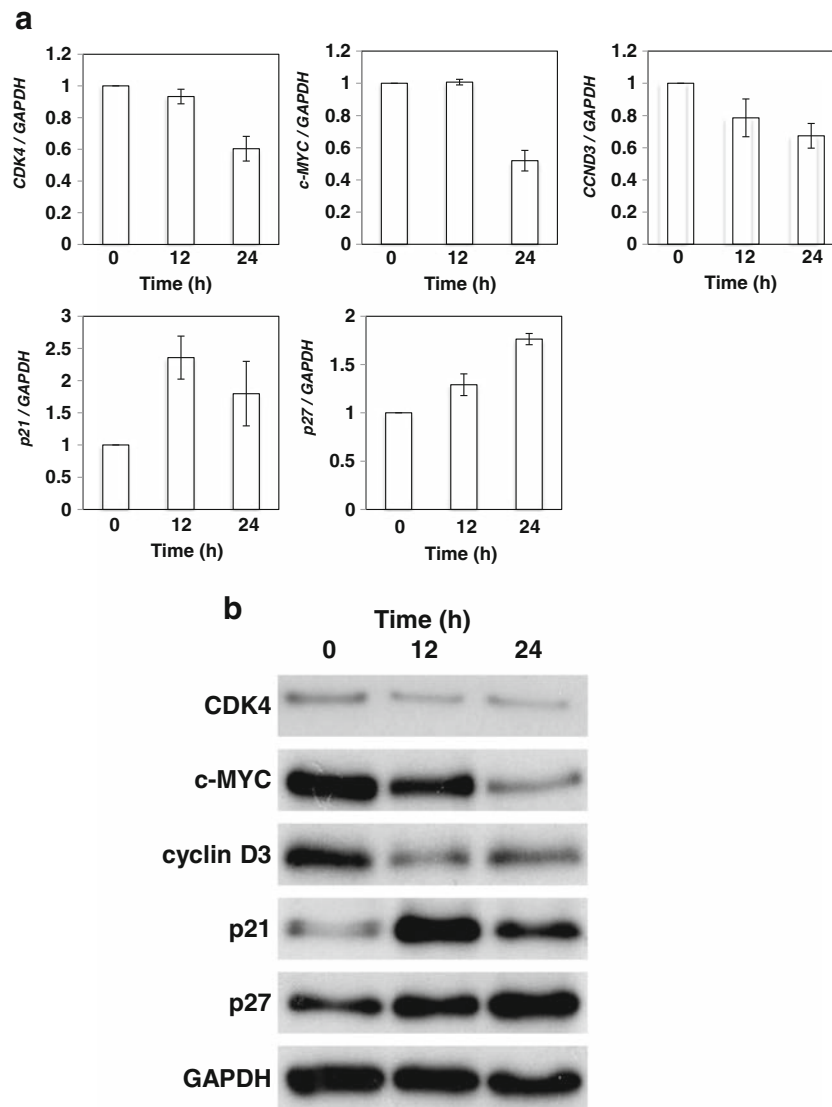


Fig. 5 SAL treatment alters the gene and protein expression of CDK4, c-MYC, cyclin D3, p21, and p27. **a.** Cells (1×10^6) were treated with SAL (100 $\mu\text{g/ml}$) at 37 °C for 12 or 24 h. Total RNAs extracted from SAL-untreated and -treated cells were analyzed by qRT-PCR using specific primers for *CDK4*, *c-MYC*, *CCND3*, *p21*, *p27*, and *GAPDH*, respectively. The control value was defined as one. Fold increases in the target genes relative to the control were normalized to *GAPDH*. Results are expressed as n-fold increase over the control; means \pm SE of three independent triplicate experiments. **b.** Cells (1×10^6) were treated with SAL (100 $\mu\text{g/ml}$) at 37 °C for 12 or 24 h. Whole cell extracts obtained from SAL-untreated and -treated cells were subjected to western blotting using

anti-CDK4, anti-c-MYC, anti-cyclinD3, anti-p21, anti-p27, and anti-GAPDH antibodies. **c.** Cells (1×10^6) were exposed to SAL (100 $\mu\text{g/ml}$) and SAL/saccharide (20 mM) co-treatment for 24 h. Total RNAs extracted from SAL-treated, SAL/saccharide co-treated, and untreated Raji cells were analyzed by qRT-PCR using the specific primers for *CDK4*, *c-MYC*, *CCND3*, *p21*, *p27*, and *GAPDH*, respectively. The control value was defined as one. Fold increases in the target genes relative to the control were normalized to *GAPDH*. Results are expressed as n-fold increase over the control; means \pm SE of three independent triplicate experiments

These findings suggest that the up-regulation of the CDK inhibitors p21 and p27 by SAL treatment induced $G_{0/1}$ phase cell cycle arrest.

Activation of the MEK-ERK signaling pathway by Gb3/lectin interaction at the cell surface The MEK-ERK signaling pathway has been reported to participate in the regulation of cell growth [28]. Treatment with SAL resulted in the formation and accumulation of GTP-Ras in Raji cells in a time-

dependent manner as indicated by enhanced phosphorylation of MEK_{1/2} and ERK_{1/2} (Fig. 6). Conversely, SAL treatment had no enhancing effect on the phosphorylation of p38 MAPK or c-Jun N-terminal kinase, which are MAPK family members in the broad sense (Fig. S4). A4GALT siRNA-treatment of Raji cells suppressed Gb3 cell surface expression (Fig. 7a and b). Consequently, A4GALT-knockdown abolished SAL-induced cell agglutination and also inhibited the phosphorylation of MEK_{1/2} and ERK_{1/2} following SAL treatment (Fig. 7c

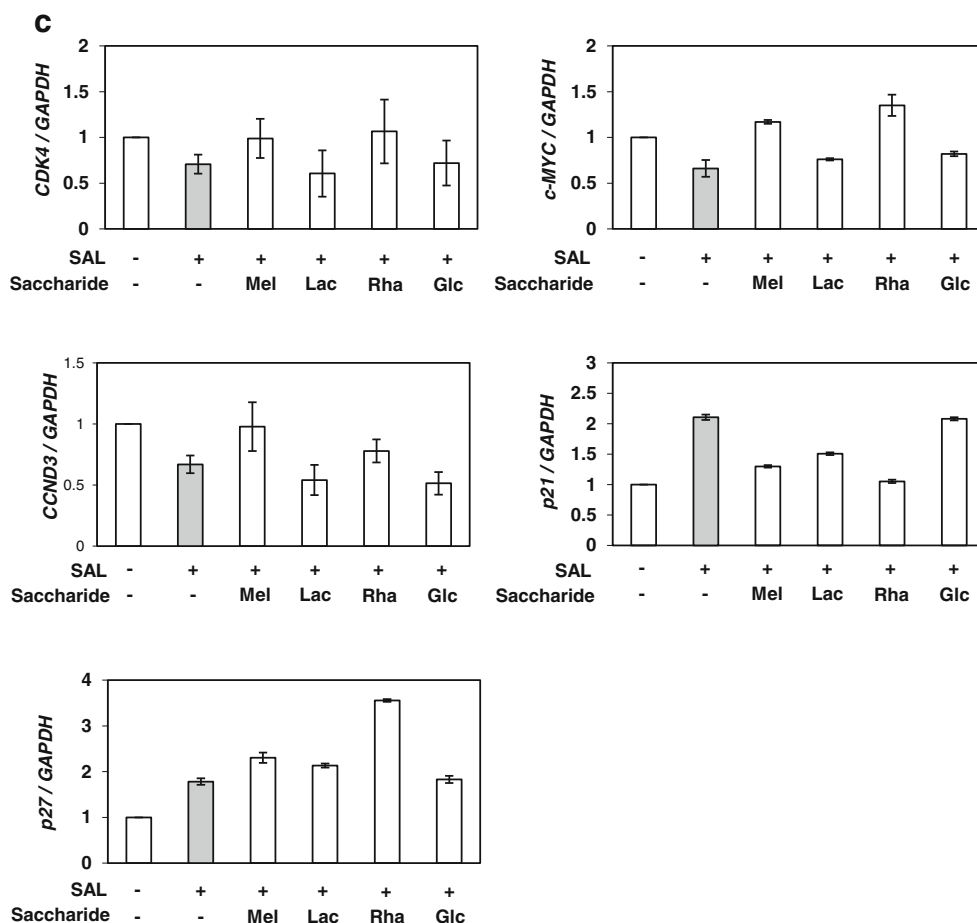


Fig. 5 (continued)

and d). Specifically, the levels of MEK_{1/2} and ERK_{1/2} phosphorylation were significantly increased by about 2 and 2.5-fold following SAL treatment in A4GALT siRNA-untreated Raji cells, whereas only 1.1 and 1.2-fold increases were

observed upon SAL treatment in A4GALT siRNA-treated Raji cells (data not shown). These results suggest that the direct interaction between Gb3 and SAL induced the MEK-ERK signaling pathway.

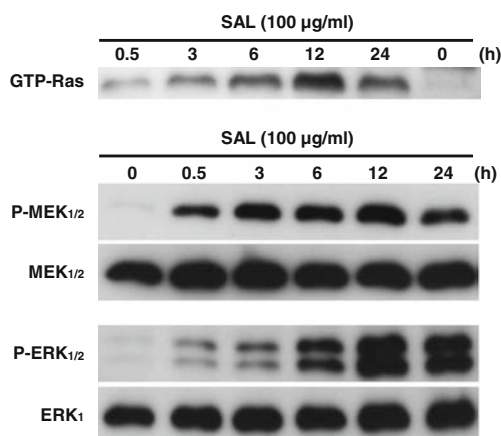


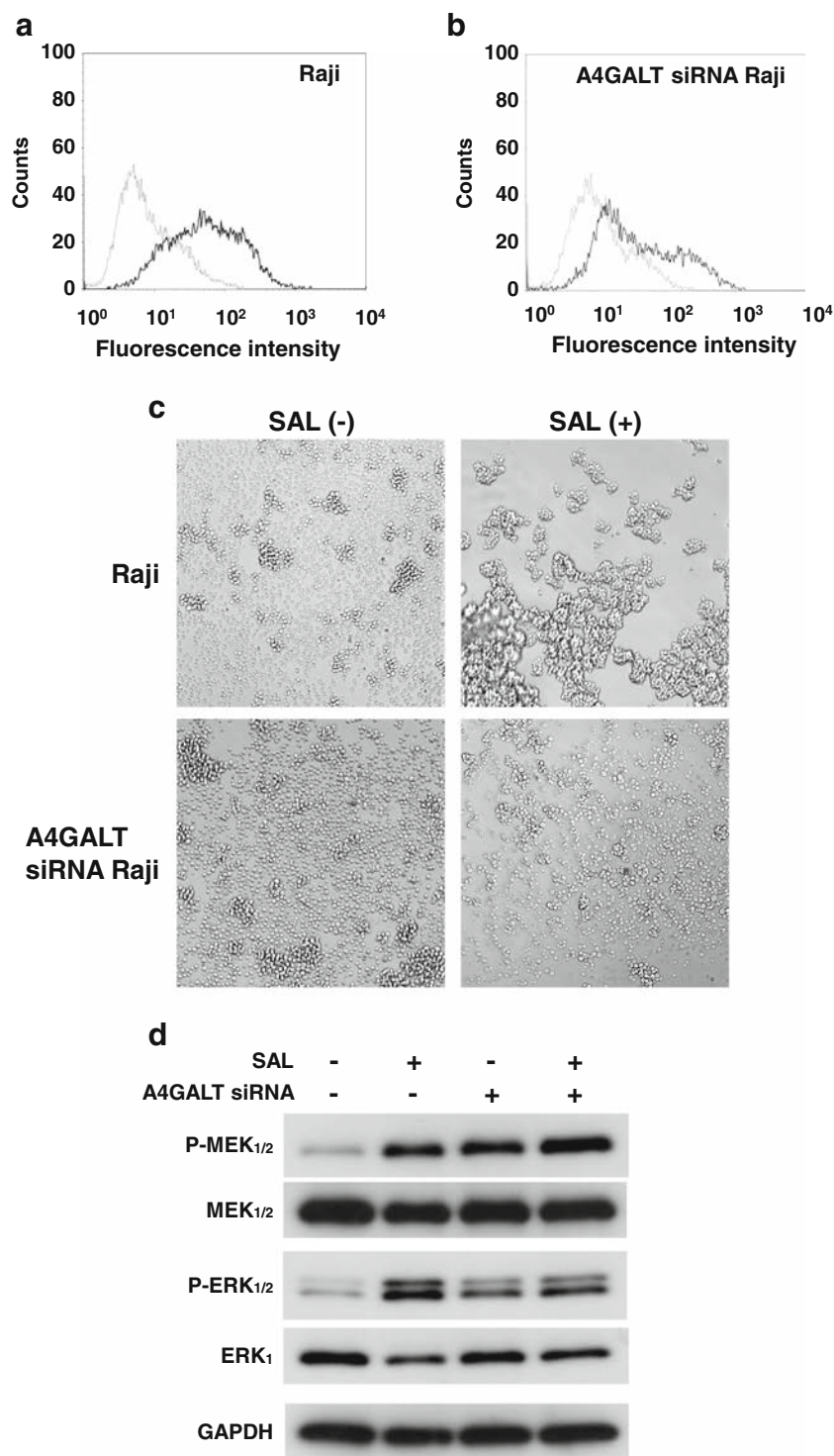
Fig. 6 SAL treatment causes activation of Ras and phosphorylation of MEK, and ERK. Cells (1×10^6) were treated with SAL (100 μ g/ml) at 37 °C for various durations from 0 to 24 h. Whole cell extracts were subjected to western blotting using antibodies directed to GTP-Ras, P-MEK_{1/2}, MEK_{1/2}, P-ERK_{1/2}, and ERK₁. Representative results from triplicate experiments are shown

Up-regulation of p21 by SAL via phosphorylation of the Ras-MEK-ERK signaling pathway We tested whether ERK_{1/2} phosphorylation was associated with the increase of p21 expression. Treatment with SAL in combination with the MEK inhibitor U0126 down-regulated p21 mRNA expression (Fig. 8a) and restored cell growth (Fig. 8b). U0126 by itself had no significant effect on cell growth (Fig. 8b). Pre-incubation with U0126 significantly decreased SAL-induced phosphorylation of ERK_{1/2} (Fig. 8c). SAL-induced enhancement of p21 protein expression was also inhibited in the presence of U0126 (Fig. 8c).

Discussion

Taken together, the results from this study indicate that the SAL/Gb3 interaction on the surface of Raji cells promotes activation of Ras (to form GTP-Ras) and phosphorylation of

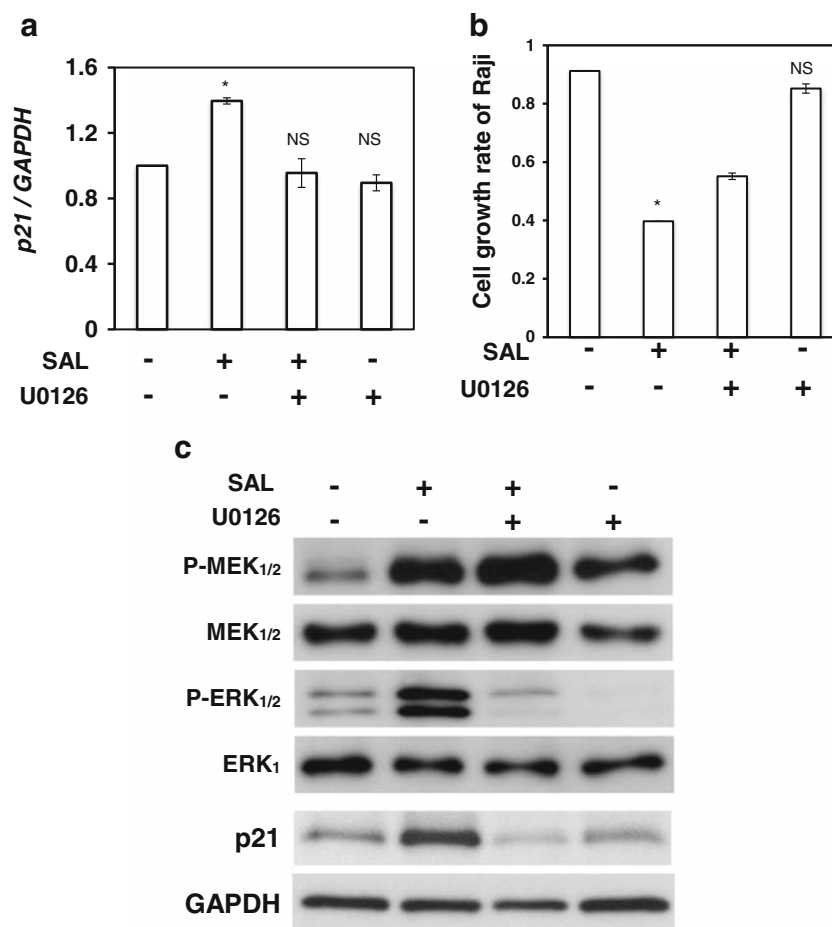
Fig. 7 Gb3 knockdown inhibits the phosphorylation of MEK and ERK. For the detection of Gb3, untreated Raji cells (**a**) and A4GALT siRNA-treated Raji cells (**b**) were stained with anti-Gb3 mAb and AF488-conjugated goat anti-mouse Ab (black line). The degree of Gb3 expression on Raji cell membranes was determined by FACSCalibur. Fluorescence intensity of control cells: gray line. **c.** Cell agglutination induced by treatment with SAL (100 μ g/ml). The images are from bright-field microscopy at 100 \times magnification. **d.** Degrees of expression and phosphorylation of MEK and ERK proteins were detected by western blotting as described in Materials and Methods



MEK_{1/2} and ERK_{1/2}. The suppression of cell growth by SAL was likely due to the enhancement of p21 expression caused by the phosphorylation of ERK_{1/2}, which derived from the Ras-MEK-ERK_{1/2} pathway. In addition, SAL reduced the protein expression levels of CDK4, c-myc, and cyclin D3. These results therefore indicate that SAL treatment induced cell cycle arrest at the G_{0/1} phase.

Gb3 is the key structure in globo-series GSLs, which contain a galactosyl α 1–4 linkage to lactosylceramide. Cell surface Gb3 is involved in the transmission of various signals into the cytoplasm via α -galactoside-binding lectins such as SAL, pierisin, and the mussel *Mytilus galloprovincialis* lectin (MytiLec) [9–11, 29]. Park *et al.* elucidated that the other globo-series GSL, globotetraosylceramide (Gb4), interacts

Fig. 8 SAL treatment enhances p21 protein expression levels through a Ras-MEK-ERK pathway. **a.** Quantitative RT-PCR showing *p21* expression, normalized relative to *GAPDH*, following treatment with SAL (100 μ g/ml) and/or the MEK inhibitor U0126 (10 μ M). The values shown are the means of triplicate experiments. Asterisk denotes $P < 0.05$ versus untreated control cells. NS denotes not significant versus untreated control cells. **b.** Growth of cells treated or untreated with SAL and/or U0126, measured by the WST-8 assay. The values shown are the means of triplicate experiments. Asterisk denotes $P < 0.05$ versus untreated control cells. NS denotes not significant versus untreated control cells. **c.** Degrees of expression and phosphorylation of Ras-MEK-ERK pathway-related proteins as detected by western blotting as described in Materials and Methods



with the epidermal growth factor receptor to promote activation of the MAPK pathway [30]. However, it has not yet been clarified whether Gb3 is involved in the activation of such a pathway. In the present study, direct interaction between Gb3 and SAL was found to transmit a regulatory signal in Raji cells through the MEK-ERK signaling pathway (Figs. 6 and 7). Phosphorylation of ERK initiates synthesis of the CDK inhibitor p21, which induces cell cycle arrest at the $G_{0/1}$ phase. External stimulation through p21 prevents damage to cellular DNA by irradiation and harmful toxins by arresting the cell cycle at the G_1/S phase transition. In comparison, p27 is involved in cell differentiation and proliferation in addition to cell cycle arrest [31]. p21 binds to the cyclin D3-CDK4 complex and suppresses cell growth. Conversely, recent reports have shown that the induction of p21 phosphorylation by ERK2 promotes cell proliferation [32]. Consistent with these properties, it has been reported that kinase-deficient forms of ERK1/2 were able to up-regulate the expression of p21 and subsequently induce $G_{0/1}$ phase cell cycle arrest [33]. Previous studies have suggested that Ras undergoes post-translational processing to be able to associate with cell membranes [34]. Thus, GDP-Ras might be located in the vicinity of GEMs on which Gb3 molecules are present. It is therefore important to

elucidate the mechanism of SAL/Gb3 interaction in the initiation of Ras activation to understand the cellular functions of lectin-induced, glycan-mediated signal transduction.

Previous reports have indicated that Ras is activated by the exchange of GTP for GDP, leading to the GTP-dependent binding of target proteins to Ras [35]. In analogy to the present findings, the activation of Ras is caused by binding between galectin-1 and the *N*-acetylglucosamine of $\alpha 5\beta 1$ integrin, which is followed by the induction of cell cycle arrest at the $G_{0/1}$ phase [36]. Thus, Ras activation might involve multiple pathways associated with various glycans and lectins. Several types of rhamnose-binding lectins having distinctive domain architectures are known [37, 38]. SAL has a unique domain construction with 9 binding sites based on a trimer of polypeptides, each consisting of triple tandem repeat domains [39]. For example, mAb raised against Gb3, which has divalent high-affinity binding sites, did not cause phosphorylation of GDP-Ras-MEK-ERK_{1/2} or induce Raji cell cycle arrest (Fig. 2). Binding of inadequate ligands to Gb3 therefore evidently do not cause the transmission of a phosphorylation signal to GDP-Ras. Studies of the cell regulatory effects of various Gb3-binding lectins will likely help to elucidate the novel mechanisms whereby multiple lectins are able to

transmit different growth-regulatory signals through the same glycan. This phenomenon is highlighted by our recent discoveries regarding MytiLec, which has a completely different primary sequence than SAL and causes direct apoptosis by binding to Gb3 [29]. This report raises the possibility that these lectins lead to different cell-regulatory signals [29].

In the current study, phosphorylated ERK_{1/2} increased the expression of the CDK inhibitor p21. This protein contains CDK-binding domains at its N-terminus and interacts with CDK to inhibit its activity, resulting in cell cycle arrest at the G_{0/1} phase [40]. In general, the expression of CDK inhibitors is regulated by the tumor suppressor p53, a transcription factor that is expressed consequent to DNA damage [41]. The p21 and p27 peptides have differing molecular masses of 21 and 27 kDa, respectively, and their C-terminal domains also play different roles. We observed that the time-dependent up-regulation of p27 occurred simultaneously with the down-regulation of cyclin D3 during a 24-h period to promote cell cycle arrest at the G₁ phase. In contrast, p21 was strongly up-regulated during a 12-h period following treatment with SAL and then decreased slightly during the subsequent 24-h period (Fig. 5).

Consistently with the phenomena described above, we found that SAL treatment is affected by the up-regulation of p21 (Fig. 5) and that production of p21 interfered with cyclin D3/CDK4 complex formation. Oligosaccharides containing α -galactoside are not a common type of glycan in human cells. Gb3 has been identified as the target of hemorrhagic toxins (e.g., verotoxin secreted by pathogenic bacteria, O157 strain) and has been proposed as a rejection antigen of pig organs that carry an α -galactose residue 1–3 linked to lactosylceramide following xenotransplantation into humans. The present results, using a lectin isolated from a fish, indicate a novel role of Gb3 as the trigger for activation of signal transduction molecules to induce cell cycle arrest of human lymphoma cells. Notably, α -galactoside-binding lectins (with diverse primary structures) are isolated more frequently from lower vertebrates and invertebrates than from higher vertebrates (mammals and birds) [42–47]. The physiological functions of these “primitive” lectins remain to be clarified in almost all cases. However, it is becoming increasingly clear that such knowledge will greatly promote biomedical studies focused on novel regulatory systems in human cells.

Acknowledgments This study was supported by the “Academic Frontier” Project for Private Universities and the “Strategic Project to Support the Formation of Research Bases at Private Universities (SENRYAKU)” from the Ministry of Education, Culture, Sports, Science, and Technology (MEXT), Japan. We would like to thank Editage (www.editage.jp) for English language editing.

Compliance with ethical standards

Conflict of interest The authors declare that there are no conflicts of interest regarding the publication of this paper.


Ethical approval This article does not contain any studies with human participants or animals performed by any of the authors.

References

- Krajhanzl A., Horejsi V., Kocourek K.: Studies on lectins. XLI. Isolation and characterization of a blood group B specific lectin from the roe of the powan (*Coregonus lavaretus maraena*). *Biochem. Biophys. Acta.* **532**, 209–214 (1978)
- Krajhanzl A., Horejsi V., Kocourek K.: Studies on lectins. XLII. Isolation, partial characterization and comparison of lectins from the roe of five fish species. *Biochem. Biophys. Acta.* **532**, 215–224 (1978)
- Sakakibara F., Kawauchi H., Takayanagi G.: Blood group B-specific lectin of *Plecoglossus altivelis* (Ayu fish) eggs. *Biochim Biophys Acta.* **841**, 103–111 (1985)
- Ozeki Y., Matsui T., Suzuki M., Titani T.: Amino acid sequence and molecular characterization of a D-galactoside-specific lectin purified from sea urchin (*Anthocidaris crassispina*) eggs. *Biochemistry.* **30**, 2391–2394 (1991)
- Hosono M., Ishikawa K., Mineki R., Murayama K., Numata C., Ogawa Y., Takayanagi Y., Nitta K.: Tandem repeat structure of rhamnose-binding lectin from catfish (*Silurus asotus*) eggs. *Biochim Biophys Acta.* **1472**, 668–675 (1999)
- Kawano T., Sugawara S., Hosono M., Tatsuta T., Nitta K.: Alteration of gene expression induced by *Silurus asotus* lectin in Burkitt's lymphoma cells. *Biol Pharm Bull.* **31**, 998–1002 (2008)
- Sugawara S., Hosono M., Ogawa Y., Takayanagi M., Nitta K.: Catfish egg lectin causes rapid activation of multidrug resistance 1 P-glycoprotein as a lipid translocase. *Biol Pharm Bull.* **28**, 434–441 (2005)
- Shirai T., Watanabe Y., Lee M.S., Ogawa T., Muramoto K.: Structure of rhamnose-binding lectin CSL3: unique pseudo-tetrameric architecture of a pattern recognition protein. *J Mol Biol.* **391**, 390–403 (2009)
- Watanabe M., Kono T., Matsushima-Hibiya Y., Kanazawa T., Nishisaka N., Kishimoto T., Koyama K., Sugimura T., Wakabayashi K.: Molecular cloning of an apoptosis-inducing protein, pierisin, from cabbage butterfly: possible involvement of ADP-ribosylation in its activity. *Proc Natl Acad Sci U S A.* **96**, 10608–10613 (1999)
- Shiotani B., Kobayashi M., Watanabe M., Yamamoto K., Sugimura T., Wakabayashi K.: Involvement of the ATR- and ATM-dependent checkpoint responses in cell cycle arrest evoked by pierisin-1. *Mol Cancer Res.* **4**, 125–133 (2006)
- Matsushima-Hibiya Y., Watanabe M., Hidari K.I., Miyamoto D., Suzuki Y., Kasama T., Kanazawa T., Koyama K., Sugimura T., Wakabayashi K.: Identification of glycosphingolipid receptors for pierisin-1, a guanine-specific ADP-ribosylation toxin from the cabbage butterfly. *J Biol Chem.* **278**, 9972–9978 (2003)
- Katagiri Y.U., Mori T., Nakajima H., Katagiri C., Taguchi T., Takeda T., Kiyokawa N., Fujimoto J.: Activation of Src family kinase yes induced by Shiga toxin binding to globotriaosyl ceramide (Gb3/CD77) in low density, detergent-insoluble microdomains. *J Biol Chem.* **274**, 35278–35282 (1999)
- Hosono M., Kawauchi H., Nitta K., Takayanagi Y., Shiokawa H., Mineki R., Murayama K.: Purification and characterization of *Silurus Asotus* (catfish) roe lectin. *Biol Pharm Bull.* **16**, 1–5 (1993)
- Tennant J.R.: Evaluation of the trypan blue technique for determination of cell viability. *Transplantation.* **2**, 685–694 (1964)

15. Laemmli U.K.: Cleavage of structural proteins during the assembly of the head of bacteriophage T4. *Nature*. **227**, 680–685 (1970)
16. Lowry O.H., Rosebrough N.J., Farr A.L., Randall R.J.: Protein measurement with the Folin phenol reagent. *J Biol Chem*. **193**, 265 (1951)
17. Matsudaira P.T.: Sequence from picomole quantities of proteins electrophoretically onto polyvinylidene difluoride membranes. *J Biol Chem*. **262**, 10035–10038 (1987)
18. Taylor S.J., Shalloway D.: Cell cycle-dependent activation of ras. *Curr Biol*. **6**, 1621–1627 (1996)
19. Taylor S.J., Resnick R.J., Shalloway D.: Nonradioactive determination of ras-GTP levels using activated ras interaction assay. *Methods Enzymol*. **333**, 333–342 (2001)
20. Yamauchi N., Takezawa T., Kizaki K., Herath C.B., Hashizume K.: Proliferative potential of endometrial stromal cells, and endometrial and placental expression of cyclin in the bovine. *J Reprod Dev*. **49**, 553–560 (2003)
21. Schmidt B.A., Rose A., Steinhoff C., Strohmeyer T., Hartmann M., Ackermann R.: Up-regulation of cyclin-dependent kinase 4/cyclin D2 expression but down-regulation of cyclin-dependent kinase 2/cyclin E in testicular germ cell tumors. *Cancer Res*. **61**, 4214–4221 (2001)
22. Mateyak M.K., Obaya A.J., Sedivy J.M.: c-Myc regulates Cyclin D-Cdk4 and -Cdk6 activity but affects cell cycle progression at multiple independent points. *Mol Cell Biol*. **19**, 4672–4683 (1999)
23. Colo M.D., McMahon S.B.: The myc oncoprotein: a critical evaluation of transactivation and target gene regulation. *Oncogene*. **18**, 2916–2924 (1999)
24. Pines J.: Cyclins and cyclin-dependent kinases: a biochemical view. *Biochem J*. **308**, 697–711 (1995)
25. Sherr C.J.: Cancer cell cycles. *Science*. **274**, 1672–1677 (1996)
26. Eguchi H., Carpentier S., Kim S.S., Moss S.F.: p27kip1 regulates the apoptotic response of gastric epithelial cells to *Helicobacter pylori*. *Gut*. **53**, 797–804 (2004)
27. Russo A.A., Jeffrey P.D., Patten A.K., Massagué J., Pavletich N.P.: Crystal structure of the p27Kip1 cyclin-dependent-kinase inhibitor bound to the cyclin A-Cdk2 complex. *Nature*. **382**, 325–331 (1996)
28. McCubrey J.A., Steelman L.S., Chappell W.H., Abrams S.L., Wong E.W., Chang F., Lehmann B., Terrian D.M., Milella M., Tafuri A., Stivala F., Libra M., Basecke J., Evangelisti C., Martelli A.M., Franklin R.A.: Roles of the Raf/MEK/ERK pathway in cell growth, malignant transformation and drug resistance. *Biochim Biophys Acta*. **1773**, 1263–1284 (2007)
29. Fujii Y., Dohmae N., Takio K., Kawsar S.M., Matsumoto R., Hasan I., Koide Y., Kanaly R.A., Yasumitsu H., Ogawa Y., Sugawara S., Hosono M., Nitta K., Hamako J., Matsui T., Ozeki Y.: A lectin from the mussel *Mytilus galloprovincialis* has a highly novel primary structure and induces glycan-mediated cytotoxicity of globotriaosylceramide-expressing lymphoma cells. *J Biol Chem*. **287**, 44772–44783 (2012)
30. Park S.Y., Kwak C.Y., Shayman J.A., Kim J.H.: Globoside promotes activation of ERK by interaction with the epidermal growth factor receptor. *Biochim Biophys Acta*. **1820**, 1141–1148 (2012)
31. Nadeem L., Brkic J., Chen Y.F., Bui T., Munir S., Peng C.: Cytoplasmic mislocalization of p27 and CDK2 mediates the anti-migratory and anti-proliferative effects of nodal in human trophoblast cells. *J Cell Sci*. **126**, 445–453 (2013)
32. Hong S.K., Kim J.H., Lin M.F., Park J.I.: The Raf/MEK/extracellular signal-regulated kinase 1/2 pathway can mediate growth inhibitory and differentiation signaling via androgen receptor downregulation in prostate cancer cells. *Exp Cell Res*. **317**, 2671–2682 (2011)
33. Hwang C.Y., Lee C., Kwon K.S.: Extracellular signal-regulated kinase 2-dependent phosphorylation induces cytoplasmic localization and degradation of p21Cip1. *Mol Cell Biol*. **29**, 3379–3389 (2009)
34. Hancock J.F.: Ras proteins: different signals from different locations. *Nat Rev Mol Cell Biol*. **4**, 373–385 (2003)
35. Avruch J., Zhang X.F., Kyriakis J.M.: Raf meets ras: completing the framework of a signal transduction pathway. *Trends Biochem Sci*. **19**, 279–283 (1994)
36. Fischer C., Sanchez-Ruderisch H., Welzel M., Wiedenmann B., Sakai T., André S., Gabius H.J., Khachigian L., Detjen K.M., Rosewicz S.: Galectin-1 interacts with the $\alpha 5 \beta 1$ fibronectin receptor to restrict carcinoma cell growth via induction of p21 and p27. *J Biol Chem*. **280**, 37266–37277 (2005)
37. Ogawa T., Watanabe M., Naganuma T., Muramoto K.: Diversified carbohydrate-binding lectins from marine resources. *J Amino Acids*. **2011**(838914), (2011)
38. Tateno H.: SUEL-related lectins, a lectin family widely distributed throughout organisms. *Biosci Biotechnol Biochem*. **74**, 1141–1114 (2010)
39. Murayama K., Taka H., Kaga N., Fujimura T., Mineki R., Shindo N., Morita M., Hosono M., Nitta K.: The structure of *Silurus asotus* (catfish) roe lectin (SAL): identification of a noncovalent trimer by mass spectrometry and analytical ultracentrifugation. *Anal Biochem*. **247**, 319–326 (1997)
40. Harper J.W., Adami G.R., Wei N., Keyomarsi K., Elledge S.J.: The p21 Cdk-interacting protein Cip1 is a potent inhibitor of G1 cyclin-dependent kinases. *Cell*. **75**, 805–816 (1993)
41. Jänicke R.U., Sohn D., Essmann R., Shulze-Osthoff K.: The multiple battles fought by anti-apoptotic p21. *Cell Cycle*. **6**, 407–413 (2007)
42. Franchi N., Schiavon F., Carletto M., Gasparini F., Bertoloni G., Tosato S.C., Ballarin L.: Immune roles of a rhamnose-binding lectin in the colonial ascidian *Botryllus schlosseri*. *Immunobiology*. **216**, 725–736 (2011)
43. Kawsar S.M.A., Matsumoto R., Fujii Y., Matsuoaka H., Masuda N., Chihiro I., Yasumitsu H., Kanaly R.A., Sugawara S., Hosono M., Nitta K., Ishizaki N., Dogasaki C., Hamako J., Matsui T., Ozeki Y.: Cytotoxicity and glycan-binding profile of a D-galactose-binding lectin from the eggs of a Japanese sea hare (*Aplysia kurodai*). *Protein J*. **30**, 509–519 (2011)
44. Watanabe Y., Tateno H., Nakamura-Tsuruta S., Kominami J., Hirabayashi J., Nakamura O., Watanabe T., Kamiya H., Naganuma T., Ogawa T., Naudé R.J., Muramoto K.: The function of rhamnose-binding lectin innate immunity by restricted binding to Gb3. *Dev Comp Immunol*. **33**, 187–197 (2009)
45. Kawsar S.M., Matsumoto R., Fujii Y., Yasumitsu H., Dogasaki C., Hosono M., Nitta K., Hamako J., Matsui T., Kojima N., Ozeki Y.: Purification and biochemical characterization of a D-galactose binding lectin from Japanese sea hare (*Aplysia kurodai*) eggs. *Biochemistry (Mosc)*. **74**, 709–716 (2009)
46. Naganuma T., Ogawa T., Hirabayashi J., Kasai K., Kamiya H., Muramoto K.: Isolation, characterization and molecular evolution of a novel pearl shell lectin from a marine bivalve. *Pteris penguin* *Mol Divers*. **10**, 607–618 (2006)
47. Lee J.K., Buckhaults P., Wilkes C., Teilhet M., King M.L., Moremen K.W., Pierce M.: Cloning and expression of a *Xenopus laevis* oocyte lectin and characterization of its mRNA levels during early development. *Glycobiology*. **7**, 367–372 (1997)

Lissoclibadin 1, a Polysulfur Aromatic Alkaloid from the Indonesian Ascidian *Lissoclinum* cf. *badium*, Induces Caspase-Dependent Apoptosis in Human Colon Cancer Cells and Suppresses Tumor Growth in Nude Mice

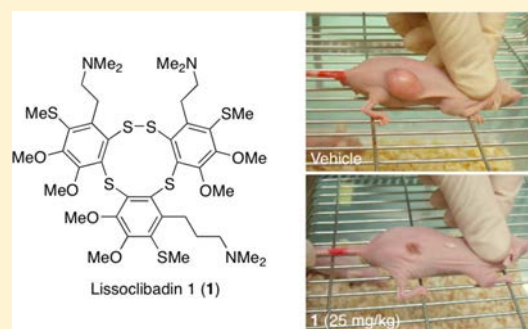
Takeo Tatsuta,[‡] Masahiro Hosono,^{*,‡} Henki Rotinsulu,^{‡,§} Defny S. Wewengkang,^{‡,§} Deiske A. Sumilat,^{‡,⊥} Michio Namikoshi,[‡] and Hiroyuki Yamazaki^{*,‡} 

[‡]Department of Natural Product Chemistry, Faculty of Pharmaceutical Sciences and [‡]Division of Cell Recognition Study, Institute of Molecular Biomembrane and Glycobiology, Tohoku Medical and Pharmaceutical University, Aoba-ku, Sendai 981-8558, Japan

[§]Faculty of Mathematic and Natural Sciences and [⊥]Faculty of Fisheries and Marine Science, Sam Ratulangi University, Kampus Bahu, Manado 95115, Indonesia

Supporting Information

ABSTRACT: Lissoclibadins, polysulfur aromatic alkaloids, were isolated from the Indonesian ascidian *Lissoclinum* cf. *badium*. Lissoclibadins 1 (1), 3 (2), 4 (3), 7 (4), 8 (5), and 14 (6) inhibited the growth of four human solid cancer cell lines: HCT-15 (colon adenocarcinoma), HeLa-S3 (cervix adenocarcinoma), MCF-7 (breast adenocarcinoma), and NCI-H28 (mesothelioma). Lissoclibadin 1 (1) exerted the most potent cytotoxic effects *in vitro* and mainly promoted apoptosis through an intrinsic pathway with the activation of a caspase-dependent pathway in HCT-15 cells. *In vivo* studies demonstrated that 1 suppressed tumor growth in nude mice carrying HCT-15 cells without significant secondary adverse effects. In conclusion, the results obtained in the present study demonstrate that 1 has potential as a chemotherapeutic candidate for preclinical investigations.



Marine natural products possess unique structural features and various biological activities.^{1–3} A number of marine-derived compounds have exhibited potent inhibitory activities against human tumor cells in *in vitro* and *in vivo* experiments. Some marine substances have entered clinical trials for the treatment of cancers, and cytarabine, trabectedin (ET743), eribulin (a synthetic derivative of halichondrin B), and monomethylauristatin E (MMAE) as the warhead of a monoclonal antibody (Adcetris) have been approved as anticancer agents.^{4–7}

In the course of our studies on bioactive metabolites from marine organisms, we have reported the isolation and structures of three novel sulfur-containing alkaloids, lissoclibadins 1–3, together with four known congeners from the Indonesian ascidian *Lissoclinum* cf. *badium*, which have rare polysulfur aromatic amine structures.⁸ Further studies on this ascidian led to the discovery of 11 related compounds, lissoclibadins 4–14.⁹ We previously reported their antimicrobial activities, inhibition of cell proliferation in murine and human cancer cell lines, and effects on IL-8 production in PMA-stimulated human promyelocytic leukemia (HL-60) cells.¹⁰

We have now further evaluated the antitumor properties of lissoclibadins *in vitro* and *in vivo*, and the findings obtained indicated that lissoclibadin 1 induced caspase-dependent apoptosis in the human colon cancer cell line HCT-15 and

exerted suppressive effects on HCT-15 cells in antitumor experiments using xenograft model nude mice.

RESULTS AND DISCUSSION

Lissoclibadins 1–3 were obtained as cytotoxic components against HL-60 cells⁸ and exhibited inhibitory activities against colony formation by Chinese hamster V79 cells and cell proliferation in nine human solid-tumor cell lines.^{10a} The effects of lissoclibadins 4–14 have also been investigated against V79 and murine leukemia L1210 cells.⁹

Further cytotoxicity studies were performed using lissoclibadins 1 (1), 3 (2), 4 (3), 7 (4), 8 (5), and 14 (6). The cytotoxicities of compounds 1–6 were initially investigated in four human cancer cell lines: HCT-15 (colon adenocarcinoma), HeLa-S3 (cervix adenocarcinoma), MCF-7 (breast adenocarcinoma), and NCI-H28 (mesothelioma). These cancer cells were treated with each test compound at various concentrations for 24 h, and cell viabilities were measured using the WST-1 assay.¹¹ The effects of compounds 1–6 on the viabilities of four cancer cell lines are summarized in Table 1. Among these lissoclibadins, compounds 1, 5, and 6 exhibited stronger

Received: November 14, 2016

Published: February 9, 2017

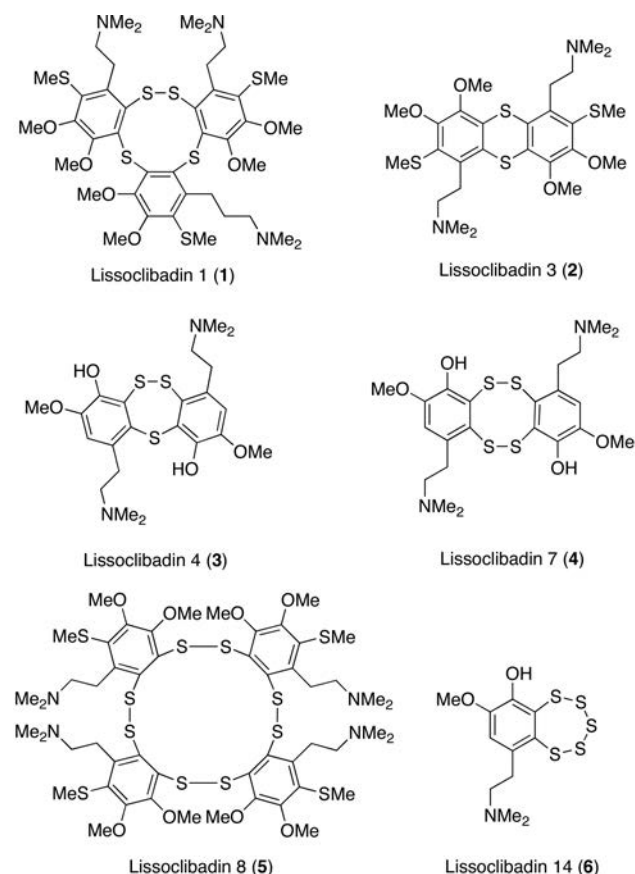


Table 1. Cytotoxicities of Compounds 1–6 against Four Human Cancer Cell Lines: HCT-15, HeLa-S3, MCF-7, and NCI-H28^a

compound	cytotoxicity (IC ₅₀ , μ M)			
	HCT-15	HeLa-S3	MCF-7	NCI-H28
lissoclibadin 1 (1)	4.0 \pm 1.8	6.3 \pm 1.4	7.6 \pm 4.0	7.1 \pm 2.3
lissoclibadin 3 (2)	13.2 \pm 1.4	16.0 \pm 1.8	n.d. ^b	n.d.
lissoclibadin 4 (3)	17.2 \pm 5.2	17.8 \pm 5.3	n.d.	n.d.
lissoclibadin 7 (4)	15.7 \pm 1.2	14.2 \pm 1.3	n.d.	n.d.
lissoclibadin 8 (5)	4.9 \pm 1.9	6.3 \pm 0.5	11.8 \pm 3.1	7.1 \pm 1.0
lissoclibadin 14 (6)	4.2 \pm 2.4	5.9 \pm 1.6	6.4 \pm 2.7	6.4 \pm 1.6
etoposide	19.7 \pm 5.7	43.1 \pm 6.5	n.d.	n.d.

^aEach value indicates the mean \pm SD of three different experiments performed in triplicate. ^bNot determined.

cytotoxicity against all cancer cell lines and were more potent than etoposide, an anticancer drug. Moreover, compounds 1, 5, and 6 showed the lowest IC₅₀ values of 4.0, 4.9, and 4.2 μ M, respectively, against HCT-15 cells (Table 1). On the other hand, compounds 2–4 exhibited weaker activities than 1, 5, and 6 (Table 1).

Among the six lissoclibadins tested, lissoclibadins 1 (1) and 14 (6) were roughly equipotent, but compound 1 was selected for further studies. Thus, morphological changes in cancer cells treated with 1 (0–10 μ M) were examined using light microscopy. Lissoclibadin 1 (1) influenced cell adhesion and morphology in a dose-dependent manner in the four cell lines

(Figure S1). These results suggest that compound 1 possesses potent cytotoxic effects.

Some anticancer agents are known to eliminate cancer cells through apoptotic processes.¹² Apoptosis is essential for tissue development and homeostasis and also functions as a defense system to avoid the effects of many toxic substances.¹² Therefore, nuclear morphological observations by fluorescent staining and a flow cytometric analysis by double staining were performed in order to investigate whether the cytotoxicity of lissoclibadin 1 (1) is triggered by an apoptotic pathway. HCT-15 cells treated with 5 μ M 1 for 24 h were stained with Hoechst-33258, and nuclear morphological effects were observed using a fluorescence microscope. Nuclear morphological observations of 5 μ M 1 revealed the condensation of chromatin and fragmentation of nuclei in a few cells, as shown in Figure 1. Moreover, similar nuclear morphological changes were detected in HeLa-S3, MCF-7, and NCI-H28 cells treated with 10 μ M 1 for 24 h (Figure 1).

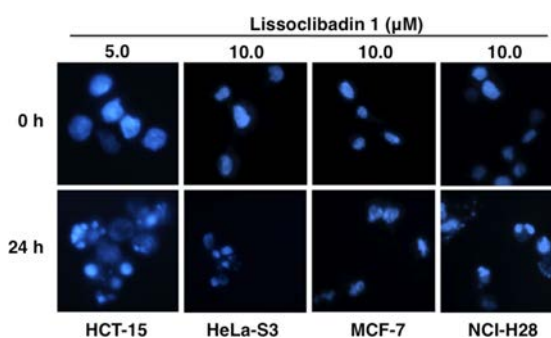


Figure 1. Nuclear morphological changes induced by lissoclibadin 1 (1) in HCT-15, HeLa-S3, MCF-7, and NCI-H28 cells. Each cell line (5×10^4 cells/mL) was precultured for 24 h, and compound 1 was then added at the indicated concentrations and cultured for 24 h. Cells were stained with Hoechst-33258 and observed using a fluorescent microscope.

The occurrence of apoptosis was analyzed using flow cytometry. HCT-15 cells were treated with 5 μ M 1 for 3, 6, 12, and 24 h and then stained with fluorescein isothiocyanate (FITC)-conjugated annexin V (annexin V) and propidium iodide (PI) in order to confirm the apoptotic actions induced by compound 1. Annexin V staining (lower right) signified early apoptotic events, while dual annexin V and PI staining (upper right) indicated the late phase of apoptosis (Figure 2). On the other hand, PI staining (upper left) showed necrosis, and nonstained cells (lower left) were viable cells (Figure 2). As shown in Figure 2, the proportion of early apoptotic cells (lower right) significantly increased to 11%, 37%, 43%, and 40% after the incubation with 1 at 5 μ M for 3, 6, 12, and 24 h, respectively. The late apoptotic cell proportion (upper right) was also increased after the 24 h incubation with 5 μ M 1 in a time-dependent manner (Figure 2). These results indicate that the cytotoxic effects of lissoclibadin 1 are attributable to the induction of apoptosis.

The apoptotic response in HCT-15 cells to 1 was significantly decreased by the addition of the pan-caspase inhibitor z-VAD-fmk (Figure 3). The percentage of apoptotic cells (upper right and lower right) decreased from 64% to 11%. Therefore, compound 1 induced apoptotic death in HCT-15 cells through a caspase-dependent pathway.

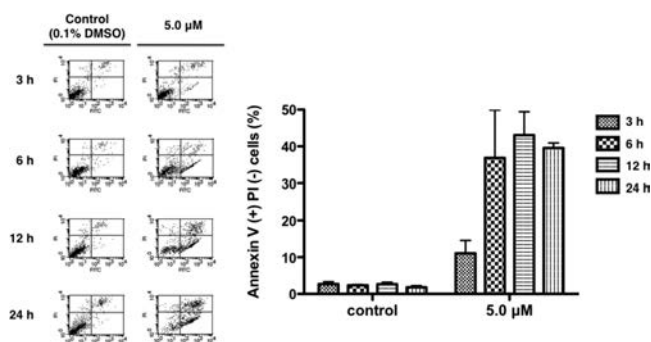


Figure 2. Analysis of apoptosis stages in HCT-15 cells assessed by flow cytometry with double staining (annexin V and PI). HCT-15 cells (5×10^4 cells/mL) were precultured for 24 h in 1 mL, lissoclibadin 1 in DMSO ($5.0 \mu\text{M}$) or DMSO alone (final concentration 0.1%) was then added, and the cells were incubated for the indicated time. Analyses of annexin V binding and PI incorporation were performed by FACSCalibur. The percentages of annexin V-positive cells are presented in the right panel. Each value is the mean \pm SD of three independent experiments.

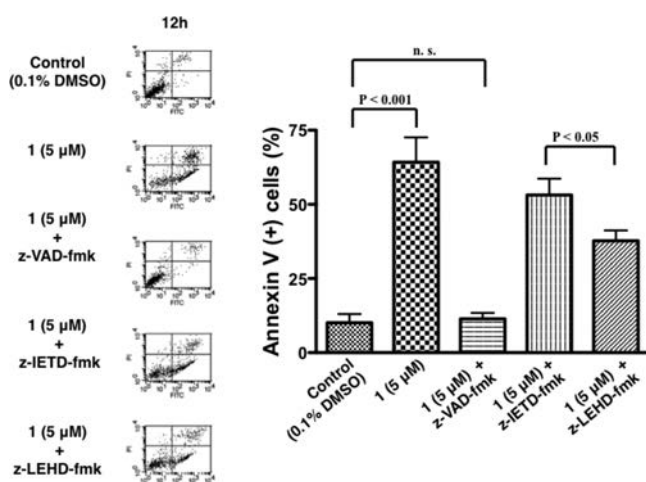


Figure 3. Effects of pan-caspase, caspase-8, and caspase-9 inhibitors on apoptosis induced by lissoclibadin 1 (**1**). HCT-15 cells (5×10^4 cells/mL) were precultured for 24 h in 1 mL. Each caspase inhibitor was added at $50 \mu\text{M}$, and the cells were incubated for 30 min. Lissoclibadin 1 in DMSO ($5.0 \mu\text{M}$) or DMSO alone (final concentration 0.1%) was then added, and the cells were incubated for the indicated time. Analyses of annexin V binding and PI incorporation were performed by FACSCalibur. The percentages of annexin V-positive cells are presented in the right panel. Each value is the mean \pm SD of three independent experiments.

The caspase cascade is transmitted through two kinds of pathways: intrinsic and extrinsic pathways.¹³ Therefore, the pathway activated by the treatment with **1** was investigated in the annexin V–PI dual-staining analysis using specific caspase-8 (z-IETD-fmk) and caspase-9 (z-LEHD-fmk) inhibitors. As shown in Figure 3, the prevention of annexin V-positive staining by z-LEHD-fmk was more potent than that by z-IETD-fmk, which indicated that apoptosis induced by **1** was caused by the intrinsic pathway rather than the extrinsic pathway. z-LEHD-fmk could not completely prevent the apoptosis in contrast to z-VAD-fmk, indicating that **1** triggers the apoptotic signal cascade so strongly that inhibition of caspase-9 alone is not sufficient for complete prevention of **1**-induced apoptosis. The treatment with caspase inhibitors did not suppress the

effects of **1** on cell adhesion and morphology (Figure S2). It may be demonstrated that the treatment with **1** causes an irreversible lethal stress in cancer cells upstream of caspase cascade activation or prevention of **1**-induced caspase activation triggers induction of other cell death signaling. Taken together, we have concluded that compound **1** induces potent cytotoxicity attributed to strong activation of caspase cascade originating in caspase-9 activation.

BALB/c nu/nu nude mice were used as a xenograft model to evaluate the *in vivo* antitumor effects of lissoclibadin 1 (**1**) on the HCT-15 cell line. Tumor growth on day 28 in the group treated with **1** at 25 mg/kg per day ($n = 6$) was approximately 60% less than that in the control group, whereas the administration group at 5 mg/kg per day ($n = 6$) showed no effect (Figure 4A). Neither obvious toxicities nor body weight changes were observed during the experimental period (Figure 4B). These results show that compound **1** suppressed tumor growth in nude mice.

The present study revealed that lissoclibadin 1 (**1**) induced cell death via apoptosis due to the mitochondrial cytochrome *c*-dependent activation (intrinsic pathway) of the caspase-9 and caspase-3 cascade pathway. Moreover, compound **1** exhibited antineoplastic activity in HCT-15 cells *in vivo* at 25 mg/kg per day with relative safety. This is the first study on the *in vivo* antitumor efficacy of **1**, and, accordingly, lissoclibadin 1 has potential as a lead compound for further development as a cancer chemotherapy agent.

EXPERIMENTAL SECTION

General Experimental Procedures. Lissoclibadins **1** (**1**), **3** (**2**), **4** (**3**), **7** (**4**), **8** (**5**), and **14** (**6**) were isolated from the ascidian *L. cf. badium* collected in Indonesia as described previously.^{8,9} A cell counting kit (WST-assay) was purchased from Dojindo Molecular Technologies, Inc. Caspase inhibitors (z-VAD-fmk, z-IETD-fmk, and z-LEHD-fmk) were purchased from Medical & Biological Laboratories Co., Ltd. (MBL).

Cell Cultures. HCT-15 (colon adenocarcinoma), HeLa-S3 (cervix adenocarcinoma), and MCF-7 (breast adenocarcinoma) cell lines were obtained from the Cell Resource Center for Biomedical Research, Institute of Development, Aging and Cancer, Tohoku University. The NCI-H28 cell line (malignant mesothelioma) was purchased from the American Type Culture Collection. Cells were routinely kept in RPMI 1640 medium (Nissui Pharmaceutical Co. Ltd.) supplemented with 10% fetal calf serum, penicillin (100 U/mL), and streptomycin ($100 \mu\text{g/mL}$) at 37°C in a 95% air and 5% CO_2 atmosphere.

WST Assay. WST-1 assays were performed in accordance with the manufacturer's instructions. Briefly, cells were plated at 5×10^3 cells/well on 96-well plates and grown for 24 h. Various concentrations of lissoclibadins (0.1 – $40 \mu\text{M}$) and etoposide (1.0 – $100 \mu\text{M}$) were added in triplicate to the cultures and incubated for 24 h before adding the WST-1 solution. The absorbance of the resulting product was measured 4 h later at a wavelength of 450 nm with background subtraction at 650 nm . The cytostatic/cytotoxic effects of compounds were expressed as relative cell viability (% of control). The experiments were conducted three times, and the IC_{50} value showing the compound concentration required for the 50% inhibition of cell viability was calculated employing GraphPad Prism 3.0 software.

Observation of Nuclear Morphology. Cells (5×10^4 cells/mL) were cultured in 5 mL on six-well plates and grown for 24 h. After the treatment, cells were trypsinized, collected by centrifugation, and washed with PBS. Cells were then fixed with $100 \mu\text{L}$ of 1.0% paraformaldehyde at 4°C for 15 min and stained with $50 \mu\text{L}$ of 1 mg/mL Hoechst-33258 at 4°C for 15 min. After three washes with PBS, cells were mounted on glass slides using Prolong gold antifade reagents (Molecular Probes). Fluorescence was visualized with a Zeiss AxioScope 2 fluorescence microscope (Carl Zeiss).

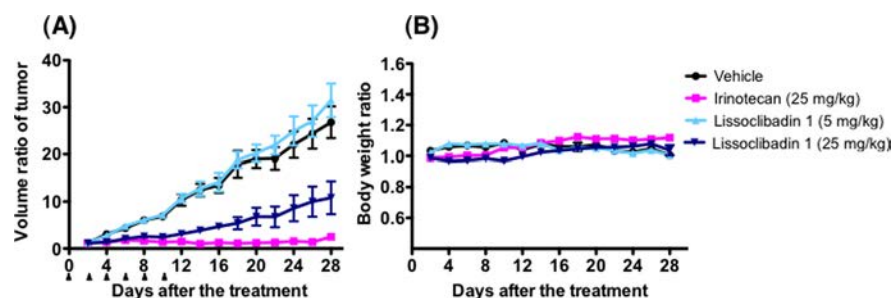


Figure 4. Antitumor effects of lissoclibadin 1 (**1**) in a tumor xenograft model bearing HCT-15 cells. HCT-15 cells (5×10^6 cells) were implanted into each nude mouse. When the tumor size reached 50–80 mm³, mice were injected intratumorally with 5 mg/kg of **1**, 25 mg/kg of **1**, and 25 mg/kg of irinotecan (as a positive control) six times every second day from day 0 (indicated by arrowhead). Tumor sizes for calculating the volume (A) and body weight (B) were measured every second day. The body weight was monitored for toxicity.

Annexin V/PI Staining. Annexin V binding and PI incorporation were detected with a MEBCYTO apoptosis kit (MBL) according to the manufacturer's directions. Briefly, cells (5×10^4 cells/mL) were cultured in 1 mL on 24-well plates. After the treatment with 5 μ M lissoclibadin 1 (**1**), adherent cells were trypsinized, pooled, and stained with annexin V-FITC and PI. The fluorescence intensities of FITC-annexin V and PI were measured using a FACSCalibur flow cytometer (Becton Dickinson).

The role of caspase activation in this process was examined by the addition of the pan-caspase inhibitor z-VAD-fmk, caspase-8-specific inhibitor z-IETD-fmk, and caspase-9-specific inhibitor z-LEHD-fmk. Each caspase inhibitor (50 μ M) was added to cultured cells 30 min before the addition of **1** (5 μ M). The analysis of annexin V binding and PI incorporation was then completed, as described above. The results from three independent experiments were expressed as the mean \pm SD. Statistical analyses were conducted using GraphPad Prism 3.0, and comparisons were made using one-way analysis of variance (ANOVA) followed by Bonferroni's *post hoc* tests.

In Vivo Antitumor Experiment. All animal experiments were performed in accordance with the Guidelines for Animal Experiments of the Tohoku Medical and Pharmaceutical University (permission number 08029). HCT-15 cells (1×10^8 /mL) were mixed with an equal volume of ice-cooled Matrigel (Becton Dickinson Labware), and an aliquot of the cell suspension (100 μ L) was injected subcutaneously into the lower backs of 6-week-old female athymic nude mice (Balb/c nu/nu, Charles River Lab. Inc.). One week after the inoculation (day 0), mice bearing tumor volumes from 50 to 100 mm³ were randomly divided into 4 groups with 6 mice in each group. Lissoclibadin 1 (**1**) and irinotecan, used as a reference antitumor drug, were dissolved in sterile PBS containing 5% DMSO and 5% glucose (solvent). Groups 1, 2, and 3 were injected intratumorally with 5 and 25 mg/kg of **1** and 25 mg/kg of irinotecan, respectively, on days 0, 2, 4, 6, 8, and 10. Group 4 was administered vehicle (solvent only). Body weights and tumor sizes were measured every other day from day 2 until 28. Solid tumor volumes were calculated as follows: length (mm) \times width (mm) \times depth (mm) $\times \pi/6$. Tumor growth and body weight changes were evaluated by the ratio of each value against the initial values on day 0.

■ ASSOCIATED CONTENT

● Supporting Information

The Supporting Information is available free of charge on the ACS Publications website at DOI: 10.1021/acs.jnatprod.6b01051.

Experimental data for antitumor effects of **1** and ¹H NMR spectra for **1**–**6** (PDF)

■ AUTHOR INFORMATION

Corresponding Authors

*Tel/fax: +81 22 727 0114. E-mail: mhosono@tohoku-mpu.ac.jp (M. Hosono).

*Tel/fax: +81 22 727 0218. E-mail: yamazaki@tohoku-mpu.ac.jp (H. Yamazaki).

ORCID

Hiroyuki Yamazaki: 0000-0002-1540-7255

Notes

The authors declare no competing financial interest.

■ ACKNOWLEDGMENTS

This work was supported in part by the Japan Science and Technology Agency (JST) (2007 Research for Promoting Technological Seeds) to M.N., Kanae Foundation for the Promotion of Medical Science to H.Y., and a Grant for Basic Science Research Projects from The Sumitomo Foundation to H.Y.

■ REFERENCES

- (1) Blunt, J. W.; Copp, B. R.; Keyzers, R. A.; Munro, M. H.; Prinsep, M. R. *Nat. Prod. Rep.* **2016**, *33*, 348–364 and previous reports in this series.
- (2) Faulkner, D. J. *Nat. Prod. Rep.* **2002**, *19*, 1–48 and previous reports in this series.
- (3) Skropeta, D.; Wei, L. *Nat. Prod. Rep.* **2014**, *31*, 999–1025.
- (4) Newman, D. J.; Cragg, G. M. *Mar. Drugs* **2014**, *12*, 255–278.
- (5) Stonik, V. A.; Fedorov, S. N. *Mar. Drugs* **2014**, *12*, 636–671.
- (6) Bhatnagar, I.; Kim, S. K. *Mar. Drugs* **2010**, *8*, 2702–2720.
- (7) Petit, K.; Biard, J. F. *Anti-Cancer Agents Med. Chem.* **2013**, *13*, 603–631.
- (8) (a) Liu, H.; Pratasik, S. B.; Nishikawa, T.; Shida, T.; Tachibana, K.; Fujiwara, T.; Nagai, H.; Kobayashi, H.; Namikoshi, M. *Tetrahedron Lett.* **2004**, *45*, 7015–7017. (b) Liu, H.; Fujiwara, T.; Nishikawa, T.; Mishima, Y.; Nagai, H.; Shida, T.; Tachibana, K.; Kobayashi, H.; Mangindaan, R. E. P.; Namikoshi, M. *Tetrahedron* **2005**, *61*, 8611–8615.
- (9) (a) Nakazawa, T.; Xu, J.; Nishikawa, T.; Oda, T.; Fujita, A.; Ukai, K.; Mangindaan, R. E.; Rotinsulu, H.; Kobayashi, H.; Namikoshi, M. *J. Nat. Prod.* **2007**, *70*, 439–442. (b) Wang, W.; Takahashi, O.; Oda, T.; Nakazawa, T.; Ukai, K.; Mangindaan, R. E. P.; Rotinsulu, H.; Wewengkang, D. S.; Kobayashi, H.; Tsukamoto, S.; Namikoshi, M. *Tetrahedron* **2009**, *65*, 9598–9603.
- (10) (a) Oda, T.; Kamoshita, K.; Maruyama, S.; Masuda, K.; Nishimoto, M.; Xu, J.; Ukai, K.; Mangindaan, R. E. P.; Namikoshi, M. *Biol. Pharm. Bull.* **2007**, *30*, 385–387. (b) Oda, T.; Fujiwara, T.; Liu, H.; Ukai, K.; Mangindaan, R. E. P.; Mochizuki, M.; Namikoshi, M. *Mar. Drugs* **2006**, *4*, 15–21.
- (11) Berridge, M. V.; Herst, P. M.; Tan, A. S. *Biotechnol. Annu. Rev.* **2005**, *11*, 127–152.
- (12) Häcker, G. *Cell Tissue Res.* **2000**, *301*, 5–17.
- (13) Lavrik, I. N. *Curr. Opin. Biotechnol.* **2010**, *21*, 551–555.

Synergistic anti-tumor effect of bullfrog sialic acid-binding lectin and pemetrexed in malignant mesothelioma

Toshiyuki Satoh^{1,2}, Takeo Tatsuta², Shigeki Sugawara², Akiyoshi Hara¹ and Masahiro Hosono²

¹Department of Clinical Pharmacotherapeutics, Tohoku Medical and Pharmaceutical University, Aobaku, Sendai, Miyagi 981-8558, Japan

²Division of Cell Recognition Study, Institute of Molecular Biomembrane and Glycobiology, Tohoku Medical and Pharmaceutical University, Aobaku, Sendai, Miyagi 981-8558, Japan

Correspondence to: Masahiro Hosono, email: mhosono@tohoku-mpu.ac.jp

Keywords: malignant mesothelioma, apoptosis, cell cycle, sialic acid-binding lectin, combination treatment

Received: December 28, 2016

Accepted: April 06, 2017

Published: April 18, 2017

Copyright: Satoh et al. This is an open-access article distributed under the terms of the Creative Commons Attribution License 3.0 (CC BY 3.0), which permits unrestricted use, distribution, and reproduction in any medium, provided the original author and source are credited.

ABSTRACT

Malignant mesothelioma is an aggressive cancer with limited therapeutic options. Sialic acid-binding lectin isolated from *Rana catesbeiana* oocytes (cSBL) is a multifunctional protein with anti-cancer activity. The effects of pemetrexed, cisplatin, and cSBL were evaluated in mesothelioma and normal mesothelial cell lines. We evaluated cytotoxicity, apoptosis, caspase-3 cleavage and activation, cell proliferation, cell cycle arrest, and levels of cell cycle proteins in H28 cells treated with pemetrexed, cisplatin, and cSBL alone or in combination. Treatment with cSBL alone was cytotoxic to mesothelioma cells. The anti-cancer effect of cSBL was observed in a broader range of cell lines and exhibited greater cancer cell selectivity than pemetrexed or cisplatin. Combination treatment with pemetrexed + cSBL resulted in greater dose-dependent cytotoxicity than pemetrexed + cisplatin, the standard of care in mesothelioma. The synergistic effect of pemetrexed + cSBL was mediated by the cytostatic effect of pemetrexed and the cytotoxic effect of cSBL. It thus appears that cSBL has therapeutic potential for the treatment of mesothelioma.

INTRODUCTION

Malignant mesothelioma is an aggressive cancer of mesothelial cell origin that results from exposure to asbestos [1, 2]. Asbestos was extensively used in industry and construction during the 20th century. It was first associated with the incidence of mesothelioma in the 1960s [3–6]. Because mesothelioma develops 20–30 years after asbestos exposure, the number of mesothelioma patients is expected to increase [7–9]. There are few therapeutic options for mesothelioma. The folate antimetabolite pemetrexed is a chemotherapeutic that is typically used in combination with platinum-containing drugs such as cisplatin [10, 11]. Compared to cisplatin monotherapy, combination treatment with pemetrexed + cisplatin improves response rate, progression-free survival, overall survival, and quality of life in mesothelioma patients [10]. However, most patients treated with pemetrexed and cisplatin experience tumor progression or relapse within a year [12, 13]. Drug resistance is

also commonly observed [14]. Therefore, alternative therapeutic agents for mesothelioma are needed.

Sialic acid-binding lectin isolated from *Rana catesbeiana* oocytes (cSBL) is a multifunctional protein with lectin-binding [15, 16], ribonuclease (RNase) [17], and anti-tumor activity [16]. cSBL is cytotoxic to cancer cells including leukemia [18–21], breast carcinoma [21–24], mesothelioma [25], and hepatoma cells [21, 26, 27]. It has little effect on normal cells such as fibroblasts, melanocytes, keratinocytes, and mesothelial cells [20, 21, 25, 26, 28]. cSBL-induced cell death involves at least three steps: (1) binding to the cell surface via carbohydrate chain containing sialic acid, (2) cell internalization, and (3) RNA cleavage and activation of apoptosis. The cytotoxic effects of cSBL are mediated by the induction of apoptosis in response to mitochondrial perturbation. RNase activity is essential for cSBL-induced cytotoxicity [24]. Treatment of tumor-bearing mice (transplanted with sarcoma 180 cells, Ehrlich, or Mep 2 ascites cells) with cSBL at a non-toxic dose prolonged

survival [16]. In contrast to commonly used DNA-targeting agents, the cytotoxic effects of RNases are non-genotoxic [29]. Thus, cSBL has therapeutic potential as a novel RNA-targeting anti-cancer agent.

Combination chemotherapy is the standard of care for many cancers. It allows for the use of doses that maximize the therapeutic effects while preventing chemoresistance. cSBL has an anti-cancer effect in mesothelioma cell lines (e.g. NCI-H28 [H28], ACC-MESO-1 [MESO-1], and ACC-MESO-4 [MESO-4]), and exhibited synergistic effects with tumor necrosis factor-related apoptosis-inducing ligand (TRAIL) in H28 cells [25] and interferon- γ in hepatoma cell lines [27]. We investigated whether cSBL exhibited greater tumor selectivity than pemetrexed and cisplatin, and whether combination treatment with cSBL + pemetrexed was comparable or superior to combination treatment with pemetrexed + cisplatin.

RESULTS

cSBL exhibits greater cancer cell selectivity than pemetrexed and cisplatin

We evaluated the effects of cSBL, pemetrexed, and cisplatin on the viability of epithelioid mesothelioma cells (NCI-H2452 [H2452], MESO-1, and MESO-4), biphasic mesothelioma cells MSTO-211H (MSTO) and sarcomatoid mesothelioma cells (H28), and non-malignant mesothelial cells (MeT5A) using WST-8 assays. All three agents reduced mesothelioma cell viability. However, cSBL had the least effect on MeT5A cells (Figure 1). Even at the highest concentration (20 μ M), cSBL only inhibited MeT5A cell viability by 40% (Figure 1C). In contrast, pemetrexed decreased MeT5A cell viability by 50% at 0.01 μ M and cisplatin decreased viability by 70% at 10 μ M. We calculated the half maximal inhibitory concentration (IC_{50}), defined as the concentration required to inhibit cell growth by 50%, from dose-response curves. The relative sensitivity (RS) of each agent represents the ratio of the IC_{50} value in a cancer cell line to the IC_{50} value in MeT5A cells (Table 1). H2452, MESO-1, and MESO-4 cells were resistant to pemetrexed (RS: 0.37, 0.06, and 0.06, respectively), and H28, H2452, and MESO-1 cells were resistant to cisplatin (RS: 0.66, 0.24, and 0.26, respectively). In contrast, cSBL was cytotoxic in these drug-resistant cell lines. The RS of cSBL was higher (9.48–247.02) than the RS values of pemetrexed and cisplatin in mesothelioma cells, indicating that the cytotoxic effect of cSBL was more selective to cancer cells.

cSBL and pemetrexed exert a strong synergistic effect

We investigated the pharmacological interaction between the three agents by evaluating the viability of H28 cells treated with pemetrexed + cisplatin, pemetrexed + cSBL, or cisplatin + cSBL. H28 cells are moderately

sensitive to pemetrexed (Figure 1 and Table 1). We previously demonstrated that combination treatment with cSBL + TRAIL has a synergistic effect H28 cells [25]. The concentration of each drug in the combination regimen was based on the IC_{50} value of each agent as a single treatment. Pemetrexed + cisplatin and pemetrexed + cSBL reduced cell viability to a similar extent (Figure 2A). To evaluate the synergistic effect of each drug combination, we calculated combination index (CI) values. The CI curves shown in Figure 2B indicated that pemetrexed + cSBL had a stronger synergistic effect and broader fraction affected (Fa) range than the other combinations. Cisplatin + cSBL exhibited the weakest cytotoxic and synergistic effects. We also calculated the concentration of each agent at Fa = 0.5 (i.e., the concentration predicted to reduce cell viability by 50%) (Table 2). Lower concentrations of each agent were required to inhibit cell viability by 50% when they were combined rather than administered a single agents. The concentration of pemetrexed decreased by nearly 50% when used in combination with cSBL (0.38 μ M) compared to cisplatin (0.65 μ M).

Pemetrexed and cSBL induce apoptosis in mesothelioma cells

We previously demonstrated that cSBL induces apoptosis in H28 (sarcomatoid histological type) as well as MESO-1 and MESO-4 (epithelioid type) cells, and that the synergistic anti-tumor effect of cSBL + TRAIL in H28 cells was mediated by an increase in apoptosis [25]. To elucidate the mechanism underlying the synergistic effect of pemetrexed + cSBL in H28 cells, we evaluated markers of apoptosis. In the initial combination treatment experiments (Figure 2A), pemetrexed (20 μ M), cisplatin (40 μ M), and cSBL (1 μ M) reduced the viability of H28 cell lines to similar levels (approximately 30%). Therefore, we used these concentrations in all subsequent experiments. After 72 h of treatment, the percentage of annexin V-positive cells was 27.3%, 38.7%, and 44.3% in cells treated with pemetrexed, cisplatin, and cSBL, respectively, and 44.8%, 47.3%, and 46.0% in cells treated with pemetrexed + cisplatin, pemetrexed + cSBL, and cisplatin + cSBL, respectively (Figure 3). There were no statistically significant differences between the individual and combination treatments.

The synergistic effect of pemetrexed + cSBL is not mediated by changes in caspase-3 activity

To investigate whether the synergistic anti-tumor effect of pemetrexed + cSBL was mediated by apoptosis, we analyzed activated caspase-3 levels. Western blot analysis demonstrated that all of the treatments increased activated caspase-3 levels (Figure 4A). Caspase-Glo™ 3/7 assays indicated pemetrexed and cisplatin did not induce caspase-3 activation. In contrast, a significant increase in activated caspase-3 was observed in cells treated

with cSBL alone or with any of the three combination treatments (Figure 4B). There were no significant differences in caspase-3 activity between cells treated with cSBL alone or the combination treatments.

Pemetrexed and cisplatin inhibit cell proliferation, but cSBL has a cytotoxic effect in H28 cells

Because apoptosis was not upregulated with the addition of pemetrexed to cSBL, we investigated the mechanism by which pemetrexed and cSBL inhibited mesothelioma cell viability. Previous reports have indicated that the anti-tumor effect of both pemetrexed and cisplatin is mediated by the induction of apoptosis in response to cell cycle arrest [30–35]. Therefore, we analyzed the effect of pemetrexed and cisplatin on cell proliferation. The total number of cells decreased by 10.4%, 14.2%, and 32.7% in cells treated with pemetrexed, cisplatin, and cSBL, respectively, for 72 h compared to control (PBS-treated) cells (Figure 5A). The ratio of annexin V- and propidium iodide (PI)-positive cells indicated that the number of dead cells barely increased in response to pemetrexed-

or cisplatin treatment, whereas the number of dead cells significantly increased with cSBL treatment (Figure 5B).

The anti-tumor activity of pemetrexed + cSBL is mediated by cytostatic and cytotoxic effects

Cell viability assays suggested that pemetrexed and cisplatin inhibited proliferation. Therefore, we analyzed cell cycle progression in H28 cells treated with these agents. Flow cytometry analysis revealed that pemetrexed and cisplatin induced cell cycle arrest in S phase and the S or G2 phase, respectively. In contrast, cSBL had a minimal effect on cell cycle progression. However, it promoted a significant increase in the number of cells in the sub-G1 phase, indicative of apoptosis. DNA histograms of cells treated with the combination treatments resembled the histograms of cells treated with the individual agents (pemetrexed + cisplatin: S phase arrest, pemetrexed + cSBL: S phase arrest and sub-G1 increment, and cisplatin + cSBL: S or G2 phase arrest and sub-G1 increment) (Figure 6A and 6B). To investigate the molecular mechanisms underlying these effects, we assessed the levels of proteins that regulate

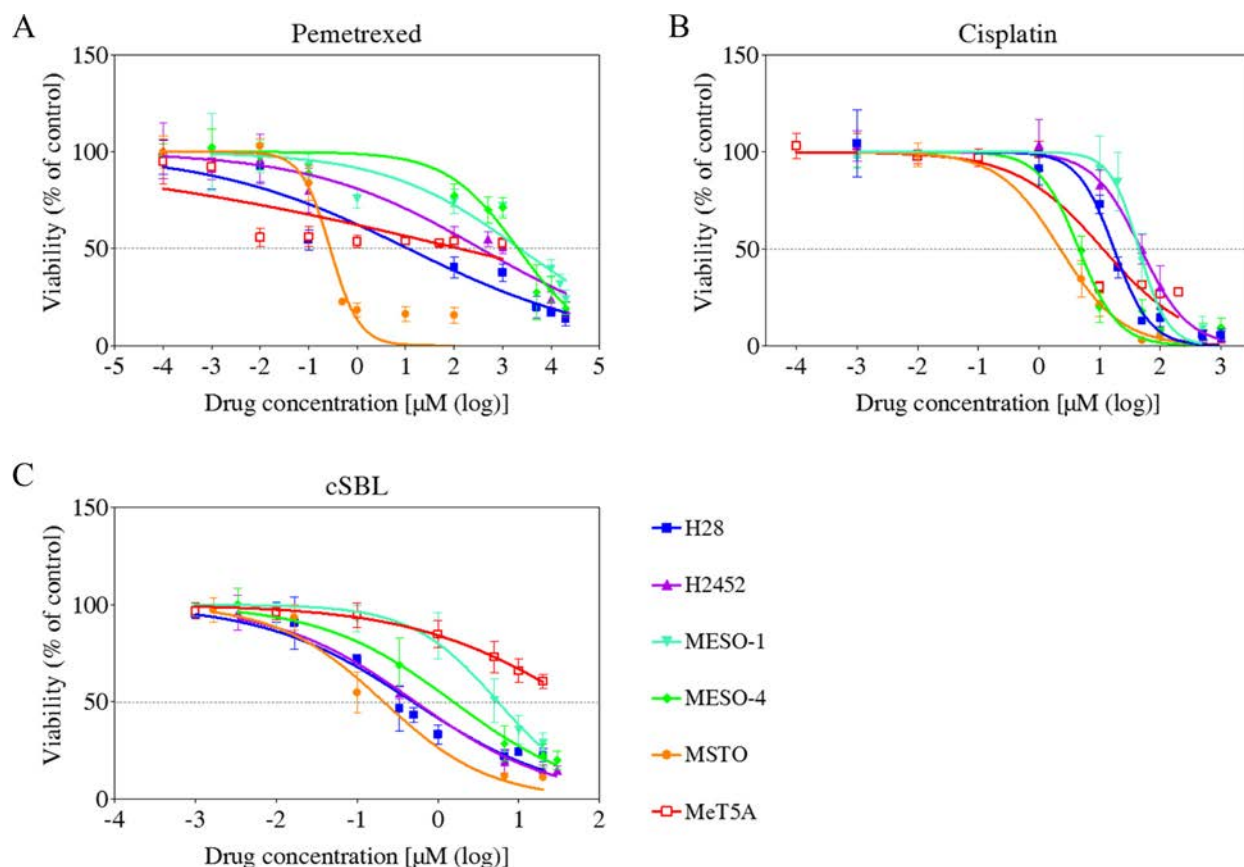


Figure 1: Dose-response curves in the mesothelioma cell lines (H28, H2452, MESO-1, MESO-4, and MSTO), and MeT5A mesothelial cells treated with pemetrexed (A), cisplatin (B), or cSBL (C). Cells were treated with pemetrexed (0.1 nM–20 mM), cisplatin (1 nM–1 mM), or cSBL (1 nM–30 μM) for 72 h. The dots and bars represent the mean and SD, respectively. Dose-response curves are depicted as lines or dotted lines. Each data point represents the mean ± SD of at least three independent WST-8 assays. Each sample was plated in triplicate.

Table 1: IC₅₀ values (μM) and RS of pemetrexed, cisplatin, and cSBL in mesothelioma cells

Drugs	Drug targets		MeT5A	H28	H2452	MESO-1	MESO-4	MSTO
Pemetrexed	TS	IC ₅₀	129.50	11.27	353.00	2267.00	2077.00	0.28
	DHFR		(24.20–693.20)	(5.67–22.39)	(208.6–597.3)	(1393–3691)	(1634–2639)	(0.23–0.34)
	GRAFT	RS	1.00	11.49	0.37	0.06	0.06	465.99
Cisplatin	DNA	IC ₅₀	11.27	17.18	47.62	44.14	4.54	2.23
			(8.07–15.73)	(15.14–19.50)	(41.23–55.00)	(38.62–50.46)	(3.87–5.33)	(1.62–3.06)
		RS	1.00	0.66	0.24	0.26	2.48	5.06
cSBL	RNA	IC ₅₀	52.22	0.46	0.52	5.51	1.54	0.21
			(33.94–80.36)	(0.35–0.68)	(0.41–0.66)	(4.67–6.50.)	(1.10–2.17)	(0.15–0.29)
		RS	1.00	113.89	100.00	9.48	33.91	247.02

The 95% confidence intervals for each IC₅₀ value are shown in parentheses. The RS value was calculated as the IC₅₀ value of each agent in MeT5A cells divided by the IC₅₀ value in each cancer cell line.

cell cycle progression (cyclin, p21^{Waf1/Cip1}, and Akt) by western blotting. The levels of cyclin A and p21^{Waf1/Cip1} were unchanged in cells treated with pemetrexed alone, while the levels of phosphorylated Akt significantly increased. Cyclin A and B1 levels significantly decreased in cisplatin-treated cells, while p21^{Waf1/Cip1} levels increased. In contrast, cyclin A, B1, D1, and E levels, and as well as p21^{Waf1/Cip1} and phosphorylated Akt levels, significantly decreased in cSBL-treated cells. The levels of cyclin A and B1 decreased, whereas p21^{Waf1/Cip1} levels increased in cells treated with pemetrexed + cisplatin. Pemetrexed + cSBL, and cisplatin + cSBL, significantly decreased cyclin B1, p21^{Waf1/Cip1}, and phosphorylated Akt levels, similar to those observed in cells treated with cSBL alone, whereas pemetrexed + cSBL had the same effect on cyclin A levels as treatment with pemetrexed alone (Figure 6C).

DISCUSSION

Mesothelioma is categorized as one of three histological subtypes: epithelioid, biphasic, or sarcomatoid [1, 36]. Previous studies have demonstrated that the epithelioid subtype is associated with more favorable survival outcomes compared to non-epithelioid subtypes [1, 37, 38]. We found that cSBL had strong cytotoxic effects in a broader range of mesothelioma cell types including pemetrexed- or cisplatin-resistant cells. We previously demonstrated that cSBL selectively bound to 20 human and animal cancer cell lines but not to 10 normal cell lines [15]. A comprehensive analysis of cSBL cytotoxicity and cancer selectivity was performed previously [39, 40]. We found that cSBL preferentially binds and internalizes into cancer cells compared to

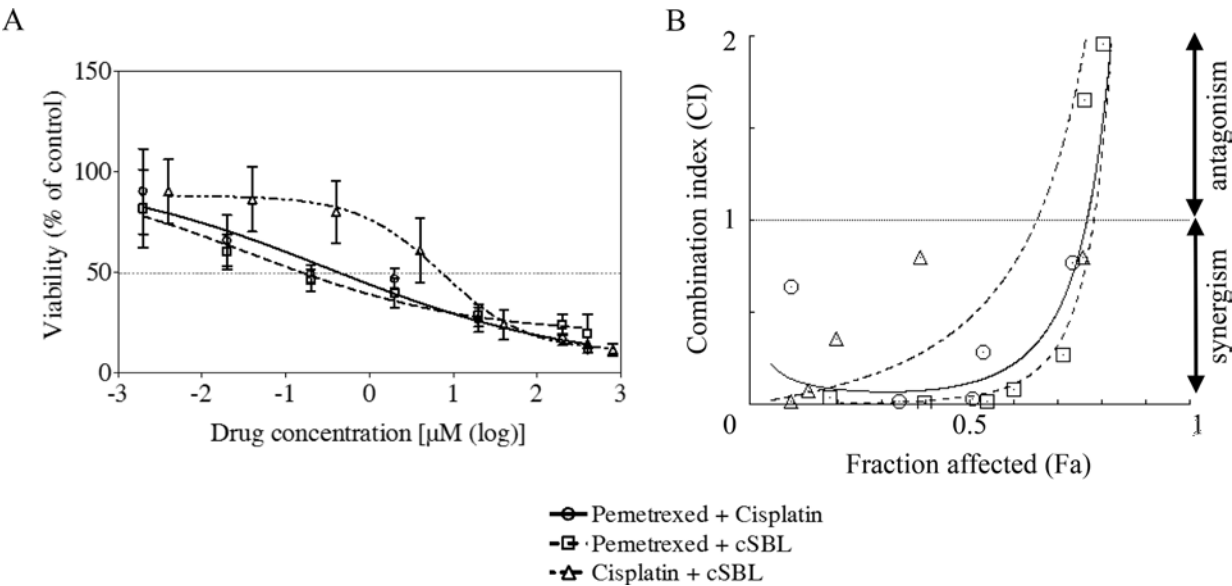


Figure 2: Pharmacological interactions between pemetrexed, cisplatin, and cSBL in H28 cells. (A) The drug concentration ratios were as follows: pemetrexed + cisplatin (1:2), pemetrexed + cSBL (20:1), cisplatin + cSBL (40:1). Cells were treated with pemetrexed (2 nM–400 μM), cisplatin (4 nM–800 μM), or cSBL (0.1 nM–20 μM) for 72 h. The horizontal axis indicates the concentration of pemetrexed in the pemetrexed + cisplatin or pemetrexed + cSBL combination or the concentration of cisplatin in the cisplatin + cSBL combination. (B) CI-Fa curves for H28 cells treated with pemetrexed + cisplatin, pemetrexed + cSBL, or cisplatin + cSBL. CI values < 1 indicate a synergistic effect, and CI values > 1 indicate an antagonistic effect. Each data point represents the mean ± SD of three independent WST-8 assays. Each sample was plated in triplicate.

Table 2: CI values and drug concentrations at Fa = 0.5 in H28 cells

	Drug/Combo	CI value	Concentration at Fa = 0.5		
			Pemetrexed (μM)	Cisplatin (μM)	cSBL (μM)
Single	Pemetrexed	—	20.44	—	—
	Cisplatin	—	—	15.2	—
	cSBL	—	—	—	0.69
Combination	Pemetrexed + Cisplatin	0.12	0.65	1.31	—
	Pemetrexed + cSBL	0.05	0.38	—	0.02
	Cisplatin + cSBL	0.47	—	4.6	0.12

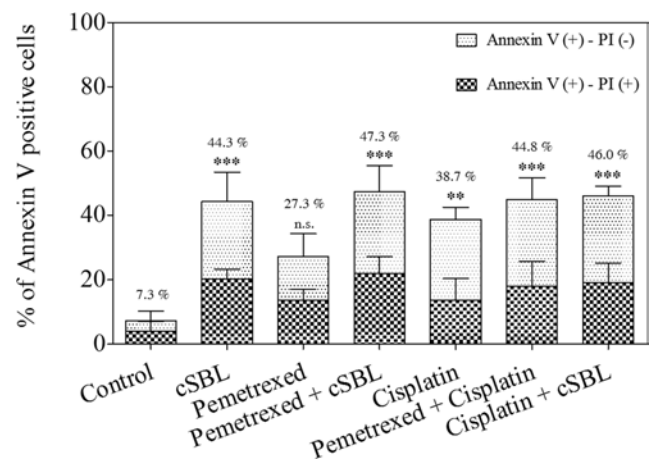


Figure 3: Pemetrexed, cisplatin, and cSBL, either alone or in combination, induced apoptosis in H28 cells. Cells were treated with pemetrexed (20 μM), cisplatin (40 μM), or cSBL (1 μM) for 72 h. The y-axis indicates the percentage of annexin V-positive cells. The percentage of PI-positive and negative cells is indicated by the different column patterns. The statistical significance of the percentage of annexin V-positive cells compared to the control is shown. ***p* < 0.01, ****p* < 0.001; n.s.: not significant.

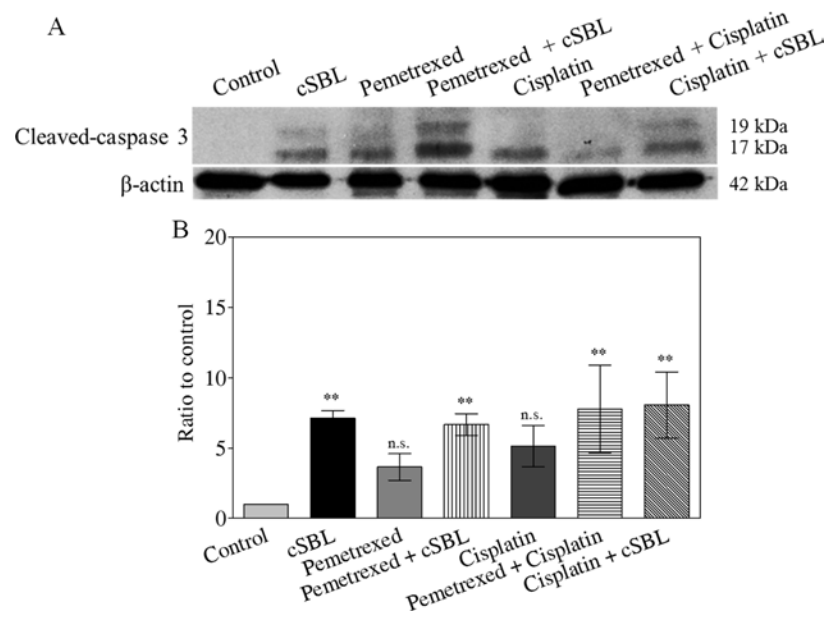


Figure 4: Caspase-3 activation is not enhanced by combination treatment. Cells were treated with pemetrexed (20 μM), cisplatin (40 μM), or cSBL (1 μM) for 72 h. (A) Cleaved (activated) caspase-3 was detected using western blot analysis. (B) Caspase-3 activity was analyzed using a Caspase-Glo™ 3/7 assay. **p* < 0.05; n.s.: not significant.

normal cells, and exerts cytotoxic effects through its RNase activity [16]. Internalization-defective P-388 mutant (RC-150) cells, which are cSBL-resistant, can bind cSBL but show no cytotoxicity [41]. Therefore, we hypothesize that the lack of specific internalization of cSBL could make normal cells non-sensitive.

Although the effects of cSBL in combination with other agents have been investigated in various cancer cell lines [21, 25, 27], there have been no reports describing the effects of cSBL in combination with pemetrexed or cisplatin. We have demonstrated that the synergistic effect of pemetrexed + cSBL is comparable to that of pemetrexed + cisplatin (Figure 2A and 2B). Treatment with pemetrexed + cSBL could decrease the risk of dose-dependent adverse effects associated with pemetrexed and/or the development of pemetrexed resistance. The synergistic effect of pemetrexed + cSBL is not mediated by increased apoptosis (Figures 3, 4). Apoptosis is commonly observed in cancer

cells treated with relatively high concentrations of anti-cancer agents, whereas a cytostatic effect (i.e. transient growth arrest) is typically observed with relatively low concentrations [42]. We found that the percentages of annexin V/PI double-positive cells (Figure 3) and dead cells in the Muse™ analysis (Figure 5) of pemetrexed- or cisplatin-treated cells were comparable and relatively low (13–17%). Cell cycle analysis (Figure 6) indicated that pemetrexed and cisplatin exert cytostatic effects, whereas cSBL exerts cytotoxic effects. These data suggest that pemetrexed- and cisplatin-treated cells proceed to an early apoptotic stage, but that cSBL is required for completion of apoptosis. The differential effects of each agent on cell cycle proteins suggest that the molecular mechanisms underlying cell cycle arrest are dependent on the cell type and the specific treatment. Pemetrexed reportedly induces S-phase arrest in A549 lung cancer cells by prolonging Akt activation, thereby sustaining

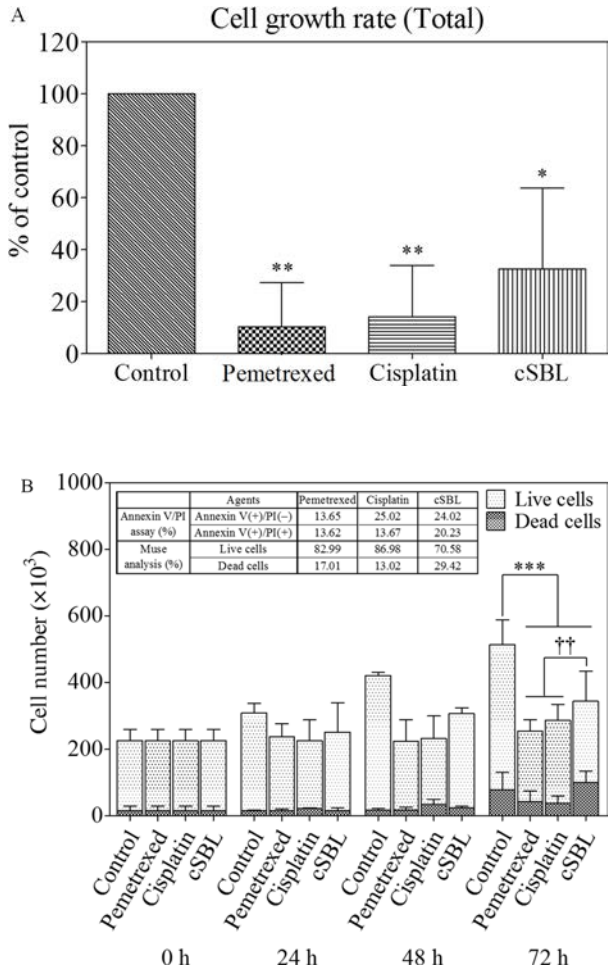


Figure 5: Pemetrexed and cisplatin inhibit proliferation, whereas cSBL has a cytotoxic effect in H28 cells. Cells were treated with pemetrexed (20 μ M), cisplatin (40 μ M), or cSBL (1 μ M) for 0–72 h. The number of cells was estimated using a Muse™ Count & Viability Kit. **(A)** Cell growth rates were calculated as the ratio of the cell number at 72 h to the cell number at 0 h and presented as a fraction of the controls. **(B)** The number of live and dead cells every 24 h is shown. Statistically significant differences in the live cell number at 72 h were observed in the treatment groups compared to the control (***). Statistically significant differences in the dead cell number at 72 h were observed in cSBL-treated cells compared to cisplatin- or pemetrexed-treated cells (**). * $p < 0.05$, ** $p < 0.01$, *** $p < 0.001$, ** $p < 0.01$.

activation of CDK2/cyclin A kinase [31]. In our study, pemetrexed treatment did not significantly alter the levels of cyclin A. However, pemetrexed induced an increase in phosphorylated Akt levels and arrested cells cycle in S-phase (Figure 6). The levels of the cyclins evaluated as well as p21^{Waf1/Cip1} levels significantly decreased in cSBL-

treated cells. Since cSBL inhibits RNA translation through degradation, short-lived proteins such as cyclins are likely to be sensitive to cSBL treatment. Interestingly, in cells treated with pemetrexed + cSBL, although the levels of cyclin B1, D1, and E, p21^{Waf1/Cip1}, and phosphorylated Akt significantly decreased to levels similar to those observed

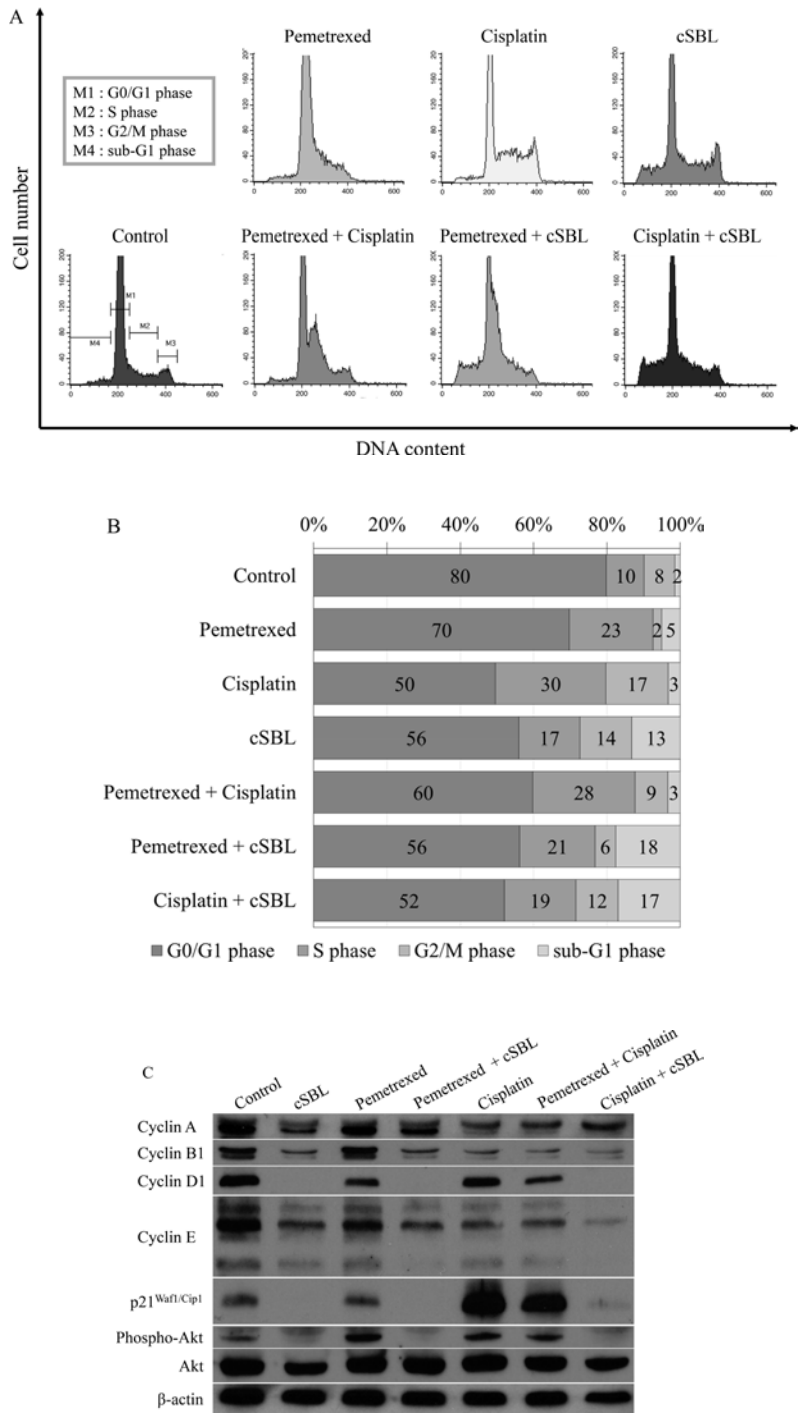


Figure 6: Pemetrexed, cisplatin, and cSBL, either alone or in combination, alter cell cycle dynamics in H28 cells. Cells were treated with pemetrexed (20 μ M), cisplatin (40 μ M), or cSBL (1 μ M) for 72 h. (A, B) Flow cytometry analysis of cell cycle progression in H28 cell lines after 72 h of treatment. (C) Western blot analysis of cyclin (A, B1, D1, and E), p21^{Waf1/Cip1}, pan-Akt, and phospho-Akt levels.

in cells treated with cSBL alone, cyclin A levels did not significantly change. Although cSBL may inhibit cyclin A translation, pemetrexed might stabilize cyclin A levels and enhance CDK2/cyclin A kinase activity, thereby inducing S-phase arrest and/or apoptosis when used in combination with cSBL [43–45]. The strong synergism of pemetrexed + cSBL is mediated by the cytostatic action of pemetrexed triggered by sustained CDK2/cyclin A activation, and the proapoptotic effect of cSBL.

The levels of p21^{Waf1/Cip1} were differentially affected by each treatment. The tumor suppressor p21^{Waf1/Cip1} arrests cell cycle progression by inhibiting the function of cyclin-CDK complexes or DNA polymerase [46–48]. Overexpression of p21^{Waf1/Cip1} induces cell cycle arrest in G1-, G2- [49], or S-phase [50, 51]. Pemetrexed and cisplatin induce cell cycle arrest by increasing p21^{Waf1/Cip1} levels [30, 52]. As a single treatment, pemetrexed did not change p21^{Waf1/Cip1} levels. However, cisplatin and cSBL significantly increased and decreased p21^{Waf1/Cip1} levels, respectively. Of the combination treatments evaluated, only pemetrexed + cisplatin substantially increased p21^{Waf1/Cip1} levels. Therefore, p21^{Waf1/Cip1} may be important for cisplatin-induced cell cycle arrest in H28 cells. Indeed, p21^{Waf1/Cip1} induced apoptosis in MSTO cells treated with a combination of cisplatin and piroxicam. Silencing p21^{Waf1/Cip1} inhibited this effect [53]. Because cisplatin strongly increased p21^{Waf1/Cip1} in H28 cells (Figure 6), we propose that the decrease of p21^{Waf1/Cip1} levels in cSBL-treated cells might explain the lack of synergy between cisplatin and cSBL. Lazzarini *et al.* reported that shRNA-mediated inhibition of p21^{Waf1/Cip1} enhanced the anti-tumor effects of DNA-damaging agents such as doxorubicin, etoposide, and CPT11 in H28

and H2052 cells [54]. Inoue *et al.* reported that sorafenib downregulated p21^{Waf1/Cip1} levels and promoted cell death in renal cell carcinoma and hepatocellular carcinoma when used in combination with DNA-damaging agents such as paclitaxel or doxorubicin [55]. Therefore, cSBL + DNA-damaging agents (with the exception of cisplatin) might be an effective therapeutic strategy for mesothelioma. The proposed mechanisms of action of the combination treatments are shown in Figure 7.

In conclusion, cSBL exhibits a potent anti-tumor effect in multiple mesothelioma cell lines due to its cytotoxic activity and high selectivity for cancer cells compared to either pemetrexed or cisplatin. Pemetrexed + cSBL exhibited a strong synergistic effect that was comparable or even superior to the standard regimen of pemetrexed + cisplatin. We propose that the synergistic effect results from the combination of the cytostatic effect of pemetrexed and the cytotoxic effect of cSBL. Therefore, cSBL has therapeutic potential for mesothelioma.

MATERIALS AND METHODS

Cell culture

The H28, H2452, and MSTO mesothelioma cell lines and immortalized, non-malignant MeT-5A mesothelial cell line were purchased from American Type Cell Culture Collection (Manassas, VA, USA). The MESO-1 and MESO-4 mesothelioma cell lines were obtained from Riken Cell Bank (Tsukuba, Japan). H28, H2452, MSTO, MESO-1, and MESO-4 cells were cultured in RPMI-1640 medium supplemented with 10%

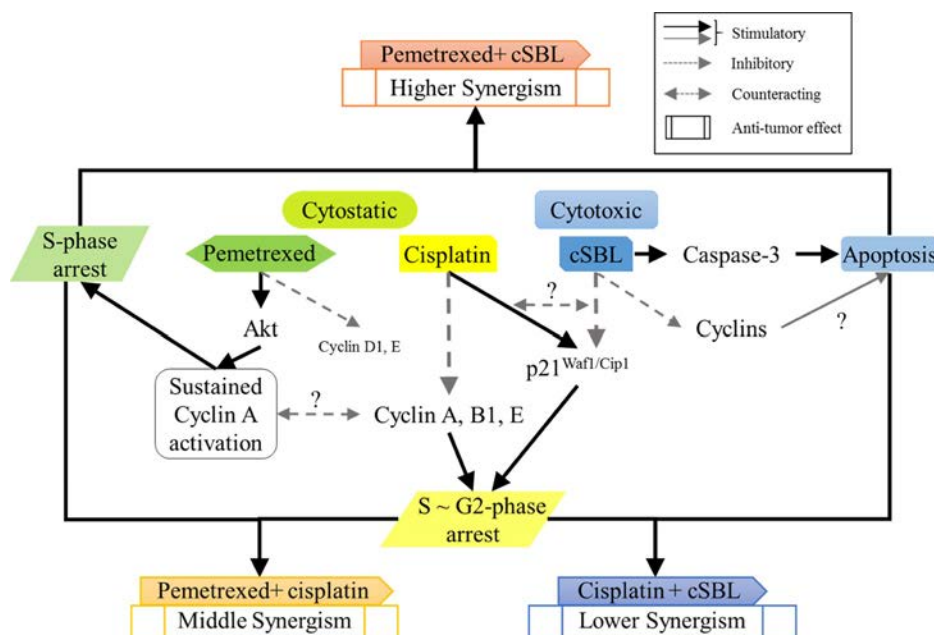


Figure 7: Schematic representation of the molecular mechanisms underlying the synergistic effects of each combination treatment in H28 cells.

fetal bovine serum (FBS). MeT-5A cells were cultured in Medium 199 with Earle's balanced salt solution (75 mM L-Gln and 1.25 g/L sodium bicarbonate) supplemented with 3.3 nM epidermal growth factor (EGF), 400 nM hydrocortisone, 870 nM insulin, 20 mM HEPES, and 10% FBS. All cells were cultured with 100 U/mL penicillin and 100 µg/mL streptomycin at 37°C in a 95% air and 5% CO₂ atmosphere.

Reagents

cSBL was isolated using sequential chromatography with Sephadex G75, DEAE-cellulose, hydroxyapatite, and SP-Sepharose as previously described [15]. Pemetrexed disodium heptahydrate was purchased from LC Laboratories (Woburn, MA, USA). Cisplatin was purchased from WAKO Pure Chemical Industries, Ltd. (Osaka, Japan). The caspase-3 polyclonal antibody and cyclin B1 (D5C10), cyclin D1 (92G2), p21^{Waf1/Cip1} (12D1), Akt (pan) (11E7), and phospho-Akt (Ser473) rabbit monoclonal antibodies were purchased from Cell Signaling Technology (Beverly, MA, USA). The cyclin A rabbit polyclonal antibody (H-432) and cyclin E mouse monoclonal antibody (HE12) were purchased from Santa Cruz Biotechnology Inc. (CA, USA). The β-actin antibody from Sigma-Aldrich (Tokyo, Japan) and horseradish peroxidase (HRP)-conjugated anti-mouse IgG were purchased from Zymed (South San Francisco, CA, USA). HRP-conjugated anti-rabbit IgG was purchased from Cedarlane (Hornby, Ontario, Canada), and the Caspase-Glo™ 3/7 Assay was purchased from Promega (Madison, WI, USA).

Cell viability assays

Cell viability was determined using the WST-8 assay. Cells (5×10^4 cells/mL) cultured in 96-well plates (100 µL/well) were treated with various concentration of pemetrexed, cisplatin, or cSBL for 72 h. The cells were incubated with Cell Count Reagent SF (Nacalai Tesque Inc., Kyoto, Japan) at 37°C in a 5% CO₂ atmosphere for 1–4 h. The absorbance of the resulting product at 450 nm was measured and the background absorbance at 650 nm subtracted. The IC₅₀ was calculated using GraphPad Prism 5.0 (San Diego, CA, USA). Experiments were conducted in triplicate.

Drug combination studies

The effect of combination treatment on cell viability was assessed using WST-8 assays. The concentration of the individual components was based on IC₅₀ values obtained in the single treatment experiments. CI values were calculated using the CompuSyn software (ComboSyn Inc., Paramus, NJ, USA) as previously described [56]. CI values < 1 indicated a synergistic effect and CI values > 1 indicated an antagonistic effect.

Annexin V staining and PI incorporation assays

To evaluate apoptosis, we evaluated annexin V binding and PI incorporation using a MEBCYTO apoptosis kit (MBL, Nagoya, Japan) according to the manufacturer's instructions. Cells (5×10^4 cells/mL) cultured in 12-well plates (1 mL/well) were treated with pemetrexed (20 µM), cisplatin (40 µM), or cSBL (1 µM). Fluorescence intensity was detected using a FACScalibur flow cytometer, and the data analyzed using the CELLQuest software (BD Biosciences, Franklin Lakes, NJ, USA).

Detection of caspase-3 activity

The level of activated caspase-3 was analyzed using western blot assays with an antibody against cleaved (activated) caspase-3. Cells (5×10^4 cells/mL) cultured in 6-well plates (2 mL/well) were treated with pemetrexed (20 µM), cisplatin (40 µM), or cSBL (1 µM) for 72 h. Whole cell lysates were prepared using extraction buffer (150 mM NaCl, 10 mM Tris-HCl [pH 7.4], 5 mM EDTA, 1% Nonidet P-40, 0.1% sodium deoxycholate, and 0.1% sodium dodecyl sulfate) supplemented with 1 tablet/10 mL cComplete, Mini, EDTA-free Protease Inhibitor Cocktail (Roche Applied Science, Indianapolis, IN, USA) and 1 tablet/10 mL PhosSTOP phosphatase inhibitor (Roche Applied Science). Soluble proteins were collected and protein concentration measured using a BCA Protein Assay Kit (Thermo Fisher Scientific, Waltham, MA, USA) according to the manufacturer's instructions. The proteins were separated using SDS-PAGE and transferred to Immobilon-P Transfer Membranes (Merck Millipore, Billerica, MA, USA). Membranes were sequentially incubated with primary and secondary antibodies diluted in Can Get Signal (Toyobo CO., LTD., Osaka, Japan). The protein bands were detected using ECL Prime Western Blotting Detection Reagent (GE Healthcare, Little Chalfont, UK).

Caspase-3 enzymatic activity was measured using a Caspase-Glo™ Assay. Cells (5×10^4 cells/mL) cultured in white 96-well plates (25 µL/well) were treated with pemetrexed (20 µM), cisplatin (40 µM), or cSBL (1 µM) for 72 h in triplicate. Caspase-Glo™ Reagent (25 µL) was added to each well and the contents of the wells mixed using a plate shaker for 30 seconds. The cells were incubated at 37°C in a 5% CO₂ atmosphere for 1 h. The luminescence in each well was measured using GloMax™ Multi Detection System (Promega, Madison, WI, USA).

Cell proliferation assays

Cell proliferation was quantified using a Muse™ Count & Viability Kit (Merck Millipore, Billerica, MA, USA). Cells (5×10^4 cells/mL) cultured in 24-well plates (500 µL/well) were treated with pemetrexed (20 µM), cisplatin (40 µM), or cSBL (1 µM) for 0–72 h. The cells

were collected at 24 h intervals and combined with Muse™ Count & Viability Reagent in which both viable and non-viable cells are differentially stained based on their permeability to the DNA-binding dyes (cells:reagent = 1:9). The total number of viable or dead cells was counted using a Muse™ Cell Analyzer (Merck Millipore).

Cell cycle analysis

Changes in cell cycle progression induced by 72 h of treatment with pemetrexed (20 µM), cisplatin (40 µM), or cSBL (1 µM) were evaluated using a CycleTEST™ Plus DNA Reagent Kit (BD Biosciences) according to the manufacturer's instructions. Cells (5×10^4 cells/mL) were cultured in 12-well plates (1 mL/well). Fluorescence intensity was detected using a FACScalibur flow cytometer and the data analyzed using the CELLQuest software (BD Biosciences). Cell cycle progression was analyzed using Flowing Software 2 (Perttu Terho, Turku Centre for Biotechnology, Finland). The levels of cell cycle regulators (cyclin A, B1, D1, E, and p21^{Waf1/Cip1}), pan-Akt, and phospho-Akt were evaluated by western blot analysis.

Statistical analysis

The results from at least three independent experiments performed in triplicate are expressed as the mean ± standard deviation (SD). Statistical analyses were conducted using GraphPad Prism 5.0 and comparisons made using one-way analysis of variance (ANOVA) followed by Bonferroni post-hoc tests.

CONFLICTS OF INTEREST

The authors declare that there are no conflicts of interest.

FUNDING

This study was supported by the 'Strategic Research' Project (2012–2017) for Private Universities from the Ministry of Education, Culture, Sports, Science and Technology of Japan and a Grant-in-Aid for Young Scientists (B) (No. 26870527 to Takeo Tatsuta).

REFERENCES

1. Tsao AS, Wistuba I, Roth JA, Kindler HL. Malignant pleural mesothelioma. *J Clin Oncol*. 2009; 27:2081–90.
2. Robinson BW, Lake RA. Advances in malignant mesothelioma. *N Engl J Med*. 2005; 353:1591–603.
3. Owen WG. Diffuse Mesothelioma and Exposure to Asbestos Dust in the Merseyside Area. *Br Med J*. 1964; 2:214–8.
4. Matsuzaki H, Lee S, Maeda M, Kumagai-Takei N, Nishimura Y, Otsuki T. FoxO1 regulates apoptosis induced by asbestos in the MT-2 human T-cell line. *J Immunotoxicol*. 2016; 13:620–7.
5. Mensi C, De Matteis S, Dallari B, Riboldi L, Bertazzi PA, Consonni D. Incidence of mesothelioma in Lombardy, Italy: exposure to asbestos, time patterns and future projections. *Occup Environ Med*. 2016; 73:607–13.
6. Albin M, Magnani C, Krstev S, Rapiti E, Shefer I. Asbestos and cancer: An overview of current trends in Europe. *Environ Health Perspect*. 1999 (Suppl 2); 107:289–98.
7. Lanphear BP, Buncher CR. Latent period for malignant mesothelioma of occupational origin. *J Occup Med*. 1992; 34:718–21.
8. Selikoff IJ, Hammond EC, Seidman H. Latency of asbestos disease among insulation workers in the United States and Canada. *Cancer*. 1980; 46:2736–40.
9. Niklinski J, Niklinska W, Chyczewska E, Laudanski J, Naumnik W, Chyczewski L, Pluygers E. The epidemiology of asbestos-related diseases. *Lung Cancer*. 2004; 45:S7–15.
10. Vogelzang NJ, Rusthoven JJ, Symanowski J, Denham C, Kaukel E, Ruffie P, Gatzemeier U, Boyer M, Emri S, Manegold C, Niyikiza C, Paoletti P. Phase III study of pemetrexed in combination with cisplatin versus cisplatin alone in patients with malignant pleural mesothelioma. *J Clin Oncol*. 2003; 21:2636–44.
11. Krug LM. An overview of chemotherapy for mesothelioma. *Hematol Oncol Clin North Am*. 2005; 19:1117–36.
12. Leon L, Gemelli M, Sciarillo R, Avan A, Funel N, Giovannetti E. Synergistic Activity of the c-Met and Tubulin Inhibitor Tivantinib (ARQ197) with Pemetrexed in Mesothelioma Cells. *Curr Drug Targets*. 2014; 15:1331–40.
13. Hazarika M, White RM, Booth BP, Wang YC, Ham DY, Liang CY, Rahman A, Gobburu JVS, Li N, Sridhara R, Morse DE, Lostritto R, Garvey P, et al. Pemetrexed in malignant pleural mesothelioma. *Clin Cancer Res*. 2005; 11:982–92.
14. Kitazono-Saitoh M, Takiguchi Y, Kitazono S, Ashinuma H, Kitamura A, Tada Y, Kurosu K, Sakaida E, Sekine I, Tanabe N, Tagawa M, Tatsumi K. Interaction and cross-resistance of cisplatin and pemetrexed in malignant pleural mesothelioma cell lines. *Oncol Rep*. 2012; 28:33–40.
15. Nitta K, Takayanagi G, Kawauchi H, Hakomori S. Isolation and characterization of Rana catesbeiana lectin and demonstration of the lectin-binding glycoprotein of rodent and human tumor cell membranes. *Cancer Res*. 1987; 47:4877–83.
16. Nitta K, Ozaki K, Ishikawa M, Furusawa S, Hosono M, Kawauchi H, Sasaki K, Takayanagi Y, Tsuki S, Hakomori S. Inhibition of cell proliferation by Rana catesbeiana and Rana japonica lectins belonging to the ribonuclease superfamily. *Cancer Res*. 1994; 54:920–7.
17. Nitta K, Oyama F, Oyama R, Sekiguchi K, Kawauchi H, Takayanagi Y, Hakomori S, Titani K. Ribonuclease activity of sialic acid-binding lectin from Rana catesbeiana eggs. *Glycobiology*. 1993; 3:37–45.

18. Tatsuta T, Hosono M, Miura Y, Sugawara S, Kariya Y, Hakomori S, Nitta K. Involvement of ER stress in apoptosis induced by sialic acid-binding lectin (lectzyme) from bullfrog eggs. *Int J Oncol*. 2013; 43:1799–808.
19. Tatsuta T, Hosono M, Sugawara S, Kariya Y, Ogawa Y, Hakomori S, Nitta K. Sialic acid-binding lectin (lectzyme) induces caspase-dependent apoptosis-mediated mitochondrial perturbation in Jurkat cells. *Int J Oncol*. 2013; 43:1402–12.
20. Ogawa Y, Sugawara S, Tatsuta T, Hosono M, Nitta K, Fujii Y, Kobayashi H, Fujimura T, Taka H, Koide Y, Hasan I, Matsumoto R, Yasumitsu H, et al. Sialyl-glycoconjugates in cholesterol-rich microdomains of P388 cells are the triggers for apoptosis induced by *Rana catesbeiana* oocyte ribonuclease. *Glycoconj J*. 2014; 31:171–84.
21. Tang CH, Hu CC, Wei CW, Wang JJ. Synergism of *Rana catesbeiana* ribonuclease and IFN- γ triggers distinct death machineries in different human cancer cells. *FEBS Lett*. 2005; 579:265–70.
22. Tseng HH, Yu YL, Chen YL, Chen JH, Chou CL, Kuo TY, Wang JJ, Lee MC, Huang TH, Chen MH, Yiang GT. RC-RNase-induced cell death in estrogen receptor positive breast tumors through down-regulation of Bcl-2 and estrogen receptor. *Oncol Rep*. 2011; 25:849–53.
23. Hu CC, Tang CH, Wang JJ. Caspase activation in response to cytotoxic *Rana catesbeiana* ribonuclease in MCF-7 cells. *FEBS Lett*. 2001; 503:65–8.
24. Kariya Y, Tatsuta T, Sugawara S, Kariya Y, Nitta K, Hosono M. RNase activity of sialic acid-binding lectin from bullfrog eggs drives antitumor effect via the activation of p38 MAPK to caspase-3/7 signaling pathway in human breast cancer cells. *Int J Oncol*. 2016; 49:1334–42.
25. Tatsuta T, Hosono M, Takahashi K, Omoto T, Kariya Y, Sugawara S, Hakomori S, Nitta K. Sialic acid-binding lectin (lectzyme) induces apoptosis to malignant mesothelioma and exerts synergistic antitumor effects with TRAIL. *Int J Oncol*. 2014; 44:377–84.
26. Liao YD, Huang HC, Chan HJ, Kuo SJ. Large-scale preparation of a ribonuclease from *Rana catesbeiana* (bullfrog) oocytes and characterization of its specific cytotoxic activity against tumor cells. *Protein Expr Purif*. 1996; 7:194–202.
27. Hu CC, Lee YH, Tang CH, Cheng JT, Wang JJ. Synergistic cytotoxicity of *Rana catesbeiana* ribonuclease and IFN- γ on hepatoma cells. *Biochem Biophys Res Commun*. 2001; 280:1229–36.
28. Lee YH, Wei CW, Wang JJ, Chiou CT. *Rana catesbeiana* ribonuclease inhibits Japanese encephalitis virus (JEV) replication and enhances apoptosis of JEV-infected BHK-21 cells. *Antiviral Res*. 2011; 89:193–8.
29. Vert A, Castro J, Ribó M, Benito A, Vilanova M. A nuclear-directed human pancreatic ribonuclease (PE5) targets the metabolic phenotype of cancer cells. *Oncotarget*. 2016; 7:18309–24. doi: 10.18632/oncotarget.7579.
30. Qu K, Lin T, Wei J, Meng F, Wang Z, Huang Z, Wan Y, Song S, Liu S, Chang H, Dong Y, Liu C. Cisplatin induces cell cycle arrest and senescence via upregulating P53 and P21 expression in HepG2 cells. *Nan Fang Yi Ke Da Xue Xue Bao*. 2013; 33:1253–9.
31. Chen KC, Yang TY, Wu CC, Cheng CC, Hsu SL, Hung HW, Chen JW, Chang GC. Pemetrexed induces S-phase arrest and apoptosis via a deregulated activation of Akt signaling pathway. *PLoS One*. 2014; 9:e97888.
32. Wu DM, Zhang P, Xu GC, Tong AP, Zhou C, Lang JY, Wang CT. Pemetrexed induces G1 phase arrest and apoptosis through inhibiting Akt activation in human non small lung cancer cell line A549. *Asian Pac J Cancer Prev*. 2015; 16:1507–13.
33. Buqué A, Muhialdin JS, Muñoz A, Calvo B, Carrera S, Aresti U, Sancho A, Rubio I, López-Vivanco G. Molecular mechanism implicated in Pemetrexed-induced apoptosis in human melanoma cells. *Mol Cancer*. 2012; 11:25.
34. Jia Y, Sun H, Wu H, Zhang H, Zhang X, Xiao D, Ma X, Wang Y. Nicotine Inhibits Cisplatin-Induced Apoptosis via Regulating $\alpha 5$ -nAChR/AKT Signaling in Human Gastric Cancer Cells. *PLoS One*. 2016; 11:e0149120.
35. Vandermeers F, Hubert P, Delvenne P, Mascaux C, Grigoriu B, Burny A, Scherpereel A, Willems L. Valproate, in combination with pemetrexed and cisplatin, provides additional efficacy to the treatment of malignant mesothelioma. *Clin Cancer Res*. 2009; 15:2818–28.
36. Indovina P, Marcelli E, Di Marzo D, Casini N, Forte IM, Giorgi F, Alfano L, Pentimalli F, Giordano A. Abrogating G₂/M checkpoint through WEE1 inhibition in combination with chemotherapy as a promising therapeutic approach for mesothelioma. *Cancer Biol Ther*. 2014; 15:380–8.
37. Kataoka Y, Yamamoto Y, Otsuki T, Shinomiya M, Terada T, Fukuma S, Yamazaki S, Hirabayashi M, Nakano T, Fukuhara S. A new prognostic index for overall survival in malignant pleural mesothelioma: the rPHS (regimen, PS, histology or stage) index. *Jpn J Clin Oncol*. 2015; 45:562–8.
38. Ortolan E, Giacomino A, Martinetto F, Morone S, Lo Buono N, Ferrero E, Scagliotti G, Novello S, Orecchia S, Ruffini E, Rapa I, Righi L, Volante M, Funaro A. CD157 enhances malignant pleural mesothelioma aggressiveness and predicts poor clinical outcome. *Oncotarget*. 2014; 5:6191–205. doi: 10.18632/oncotarget.2186.
39. Tatsuta T, Sugawara S, Takahashi K, Ogawa Y, Hosono M, Nitta K. Lectzyme: A New Candidate Drug for Cancer Therapy. *Biomed Res Int*. Hindawi Publishing Corporation. 2014; 2014:1–10.
40. Tatsuta T, Sugawara S, Takahashi K, Ogawa Y, Hosono M, Nitta K. Cancer-selective induction of apoptosis by lectzyme. *Front Oncol*. 2014; 4:139.
41. Nitta K, Ozaki K, Tsukamoto Y, Furusawa S, Ohkubo Y, Takimoto H, Murata R, Hosono M, Hikichi N, Sasaki K. Characterization of a *Rana catesbeiana* lectin-resistant mutant of leukemia P388 cells. *Cancer Res*. 1994; 54:928–34.

42. Chang BD, Broude EV, Dokmanovic M, Zhu H, Ruth A, Xuan Y, Kandel ES, Lausch E, Christov K, Roninson IB. A senescence-like phenotype distinguishes tumor cells that undergo terminal proliferation arrest after exposure to anticancer agents. *Cancer Res.* 1999; 59:3761–7.
43. Ding H, Han C, Guo D, Wang D, Chen CS, D'Ambrosio SM. OSU03012 activates Erk1/2 and Cdk5 leading to the accumulation of cells in the S-phase and apoptosis. *Int J Cancer.* 2008; 123:2923–30.
44. Adachi S, Ito H, Tamamori-Adachi M, Ono Y, Nozato T, Abe S, Ikeda Ma, Marumo F, Hiroe M. Cyclin A/cdk2 activation is involved in hypoxia-induced apoptosis in cardiomyocytes. *Circ Res.* 2001; 88:408–14.
45. Zhan Z, He K, Zhu D, Jiang D, Huang YH, Li Y, Sun C, Jin YH. Phosphorylation of Rad9 at Serine 328 by Cyclin A-Cdk2 Triggers Apoptosis via Interfering Bcl-xL. *PLoS One.* 2012; 7:e44923.
46. Pestell RG, Albanese C, Reutens AT, Segall JE, Lee RJ, Arnold A. The cyclins and cyclin-dependent kinase inhibitors in hormonal regulation of proliferation and differentiation. *Endocr Rev.* 1999; 20:501–34.
47. Cheng M, Olivier P, Diehl JA, Fero M, Roussel MF, Roberts JM, Sherr CJ. The p21(Cip1) and p27(Kip1) CDK “inhibitors” are essential activators of cyclin D-dependent kinases in murine fibroblasts. *EMBO J.* 1999; 18:1571–83.
48. Flores-Rozas H, Kelmant Z, Dean FB, Pan ZQ, Harper JW, Elledge SJ, O'Donnell M, Hurwitz J. Cdk-interacting protein 1 directly binds with proliferating cell nuclear antigen and inhibits DNA replication catalyzed by the DNA polymerase δ holoenzyme (cell cycle regulation/processivity/protein-protein interaction). *Biochemistry.* 1994; 91:8655–9.
49. Niculescu AB, Chen X, Smeets M, Hengst L, Prives C, Reed SI. Effects of p21(Cip1/Waf1) at both the G1/S and the G2/M cell cycle transitions: pRb is a critical determinant in blocking DNA replication and in preventing endoreduplication. *Mol Cell Biol.* 1998; 18:629–43.
50. Ogryzko VV, Wong P, Howard BH. WAF1 retards S-phase progression primarily by inhibition of cyclin-dependent kinases. *Mol Cell Biol.* 1997; 17:4877–82.
51. Radhakrishnan SK, Feliciano CS, Najmabadi F, Haegbarth A, Kandel ES, Tyner AL, Gartel AL. Constitutive expression of E2F-1 leads to p21-dependent cell cycle arrest in S phase of the cell cycle. *Oncogene.* 2004; 23:4173–6.
52. Ramirez JM, Ocio EM, San Miguel JF, Pandiella A. Pemetrexed acts as an antimyeloma agent by provoking cell cycle blockade and apoptosis. *Leukemia.* 2007; 21:797–804.
53. Baldi A, Piccolo MT, Boccellino MR, Donizetti A, Cardillo I, La Porta R, Quagliuolo L, Spugnini EP, Cordero F, Citro G, Menegozzo M, Calogero RA, Crispi S. Apoptosis induced by piroxicam plus cisplatin combined treatment is triggered by p21 in mesothelioma. *PLoS One.* 2011; 6:e23569.
54. Lazzarini R, Moretti S, Orecchia S, Betta PG, Procopio A, Catalano A. Enhanced antitumor therapy by inhibition of p21waf1 in human malignant mesothelioma. *Clin Cancer Res.* 2008; 14:5099–107.
55. Inoue H, Hwang SH, Weckslar AT, Hammock BD, Weiss RH. Sorafenib attenuates p21 in kidney cancer cells and augments cell death in combination with DNA-damaging chemotherapy. *Cancer Biol Ther.* 2011; 12:827–36.
56. Chou TC. Drug combination studies and their synergy quantification using the Chou-Talalay method. *Cancer Res.* 2010; 70:440–6.



Sialidase NEU3 defines invasive potential of human glioblastoma cells by regulating calpain-mediated proteolysis of focal adhesion proteins

Kohta Takahashi^{a,b}, Sergei Proshin^c, Kazunori Yamaguchi^d, Yoji Yamashita^e, Ryuichi Katakura^e, Koji Yamamoto^{a,f}, Hiroshi Shima^f, Masahiro Hosono^{b,*}, Taeko Miyagi^{a,f,**}

^a Division of Cancer Glycosylation Research, Tohoku Medical and Pharmaceutical University, Sendai, Japan

^b Division of Cell Recognition Study, Tohoku Medical and Pharmaceutical University, Sendai, Japan

^c St Petersburg State Pediatric Medical University, Litovskaya ul., 2, St Petersburg, 194100, Russia

^d Division of Molecular and Cellular Oncology, Miyagi Cancer Center Research Institute, Natori, Japan

^e Department of Neurosurgery, Miyagi Cancer Center, Natori, Japan

^f Division of Cancer Chemotherapy, Miyagi Cancer Center Research Institute, Natori, Japan

ARTICLE INFO

Keywords:

Sialidase
Glioblastoma
Invasion
Calpain
Focal adhesion
Gangliosides

ABSTRACT

Background: Glioblastoma multiforme is one of the most malignant tumors of the human central nervous system characterized by high degree of invasiveness. Focusing on this invasive nature, we investigated whether ganglioside-specific sialidase NEU3 might be involved, because gangliosides are major components of brain tissues, and cell surface sialic acids, as target residues of sialidase catalysis, are thought to be closely related to cell invasion.

Methods: NEU3 mRNA levels of human glioblastoma specimens were evaluated by quantitative RT-PCR. Human glioblastoma cell lines, U251, A172, and T98G were used for cell invasion and migration by transwell and cell scratching assay. The molecules involved in the signaling cascade were investigated by western blot and immunofluorescent microscopy.

Results: NEU3 expression was down-regulated in human glioblastoma specimens. In the human glioblastoma cell lines, NEU3 overexpression reduced invasion and migration by promoting the assembly of focal adhesions through reduced calpain-dependent proteolysis, but NEU3 silencing resulted in accelerating cell invasion via disassembly of focal adhesions. In NEU3-silenced cells, elevation of calpain activity and GM3 accumulation were observed, as results of reduced sialidase hydrolysis, localization of calpain and GM3 at the cell lamellipodium being demonstrated by immunofluorescence microscopy.

Conclusion: Sialidase NEU3 was found to exert a great influence on cell invasion in regulation of calpain activity and focal adhesion disassembly and consequent invasive potential of glioblastoma cells.

General significance: This first demonstration of sialidase involvement in invasive potential of glioblastoma cells may point to NEU3 as an attractive treatment target of human gliomas.

1. Introduction

Glioblastoma multiforme is the commonest and most malignant tumor of the human central nervous system, and characterized by massive and diffuse infiltration into surrounding normal brain tissues. Even with intensive treatment, median survival of affected patients is only in the order of 14 months after diagnosis [1,2]. Local invasion and

distant migration are considered leading causes of tumor recurrence and treatment failure, but the underlying mechanisms in glioblastomas are not fully understood, despite reports of potential targets [3]. With the aim of providing pointers to novel effective treatments, we have focused on the highly invasive nature of this tumor by investigating sialidase (EC 3.2.1.18), a key enzyme for the control of cellular sialic acid contents through the removal of sialic acid residues from

Abbreviations: FAK, Focal adhesion kinase; FA, Focal adhesion; ECM, Extracellular matrix; Suc-LLVY-AMC, Succinyl-L-leucyl-L-leucyl-L-valyl-L-tyrosine 4-methylcoumaryl-7-amide; PIP₂, Phosphatidylinositol 4, 5-bisphosphate; TLC, Thin-layer chromatography; Sulfo-NHS-biotin, Sulfo-succinimidyl-6-[biotin-amido]hexanoate; PBS, Phosphate buffered saline; RIPA, Radio-immunoprecipitation assay; Phalloidin-TRITC, Phalloidin-tetramethylrhodamine B isothiocyanate; Lac-Cer, Lactylceramide; Gb3, Globotriaosylceramide; PLCdelta, Phospholipase C delta; PH, Pleckstrin homology

* Correspondence to: M. Hosono, Divisions of Cell Recognition Study, Tohoku Medical and Pharmaceutical University, 4-4-1, Komatsushima, Aoba-ku, Sendai 981-8558, Japan.

** Correspondence to: T. Miyagi, Division of Cancer Chemotherapy, Miyagi Cancer Center Research Institute, 47-1 Nodayama, Medeshima-Shiode, Natori 981-1293, Japan.

E-mail addresses: mhosono@tohoku-mpu.ac.jp (M. Hosono), miyagi-ta@nifty.com (T. Miyagi).

<http://dx.doi.org/10.1016/j.bbagen.2017.07.023>

Received 3 February 2017; Received in revised form 26 July 2017; Accepted 27 July 2017

Available online 29 July 2017

0304-4165/ © 2017 Published by Elsevier B.V.

glycoproteins and glycolipids [4,5], aberrant sialylation being implicated in invasion and metastasis of cancer cells. Sialidases regulate cell surface sialylation in collaboration with sialyltransferases that transfer sialic acid residues to glycoconjugates. With the context of sialylation of glycoproteins, there is evidence that sialyltransferases may thereby participate in glioma malignancy [6,7]. Understanding of the roles of sialic acid-containing glycosphingolipids is clearly important given their involvement in neuronal function.

Gangliosides are ubiquitously expressed in mammalian cells and are particularly abundant in the nervous system. Accumulating evidence indicates that they play specific functional roles essential for cell survival, proliferation, and differentiation during brain development under desialylation control by sialidase catalytic reactions. In very early stages of brain development, the pattern of ganglioside expression is limited to simple gangliosides, predominantly GM3 and GD3, but these are soon lost after birth, becoming replaced by more complex forms, particularly GM1, GD1a, GD1b, and GT1b, as major components [8,9]. In human gliomas, however, re-expression of simple gangliosides has been reported [10,11]. While functional roles have yet to be fully clarified, it was recently reported that GD3 enhances invasiveness by complex formation with PDGF receptor and Yes kinase [12], and playing an important role in tumorigenicity [13].

Among the four types of human sialidases so far identified (NEU1-NEU4), differing in major subcellular localization and enzymatic properties, as well as position of the encoding genes [4], NEU3 and NEU4 appear to be involved in neuronal differentiation, neuritogenesis, and axonal growth in opposing ways. The level of NEU3 expression increases during the development of the mouse brain and during retinoic acid-induced neuronal differentiation whereas NEU4 decreases and is known to suppress differentiation [14,15]. Additionally, in a recent study, involvement of NEU4 in stem cell survival of some glioblastoma cells was indicated [16]. NEU3 would be mostly expected to participate in cell invasion and motility, because it hydrolyzes almost specifically gangliosides and is up-regulated in various carcinomas [5]. In fact, it has been observed to participate in promotion of cell invasion and motility in renal cell carcinoma [17] and head and neck squamous cell carcinoma [18]. In the present study, we focused on NEU3 by observing whether and how it is involved in invasiveness and motility of glioblastoma cells, and obtained evidence that it modulates invasion and migration through regulation of calpain-dependent disassembly of focal adhesion proteins.

2. Material and methods

2.1. Patient samples

Surgical specimens of human glioblastoma, classified as grade IV using the criteria of the World Health Organization, were obtained at the time of surgical removal at the Division of Neurosurgery, Miyagi Cancer Center. Informed consent was obtained from each patient to allow the use of portions of tissue for research purposes, and the study was approved by the Committee on Human Rights in Research at Miyagi Cancer Center. Histological diagnoses were based on WHO (World Health Organization) criteria by a neuropathologist.

2.2. Antibodies and reagents

Antibodies for integrin $\alpha 3$ (ASC-1), $\alpha 5$ (P1D6), $\beta 1$ (6S6) and $\beta 4$ (ASC-8) were obtained from Millipore, for transferrin receptor (H-300), paxillin (H-114), and FAK (A17) from Santa Cruz Biotechnology, and for Talin (8d4) from Sigma. Fibronectin was from BD Biosciences, and Suc-LVY-AMC and calpeptin were from Sigma.

2.3. Cell culture and transfection

Human glioblastoma cell lines, U251, A172 and T98G (Japan

Collection Research Bioresources) were maintained in Dulbecco's modified Eagle's medium with 10% heat-inactivated fetal bovine serum at 37 °C in a 5% CO₂ atmosphere. For astrocyte culture, Gibco Human Astrocytes (Life Technologies, N7805-100) were cultured in Gibco Astrocyte Medium (A1261301), and Geltrex matrix-coated plates (A1413202) with 25,000 cells per well in 6-well plates were used according to the manufacturer's instructions. For *NEU3* gene transfection, the entire open reading frame (1.2 kb) of the human *NEU3* gene was inserted into a retrovirus vector pMXs-neo and the plasmid was introduced into PlatA, and targeted cells were then incubated with culture media containing infectious viruses for two days and selected by cultivation in the presence of 300 µg/ml G418 for 10–14 days, as described previously [19]. Several experiments were performed with transient transfection of the pCAGGS-NEU3 expression plasmid [20] by Eugene HD (Promega). GFP-PLCdelta-PH was obtained from Addgene (Plasmid 21,179). For silencing, siRNAs targeting NEU3 was synthesized by Dharmacon Inc. (Thermo Fisher Scientific) as described [20], and transfected using Lipofectamine RNAiMAX reagent (Invitrogen). One sample was 5'-AAGGGAGTGTGGTAAGTTT-3' beginning at nucleotide 839 of the NEU3 open reading frame sequence, and the scrambled control was 5'-GCGATTAATGTAGGTT CGA-3'. Another siRNA targeting NEU3 synthesized by iGENE Therapeutics (Tsukuba, Japan) featured 5'-GGTTACAGTAGAATGTGAAGTGGA-3'. These two siRNAs targeting NEU3 caused 75–95% NEU3 reduction and almost the same results in various experiments, and therefore, the former was routinely utilized for the present study. The efficiency of NEU3 silencing was evaluated by real time PCR as described [21]. Transiently transfected cells were used for experimentation at 48–72 h.

2.4. Sialidase activity assays

Crude extracts were used for sialidase assays with bovine brain GM3 (Alexis Biochemicals, Lansen, Switzerland) as the substrate in the presence of Triton X-100. After incubation at 37 °C for 10–30 min, the amount of sialic acid released was determined by a modified thio-barbituric acid method or by fluorometric high-performance liquid chromatography with malononitrile as previously described [20]. One unit of activity was defined as the amount of enzyme that cleaved 1 nmol sialic acid from the substrates. Protein concentrations were determined by dye-binding assay (Bio-Rad Laboratories, Hercules, CA, USA).

2.5. Cell adhesion, migration and invasion assays

For cell adhesion assays, extracellular matrix-coated 96-well plates (BD Biosciences) were blocked with 1% bovine serum albumin in PBS. Cell suspensions in serum-free medium were then applied to these coated 96-well plates. After incubation for 30 min and fixation, attached cells were stained with 0.5% crystal violet, and incorporated dye was eluted with 2% deoxycholate, and measured spectrophotometrically at A₅₅₀. In cell-adhesion-inhibition assays, suspended cells were incubated with 1 µg/ml neutralizing anti- $\beta 1$ integrin antibody at 37 °C for 30 min before plating. Migration and invasion assays were carried out using fibronectin-coated cell culture inserts (Falcon) and BD Biocoat Matrigel invasion chambers (BD Bioscience), respectively. Cells were seeded at 2×10^4 cells/well with serum-free medium onto the upper chamber, and lower chamber was filled with medium containing 10% fetal bovine serum. After 24 h, cells were fixed and stained with 0.1% crystal violet and the invading or migrating cells on the lower membrane surface were counted under a microscope. For wound healing assay, cells were grown on 24-well plate. Once confluence was reached, wound was made by using a pipette tip. Wound scratches were imaged immediately after scratching and overnight migration. The area covered by the cell sheets during migration was measured. At least three experiments per conditions were performed.

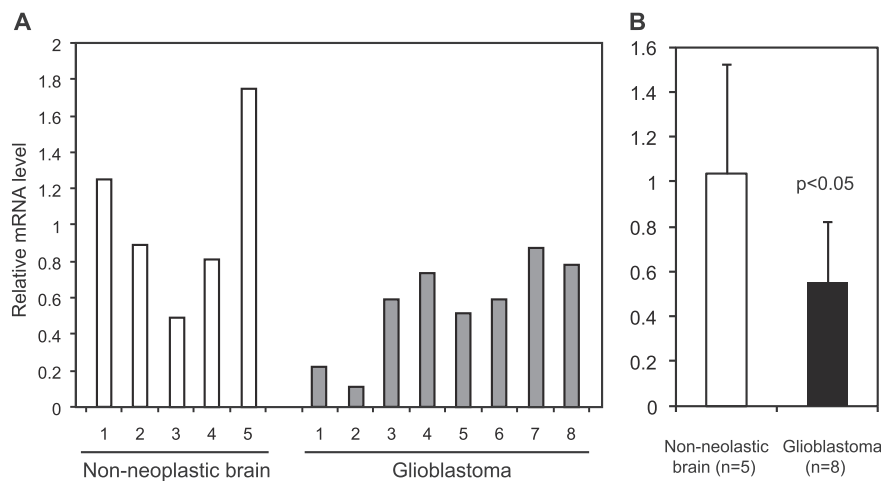


Fig. 1. Down-regulation of sialidase NEU3 expression in human glioblastoma specimens. Sialidase NEU3 mRNA levels were evaluated in human glioma tissues and non-neoplastic brain tissues (A) by quantitative real-time PCR according to the methods described previously [21], and statistical significance of the differences in levels was determined (B).

2.6. Cell surface biotinylation assay

Cells were washed three times with chilled PBS containing 1 mM $MgCl_2$ and 0.1 mM $CaCl_2$, and then incubated with sulfo-NHS-biotin (Pierce) (0.5 mg/ml) in the same buffer at 4 °C for 30 min. Reactions were terminated by incubation of the cells with 100 mM glycine in PBS. Cells were lysed in modified RIPA buffer (50 mM Hepes, pH 7.5, 150 mM NaCl, 1% Nonidet P-40, 2 mM EDTA, 7.5 µg/ml of aprotinin, 10 µg/ml of leupeptin, 10 mM NaF, 2 mM PMSF), and the biotinylated proteins were precipitated with streptavidin-conjugated agarose (Sigma) for analysis by immunoblotting.

2.7. Immunoblotting

Cells were lysed with modified RIPA buffer. Lysates were clarified by centrifugation at 12000 × g for 10 min and then resolved on SDS-PAGE. After transfer to PVDF membranes, specific proteins were detected using appropriate primary antibodies, and peroxidase-coupled secondary antibodies with ECL Plus Western blotting reagent (GE Healthcare). For the immunoprecipitation assay with anti-FAK antibodies, cells were allowed to adhere for 1 h to cell-culture dishes coated with fibronectin, and then lysed with modified RIPA buffer. The lysates were incubated with anti-FAK antibody at 4 °C for overnight, and then incubated with protein G-Sepharose at 4 °C for 2 h. The immunoprecipitates were analyzed by immunoblotting as described above.

2.8. Immunofluorescence microscopy

Cells grown on fibronectin-coated coverslip were fixed with 4% paraformaldehyde for 15 min and then incubated with 0.1% Triton X-100. After blocking with 1% BSA, cells were incubated with anti-paxillin antibody for 1 h, followed by incubation with Alexa 488 anti-rabbit IgG. The cells were then washed and mounted under Fluoromount/Plus (Diagnostic BioSystems) as an anti-fading reagent. Fluorescence images were obtained using a confocal laser-scanning microscope (FluoView FV1000, Olympus). To visualize F-actin and nucleus, phalloidin-tetramethylrhodamine B isothiocyanate (phalloidin-TRITC, Sigma) and DRAQ5 were used. To assess localization of calpain and GM3, cells were seeded at 0.5×10^5 cells/well onto fibronectin-coated cover slips, after 24 h transfected with siRNA targeting NEU3 by RNAiMAX, and on the following day treated with EGCase (EGCase II ACT RE, TAKARA 4463) at the concentration of 20 min/ml in 5% FBS containing DMEM at 37 °C overnight. Cells were fixed with 4% PFA for 20 min, permeabilized and blocked by 0.2% saponin and 0.2% gelatin in PBS, each for 30 min, respectively, at room temperature, and then stained using anti-GM3 (M2590) 1/100 or anti-Calpain (CST) 1/25 antibodies. Lamellipodia

were defined as having an arc shape and size of the F-actin structure, and cells bearing lamellipodia with a greater than 20 µm width from one end of a lamellipodia to another were counted as lamellipodia-bearing cells. At least 200 cells per coverslip were analyzed and values are means ± SD from three independent experiments.

2.9. Intracellular calcium release

U251 cells were seeded in 96-well-plate at a density of 20,000 per well and cultured for 24 h. The cells were rinsed three times with assay buffer (130 mM NaCl, 5 mM KCl, 10 mM HEPES, 8 mM D-glucose, 1.2 mM $MgCl_2$ and 1.5 mM $CaCl_2$, pH 7.4), and then incubated with this buffer supplemented with the organic anion transport inhibitor probenecid (2.5 mM), 1 µM Fluo 4-AM and 0.1% Pluronic F-127 for 60 min at 37 °C. Before measurement fluorescence emission at 525 nm following excitation at 480 nm, cells were rinsed a further three times with assay buffer.

2.10. Calpain activity

Cells from confluent dishes were harvested with 0.1% trypsin-EDTA solution, neutralized with 10% fetal bovine serum containing media, and washed twice with HEPES-buffered Hank's balanced salt solution, pH 7.4, without phenol red. Equal numbers of cells were resuspended in 100 µl of HEPES-buffered Hank's balanced salt solution at 5×10^4 cells in 96-well plate at 37 °C in a 5% CO_2 incubator for 10 min. To assay calpain activity, calpain specific hydrolysis of the peptidyl 7-amino bond of the cell-permeable fluorogenic calpain substrate, Suc-LLVY-AMC fluorescence emission at 525 nm following excitation at 480 nm was added at 20 µM to cell suspensions, followed by incubation at 37 °C for 15–30 min. AMC fluorescence was measured by fluorometer (GloMax-Multi detection system; Promega) with excitation/emission wave lengths of 365 nm/410 to 460 nm.

2.11. Calpain translocation

GM3 dissolved in sterile water was sonicated in serum-free medium, kept on ice for 10 min and added to the cells in serum-free medium at concentration of 50 µM. After incubation at 37 °C for 24 h, cells were lysed in the buffer (20 mM HEPES, pH 7.4, 20 mM NaCl, 1.5 mM $MgCl_2$, 250 mM sucrose, 1 mM EDTA, 2 mM PMSF, 7.5 µg/ml aprotinin and 10 µg/ml leupeptin) by passing through 27G needle for 10 times and left on ice for 20 min. After homogenization, the lysates were centrifuged at 4 °C 1000 × g for 5 min and supernatants were collected as total protein fractions. The supernatants were then centrifuged at 150,000 × g for 30 min at 4 °C in an Optima MAX-XP ultracentrifuge (Beckman coulter). The resulting supernatants were collected as

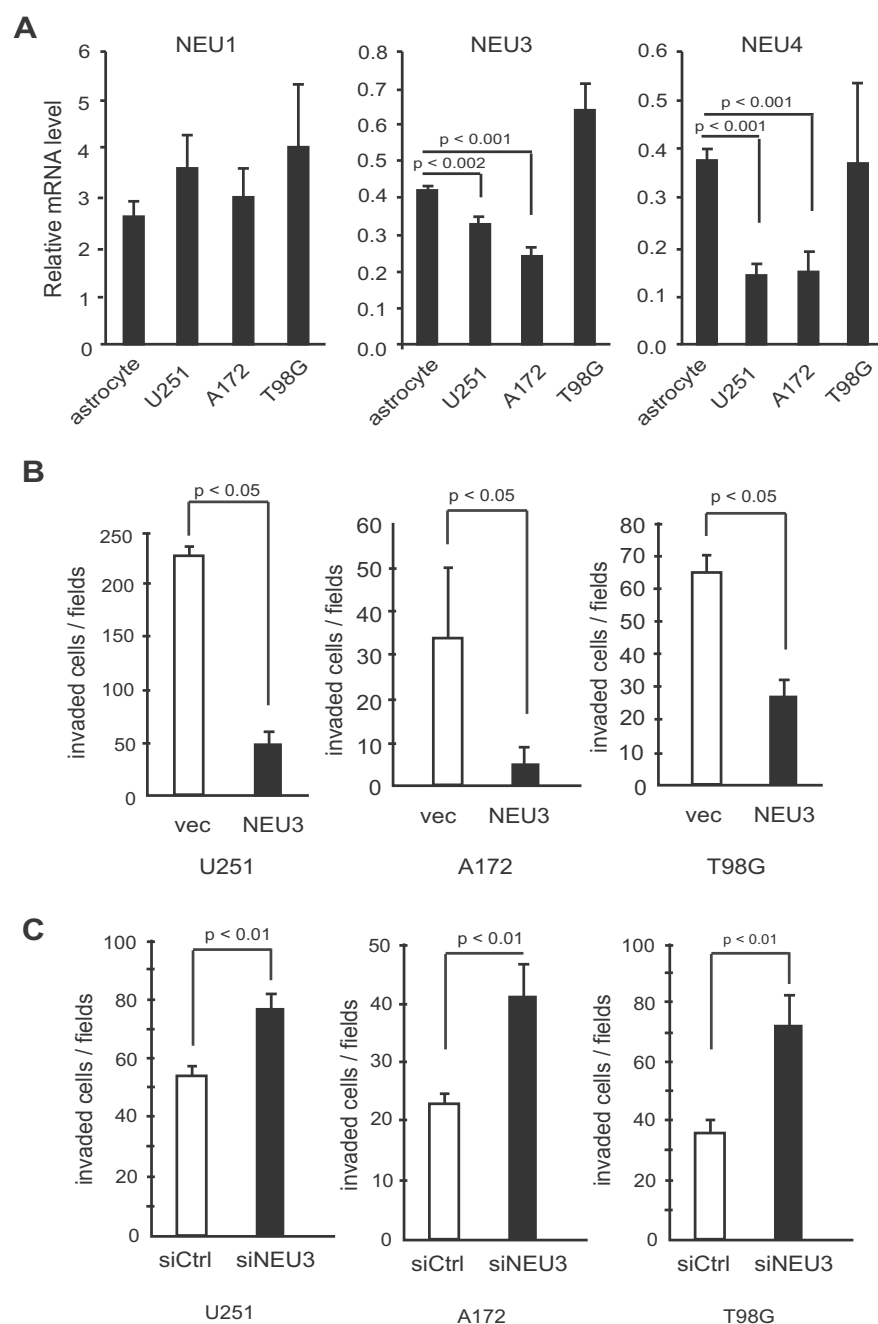


Fig. 2. Sialidase expression of human glioblastoma cell lines and the influence of alteration of sialidase NEU3 expression on cell invasiveness. The mRNA levels of the four human sialidases were evaluated in the three glioblastoma cell lines as compared to those of astrocytes (A) by real-time PCR, as described earlier [21]. NEU2 expression was undetectable in these human cells. Decreased invasiveness was shown in NEU3 overexpressing cells (B), whereas enhanced invasiveness was noted in the siRNA-mediated silenced cells (C). Sialidase activity was determined with GM3 as substrate in NEU3-transfected cells compared with control cells, and the efficiency of siRNA-mediated NEU3 silencing was evaluated by real time PCR in U251 cells.

cytosolic fractions, and the pellets containing the membrane fractions were resuspended in the lysis buffer with 1% Nondet P-40 and homogenized for 10 min. The amount of calpain was determined by immunotting as described above using anti-calpain antibody.

2.12. Thin-layer chromatography

Glycolipids were extracted from cells (1×10^7) in sequence with 2 ml of isopropanol/hexane/water (55:25:20, v/v/v) and hydrolyzed with 0.1 M NaOH/methanol. After desalting with a Sep-Pak C₁₈ cartridge, total lipid extracts were applied to DEAE-Sephadex A-25 mini-columns, fractionated into neutral and acidic glycolipids, and analyzed by thin-layer chromatography on high-performance thin-layer chromatography plates (Merck) with orcinol-H₂SO₄ reagent for detection, as described elsewhere [17]. Densitometric analyses were performed with VersaDoc and Quantity One software (Bio-Rad).

2.13. Statistical analysis

Results are expressed as mean \pm SD. All values were compared using the Student's *t*-test or the Welch's *t*-test.

3. Results

3.1. Sialidase expression in human glioma tissues and glioblastoma cell lines

Fig. 1 shows the results of NEU3 expression in human glioblastoma and non-neoplastic brain tissues as assessed by quantitative RT-PCR. Significant decrease in NEU3 mRNA levels in tumor compared with non-tumor tissues was detected (relative levels were 0.55 ± 0.27 and 1.04 ± 0.48 , respectively). To determine whether decrease of NEU3 expression might be involved in cell invasion, we employed three glioma cell lines, U251, A172 and T98G. The expression levels of four

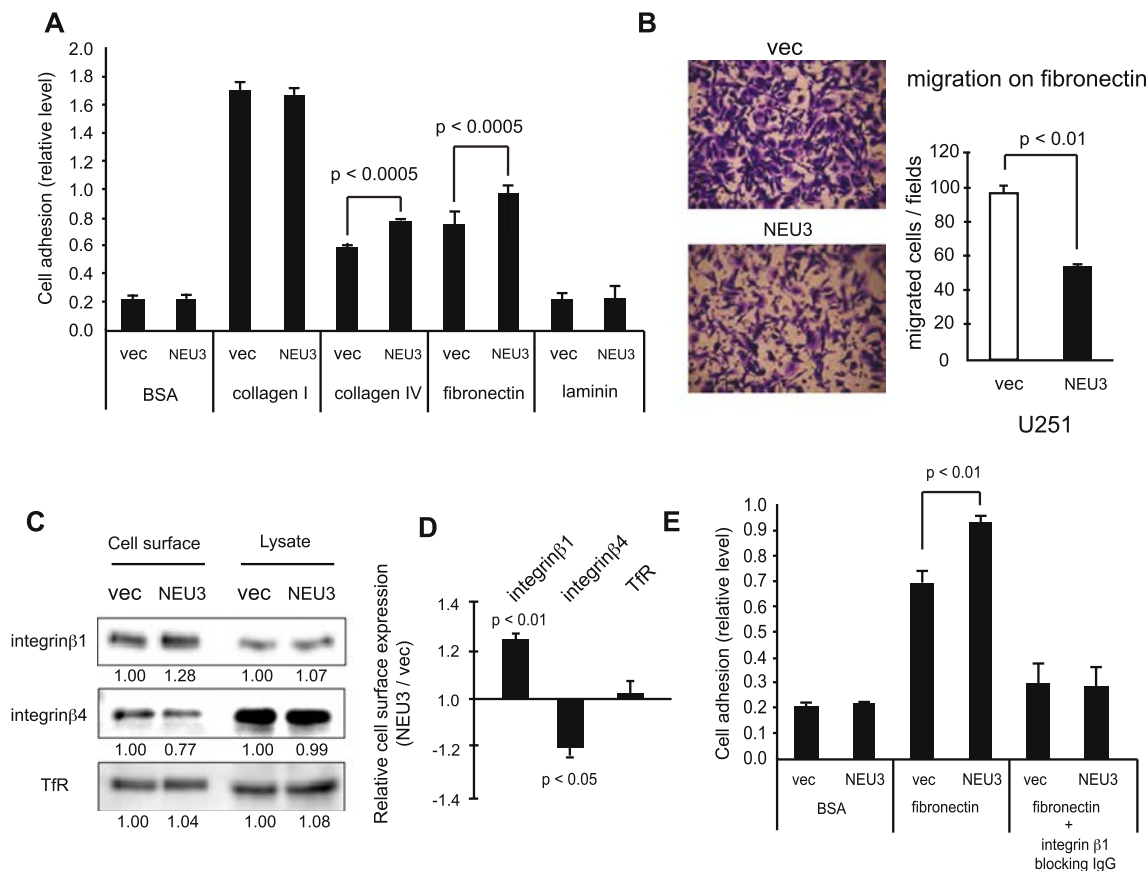


Fig. 3. Sialidase NEU3 stabilizes cell adhesion and suppresses cell invasion in glioblastoma cells. Enhanced adhesion to collagen IV and fibronectin (A), and suppression of cell migration on fibronectin (B). Changes in cell surface expression of integrin $\beta 1$ and $\beta 4$ by cell surface biotinylation assay followed by immunoblotting (C) and its quantification ($n = 3$) (D). Attenuation of the NEU3-mediated enhanced adhesion to fibronectin by treatment with a blocking antibody for integrin $\beta 1$ binding (E).

human sialidases were firstly evaluated in these cell lines (Fig. 2A). When compared to those of astrocytes derived from normal human brain, U251 and A172 cells clearly showed reduced levels of NEU3 and NEU4, but no significant change in the NEU1 level, whereas T98G cells possessed the relatively similar levels of the three forms as to astrocytes. In line with our previous report that NEU2 expression is hardly detectable in human cells [22], these cells also exhibited undetectable NEU2. To clarify the influence of NEU3 on glioma cell invasiveness, we examined invasion by three glioma cell lines, U251, A172 and T98G, using Transwell Matrigel invasion assays. Transfection of NEU3 resulted in marked decrease in the number of invaded cells (Fig. 2B), and on the other hand, NEU3 siRNA-mediated silencing increased invasiveness (Fig. 2C). NEU3 transient expression in these cells yielded approximately 25–60-fold increase in the sialidase activity with ganglioside GM3 as substrate as compared with control cells, and silencing yielded 35–15% mRNA level of the controls. Stable U251 cell NEU3 transfectants showed 31-fold increase in the activity, and the gene-silencing efficiency was about 80% relative to control cells.

3.2. NEU3 stabilizes cell adhesion to collagen IV and fibronectin and suppresses invasion of glioma cells

Cellular invasiveness is generally dependent on multi-processes including adhesion, movement, and penetration involving the extracellular matrix (ECM). To understand the molecular basis of NEU3-mediated suppression of invasion, we then examined the effect of alteration of NEU3 expression using stably transfected U251 cells. When cell adhesion to ECM, as an initial step of invasion, was analyzed, NEU3 overexpression was found to enhance the adhesion to collagen IV and fibronectin (Fig. 3A), while cell migration on fibronectin was

significantly suppressed (Fig. 3B). As integrins have been implicated in glioma invasion [23], cell surface integrin expression was then examined by cell surface biotinylation analysis. In agreement with increased cell adhesion, NEU3 transfection yielded a slight but significant increase of integrin $\beta 1$, a receptor for collagen IV and fibronectin, whereas integrin $\beta 4$ showed reduction, although the levels in whole cell lysates were unaffected (Fig. 3C, D). NEU3 did not give an influence on the cell surface expression of other integrins, and there was no change in the level of biotin-labeled transferrin receptors. Since several previous observations [24,25] suggested integrin $\beta 4$ to not actually participate in invasion of glioma cells, we next focused on integrin $\beta 1$ in glioma U251 cells. On treatment with an antibody blocking binding of integrin $\beta 1$ to the ECM, NEU3-mediated enhanced adhesion to fibronectin was almost fully abrogated (Fig. 3E), indicating stabilization of cell surface integrin $\beta 1$. It should be noted here that similar results were also obtained with NEU3-transiently expressed U251 cells.

3.3. NEU3 stabilizes focal adhesion and suppresses cell spreading

Attachment of cells to ECM components induces clustering of integrins on cell surface, triggers formation of focal adhesion (FA) complexes, and then is followed by rapid turnover of the FA assembly and disassembly, essential for cell spreading and migration. The change in the level of integrin $\beta 1$ localized at surface membranes, therefore, might influence on the FA assembly and disassembly. To verify the possibility, we analyzed FAs of the cells by immunocytochemistry using antibodies for FA-resident protein, paxillin. NEU3 overexpressing cells showed prominent increase in the number of FAs and in formation of actin stress fibers on a fibronectin matrix (Fig. 4A, B). Formation of cell lamellipodia was also significantly suppressed compared with control

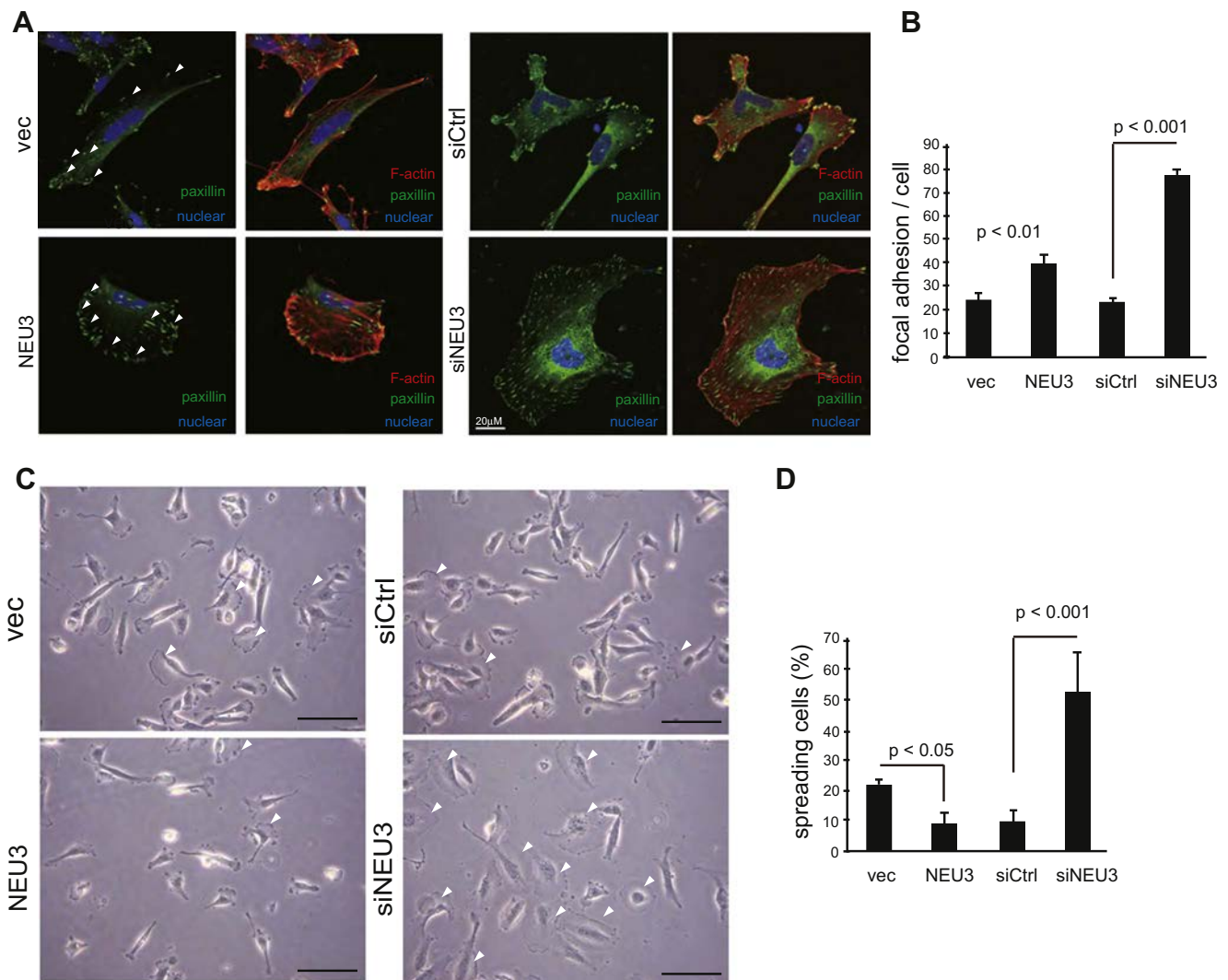


Fig. 4. Sialidase NEU3 enhances focal adhesion formation on fibronectin and reduces glioblastoma cell spreading. The number of focal adhesions on fibronectin matrix in NEU3 overexpressing cells and in its silenced cells (A), and the representative images are shown. Means \pm SD values from three independent experiments are graphically illustrated in (B). Cell spreading and lamellipodium formation in the NEU3 overexpressing and its silenced cells, and the representative images are shown in (C). The number of spreading cells was normalized to the total number of cells (D). Values are means \pm SD from three independent experiments.

cells (Fig. 4C, D). Furthermore, NEU3 silencing markedly enhanced the lamellipodia formation on leading edges (Fig. 4C, D). NEU3 thus appeared to down-regulate glioma cell migration and invasion by FA stabilization and suppression of turnover, whereas NEU3 silencing causes the opposite.

3.4. NEU3 suppresses calpain activity and FA protein degradation

To elucidate how NEU3 regulates FAs turnover, we focused on calpain, catalyzing degradation of FAs proteins. The amount of cleaved form of Talin and FAK, major substrates of calpain, was firstly observed. When U251 cells were attached on fibronectin-coated tissue culture for 1 h, and then the level of Talin and FAK were quantified by western blotting with anti-Talin and anti-FAK antibodies. Cleaved forms observed at 190 and 80 kDa respectively, were reduced by NEU3 overexpression (Fig. 5A). Diminution of the cleaved products in the presence of the calpain inhibitor, calpeptin, confirmed their origin through proteolytic cleavage by calpain (Fig. 5A). In contrast, NEU3 silencing promoted degradation of FAK and Talin, which was inhibited by calpeptin treatment (Fig. 5B). With a cell permeable fluorogenic calpain substrate, Suc-LLVY-AMC, NEU3 was found to suppress calpain activity (Fig. 5C) whereas NEU3 silencing exerted the opposite effects (Fig. 5D).

3.5. Regulation of calpain activity by NEU3-mediated glycolipid alteration

To elucidate the mechanism of calpain regulation by NEU3, we analyzed intracellular calcium ion, an activator of calpain, but no influence was evident (data not shown). Since calpain might be activated by interaction with phosphatidylinositides such as phosphatidylinositol 4, 5-bisphosphate (PIP₂) at inner leaflets of plasma membrane [26,27], we then examined if NEU3-mediated glycolipid alteration might affect PIP₂ localization and subsequent calpain activation at plasma membranes. To observe what glycolipids are expressed in glioblastoma cells and how they are altered by NEU3 expression, the glycolipid pattern of U251 cells was analyzed by thin-layer chromatography (TLC). The profile of neutral glycolipids revealed clearly detectable glycolipids, with TLC bands having the similar mobility to lactosyl-ceramide (Lac-Cer), globotriaosylceramide (Gb3), and globoside (Gb4) (Fig. 6A, left). The acidic glycolipid profile exhibited a very pronounced band showing similar TLC mobility to GM2, others distinctly recognized with similar mobility to GM3 and GM1, and more hydrophilic gangliosides modestly detectable (Fig. 6A, middle). Consistent with the recent reports by Fabris et al. [28] describing glioblastoma gangliosides compared to those of healthy brain tissues to be characterized by diverse ceramide composition with fatty acyl chains, the doublets of glycolipids observed

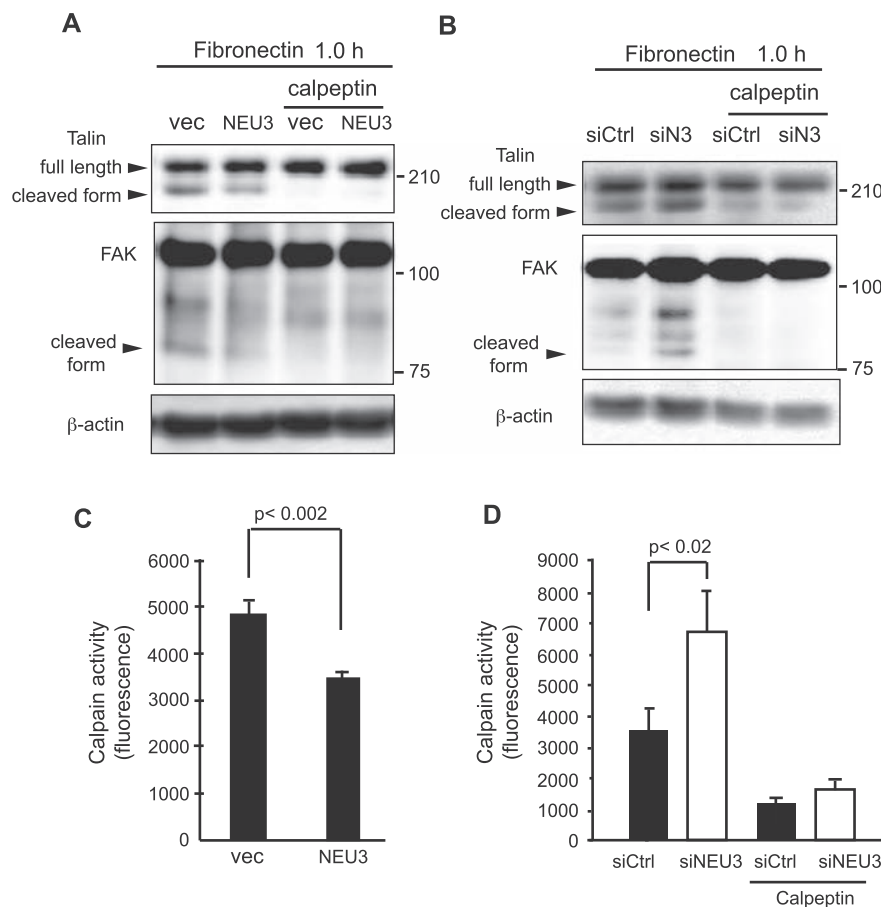


Fig. 5. Sialidase NEU3 suppresses calpain activity and degradation of FA proteins. Note reduced amount of cleaved forms of Talin and FAK in fibronectin-coated tissue culture with NEU3, and attenuation of the NEU3-mediated effects in the presence of calpeptin (A). Enhanced degradation of FAK and Talin by NEU3 silencing, and its attenuation by calpeptin (B). Calpain activity in intact cells was determined with the cell permeable fluorogenic substrate, Suc-LLVY-AMC. Suppression of the calpain activity by NEU3 (C) and its promotion by NEU3 silencing that was attenuated by calpeptin (D).

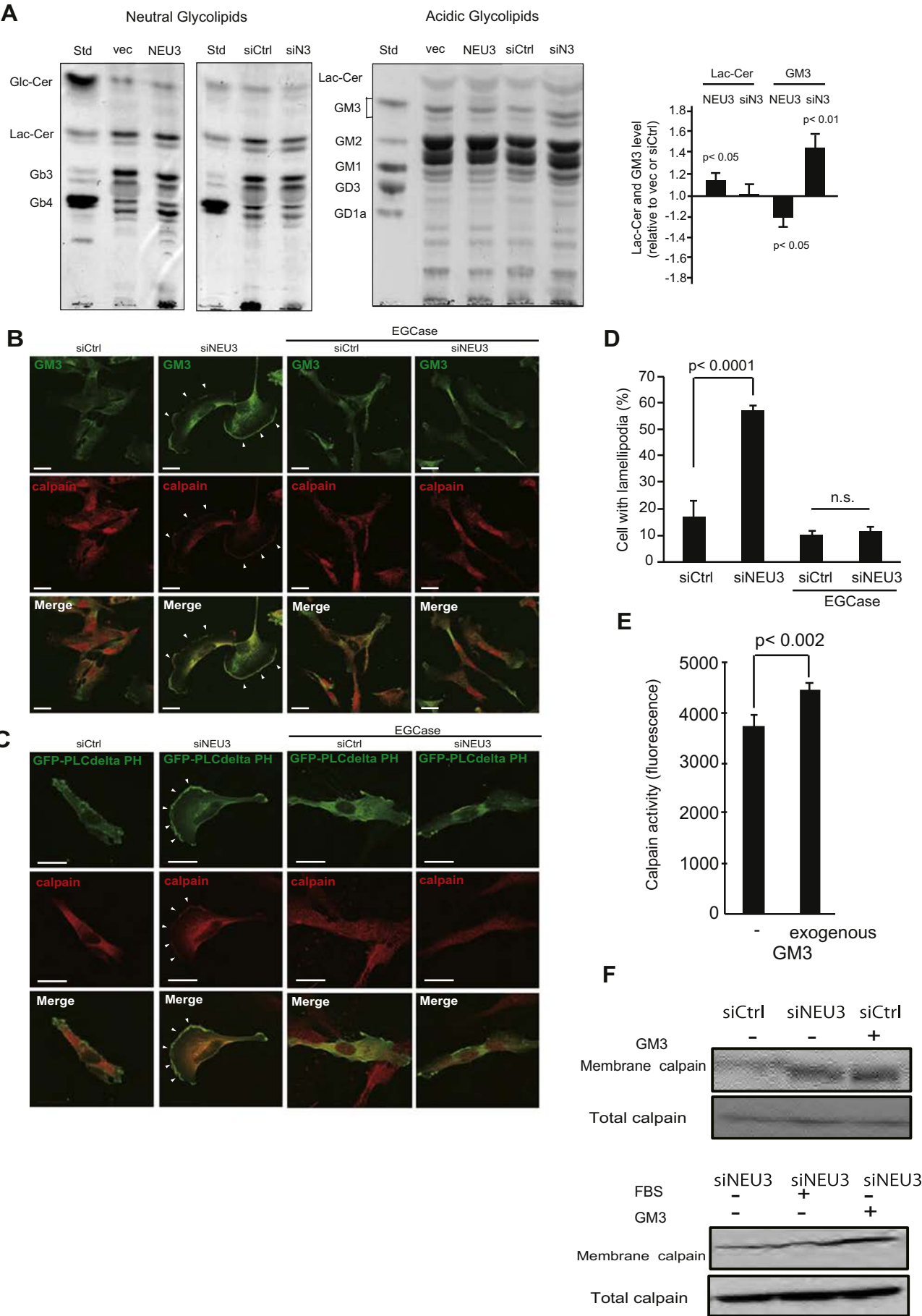
in this glioblastoma cells are likely due to the heterogeneity on the ceramide moiety. In comparison of the glycolipids in NEU3-overexpressing and -silenced cells with those of respective control cells, changes in Lac-cer and Gb4 in neutral glycolipids and in GM3 and GM1 in gangliosides were recognizable. Interestingly, modifications induced by NEU3 silencing were a decrease in both Lac-cer and Gb4, and on the other hand, an increase in GM3 and GM1, whereas NEU3 overexpression mostly caused the opposite changes. Decreased Gb4 has been suggested to reduce cell proliferation via suppressing EGFR-induced ERK pathway but less effects on cell motility of cancer cells as presented by Park et al. [29], and in neuroblastoma cells, switching from cell proliferation to migratory signaling has been proposed through phosphorylation of PDGF receptors mainly in GM1-rich lipid microdomains [30]. Although the mechanism of the metabolic changes in Gb4 and GM1 in U251 cells remains to be elucidated, they may be closely related to exert effect on a cell motility and invasiveness rather than on cell proliferation, which is not contradictory to the phenomena induced concomitantly by GM3 resulting in promotion of cell motility and invasion described below.

As shown in our previous studies with various cells [4], the changes in Lac-Cer and GM3, a product and a substrate of NEU3, respectively, were confirmed here in the neuroblastoma cells (Fig. 6A, left and middle), as quantified in the graph (right). Since Morford et al. and Nuzzi et al. have suggested in Jurkat T-cells and in neutrophils, respectively [31,32], that calpain might exist in the raft fraction together with GM3 and get activated, we examined whether the amount of calpain in the lipid raft fraction is affected by NEU3 silencing, and found that any significant change in calpain distribution was not detectable in U251 cells as assessed by raft fractionation followed by immunoblotting (data not shown). Then we performed immunostaining analysis by immunofluorescence microscopy. Interestingly, in NEU3

silenced cells, strongly polarized GM3 and calpain on the lamellipodium were observed, and the lamellipodia and polarization were abrogated after treatment of EGCase, which hydrolyses the linkage between the oligosaccharide and ceramide (Fig. 6B, C). Furthermore, we detected PIP₂ production in the cells using the PH-green fluorescent protein (GFP) probe, which contains the PH domain from PLCdelta [33]. By NEU3 silencing, GFP-PLCdelta-PH and calpain also strongly colocalized at lamellipodia and it diminished by EGCase treatment for overnight, (Fig. 6D). The treatment for 6–7 h hardly showed any effect, as GM3 observed to be almost hydrolyzed for 12–16 h. Because PIP₂ is one of the activator for calpain, polarized GM3 and lamellipodia formation may support PIP₂ production at and/or localization to plasma membrane and subsequent activation of calpain at the membranes. Cellular calpain activity was, in fact, increased by exogenous addition of GM3 (Fig. 6E). To verify that calpain translocates to plasma membrane and is activated by GM3, the effect of GM3 exogenously added to the cell culture was observed. As shown in Fig. 6F, a larger amount of calpain was indeed detected in the membrane fractions by NEU3 silencing or GM3 addition. These results suggest that NEU3 down-regulation leads to accumulation of GM3, which may be important for NEU3-mediated lamellipodia formation and calpain regulation resulting promotion of cell motility and invasion.

3.6. Calpain inhibitor abrogates invasion by NEU3 silencing

As shown in Fig. 2, in contrast to reduction of cell invasion in NEU3 overexpressing glioblastoma cells, silencing exerted an enhancing effect. To verify the effect of calpain activity on the cell invasion, wound healing assay and invasion assay were carried out in NEU3-silenced U251 cells. As shown in Fig. 7A and B, wound healing assays revealed that NEU3 down-regulation resulted in promotion of cell migration as



(caption on next page)

Fig. 6. Regulation of calpain activity by NEU3-mediated glycolipid modulation

(A) Alteration of glycolipid pattern in NEU3 overexpressing or NEU3-silenced U251 cells (1×10^7) analyzed by thin-layer chromatography (TLC). Neutral glycolipids were separated in a solvent system of chloroform/methanol/0.02% aqueous CaCl_2 (60:40:9, v/v/v), and acidic glycolipids in chloroform/methanol/0.02% aqueous CaCl_2 (60:35:8, v/v/v). The doublets are due to the heterogeneity of the ceramide moiety. The values in the graph (right panel) indicate changes in the amounts of Lac-cer and GM3 in NEU3 overexpressing and silenced cells, relative to vector and siRNA controls, respectively, of four independent experiments, as analyzed with Quantity One software (Bio-Rad).

(B) Polarized GM3 and calpain at lamellipodia in NEU3-silenced cells as assessed by immunofluorescent microscopy. Note abrogation of the polarization of GM3 and calpain (right in B) and lamellipodia formation (C) after EGCase treatment for overnight. (D) GFP-PLCdelta-PH, PIP_2 probe, was transiently expressed in U251 cells, and its co-localization with calpain was analyzed. Scale bar, 20 μm . (E) Stimulation of cellular calpain activity by GM3 (50 μM) exogenously added and incubated for 16 h. (F) Translocation of calpain to membranes by NEU3 silencing or addition of GM3, as assessed by immunoblotting.

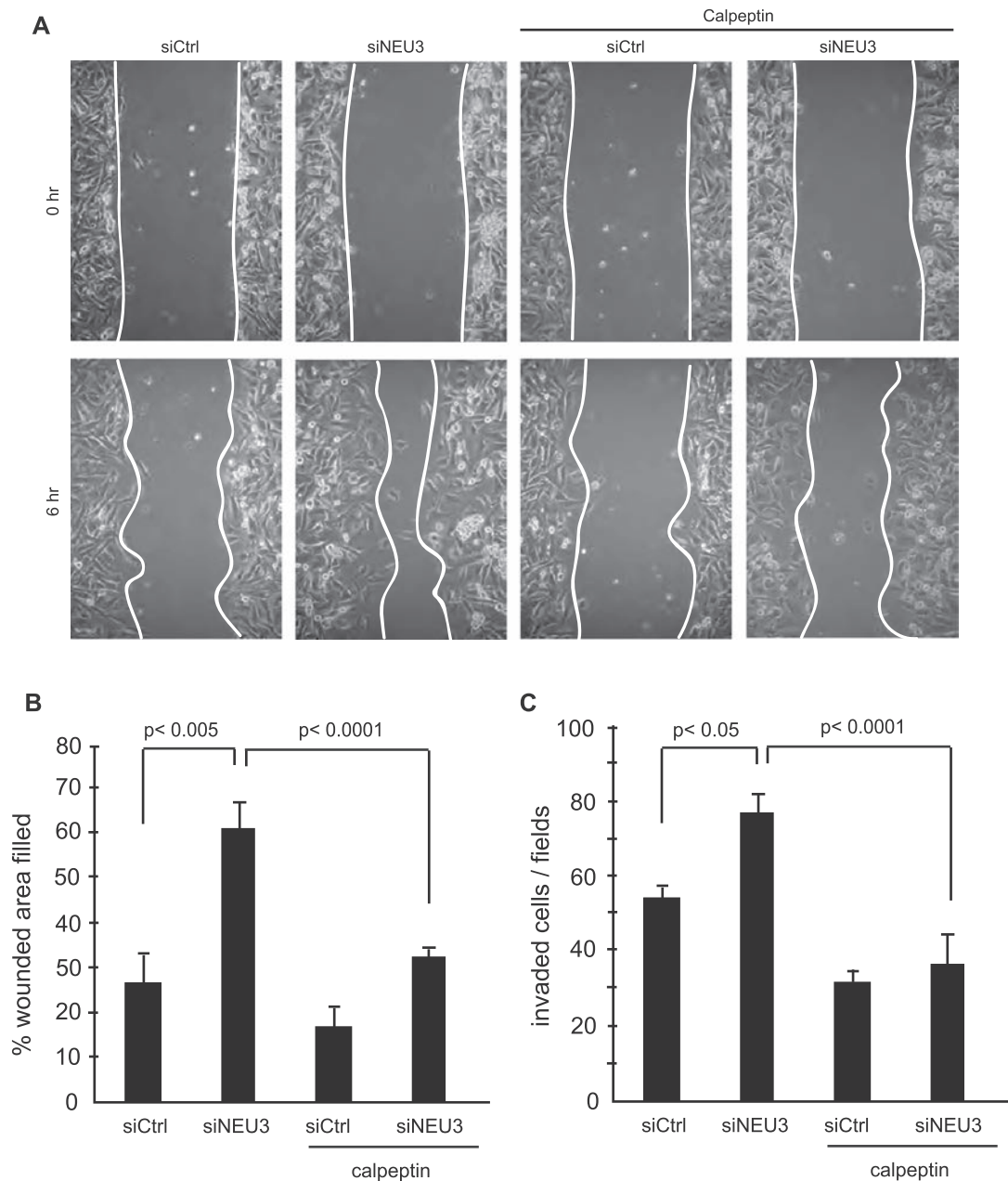


Fig. 7. Calpain inhibitor abrogation of enhanced cell invasion by NEU3 down-regulation.

(A) Promotion of cell migration in NEU3-silenced cells as assessed by wound healing assays and abrogation of the effects by treatment with the calpain inhibitor, calpeptin. (B) The values in the graph indicate changes in the wounded area in NEU3-silenced cells, obtained from three independent experiments. (C) Promotion of cell invasion in NEU3-silenced cells assessed using Biocoat Matrigel invasion chambers, and inhibition of the effects by calpeptin.

compared to control cells, but the augmentation was abrogated by the calpain inhibitor, calpeptin. Similarly, invasion assays using Biocoat Matrigel invasion chambers demonstrated promotion of cell invasion, which was also inhibited by calpeptin (Fig. 7C). These results suggest that NEU3 down-regulation observed in human glioblastoma tissues (Fig. 1) would contribute to the invasiveness, a characteristic feature of this malignancy, probably by causing calpain activation and acceleration of focal adhesion turnover through ganglioside modulation including GM3 accumulation as outlined in Fig. 8.

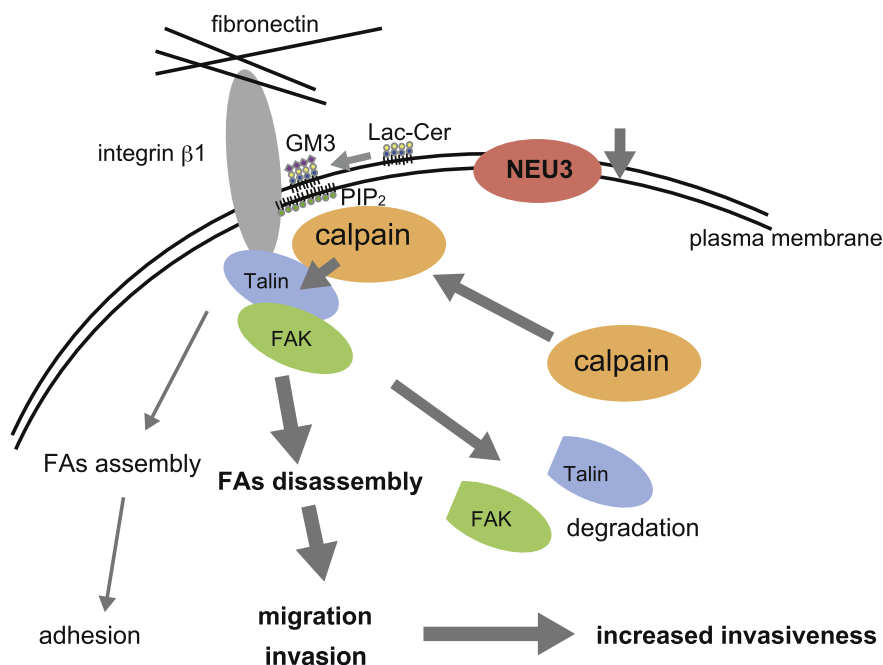


Fig. 8. A possible pathway of sialidase NEU3 contributions to invasiveness of human glioblastoma. NEU3 down-regulation in human glioblastoma tissues and glioblastoma cells could contribute to the increased invasiveness, by causing calpain activation and acceleration of FAs turnover through ganglioside modulation, including GM3 accumulation.

4. Discussion

In the present study, we examined whether sialidase is involved in the invasiveness of human glioblastoma cells, because a ganglioside-hydrolyzing sialidase, NEU3, is known to be associated with invasion and migration of carcinoma cells. As expected, but opposite to various carcinomas, human glioblastoma tissues showed down-regulation of NEU3, and siRNA-mediated NEU3 silencing of glioblastoma cells actually caused enhancement of invasiveness as compared with control cells. In this context, it is especially interesting that NEU3 silencing resulted in decreased cell motility of renal cell carcinoma through inhibition of IL6-mediated Akt/Rho signaling pathway [17], and also through blocking of β1 integrin recycling and FAK/AKT pathway [34]. The mechanism here for the increased cell invasion on down-regulation of the sialidase was found to involve promotion of degradation of focal adhesion proteins subsequent to calpain activation, with GM3 accumulation. It is uncertain at present what factors are responsible for the NEU3 effects different from those in other epithelial cancers, but may be attributed to the origin of most gliomas. According to current consensus [35], neural stem cells located in the subventricular zone of the brain are thought to be the source of glioma. They accumulate enough genomic mutations leading to diverse forms of glioma and undergo epithelial to mesenchymal transition, which is required for migratory phenotype and characterized by loss of epithelial morphology. This feature is likely to be the one of the factors for the differential effects of NEU3.

Previous studies have generally reported [10,11] that increase of GD3 and GM3 and decrease of gangliosides normally present in adult brain (GM1, GD1a, GD1b and GT1b) are characteristic features of human glioblastomas, correlating with a higher grade of malignancy. It is feasible that proportions of simple gangliosides such as GD3 and GM3 in glioma tissues would increase, because these are good substrates for NEU3 and would be expected to accumulate on its down-regulation. GD3 has recently been proposed as a key molecule contributing to glioblastoma invasiveness [12] and tumorigenicity [13]. In addition to causing calpain activation through GM3 accumulation, the NEU3 down-regulation observed in human gliomas might influence malignant properties through GD3 accumulation with GD3 synthase up-regulation.

Calpains are known to play roles in numerous physiological and

pathological phenomena. Calpain activity is altered during carcinogenesis and may be involved in processes contributing to cancer development and progression [36,37] by proteolysis of various substrates including focal adhesion proteins and proto-oncogene products. Interestingly, in our U251 cells, NEU3 down-regulation was found to activate calpain activity and cause accelerated degradation of focal adhesion proteins, such as Talin and FAK, leading to enhanced cell migration and invasion. This calpain activation was likely induced by increased GM3, as a result of decreased sialidase reactions. Previous work by Jan et al. also pointed to a requirement of calpain for glioblastoma cell invasion in calpain 2-silenced cells, calpain maintaining the level of extracellular metalloprotease 2 [38]. Our present study indicated that NEU3 gives rise to glioblastoma invasion by regulating the activity and cellular distribution of calpain through ganglioside modulation. Although the detailed mechanisms remains unclear at present, ganglioside changes including GM3 accumulation as the result of altered NEU3 expression might cause translocation of calpain to the cell surface and bring about potentiation of its activity. Consistent with our results, Chakrabarti et al. have described a ganglioside mixture to stimulate calpain activity [39], and Nuzzi et al. also have suggested in neutrophils that GM3-containing lipid rafts at the leading edge recruit phosphoinositides, such as PIP₃, and translocate calpain to membrane and lead to its activation [32]. It has also been reported that formation of sphingolipid-rich domain in the outer leaflet is required for accumulation of PIP₂ in the inner leaflet of the plasma membrane [40,41]. Our present findings that GM3 accumulation on NEU3 down-regulation can contribute to enhanced glioblastoma cell invasion by calpain activation point to a new mechanism of NEU3 for cell invasion and may provide a basis for the development of novel therapeutics targeting NEU3 in glioma patients.

Transparency document

The <http://dx.doi.org/10.1016/j.bbagen.2017.07.023> associated with this article can be found, in the online version.

Acknowledgments

We appreciate Dr. Akemi Suzuki (Tohoku Medical and Pharmaceutical University) for his helpful discussion, and also Mrs.

Setsuko Moriya (Tohoku Medical and Pharmaceutical University) and Mr. Tadashi Wada (Miyagi Cancer Center Research Institute) for their valuable technical assistance. This study was supported in part by Grants-in-Aid for Scientific Research on Innovative Areas (No. 3301) from the Ministry of Education, Culture, Sports, Science and Technology of Japan (24110514).

References

- [1] P.Y. Wen, S. Kesari, Malignant gliomas in adults, *N. Engl. J. Med.* 359 (2008) 492–507.
- [2] G.P. Dunn, M.L. Rinne, J. Wykosky, G. Genovese, S.N. Quayle, L.F. Dunn, P.K. Agarwalla, M.G. Chheda, B. Campos, A. Wang, C. Brennan, K.L. Ligon, F. Furnari, W.K. Cavenee, R.A. Depinho, L. Chin, W.C. Hahn, Emerging insights into the molecular and cellular basis of glioblastoma, *Genes Dev.* 26 (2012) 756–784.
- [3] I. Paw, R.C. Carpenter, K. Watabe, W. Debinski, H.W. Lo, Mechanisms regulating glioma invasion, *Cancer Lett.* 362 (2015) 1–7.
- [4] T. Miyagi, K. Yamaguchi, Mammalian sialidases: physiological and pathological roles in cellular functions, *Glycobiology* 22 (2012) 880–896.
- [5] T. Miyagi, K. Takahashi, K. Hata, K. Shiozaki, K. Yamaguchi, Sialidase significance for cancer progression, *Glycoconj. J.* 29 (2012) 567–577.
- [6] H. Yamamoto, A. Oviedo, C. Sweeley, T. Saito, J.R. Moskal, Alpha2,6-sialylation of cell-surface N-glycans inhibits glioma formation in vivo, *Cancer Res.* 61 (2001) 6822–6829.
- [7] Y.K. Chong, E. Sandanaraj, L.W.H. Koh, M. Thangaveloo, M.S.Y. Tan, G.R.H. Koh, T.B. Toh, G.G.Y. Lim, J.D. Holbrook, O.L. Kon, M. Nadarajah, I. Ng, W.H. Ng, N.S. Tan, K.L. Lim, C. Tang, B.T. Ang, *ST3GAL1*-associated transcriptomic program in glioblastoma Tumor Growth, Invasion, and Prognosis, *J. Natl. Cancer Inst.* 108 (2016) djv326.
- [8] K. Vajn, B. Viljetic, I.V. Degmeic, R.L. Schnaar, M. Heffer, Differential distribution of major brain gangliosides in the adult mouse central nervous system, *PLoS One* 8 (2013) e75720.
- [9] R.K. Yu, Y. Nakatani, M. Yanagisawa, The role of glycosphingolipid metabolism in the developing brain, *J. Lipid Res.* 50 (2009) S440–S445.
- [10] C.C. Sung, D.K. Pearl, S.W. Coons, B.W. Scheithauer, P.C. Johnson, A.J. Yates, Gangliosides as diagnostic markers of human astrocytomas and primitive neuroectodermal tumors, *Cancer* 74 (1994) 3010–3022.
- [11] R. Wagener, G. Röhn, G. Schillinger, R. Schröder, B. Kobbe, R.I. Ernestus, Ganglioside profiles in human gliomas: quantification by microbore high performance liquid chromatography and correlation to histomorphology and grading, *Acta Neurochir.* 141 (1999) 1339–1345.
- [12] Y. Ohkawa, H. Momota, A. Kato, N. Hashimoto, Y. Tsuda, N. Kotani, K. Honke, A. Suzumura, K. Furukawa, Y. Ohmi, A. Natsume, T. Wakabayashi, K. Furukawa, Ganglioside GD3 enhances invasiveness of gliomas by forming a complex with platelet-derived growth factor receptor α and yes kinase, *J. Biol. Chem.* 290 (2015) 16043–16058.
- [13] S.C. Yeh, P.Y. Wang, Y.W. Lou, K.H. Khoo, M. Hsiao, T.L. Hsu, C.H. Wong, Glycolipid GD3 and GD3 synthase are key drivers for glioblastoma stem cells and tumorigenicity, *Proc. Natl. Acad. Sci. U. S. A.* 113 (2016) 5592–5597.
- [14] T. Hasegawa, K. Yamaguchi, T. Wada, A. Takeda, Y. Itoyama, T. Miyagi, Molecular cloning of mouse ganglioside sialidase and its increased expression in Neuro2a cell differentiation, *J. Biol. Chem.* 275 (2000) 8007–8015.
- [15] K. Shiozaki, K. Koseki, K. Yamaguchi, M. Shiozaki, H. Narimatsu, T. Miyagi, Developmental change of sialidase neu4 expression in murine brain and its involvement in the regulation of neuronal cell differentiation, *J. Biol. Chem.* 284 (2009) 21157–21164.
- [16] C. Tringali, F. Cirillo, G. Lamorte, N. Papini, L. Anastasia, B. Lupo, I. Silvestri, G. Tettamanti, B. Venerando, NEU4L sialidase overexpression promotes β -catenin signaling in neuroblastoma cells, enhancing stem-like malignant cell growth, *Int. J. Cancer* 131 (2012) 1768–1778.
- [17] S. Ueno, S. Saito, T. Wada, K. Yamaguchi, M. Satoh, Y. Arai, T. Miyagi, Plasma membrane-associated sialidase is up-regulated in renal cell carcinoma and promotes interleukin-6-induced apoptosis suppression and cell motility, *J. Biol. Chem.* 281 (2006) 7756–7764.
- [18] K. Shiga, K. Takahashi, I. Sato, K. Kato, S. Saijo, M. Moriya, M. Hosono, T. Miyagi, Up-regulation of sialidase NEU3 in head and neck squamous cell carcinoma associated with lymph node metastasis, *Cancer Sci.* 106 (2015) 1544–1553.
- [19] S. Kawamura, I. Sato, T. Wada, K. Yamaguchi, Y. Li, D. Li, X. Zhao, S. Ueno, H. Aoki, T. Tochigi, M. Kuwahara, T. Kitamura, K. Takahashi, S. Moriya, T. Miyagi, Plasma membrane-associated sialidase (NEU3) regulates progression of prostate cancer to androgen-independent growth through modulation of androgen receptor signaling, *Cell Death Differ.* 19 (2012) 170–179.
- [20] T. Wada, K. Hata, K. Yamaguchi, K. Shiozaki, K. Koseki, S. Moriya, T. Miyagi, A crucial role of plasma membrane-associated sialidase in the survival of human cancer cells, *Oncogene* 26 (2007) 2483–2490.
- [21] T. Yamaguchi, K. Hata, K. Koseki, K. Shiozaki, H. Akita, T. Wada, S. Moriya, T. Miyagi, Evidence for mitochondrial localization of a novel human sialidase (NEU4), *Biochem. J.* 390 (2005) 85–93.
- [22] K. Koseki, T. Wada, M. Hosono, K. Hata, K. Yamaguchi, K. Nitta, T. Miyagi, Human cytosolic sialidase NEU2-low general tissue expression but involvement in PC-3 prostate cancer cell survival, *Biochem. Biophys. Res. Commun.* 428 (2012) 142–149.
- [23] G.M. D'Abaco, A.H. Kaye, Integrins: molecular determinants of glioma invasion, *J. Clin. Neurosci.* 14 (2007) 1041–1048.
- [24] W. Paulus, I. Baur, A.S. Beutler, S.A. Reeves, Diffuse brain invasion of glioma cells requires beta 1 integrins, *Lab. Invest.* 75 (1996) 819–826.
- [25] B.B. Tysnes, L.F. Larsen, G.O. Ness, R. Mahesparan, K. Edvardsen, I. Garcia-Cabrera, R. Bjerkvig, Stimulation of glioma-cell migration by laminin and inhibition by anti-alpha3 and anti-beta1 integrin antibodies, *Int. J. Cancer* 67 (1996) 777–784.
- [26] T.C. Saïdo, M. Shibata, T. Takenawa, K. Suzuki, Positive regulation of mu-calpain action by polyphosphoinositides, *J. Biol. Chem.* 267 (1992) 24585–24590.
- [27] L. Leloup, H. Shao, Y.H. Bae, B. Deasy, D. Stolz, P. Roy, A. Wells, m-Calpain activation is regulated by membrane localization and by its binding to phosphatidylinositol 4, 5-bisphosphate, *J. Biol. Chem.* 285 (2010) 33549–33566.
- [28] D. Fabris, M. Rozman, T. Saiko, Z. Vukelic, Aberrant ganglioside composition in glioblastoma multiforme and peritumoral tissue: a mass spectrometry characterization, *Biochimie* 137 (2017) 56–68.
- [29] S.-Y. Park, C.-Y. Kwak, J.A. Shayman, J.H. Kim, Globoside (Gb4) promotes activation of ERK by interaction with the epidermal growth factor receptor, *Biochim. Biophys. Acta* 1820 (2012) 1141–1148.
- [30] A. Szoor, L. Ujlaky-Nagy, G. Toth, J. Szollosi, G. Vereb, Cell confluence induces switching from proliferation to migratory signaling by site-selective phosphorylation of PDGF receptors on lipid raft platforms, *Cell. Signal.* 28 (2016) 81–93.
- [31] L.A. Morford, K. Forrest, B. Logan, L.K. Overstreet, J. Goebel, W.H. Brooks, T.L. Roszman, Calpain II colocalizes with detergent-insoluble rafts on human and Jurkat T-cells, *Biochem. Biophys. Res. Commun.* 295 (2002) 540–546.
- [32] P.A. Nuzzi, M.A. Senetar, A. Huttenlocher, Asymmetric localization of calpain 2 during neutrophil chemotaxis, *Mol. Biol. Cell* 19 (2007) 795–805.
- [33] S. Choi, N. Thapa, A.C. Hedman, Z. Li, D.B. Sacks, R.A. Anderson, IQGAP1 is a novel phosphatidylinositol 4, 5 bisphosphate effector in regulation of directional migration, *EMBO J.* 32 (2013) 2617–2630.
- [34] C. Tringali, B. Lupo, I. Silvestri, N. Papini, L. Anastasia, G. Tettamanti, B. Venerando, The plasma membrane sialidase NEU3 regulates the malignancy of renal carcinoma cells by controlling β 1 integrin internalization and recycling, *J. Biol. Chem.* 287 (2012) 42835–42845.
- [35] J. De Weille, On the genesis of neuroblastoma and glioma, *Int. J. Brain Sci* 2014 (2014) ID217503(14 pages Hindawi).
- [36] S.J. Storr, N.O. Carragher, M.C. Frame, T. Parr, S.G. Martin, The calpain system and cancer, *Nat. Rev. Cancer* 11 (2011) 364–374.
- [37] L. Leloup, A. Wells, Calpains as potential anti-cancer targets, *Expert Opin. Ther. Targets* 15 (2011) 309–323.
- [38] H.S. Jang, S. Lai, J.A. Greenwood, Calpain 2 is required for glioblastoma cell invasion: regulation of matrix metalloproteinase 2, *Neurochem. Res.* 35 (2010) 1796–1804.
- [39] A.K. Chakrabarti, S. Dasgupta, R.H. Gadsden Sr., E.L. Hogan, N.L. Banik, Regulation of brain m calpain Ca²⁺ sensitivity by mixtures of membrane lipids: activation at intracellular Ca²⁺ level, *J. Neurosci. Res.* 44 (1996) 374–380.
- [40] M. Abe, A. Makino, F. Hullin-Matsuda, K. Kamijo, Y. Ohno-Iwashita, K. Hanada, H. Mizuno, A. Miyawaki, T. Kobayashi, A role for sphingomyelin-rich lipid domains in the accumulation of phosphatidylinositol-4,5-bisphosphate to the cleavage furrow during cytokinesis, *Mol. Cell. Biol.* 32 (2012) 1396–1407.
- [41] H. Watanabe, K. Okahara, Y. Naito-Matsui, M. Abe, S. Go, J. Inokuchi, T. Okazaki, T. Kobayashi, Y. Kozutsumi, S. Oka, H. Takematsu, Psychosine-triggered endomitosis is modulated by membrane sphingolipids through regulation of phosphoinositide 4,5-bisphosphate production at the cleavage furrow, *Mol. Biol. Cell* 27 (2016) 2037–2050.

東北医科薬科大学分子生体膜研究所年報

2018年3月1日発行

発行者・発行所 東北医科薬科大学分子生体膜研究所
宮城県仙台市青葉区小松島4-4-1